



**HAL**  
open science

# Identification and characterisation of host factors governing Crimean-Congo Hemorrhagic Fever Virus entry

Maureen Ritter

► **To cite this version:**

Maureen Ritter. Identification and characterisation of host factors governing Crimean-Congo Hemorrhagic Fever Virus entry. Molecular biology. Ecole normale supérieure de lyon - ENS LYON, 2024. English. NNT: 2024ENSL0042 . tel-04784612

**HAL Id: tel-04784612**

**<https://theses.hal.science/tel-04784612v1>**

Submitted on 15 Nov 2024

**HAL** is a multi-disciplinary open access archive for the deposit and dissemination of scientific research documents, whether they are published or not. The documents may come from teaching and research institutions in France or abroad, or from public or private research centers.

L'archive ouverte pluridisciplinaire **HAL**, est destinée au dépôt et à la diffusion de documents scientifiques de niveau recherche, publiés ou non, émanant des établissements d'enseignement et de recherche français ou étrangers, des laboratoires publics ou privés.



# THESE

en vue de l'obtention du grade de Docteur, délivré par  
l'ECOLE NORMALE SUPERIEURE DE LYON

**Ecole Doctorale N°340**  
Biologie Moléculaire, Intégrative et Cellulaire (BMIC)

**Discipline : Sciences de la vie et de la santé**

Soutenue publiquement le 27/09/2024, par :

**Maureen RITTER**

---

## **Identification and characterisation of host factors governing Crimean-Congo Hemorrhagic Fever Virus entry**

Identification et caractérisation des facteurs cellulaires gouvernant l'entrée du virus de la  
Fièvre Hémorragique de Crimée-Congo

---

Sous la direction de : François-Loïc COSSET et Chloé JOURNO

Devant le jury composé de :

**Aurélié ALBERTINI**, CR - HDR, I2BC, Université Paris-Saclay  
**Jean-Luc BATTINI**, DR2, IRIM, Université de Montpellier  
**Pierre-Yves LOZACH**, DR2, IVPC, Université Claude Bernard Lyon 1  
**Chloé JOURNO**, MCU - HDR, CIRI, Ecole normale supérieure de Lyon

Rapporteuse  
Rapporteur  
Examineur  
Co-directrice de thèse



## Summary

The Crimean-Congo Hemorrhagic Fever Virus (CCHFV) is a deadly emerging pathogen from the *Orthonairovirus* genus. The virus is transmitted through ticks and has a broad tropism, infecting humans, cattle, small mammals, or birds.

Until recently, the CCHFV entry receptor was unidentified. Indeed, nucleolin was suggested but was not further characterised. In this context and using transcription- and entry-competent virus-like particles (tecVLPs), I first assessed the role of nucleolin. Unexpectedly, while performing this experiment, I found that, another cellular factor, the low-density lipoprotein receptor (LDL-R) was playing a crucial role in CCHFV infection.

LDL-R is a lipid transfer receptor that allows the uptake of cholesterol, contained in lipoproteins, from the circulation. This internalisation is mediated by the apolipoprotein E (apoE), that is present onto the lipoproteins, and that binds to the LDL-R.

Using antibodies, soluble proteins and knockdowns, I was able to determine that LDL-R promotes CCHFV infection. Then, by inhibiting endocytosis and increasing the cell surface expression of the receptor, I showed that LDL-R was a binding and internalisation factor. Moreover, I showed that this entry pathway was not used in bovine cells.

Then, I was able to determine that apoE is present onto the virion and promotes binding to the receptor, thus facilitating the virus entry.

Finally, thanks to a collaboration, I was able to confirm my results using the authentic virus in the biosafety level 4 laboratory.

To summarise, I discovered LDL-R as an entry factor allowing the binding and internalisation of CCHFV into human cells. Furthermore, I characterised that the interaction virus – receptor happens through apoE incorporated onto the particles. This results open the possibility for new therapeutic treatments targeting these factors.



## Résumé

Le virus de la fièvre hémorragique de Crimée-Congo (VFHCC) est un pathogène émergent mortel appartenant au genre des *Orthonairovirus*. Le virus est transmis par les tiques et a un large tropisme, infectant l'homme, le bétail, les petits mammifères ou les oiseaux.

Jusqu'à récemment, le récepteur d'entrée du VFHCC n'était pas identifié. Dans ce contexte et en utilisant des particules virales compétentes pour la transcription et l'entrée (tecVLPs), j'ai évalué le rôle de la nucléoline. De façon inattendue, lors de cette expérience, j'ai mis en évidence que le récepteur des lipoprotéines de basse densité (LDL-R), et déterminé qu'il jouait un rôle crucial dans l'infection par le VFHCC.

Le LDL-R est un récepteur de transfert de lipides qui permet l'absorption du cholestérol en circulation dans les lipoprotéines. Cette internalisation se fait par l'intermédiaire des apolipoprotéines E (apoE), présents sur les lipoprotéines, et qui se lie aux récepteurs de type LDL-R.

En utilisant des anticorps, des protéines solubles et des knock-downs, j'ai pu déterminer que LDL-R favorise l'infection par le VFHCC. En inhibant l'endocytose et en augmentant l'expression du récepteur à la surface des cellules, j'ai montré que le LDL-R était un facteur d'attachement et d'internalisation en cellules humaines. De plus, j'ai démontré que LDL-R n'était pas un facteur d'entrée en cellules bovines.

Ensuite, j'ai pu déterminer qu'apoE est présente sur le virion et promeut la liaison au récepteur LDL-R, donc l'entrée du virus.

Enfin, grâce à une collaboration, j'ai pu confirmer mes résultats en utilisant le virus authentique, manipulé en laboratoire de biosécurité de niveau 4.

En résumé, j'ai découvert un facteur d'entrée permettant l'attachement et l'internalisation du VFHCC dans les cellules humaines. De plus, j'ai caractérisé que l'interaction virus-récepteur se fait par l'intermédiaire de l'apoE incorporée dans les particules. Ces résultats ouvrent de nouvelles possibilités de traitements thérapeutique ciblant ces facteurs.



## Acknowledgments

I would like to thank my jury members, Dr. Aurélie Albertini, Dr. Jean-Luc Battini and Dr. Pierre-Yves Lozach for accepting to evaluate this work and taking part in my PhD defence jury. I would like to also thank my thesis committee, Dr. Mathieu Mateo and Dr. Laurence Briant for their time and advice.

I would like to thank my supervisor Dr. François-Loïc Cosset, which gave me the opportunity to do a PhD and thanks Dr. Solène Denolly for the meetings I had in videoconference, since you were doing a post-doc in Germany. Thanks to you and François-Loïc, the PhD project that I started was successfully published.

I am more than grateful to Dr. Chloé Journo, my co-supervisor, which adopted me and my project for the last year. You gave a lot of your time to allow me to successfully complete my PhD. You were there for the meetings and the rehearsals. You worked with me on this manuscript and taught me how to improve myself on so many levels. Working with you was extremely enriching, and I really want to say “thank you” for accepting being my co-supervisor.

I will also thank the EVIR members, and the collaborators who participate in the receptor project.

Anupriya, Apoorv, Li, Bertrand, Vincent and Sergueï for your great inputs, and Christelle and Chloé for the HCV experiments.

I also want to thank the Nitrovire team: Dr. Cyrille Mathieu, Alexandre Lalande, and Lola Canus, who made it possible to verify our results in the BSL-4 laboratory, for our discussions and your kindness. Thank you Cyrille for always being available and for your great help on this manuscript.

More than the EVIR members, I need to express my gratitude to all the friends I gained in the team.

It all started with Dr. Natalia Freitas, my first internship supervisor, which became my first scientific mentor and then my PhD supervisor. You are the reason why I had to write all of



these, why I never pipet less than 2 $\mu$ L, why I have milk in my secondary antibody and why my liver is starting to show signs of weakness.

I also thank Dr. Margot Enguehard, who taught me how to manipulate and is the reason I only think of cocktails when preparing my sucrose for ultracentrifugation.

I need to talk about Dr. Didier Negre, the father figure I was not expecting to find at work. You were always there for my technical and sentimental issues. You showed me how to fix a hood, a pipet, a bike and a door. Didier, you made everything better, and I hope you will enjoy your retirement.

I also complained a lot to Caroline Costa and Séverine Périán who took the time to listen to me. Thank you very much for all the time spend in your office and all the support you gave me.

Thank you Gisèle Froment for your kindness and the great food.

Then I want to thank my fellow labmates, “les Djeuns EVIR”. I don’t even know where to start. I am grateful for all your scientific inputs, for your helps during my experiments, for the hugs when I needed it, for the motivation when I had none but most importantly, thank all of you for the memories.

Clélia for your incredible patisserie, and please, I beg you, can you do a strawberry / pistachio cake for my PhD defence? But also thank you for your kindness that I really appreciated and needed.

Thomas for the language skills I had to develop to be able to insult you, or just for your presence, you were able to brighten my day with your face. I will always remember the “Padre” or our series of pictures in St Raphael. Oh, and my mom hopes you are doing well in Singapore.

Marie and Audrey, the incredible and officially inseparable duo. You saw me through a lot of stages of my life and were a main support during the PhD. I loved every talk, every laugh and every moment requiring closing the door of Caroline’s office.

Solène a.k.a. Babyso, my CCHFV teammate, thank you for everything. From small talks to experimentations, your input was valuable. You probably taught me more than everyone else, not only in science but also in life, where I saw you giving all you had and even more.

Finally for the team, thank you Johan, my partner in crime, the “tic” to my “tac” and my second neuron. There are so many things to say. You were there for the nights in the lab, for my coffees, for my beers and simply for me. I do not remember being without you for more

than an hour. Always together to prepare for trouble and make it double. To protect the lab from devastation. To unite all PhD students within the CIRI. To denounce the evils of truth and love. To extend our reach to the stars above. Momo and Jojo blast off at the speed of light.

I also thank your cousin Roman, who helped motivate me for the writing by forcing me to stay late in the library and for the great food he cooked. Same, please, I would like a cake for the defence.

I have been very well supported, not only in the team but also within the CIRI. I would like to thank Sandrine Alais, Clara Blasco, Philippe Mangeot and Lionel Condé in the M5. I also thank the UBIVE team (especially Xavier, Caro, Alex, and Blaise), and Olivier and Emeric from the tour Cervi. Doing this PhD with your support changed everything.

A special mention to Clément Luy, Ludivine Vagneur, the whole CHSCT and the cellule signalement de l'ENS for their help, and for everything they have done for so many PhD students. Also, thank you Muriel Grammont and BMIC for the time spent for me.

It will also probably be the only opportunity I have to thank Dr. Maria Dimitrova that gave me the passion for the virology.

But all of these would not have happened without my long-time friends and family.

Thank you, mom, for the education you gave me. I inherited your temperament that was more than useful during these 3 years. You taught me not to take the easy way out and to fight. Thank you also, Christophe, for the invaluable support you gave me and my sister during all these years.

I also got the support of one of the most incredible woman, my godmother Jenny.

Thank you Gaëlle, my little sister, for not being that annoying. I am immensely proud of you and how you've grown. You will be a fantastic teacher.

I also thank my dad for everything. First, for everything you taught me. The patience, the kindness and for the thousands of bad jokes. And finally, for your support during all my years of study. For being there in Lyon as you were in Strasbourg. I would never have been able to

be here today without you. Finally, thank you Mamouma for everything. Vun deiner Ankeltochter un vu de, vielleicht, Dr. Ritter, merci vielmols.

I am grateful to Dr. Kodie Noy. I am so glad I met you, so glad I shared my days, my thoughts, my mistakes and my madness with you. You are the most unique person, and I enjoyed the time spent by your side. Thank you for this 3 years campaign of Dungeon and Dragons, for the rehearsals in frenglish, the game nights, and for all the incredible food you made and helped me survived (food is really important during a PhD, it should not be underestimated). Also, thanks to my cat, Brioche. She is not the smartest little girl, not the most beautiful princess, nor the cuddliest ball of fur, but she helped with the PowerPoint by adding random characters (I am sorry in advance, I would probably not find them all).

I would like to thank Loïc Bertin, for the incredible riddles, and fantastic discussions we had. I have great hopes for the genius that you are.

Thanks to MTPLBG, Elodie Chabrol, Laëtitia Lebec, Lucie Boël and Valentin Gauthier. For everything I learned by your side during the preparation of Ma Thèse pour les nuls, and for all the emergencies meetings we had.

I am grateful to all the BMC master students, especially to Léa, Juliette, Jonathan, Maxime, Agathe, Quentin, Nicolas, Olwenn,... for the evenings spent at studying, and in the worst case scenario, drinking. I could not have imaging being part of such an incredible master.

Then, for the 4-4-2 team from Strasbourg: thank you Amélie Schäfer, future Dr. Amira Slama, Dr. Valod, Dr. Robin Kuster, Daniel Rusu and David Nguyen for all the nights in the library, for our great buffets in the PEGE and for the study Sundays. But mainly, thanks all of you for the incredible memories, the laughs, and the drinks.

I go back a bit further in time and thanks my high school and adulthood best friends, Julien and Pauline. You are true to yourself and are always there for me. I just love being with you and living the same moment we had in high school, but with money.

Finally, thanks to all of you who crossed my path and shaped the person I am and proud to be, and to you, who are reading this manuscript.



## Table of contents

<b>CHAPTER I. INTRODUCTION .....</b>	<b>25</b>
A. The Crimean-Congo Hemorrhagic Fever virus, an emerging threat .....	25
1. CCHFV discovery and transmission .....	25
a. Discovery and historical perspective .....	25
b. Geographic distribution .....	26
c. Vectors of CCHFV .....	28
d. Transmission dynamics to vertebrates .....	29
e. Human transmission .....	31
f. A global health concern .....	31
2. CCHF pathogenesis, diagnostics, and treatments .....	32
a. Symptoms .....	32
b. Histopathologic studies and biochemical changes .....	33
c. Diagnosis .....	34
d. Treatment .....	34
e. Prevention .....	35
B. CCHFV characteristics and structure .....	37
1. Taxonomy .....	37
2. Genome and virion structure .....	38
3. Viral proteins and their roles .....	39
a. Proteins encoded by the S-segment .....	39
b. Proteins encoded by the M-segment .....	41
c. Proteins encoded by the L-segment .....	43
4. Production of new CCHFV virions .....	44
a. Replication step .....	45
b. GPC maturation and viral production .....	47
c. Assembly and egress .....	49
C. Viral entry of CCHFV and other members of the <i>Bunyaviricetes</i> class .....	49
1. Putative attachment factors for CCHFV .....	50
a. Nucleolin .....	50
b. DC-SIGN .....	51
c. Heparan Sulfate Proteoglycans .....	51
2. Internalisation routes for CCHFV .....	52
a. CCHFV relies on clathrin-mediated endocytosis .....	52
b. Cholesterol-dependant endocytosis in CCHFV entry .....	52
3. Fusion .....	53
4. CCHFV cellular tropism .....	54
5. Tools to identify entry factors .....	56
a. Affinity purification–mass spectrometry .....	56
b. Genome modifications: gain of function and loss of function screens .....	57
c. Pooled vs arrayed screens .....	59
6. <i>Bunyaviricetes</i> entry .....	60

D.	Low-density lipoprotein receptors in viral entry .....	63
1.	Lipoproteins and cholesterol.....	63
a.	Formation of lipoproteins.....	63
b.	Apolipoproteins on VLDL, IDL and LDL .....	65
2.	LDL-R family: pattern of expression, structure, and functions independent of viral infection.....	66
a.	Common features of the LDL receptors .....	66
b.	LRP1 .....	68
c.	LRP1B .....	68
d.	Megalin .....	69
e.	ApoER2.....	69
f.	VLDL-R.....	70
g.	LDL-R .....	70
3.	Roles of LDL receptors in viral infection.....	72
E.	Tools to study CCHFV .....	76
1.	Minigenome system .....	76
2.	Pseudotyped particles .....	77
3.	Transcription- and entry- competent virus-like particles .....	78
4.	Viral replicon particles.....	79
5.	Recombinant CCHFV .....	80
6.	Animal models.....	81

**CHAPTER II. OBJECTIVE OF THE WORK, AND SCIENTIFIC CONTRIBUTIONS TO OTHER PROJECTS .....83**

1.	CCHFV_tecVLPs are protected by a secreted cellular factor. ....	83
2.	Trafficking motifs in CCHFV Gn and Gc cytoplasmic tails govern CCHFV assembly.....	84
3.	Identification and characterisation of LDL-R as an entry factor for CCHFV.....	84

**CHAPTER III. RESULTS .....87**

A.	CCHFV_tecVLPs are protected by a secreted cellular factor. ....	87
1.	Context .....	87
2.	Results .....	87
3.	Conclusion .....	89
B.	Trafficking motifs in CCHFV Gn and Gc cytoplasmic tails govern CCHFV assembly.....	90
1.	Context .....	90
2.	Results .....	91
3.	Conclusion .....	94
C.	LDL-R and apoE associated with CCHFV particles mediate the virus entry into human cells. ....	95
1.	Context .....	95
2.	Results .....	95
3.	Conclusion .....	109

<b>CHAPTER IV. DISCUSSION.....</b>	<b>111</b>
A. Perspectives on the identified lipid's receptors.....	111
1. LDL-R as an entry factor for CCHFV .....	111
2. LDL-R is not the only entry factor for CCHFV .....	112
a. LRP8 .....	113
b. VLDL-R.....	114
c. LRP1 .....	114
B. Role of apolipoproteins in CCHFV infection .....	116
1. Incorporation onto particles .....	116
a. Incorporation during production or after secretion?.....	116
b. Linked lipoproteins or apoE incorporation?.....	117
2. Role of apolipoproteins in the production of CCHFV particles .....	119
3. Impact of apolipoproteins incorporation.....	120
a. Cell-cell transmission .....	120
b. Hiding CCHFV epitopes .....	121
c. Indirect treatments against CCHFV .....	121
C. Relevance in non-human hosts .....	122
1. Murine hosts .....	122
2. Bovine hosts .....	123
3. Ticks, main vector of CCHFV.....	124
 <b>CHAPTER V. GENERAL CONCLUSION .....</b>	 <b>126</b>
 <b>CHAPTER VI. MATERIAL AND METHODS .....</b>	 <b>129</b>
 <b>CHAPTER VII. REFERENCES .....</b>	 <b>139</b>
 <b>CHAPTER VIII. LIST OF PUBLICATIONS, PATENTS, AND PARTICIPATIONS TO SCIENTIFIC EVENTS.....</b>	 <b>167</b>
 <b>CHAPTER IX. ANNEXE.....</b>	 <b>169</b>





## List of figures

Figure 1: Phylogenetic tree and map of the geographic distribution of CCHFV .....	27
Figure 2: Schematic overview of the life cycle of Hyalomma ticks and its role in CCHFV circulation.....	29
Figure 3: Total worldwide CCHFV seroprevalence reported in domestic animals by species.	30
Figure 4: Schematic representation of symptoms and biological changes occurring during CCHFV infection.....	33
Figure 5: Bunyaviricetes phylogenetic tree.....	37
Figure 6: Schematic representation of CCHFV virion.....	38
Figure 7: Negatively stained CCHFV particle from a porcine kidney cell culture preparation.	39
Figure 8: Crystal structure of CCHFV NP .....	40
Figure 9: X-ray structure of CCHFV Gc IbAr10200 strain .....	42
Figure 10: Schematic representation of the CCHFV replication cycle .....	45
Figure 11: Model of bunyaviruses transcription and translation .....	47
Figure 12: Schematic representation of the CCHFV glycoproteins processing.....	48
Figure 13: Mechanism of bunyaviruses class II membrane fusion protein .....	54
Figure 14: Formation of LDL (endogenous lipid metabolism).....	64
Figure 15: Structure of the core members of the low-density lipoprotein receptor family....	67
Figure 16: LDL endocytosis by LDL-R.....	71
Figure 17: Models of HCV association with lipoproteins .....	73
Figure 18: CCHFV minigenome assay.....	77
Figure 19: CCHFV_tecVLP assay .....	79
Figure 20: CCHFV VRP assay.....	80
Figure 21: CCHFV particles are slightly sensitive to a 37°C incubation period .....	88
Figure 22: Intracellular particles are stable at 37°C.....	88
Figure 23: Purified CCHFV_tecVLPs are protected from temperature-sensitive degradation by secreted factors.....	89
Figure 24: Infectivity of CCHFV Gc cytoplasmic tail mutants.....	92
Figure 25: Infectivity and viral incorporation of CCHFV Gn cytoplasmic tail mutants.....	93
Figure 26: Production of infectious CCHFV particles from PACS-1 knockdown cells .....	94
Figure 27: NCL is not an essential factor for CCHFV infection contrary to LDL-R.....	96
Figure 28: LDL-R is a cofactor of CCHFV infectivity .....	97
Figure 29: Expression of LDL-R at the surface of Huh-7.5, A549, TE-671, EBL, MDBK and PHH cells assessed by flow cytometry .....	97
Figure 30: Levels of tecVLPs infection in different cell types.....	98
Figure 31: LDL-R is a factor of CCHFV infection in human but not in bovine.....	99
Figure 32: LDL-R play a role in the early steps of CCHFV infection.....	100
Figure 33: LDL-R promotes CCHFV entry.....	101
Figure 34: TyrA23 treatment inhibits LDL-R endocytosis and thus LDL uptake.....	103
Figure 35: TyrA23 treatment inhibits CCHFV_tecVLPs endocytosis but may increase CCHFV_tecVLPs binding .....	105
Figure 36: ApoE promote CCHFV infection .....	107

Figure 37: ApoE is associated with CCHFV particles .....	108
Figure 38: ApoE is a cellular factor contributing CCHFV particles assembly, secretion, or infectivity.....	109
Figure 39: Possible models of CCHFV particles, associated to apolipoproteins and/or lipoproteins. ....	118
Figure 40: Schematic representation of CCHFV IbAr10200 GPC and highlight on the CARC-CRAC motifs.....	119
Figure 41: Comparison of LDL-R and VtgR structures .....	125
Figure 42: Schematic representation of the factors involved in CCHFV entry into human cells. ....	127

## List of tables

Table 1: Table summarising the known roles of CCHFV's proteins .....	44
Table 2: List of 25 common plasma membrane proteins genes expressed in permissive cells with low or no expression in non-permissive cells .....	55
Table 3: Summary table of Bunyaviricetes receptors or co-factors of entry.....	62
Table 4: Different class of human lipoproteins .....	65
Table 5: LDL receptors playing a role in viral entry.....	75
Table 6: Summarised results from the Xu et al., Monteil et al., and Ritter et al .....	115
Table 7: List of the antibodies.....	130



## Abbreviations

<b>Abbreviation</b>	<b>Complete name</b>
AGDP	Agar gel diffusion precipitation
ALT	Alanine transferase
AP-2	Adaptor protein 2
AP-MS	Affinity purification-mass spectrometry
ApoE	Apolipoprotein E
ApoER2	Apolipoprotein E receptor 2
AST	Aspartate transaminase
BSL	Biosafety level
BUNV	Bunyamwera virus
BVDV	Bovine viral diarrhea virus
CCHFV	Crimean-Congo Hemorrhagic Fever virus
CD	Cytoplasmic domain
CDC	Center for Disease Control and Prevention
CETP	Cholesterol ester transfer protein
CF	Complement-fixation
CME	Clathrin-mediated endocytosis
CPK	Creatinine phosphokinase
CPZ	Chlorpromazine
CRISPR/Cas9	Clustered Regularly Interspaced Short Palindromic Repeats/CRISPR associated protein 9
CRISPRi	CRISPR/Cas9 interference
cRNA	Complementary RNA
CT	Cytoplasmic tail
dCas9	Deactivated Cas9
DC-SIGN	Dendritic Cell-Specific Intracellular-3-Grabbing Non-integrin
DRC	Democratic Republic of the Congo
dsRNA	Double-stranded RNA
EBIV	Ebinur Lake Virus
EE	Early endosome
EEEV	Eastern equine encephalitis virus
EGF	Epidermal growth factor
ELISA	Enzyme-linked immunosorbent assays
EM	Electron microscopy
ER	Endoplasmic reticulum
ESCRT	Endosomal sorting complex required for transport
FBS	Foetal bovine serum
Gc	Glycoprotein c
GETV	Getah Virus
GFP	Green fluorescent protein
Gn	Glycoprotein n

<b>Abbreviation</b>	<b>Complete name</b>
GOF	Gain of function
GP	Glycoprotein
GPC	Glycoprotein precursor complex
HAZV	Hazara virus
HBV	Hepatitis B virus
HCV	Hepatitis C virus
HDL	High-density lipoprotein
HI	Hemagglutination-inhibition
HIV	Human immunodeficiency virus
HSP70	Heat shock protein 70
HSPG	Heparan sulfate proteoglycan
IDL	Intermediate-density lipoprotein
IFN	Interferon
IFN-I	Type I interferon
Ig	Immunoglobulin
JEV	Japanese Encephalitis Virus
Kb	Kilobase
KD	Knock down
KO	Knock out
LACV	La Crosse encephalitis virus
LDH	Lactate dehydrogenase
LDLR	Low-density lipoprotein receptor
LE	Late endosome
LOF	Loss of function
LRP1	LDL-R related protein 1
MA-CCHFV	Mouse adapted CCHFV
mgRNA	Minigenome RNA
MLD	Mucin-like domain
MLV	Murine Leukemia Virus
MOI	Multiplicity of infection
MTP	Microsomal triglyceride transfer protein
MVB	Multivesicular bodies
NCL	Nucleolin
NGS	Next-generation sequencing
NHP	Non-human primate
NK	Natural killer
NLuc	NanoLuc luciferase
NP	Nucleoprotein
NSm	Non-structural protein m
NSs	Non-structural protein s
NT	Neutralisation test
NWM	Newborn white mouse
OE	Overexpression

<b>Abbreviation</b>	<b>Complete name</b>
ORF	Open reading frame
OROV	Oropouche virus
OTU	Ovarian tumor protease
PCSK9	Proprotein convertase subtilisin/kexin type-9
PHH	Primary human hepatocyte
p.i.	Post-infection
pp	Pseudotyped particle
RAP	Receptor-associated protein
rCCHFV	Recombinant CCHFV
RdRp	RNA-dependant RNA polymerase
RNAi	RNA interference
RNP	Ribonucleoprotein
RSV	Respiratory Syncytial Virus
RT-PCR	Reverse-transcription polymerase chain reaction
RVFV	Rift Valley Fever Virus
SFSV	Sandfly fever Sicilian virus
sgRNA	Small guide RNA
shRNA	Short hairpin RNA
SKI-1/S1P	Subtilisin kexin isozyme-1/site-1 protease
TMD	<i>Trans</i> -membrane domain
tecVLP	Transcription and entry competent viral-like particle
TGN	<i>Trans</i> -Golgi network
TL	T-lymphocyte
TNF- $\alpha$	Tumor necrosis factor $\alpha$
TyrA23	Tyrphostin A23
UTR	Untranslated region
VEEV	Venezuelan equine encephalitis virus
VLDL-R	Very-low-density lipoprotein receptor
VLP	Virus-like particles
vRNA	Viral RNA
VRP	Viral replicon particle
VSV	Vesicular stomatitis virus
VSV-G	VSV glycoprotein
VtgR	Vitellogenin receptor
WBC	White blood cell
WHO	World Health Organization
WT	Wild-type





## Chapter I. Introduction

### A. The Crimean-Congo Hemorrhagic Fever virus, an emerging threat

#### 1. CCHFV discovery and transmission

The Crimean-Congo Hemorrhagic Fever Virus, or CCHFV, is the pathogen that causes the Crimean-Congo Hemorrhagic fever disease. CCHF disease is characterised by fever, nausea, haemorrhage and can lead to death. The virus is transmitted through ticks, and with 10 000 to 15 000 cases reported each year, it is the one of the most infectious tick-borne virus known to infect humans (Patel *et al.*, 2023).

##### a. Discovery and historical perspective

The Crimean-Congo Hemorrhagic Fever Virus is described as an emerging virus, but the wide distribution of infected ticks across southern Asia, south-eastern Europe and Africa suggests that human infection may have first occurred earlier than thought. Indeed, Abū Bakr al-Rāzī (854–932), a physician of the eastern world, described three cases with symptoms similar to CCHF (Arda and Aciduman, 2007). Later in the 12<sup>th</sup> century, central Asia physicians noticed a link between tick bites and severe haemorrhagic illnesses, and in the 1970's Harry Hoogstraal suggested that these illness could be CCHF (Arda and Aciduman, 2007; Hoogstraal, 1979).

However, the first recognised outbreak took place in the Crimean Peninsula. In 1944, during the World War II, 200 Soviet military physicians in the Crimean Peninsula encountered a mysterious and severe febrile illness, and around 10% died. The viral origin of the "Crimean Hemorrhagic Fever" was discovered by the scientist Mikhail Chumakov between 1944 and 1945, by reproducing the disease through inoculation of patients' blood to non-infected individuals (Hoogstraal, 1979). At that time, the newborn white mouse (NWM) was a common experimental system used to isolate viruses, since the young mice were almost always susceptible to viral agents. In collaboration with Lev Zilber, Mikhail Chumakov isolated the virus from NWM brain and newborn rat brain tissue after intracranial injection

of sera from convalescent patients. He then linked the disease with tick exposure (Hoogstraal, 1979).

In the meantime, in 1956 in Belgian Congo (now the Democratic Republic of the Congo, DRC), Ghislaine Courtois received in the clinic a 13-year-old child with nausea and vomiting. Dr. Courtois inoculated the child's blood into 3-day-old mice. One mouse became sick. He then serially inoculated the mouse's brain into 2-day-old mice and observed similar symptoms. These serial passages suggested a viral agent. A month later, the doctor himself became ill and his blood was inoculated into infant mice after passing through a bacteria-tight filter. All mice developed symptoms, establishing the nature of the pathogen, named "Congo virus" (Woodall, 2007).

Isolates from the "Crimean Hemorrhagic Fever Virus" (CHFV) and the "Congo virus" were both received at the world reference center for arboviruses at Yale in 1969. There, Dr. Jordi Casal observed, by complement-fixation (CF), that both viruses were antigenically indistinguishable and proposed the name "CHF-Congo" (Casals, 1969). This name was then changed to "Crimean-Congo Hemorrhagic Fever Virus". At that time, the fact that the virus had been isolated from two distinct and distant geographic locations already suggested that its distribution could in fact be widespread.

#### b. Geographic distribution

Since its detection in eastern Europe or central Africa, the virus is now known to be widespread across Europe, Africa and Asia. According to the Center for Disease Control and Prevention (CDC, Centers for Disease Control and Prevention, 2014), there are more than 40 countries considered to be endemic to CCHFV, mostly in central Asia and central Africa (Figure 1). The virus is endemic in Turkey, Iraq, Iran, Afghanistan, and Uzbekistan, with more than 50 human cases reported per year in those countries. It is also present in the Balkan states, Mauritania, Sudan, and South Africa, with 5-49 cases reported per year according to the World Health Organization (WHO, Crimean-Congo haemorrhagic fever). Phylogenetic analysis of the S-segment (the most conserved viral genomic segment) led to the identification of 7 clades: Clade I (Africa 2), clade II (Africa 1), clade III (Africa 3), clade IV (Asia

1), clade V (Europe 1), clade VI (Europe 2) (see Figure 1) (Hewson *et al.*, 2004; Shahhosseini *et al.*, 2021).

More recently, sero-surveillance programs have provided evidence of CCHFV in southwestern Europe countries, such as Portugal (Filipe *et al.*, 1985), Spain (Palomar *et al.*, 2017) and France since October 2023 (Bernard *et al.*, 2024; Santé Publique France, 2023).

The spread of the virus in non-endemic areas can be attributed to human movement but also to climate change, which influences vertebrate host migration and can propagate the virus' vectors described in the following section. For instance, *Hyalomma marginatum* and *H. rufipes* ticks, that are known to be present only in areas with relatively hot and dry climates, are now also detected in Sweden (Grandi *et al.*, 2020).

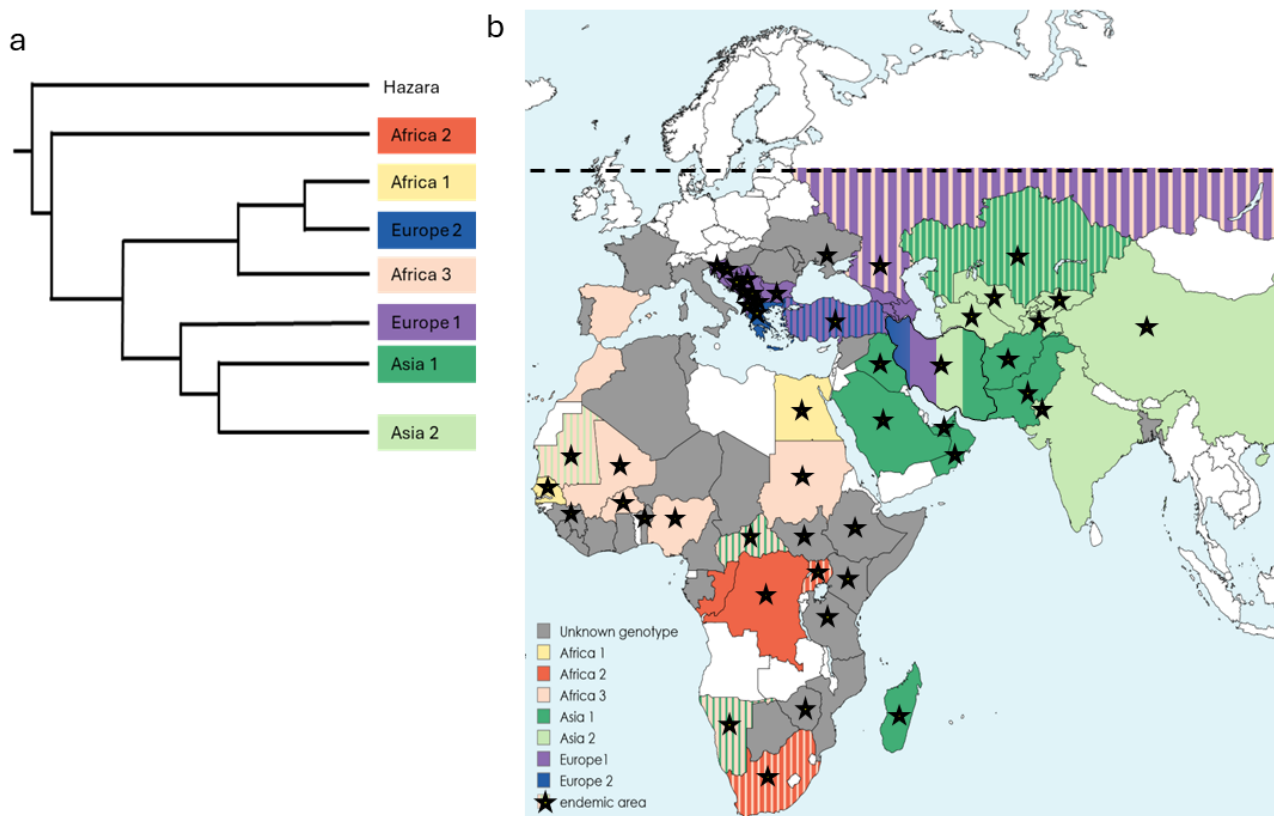


**Figure 1: Phylogenetic tree and map of the geographic distribution of CCHFV.** (a) Phylogenetic Maximum Likelihood tree based on the S-segment of CCHFV. (b) Map representing the wide distribution of CCHFV evidenced in Africa, Europe and Asia. Countries are coloured accordingly to the prevalent genotype identified. In grey, countries where CCHFV was detected but where the prevalent genotype is still unknown. Countries with several genotyped are represented with the corresponding colours. The stars indicate a country considered as endemic according to the CDC. The dotted line represents the maximum latitude were CCHFV main vector was found. Modified and updated from Shahhosseini *et al.* (2021). Created with mapchart.net.

### c. Vectors of CCHFV

By definition, a vector for an infectious agent is known as a hematophagous arthropod species that transmits a pathogen during blood feeding. In this context, vector competence is the innate ability of an arthropod to acquire, maintain, and transmit microbial agents (Kahl *et al.*, 2002). In the case of CCHFV, the vectors are ticks, especially those belonging to the *Hyalomma* genus. Consistently, the distribution of *Hyalomma* ticks overlaps with the distribution of CCHF cases (Gargili *et al.*, 2017). This genus includes several species, with *Hyalomma marginatum marginatum* being the most commonly associated with human infections (Hoogstraal, 1979).

*Hyalomma* ticks develop through three active stages (larva, nymph, and adult). Most species have a “two-host” behaviour, meaning that larva and nymph feed on the same host before dropping off, moulting and feeding as adults on a second host where they mate and later lay eggs in the vegetation. In the life cycle of the tick, the virus can be transmitted from one stage to the next one as the virus can replicate during the different metamorphoses (transstadial transmission) (Dohm *et al.*, 1996). It can also be transmitted horizontally from the male to the female during copulation and have a vertical transovarian transmission (from the female to the thousands of eggs she can lay) (Gonzalez *et al.*, 1992). Indeed, it was demonstrated that CCHFV replicates in a wide variety of tissue types but mostly in reproductive and salivary glands (Dickson and Turell, 1992). During the bloodmeal, the virus can be directly transmitted to ticks feeding nearby (or “co-feeding”) without the need for viremia in the tick host (Jones *et al.*, 1987; Nuttall and Labuda, 2004). The virus can also be transmitted to other species such as birds, small mammals, ungulates, or humans (described in the following section). All of these viral transmission events are represented in Figure 2.

CCHFV is not restricted to *Hyalomma marginatum marginatum*, as it has been identified in at least 35 ticks species, among which 32 hard tick (*Ixodidae*) and 3 soft tick (*Argasidae*) species (Gargili *et al.*, 2017; Hoogstraal, 1979). This disparity between hard vs soft ticks can be explained by the fact that while hard ticks may feed for days or even weeks, most *Argasidae* only feed for 20-70 minutes, thus reducing the probability of transmission. Moreover, experiments by Sheperd *et al.* showed that CCHFV could not be detected later than one day after inoculation into specimens of *Argas walkerae*, *Ornithodoros savignyi*, and

*Ornithodoros p. porcinus*, all members of the *Argasidae* family. These results suggest that the CCHFV-positive soft ticks described previously may have been false-positives caused by contaminated tick mouth or a fresh bloodmeal on infected animals (Shepherd *et al.*, 1989b).

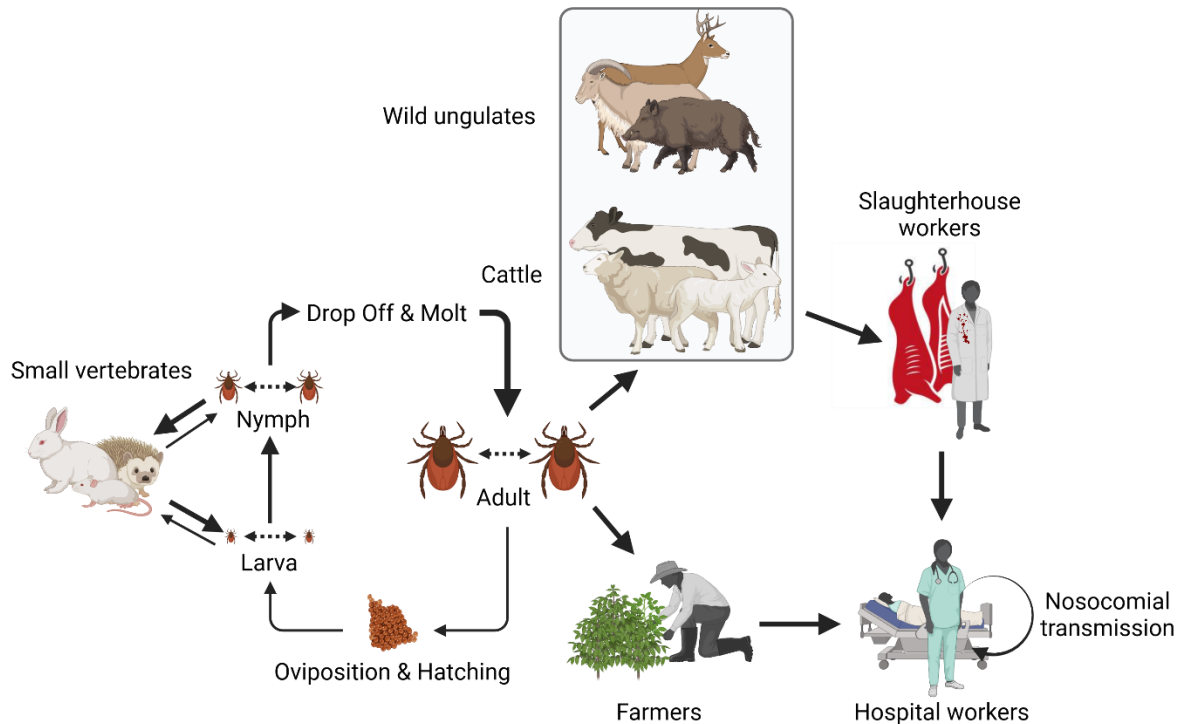


**Figure 2: Schematic overview of the life cycle of *Hyalomma* ticks and its role in CCHFV circulation.** In this representation, the infected larva feed on small vertebrates and molt to the nymph stage on the same host. After feeding again, it molts to the adult stage and change host to feed, choosing mostly wild ungulates and cattle. During the blood meal, ticks can infect each other through saliva proximity and they transmit the virus to their hosts. The virus is transmitted to human mostly by tick bites of fields workers or through the contaminated blood of slaughter cattle. The human-to-human transmission occur mainly at the hospital environment. The thickness of the arrow represents the efficiency of transmission. Modified from Bente *et al.* (2013). Created with BioRender.com.

#### d. Transmission dynamics to vertebrates

Like most arthropod-borne agents, CCHFV circulates in a tick – nonhuman vertebrate – tick cycle (Hoogstraal, 1979). Infection in nonhuman vertebrates is asymptomatic and therefore can be difficult to detect. In order to detect arbovirus infection in vertebrates, several methods have been used: inoculation of body fluids into NWM, CF, neutralisation test (NT), indirect hemagglutination-inhibition (HI) or agar gel diffusion precipitation (AGDP) (Casals and Tignor, 2008; Hoogstraal, 1979; Spengler *et al.*, 2016). More recently, reverse-transcription polymerase chain reaction (RT-PCR) and enzyme-linked immunosorbent assays

(ELISA) have been developed (Bonney *et al.*, 2017; Duh *et al.*, 2006; Saijo *et al.*, 2005). Using these methods, it was shown that a wide range of vertebrates can be infected with CCHFV.

The first animals to be tested were domestic animals in endemic areas. As reviewed in Spengler *et al.*, (2016), sheep, goats, horses, pigs, dogs, and chickens, as well as camels, donkeys, and ostriches, were tested seropositive for CCHFV.

Moreover, many wild animal species were reported positive for CCHFV, like hares, buffalo and rhinoceroses, but no nonhuman primates (reviewed in Spengler *et al.*, 2016) (Figure 3). Reptiles, including blunt-nosed vipers, and legless lizards were tested, but the only reptile case reported was a Horsfield's tortoise in Tadjikistan (Pak.TP, 1970).

Of note, birds are also involved in the life cycle of *Hyalomma* ticks; indeed, they transport ticks over long distances (Capek *et al.*, 2014; Jameson *et al.*, 2012). For instance, CCHFV-positive ticks collected on migratory birds have been reported in Greece in 2009 (Lindeborg *et al.*, 2012), and in Italy in 2017 (Mancuso *et al.*, 2019). However, CCHFV infection in avian species remains unclear as numerous species tested were sero-negative (Spengler *et al.*, 2016).

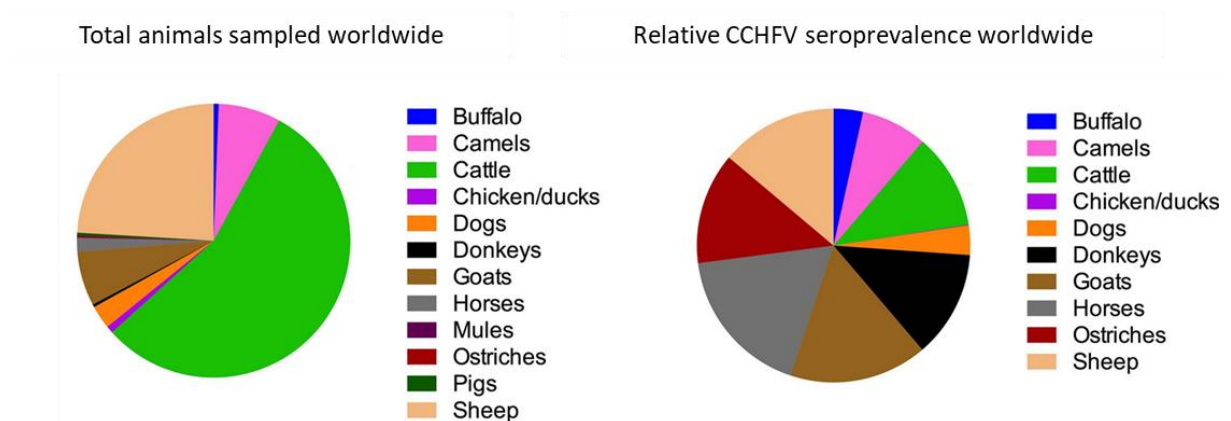


**Figure 3: Total worldwide CCHFV seroprevalence reported in domestic animals by species.** The seroprevalence is determined by sum of seropositive animals over the sum of total animals, sampled internationally. Modified from Spengler *et al.* (2016).

e. Human transmission

Humans can be infected with CCHFV through different routes (Figure 2) including through bites of infected ticks, or contact with infected animal blood or tissues during slaughter of livestock (Hoogstraal, 1979a; WHO, fact-sheet). In a study from Ergönül *et al.*, (2004), it was shown that in Turkey, 80% of the reported cases occurred in farmers, slaughterhouse workers or butchers.

Human-to-human transmission can occur from close contact with the blood, secretions, or body fluids of an infected person. These cases are mostly observed among health care workers. Three cases of sexual transmission have also been documented by Pshenichnaya *et al.*, (2016), and one by Ergönül and Battal, (2014). But in all these cases, the sexual transmission is only described as “probable” since transmission through saliva could not be excluded, and the authors were unable to detect the virus in seminal fluid (Ergönül and Battal, 2014; Pshenichnaya *et al.*, 2016). The virus can be transmitted vertically through intrauterine or perinatal routes, but this does not systematically occur. Indeed, in a paper from Ergönül *et al.*, the authors described three cases of babies from infected mother who died because of intense bleeding, two of which were positive for CCHFV by PCR (Ergönül *et al.*, 2010). In another pregnancy reported, a healthy baby was born, negative for CCHFV (Aydemir *et al.*, 2010). The risk of vertical transmission probably depends on the gestational age at the time of the acquired infection (Gozel *et al.*, 2014).

f. A global health concern

As environmental factors change, the disease might spread more widely in humans. From cases in Crimea or the DRC, cases are now reported in China, Turkey, or Spain. Since 2002, Turkey has had more than 10 000 human cases reported (Spengler *et al.*, 2018). This wide distribution, the widest for a tick-borne pathogen, can be caused by the numerous competent tick species (Hoogstraal, 1979; Randolph and Rogers, 2007). The probability of epidemic is well acknowledged since the virus is under surveillance at the European Union level, and it is included in the WHO R&D Blueprint priorities for research and product development for early diagnostics (WHO, blueprint). In order to monitor this risk, sero-surveillance has been



established as well as risk maps. However environmental and social settings evolve so fast that it might not be sufficient. For example, in a paper published in 2015, it was established that the probability of CCHF occurrence in humans in Spain was null; one year later, the country reported its first autochthonous case (Messina *et al.*, 2015; Mora-Rillo *et al.*, 2018). Moreover, a retrospective study identified a case from 2013 (Lorenzo Juanes *et al.*, 2023; Negrodo *et al.*, 2021). This demonstrates the need to increase sampling from ticks and other wild animals and to increase the sero-surveillance.

## 2. CCHF pathogenesis, diagnostics, and treatments

### a. Symptoms

Although CCHF may be fatal in humans (fatality rate from 5-30% depending on the strain and the care treatment), more than 70% of the infections are asymptomatic. In symptomatic infections, CCHF disease is divided into four clinical phases: incubation, prehaemorrhagic, haemorrhagic and convalescent phases (Hoogstraal, 1979) (Figure 4).

The incubation period usually takes place between 3-7 days after exposure (Swanepoel *et al.*, 1989). The duration of this period may differ depending on the viral dose and the route of exposure (tick bite or contaminated blood).

The prehemorrhagic period is characterised by fever, headache, myalgia, dizziness, diarrhea, nausea and vomiting. This period usually last for 1-7 days (Ergönül, 2006; Hoogstraal, 1979; Schwarz *et al.*, 1997; Swanepoel *et al.*, 1989).

The hemorrhagic period is short, 2-3 days. During this period, patients show signs of petechia, large hematomas on the mucous membranes, bleeding from the nose, the vagina, the gingiva, the gastrointestinal system, the respiratory tract, and cerebral haemorrhage (Ergönül, 2006). If the patient survives, he enters the convalescence period. This last period usually starts about 10-20 days after the first symptoms. To date, it remains unclear whether CCHFV infection leaves long-term sequelae, but the recovery is slow, and some patients showed signs of weakness and loss of hearing.

## b. Histopathologic studies and biochemical changes

Immunohistochemical analysis and *in situ* localisation of CCHFV in human tissues associated parenchymal necrosis in the liver with viral replication, suggesting a direct viral cytopathic effect (Burt *et al.*, 1997). Like other haemorrhagic viruses, patients infected with CCHFV appears to have thrombocytopenia (decrease in platelet count; PLT), leukopenia (decrease in white blood cell count; WBC) and elevated levels of aspartate transaminase (AST), alanine transferase (ALT), lactate dehydrogenase (LDH), and creatinine phosphokinase (CPK). In the case of CCHFV, as well as viruses like Lassa or Marburg, AST is generally higher than ALT. This indicates the involvement of other organs besides the liver (Ergönül, 2006; Swanepoel *et al.*, 1989). In the case of the survival of the patient, CCHFV immunoglobulin M and G (IgM and IgG) are detected by days 7 to 9 post infection (Shepherd *et al.*, 1989c) (Figure 4). In the fatal cases of CCHFV infection, high level of pro-inflammatory cytokines such as tumor necrosis factor  $\alpha$  (TNF- $\alpha$ ) or interleukin-6 were detected (Ergönül *et al.*, 2006; Saksida *et al.*, 2010). In contrast, these cases do not develop detectable level of antibodies (Swanepoel *et al.*, 1989).

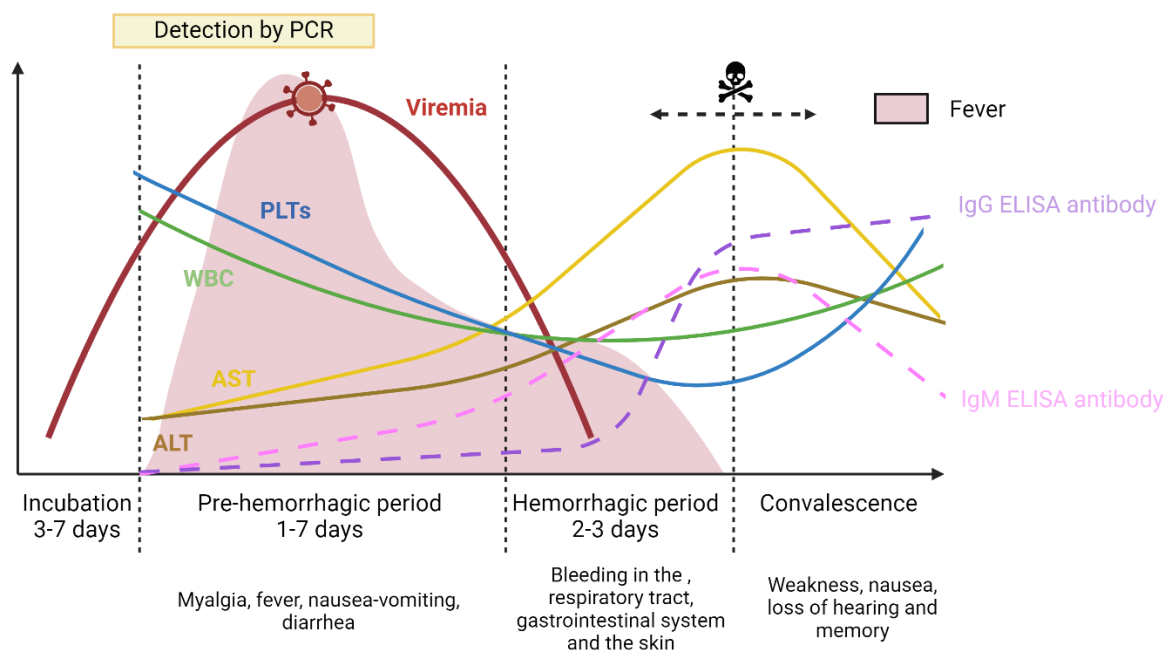


**Figure 4: Schematic representation of symptoms and biological changes occurring during CCHFV infection.** CCHF is divided into 4 periods: incubation, pre-hemorrhagic, hemorrhagic and convalescence. The zone in red represents the fever. The higher the peak is, the higher is the fever. The black dotted double arrow is the period where most deaths occur. Modified from Ergönül, (2006). Created with BioRender.com.

### c. Diagnosis

In endemic areas, CCHFV is suspected when a person shows the symptoms described above (fever, myalgia, malaise, diarrhea, etc.) with elevated serum AST and ALT, and in particular if the person has a history of tick exposure. The case is then confirmed by RT-PCR and ELISA to assess the specific IgM and/or IgG. Both these detection modes have their limitations. On the one hand, RT-PCR which is quicker, can only be performed during the first 10-12 days of the illness. And even if the method is sensitive, the high degree of sequence diversity among CCHFV genotypes (20-31%) may render it useless (Bente *et al.*, 2013). For this reason, primers targeting well-conserved sequences (such as the 5' untranslated region (UTR) of the S segment) are preferred, allowing the detection of up to 18 different strains (Atkinson *et al.*, 2012). On the other hand, with the ELISA, the CCHFV-specific IgM and IgG are detectable only a week after infection, and, as described above, most patients with fatal outcomes do not develop a measurable antibody response.

### d. Treatment

In most cases, CCHFV infections require hospitalisation or therapy. In cases of coagulation abnormalities, the patient will require the provision of fresh plasma and platelet, while for severe haemorrhage, the patient will require a blood transfusion. In addition, to counteract viral replication, ribavirin, a guanosine analogue licensed for the treatment of respiratory syncytial virus infections (RSV) and hepatitis C (HCV) (Cooper *et al.*, 2003; Mangia *et al.*, 2005), has been used to treat CCHFV for more than two decades. Ribavirin-mediated inhibition of CCHFV replication was demonstrated *in vitro* (Bergeron *et al.*, 2010; Huggins, 1989) and in mice models (Bente *et al.*, 2010; Tignor and Hanham, 1993) but the benefit for humans is still debated. In most of the trials, a control group is missing, or the trial is not randomised (Dokuzoguz *et al.*, 2013; Jabbari *et al.*, 2006; Midilli *et al.*, 2007). In papers that compare the studies on the impact of ribavirin, no clear benefit or adverse effects were observed, since no control group was included (Johnson *et al.*, 2018; Soares-Weiser *et al.*, 2010). In a recent study, the effect of the drug on the mutation rate of the CCHFV genome was assessed through next-generation sequencing (NGS). In this study including a control

group, no impact on the viral load was observed. The authors noticed also that ribavirin does have a slight impact on the mutation rate, but it is too low to affect error catastrophe, which may inhibit the viral replication (D'Addiego *et al.*, 2023).

Usually, ribavirin is combined with an interferon type I (IFN-I) treatment. The assessment of the impact of IFN-I on CCHFV was reported in one clinical study, but no benefit was observed (van Eeden *et al.*, 1985).

Other drugs were tested *in vitro* or in non-human models. Favipiravir is a pyrazine carboxamide derivative that is approved for the treatment of Influenza (Furuta *et al.*, 2005). The use of favipiravir in mice lacking the type I interferon receptor (IFNAR<sup>-/-</sup> mice) showed beneficial effects against CCHFV infection by decreasing viral replication (Hawman *et al.*, 2018; Oestereich *et al.*, 2014). A modest benefit was also demonstrated in cynomolgus macaques (Hawman *et al.*, 2020). More recently, a 65-year-old man was treated with favipiravir for its CCHFV / SARS-CoV-2 coinfection. By the end of the fifth day of treatment, his biological parameters and clinical symptoms had normalised (Dülger *et al.*, 2020). In an inhibitor screen that tested 40 nucleoside analogues, ribavirin, favipiravir, and 2'-deoxy-2'-fluorocytidine were identified to have a potent antiviral effect on CCHFV replication (Welch *et al.*, 2017).

In conclusion, several treatments are administered to people infected with CCHFV, but none of them are commercialised due to a lack of efficacy proof.

#### e. Prevention

Similar to the absence of approved and licensed treatments to date, no vaccine is currently approved by the Food and Drug Administration. One vaccine, consisting of inactivated virus derived from CCHFV-infected suckling mice brain tissue, has been used in Bulgaria since 1974. Since the beginning of the vaccination campaign, the country has reported a decline in the number of CCHFV cases, from 1105 to 279, but causality has not been demonstrated (Christova *et al.*, 2009; Papa *et al.*, 2011). Since then, several attempts to develop a vaccine have been made either with inactivated viruses, viral vectors, viral replicon particles (VRPs),

DNA vaccines or messenger RNA (mRNA) vaccines, all of which are reviewed in (Ahata and Akçapınar, 2023). To date, the most promising results seem to be vaccines targeting the glycoproteins (GPs) or the nucleoprotein (NP) (detailed later in the Chapter I.B.3). Interestingly, immunisation against CCHFV glycoprotein c (Gc) induces the production of neutralising antibodies, without being able to provide full protection. On the other hand, immunisation against NP increases the humoral response but does not induce the production of neutralising antibodies (Hawman *et al.*, 2023). This counter-intuitive observation highlights the importance of both cellular and humoral immunity required for a protection against CCHFV.

The current absence of prophylactic treatment is probably due to the absence of susceptible immunocompetent animal models for CCHFV infection that replicate the pathology of the virus typically encountered in humans. As a consequence of the absence of treatment and the high fatality rate, this pathogen is studied in biosafety level laboratories (BSL-4) in most countries. Some eastern Europe countries like Albania, Bulgaria or Greece use BSL-3, and Kosovo even uses BSL-2 (Weidmann *et al.*, 2016).

Of note, vaccination is not the only way to prevent CCHFV infection, as there are ways to reduce exposure to the virus. Farmers can wear clothing with long sleeves and pants and reduce the tick population in their farm environment, using plants or solvents as reviewed in (Kumar *et al.*, 2020). Concerning the slaughterhouse workers and health workers, they should wear protective equipment to avoid the contact of contaminated blood (boots, gloves, mask...). Finally, educational campaigns to inform people in endemic areas of the risks, such as tick bites and early symptoms, may contribute to reducing the risk of CCHFV infections.

## B. CCHFV characteristics and structure

### 1. Taxonomy

CCHFV belongs to the class *Bunyaviricetes* (represented in Figure 5), which regroups spherical, enveloped viruses with a segmented negative or ambisense-stranded RNA genome. To date, this class is composed of 15 families of viruses that can infect a wide range of hosts, from plants to humans (Kuhn *et al.*, 2023). CCHFV belongs to the *Nairoviridae* family, which is one of the five families associated with haemorrhagic fever in humans (together with the families *Arenaviridae*, *Hantaviridae*, *Peribunyaviridae* and *Phenuiviridae*). The *Nairoviridae* family consists of arthropod-borne viruses and is divided into 7 genera, of which the *Orthonairovirus* contains 51 viruses, including CCHFV and the closely related Hazara virus (HAZV), as represented in Figure 5 (Leventhal *et al.*, 2021).

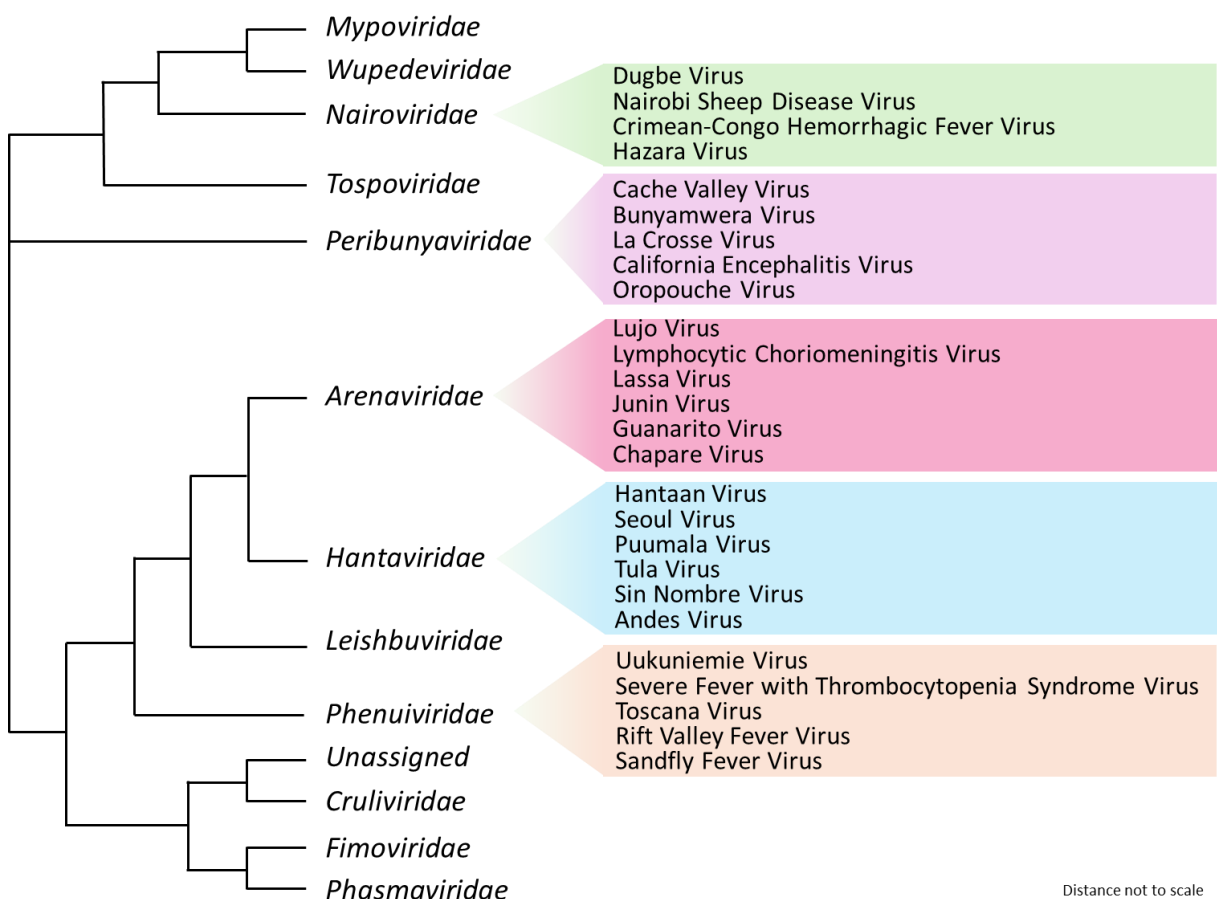


**Figure 5: Bunyaviricetes phylogenetic tree.** The phylogenetic tree of the class *Bunyaviricete* is based on nucleoprotein amino acid sequences of 13 out of the 15 families. Specific viruses of the 5 families associated with haemorrhagic fever in humans are listed in no specific order. Modified from Leventhal *et al.*(2021).

## 2. Genome and virion structure

CCHFV genome is composed of three segments of negative or ambisense polarity RNA: small (S), medium (M) and large (L) segments. These segments are associated with viral proteins to form the ribonucleoprotein (RNP) complexes (Figure 6). All 3 segments are flanked at their 5' and 3' ends by untranslated regions (UTRs). Like other bunyaviruses, the nucleotide sequences at the 5' and 3' ends are partially complementary and form a panhandle structure, giving the RNPs a pseudo-circular conformation (Jeeva *et al.*, 2017b; Morikawa *et al.*, 2002; Pettersson and von Bonsdorff, 1975; Raju and Kolakofsky, 1989).

The S-segment is approximately 1.6 kilobase (kb) long and encodes the NP along with the non-structural protein NSs in an opposite-sense reading frame. The M-segment is 5.4kb long and encodes the glycoprotein precursor complex (GPC), that will be further cleaved into the glycoproteins Gc and Gn, the non-structural protein NSm and GP160/85, later processed into GP38 and the mucin-like domain (MLD). Finally, the L-segment is 12.1kb long and encodes the RNA-dependant RNA polymerase (L protein).

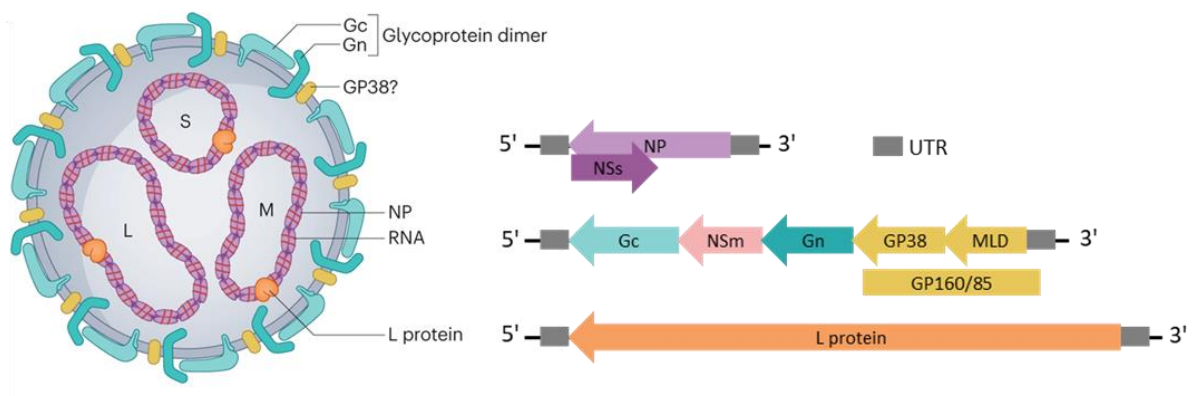


**Figure 6: Schematic representation of CCHFV virion.** CCHFV is an enveloped, tri-segmented, negative-sense RNA virus. The two glycoproteins Gc and Gn are expressed at the surface of the virion. Evidence of GP38 at the surface is still unclear. The segment S encodes NP and, in the opposite-sense, NSs. M encodes the glycoprotein precursor GPC that processed to produce Gc, NSm, Gn, and GP160/85 that is further cleaved into MLD and GP38. L encodes the RNA-dependant-RNA-polymerase (L protein). UTR: untranslated region. Modified from Hawman *et al.* (2023).

CCHFV virion is spherical and approximately 80-100nm in diameter (Figure 7) (Korolev *et al.*, 1976). Its envelope is composed of lipids and incorporates the viral glycoproteins Gn and Gc that form a lattice of putative tetrameric projections on the viral membrane surface (demonstrated for HAZV) (Punch *et al.*, 2018). The incorporation of a secreted glycoprotein, GP38 represented in Figure 6, is still unclear and discussed in Chapter I.B.3.b (Golden *et al.*, 2019).

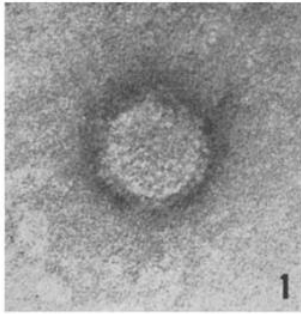


**Figure 7: Negatively stained CCHFV particle from a porcine kidney cell culture preparation. Magnification x170,000. From Korolev *et al.* (1976).**

### 3. Viral proteins and their roles

#### a. Proteins encoded by the S-segment

The first crystal structure of NP was obtained on the YL04057 strain, isolated from China, after being expressed and purified as a recombinant protein in *Escherichia coli* (Guo *et al.*, 2012). It is a 482 amino acid-long protein constituted of a globular core, “the head”, comprising 23 alpha helices, with a “stalk” composed of two long alpha helices that extend away from the core with an exposed loop at the apex, supported by a three-helix bundle (Figure 8) (Carter *et al.*, 2012; Guo *et al.*, 2012; Wang *et al.*, 2012).

The main role of NP is to interact with the viral RNA (vRNA) and form the ribonucleoprotein complex through oligomerisation. The formation of the RNP is essential in the replicative cycle and to protect the genome from degradation (Jeeva *et al.*, 2017b; Wang *et al.*, 2016, 2012). NP binds to the vRNA with high affinity through the panhandle structure formed at the 5'-3' UTRs (Jeeva *et al.*, 2017b). In addition to binding, NP enhances the translation of messenger vRNA (Jeeva *et al.*, 2017a).

By immunoprecipitation, it was also demonstrated that NP interacts with host heat shock proteins 70 (HSP70) during viral replication, and shown for HAZV NP, within the viral



particles too (Surtees *et al.*, 2016). In this study, the authors found that HSP70 is required for transcription of HAZV. It is also interesting to note that, in ticks, upon infection with the bacterium *Anaplasma phagocytophilum*, HSP70 expression is increased which reduces the risk of desiccation and increases the tick survival (Benelli, 2020). Thus, CCHFV interaction with HSP70 may play a role in the persistence in CCHFV's vector.

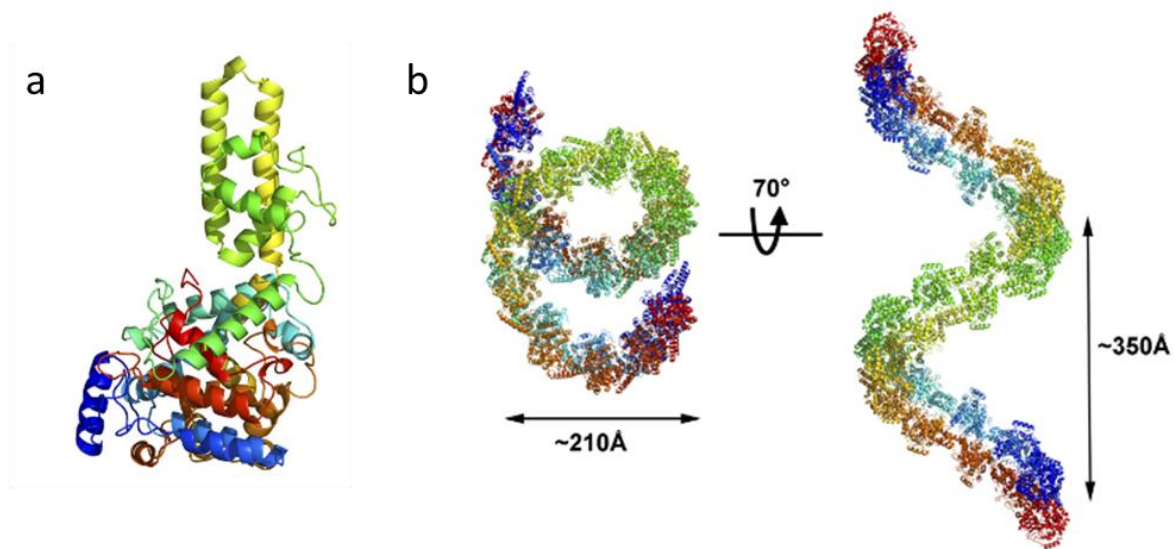


**Figure 8: Crystal structure of CCHFV NP.** (a) The structure is coloured in rainbow colours from blue at the N terminus to red at the C terminus. (b) Antiparallel double superhelix polymer of CCHFV N. Each superhelix is coloured in rainbow colours from blue to red. From Wang *et al.* (2012).

CCHFV NP has also been shown to have an intrinsic nuclease activity on single- and double-stranded DNA (Guo *et al.*, 2012). This is surprising since the NP of arenaviruses also has an exonuclease activity, but on RNA. The functional relevance of this activity in arenaviruses is the degradation of viral dsRNA so it cannot be detected by the innate immune system (Qi *et al.*, 2010). For CCHFV, this *in vitro* observation is still not explained.

In addition, it was demonstrated that the apoptotic processes that are coordinated by Bax or downstream effectors (release of cytochrome C, cleavage of caspase-9 and caspase-3) are reduced by NP during the early stages of CCHFV infection (Karlberg *et al.*, 2015). The anti-apoptotic activity contributes to the viral replication and propagation. On the other hand, NP possesses a specific cleavage motif for caspase-3: the DEVD motif. After induction of apoptosis, it was shown that NP is cleaved at the DEVD site (Karlberg *et al.*, 2011). It was also demonstrated that the caspase-3 cleavage of NP results in an incomplete digestion,

indicating that NP is a poor substrate for cleavage (Carter *et al.*, 2012). This can be explained by the fact that the cleavage motif is located in the described oligomerisation site, thus, is not accessible to the caspase-3 (Wang *et al.*, 2012). This highly conserved DEVD motif may also have another function, maybe in ticks, which differs from a cleavage by a caspase. Indeed, when mutated into an AEVA motif that is uncleavable, the virus could not grow in tick cell culture (Salata *et al.*, 2018).

Another viral factor that may play a role in the apoptosis modulation is NSs, also encoded by the S-segment. As for other bunyaviruses, the CCHFV NSs was reported to induce apoptosis by disrupting the mitochondrial membrane potential (Barnwal *et al.*, 2016; Colón-Ramos *et al.*, 2003; Xu *et al.*, 2008). These opposite effects between NP and NSs are not fully explained yet but might contribute to a fine-tuning of apoptosis in infected cells.

#### b. Proteins encoded by the M-segment

The medium-sized segment of CCHFV encodes a polyprotein, the GPC that is further cleaved into the structural proteins: Gc, and Gn, the secreted glycoproteins GP160/GP85 and GP38 as well as into non-structural proteins: mucin-like domain (MLD), and NSm (Sanchez *et al.*, 2002).

Gc and Gn are the two viral glycoproteins that are located at the surface of the virion and participate in receptor binding and entry (more details in Chapter I.C.1 ) (Mishra *et al.*, 2022; Ye *et al.*, 2022). Gc is a class II membrane fusion protein whose structure was recently revealed and is the major target of neutralising antibodies, demonstrating that it is a well-exposed and immunogenic protein (Figure 9) (Fels *et al.*, 2021; Li *et al.*, 2022; Mishra *et al.*, 2022). On the other hand, much remains unknown concerning Gn because of a lack of tools. What is known is that the protein bears a zinc finger domain and thus binds to RNA (Estrada and De Guzman, 2011)

On the M-segment, between the open reading frames of the two glycoproteins is the sequence encoding the non-structural protein NSm. This protein was reported to promote glycoproteins processing and virion assembly, but was also shown to be non-essential for CCHFV replication (Freitas *et al.*, 2020; Welch *et al.*, 2020).

During the processing of the GPC, a preGn protein is released. The preGn is cleaved by host proteases allowing the release Gn of two proteins of 85kDa and 160 kDa, respectively (GP85/160), which are further cleaved to form the highly glycosylated MLD and GP38 proteins, both secreted (detailed in Chapter I.B.4.b) (Sanchez *et al.*, 2006). GP85 and GP160 are suggested to be non-cleaved version of MLD-GP38 since they are recognised by the anti-GP38 antibody 13G8, but more investigation is required. Indeed, while it is known that GP160 is not a dimer of GP85, the exact mechanism of GP85 and GP160 production is still not known (Sanchez *et al.*, 2006), as is their role in the viral cycle.

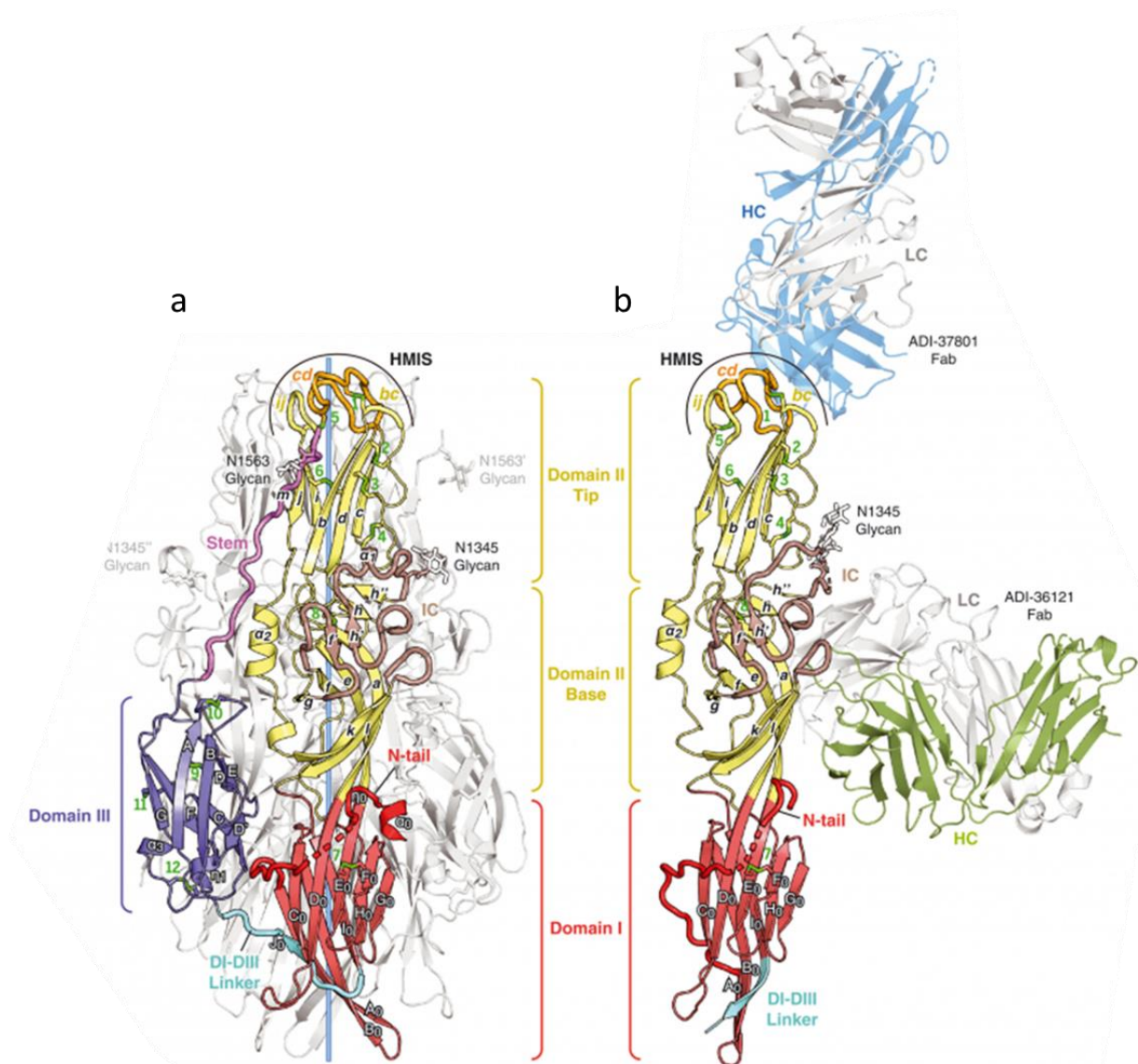


**Figure 9: X-ray structure of CCHFV Gc IbAr10200 strain.** (a) X-ray structure of the CCHFV Gc ectodomain in the post fusion conformation. The front protomer is coloured according to domain, and the trimer axis is shown in light blue. Secondary structure elements and disulfide bonds (green numbers) are labelled. An orthonairovirus-specific insertions cluster (IC) is depicted in brown. (b) X-ray structure of the CCHFV Gc monomer, in prefusion conformation, associated with the ADI-37801 and ADI-36121 Fabs. HC, heavy chain; LC, light chain. From Mishra *et al.* (2022).

Finally, GP38 was described as participating in the GPC processing and to be crucial for production of infectious particles (Freitas *et al.*, 2020). More recently, a paper was published that claimed that GP38 was found at the surface of the plasma membrane in infected cells and at the virion surface (Golden *et al.*, 2019). However, the evidence is not clear. The authors showed a localisation of GP38 at the cell surface, but this does not mean that the protein will be incorporated onto the virions. Furthermore, they could not show a colocalization of GP38 and other CCHFV' glycoproteins by electron microscopy.

### c. Proteins encoded by the L-segment

With more than 12kb, the large segment of CCHFV genome is one of the largest of the *Bunyaviricetes* (Honig *et al.*, 2004). The L-segment of CCHFV encodes the L protein that bears the RNA-dependant RNA polymerase (RdRp) and the cap-snatching activity. The cap-snatching allows the transcription of CCHFV RNAs by cellular factors. Moreover, mapping of the NP showed a binding site to the L protein, suggesting an association to form the viral RNP (Macleod *et al.*, 2015).

The L protein also has an ovarian tumour protease (OTU) domain (Devignot *et al.*, 2015; Holm *et al.*, 2018; Honig *et al.*, 2004). The OTU domain of L protein possesses a de-ISGylating and a deubiquitylation activity that reduces the innate response by blocking the RIG-I-mediated IFN- $\beta$  responses (Scholte *et al.*, 2017; Spengler *et al.*, 2015).

All of these properties of CHFV proteins are summarised in Table 1.

	Protein	Role	Ref	Limits
S	Nucleoprotein	Interaction with vRNA	(Jeeva et al., 2017)	
		Formation of RNP	(Carter et al., 2012)	
		Endonuclease activity	(Guo et al., 2012)	
			(Wang et al., 2016)	No endonuclease activity in RNP complexes (when bind to RNA)
		Interaction with HSP70 during replication and in particles	(Surtees et al., 2016)	Interaction within the particles was not shown for CCHFV but HAZV
		Promotes translation of viral mRNA	(Jeeva et al., 2017)	
		Cleaved by caspase 3 through DEVD motif	(Karlberg et al., 2011)	
			(Wang et al., 2012)	Motif not available in oligomeric conformation
(Carter et al., 2012)	CCHFV NP is a poor substrate for cleavage from the caspase 3			
Inhibition of apoptosis (Suppression of the activation of caspase 3 and 9, and induction of apoptosis triggered by BAX and the release of cytochrome c from mitochondria)	(Karlberg et al., 2015)			
NSs	Induction of apoptosis	(Barnwal et al., 2016)		
M	Gn	Binding to RNA	(Estrada and De Guzman, 2011)	
		entry ?	(Xiao et al., 2011)	
	Gc	Fusion, entry	(Mishra et al., 2022)	
		NSm	GPC processing	(Freitas et al., 2020)
	MLD	Unknown		
	GP38/ GP85/GP160	GPC processing	(Freitas et al., 2020)	
L	L	Capsnatching activity	(Jin and Elliott, 1993)	
		RNA <sup>h</sup> RNAP	(Honig et al., 2004)	
		Endonuclease activity	(Devignot et al., 2015)	
		Formation vRNP	(Macleod et al., 2015)	
		Inhibition of innate immune response (through de- <sup>h</sup> ISGylating and a deubiquitylation)	(Scholte et al., 2017)	

**Table 1: Table summarising the known roles of CCHFV's proteins.**

#### 4. Production of new CCHFV virions

CCHFV, as all viruses, is an obligate intracellular parasite that must infect a cell to replicate, form new particles, and infect naïve cells. In the following section, I will describe what is known about CCHFV infection cycle (simplified version represented in Figure 10). While it is conventional to start the viral cycle at the virus attachment step, here I start after the fusion, in order to focus with extended details on the entry steps in the next chapter.

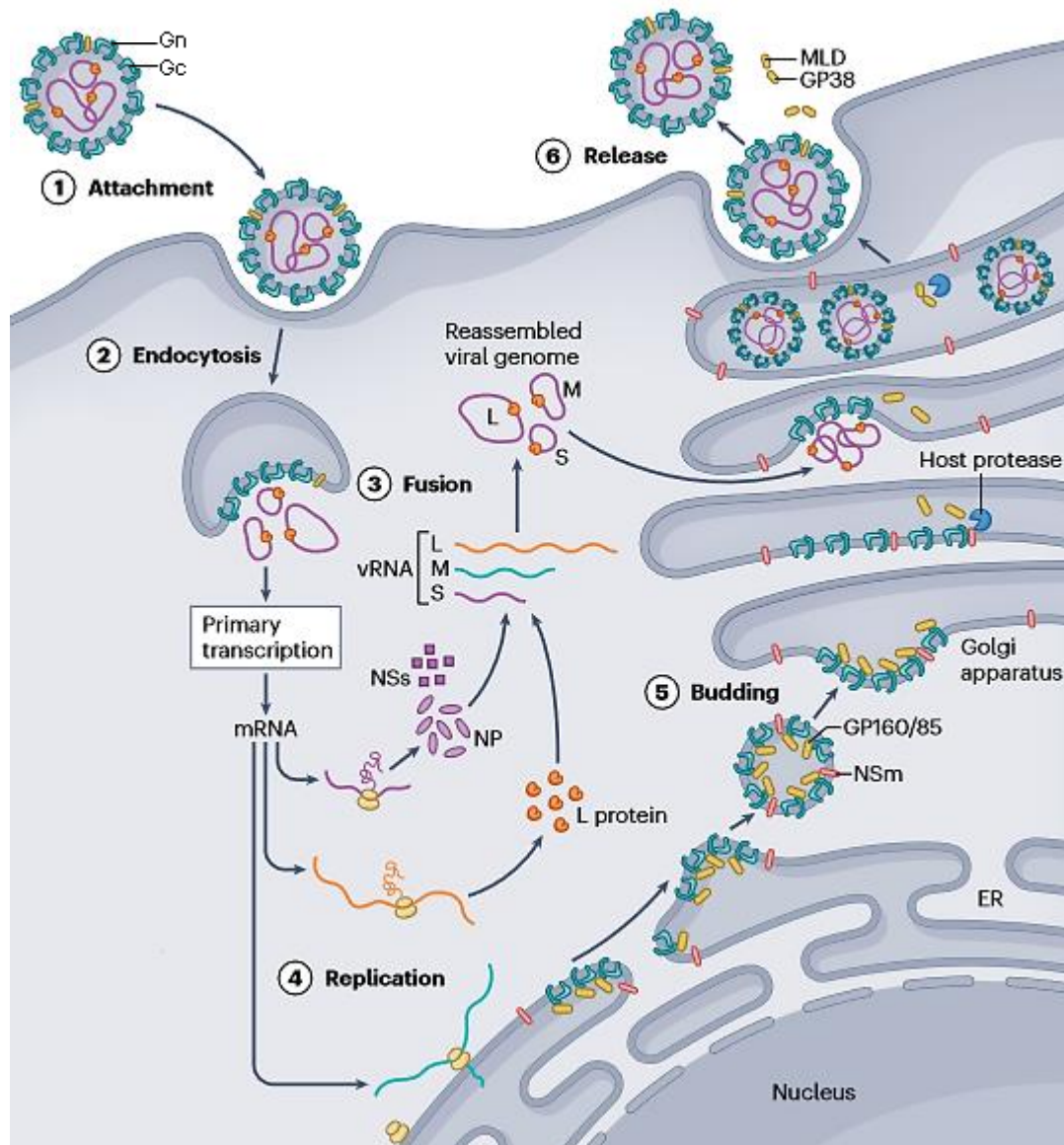


**Figure 10: Schematic representation of the CCHFV replication cycle.** After attachment, CCHFV is internalised through clathrin-mediated endocytosis, and the viral membrane fuses with the endosome membrane. Upon the fusion step, the genome is released into the cytoplasm and converted to mRNA by the RdRp while the translation is initiated to form the proteins. In parallel, the genome is replicated into positive sense vRNA and then into neo-synthesised genomic vRNA that will be associated with NP and L protein (RNP). GPC matures through the ER and the Golgi apparatus, and viral particles bud into the Golgi lumen, incorporating the RNPs, before being released into the extracellular environment. Modified from Hawman et al. (2023).

#### a. Replication step

The replication process includes the production of the viral genome and the translation of viral proteins by host ribosomes. At the time of the release in the cytoplasm, the viral genome, lacking the 5' cap and the 3' poly-A-tail, is associated with the NP and forms a RNP

(Jeeva *et al.*, 2017a). CCHFV being a negative-sense single-stranded RNA, its genome does not act as mRNA, but is transcribed into mRNA after entry (Figure 10). This step is catalysed by the viral RdRp present in the virion. As described previously, the polymerase also has a cap-snatching activity by which the viral RdRp cleaves host cell mRNA downstream of the 5' cap and uses the resulting capped oligoribonucleotide as a primer to initiate transcription (Jin and Elliott, 1993). From the transcription of the vRNA results not only the mRNA but also the positive-sense complementary RNA (cRNA), or antigenomic RNA. The cRNA serves as a template to produce neo-synthesised genomic RNA (Jeeva *et al.*, 2017b). While the cRNA is the same length as the vRNA, the mRNA is longer due to the addition of the cap (shown for Germiston virus (Bouloy *et al.*, 1990)). Even if the exact mechanism of CCHFV replication is not clear, it was demonstrated for Bunyamwera (BUNV) and Uukuniemi that, although all three segments are replicated by the viral RdRp, the degree of replication of each segment is not the same. Indeed, for BUNV and Uukuniemi, the molar abundances of the neo-synthesised genomic RNAs were quantified, and the authors showed that the M-segment was more abundant than the L-segment and, to a greater extent still, the S-segment (Barr *et al.*, 2003; Pettersson and Kääriäinen, 1973).

A fact quite unique among negative stranded viruses is that bunyaviruses transcription of mRNA requires ongoing protein synthesis (Ikegami *et al.*, 2005). This is related to the control of the transcription termination. Correct termination requires the transcribed mRNA to anneal with the genomic template RNA in regions containing a termination signal. In the case of the bunyaviruses, the coding regions (ahead from the authentic termination sites in 5') contain termination signals similar to the authentic sequence in the non-coding region in 5'. Upon transcription, ribosomes bind to the on-going synthesised RNA to translate it. These ribosomes prevent the interaction with the viral RNA and the "premature" transcription termination (Figure 11) (Barr, 2007; Raju and Kolakofsky, 1987).

Hence, upon transcription, the cellular machinery is used to translate the viral proteins. The L protein, NSs and NP are translated into the cytosol, while GPC is translated into the endoplasmic reticulum (ER) in order to mature.

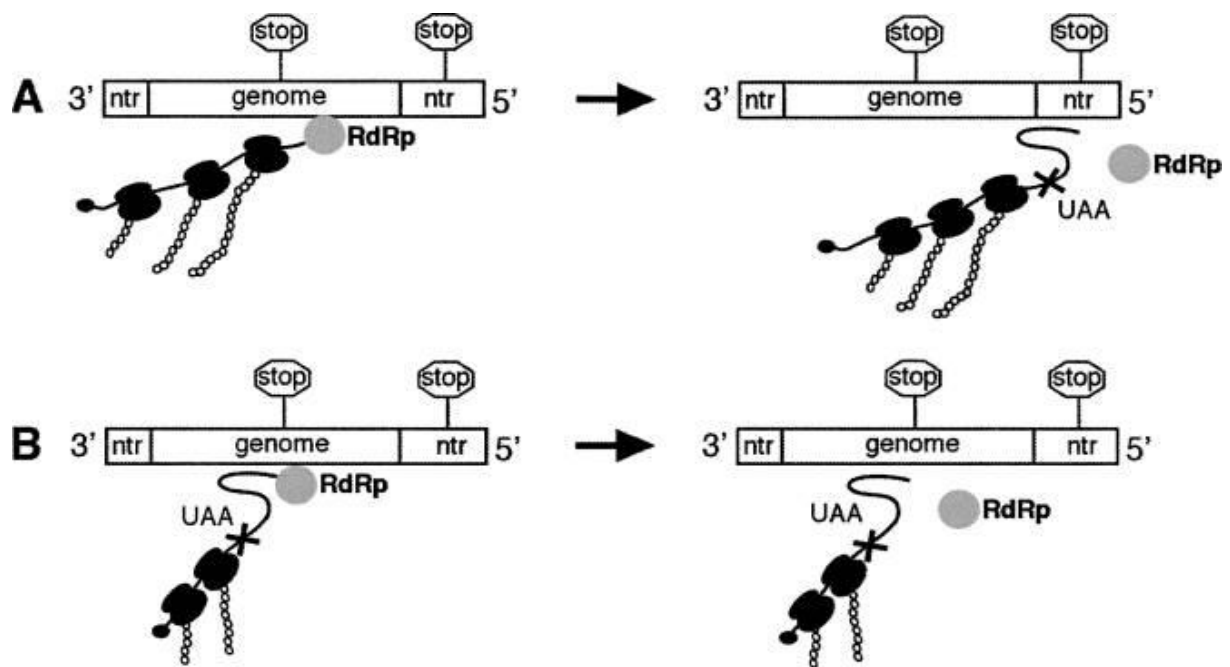


**Figure 11: Model of bunyaviruses transcription and translation.** (a) Transcription termination requires RNA interactions involving the termination signal (shown as stop signs) or its complement in mRNA. Translating ribosomes prevent formation of interactions, so termination signals within genome coding regions are suppressed. Termination signals within NTRs are active, as these regions are not translated, thus allowing RNA interactions to form (shown as a loop). (b) When translation is inhibited, RNA interactions can form, thus activating previously silent termination signals within coding regions. NTRs: Non translated region, or untranslated region in the manuscript. From Barr *et al.* (2007).

#### b. GPC maturation and viral production

As described previously, GPC is a polyprotein that goes through proteolytic processing. After its synthesis in the ER, where it is *N*-glycosylated, GPC is cleaved by a signal peptidase and/or the intramembrane cleaving proteases, into Gn precursor (PreGn), NSm, and Gc precursor (PreGc) (Altamura *et al.*, 2007; Sanchez *et al.*, 2002). These products are then transported to the Golgi complex where the PreGc is cleaved by an unknown protease. Since the cleavage site of CCHFV (RKLP) is identical to the one of Guanarito virus (arenavirus), it is believed that the enzyme is either a subtilisin kexin isozyme-1/site-1 protease (SKI-1/S1P), as for Guanarito virus, or a similar protease (SKI-1/S1P-like) (Sanchez *et al.*, 2006; Vincent *et al.*, 2003). Concerning PreGn, it is cleaved by a SKI-1/S1P protease into Gn and GP85/160, which contains the MLD. MLD acquires *O*-linked glycans at this step (Bergeron *et al.*, 2007; Sanchez *et al.*, 2002). GP85/160 is further cleaved in the *trans*-Golgi network (TGN) by a furin to



produce GP38, and together with GP85/160, they are secreted into the extracellular environment (Figure 12) (Sanchez *et al.*, 2006). More recently, it was demonstrated that GP38 deletion affects the Golgi localisation of Gc and thus, impairs the preGc cleavage (Freitas *et al.*, 2020).

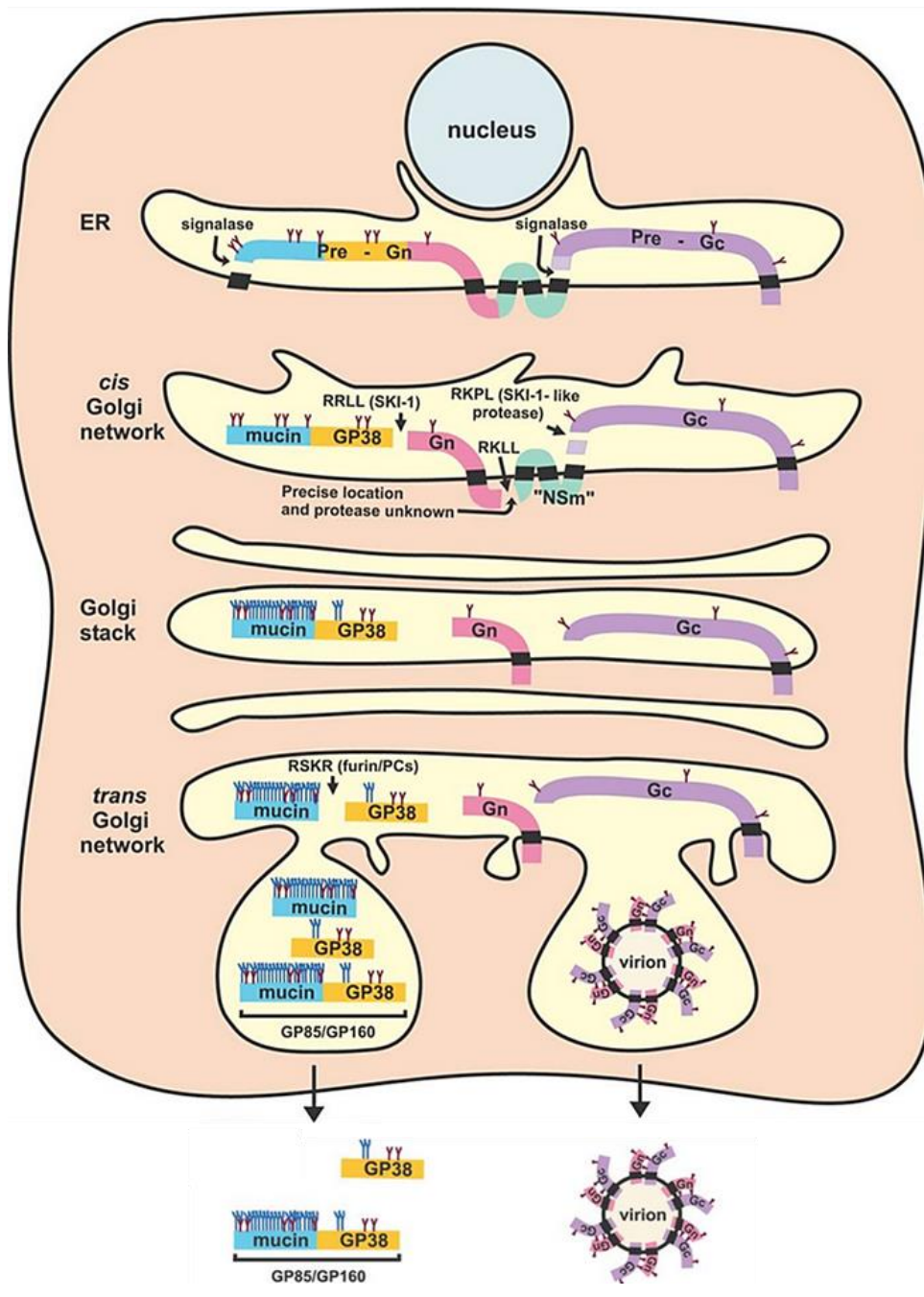


**Figure 12: Schematic representation of the CCHFV glycoproteins processing.** After synthesis in the ER, the GPC is cleaved by signal peptidase into preGn and preGc. Then in the cis Golgi network, cellular proteases SKI-1 and SKI-1 like protease cleave preGn into MLD/GP38 and Gn. This is further processed into the trans Golgi network where MLD/GP38 can be cleaved by the furin in order to give GP38, MLD/GP38 and MLD that will be secreted, with the exception of MLD alone that is not detected in the extracellular environment. Modified from Sanchez *et al.* (2006).

### c. Assembly and egress

The next step is the assembly of new virions. Once again, there are many unknowns about CCHFV assembly. For most viruses, the cellular localisation of the viral glycoproteins indicates the assembly site. In the case of CCHFV, Gn protein contains a Golgi localisation motif and co-expression of Gn and Gc results in a specific Golgi localisation (Figure 10). Interestingly, expression of Gc only leads to an ER localisation of the protein. This may indicate that the two glycoproteins have to interact, and form hetero-oligomers for their transportation to the Golgi (Bertolotti-Ciarlet *et al.*, 2005; Haferkamp *et al.*, 2005). There, the mature proteins and the viral RNAs encapsulated into RNPs can form new virions that will bud from the Golgi, acquiring their lipoprotein bilayer. They will then be transported to the plasma membrane and be secreted into the extracellular environment. Of note, CCHFV NP is able to self-assemble without the GPC into virus-like particles (VLPs), which are particles that do not contain viral genome (Zhou *et al.*, 2011).

Once newly formed virions are produced, they will infect naïve cells and start the replication cycle over again, following an entry step that will be detailed in the following section.

## C. Viral entry of CCHFV and other members of the *Bunyaviricetes* class

The viral entry regroups the different steps, starting with the initial interaction between the virus and the host cell, until the release of the viral genome into the cytoplasm. It can be separated into attachment, internalisation, and fusion steps in the case of enveloped viruses (Figure 10). Entry of most enveloped viruses is initiated by the interaction of their envelope glycoproteins with host cell surface co-factor(s) and/or receptor(s) (Boulant *et al.*, 2015).

A receptor is the molecule that, once bound to the viral particle, changes its conformation, and mediates the signalling cascade leading to the transfer of the viral genome into the target cell. The interaction with the receptor can be facilitated by co-factors, such as attachment factors. Attachment factors can bind specifically, or not-specifically, to the viral particle and concentrate the virus onto the cell surface, promoting its encounter with the receptor(s). A single virus can use several co-factors or receptors on a single cell, which

usually determines the cell tropism. It can also use different factors on different cell types (Stehle and Casasnovas, 2009).

In the case of CCHFV, its entry is still poorly understood. **As I started my PhD research, its cellular receptor(s) had not been identified yet**, nor had the glycoprotein(s) involved in the attachment or the entry. In this chapter, I will summarise the knowledge then available about the entry of CCHFV, as well as provide insight into the different *Bunyaviricetes* entry factors.

## 1. Putative attachment factors for CCHFV

### a. Nucleolin

Some studies using soluble ectodomains of CCHFV Gc and Gn suggested that Gc is the glycoprotein that binds to the cell and, most specifically, binds to nucleolin (NCL) (Xiao *et al.*, 2011). NCL is involved in ribosome production and is described as being localised in the nucleolus but also localised at the plasma membrane (Tayyari *et al.*, 2011). This protein is ubiquitously expressed, and thus is present on CCHFV-susceptible cell lines. In Xiao *et al.*, 2011, the authors incubated SW-13 (human adrenal cortex cells), VeroE6 (African green monkey kidney cells) or 293T/17 (human kidney cells) with recombinant fragments of Gn and Gc and analysed them by flow cytometry. These recombinant fragments were the Gn ectodomain and a Gc fragment of the ectodomain fused to Fc from human IgG1. It showed that Gc, and particularly the fragment 180-300, binds to the cell, contrary to the Gn ectodomain, which had limited binding. The authors then used these fusion proteins for immunoprecipitation with SW-13 and 293T/17 lysates, and obtained only one hit, NCL (Xiao *et al.*, 2011). The authors concluded that the protein was an attachment factor. It is known that NCL can serve for the attachment of several viruses and bacteria such as RSV (Tayyari *et al.*, 2011; Xiao *et al.*, 2011), enterovirus 71 (Su *et al.*, 2015), human immunodeficiency virus type 1 (HIV1) or *Francisella tularensis* (Barel *et al.*, 2008), which were reviewed in Tonello *et al.*, (2022). However, NCL is notoriously “sticky” and can easily engage in non-specific interactions, so immunoprecipitation is no robust evidence that the protein is a *bona fide* attachment factor. Furthermore, no studies including CCHFV entire particles were performed.

### b. DC-SIGN

Another paper described the Dendritic Cell-Specific Intracellular-3-Grabbing Non-integrin (DC-SIGN) as a potential co-receptor for CCHFV (Suda *et al.*, 2016). In this article, the authors used vesicular stomatitis virus (VSV) pseudotyped with CCHFV GPs to infect Jurkat cells (human T lymphocytes) that were overexpressing a control molecule, or DC-SIGN. They obtained a 4-fold increase in infectivity with DC-SIGN-overexpressing cells. Furthermore, they used an anti-DC-SIGN antibody and were able to decrease the infection by 2-fold. This receptor is expressed on dendritic cells, which are susceptible to CCHFV infection (Connolly-Andersen *et al.*, 2009), and which are recruited at the tick bite, the primary site of infection. Moreover, several bunyaviruses are known to use DC-SIGN as an attachment factor (described in Chapter I.C.6), thus strengthening the notion that this hit could be a potential co-factor for CCHFV entry. However, many CCHFV susceptible cells do not express DC-SIGN, some technical information is missing in this paper (such as the antibody concentration used for the blocking assay), and the impact on the pseudotyped particles (pp) is minor, suggesting that this factor may help with the attachment of the virus but may not be the main receptor.

### c. Heparan Sulfate Proteoglycans

Other factors that may be implicated in CCHFV attachment are the Heparan Sulfate Proteoglycans (HSPG), which are expressed in all animal tissues and have already been shown for other bunyaviruses (described in Chapter I.C.6). Due to heavily sulphated glycosaminoglycan (GAG) chains, HSPG present a negative charge that can interact with the basic residues of viral glycoproteins (Rusnati *et al.*, 2009). To date, there is only little evidence of the role of GAGs in CCHFV infection (Riblett *et al.*, 2016). In this paper, the authors engineered haploid cells (Hap1), which could not produce B3GAT3 or B4GALT7, both enzymes being required to produce HSPG. Upon infection of these cells with CCHFV, a 2-fold decrease of infection was observed. HSPG may thus play a role for CCHFV like it does for other viruses, through weak interaction, increasing the viral concentration at the entry site and thus facilitating the binding to specific receptors.

## 2. Internalisation routes for CCHFV

In most of the cases, following the attachment to the cell and the binding to the receptor(s), a signalling cascade can be triggered that leads viral particles to be internalised into the cell and release their genomes. Some viruses, such as the Herpes Simplex Virus 1 do not require endocytosis and can fuse with the plasma membrane (Fuller and Spear, 1987). Other rely on endocytosis. There are several mechanisms of endocytosis, well described in Mercer *et al.*, 2010. The most studied mechanisms are the macropinocytosis, caveolar/raft-dependant endocytosis, and the clathrin-mediated endocytosis (CME), but some clathrin- and caveolar/raft independent mechanisms have also been described. In the case of CCHFV, internalisation occurs through clathrin- and cholesterol-dependant endocytosis.

### a. CCHFV relies on clathrin-mediated endocytosis

CME is by definition an endocytic process driven by the formation of a clathrin (a molecular scaffold for vesicles) coat on the cytoplasmic leaflet of the membrane (Mercer *et al.*, 2010). In Simon *et al.*, (2009), the authors demonstrated that CCHFV endocytosis was dependant on clathrin by using chlorpromazine (CPZ) and sucrose, two inhibitors of CME, as well as downregulation of clathrin. However, these results can be challenged. Indeed, CPZ also interferes with phagosome formation (Elferink, 1979) while sucrose is not specific to CME (Guo *et al.*, 2015). Four years later in Garrison *et al.*, (2013), the authors used a more specific inhibitor: pitstop2, and downregulated the adaptor protein 2 (AP-2), the second most abundant protein after clathrin in clathrin-coated pits. Both strategies impacted the infection of CCHFV and thus confirmed the clathrin dependant entry route.

### b. Cholesterol-dependant endocytosis in CCHFV entry

In the same paper, the cholesterol dependency was demonstrated by treating Vero E6 cells with the cholesterol-depleting drug methyl- $\beta$ -cyclodextrin. Treated cells were used for binding and infection assays. The authors found that the binding was not affected, while

CCHFV RNA levels, after 6h of infection, were lower in the treated cells. Their conclusion was that cholesterol is required in a post-binding event following internalisation, possibly by interfering with CME. However, these results do not rule out the possibility that cholesterol may play a role in the replication steps since in Vero E6 mRNA is strongly synthesised as early as 6h p.i. (Simon *et al.*, 2009).

### 3. Fusion

The last step of the entry, before the release of the viral genome into the cell, is the fusion of the viral membrane with the endosome. During this step, the clathrin-coated vesicles that contain the viral particles, are sorted into endosomes that become increasingly acidic as they mature from early endosomes (EE) to late endosomes (LE). This change of pH is required for conformational changes in the glycoproteins, which trigger the fusion process. Indeed, using NH<sub>4</sub>Cl (that neutralise luminal pH), it was demonstrated that CCHFV entry is pH-dependant (Garrison *et al.*, 2013; M. Simon *et al.*, 2009). It was shown in Garrison *et al.*, (2013) that Rab5 (an EE-specific protein) but not Rab7 (a LE-specific protein) is required for CCHFV infectivity, demonstrating that CCHFV does not require LE trafficking for entry. However, a paper was published a year later where the authors showed that, 30min after the infection, CCHFV starts to localise to multivesicular bodies (MVBs), which correspond to LE (Shtanko *et al.*, 2014). MVBs are formed from early endosomes by the inward budding of the limiting membrane into the lumen, and their formation is dependent on the endosomal sorting complex required for transport (ESCRT) (Piper and Katzmann, 2007). This complex requires proteins such as Vps24, Tsg101, Alix/Aip1 that were shown to regulate CCHFV entry (Shtanko *et al.*, 2014).

The process of fusion in CCHFV infection is believed to be similar to the one observed in Rift Valley Fever Virus (RVFV) and HAZV. It was revealed that Gn acts as a shield to bury the fusion loop of Gc and prevent premature fusion of the virions (Halldorsson *et al.*, 2018; Punch *et al.*, 2018). At a low pH (endosomal pH), the Gn shield is repositioned, Gn-Gc heterodimer dissociates, followed by the extension of Gc into a trimer hairpin to expose its fusion loop and drive the membrane fusion (represented in Figure 13) (Mishra *et al.*, 2022; Punch *et al.*, 2018), followed by the release of the viral genome, into the host cell.

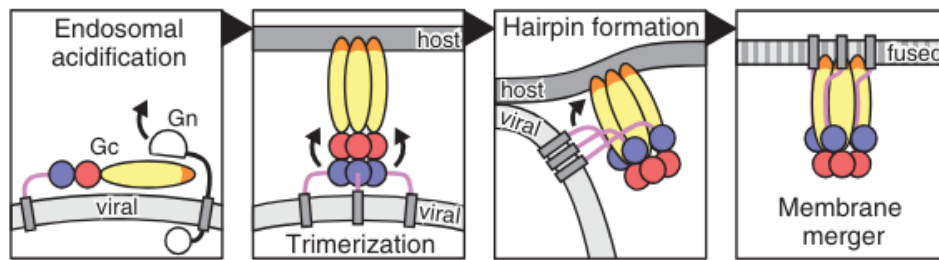


**Figure 13: Proposed model of the mechanism of bunyaviruses class II membrane fusion protein.** CCHFV Gn and Gc form a heterodimer where Gn acts as a shield on Gc. Upon endosomal acidification, the heterodimer dissociates and Gc changes conformation to form a trimer hairpin that expose its fusion loop (in orange), causing the fusion. From Mishra *et al.* (2022).

#### 4. CCHFV cellular tropism

CCHFV ability to complete an infection cycle in a cell depends on several host factors that contribute to defining the virus tropism. Indeed, for a cell to be able to produce new virions, the cell must be susceptible and permissive to the infection. A susceptible cell expresses at its surface host factors required for the virus entry, and a permissive cell is able to replicate the virus once it has entered.

Since the presence or absence of a receptor/co-factor might explain the capacity of a virus to infect varied species or different organs and cell types, it is interesting to consider CCHFV host range and cellular tropism as hints for candidate receptors/co-factors. A retrospective study indicated that, in humans, mononuclear phagocytes, endothelial cells and hepatocytes are the main targets of infection (Burt *et al.*, 1997). More recently, a paper was published in which the authors infected 16 human cell lines and 6 animal cell lines (monkey, pig, hamster, and dog) and measured the viral RNA load in the supernatant and NP expression in infected cells, 4 days post-infection (Dai *et al.*, 2021). They described HepG2 (hepatocytes) as non-permissive, even if they showed, in the supernatant, a viral load comparable to Huh7. They suggested that HepG2 support transcription and replication but produce defective particles. A-431 cells (epidermal carcinoma) did not show signs of infection/replication and THP-1 (monocytes) did not support CCHFV replication, probably because of a high interferon response (Dai *et al.*, 2021).

During her PhD in 2012 at the United States Army Medical Research Institute of Infectious Diseases, Aura Garrison used a library of 59 human cancer cell lines and screened their ability to support CCHFV replication (Garrison, 2012). The experiment was done using authentic CCHFV and the read-out was done by staining the infected cells for NP after 3, 5 and 7 days. From the 59 cell lines, only 3 did not show signs of infection/replication: Molt-4 and CCRF-CEM, both T-lymphocytes (TL), and HL-60 (promyeloblast). She then assessed a third TL cell line, Jurkat, and it showed no sign of replication either. Therefore, it is possible that TL do not express the CCHFV receptor, or that they cannot support virus replication. Using these candidate cell lines, she did a bioinformatics screen to identify which receptors could be expressed in the 56 other cell lines, but not in TL, and obtained a list of 25 plasma membrane proteins that could be receptor/co-factor candidates, as shown below (Table 2).

All these data indicate that CCHFV can infect a wide range of cell lines of human and non-human origin, with the exception of TL, and thus, can either use several entry factors or use a receptor ubiquitously expressed and well conserved between species.

Gene symbol	Gene name
ACTR2	actin-related protein 2 homolog (yeast)
AGRN	Agrin
B2M	beta-2-microglobulin
CALM1	calmodulin 1
CD59	CD59 molecule, complement regulatory protein
CD63	CD63 molecule
CD9	CD9 molecule
CNIH4	cornichon homolog 4 (Drosophila)
CTNNA1	cadherin-associated protein
CTTN	Cortactin
DSP	Desmoplakin
EPCAM	Epithelial cell adhesion molecule
HNRNPM	Heterogeneous nuclear ribonucleoprotein M
JUP	Junction plakoglobin
LAMP1	lysosomal-associated membrane protein 1
LDLR	low density lipoprotein receptor
MCAM	melanoma cell adhesion molecule
PLXNB2	Plexin-B2
PPAP2C	Lipid phosphate phosphohydrolase 2
PTPRF	Receptor-type tyrosine-protein phosphatase F
SPTBN1	Spectrin beta chain, brain 1
STOM	stomatin
TFRC	Transferrin receptor
VAPA	vesicle-associated membrane protein

**Table 2:** List of 25 common plasma membrane proteins genes expressed in permissive cells with low or no expression in non-permissive cells. Two transcript data sets were used to perform a bioinformatics screen comparing plasma membrane protein expression between permissive and non-permissive cells. From Garrison (2012).



## 5. Tools to identify entry factors

As it was highlighted above, there are many unknowns about CCHFV entry. To elucidate the mystery of its entry factors, there are many different assays and tools that can be used. Here, I will describe some of the methods currently used for identifying a virus entry factor, and in the next section (Chapter I.C.6), I will provide more insight on how they were used on bunyaviruses.

### a. Affinity purification–mass spectrometry

A common way to identify a viral entry factor is by characterisation of the interactome of the viral glycoproteins. Previously, the most used technique was the virus overlay protein binding assays. During an overlay assay, total cell lysate is subjected to gel electrophoresis, transferred onto a membrane which is then incubated with viral particles, or purified viral glycoproteins. The band(s) where the virus interacts with a cellular protein is revealed with an antibody targeting a viral component. In a duplicate gel, non-incubated with the virus, this band is identified by mass spectrometry (MS). However, this technique fails to identify entry factors requiring complexes or a specific conformation and cannot be used for viruses having low binding affinities with their receptors.

More recently, in order to avoid the denaturation step of the gel electrophoresis, the most common interactome approach became affinity purification followed by mass spectrometry (AP-MS). This method involves bringing in contact the whole virus, or its glycoproteins, with the lysate of target cells. Then the complex glycoprotein/entry factor(s) or virus/entry factor(s) is purified using specific high affinity antibodies directed against a viral component, followed by an enzymatic digestion of the co-purified proteins. These co-purified proteins are then identified using Liquid Chromatography coupled to tandem mass spectrometry. This is efficient for viruses having a high affinity with their receptor, but in the case of a weaker interaction, a chemical cross-linking reaction can be performed. The AP-MS depends on the quality of the affinity purification. The choice of the antibody is important because it should recognise a conformational epitope that is not hidden upon binding to the unknown entry

factor. Most of the time the antibodies are targeting other viral proteins than the GPs, since the protein's epitope could already be involved in the interaction virus/entry factor. Another solution is to use tagged viral components, but this method is limited because it requires to genetically modify the viral proteins, and again, the tag should not sterically hinder the receptor binding. In addition, AP-MS screens can result in false-positive candidates through non-specific binding.

b. Genome modifications: gain of function and loss of function screens

Genomic approaches consist in modifying the target cell genome in order to identify an entry factor. These are divided into gain of function (GOF) and loss of function (LOF). GOF consists in introducing new functionalities, such as the expression of cellular entry factors, into target cells. If these cells become more infected, the newly expressed gene encodes a pro-viral factor, and in contrast, if they become less permissive, it encodes an anti-viral factor. The most common tool for GOF is cDNA libraries. cDNA libraries are synthesised from the total mRNA of a susceptible cell line, that is reverse transcribed and cloned into plasmid or lentiviral expression systems (Kawano *et al.*, 2004). This approach has several limitations. It requires a suitable non-susceptible cell line that can be modified. Moreover, the reverse transcriptase step is prone to error and mutations, thus possibly producing truncated ORF creating false-negative.

In contrast to GOF approaches, LOF screens start with a susceptible cell line that is further modified to knock down (KD), impair (truncation) or knock out (KO) a host factor. Down regulation can be produced using RNAi or Clustered Regularly Interspaced Short Palindromic Repeats/CRISPR associated protein 9 (CRISPR/Cas9) interference (CRISPRi).

RNAi screens are commonly used and are well described in several reviews (Mohr *et al.*, 2010; Panda and Cherry, 2012). siRNAs are delivered through transfection in the cytosol. In order to obtain a more stable integration, short hairpin RNAs (shRNAs) are also used. Those RNAs can also be stably expressed through integration of their DNA sequence after integration into lentiviral vectors. However, RNAi screen have false positives, caused by off-

target effects, and false negatives, caused by gene duplication preventing phenotypic manipulation by single gene knock downs.

In CRISPRi screens, the nuclease-deactivated Cas9 (dCas9) is fused to gene repressors, such as Krüppel associated box, which inhibit a targeted gene activity and its transcription. During CRISPRi screens, small guide RNAs (sgRNAs) are delivered into the cell with the modified Cas9 using lentiviral vectors. The sgRNA can also be delivered without the Cas9, in cells modified to stably express the protein. Once delivered, the sgRNA guides the complex to a specific region of the DNA where the dCas9 inhibits the gene transcription. This tool results in more efficient knock down and less off-target effects than siRNA. A limit to KD screen is that, since the total repression of the gene cannot be achieved, there is a higher risk of false-negative results than in total KO screen.

However, the CRISPR/Cas technology can also be used to achieved site-specific mutagenesis that causes the KO of a gene. The KO occurs when a sgRNA assembles with a Cas9 nuclease to form the CRISPR/Cas9 complex. In this case, the sgRNA guides the complex where the Cas9 causes a double-stranded DNA break. The DNA is then repaired in a non-homologous manner, causing the null phenotype. The delivery system is identical to the one described for CRISPRi. CRISPR/Cas9 screens being widely used recently, different libraries of sgRNA have been set up and optimised in order to reach the lowest levels of off-target effects (Sanson *et al.*, 2018).

Furthermore, KO can also be achieved by random mutagenesis. Random mutagenesis is usually done using retroviral gene-trap vectors containing a reporter gene flanked by strong splice acceptor sites (to target introns) and a polyadenylation sequence. After transduction, the gene-trap vectors are integrated into introns, leading to the production of truncated mRNA fused to the reporter gene and ending at the polyadenylation sequence, disrupting the expression of the gene (De-Zolt *et al.*, 2009). The gene of interest that is KO can be identified by sequencing from the inserted reporter gene. However, this method is inefficient in diploid cells, in which both alleles should be targeted to allow the null phenotype.

The main issue with KO screens is that there is a total loss of the expression of the host factor, leading in the case of essential genes, to cell death. This is not the case in KD studies, giving them the advantage of the ability to study essential genes.

c. Pooled vs arrayed screens

These tools can be used either pooled or arrayed. Arrayed screens are done by targeting one gene per well in a multiwell plate format. This method does not require selection and sequencing in order to identify the factors of interest but is tedious and can be limited in terms of numbers of targeted genes. In contrast, in pooled screens, a single population of cells is introduced to a mix of cDNA or sgRNA. In this case, cells that exhibit a phenotype of interest need to be sorted. This can be done by fluorescence-activated cell sorting, antibiotic selection, or cytopathic death resulting from the viral infection. The identification of the factor involved in the virus cycle is then done by next generation sequencing (NGS), comparing the enrichment of particular cDNA or sgRNA sequences in the selected population, and in the initial population. All the methods described above are well reviewed in Barrass and Butcher, (2020).

Screens can highlight receptors or co-factors of entry, but also factors mediating viral replication itself. They only represent the first step of the long process required for the validation and characterisation of viral receptors. For example, high-throughput screens are followed by a smaller screen with the potential hits to validate them. Then it is required to assess the impact of the candidates on the cell, independently of the infection, before starting to characterise the precise role of the protein on the viral cycle.

Even if high-throughput screens are more used because of their capacity of evaluate many factors simultaneously, they are time-consuming, tedious, and sometimes, they may not highlight any factors. In the following paragraph, I will present the receptors or co-factors of the *Bunyaviricetes* class, highlighting that sometimes discoveries are also made by targeting specific hypothesis-driven candidates, based on the literature. However, serendipity can also be a factor in discovery.

## 6. *Bunyaviricetes* entry

As described earlier, CCHFV is a virus from the *Bunyaviricetes* class. This class is now classified in 15 families: *Arenaviridae*, *Cruliviridae*, *Discoviridae*, *Fimoviridae*, *Hantaviridae*, *Konkoviidae*, *Leishbuviridae*, *Mypoviridae*, *Nairoviridae*, *Peribunyaviridae*, *Phasmaviridae*, *Phenuiviridae*, *Tospoviridae*, *Tulasviridae* and *Wupedeviridae* (Kuhn *et al.*, 2023). Even if the majority of the bunyaviruses are of little public interest, some of them are recognised as priority pathogens by the WHO, such as CCHFV and RVFV (Mehand *et al.*, 2018). From these 15 families, 5 are known to contain viruses that infect or cause disease in vertebrates or humans more specifically: *Arenaviridae*, *Hantaviridae*, *Nairoviridae*, *Phenuiviridae* and *Peribunyaviridae*. In the Table 3, I listed the host receptor(s) or co-factors(s) that mediate the entry of these viruses. In the case of the arenaviruses, only the viruses known for causing human disease are described.

From this table, it can be noticed that viruses that are closely related can use the same entry factors, such as TfR1 for the New World arenaviruses, or DC-SIGN for the phleboviruses. This can be explained by similarities in their glycoproteins and thus, in their receptor-binding domains. However, this can be biased by the fact that researchers tend to first investigate given factors already described for closely related viruses.

It can also be noticed that, depending on the vector, viruses use different receptors. For example, the arboviruses commonly use HSPG or DC-SIGN, in contrast to viruses transmitted by rodents.

Finally, and highlighted in bold in Table 3, since 2021, more and more *Bunyaviricetes* are described using low-density lipoprotein receptor (LDL-R) related protein 1 (LRP1). LRP1 is a receptor of the LDL receptor family, which is shown to be used by a wide diversity of viruses for their entry and is discussed in more details in the following section (Chapter I.D).

	Virus	Main vector	Factor	Entry step	Tool			Ref
					Virus / Peptide	Cell line	Assay	
Peribunyaviridae	Cache Valley virus (CVV)	Mosquito	Unkown					
	Bunyamwera Virus (BUNV)	Mosquito	DC-SIGN	ND	GERV		Not shown	(Lozach et al., 2011)
	La Crosse Virus (LACV)	Mosquito	DC-SIGN	ND	VSV_LACV GPs	Raji	OE DC-SIGN	(Hofmann et al., 2013)
			LRP1	D: Attachment	FA	Huh-7	Binding assay,	(Devignot et al., 2023)
	California Encephalitis Virus (CEV)	Mosquito	Unkown					
	Oropouche Virus (OROV)	Culicoide	LRP1	ND	OROV strain BeAn19991 and VSV_OROV GPs	BV2, HEK293T, A549 and N2a	LRP1 KO cells, competition assay	(Schwarz et al., 2022)
	Akabane Virus (AKAV)	Mosquito ?	HSPG	D: Attachment	rAKAV OBE-1 and Iriki strains and VSVpp AKAV_GPC	HmLu-1	Competition assay, enzymatic removal, KO HSPG-KO cells and binding assay,	(Murakami et al., 2017)
Schmallenberg virus (SBV)	Culicoide	HSPG	D: Attachment	SBV	HmLu-1 cells	Competition assay, enzymatic removal, KO HSPG-KO cells and binding assay	(Murakami et al., 2017)	
Hantaviridae	Hantaan Virus (HTNV)	rodent	$\alpha\beta 3$ integrins	ND	HTNV 76-118 strain	VeroE6, CHO and HUVEC	Competition, neutralisation assay and OE	(Gavrilovskaya et al., 1999)
			$\beta 2$ integrin	ND	HTNV 76-118 strain, VSV_HNTV GPs	CHO	OE, NF-kB assement after infection with UV inactivated virus.	(Raftery et al., 2014)
			DAF	ND	HTNV 76-118 strain	Vero C1008 and HUVEC	Neutralisation assay	(Krautkrämer and Zeier, 2008)
			gC1qR	ND	HTNV 76-118 strain	VeroE6 and HUVEC, A549	Overlay assay and mass spectrometry, KD and OE	(Choi et al., 2008)
			70-kDa protein	ND	HTN A9 strain	CHO	Overlay assay and neutralisation	(Mou et al., 2006)
	Seoul Virus (SEOV)	rodent	$\alpha\beta 3$ integrins	ND	SEOV SR-11 strain	VeroE6, CHO and HUVEC	Competition, neutralisation assay and OE	(Gavrilovskaya et al., 1999)
	Puumala Virus (PUUV)	rodent	$\alpha\beta 3$ integrins	ND	PUUV-K27 strain	VeroE6, CHO and HUVEC	Competition, neutralisation assay and OE	(Gavrilovskaya et al., 1999)
	Propect Hill Virus (PHV)	rodent	$\alpha 5\beta 1$ integrin	ND	PHV	VeroE6, CHO and HUVEC	Competition, neutralisation assay and OE	(Gavrilovskaya et al., 1999)
	Tula Virus (TULV)	rodent	unknown					
	Sin Nombre Virus (SNV)	rodent	$\alpha\beta 3$ integrins	ND	SNV CC107	VeroE6, CHO and HUVEC	Neutralisation assay, OE and inhibition	(Gavrilovskaya et al., 1998)
			PCDH1	D: Attachment	VSV_SNV GPs and SNV CC107	Haploid HAP1, U2OS, HUVEC and HPMEC	KO and OE, neutralisation and binding assay	(Jangra et al., 2018)
			DAF	D: Attachment	SNV SN77734 strain	Tanoue B cells	Binding assay,	(Buranda et al., 2010)
Andes Virus (ANDV)	rodent	$\alpha\beta 3$ integrins	ND	ANDV	VeroE6 and BHK-21	Competition assay and neutralisation assay	(Matthys et al., 2010)	
		PCDH1	D: Attachment	VSV_ANDV GPs, ANDV Chile-9717869	Haploid HAP1, U2OS, HUVEC and HPMEC	Genetic gene-trap screen, KO, OE, neutralisation and binding assay	(Jangra et al., 2018)	
Arenaviridae	Lujovirus (LUJV)	rodent	CD63	D: fusion	LUJV and VSV_LUJV GPs	Haploid HAP1	Genetic gene-trap screen, KO, and cell-cell fusion,	(Raaben et al., 2017)
			NRP2	D: attachment	LUJV and VSV_LUJV GPs	Haploid HAP1, HUVEC, HEK293T and BSR-T7	Genetic gene-trap screen, KO, OE and neutralisation	(Raaben et al., 2017)
	Lymphocytic Choriomeningitis Virus (LCMV)	rodent	Axl, Tyro3	ND	HIV lentiviral_LCMV GPs strain CI 13, WE54, ARMS3b and WE2.2	Jurkat	OE	(Shimajima and Kawaoka, 2012)
			DC-SIGN, LSEctin	ND	HIV lentiviral_LCMV GPs strain CI 13, WE54, ARMS3b and WE2.2	Jurkat	OE	(Shimajima and Kawaoka, 2012)
			$\alpha$ -dystroglycan	H: main receptor	LCMV strain CI 13, Arm5, WE54, MC57	VeroE6, MC57, ES	Overlay assay and blocking	(Cao et al., 1998)
	Lassa Virus (LASV)	rodent	$\alpha$ -dystroglycan	H: main receptor	LASV	VeroE6 and MC57	Overlay assay and neutralisation	(Cao et al., 1998)
			LAPM1	H: pre-fusion	VSV_LASV GPs	Haploid HAP1	Genetic gene-trap screen, cell-cell fusion and fusogenic defective mutant of LASV GP1.	(Jae et al., 2014), (Cohen-Dvashi et al., 2016)
			DC-SIGN and LSEctin	D: binding	HIV lentiviral vector LASV GPs strain Josiah and VSV_LASV GPs strain Josia	Jurkat	cDNA library screen from VeroE6 and binding assay	(Shimajima et al., 2012)
		Axl, Tyro3	H: internalisation	HIV lentiviral vector LASV GPs strain Josiah and VSV_LASV GPs strain Josia	Jurkat	cDNA library screen from VeroE6, binding assay and internalisation defective mutants,	(Shimajima et al., 2012)	

	Virus	Main vector	Factor	Entry step	Tool			Ref
					Virus / Peptide	Cell line	Assay	
<b>Arenaviridae</b>	Junin Virus (JUNV)	rodent	VGCCs	D: attachment H: main receptor in some species	MLV_JUNV GPs retroviral vector and Candid 1 strain	U2OS	siRNA screen, inhibitor, binding assay and KD in mice	(Lavanya et al., 2013)
			TFR1	D: Attachment	MLV_JUNV GPs retroviral vector and Candid 1 strain	U2OS	siRNA screen	(Lavanya et al., 2013)
					JUNV strain XI-13	293T, CHO and BHK	Neutralisation, OE and binding assay	(Radoshitzky et al., 2007), (Flanagan et al., 2008)
	Whitewater Arroyo Virus (WWAV)	rodent	TFR1	ND	MLV retroviral vector WWAV GPs strain AV96	293T	OE	(Zong et al., 2014)
	Guanarito Virus (GTOV)	rodent	TFR1	D: Attachment	GTOV strain VINH-9551	293T, CHO and BHK	Neutralisation, OE and binding assay	(Radoshitzky et al., 2007), (Flanagan et al., 2008)
	Sabia Virus (SBAV)	rodent ?	TFR1	ND	SABV	293T, CHO and BHK	Neutralisation and OE	(Radoshitzky et al., 2007)
Chapare Virus (CHAPV)	rodent ?	TFR1	ND	MLV retroviral vector MACV GPs	HEK23T	Neutralisation	(Helguera et al., 2012)	
<b>Nairoviridae</b>	Dugbe Virus (DUGV)	Tick	Unkown					
	Nairobi Sheep Disease Virus (NSDV)	Tick	Unkown					
	Crimean-Congo Hemorrhagic Fever Virus (CCHFV)	Tick	Nudeolin	ND	Soluble ectodomain of Gc and Gn lbar 10200	SW-13 and 293T/17	CoIP	(Suda et al., 2016)
			DC-SIGN	ND	VSVpp CCHFV_GPs lbar 10200	Jurkat	OE of DC-SIGN, neutralisation and competition assay	(Xiao et al., 2011)
Hazara Virus (HAZV)	Tick	Unkown						
<b>Hantaviridae</b>	Uukuniemie Virus (UUKV)	tick	DC-SIGN	D: Main receptor	UUKV S23 strain	HeLa, Vero	Neutralisation assay, OE, inhibitor, particles dyed and binding assay and OE, inhibitor, neutralisation, binding assay, endocytic deficient mutant	(Lozach et al., 2011)
			L-SIGN	D: Attachment	UUKV S23 strain	Raji, HeLa		(Léger et al., 2016)
	Heartland Virus (HRTV)	tick	unkown					
	Severe Fever with Thrombocytopenia Syndrome Virus (SFTSV)	tick	DC-SIGN	ND	VSV_SFTSV GPs	Raji	OE, competition assay and	(Hofmann et al., 2013)
			DC-SIGNR, LSECTin	H: Attachment	VSV_SFTSV GPs	Jurkat and Raji	OE	(Tani et al., 2016)
			NMMHC-IIA	H: Attachment	SFTSV	HUVEC and HeLa	CoIP recombinant ectodomaine Gn-mFc, mass spectrometry, KD and OE	(Sun et al., 2014)
	Toscana Virus (TOSV)	phlebotome	DC-SIGN	ND	TOSC ISS strain	Raji	OE and inhibitors	(Lozach et al., 2011)
			L-SIGN	ND	TOSC ISS strain	Raji, HeLa	OE	(Léger et al., 2016)
			HSPG	H:Attachment	TOSC ISS strain	Vero	Vero cells, inhibitors	(Pietrantoni et al., 2015)
	Rift Valley Fever Virus (RVFV)	mosquito	DC-SIGN	ND	RVFV ZH548 strain	Raji	Neutralisation assay, OE and inhibitor	(Lozach et al., 2011)
L-SIGN			ND	rHAZV ZH548 strain	Raji, HeLa	OE	(Léger et al., 2016)	
RNASEK			D: internalisation	RVFV MP 12 strain	U2OS	RNAi screen, KD, binding and internalisation assay	(Hackett et al., 2015)	
HSPG			H: Attachment	Non-spreading RVFV	CHO deficient cells, A549	Inhibitors	(De Boer et al., 2012)	
LRP1			D: Attachment and internalisation	RVFV ZH501, RVFV-MP12GFP	BV2, MEF	CRISPR/Cas9 screen, KO, competition assay, BLI, neutralisation, binding and internalisation assay	(Ganaie et al., 2021)	
Punta Toro Virus (PTV)	phlebotome	DC-SIGN	ND	PTV	Raji	Inhibitor	(Lozach et al., 2011)	
Sandfly Fever Sicilian Virus (SFSV)	phlebotome	LRP1	D: Attachment	Sabin	Huh-7	Binding assay	(Devignot et al., 2023)	

**Table 3: Summary table of Bunyaviricetes receptors or co-factors of entry.** In this exhaustive list are represented viruses known to infect vertebrates, or more specifically to infect humans in the case of the Arenaviridae and the Hantaviridae. The accepted vector transmitting the virus is indicated. If the vector is only putative, it is followed by a question mark. The factors are listed followed by the precise step of the entry where they act. ND: not determined, D: determined, H: hypothesised. BLI: Bio-layer Interferometry. Receptors from the family of the LDL-receptors are highlighted in bold.

## D. Low-density lipoprotein receptors in viral entry

LRP1, but also other LDL receptors, have been increasingly cited as viral cofactors over the past few years and not only for the bunyaviruses. In this section, I will detail the core members of the LDL-R family, and their implication in viral cycles.

### 1. Lipoproteins and cholesterol

#### a. Formation of lipoproteins

As indicated in their names, LDL receptors bind to low-density lipoproteins. Lipoproteins are particles constituted of a core of lipids, such as cholesterol ester (product of an esterification reaction between the cholesterol molecule and a fatty acid) and triglycerides. Both molecules are insoluble in water and require to be surrounded by phospholipids and proteins, such as apolipoproteins (amphipathic proteins binding to lipids) for their transport between tissues. Cholesterol is essential for cell metabolism (synthesis of hormones for example) and cell integrity. Regulation of plasma cholesterol levels is crucial, and default in this regulation can cause cholesterol accumulation in the arteries, leading to atherosclerosis (Brown and Goldstein, 1986).

In the endogenous lipid metabolism, lipoproteins are formed in the ER of hepatocytes. Triglycerides and cholesterol ester accumulate in the ER, leading to the formation of lipid droplets, and associate with apoB-100 by the action of the microsomal triglyceride transfer protein (MTP). The association forms lipoproteins called nascent very-low-density lipoproteins (VLDLs). Nascent VLDLs are secreted and capture apolipoprotein E (apoE) and C (described in the following section) from circulating high-density lipoprotein (HDL) to form mature VLDLs (Gibbons *et al.*, 2004). Mature VLDLs are then transported from the liver to adipose, cardiac and muscle tissues through the circulation. In the capillary endothelium, mature VLDLs, and more precisely, the apoC presents at their surface, activates the lipoprotein lipase, which hydrolyses the triglycerides and releases free fatty acids (Nimpf and Schneider, 2000). VLDLs are reduced by the activity of the lipoprotein lipase and form now intermediate-density lipoprotein (IDL) that will be further reduced by hepatic lipase into LDL (Figure 14).



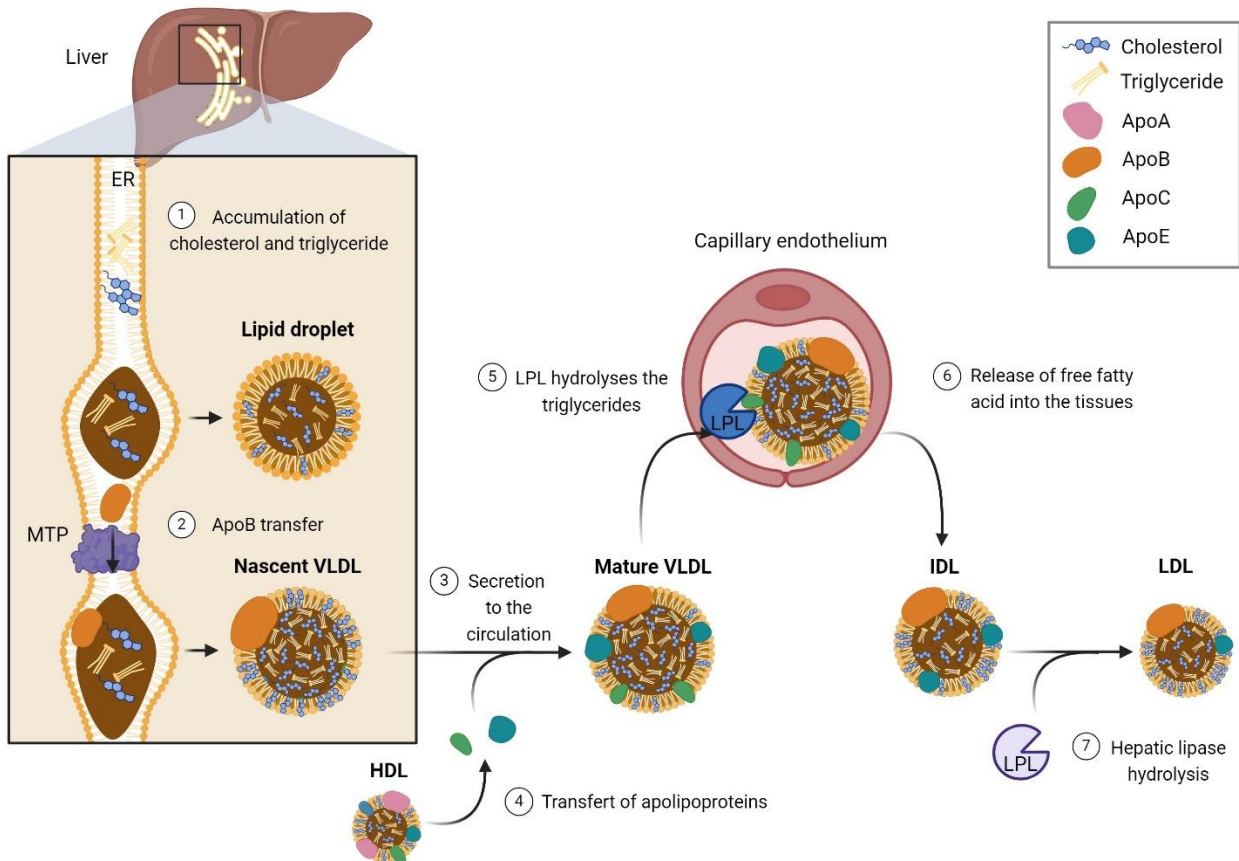


**Figure 14: Formation of LDL (endogenous lipid metabolism).** After accumulation into the ER of hepatic cells, cholesterol ester and triglyceride associate with apoB-100 through the activity of the microsomal triglyceride transfer protein (MTP). The nascent VLDL formed is secreted and associated with apoE and apoC from free HDL to form mature VLDL that will be reduced by the activity of lipoprotein lipases on capillary endothelium cells. The product of the hydrolysis is IDL that will be further reduced into LDL by hepatic lipase. Created with BioRender.com.

While in the circulation, HDLs exchange their cholesterol ester to triglyceride contained in HDL, IDL or LDL through the activity of the cholesterol ester transfer protein (CETP).

As indicated above and in the Figure 14, there are different forms of lipoproteins, that differ in size, density, lipid composition, and incorporated apolipoproteins. All of them are described in Feingold, (2000) and summarised in the Table 4 below.

Lipoprotein	Density (g/ml)	Size (nm)	Major Lipids	Major Apoproteins
VLDL	0.930-1.006	30-80	Triglycerides	Apo B-100, Apo E, Apo C
IDL	1.006-1.019	25-35	Triglycerides Cholesterol	Apo B-100, Apo E, Apo C
LDL	1.019-1.063	18- 25	Cholesterol	Apo B-100
HDL	1.063-1.210	5-12	Cholesterol Phospholipids	Apo A-I, Apo A-II, Apo C, Apo E

**Table 4: Different class of human lipoproteins.** Modified from Feingold (2000).

#### b. Apolipoproteins on VLDL, IDL and LDL

The human genome encodes 21 apolipoproteins, among which apoA-I, II, IV, V; apoC-I, II, III; apoB and apoE (Zhou *et al.*, 2018) that are secreted in the plasma in their free form, or on lipoproteins. Here, I will only detail the ones mainly present on human VLDL, IDL and LDL.

ApoB-100 is the mandatory structural component of VLDL, IDL and LDL. It is a protein of 513 to 550 kDa. The protein is synthesised in the ER of hepatocytes and possesses a globular amino-terminal domain reacting with MTP, allowing its transfer into lipids droplets to form lipoproteins (Hussain *et al.*, 2003; Knott *et al.*, 1986). ApoB is not an exchangeable protein and requires the activity of the MTP to be incorporated onto particles.

ApoC-I is a 6.6 kDa protein synthesised in the liver and the intestine (Cohn *et al.*, 2002; Jackson *et al.*, 1974; Polz *et al.*, 1980). ApoC is a highly exchangeable protein. When it is incorporated on VLDLs, ApoC-I inhibits the VLDL hydrolysis by LPL (Conde-Knape *et al.*, 2002), and when it is associated with HDLs, it inhibits the CETP activity (Gautier *et al.*, 2000), thus regulating the HDL clearance.

ApoC-II is an 8.8 kDa protein also mainly synthesised mainly in the liver and, to a lesser extent, in the intestine. ApoC-II activates the LPL in the capillary endothelium (MacPhee *et al.*, 2000).

ApoC-III is the more abundant C apolipoprotein in human plasma and is expressed in similar organs than apoC-II (Nestel and Fidge, 1982). In the opposite of apoC-II, apoC-III protein is an inhibitor of the LPL (Brown and Baginsky, 1972).

ApoE is secreted in the liver and intestine, but also in the kidney, spleen and brain, and has an approximately mass of 34 kDa (Pitas *et al.*, 1987). ApoE is an exchangeable protein and can be incorporated from IDL to HDL. In humans, 3 common isoforms of *APOE* exist:  $\epsilon 2$ ,  $\epsilon 3$ ,  $\epsilon 4$  (Rall Jr and Mahley, 1992). Even if the three isoforms differ by only a single amino acid substitution, it impacts their stability and affinity to receptors (Morrow *et al.*, 2000). Indeed, apoE2 binds less to receptors than apoE3 or apoE4 (Morrow *et al.*, 2000). Moreover, the amino acid change also impacts the binding to lipoproteins. ApoE3 and E2 bind preferentially to HDLs and apoE4 to VLDLs (Saito *et al.*, 2003). ApoE is involved in cellular proliferation. It was demonstrated that apoE inhibits smooth muscle cells proliferation, probably through activation of signalling cascades upon binding to HSPG (Swertfeger and Hui, 2001). But the main role of apoE is to bind core members of LDL receptors, and thus, as such, it plays a role in hepatic uptake of lipoprotein particles as described in the following section.

## 2. LDL-R family: pattern of expression, structure, and functions independent of viral infection

### a. Common features of the LDL receptors

The family of low-density lipoprotein receptors regroups several surface receptors that share similar motifs in their extracellular regions. They were discovered in 1947 after the identification of a cellular pathway for the binding, internalisation and degradation of LDL (Goldstein and Brown, 1974). The core members are the LDL-R, apolipoprotein E receptor 2 (apoER2), very low-density lipoprotein receptor (VLDL-R), LRP1, LRP1B, and the megalin. All of these proteins present several repetitions of a ligand-binding motif of approximately 40 amino acids with 6 cysteine residues, called LDL-R type A repeats, or cysteine-rich repeats. The large members of the family (LRP1, LRP1B and megalin) contain four cluster of repeats of this ligand-binding motif, when the other members only have one. The receptors of the family also contain epidermal growth factor (EGF)-like domains along with a  $\beta$ -propeller (YWTD) domain, a transmembrane anchor, and a cytoplasmic tail.

The cytoplasmic domain of LDL receptors contains several endocytosis signals. Indeed, four classes of motifs were identified. There are two tyrosine-based signals: a NPxY motif, and a Yxx $\emptyset$  motif ( $\emptyset$  is an amino acid with a bulky hydrophobic group sequence). The NPxY motif

directs the receptors to clathrin-coated pits (Brown and Goldstein, 1986; Chen *et al.*, 1990). There is also a di-leucine motif, a serine phosphorylation and a ubiquitin motif (Li *et al.*, 2001) (Figure 15).

An interesting feature of the receptors of the LDL-R family is that their interaction with their ligand can be antagonised by the receptor-associated protein (RAP) (Bu, 1998).

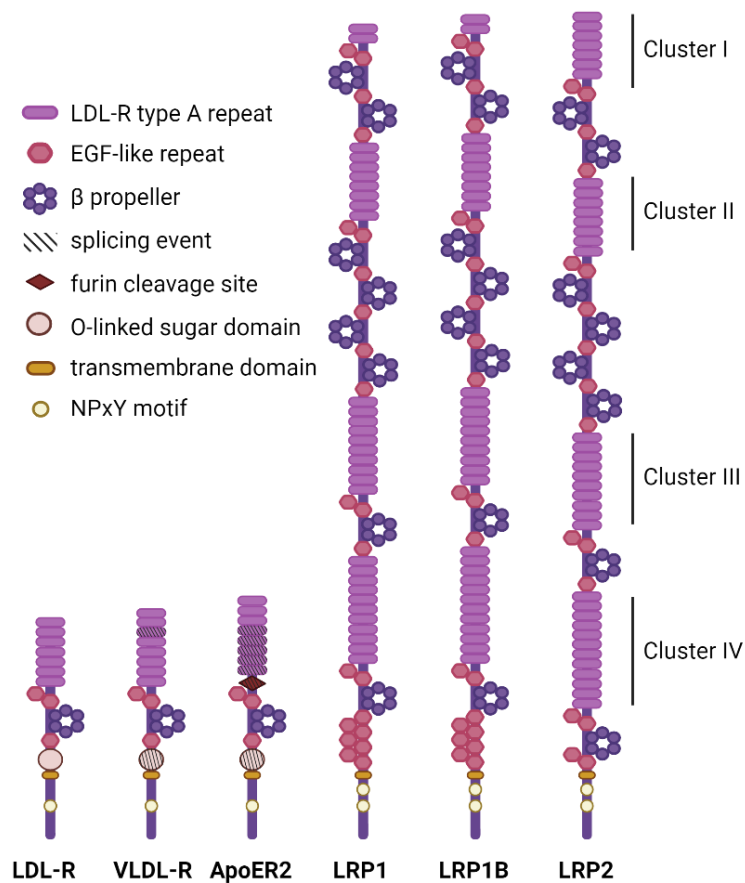


**Figure 15: Structure of the core members of the low-density lipoprotein receptor family.** LDL receptors contain five distinct modules present in characteristic numbers: LDL receptor type A (LA) repeats for ligand binding, EGF-like domains, YWTD beta propellers, O-linked sugar domain, transmembrane domain, and a cytoplasmic tail harbouring one or more NPxY motifs essential for binding of intracellular adapter proteins. Differentially spliced domains are depicted hatched. Cluster I, II, III, IV are corresponding to the clusters of LA repeats for LRP1, LRP1B and LRP2. Created with BioRender.com.

### b. LRP1

LRP1, or  $\alpha$ 2-macroglobulin receptor, is ubiquitously expressed but is expressed at the highest level in the brain and the liver. Being one of the largest members of the family, it is constituted of 4 cluster of ligand-binding motifs repeats (Figure 15). These domains interact with at least 40 different ligands, listed in Boucher and Herz (2011). For example, its extracellular domain is known to interact with the amyloid precursor protein,  $\alpha$ 2-macroglobulin (a protease inhibitor acting in the coagulation cascade) or apoE (Mikhailenko *et al.*, 2001) (Moestrup *et al.*, 1993; Willnow *et al.*, 1994). Interestingly, ligands bind specifically to particular clusters in LRP1 sequence. Indeed, most of the ligands bind to the cluster II and IV (Neels *et al.*, 1999). It was also demonstrated that its cytoplasmic tail also binds to several ligands, such as Dab1 (acting on neural migration), or OMP25 (involved in mitochondrial transport) (Kwon *et al.*, 2010).

Its main functions are the endocytosis of the different ligands (lipoprotein metabolism in the liver), the regulation of cell signalling pathway (Willnow, 1999) and neurite growth (in the brain) (Holtzman *et al.*, 1995)

### c. LRP1B

LRP1B was first identified as a candidate tumour suppressor, since it is deleted in cell lung cancer cell lines (Liu *et al.*, 2000). The receptor is expressed in multiple tissues, such as the cerebral cortex, the lung, the liver or the placenta (Li *et al.*, 2005). LRP1B is a close homolog of LRP1 (52% homology), and the number of ligand-binding repeats is identical to LRP1, except for the one additional ligand-binding motif in the cluster IV. Both receptors share several ligands, such as RAP or apoE, listed in Príncipe *et al.*, (2021). Similar to LRP1, the ligands bind preferentially to the cluster II and IV.

Nonetheless, LRP1B and LRP1 also differ in some aspects. For example, it was demonstrated that the kinetics of RAP endocytosis and the efficiency of this internalisation is lower for LRP1B (Liu *et al.*, 2001). This suggests that LRP1B might not be an efficient clearance receptor.

It has to be considered that the ORF of LRP1B is 13.8 kb and thus, overexpression (OE) of a vector encoding the protein is challenging. In this context, a mini receptor, mLRP1B4, comprising the fourth cluster (IV), the transmembrane domain and the intracellular domain, was designed and used for most experiments (Liu *et al.*, 2001).

#### d. Megalin

Megalin, also known as LRP2, is the third and last large member of the LDL-R family (Figure 15). In contrast to the above mentioned LDL receptors that were ubiquitously expressed, megalin is mainly expressed at the apical side of epithelial cells (Hermo *et al.*, 1999; Zheng *et al.*, 1998). Interestingly, megalin can be internalised upon interaction with some ligands and traffic to the opposite side of the polarized cell, to release the ligand in the extracellular environment without degradation. This was demonstrated for the retinol binding protein, the thyroglobulin or the albumin (Marinò *et al.*, 2000; Marínó *et al.*, 2001; Russo *et al.*, 2007). Just like the other large LDL receptors, it is known to have a great diversity of ligands listed in Marzolo and Farfán, (2011).

Megalin was shown to have several roles. In the central nervous system, it is implicated in the formation of brain structures such as the olfactory bulb or the forebrain. This is probably caused by a requirement of cholesterol uptake during the brain formation (Willnow *et al.*, 1996). In the liver or the lung, the main role is the internalisation of its ligands, like selenoproteins, apoE or insulin (Morales *et al.*, 1996; Olson *et al.*, 2008; Orlando *et al.*, 1998)

#### e. ApoER2

ApoER2, also named LRP8, is preferentially expressed in the central nervous system, but can also be found in the placenta or the ovaries (Kim *et al.*, 1996; Reddy *et al.*, 2011). The receptor has 8 ligand binding motifs and an unique proline-rich domain displayed in its cytoplasmic tail (Figure 15). ApoER2 is mostly known for its role as the Reelin receptor, and thus, in the Reelin pathway controlling the neuronal migration during brain development. ApoER2 also interacts with several factors such as Sepp1, a selenoprotein (ligands listed in

Dlugosz and Nimpf, (2018)). The receptor allows the uptake of selenium at the blood brain barrier as well as within the brain, on neurons. Selenium is particularly important to prevent neurodegeneration (Olson *et al.*, 2007).

A particularity of apoER2 is that it undergoes several splicing events. The ligand-binding motifs 4 to 6 are spliced out of all transcripts (Clatworthy *et al.*, 1999). Some transcripts contain a furin cleavage site in the ligand-binding motif 8, and some have the additional proline-rich domain in their cytoplasmic tail (Brandes *et al.*, 2001).

#### f. VLDL-R

VLDL-R has 8 ligand-binding repeats and shares around 50% homology with apoER2 (Kim *et al.*, 1996) (Figure 15). Similar to apoER2, the receptor is mostly expressed in the central nervous system, but can also be found in skeletal muscles or in the heart (Oka *et al.*, 1994). While both apoER2 and VLDL-R were shown to be expressed in the central nervous system, they do not co-localise in the same neurons at the same time. Interestingly, both receptors bind to Reelin (apoER2 with a stronger affinity), contributing to distinct actions on the development of the cerebral cortex. ApoER2 is mainly involved in the early steps of migration, and VLDL-R in its termination (Hirota *et al.*, 2015).

VLDL-R also undergoes splicing events producing 4 transcript variants. The transcript III lacks the third ligand-binding motif, and the variant IV lacks the same motif as well as the O-linked sugar domain. Similar to LRP1 and LRP1B, VLDL-R shares several ligands with apoER2, but also has specific ligands such as the vitellogenin or apoB.

#### g. LDL-R

LDL-R was the first receptor of the family to be discovered, and the most studied one. It was identified by Brown and Goldstein, (1986) after comparing the LDL uptake by normal fibroblasts and fibroblasts from patients presenting a familial hypercholesterolemia. LDL-R is ubiquitously expressed and binds to apoB, apoE and the proprotein convertase subtilisin/kexin type-9 (PCSK9) (Lagace *et al.*, 2006). PCSK9 is mainly secreted in the liver and

binds specifically to LDL-R (Kosenko *et al.*, 2013; Seidah *et al.*, 2003) and, once bound to LDL-R, inhibits its endocytic recycling, causing the lysosomal degradation of both proteins (Surdo *et al.*, 2011). The prototypic LDL receptor is constituted of 7 LDL receptor type A repeats, followed by two EGF-like repeats, a YWTD domain, a third EGF-like repeat, the transmembrane domain and the cytoplasmic tail containing an endocytic NPxY motif (Figure 15).

LDL-R mediates the clearance of LDL (discussed in Chapter I.D.1.a), though the binding of apoB and apoE followed by endocytosis via clathrin pits. In the endosome, the acidification of the compartment (pH below 6.5) causes the dissociation of the receptor and its ligand (Brown and Goldstein, 1986). After dissociation, the ligand is targeted to the lysosome, and the receptor is recycled to the cell surface where it binds another apolipoprotein. Once in the endolysosome, the LDL is hydrolysed to liberate cholesterol (Figure 16).

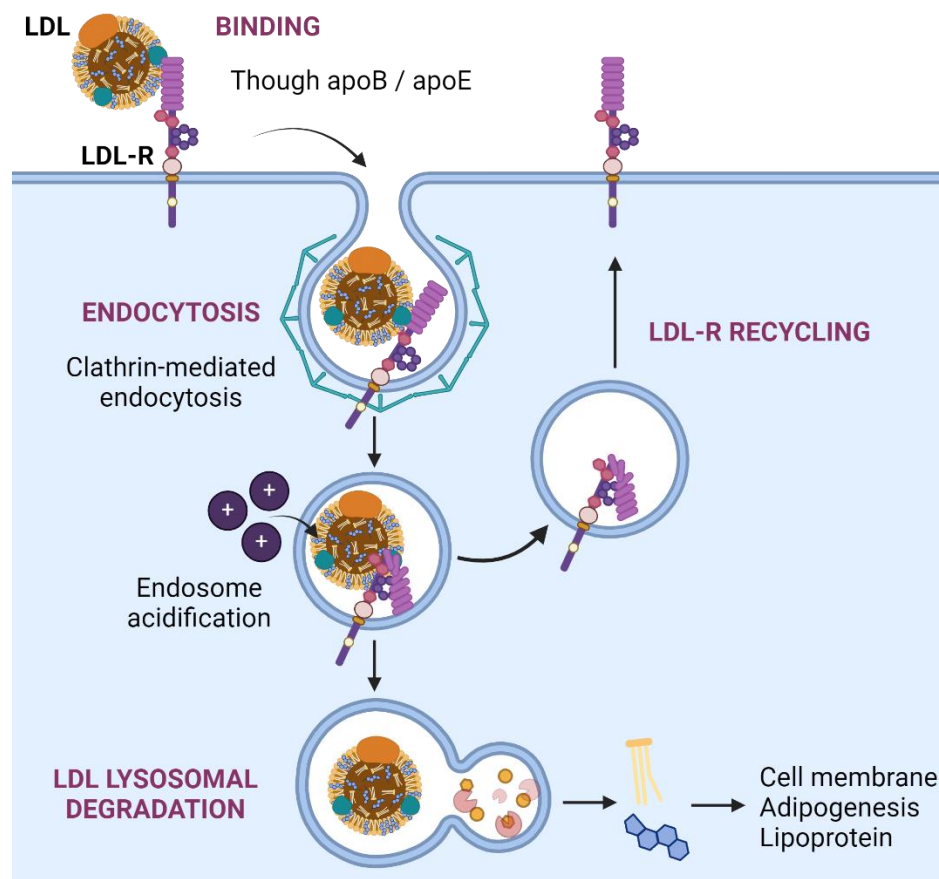


**Figure 16: LDL endocytosis by LDL-R.** LDL-R binds to LDL through apoB or apoE and internalises it by clathrin-mediated endocytosis. Upon acidification of the endosome, the ligand and the receptor dissociate. LDL-R is recycled to the cell surface and LDL is degraded to release into the cell the triglycerides and cholesterol. Created with BioRender.com.



### 3. Roles of LDL receptors in viral infection

Since the discovery of LDL-R, it was demonstrated that the receptors from the family have several roles outside of the uptake of cholesterol, one of them being a host factor promoting viral infection. The first paper describing a role as a viral receptor was published in 1993 by Paul Bates on the Rous Sarcoma Virus. Using a library of chicken genomic DNA transfected into COS7 cells (chicken being infected by the virus in contrast to COS7 cells), the authors had previously isolated, but not identified, a gene conferring susceptibility to the virus (GOF screen) (Young *et al.*, 1993). In Bates *et al.*, (1993), the authors were able to identify a 819 nucleotide sequence encoding an ectodomain related to the ligand-binding motif of LDL-R. At that time, there were no other virus known to interact with the receptors of the family, and it was thought that the only ligands were apolipoproteins. Thus, despite failing to find other corresponding proteins in the GeneBank database, they referred to the protein as “the RSV(A) receptor” or as “pg800” (Bates *et al.*, 1993).

One year later, Franz Hofer identified a fragment of LDL-R and LRP1 as proteins binding to a minor-group human rhinovirus (HRV2) (Hofer *et al.*, 1994). Then, in 1998, it was determined that the fragment previously identified by Hofer *et al.* was in fact from VLDL-R (Marlovits *et al.*, 1998).

The following year, it was reported that HCV and the bovine viral diarrheal virus (BVDV), both from the *Flaviviridae* family, use LDL-R for their entry. In the case of HCV, using neutralising antibodies against apoE and apoB, it was further shown that the virus could interact with the receptor through the apolipoproteins. Since a total inhibition was never achieved in these neutralisation assays, the authors could not exclude a direct endocytosis of HCV by LDL-R (Agnello *et al.*, 1999). In 2016, a role of VLDL-R in HCV entry was also demonstrated (Ujino *et al.*, 2016).

HCV is a particular virus. Its particles are called lipo-viro-particles (André *et al.*, 2002). The viral particles are associated with triglycerides, cholesterol ester and apolipoproteins, similar to VLDL or LDL (Merz *et al.*, 2011; Nielsen *et al.*, 2006). Currently, the exact association between particles and lipoproteins is still unclear and two models have been proposed (Figure 17). On the one hand, the “one-particle” model represents the incorporation of the viral particle inside a lipoprotein. On the other hand, the “two-particles” model results from

the non-covalent link between E1/E2 viral glycoproteins and apolipoproteins at the surface of lipoproteins (Figure 17) (Cosset *et al.*, 2020).

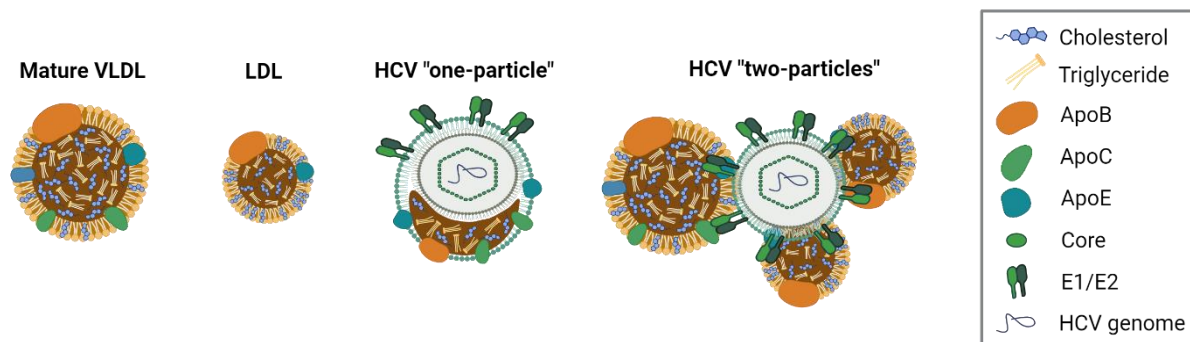


**Figure 17: Models of HCV association with lipoproteins.** Created with BioRender.com.

In 2008, the Japanese Encephalitis Virus (JEV), another flavivirus, was described to use to LDL-R, using neutralisation assays with antibodies and soluble LDL-R (Chien *et al.*, 2008). Later, Liu *et al.*, (2020) demonstrated that defensin, an antimicrobial peptide from mosquitoes is able to bind to the E protein of JEV and increase the virus binding to host cells. They in fact showed that defensin binds to LRP2 (megalin), and concluded that JEV uses LRP2 as an entry factor through the interaction with defensin (Liu *et al.*, 2020).

It is only in 2013 that LDL-R was identified as a receptor for VSV, that became the classic control to study the receptor. Previously, in 1993, it was observed that a soluble form of the LDL-R was secreted upon IFN treatment, and that this correlated with the inhibition of VSV infection (Fischer *et al.*, 1993). Twenty years later, the same team was able to link their previous discovery with the capacity of VSV to use LDL-R for entry. They identified the ligand-binding motif as the epitope for VSV binding. This motif, as described previously, is shared among the LDL receptors family and thus, VSV probably uses other LDL receptors in addition to LDL-R. This was demonstrated using fibroblasts that do not express the LDL-R, or later using haploid cells KO for LDL-R (Finkelshtein *et al.*, 2013; Nikolic *et al.*, 2018). In the later paper, in 2018, the interaction between VSV and LDL-R was further characterised. From the 7 repeated ligand-binding motifs (also known as cysteine-rich repeats, CR), the second and the third (CR2 and CR3) were found to bind the VSV glycoprotein (VSV-G).

Then, from 2021 to 2024, more than 15 viruses were described to use receptors from the LDL-R family (see Table 5) among which the Hepatitis B virus (HBV) (Li and Luo, 2021). In this

paper, the authors claimed that the interaction is similar to the one described for HCV and occurs through apoE. However, they did not show an interaction between apoE and the virus, but only an interaction between apoE and its receptor (Li and Luo, 2021). Nevertheless, prior to this publication, it was demonstrated that HBV particles are enriched in apoE and thus, we can hypothesise that the interaction with the LDL-R can be apoE-mediated (Qiao and Luo, 2019).

SARS-CoV-2 was also reported to depend on LDL-R for entry. Indeed, LDL-R was shown to increase the entry of lentiviral particles pseudotyped with SARS-CoV-2 spike protein (Uppal *et al.*, 2023). The same year, it was demonstrated that there is also an impact of LRP1 on the replication of the virus (Devignot *et al.*, 2023). The basis of the observation was not investigated, but in 2020 it was reported that the spike protein interacts with cholesterol and thus, the interaction could also happen through apoE (Qiao and Luo, 2019).

Most of the recent viruses identified as dependent on LDL receptors are from the *Alphaviruses* family (see Table 5). Indeed, several of them were shown to use LDL-R for their entry, but also LRP8 (apoER2) and VLDL-R (Adams *et al.*, 2024; Cao *et al.*, 2023; Clark *et al.*, 2022; Ma *et al.*, 2024; Zhai *et al.*, 2024). The interaction of those alphaviruses with their receptor seems to occur directly through their protein E2E1 and the CR4 and CR5 of LDL-R (Zhai *et al.*, 2024).

Finally, as stated in the “*Bunyaviricetes* entry” section, several bunyaviruses were recently shown to interact with LRP1 (see Table 5) (Devignot *et al.*, 2023; Ganaie *et al.*, 2021; Schwarz *et al.*, 2022). The interaction between these viruses and the receptor is described as direct since the glycoprotein of RVFV is used to compete with Oropouche virus (OROV) infections and since the authors used VSV pseudotyped with OROV glycoprotein (Schwarz *et al.*, 2022). More precisely, the viruses were shown to bind specifically to the cluster II and IV of ligand-binding domain repeats of LRP1 (Ganaie *et al.*, 2021; Schwarz *et al.*, 2022).

We can notice that the human hepatotropic viruses discussed above, such as HBV and HCV, were shown to bind to apolipoproteins, in contrast to other non-hepatotropic viruses. This may be explained by the fact that viruses take advantages of factors highly expressed in the liver. It can also be explained by oriented research on these highly expressed factors since the non-hepatotropic viruses were not assessed for a possible interaction with apolipoproteins. We can also notice that LRP1B is not listed as entry factors for viruses, even

if it shares the same ligand-binding motifs than LRP1. This can be explained either by the fact that LRP1B is less investigated than LRP1, or by the fact that viruses may require co-factors to allow their entry, and these co-factors may differ depending on the LDL receptor.

Receptor	Virus	Step	Type of interaction	Reference
LDLR	Subgroup A Rous Sarcoma Virus	Entry	Not shown	(Bates et al., 1993)
	Minor group HRV	Entry	Not shown	(Hofer et al., 1994)
	<b>HCV</b>	<b>Entry and replication</b>	<b>Indirect through apoE and apoB</b>	(Agnello et al., 1999)(Owen et al., 2009)
	BVDV	Entry	Not shown	
	JEV	Entry	Not shown	(Chien et al., 2008) (Huang et al., 2021)
	VSV	Entry and later stages	Direct with VSV-G	(Finkelshtein et al., 2013) (Nikolic et al., 2018) (Devignot et al., 2023)
	<b>HBV</b>	<b>Entry</b>	<b>Seems indirect through apoE</b>	(Li and Luo, 2021)
	SARS-CoV-2	Entry	Not shown	(Uppal et al., 2023)
	GETV	Entry	Direct with GETV-E2E1	(Zhai et al., 2024) (Ma et al., 2024)
	SFV	Entry	Direct with SFV-E2E1	
	RRV	Entry	Direct with RRV-E2E1	
	BEBV	Entry	Direct with BEBV-E2E1	
	EEEV	Entry	Direct	(Ma et al., 2024)
	WEEV	Entry	Direct	
CFSV	Later stages	Not shown	(Leveringhaus et al., 2024)	
LRP1	Minor group HRV	Entry	Not shown	(Hofer et al., 1994)
	RVFV	Entry	Direct	(Devignot et al., 2023) (Ganaie et al., 2021)
	OROV	Entry	Direct	(Schwarz et al., 2022)
	SFSV	Entry	Not shown	(Devignot et al., 2023)
	LACV	Entry	Not shown	
	SARS-CoV-2	Later stages	Not shown	
VLDLR	Minor group HRV	Not shown	Not shown	(Marlovits et al., 1998)
	<b>HCV</b>	<b>Entry</b>	<b>Indirect through apoE</b>	(Ujino et al., 2016)
	SFV	Entry	Direct	(Clark et al., 2022)(Cao et al., 2023)(Adams et al., 2024)
EEEV	Entry	Direct		
LRP8	SFV	Entry	Direct	
	SINV	Entry	Direct	
	EEEV	Entry	Direct	
LRP2	JEV	Entry	Indirect through defensin in mosquito cells	(Liu et al., 2020)

**Table 5: LDL receptors playing a role in viral entry.** Retroviridae in light grey, Picornaviridae in dark grey, Flaviviridae in green, Rhabdoviridae in orange, Hepadnaviridae in light blue, Coronaviridae in blue, Alphaviruses in yellow and Bunyaviricetes in pink. Viruses in bold highlight the hepatotropic viruses which binds to LDL-R through apolipoproteins. HRV: Human Rhinovirus; HCV: Hepatitis C virus; HBV: Hepatitis B virus; BVDV: Bovine viral diarrhea virus; JEV: Japanese encephalitis virus; VSV: Vesicular stomatitis virus; GETV: Getah virus; SFV: Semliki Forest virus; RRV: Ross River virus; BEBV: Bebaru virus; EEEV: Eastern equine encephalitis virus; WEEV: Western equine encephalitis virus; CFSV: Classical swine fever virus; RVFV: Rift Valley fever virus; OROV: Oropouche virus; SFSV: Sandfly fever Sicilian virus; LACV: La Crosse encephalitis virus; SINV: Sindbis virus.

## E. Tools to study CCHFV

As described above, the authentic CCHFV is classified as a BSL-3 to 4 virus in most countries, making its study more rare, expensive, and time-consuming. In order to boost the research required to find anti-viral drugs, vaccines, or simply to dissect its replication cycle, powerful tools have been developed.

### 1. Minigenome system

The minigenome system, depicted in Figure 18, is used to study viral transcription, replication, and encapsidation independently of viral entry. The minigenome is analogue to the viral RNA. It contains the 5' and 3' UTR of a viral segment, and in between, the CCHFV genome is replaced by a reporter gene (Bergeron *et al.*, 2010; Devignot *et al.*, 2015). The minigenome is cloned into a plasmid, most of the time under the control of a T7 promotor, thus requiring the transfection of an expression plasmid encoding the T7 RNA polymerase *trans*, or the use of cells stably expressing it. The expression of the reporter gene then relies on the viral replication machinery, the NP and L proteins, that is provided by transfection of expression plasmids (Bergeron *et al.*, 2010), or by superinfection in BSL-4 conditions with authentic CCHFV (Flick *et al.*, 2003). The minigenome RNA (mgRNA) is transcribed, encapsidated with NP and acts as a template for replication and transcription, resulting in the expression of the reporter signal. To study the replication alone, the L plasmid can be replaced with an L protein mutated at the D693, which loses its cap-snatching activity and is unable to transcribe mRNA (Devignot *et al.*, 2015). Since this system does not produce infectious particles, it can be studied in BSL-2 laboratories.

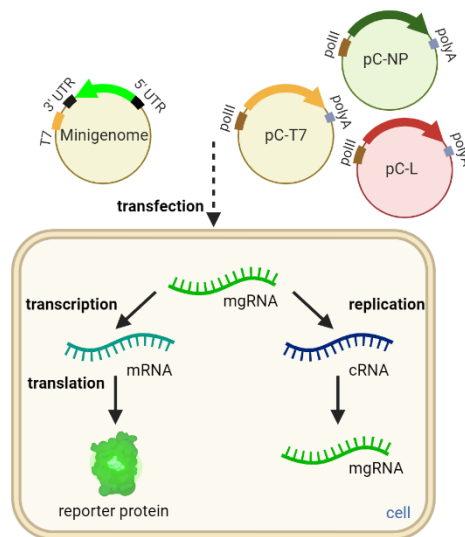


**Figure 18: CCHFV minigenome assay.** Cells are transfected with plasmids expressing the replication machinery (NP and L protein), as well as a minigenome encoding a reporter molecule whose open reading frame is flanked by 5' and 3' UTRs. Generation of the minigenome RNA (mgRNA) is achieved by transfection of the reporter minigenome plasmid under a T7 promoter as well as a T7 RNA polymerase helper plasmid (right). In the cell, mgRNA is replicated into complementary RNA (cRNA) or transcribed into messenger RNA (mRNA) that is translated into the reporter molecule. Created with BioRender.com.

## 2. Pseudotyped particles

Pseudotyped particles are chimeric virions which consist of a viral core from a parental virus and viral envelope proteins from another virus. Contrary to the minigenome system, this tool is used to study cellular tropism or entry steps. Most pp are based on specific parental viruses such as retroviruses (Murine Leukemia Virus, MLV; or HIV), or rhabdoviruses (VSV), and are modified to become defective for a complete replication cycle (Evans *et al.*, 2007; Ma *et al.*, 1999; Whitt, 2010). Generation of pp is more efficient when the glycoprotein of the virus of interest assembles at the same site as the parental virus. For VSV particles pseudotyped using CCHFV GPC, it is not the case. Indeed, VSV buds at the plasma membrane, while CCHFV buds at the Golgi (Bertolotti-Ciarlet *et al.*, 2005; Brown and Lyles, 2005). In order to target CCHFV GPC at the plasma membrane, a mutant was generated with the deletion of 53 amino acids at the Gc cytoplasmic tail, increasing its localisation at the plasma membrane (Suda *et al.*, 2016). In this paper, the gene for the VSV-G was deleted (VSVΔG) and replaced by a reporter gene such as the green fluorescent protein (GFP) or the NanoLuc luciferase (NLuc). To produce VSVpp CCHFV GPC, the authors transfected target

cells with a plasmid encoding for the Gc mutant, which was produced and targeted at the plasma membrane, and infected these cells with VSV $\Delta$ G. VSV virion progeny incorporated the CCHFV GP during the budding, and produced VSV $\Delta$ G\_GFP\_CCHFV GP, which genome lacked a gene encoding a glycoprotein, and hence, was not replicative. It is important to note that infection with VSV $\Delta$ G\_GFP\_CCHFV GP must be performed with an anti VSV-G antibody to ensure that there is no impact of residual VSV-G present on the particle.

To produce a replication-competent VSVpp\_CCHFV GPC, an ORF encoding a truncated GPC can be introduced into the VSV genome (Rodriguez *et al.*, 2019). This truncated GPC was obtained after several passages of VSV $\Delta$ Gpp\_CCHFV GPC and has 4 mutations in the Gc ORF and 2 in the preGn. This system has to be handled in a BSL-3 laboratory.

### 3. Transcription- and entry- competent virus-like particles

The previous systems have the disadvantage that the virion structures and machinery are not similar to CCHFV virions. In order to overcome this limitation, transcription- and entry-competent VLPs were developed (tecVLPs, represented in Figure 19). These particles, unlike the CCHFV GPC-pseudotyped particles derived from VSV, contain all CCHFV proteins, and a minigenome usually flanked by the L segment UTRs. The tecVLPs mimic authentic CCHFV virion morphology, entry, and primary transcription (Zivcec *et al.*, 2015). Nonetheless, they do not contain any authentic viral genome, and therefore are unable to express viral proteins upon entry. To produce VLPs, producer cells are transfected with plasmids encoding NP, GPC, L protein, T7 RNA polymerase, and a minigenome (as described previously), resulting in the encapsidation and incorporation of the mgRNA into the particles. Depending on the reporter gene, indicator cells that will further be infected, require being “pre-transfected” with the replication machinery: NP- and L- encoding plasmids. Indeed, a robust *Renilla* or GFP signal can be obtained only if the indicator cells strongly express NP and L protein (Devignot *et al.*, 2015), while NLuc signals can be obtained in the absence of pre-transfection (Zivcec *et al.*, 2015). Moreover, tecVLPs can also infect “amplifier cells” that have been pre-transfected with NP, L protein but also GPC prior to infection, and thus form new virions, only containing the encapsidated minigenome. This provides a view of the

assembly and egress steps, which is not possible in indicator cells since they do not express the structural proteins required for the virion production (GPC) (Devignot *et al.*, 2015).

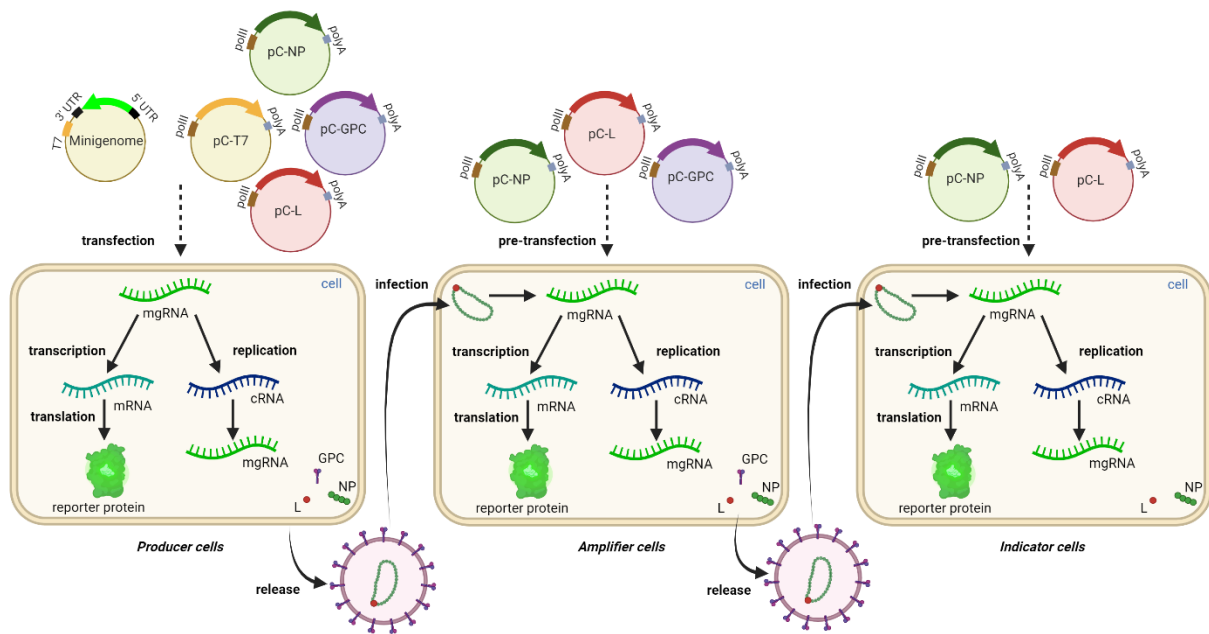


**Figure 19: CCHFV\_tecVLP assay.** Producer cells are transfected with plasmids encoding the replication machinery (NP and L protein), the glycoprotein precursor complex (GPC), a minigenome encoding a reporter molecule whose ORF is flanked by CCHFV 5' and 3' UTRs, and a T7 RNA polymerase. In the cell, the minigenome RNA (mgRNA) is replicated into complementary RNA (cRNA) or transcribed into messenger RNA (mRNA) which is translated into the reporter molecule. Moreover, assembly and budding of newly formed particles occur. TecVLPs are used to infect amplifier cells (that express NP, L protein and GPC) or indicator cells (that express NP and L protein, or that are left untransfected) depending on the reporter protein expressed. Created with BioRender.com.

#### 4. Viral replicon particles

The tecVLPs system has the disadvantage of requiring a step of pre-transfection, depending on the reporter gene, limiting the population of “detectable infected cells” to the one that is doubly transfected with NP and L plasmids. Moreover, the particles only incorporate one RNP, containing the mgRNA, possibly causing differences in the replication process compared to the authentic virus (with 3 segments). To get closer to the authentic virus, viral replicon particles were developed (represented in Figure 20). These particles do not contain a minigenome as previously, but the full-length S-segment and L-segment, allowing them to perform authentic entry, transcription, and replication. Moreover, since they do not encapsidate the M-segment, they do not produce the GPC necessary to form new virions (Scholte *et al.*, 2019; Spengler *et al.*, 2019). In order to produce VRPs, cells are transfected



with plasmids containing the full S- and L-segment, under the control of the T7 promoter, but also encoding the T7 RNA polymerase, the GPC without the UTRs, and with the helper plasmids encoding NP and L protein under a strong cellular RNA polymerase II promoter (Scholte *et al.*, 2019). To easily detect infected cells, VRPs expressing ZsGreen were developed by cloning the ZsGreen ORF into the S-segment plasmid, with a P2A cleavage site (Scholte *et al.*, 2019). Similar to tecVLPs, a step of “amplification” can be done by transfecting amplifier cells with the plasmid encoding GPC. This single-cycle infection allows this system to be manipulated in BSL-2 conditions.

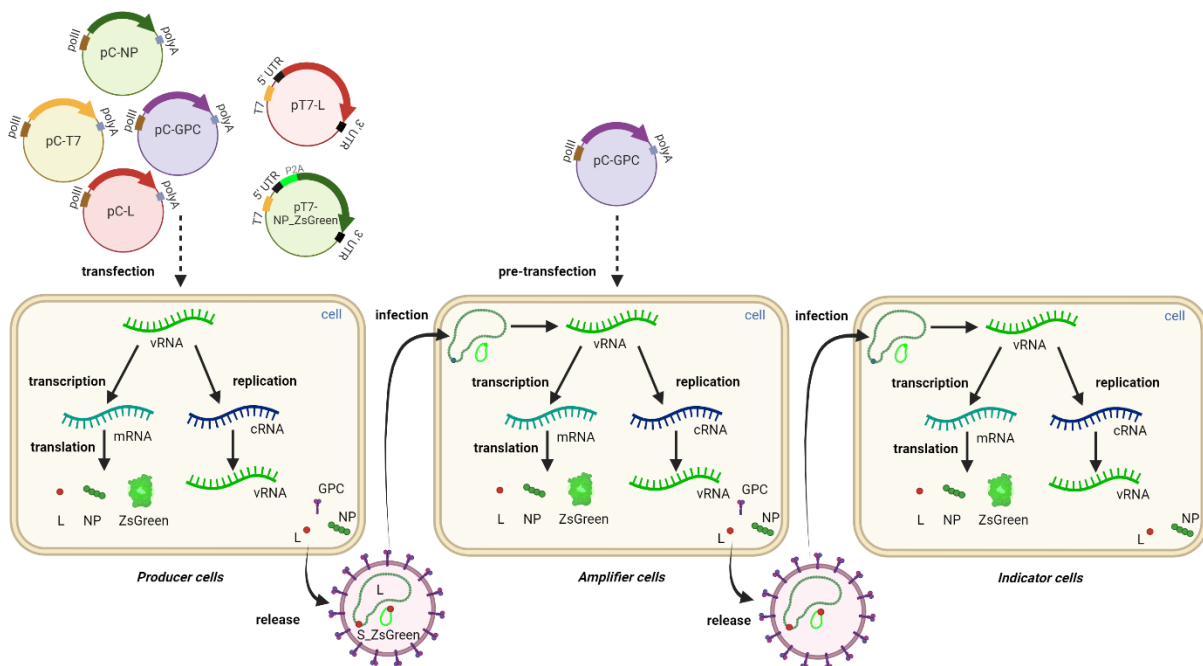


**Figure 20: CCHFV VRP assay.** Producer cells are transfected with plasmids encoding the replication machinery (NP and L protein), the glycoprotein precursor complex (GPC), the S\_ZsGreen and L segments and a T7 RNA polymerase. In the cell, viral RNAs (vRNAs) are replicated into complementary RNAs (cRNAs) or transcribed into messenger RNA (mRNA) that are translated into L and NP\_ZsGreen proteins, the latter being then cleaved into NP and ZsGreen. Moreover, assembly and budding of newly formed particles occur. VRPs are used to infect amplifier cells (that express GPC) or indicator cells (that are left untransfected). Created with BioRender.com.

## 5. Recombinant CCHFV

Finally, complete CCHFV can be produced by adding the M-segment to the VRP system, resulting in the production of recombinant CCHFV (rCCHFV). As described previously, to facilitate the monitoring of the infection, a ZsGreen can be added to the S-segment

(Bergeron *et al.*, 2015; Flick *et al.*, 2003; Welch *et al.*, 2017). Even if this tool must be manipulated under BSL-4 conditions, recombinant CCHFV allows the functional assessment of mutations on the complete virus genome.

## 6. Animal models

As previously stated, there is a lack of animal model to study CCHFV, slowing the development of vaccines and treatments. CCHFV does not cause disease in immunocompetent adult rodents (Shepherd *et al.*, 1989a; Zeller *et al.*, 1994). The only model available has long been neonatal mice or rats used since 1967 by Chumakov (Hoogstraal, 1979). This changed with the discovery that CCHFV infection was lethal in adult IFNAR<sup>-/-</sup> mice (Bereczky *et al.*, 2010; Zivcec *et al.*, 2013). Then, a model of immunocompetent mice treated with anti IFN-I receptor A (MAR1-5A3), and thus producing a transient IFN-I blockade, resulted in lethal CCHFV infection (Garrison *et al.*, 2017; Sheehan *et al.*, 2006). In 2017, a model of humanised mice was described (Spengler *et al.*, 2017). The authors used NOD-SCID-g (NSG)-SGM3 mice, which have inherited severe combined immune deficiency (SCID) combined to a defect in cytokine signalling and expressing human Stem cell factor, GM-CSF and IL-3 (SGM3). This genetic background renders the mice deficient for natural killer, B, and T cells, allowing them to be humanised, and the expression of the SGM3 transgenes supports the stable engraftment of myeloid lineages. After infection, the mice show endothelial damage, plasma leakage and several neurological symptoms as described in humans (Spengler *et al.*, 2017).

However, all these rodent models, well described in Garrison *et al.*, (2019), cannot be used to study the role of adaptive immunity in CCHFV infection. In 2021, a mouse-adapted variant of CCHFV (MA-CCHFV) was developed. A clinical isolate of the Hoti strain of CCHFV was inoculated into *Rag2*<sup>-/-</sup> mice (lacking adaptive immunity), and after serial passages, the authors observed a decrease in time of onset of severe disease. This MA-CCHFV was then inoculated into wild-type mice and was able to cause severe symptoms. After sequencing, it was demonstrated that MA-CCHFV was mutated twice in the S-segment, resulting in a coding change in NP but also in NSs. In addition, one mutation was identified in the M-segment, changing the protein sequence for NSm. Finally, two changes were observed in the

L protein. No further study has been conducted yet, but we can hypothesise that these mutations, mostly the one in NSs, can modulate the ability of MA-CCHFV to antagonise the mouse innate immune signalling (Hawman *et al.*, 2021).

Finally, the only non-rodent model known to date is a non-human primate (NHP) model: the cynomolgus macaque. Until 2018, studies using NHP (rhesus macaques and African green monkeys) infected with CCHFV did not show any clinical signs (Fagbami *et al.*, 1975). Then, it was published that cynomolgus macaques, infected with the Hoti or Afg09 strain of CCHFV, can recapitulate the severe clinical and pathological signs of a human CCHFV infection (Haddock *et al.*, 2018; Smith *et al.*, 2019). Interestingly, these results were not reproduced in Cross *et al.*, (2020) where the infected cynomolgus macaque developed only a mild clinical disease.

During my PhD, and in the following manuscript, I mainly used CCHFV\_tecVLPs.

## Chapter II. Objective of the work, and scientific contributions to other projects

As described in my introduction, CCHFV is a growing threat, without any vaccine or licenced treatment, listed in the Blueprint list of the WHO. Moreover, there is a dire need to implement knowledge about the molecular mechanisms involved in virus/host interactions. When my project started, there were no receptor or entry co-factor identified for CCHFV, with the exception of DC-SIGN and Nucleolin, but both lacking strong evidence. It is in this context that I aimed at **identifying and characterising cellular factors governing CCHFV entry into host cells**. I also contributed to several projects in the lab aiming to better understand the molecular properties of the virus, as described below.

### 1. CCHFV\_tecVLPs are protected by a secreted cellular factor.

During my PhD, I collaborated with Solène Denolly, a Post-Doctoral fellow in the Department of Infectious Diseases, Molecular Virology, Heidelberg University, Germany (Prof. Dr. Bartenschlager team) on a project related to HCV. This project highlighted the sensitivity of HCV to oxidation, and the mechanism used by the virus to prevent oxidation-mediated degradation by taking advantage of secreted factors. In this project, CCHFV, as well as several other hepatotropic viruses, were used to verify the stability of their infectious particles at body temperature, in the presence or absence of secreted cellular factors. My contribution, presented in the following “Results” section (Chapter III.A.2) allowed to demonstrate that CCHFV infectious particles are more stable if cellular proteins are present in the medium, and thus, that there are secreted factors that may protect the particles. The complete version of the published paper is presented in Annexe.

**Low-density hepatitis C virus infectious particles are protected from oxidation by secreted cellular proteins.** 2023. mBio 14: e01549-23. <https://doi.org/10.1128/mbio.01549-23>

Christelle Granier\*, Johan Toesca\*, Chloé Mialon\*, **Maureen Ritter**, Natalia Freitas, Bertrand Boson, Eve-Isabelle Pécheur, François-Loïc Cosset<sup>#</sup> and Solène Denolly<sup>#</sup>

## 2. Trafficking motifs in CCHFV Gn and Gc cytoplasmic tails govern CCHFV assembly.

The second project that I contributed to aimed to study the trafficking motifs required for the maturation of the glycoproteins of CCHFV, and to identify cellular factors involved in its assembly. It was supervised by Dr. Natalia Freitas, a Post-Doctoral fellow who later left the team, and then by Dr. Anupriya Gautam and Bertrand Boson. For this paper, the cytoplasmic tails of Gn and Gc were mutated at putative endocytic motifs. I provided information concerning the impact of the mutations on the formation of infectious particles, presented in the following Results section (Chapter III.B.2). We also assessed the impact of two cellular factors, PACS-1, and PACS-2, on CCHFV assembly, and I more specifically characterised the role of PACS-1. The complete version of the published paper is presented in Annexe.

**The PACS-2 protein and trafficking motifs in CCHFV Gn and Gc cytoplasmic tails govern CCHFV assembly.** 2024. *Emerging Microbes & Infections*  
<https://doi.org/10.1080/22221751.2024.2348508>

Anupriya Gautam, Alexandre Lalande\*, **Maureen Ritter\***, Natalia Freitas\*, Solène Lerolle, Lola Canus, Fouzia Amirache, Vincent Lotteau, Vincent Legros, François-Loïc Cosset, Cyrille Mathieu, and Bertrand Boson

## 3. Identification and characterisation of LDL-R as an entry factor for CCHFV

In parallel, I worked on the main aim of my PhD, **the identification and characterisation of host factors governing CCHFV entry**. Based on the Xiao *et al.*, (2011) report, I first attempted to confirm whether NCL was indeed an entry factor for CCHFV, using tecVLPs as an experimental system. I chose not to test DC-SIGN since it is not expressed in the susceptible Huh-7.5 cells. In the following Results section (Chapter III.C.2), I will present my data obtained for NCL, and how it led to the identification and characterisation of LDL-R and apolipoproteins as entry factors for CCHFV. This project started with experiments that I performed under the supervision of Dr. François-Loïc Cosset and Dr. Natalia Freitas. When Dr. Natalia Freitas left the team, Dr. Solène Denolly, still at Heidelberg University at the time, joined the supervision of the project, allowing me to benefit from her expertise in viral

interactions with apolipoproteins. It then turned into a massive collective effort. In the team, Dr. Anupriya Gautam, Thomas Vallet, Dr. Li Zhong, Bertrand Boson, Apoorv Gandhi, Sergueï Bodoirat and Dr. Vincent Legros also dedicated their time to this project. We were also able to collaborate, among others, with Dr. Cyrille Mathieu, Lola Canus and Alexandre Lalande, who performed the experiments in the BSL-4 using the authentic virus. Finally, it would not have been possible without the collaborators Prof. Philippe Roingard and Julien Burland-Gaillard for the electron microscopy, Dr. John N. Barr for the HAZV system, Dr. Vincent Lotteau for the BSL-4 experiments, and Chloé Journo for my PhD supervision. In the following Results section (Chapter III.C.2), I will present in detail the data that I specifically obtained or helped to obtain, while the complete version of the published paper is presented in Annexe.

**The low-density lipoprotein receptor and apolipoprotein E associated with CCHFV particles mediate CCHFV entry into cells.** 2024. Nature Communications **15**, 4542.

<https://doi.org/10.1038/s41467-024-48989-5>

**Maureen Ritter**, Lola Canus\*, Anupriya Gautam\*, Thomas Vallet\*, Li Zhong, Alexandre Lalande, Bertrand Boson, Apoorv Gandhi, Sergueï Bodoirat, Julien Burlaud Gaillard, Natalia Freitas, Philippe Roingard, John Barr, Vincent Lotteau, Vincent Legros, Cyrille Mathieu, François-Loïc Cosset and Solene Denolly

Objective of the work, and scientific contributions to other projects

## Chapter III. Results

### A. CCHFV\_tecVLPs are protected by a secreted cellular factor.

#### 1. Context

CCHFV transmission from cell to cell or from host to host can be studied not only by looking for molecular factors governing viral entry, but also by understanding the routes and parameters of viral transmission. To this end, the viral stability on surfaces or in body fluids can be assessed. As a virus that replicates in the liver, CCHFV particles are exposed to a complex environment after their secretion, such as the acidic bile or the lipoproteins. In the report Granier *et al.*, (2023), I addressed the properties of CCHFV particles stability.

#### 2. Results

To evaluate the stability of CCHFV particles, CCHFV NLuc\_tecVLPs were produced, as described in Figure 19, in Huh-7.5 cells cultured in serum-free medium, that is, in Huh-7.5 grown previously for 24h in OptiMEM without foetal bovine serum (FBS). The hepatocyte Huh-7.5 cells were used since the liver is one of the main infected organs upon CCHFV infection. Moreover, this cell line is defective in the innate immune signalling because of the expression of an inactive form of RIG-I, a cytosolic pattern recognition receptor inducing IFN-I responses (Sumpter *et al.*, 2005). Since CCHFV is sensitive to IFN, this defect allows a better viral production and a higher permissiveness.

Briefly, Huh-7.5 were transfected with plasmids harbouring the NLuc ORF flanked by the L 5' and 3' UTRs and under the control of a T7 promotor. The cells were also transfected with plasmids encoding the T7 polymerase, and ORF of the L, NP, and GPC proteins of CCHFV, to produce CCHFV particles containing only the RNA of the NLuc minigenome (Figure 19). Three days post-transfection, the supernatant was harvested and filtered through a 0.45µm filter. The infectivity of the particles produced was assessed after a 6-hour incubation period at 37°C (body temperature) following their harvest and compared to supernatants stored at 4°C immediately after harvest. The infection assay was performed on Huh-7.5 grown in serum-free medium and pre-transfected with NP and L expression plasmids 24h before



infection. Three days post-infection, indicator cells were harvested and lysed using a passive lysing buffer, and finally, the NLuc luminescence signal from the infected cells was assessed using the Nano-Glo® Luciferase Assay System (Promega).

I found that CCHFV\_tecVLPs infectivity decreased slightly, around 5 folds, when incubated at 37°C compared to 4°C (Figure 21), meaning that CCHFV\_tecVLPs are not fully stable at body temperature.

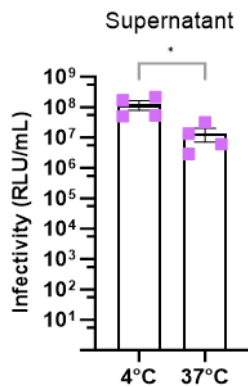


**Figure 21: CCHFV particles are slightly sensitive to a 37°C incubation period.** NLuc\_tecVLPs were either left at 4°C before infection or incubated for 6 h at 37°C before infection of Huh-7.5 cells pre-transfected with plasmids encoding NP and L. The results are represented as means ± SEM. Each dot in the graph corresponds to the value of an individual experiment. N=4. Parametric unpaired t-test.

Next, the stability of these extracellular particles was compared with their intracellular counterparts (Figure 22). Intracellular particles are particles that have been assembled in the cells but have not been released yet. Intracellular particles were retrieved after 3 cycles of freeze-thawing of the producer cells and treated as previously described for particles from the supernatant. Interestingly, after 6 hours at 37°C, intracellular CCHFV\_tecVLPs remained stable. This suggests that intracellular CCHFV\_tecVLPs can be protected from the 37°C treatment, possibly by a cellular factor.

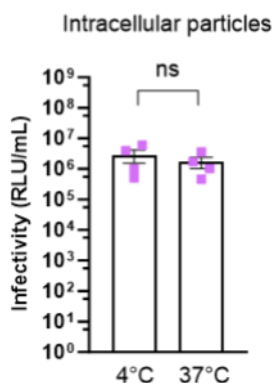


**Figure 22: Intracellular particles are stable at 37°C.** CCHFV NLuc\_tecVLPs intracellular particles were diluted in serum-free medium and treated as in Figure 19. The results are represented as means ± SEM. Each dot in the graph corresponds to the value of an individual experiment. N=4. Parametric unpaired t-test.

Since intracellular particles and particles in the supernatant are surrounded by cellular factors, secreted or not, the next step was to assess the stability of “purified extracellular particles”. For this purpose, extracellular particles and medium/cellular components were separated by an ultracentrifugation step with a 20% sucrose cushion. Here, I observed a strong decreasing trend (more than 3 log) in the infectivity of purified particles incubated at 37°C, compared to the purified particles kept at 4°C (Figure 23, white bars). This demonstrates that secreted particles without cellular factors are highly sensitive to temperature. Moreover, the difference of stability between supernatant and purified particles can suggest that some secreted cellular factors could stabilise extracellular tecVLPs.

Thus, to investigate the effect of potential stabilising factors secreted by virus-producer cells, purified extracellular particles were resuspended in a “Mock medium”. This medium consists of a supernatant of naïve Huh-7.5 cells incubated for 72 h in a serum-free medium. Interestingly, I found that after incubation with the mock medium, the infectivity increases of 2 log, and thus it tends to partially protect purified extracellular from temperature-dependent loss of infectivity (Figure 23, pink bars).

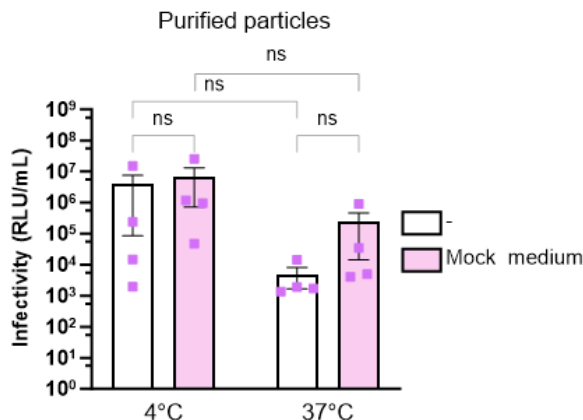


**Figure 23: Purified CCHFV\_tecVLPs are protected from temperature-sensitive degradation by secreted factors.** CCHFV\_tecVLPs were purified by ultracentrifugation. Purified extracellular particles were diluted in serum free medium (white bars) or in mock medium (pink bars) and treated as in Figure 19. The results are represented as means  $\pm$  SEM. Each dot in the graph corresponds to the value of an individual experiment. N=4. Two-way ANOVA test with Sidak's multiple comparisons.

Altogether, these results showed that CCHFV\_tecVLPs are characterised by their high instability at 37°C, which can be overcome by cellular secreted factors.

### 3. Conclusion

In a previous report about the tecVLPs, it was shown that the particles were almost not infectious after 3 days at 4°C (Devignot *et al.*, 2015), highlighting a poor stability of the

system. Thus, the slight reduction in infectivity observed in the supernatant incubated at 37°C vs 4°C is not surprising. Interestingly, in purified particles, this loss in infectivity is stronger. These observations were not the same for all the viruses tested in the paper. Indeed, HCV was highly unstable, even its intracellular particles. Using HCV, it was demonstrated that several factors produced by hepatocytes, such as human serum albumin, alpha-1-antitrypsin and iron-free transferrin, can protect the particles from a loss of infectivity following an incubation at 37°C.

## B. Trafficking motifs in CCHFV Gn and Gc cytoplasmic tails govern CCHFV assembly.

### 1. Context

Capitalising on the experience I gained working on the HCV stability project, and following the report about CCHFV assembly previously published in the team (Freitas *et al.*, 2020), I took part in a follow-up project that aimed at studying the role of trafficking motifs in Gn and Gc cytoplasmic tails. As described in the Introduction section, CCHFV glycoproteins need to traffic through the secretory pathway for their maturation. Thus, viral proteins need to interact with several cellular factors. Different types of trafficking motifs are typically contained in the cytoplasmic tails (CT) of viral surface glycoproteins (de Zarate *et al.*, 2004). For CCHFV, the Gc glycoprotein contains an ectodomain of 481 residues (Mishra *et al.*, 2022) that is followed by a single *trans*-membrane domain (TMD) and by a 63 residue-long cytoplasmic domain (CD) of unknown function (Guardado-Calvo and Rey, 2021). On the other hand, the Gn glycoprotein contains an ectodomain of 176 residues that is followed by two TMDs with, in between, a particularly long CT of 94 residues (Altamura *et al.*, 2007; Haferkamp *et al.*, 2005; Vincent *et al.*, 2003). In this paper, we aimed at understanding how CCHFV GPs make use of host factors and pathways to reach the site of assembly and promote envelopment of its viral particles. In order to investigate the role of putative membrane trafficking motifs, we used mutagenesis and studied how it could impact envelopment and production of infectious viral particles.

## 2. Results

### **Gc cytoplasmic determinants are essential for the formation of infectious particles.**

We identified several putative membrane trafficking motifs in the CT of CCHFV Gc glycoprotein (Figure 24a): two tyrosine-based motifs (Y1 and Y2), an acidic cluster motif (AC), a dileucine motif (LL), and an ER retrieval motif (ERR). These potential determinants were mutated (Figure 24b). We evaluated the role of these putative trafficking motifs on virion assembly, GP incorporation, and infectivity in Huh-7.5 hepatoma cells. I examined the ability of the GPC mutants generated in the identified Gc CT motifs (Figure 24b) to support the formation and release of intracellular and extracellular infectious CCHFV\_tecVLPs (Figure 24c). Comparing intracellular and extracellular infectivity allows the distinction between assembly/egress and infectious capacity. Indeed, if a mutant fails to produce infectious particles in the supernatant, this could mean either that particles are less infectious, or that particles were less produced/assembled. This last hypothesis is verified if there is also a defect in the intracellular infectivity.

For this purpose, Huh-7.5 cells grown in media containing FBS were transfected with the different plasmids required to produce GFP\_tecVLPs, including the wild-type (WT) GPC plasmid, a mutated GPC, or no GPC as control (Figure 24b). After 72h, supernatant was harvested and filtered through a 0.45 $\mu$ m filter. In parallel, intracellular particles were harvested after 3 cycles of freeze-thawing of cells. The infectivity of both types of particles was quantified after infection of Huh-7.5 cells pre-transfected with NP- and L-expressing plasmids. Indicator cells were harvested 24h post-infection and the GFP signal was analysed by flow cytometry (Figure 24c). The “no GPC condition” represents the background. It can be noticed that one replicate causes the mean background to be around 1,1e<sup>2</sup> IU/mL for the extracellular particles and 3 IU/mL/10<sup>6</sup> cells for intracellular particles.

When comparing the titers obtained with mutant tecVLPs, I found that, while the Y1 mutant allowed the formation and release of infectious tecVLPs at levels identical to WT tecVLPs, the other CT mutants yielded 5-fold to 1 log lower (AC mutant), or hardly detectable (Y2, LL, ERR mutants), infectivity, for both intracellular and extracellular tecVLPs (Figure 24c).

Collectively, these results indicate that several Gc CT determinants play important roles in the assembly and release of infectious tecVLPs.

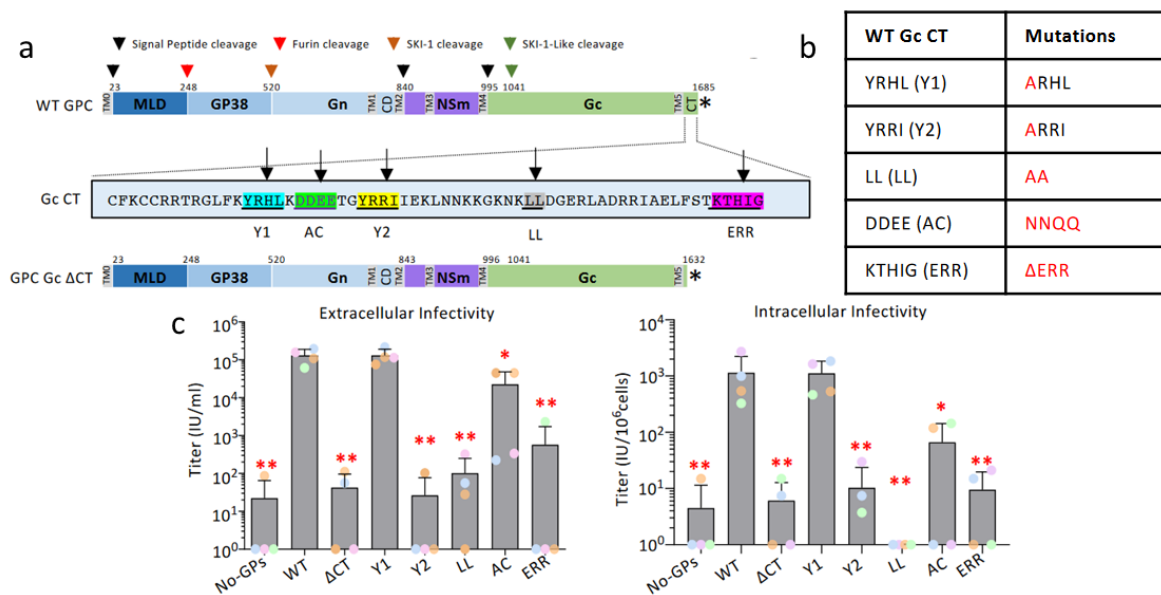


**Figure 24: Infectivity of CCHFV Gc cytoplasmic tail mutants.** (a) Schematic representation of the GPC polyprotein encoded by CCHFV WT-M cDNA (WT GPC) and mutant GPC harbouring deletion of Gc cytoplasmic tail (GPC Gc ΔCT). The stars indicate the position of the stop codon. The N-terminal signal peptide (TMD0) and putative transmembrane domains (TM1 to TM5) are shown as grey boxes, signal peptidase cleavage sites are indicated by black arrows and other host protein convertase cleavage sites are indicated by red, orange, and green arrows. The bottom part shows the CT sequence of Gc. Several trafficking motifs were identified, underlined, and boxed in different colours: two tyrosine-based motifs, Y1 and Y2 (blue and yellow); di-leucine motif, LL (grey); acidic cluster, AC, (green); endoplasmic reticulum retrieval domain, ERR (pink). Deletion of the putative trafficking motifs in the cytoplasmic tail of Gc is indicated as ΔCT. (b) The mutations introduced in the above Gc motifs are shown in the Table. (c) Titers of intracellular and extracellular CCHFV\_tecVLPs bearing mutant Gc CT proteins. At 72h post-transfection, clarified supernatants and cell associated tecVLPs were used to infect Huh-7.5 cells pre-transfected with L and NP expression vectors, and titers were determined by flow cytometry analysis at 24h post-infection. The results are represented as means ± SEM. Each dot in the graphs corresponds to the value of an individual experiment. N=4. Parametric unpaired t-test.

### Mutations in Gn cytosolic determinants impact the formation of CCHFV infectious particles.

We identified several putative membrane trafficking motifs in the CD of CCHFV Gn glycoprotein (Figure 25a). Similar to Gc CT, we highlighted two tyrosine-based motifs (Y1 and Y2), an acidic cluster motif (AC) and a di-leucine motif (LL). These potential determinants were mutated in the context of the GPC expression vector to raise mutant Gn proteins upon CCHFV\_tecVLP production (Figure 25b). Using the same assays as previously described for Gc mutants, I determined the capacity of the Gn mutants to support the formation and release of extracellular and intracellular infectious CCHFV\_tecVLPs (Figure 25c).

I found that while the mutation of the Y1 motif allowed the formation and release of infectious tecVLPs at levels identical to WT tecVLPs, the other CD mutants (Y2, LL, and AC mutants) yielded strongly reduced or no infectivity for both intracellular and extracellular tecVLPs (Figure 25c). These results indicated that the latter determinants play essential roles in GP incorporation and release of infectious virions.

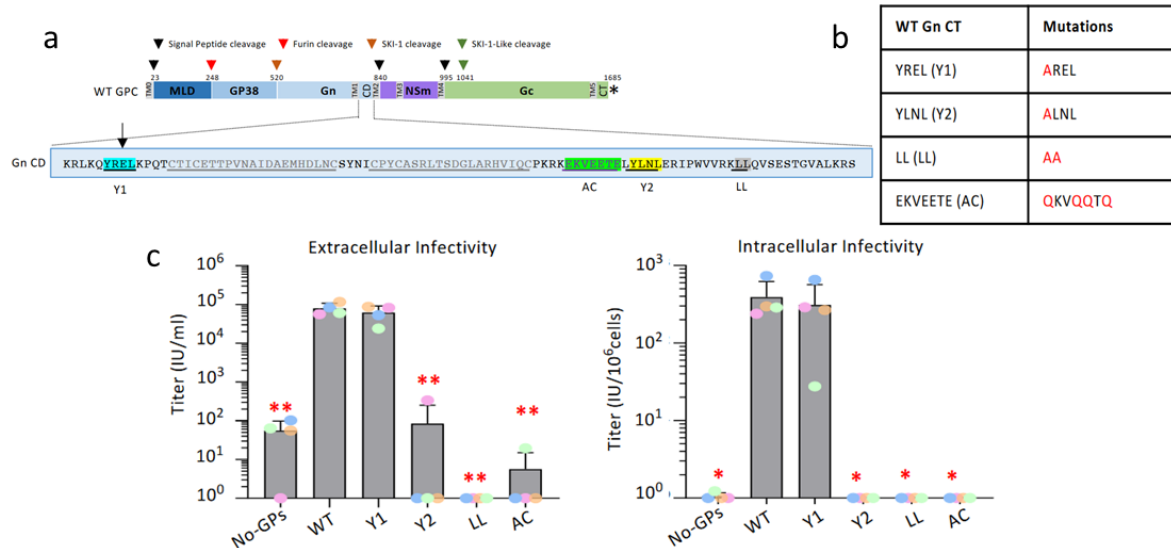


**Figure 25: Infectivity and viral incorporation of CCHFV Gn cytoplasmic tail mutants.** (a) Schematic representation of the GPC polyprotein encoded by CCHFV WT-M (WT GPC). The star indicates the position of the stop codon. The N-terminal signal peptide (TM0) and putative transmembrane domains (TM1 to TM5) are shown as grey boxes, signal peptidase cleavage sites are indicated by black arrows and other host protein convertase cleavage sites are indicated by red, orange and green arrows. The bottom part shows the CD of Gn. Several trafficking motifs were identified, underlined, and boxed in different colours: two tyrosine-based motifs, Y1 and Y2 (blue and yellow); di-leucine motif, LL (grey); acidic cluster, AC (green). (b) The mutations introduced in the above Gn motifs are shown in the Table. (c) Titers of intracellular and extracellular CCHFV tecVLPs bearing mutant Gn CD proteins. At 72h post-transfection, clarified supernatants and cell-associated tecVLPs were used to infect Huh-7.5 cells pre-transfected with L and NP expression vectors, and titers were determined by flow cytometry analysis at 24h post-infection. The results are represented as means  $\pm$  SEM. Each dot in the graphs corresponds to the value of an individual experiment. N=4. Parametric unpaired t-test.

### PACS-1 adaptor is not a critical factor for production and secretion of CHFV particles.

Several Golgi-resident transmembrane proteins have been shown to use AP-1-mediated retrograde transport from endosomes to TGN, following the binding of the cellular adaptor PACS-1 to their acidic cluster. Since our results revealed that the AC motif in Gc, but even more in Gn, is important to promote CCHFV GP intracellular trafficking and/or incorporation on viral particles (Figure 24c and Figure 25c), I investigated whether PACS-1 down-regulation could impair CCHFV particles assembly. We downregulated PACS-1 through expression of a short hairpin RNA (ShPACS-1) in producer cells. While we achieved a knock down efficiency of PACS-1 of up to 80% in Huh7.5 cells (Figure 26a), this did not influence the production of

infectious viral particles (Figure 26b). Hence, I concluded that PACS-1 is not a crucial host factor for the transportation of CCHFV GPs to the assembly site.

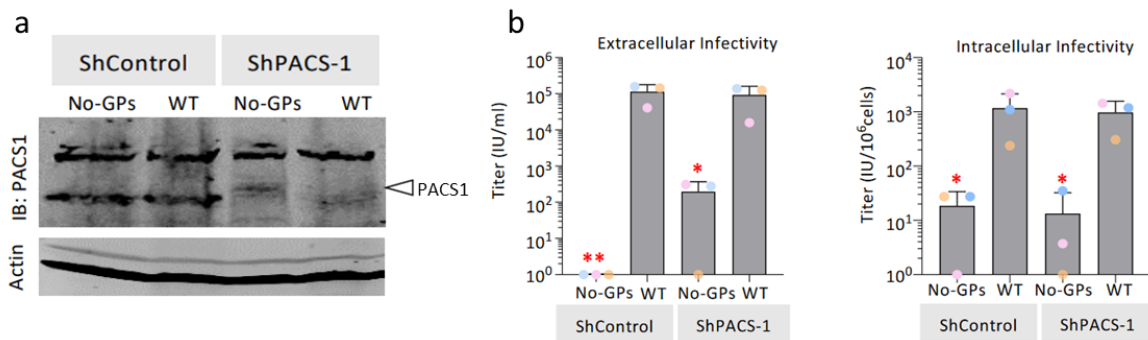


**Figure 26: Production of infectious CCHFV particles from PACS-1 knockdown cells.** Downregulation of PACS-1 was achieved in Huh-7.5 cells via lentiviral vectors expressing PACS-1 (ShPACS-1), or control shRNA (ShControl). The cells were then used to produce CCHFV\_tecVLPs harbouring WT GPC or no GPC (No-GPs). (a) Representative Western blot analysis. (b) Infectivity titers of CCHFV\_tecVLPs produced in the presence vs. in the absence of PACS-1 shRNA. At 72h post-transfection, clarified supernatants and intracellular tecVLPs were used to infect Huh-7.5 cells pre-transfected with L and NP expression vectors, and titers were determined by flow cytometry analysis at 24h post-infection. The results are represented as means  $\pm$  SEM. Each dot in the graphs corresponds to the value of an individual experiment. N=3.

### 3. Conclusion

In this study, I confirmed that the cytoplasmic domains of CCHFV GPs contain trafficking motifs important for assembly and secretion of infectious particles, since their mutation affected the infectivity of extracellular and intracellular particles. I also showed that PACS-1 is not a critical factor for the production of infectious CCHFV\_tecVLPs. In the paper, these motifs were further characterised for their role in the traffic of CCHFV GPs and assembly, by biochemical and intracellular imaging analyses. We highlighted that CCHFV GPs are targeted to the plasma membrane before returning the Golgi to reach the assembly site. This retrograde trafficking could be essential for the maturation of the GPs. More precisely, the Gc Y1 motifs allow the retrograde transport from the plasma membrane to the early endosomes, then to the late endosomes, and the Gc and Gn Y2 target the GPs to the TGN. Finally, the Gc ER retrieval motif and the Gn acidic cluster motif redirect them to the *cis*-Golgi network.

This transport seems to be completed by PACS-2 protein. PACS-2 binds acidic cluster motifs present on the GPs, and probably connects them to COPI along the retrograde pathway to reach the assembly site.

## C. LDL-R and apoE associated with CCHFV particles mediate the virus entry into human cells.

### 1. Context

My contribution to the previous reports allowed me to gain a better insight into CCHFV assembly and its interaction with cellular factors. However, my main project focused on the identification of specific cellular factors, those implicated in the viral entry. As described in the Introduction section, the cellular receptors and co-factors involved in CCHFV entry into host cells remained poorly identified at the start of my PhD. Only the human C-type lectin DC-SIGN and the NCL had been proposed to be involved in CCHFV entry, but as discussed earlier, they might not be sufficient for CCHFV entry (Suda *et al.*, 2016; Xiao *et al.*, 2011), and no further study had been conducted since their identification as candidate factors. I therefore started by assessing the involvement of NCL in CCHFV entry using our experimental systems.

### 2. Results

**Nucleolin is not a critical factor for CCHFV infectivity, but the low-density-lipoprotein receptor is.**

I decided to analyse the effect of blocking the NCL at the surface of Huh-7.5 cells by using an anti-NCL antibody added before infection with CCHFV\_tecVLPs harbouring a NanoLuc luciferase reporter gene (NLuc\_tecVLP). As a negative control, I used vesicular stomatitis virus glycoprotein pseudoparticles (VSVpp), which consist in retroviral vector particles pseudotyped with VSV-G, and which are independent on NCL for entry into cells, but instead depend on LDL-R (Amirache *et al.*, 2014; Finkelshtein *et al.*, 2013). Thus, I also used an anti-LDL-R antibody to block the VSVpp entry, as a control. As expected, anti-NCL did not block VSVpp infection, but anti-LDL-R did, with up to a 50% inhibition (Figure 27). The decrease of 50% observed for VSVpp can be explained by its ability to use other receptors from the LDL-R family.



Surprisingly, the anti-NCL antibody only blocked CCHFV\_tecVLPs infection up to 35% with 4 $\mu$ g/mL, when the anti-LDL-R antibody allowed a stark decrease of 80% (Figure 27). These results suggest that NCL may indeed play a minor role in CCHFV entry, but mainly that LDL-R is a key factor in CCHFV infection.

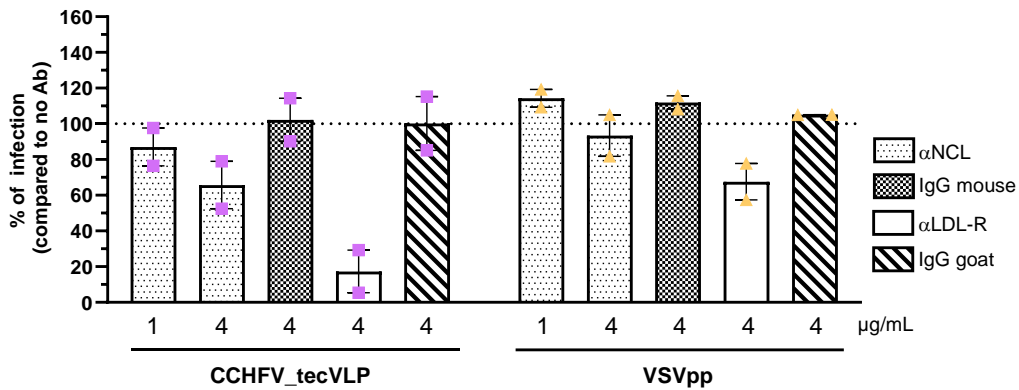


**Figure 27: NCL is not an essential factor for CCHFV infection contrary to LDL-R.** Huh-7.5 cells were incubated with different concentrations of anti-NCL antibody (dot bars), anti-LDL-R antibody (open bar) or control isotype (IgG mouse in grid bar; IgG goat in dashed bar) for 1h at 37°C before infection with CCHFV NLuc\_tecVLP. The media was replaced 3h post-infection (p.i.) and the cells were harvested at 48h p.i. to determine the levels of infection by measurement of NLuc level. The results are represented as means  $\pm$  SEM. Each dot in the graph corresponds to the value of an individual experiment. N=2.

Following this serendipitous observation, I decided to further study LDL-R in CCHFV infection. I repeated the previous assay but this time by only blocking the LDL-R in a dose response manner and using tecVLPs harbouring a GFP reporter gene (GFP\_tecVLP), for a more precise quantification of the infection level. For this experiment, VSVpp were used as a positive control. As a negative control, I used retroviral vector particles pseudotyped with the Env glycoprotein from amphotropic Murine Leukemia Virus (MLVpp). Amphotropic MLV entry depends on interaction with the PiT-2, a type III sodium-dependent phosphate transporter (Lavillette *et al.*, 2002) and thus, is independent of LDL-R. I also tested the dependency to LDL-R of HAZV, another member of the genus *Orthonavivirus*, using a GFP-expressing recombinant virus (Fuller *et al.*, 2020) produced in Huh-7.5 cells. In agreement with the previous results, I found that LDL-R blocking inhibited infection of both CCHFV\_tecVLP and VSVGpp particles in an anti-LDL-R antibody dose-dependent manner (inhibition up to 80% and 60% respectively) but did not affect MLVpp infection (Figure 28a). Interestingly, the blocking of LDL-R at the surface of Huh-7.5 cells did not impair HAZV infection as assessed by flow cytometry (Figure 28a), suggesting that LDL-R is not a *pan-Orthonavivirus* entry factor.

Then, I sought to confirm this result using authentic CCHFV of the Ibar10200 strain (WT CCHFV virus) that our collaborators produced in Huh-7.5 cells in a BSL-4 laboratory. For this experiment, I prepared the Huh-7.5 cells and added the antibody before our collaborators infected them in the BSL-4 facility. Upon infection and the subsequent assessment of the levels of infection at 24h post-infection (p.i.), *via* quantification of viral RNAs in infected cell lysates by Anupriya Gautam, we confirmed that blocking LDL-R could dose-dependently inhibit authentic CCHFV infection. The level of inhibition, around 75%, is similar to the one observed using tecVLPs (Figure 28b).

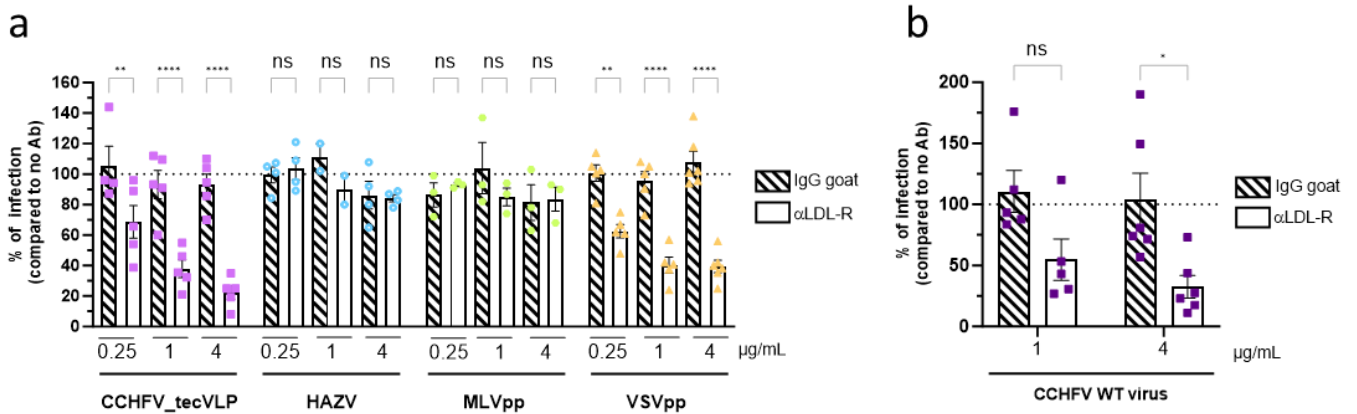


**Figure 28: LDL-R is a cofactor of CCHFV infectivity.** (a) Huh-7.5 cells pre-transfected with NP and L expression plasmids were incubated with different concentration of an anti-LDL-R antibody (open bars) or control isotype (IgG goat, dashed bars) for 1h at 37°C before infection with CCHFV GFP\_tecVLP (pink), MLVpp (green), and VSVpp (yellow) or infection with HAZV (blue). The media was replaced 3h p.i. and the cells were harvested at 16h p.i. for HAZV or 48h p.i. for the other viral particles to determine the levels of infection by flow cytometry. The results are represented as means ± SEM. Each dot in the graphs corresponds to the value of an individual experiment. N=2-5. Two-way ANOVA test with Sidak’s multiple comparisons. (b) Same experiment using WT CCHFV. Media was removed 1h post-infection and cells were lysed at 24h p.i. for determination of the levels of infection by RT-qPCR of viral RNA in cell lysates. The results are represented as means ± SEM. Each dot in the graphs corresponds to the value of an individual experiment. N=4-5. Mann-Whitney test.

Next, I aimed at confirming the LDL-R-dependent CCHFV entry in primary human hepatocytes (PHH), which express LDL-R at their surface (Figure 29).

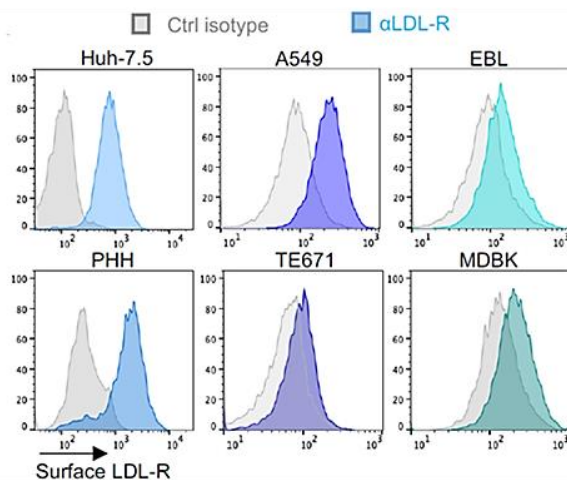


**Figure 29: Expression of LDL-R at the surface of Huh-7.5, A549, TE-671, EBL, MDBK and PHH cells assessed by flow cytometry.** Different cell types were stained with an anti-LDL-R (αLDL-R) or a goat IgG (ctrl isotype) followed by an anti-goat-PE and analysed by flow cytometry. This chart is representative of 3-4 independent experiments.

To do so, I started by confirming that PHH can be infected by NLuc\_tecVLPs (Figure 30a) although I observed that they are less permissive than the Huh-7.5 cells. The NLuc minigenome was used in this experiment in order to not be dependent on the transfection efficiency, which might be low in this system, and required for the NP and L pre-transfection.

Then, I assessed the PHH sensitivity to the LDL-R blocking with using 4 $\mu$ g/mL of anti-LDL-R. I found that infection of PHH was sensitive to LDL-R blocking at a similar level than the Huh-7.5 (up to 80% inhibition) (Figure 31a)

I also tested the involvement of LDL-R for CCHFV infection in cells from different tissues and species. First, I tested other human cells than Huh-7.5 hepatoma cells, either A549 lung epithelial cells or TE-671 rhabdomyosarcoma cells, which express the receptor at their surface (Figure 29). We can notice that the TE-671 cells have a low but detectable level of LDL-R expression at their cell surface. Then, I assessed if these cells can be infected with NLuc\_tecVLPs (Figure 30b). Interestingly, the level of LDL-R at the cell surface does not correlate with the RLU signal. Indeed, TE-671 with a low expression of the receptor provide a luminescence signal equivalent to the Huh-7.5 and A549 cells that highly express LDL-R. This can be caused by a difference in replication/translation efficiency, since the RLU signal is dependent not only on the entry, but also reflects the replication and translation level of the NLuc minigenome.

Finally, by LDL-R blocking assay, I found that infection of both A549 and TE-671 cells, was sensitive to LDL-R blocking (around 80% and 90% inhibition respectively) (Figure 31b).

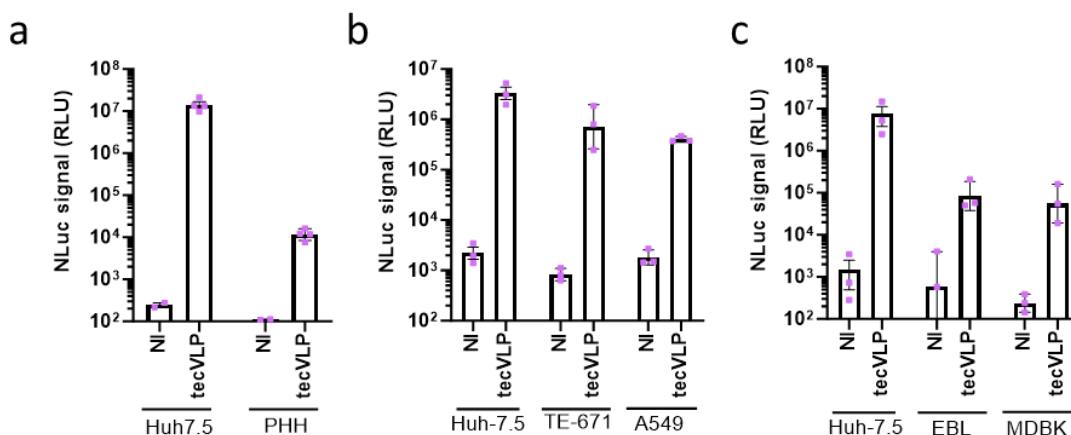


**Figure 30: Levels of tecVLPs infection in different cell types.** (a) Levels of NLuc signals detected at 24h after infection of Huh-7.5 cells or PHH with 100 $\mu$ L of NLuc\_tecVLPs. (b) Level of NLuc signals detected 48h after infection of Huh-7.5, TE-671 and A549 cells with 100 $\mu$ L of NLuc\_tecVLPs. (c) Levels of NLuc signals detected 48h after infection of Huh-7.5, EBL and MBDK cells with 100 $\mu$ L of NLuc\_tecVLPs. NI: non infected control. The results are represented as means  $\pm$  SEM. Each dot in the graphs corresponds to the value of an individual experiment. N=3-4.

Since CCHFV can also infect cattle, I tested the LDL-R dependency of CCHFV entry in bovine cells, either EBL embryonic lung cells or MDBK kidney cells, which express low but detectable levels of LDL-R at their surface (Figure 29), and which are permissive, although less than Huh-7.5 cells, to NLuc\_tecVLP infection (Figure 30c). Yet, while the LDL-R blocking antibody could bind LDL-R expressed at the surface of bovine cells (Figure 29), it had no effect on NLuc\_tecVLP infection in these blocking assays (Figure 31c), thus suggesting that CCHFV infection in EBL and MDBK cells may not depend on LDL-R.

Altogether, these results suggested that LDL-R is used by CCHFV for infection of human cells but not of bovine cells.

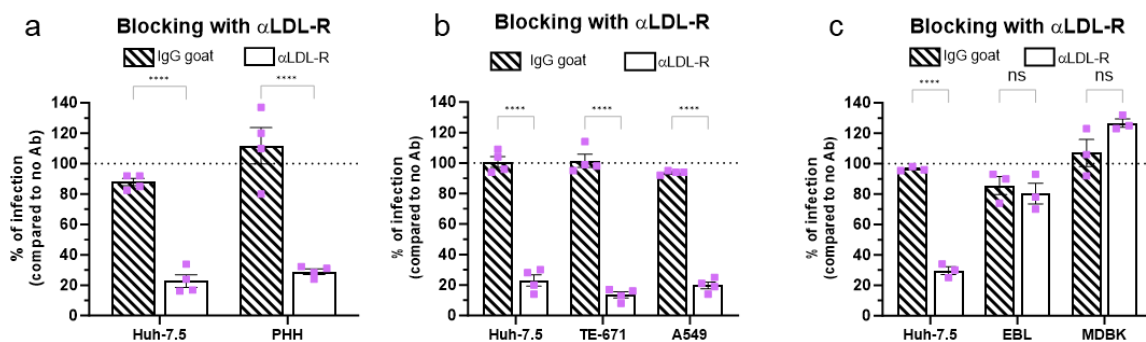


**Figure 31: LDL-R is a factor of CCHFV infection in human but not in bovine.** (a) Huh-7.5 cells or PHH were incubated with 4  $\mu$ g/mL of LDL-R antibody (open bars) or control isotype (IgG goat, dashed bars) for 1h at 37°C before infection with CCHFV NLuc\_tecVLP. The media was replaced 3h p.i. and the cells were harvested at 24h p.i. for determination of the levels of infection by NLuc measurement. (b) Same as (a) with Huh-7.5, TE-671, A549 cells with harvesting at 48h p.i.. (c) Same as (b) with Huh-7.5, EBL, MDBK cells. The results are represented as means  $\pm$  SEM. Each dot in the graphs corresponds to the value of an individual experiment. N=3-4. Two-way ANOVA test with Sidak's multiple comparisons.

### LDL-R is involved at cell entry steps of CCHFV.

Since the levels of infection of CCHFV tecVLPs reflect both the efficiency of cell entry and the subsequent transcription and replication of their minigenome, I sought to determine if LDL-R is involved at the entry and/or transcription/replication steps. To discriminate either possibility, I added the anti-LDL-R antibody at different time points before and/or after infection of Huh-7.5 cells (Figure 32a). I found that while addition of the antibody either before or concomitantly to the infection step inhibited GFP\_tecVLP infectivity to up to 80% (Figure 32b: H-1, H-1 & H0, H0), addition of the anti-LDL-R antibody from 2h post-infection onward had no effect on infectivity (Figure 32b: H+2, H+4, H+6), hence suggesting that LDL-R is involved at an entry step rather than at a later step of transcription/replication.

Of note, this result was obtained after 3 independent experiments. In order to have a significant decrease, it would have required a 4<sup>th</sup> replicate.

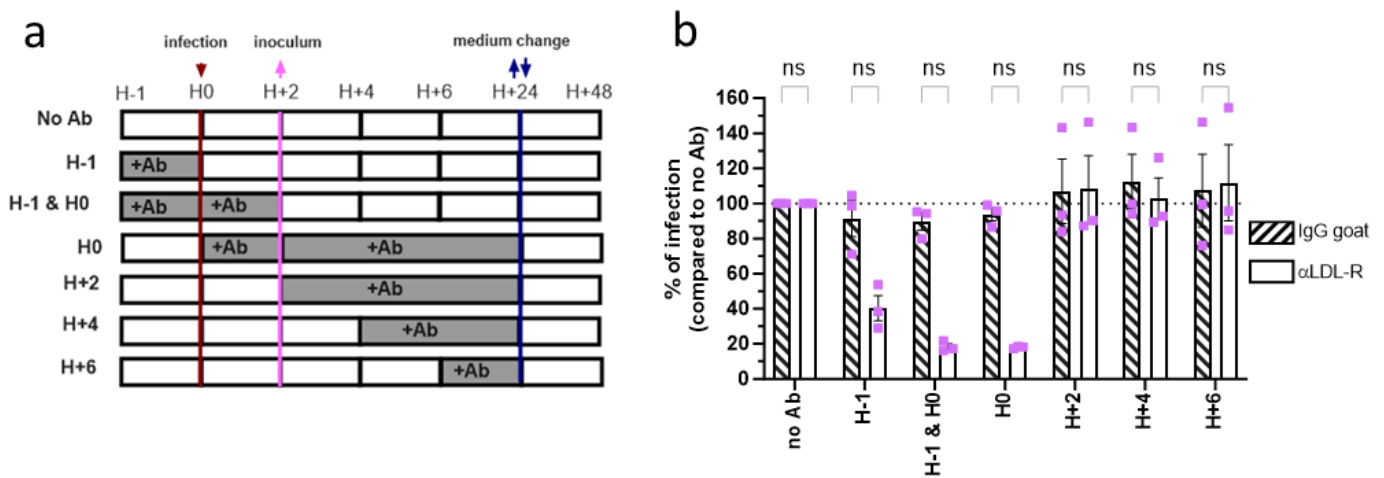


**Figure 32: LDL-R play a role in the early steps of CCHFV infection.** (a) Schematic representation of the experimental setting. Huh-7.5 cells were incubated with 4µg/mL of anti-LDL-R antibody or control isotype (as indicated in grey), before, during or after infection (red line) with CCHFV GFP\_tecVLPs as indicated in grey. The inoculum was removed 2h p.i. (pink line) and the media changed after 24h (blue line). Cells were harvested 48h p.i. and the level of infection was determined by flow cytometry. (b) Percentage of infectious titers of CCHFV GFP\_tecVLP relative to control isotype as in the experimental set up described in (a). The results are represented as means ± SEM. Each dot in the graphs corresponds to the value of an individual experiment. N=3. Mann-Whitney test.

I thus hypothesised that LDL-R could serve as a CCHFV entry factor through its expression at the cell surface. To test this hypothesis, I saturated the GFP\_tecVLPs or authentic WT CCHFV particles with a soluble recombinant form of LDL-R (sLDL-R) before infection of Huh-7.5 cells, to limit their access to LDL-R and thus, their entry. As a control soluble protein, I used a soluble form of CD81 (CD81-LEL) (Douam *et al.*, 2014). CD81 is a crucial receptor for HCV expressed at the surface of Huh-7.5 cells (Akazawa *et al.*, 2007), that should not play a role in CCHFV infection. I also used VSVpp as a positive control and MLVpp as a negative control. For the BSL-4 experiment, once again I prepared the cells and reagents for our collaborators in Cyrille Mathieu’s team and the RNA quantification was done by Anupriya Gautam. While the soluble form of CD81 had no effect on all viral infections tested, I found that sLDL-R inhibited VSVpp up to 95% as expected. More importantly, sLDL-R inhibited CCHFV infection in a dose-dependent manner in both GFP\_tecVLP infection (Figure 33a) and authentic CCHFV infection (Figure 33b), up to 70% inhibition and 55% respectively.

These results suggest that sLDL-R could prevent cell entry through interaction with CCHFV particles.

Like for the LDL-R blocking experiment (Figure 28a), I did not observe any impact of sLDL-R neutralisation on HAZV infection (Figure 33a). Of note, while the blocking of LDL-R with an antibody impaired VSVpp and CCHFV\_tecVLP at similar levels (Figure 28a), sLDL-R impaired CCHFV entry at a lesser extent as compared to VSVpp (Figure 33a). This difference between both viruses could be due to a different role or affinity of LDL-R for the two types of viral particles. Alternatively, this could also be due to the production of CCHFV tecVLPs in Huh-7.5 cells that express competitors for binding to sLDL-R, such as apoB or apoE, which is not the case for HEK293T cells that were used to produce VSVpp.

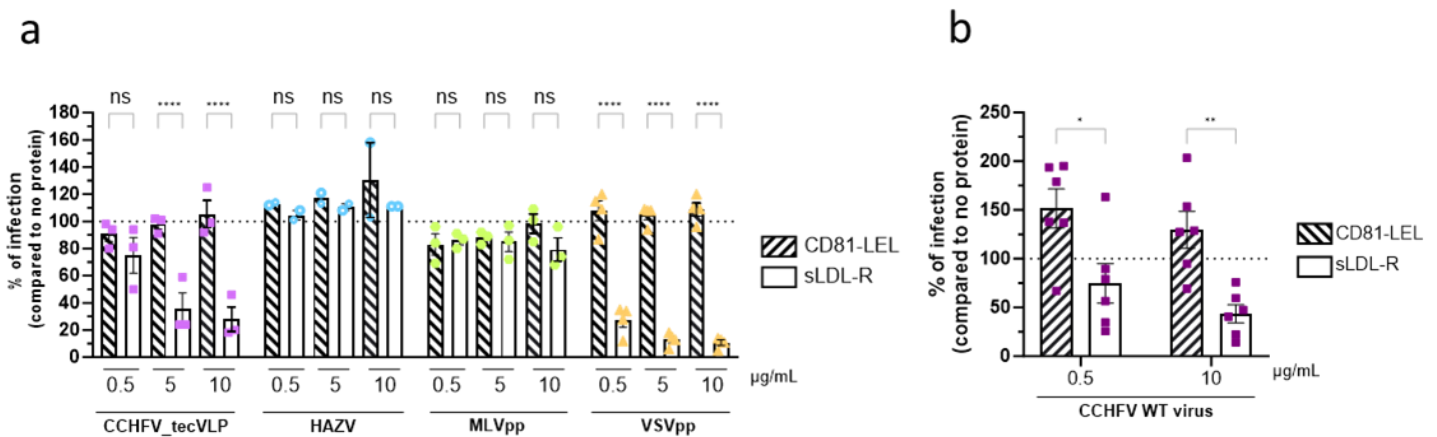


**Figure 33: LDL-R promotes CCHFV entry.** (a) CCHFV GFP\_tecVLP (pink), MLVpp (green), VSVGpp (yellow) or HAZV (blue) were incubated for 1h at room temperature with soluble LDL-R (sLDL-R, open bars) or with soluble CD81 (CD81-LEL, dashed bars) at different concentrations before infection of Huh-7.5 cells. For CCHFV infection, cells were pre-transfected with NP and L expression plasmids. The media was replaced 3h p.i. and the cells were harvested 16h p.i. (HAZV) or 48h p.i. and the level of infection was determined by flow cytometry. The results are represented as means  $\pm$  SEM. Each dot in the graphs corresponds to the value of an individual experiment. N=2-4. Two-way ANOVA test with Sidak's multiple comparisons. (b) Same experiment using WT CCHFV. Media was removed 1h p.i. and cells were lysed 24h p.i. The level of infection was quantified by RT-qPCR. The results are represented as means  $\pm$  SEM. Each dot in the graphs corresponds to the value of an individual experiment. N=6. Two-way ANOVA test with Sidak's multiple comparisons.

### LDL-R promotes CCHFV entry by facilitating binding and endocytosis into cells.

Next, I wondered whether LDL-R could promote CCHFV tecVLPs endocytosis. Taking advantage of the presence of a tyrosine motif within the LDL-R cytoplasmic tail that is essential for its endocytosis (Chen *et al.*, 1990), I used Tyrphostin A23 (TyrA23). TyrA23 is a small molecule that binds to AP-2 where AP-2 binds to tyrosine motifs: YXX $\phi$  (X being any amino acid and  $\phi$  a bulky hydrophobic amino acid) present on the CT of surface protein.

(Crump *et al.*, 1998). By binding the tyrosine motif, AP-2 will allow the internalisation of the protein. Thus, by competition, TyrA23 decreases retrograde transport of surface protein expressing the YXX $\phi$  motif. I hypothesised that inhibiting the endocytosis of the receptor, but not its production nor its whole recycling cycle, will result in an increase of its cell surface expression. Thus, if LDL-R plays a role in the endocytosis of the virus, then, the treatment will decrease the infection by CCHFV\_tecVLPs, and in contrast, if it allows the binding, the treatment will increase the infection.

First, with the help of Vincent Legros for the live imaging assay, I determined the effect of TyrA23 on LDL-R endocytosis by using LDLs labelled with pHrodo that fluoresce only after their endocytosis (Ritter *et al.*, 2018). As a positive control, I used chlorpromazine (CPZ), which efficiently blocks clathrin-mediated endocytosis (Wang *et al.*, 1993) (Figure 34a; left). As expected, upon CPZ treatment, almost no fluorescence from the labelled LDLs was observed, meaning that it inhibited the LDL receptor endocytosis (Figure 34a; right).

Then, I assessed the effect of a 30min pre-treatment with TyrA23 before addition of labelled LDLs along with fresh drug (Figure 34b; left). This treatment led to a partial diminution of the fluorescence from the LDL-pHrodo, and thus, a partial inhibition of LDL-R endocytosis (Figure 34b; right). Furthermore, I assessed the effect of a 24h pre-treatment with or without addition of fresh TyrA23 (Figure 34c; left). This experiment was done after the observation that 24h after incubation with the drug, the media that had turned yellow (from the TyrA23 addition), was back to normal, suggesting that the drug was fully degraded. I hypothesised that the transient inhibition of endocytosis would have increased the expression of LDL-R at the cell surface, which could undergo endocytosis once the drug become inactive, and thus, maybe increase LDL binding and internalisation. I observed that after 24h incubation with TyrA23, LDL could be endocytosed at a similar rate compared to mock treated cells (Figure 34b; right), showing that the drug is not effective at this time point. A partial inhibition could be restored after addition of fresh TyrA23 (Figure 34c; right). In this experiment, I could not conclude on the increase of LDL-R at the cell surface.

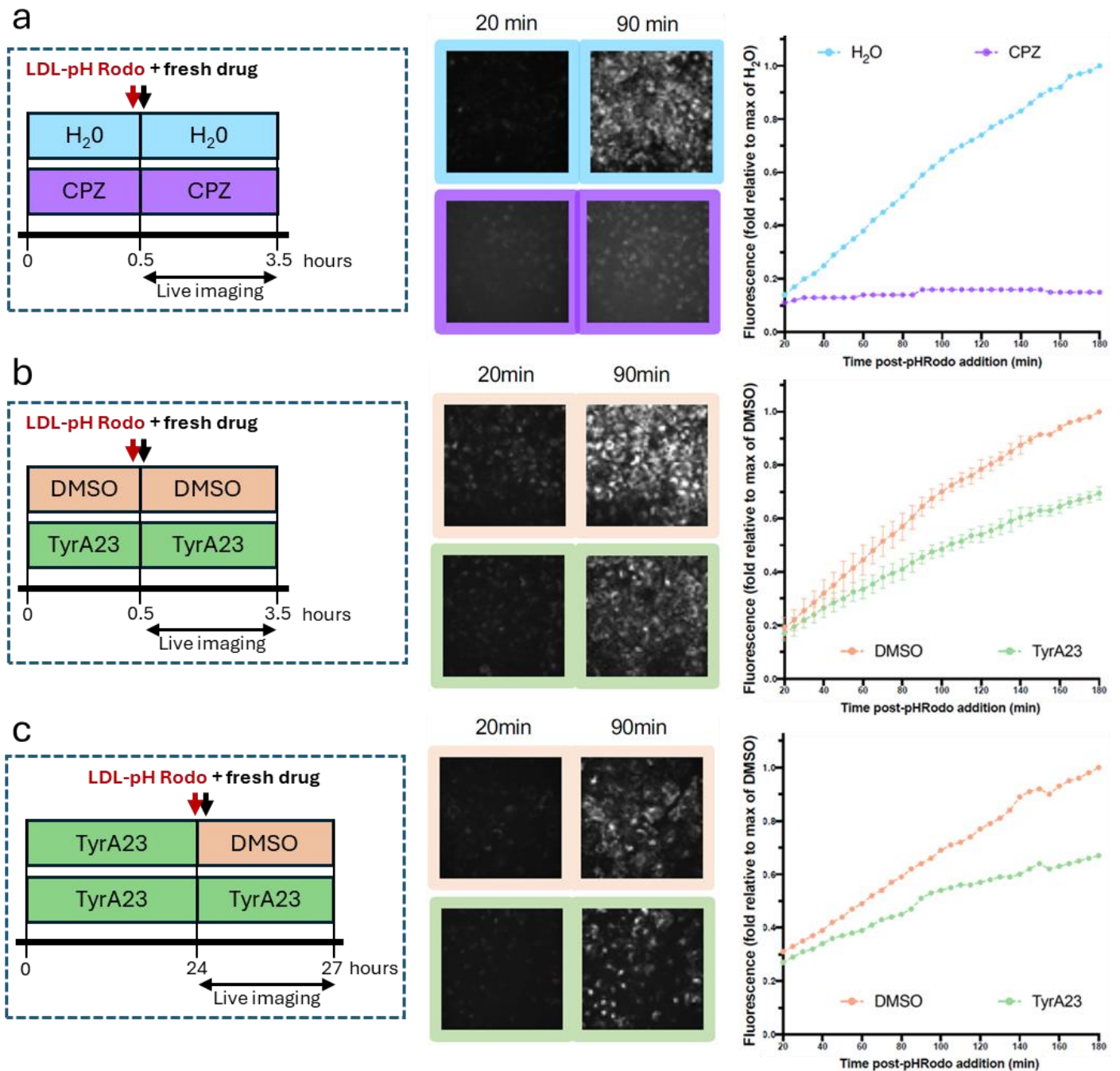


**Figure 34: TyrA23 treatment inhibits LDL-R endocytosis and thus LDL uptake.** (a) Huh-7.5 cells were treated with H<sub>2</sub>O (blue) or Chlorpromazine (CPZ, 100 $\mu$ M - violet) for 30 minutes. 20 minutes before live imaging analysis, fresh H<sub>2</sub>O or CPZ was added before adding LDL-pHrodo (10 $\mu$ g/mL) to the media and fluorescence was measured every 5 minutes for 3 hours (left). Two representative image of the fluorescence 20min and 90 minutes after addition of LDL-pHrodo (middle). Level of fluorescence for each time point expressed as fold relative to the max fluorescence of H<sub>2</sub>O (right). (b) Huh-7.5 cells were treated with DMSO (orange) or TyrA23 (100 $\mu$ M - green) for 30 minutes. 20 minutes before live imaging analysis, fresh DMSO or TyrA23 were added before adding LDL-pHrodo (10 $\mu$ g/mL) to the media and fluorescence was measured every 5 minutes for 3 hours (left). Two representative image of the fluorescence 20min and 90 minutes after addition of LDL-pHrodo (middle). Level of fluorescence for each time point expressed as fold relative to the max fluorescence of DMSO (right). (c) Huh-7.5 cells were treated with TyrA23 (100 $\mu$ M - green) for 24 hours. 20 minutes before live imaging analysis, fresh DMSO (green) or TyrA23 were added before adding LDL-pHrodo (10 $\mu$ g/mL) to the media and fluorescence was measured every 5 minutes for 3 hours (left). Two representative image of the fluorescence 20min and 90 minutes after addition of LDL-pHrodo (middle). Level of fluorescence for each time point expressed as fold relative to the max fluorescence of DMSO (right).



Once the impact of the TyrA23 treatment was characterised, I determined the effect of the pre-treatment on cell viability, on LDL-R surface expression levels by flow cytometry, and on CCHFV\_tecVLPs infection. A 30min pre-treatment with TyrA23 did not impact the cell viability, nor the cell surface expression of LDL-R, but resulted in a slight but reproducible inhibition of tecVLP infection (Figure 35a). So, a moderate inhibition of LDL-R internalisation causes a moderate diminution of CCHFV\_tecVLPs infection, suggesting a role of the receptor in the particles' endocytosis.

Furthermore, when I tested a 24h TyrA23 pre-treatment to extend these observations, I found that it resulted in an increase of LDL-R level at the cell surface without impacting the cell viability. The increase of cells surface LDL-R coincided with an increased tecVLPs infection (Figure 35b). This result confirmed that a cell surface accumulation of LDL-R increases the tecVLPs entry level, maybe through increased binding.

To assess the effect of LDL-R endocytosis inhibition independently of an increase of LDL-R cell surface expression, I pre-treated cells with TyrA23 and added fresh drug vs. DMSO at the time of infection with CCHFV, but also the other control viruses (Figure 35c).

For CCHFV\_tecVLPs, pre-treatment of TyrA23 followed by the addition of fresh drug prevented both LDL-R endocytosis and tecVLPs infection (Figure 34c; right and Figure 35c; right), suggesting once again a role of LDL-R in CCHFV endocytosis.

In contrast, I obtained an increase of the infection if the TyrA23 was replaced by a mock (DMSO) at the time of infection. This result supports the implication of LDL-R in the particles' binding.

Interestingly, a similar pattern is observed for HAZV and, in a lesser extent, for MLVpp. TyrA23 is not a specific inhibitor of LDL-R endocytosis but inhibits the internalisation of cell surface proteins relying on the CME. Thus, the effect observed on HAZV can be the consequence of its unknown receptor endocytosis being inhibited. Concerning VSVpp, it is known that VSV-G can interact with several LDL receptor, including LRP1 (Amirache *et al.*, 2014; Finkelshtein *et al.*, 2013) which present two endocytic NPxY motifs (Figure 15), still available for AP-2 binding. It may compensate the inhibition of the binding of AP-2 to the YXX $\phi$  motif. However, the results observed for MLVpp are surprising. The virus endocytosis does not rely on the CME. Indeed, its internalisation relies on macropinocytosis, which is

clathrin-independent (Rasmussen and Vilhardt, 2014), and thus should not be impacted by the TyrA23 treatment.

Altogether, these results indicated that LDL-R promotes CCHFV entry through binding of viral particles and by facilitating their endocytosis into cells.

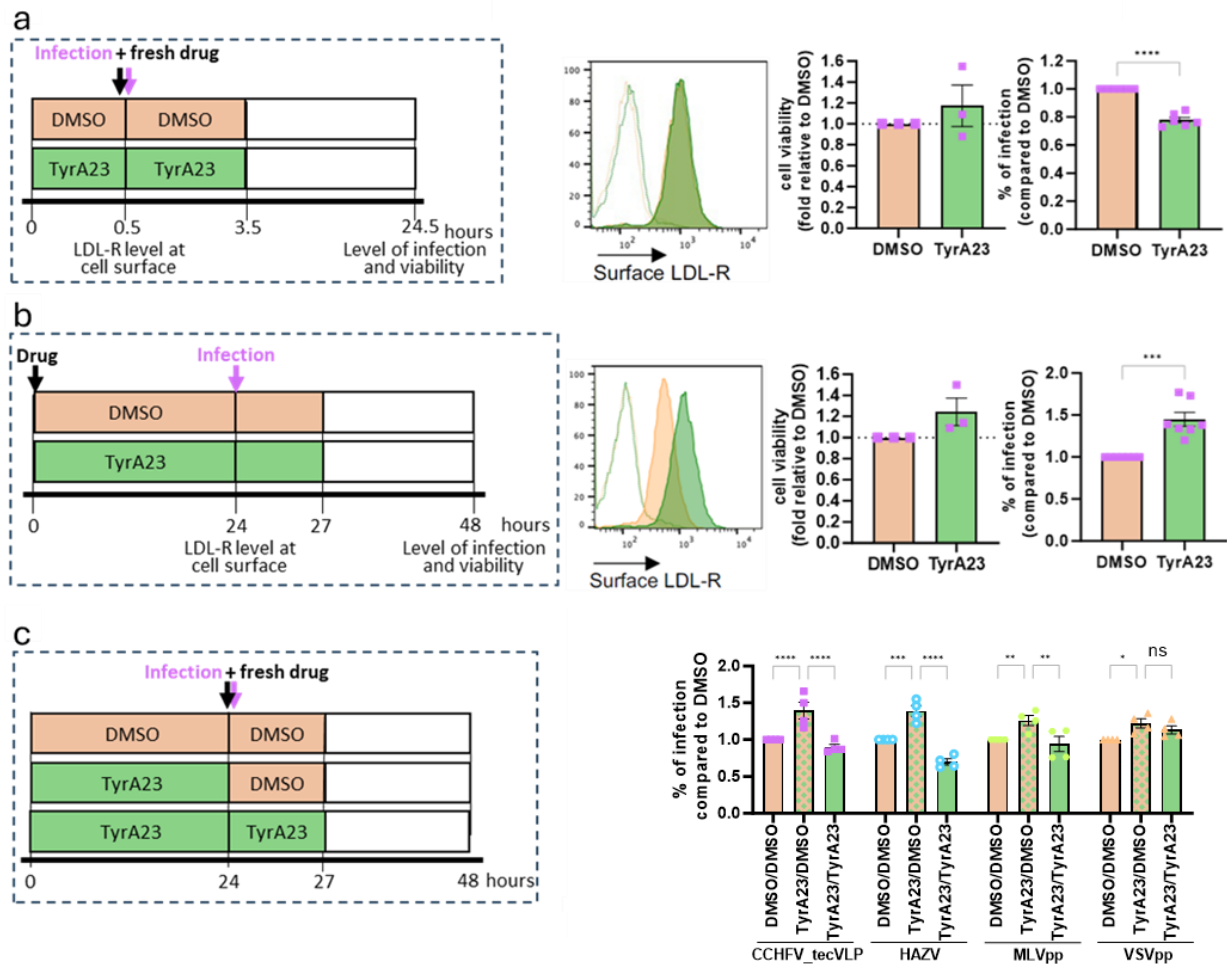


**Figure 35: TyrA23 treatment inhibits CCHFV\_tecVLPs endocytosis but may increase CCHFV\_tecVLPs binding.** (a) Huh-7.5 cells pre-transfected with NP and L expression plasmids were treated with DMSO and TyrA23 (100 $\mu$ M) and infected 30min later with GFP\_tecVLPs in presence of fresh drug. Media was removed 3h p.i. and the cells were harvested at 24h p.i. for determination of the levels of infection by flow cytometry (right). Cell surface expression of LDL-R 30min post-treatment determined by flow cytometry (2nd from left) with control isotypes as depicted in dotted lines. Representative from 6 independent experiments. Cell viability (3<sup>rd</sup> from left); N=3. Level of infection (right). The results are represented as means  $\pm$  SEM. Each dot in the graphs corresponds to the value of an individual experiment. N=6. One sample t test. (b) Huh-7.5 cells pre-transfected with NP and L expression plasmids were treated for with DMSO or TyrA23 (100 $\mu$ M) and infected 24h later with GFP\_tecVLPs. Media was removed 3h p.i. and the cells were harvested at 24h p.i. for determination of the levels of infection by flow cytometry. Cell surface expression of LDL-R 24h post-treatment determined by flow cytometry (2nd from left). Representative from 7 independent experiments. Cell viability (3<sup>rd</sup> from left); N=3. Level of infection (right). The results are represented as means  $\pm$  SEM. Each dot in the graphs corresponds to the value of an individual experiment. N=7. One sample t-test. (c) Huh-7.5 cells pre-transfected or not with NP and L expression plasmids were treated with DMSO or TyrA23 (100 $\mu$ M) for 24h before infection with CCHFV GFP\_tecVLP (pink), MLVpp (green), and VSVpp (yellow) or HAZV (blue) with addition of fresh drug or DMSO. Media was removed 3h p.i. and the cells were harvested at 16h p.i. (HAZV) or 24h p.i. for determination of the levels of infection by flow cytometry. The results are represented as means  $\pm$  SEM. Each dot in the graphs corresponds to the value of an individual experiment. N=4. Two-way ANOVA test with Sidak's multiple comparisons.

### **The exchangeable apolipoprotein E mediates CCHFV entry.**

Next, I wondered whether the interaction between LDL-R and CCHFV particles can be promoted through the use of natural ligands of the cellular receptors. Indeed, while VSV particles interact directly with LDL-R (Nikolic *et al.*, 2018), it was shown that other viruses, such as HCV, bind to LDL-R through apoE (Owen *et al.*, 2009).

First, I tested whether anti-apoE antibodies could neutralise CCHFV\_tecVLP or authentic WT CCHFV particles. As a positive control, I used HCV particles, as they can be neutralised by anti-apoE antibodies (Owen *et al.*, 2009), whereas I used VSVpp and MLVpp as negative controls, since VSV-G is a direct ligand of LDL-R binding, and since MLV Env binds an irrelevant receptor (Battini *et al.*, 1996). I incubated viral particles with anti-apoE antibodies for 1h before infection assays.

Interestingly, I found a dose-dependent inhibition for both CCHFV GFP\_tecVLP (Figure 36a) and authentic WT CCHFV particles (Figure 36b), which reaches 80% and 55% of inhibition respectively, by anti-apoE antibodies. This inhibition is similar to the one observed for HCV. Moreover, as expected, the anti-apoE antibodies did not inhibit VSVpp or MLVpp infection (Figure 36a).

The difference of level of neutralisation between tecVLPs and authentic WT virus could be due to a difference in the number of infectious particles. Conversely, when I tested the apoE dependency of HAZV infection, I found that neutralisation by anti-apoE antibodies did not significantly influence HAZV infection (Figure 36a). These results suggest that apoE is involved in CCHFV entry but not HAZV and strengthen the previous conclusion: HAZV does not enter the cell through lipid transfer receptors.

These results suggested that apoE plays a crucial role in CCHFV infectivity.

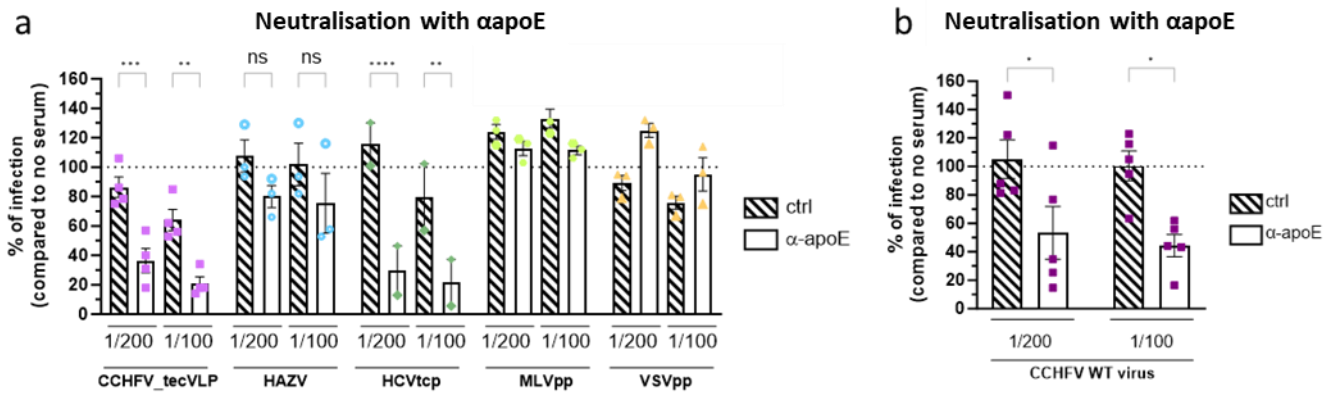


**Figure 36: ApoE promote CCHFV infection.** (a) CCHFV\_tecVLPs (pink), MLVpp (light green), VSVGpp (yellow), HAZV (blue) or HCVtcp (green) were incubated for 1h at room temperature with anti-apoE serum or control serum at different dilution before infection of Huh-7.5 cells. In the case of CCHFV\_tecVLP infection, cells were pre-transfected with NP and L expression plasmids. Cells were harvested 48h post-infection and infectivity was determined by flow cytometry or by NS5A immunostaining (for HCVtcp). The results are represented as means  $\pm$  SEM. Each dot in the graphs corresponds to the value of an individual experiment. N=2-4. Two-way ANOVA test with Sidak's multiple comparisons. (b) The same experiment was performed using WT CCHFV particles. Media was removed 1h p.i. and cells were lysed 24h p.i. The infectivity was quantified by RT-qPCR. The results are represented as means  $\pm$  SEM. Each dot in the graphs corresponds to the value of an individual experiment. N=5. Two-way ANOVA test with Sidak's multiple comparisons. The results are represented as means  $\pm$  SEM. Each dot in the graphs corresponds to the value of an individual experiment.

### **ApoE is associated with CCHFV particles and promotes their assembly/secretion and specific infectivity.**

ApoE is present at the surface of lipoproteins such as LDLs and VLDLs but it can also exist in a lipid-free form in the extracellular environment (Zhang *et al.*, 1996). Importantly, apoE belongs to the family of exchangeable apolipoproteins, implying that it can be transferred from a lipoprotein to another lipoprotein or to a viral particle, as described for HCV (Bankwitz *et al.*, 2017; Li *et al.*, 2017). Thus, there is a possibility for the apolipoprotein to be incorporated onto the viral particles, either during the production, or after the egress using the apoE present on lipoproteins from the cell or from the FBS. I therefore sought to determine if CCHFV\_tecVLPs harbour apoE at their surface, which would promote entry of CCHFV by binding to LDL-R.

First, I concentrated tecVLP particles by ultracentrifugation of producer cell supernatants onto a sucrose cushion. I found an enrichment of 2-fold of apoE in pellets of tecVLPs, as compared to pellets obtained from supernatants of mock transfected cells (empty plasmid) (Figure 37a), or to pellets obtained from supernatants of HAZV producing cells (Figure 37b). This suggests a possible association of apoE and CCHFV particles.

Then, I determined if I could capture viral particles with an anti-apoE antibody, as previously shown for HCV (Calattini *et al.*, 2015). After immuno-precipitation assay on supernatant from CCHFV\_tecVLPs producing cells, I found a 16-fold enrichment of CCHFV\_tecVLP RNAs with anti-apoE antibodies relative to control IgGs (Figure 37c), confirming an association of apoE with CCHFV particles.

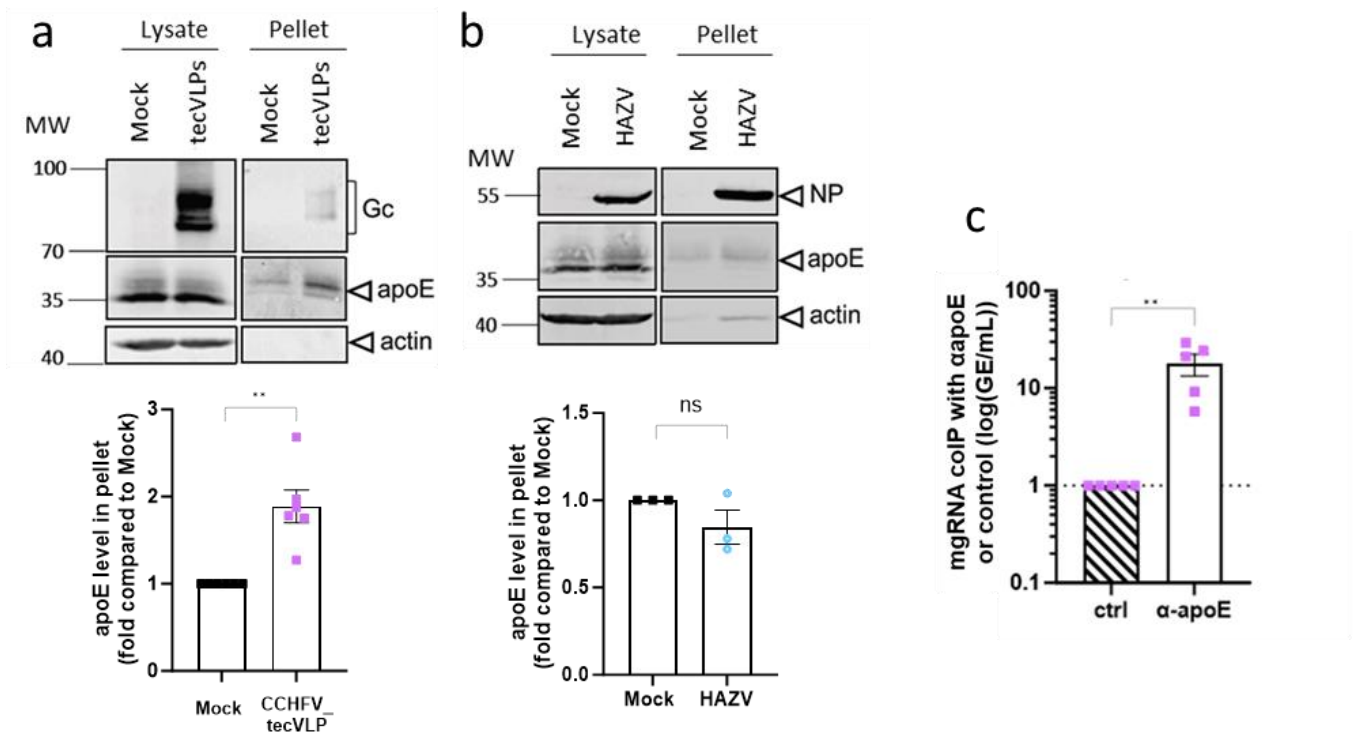


**Figure 37: ApoE is associated with CCHFV particles.** (a) Western blot analysis of cell lysates of cells producing CCHFV\_tecVLPs vs. Mock cells and of particles concentrated by ultracentrifugation (top). Representative image of 6 independent experiments. Quantification of the apoE enrichment in pellet of CCHFV\_tecVLPs relative to mock condition (bottom). The results are represented as means  $\pm$  SEM. Each dot in the graphs corresponds to the value of an individual experiment. N=6. One sample t-test. (b) Western blot analysis of cell lysates of cells producing HAZV vs. Mock cells and of particles concentrated by ultracentrifugation (top). Representative image of 3 independent experiments. Quantification of the apoE enrichment in pellet of HAZV relative to mock condition (bottom). The results are represented as means  $\pm$  SEM. Each dot in the graphs corresponds to the value of an individual experiment. N=3. Wilcoxon test. (c) Level of CCHFV minigenome RNA co-immunoprecipitated with an apoE serum vs. control IgGs and quantified by RT-qPCR. The results are represented as means  $\pm$  SEM. Each dot in the graphs corresponds to the value of an individual experiment. N=5. One sample t-test.

Finally, with the help of Anupriya Gautam, we produced CCHFV\_tecVLPs in Huh-7.5 cells transduced with a shRNA targeting apoE, which induced a robust loss of apoE expression (Figure 38a). The apoE knock down did not impair the level of expression of CCHFV NP in producer cells (Figure 38b), thus, it did not impair the transfection efficiency nor the expression of the plasmids required for the tecVLPs production. However, it resulted in a strong loss of infectivity of CCHFV\_tecVLPs, with a 2-log titer decrease (Figure 38c). These

results suggest that apoE plays a role in assembly/secretion or infectivity of CCHFV\_tecVLPs. Furthermore, by assessing the mgRNA level in the supernatant of Huh-7.5 KD apoE producing cells (see manuscript in Annexe), we observed a decrease in the RNA level in knock down cells. This demonstrated that apoE had a role in the production of CCHFV particles.

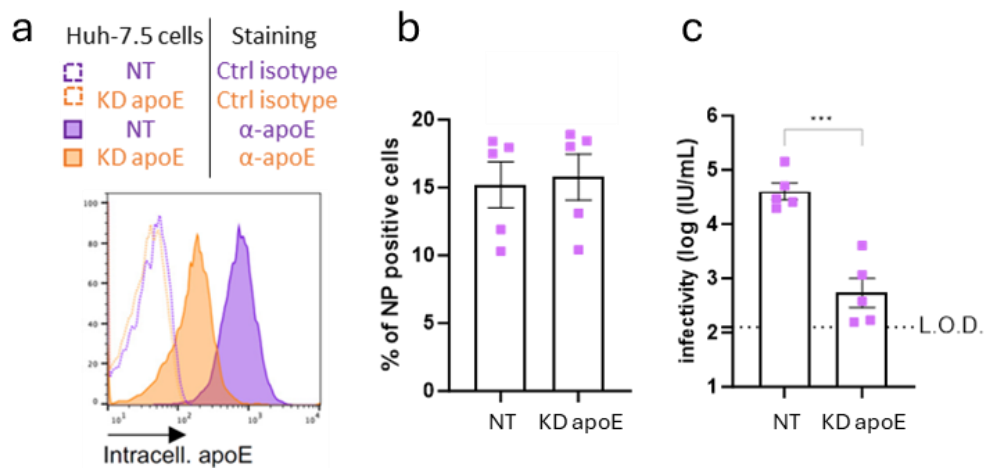


**Figure 38: ApoE is a cellular factor contributing CCHFV particles assembly, secretion, or infectivity.** (a) Intracellular level of apoE assessed by flow cytometry of cells transduced with shRNA targeting apoE or non-transduced (NT). Representative image of 3 independent experiments. (b) Cells described in (a) were used for production of CCHFV tecVLPs as described in Methods. Percentage of CCHFV NP transfected cells was assessed by staining of NP in CCHFV\_tecVLPs producing (anti-NP antibody, 9D11) followed by an anti-mouse APC and analysed by flow cytometry. The results are represented as means  $\pm$  SEM. Each dot in the graphs corresponds to the value of an individual experiment. N=5. Unpaired t-test for. (c) Infectivity of CCHFV\_tecVLPs produced in cells described in (a), as assessed by flow cytometry. The results are represented as means  $\pm$  SEM. Each dot in the graphs corresponds to the value of an individual experiment. N=5. Unpaired t-test.

### 3. Conclusion

These results have been included in a broader study published in Nature Communications (see in Annexe). This study indicates that CCHFV particles could incorporate apoE, which may therefore provide a ligand to increase interaction with the cellular factor LDL-R. This cell surface protein allows CCHFV to bind to the host cell and plays a role in the endocytosis of the viral particles.

Of note, it is probably not the only entry factor used by CCHFV, as in the report, we also highlight a potential role of VLDL-R in CCHFV infection. In addition, since LRP1, a member of the LDL-R family was recently shown to act as an entry factor for RVFV and OROV (Ganaie et

*al.*, 2021; Schwarz *et al.*, 2022), we also tested this host factor. Interestingly, CCHFV\_tecVLPs infection did not rely on LRP1 (Annexe). We finally demonstrated that apoE is a pro-viral factor for assembly/secretion of CCHFV particles.

## Chapter IV. Discussion

During my PhD I was able to identify LDL-R as a cellular factor governing CCHFV entry (Ritter *et al.*, 2024). After we submitted the paper to Nature Communication (October 2023), two teams published about LDL-R being an entry factor for the virus in January (Xu *et al.*, 2024) and March (Monteil *et al.*, 2024). The results of the three papers are summarised in Table 6. In the following sections, I will discuss my results and how they are incorporated with the current literature.

### A. Perspectives on the identified lipid's receptors

#### 1. LDL-R as an entry factor for CCHFV

LDL-R is ubiquitously expressed, which could account for the broad cellular tropism of the virus. However, its expression level varies and the virus preferentially infect specific cell types (hepatocytes or endothelial cells). As described in the introduction, the permissiveness of some cell lines is still unclear. Indeed, in Dai *et al.*, (2021), the authors claimed that the hepatocytes HepG2 cells are non-permissive, when in my hands (data not shown) and in Monteil *et al.*, (2024) this cell line shows level of infection similar to the hepatocytes Huh7 cells or adrenal cortex SW-13 cells. Both of them are commonly used for CCHFV infection assays. The discrepancy observed between laboratories may be due to cellular derivation to cells lacking the expression of factors required for CCHFV infectivity. However, in the literature, non-stimulated T and B lymphocytes are described as non-permissive to CCHFV infection (Connolly-Andersen *et al.*, 2009; Garrison, 2012). Moreover, non-stimulated T and B cells are known to express a low level of LDL-R (Amirache *et al.*, 2014; De Sanctis *et al.*, 1998). Supporting the conclusion that LDL-R is an entry factor for CCHFV

Beside the expression level, I reviewed the localisation of LDL-R in polarized cells and compared this with the reported modes of entry of CCHFV in these cells. Interestingly, it was shown that LDL-R is more expressed at the basolateral side than the apical side on polarized cells (Gan *et al.*, 2002; Kim *et al.*, 2018; Yokode *et al.*, 1992) and consistently, it was shown in Caco-2 and MDCK that CCHFV, contrary to HAZV, enters through the basolateral side



(Connolly-Andersen et al., 2007; Monteil et al., 2020). Even if tropism is a viral receptor, LDL-R being an entry factor for CCHFV is consistent with the literature.

## 2. LDL-R is not the only entry factor for CCHFV

Another point on which the three papers on LDL-R agree is that LDL-R is not the only entry factor involved in CCHFV infection. In my case, using polyclonal anti-LDL-R antibody, I never reached a complete inhibition of the infection (Figure 28). The concentrations used in the paper were 1 and 4 µg/mL, but with CCHFV\_tecVLPs, I also tested 8, 16 and 32 µg/mL (not shown). A plateau was reached at 94% of inhibition for 16µg/mL. In Monteil *et al.*, (2024), the authors used authentic CCHFV at multiplicity of infection (MOI) of 0,1 to infect haploid AN3-12, Vero and A549 cells knocked out for LDL-R. They observed each time a diminution of 1 log of the RNA level compared to WT cells. In a similar experiment, Xu *et al.*, (2024) still detected CCHFV RNA in Huh7 *Ldlr* KO after infection. In models closer to the physiologic infection, such as blood vessels organoids, the inhibition is around 80%. This suggests that, in absence of LDL-R, CCHFV entry can occur through other factors that are still unknown.

In order to identify other entry factors, a CRISPR/Cas9 screen could be done on Huh-7.5 or SW-13 cells (both permissive cell lines) knocked out for LDL-R and using VSVΔG-CCHFV GPs pseudotyped particles in presence of anti-VSV-G antibodies. This method allows to target the entry step, since only CCHFV GPs are present on the particles and residual VSV-G is neutralised. However, knockout screen can be limiting if the entry factor is an essential factor for the cell. To overcome this limitation, either a CRISPRi screen (knockdown screen) could be considered on the cells cited above, or a cDNA library screen (GOF screen), from Huh-7.5 cells or SW-13 cells RNAs, on T lymphocytes (not permissive to CCHFV), but the low transduction efficiency could be an obstacle.

Another possibility would require to determine the residues of Gc that are crucial to bind LDL-R, as it was established for VSV (Nikolic et al., 2018), to mutate them in order to produce CCHFV particles that would not bind to LDL-R, and to perform either a LOF or a GOF screen. It could be performed with CCHFV\_tecVLPs or with a rCCHFV in BSL-4 laboratories produced from apoE-free cells.

Interestingly, VSV is known to not only bind to LDL-R but also to other receptors from the LDL-R family (VLDL-R and LRP1) (Finkelshtein *et al.*, 2013). This is based on the high similarity of their ligand-binding domain. Moreover, several members of the *Bunyaviricetes* were shown to use LRP1 for their entry (Table 5). For these reasons, the authors of the different LDL-R papers (including us), assessed the role of other members of the family, such as VLDL-R, LRP1 or LRP8, which are detailed below.

a. LRP8

LRP8 or apoER2 contribution to CCHFV infection was assessed. In Xu *et al.*, (2024), the authors did a screen of LDL receptors, either by knock out in 293T cells, by double knock out in Huh7 *Ldlr* KO, or by OE in DLD1 cells, which express only a low level of LDL-R. In all those experiments, they did not observe any changes in CCHFV infectivity in the LRP8 modified cells (Table 6).

In contrast, in Monteil *et al.*, (2024), the authors used a soluble LRP8 which was able to inhibit VSV particles pseudotyped with CCHFV GPs (VSVΔG-CCHFV GPs), but had no effect on authentic CCHFV IbAr10200 or on a clinical strain (Table 6). One of the differences between these conditions is the fact that pseudotyped VSVΔG-CCHFV particles are produced in HEK293T cells, while the authentic virus is produced in SW-13 cells. The authors claimed that apoE can be incorporated onto particles when produced in HEK293T cells but not in SW-13 cells. However, the authors did not assess the level of apoE produced in the two cell lines or present on the particles. They only performed a neutralisation assay using an anti-apoE antibody which was able to decrease VSVΔG-CCHFV GPs infection but not the authentic CCHFV (both produced in media containing serum). To conclude on LRP8, the only impact observed was with a soluble protein on VSV particles pseudotyped with CCHFV GPs. However, the infection assays were not done with neutralising anti-VSV-G antibodies to assess the presence of the glycoproteins on the pseudotyped particles. Thus, we cannot exclude that the soluble LRP8 impaired the component from the VSV pseudotyped particles that are not related to CCHFV, such as the VSV-G that can still be at the surface of the particles.

### b. VLDL-R

In our paper, we observed a 2.5 fold increase in CCHFV infectivity in Huh-7.5 cells overexpressing VLDL-R, suggesting that this receptor may play a role in the virus entry (Ritter *et al.*, 2024) (Table 6). However, Monteil *et al.*, (2024) used a soluble VLDL-R on CCHFV particles and did not observe any reduction in the infectivity (Table 6). This experiment was not done on VSV-CCHFV but only on the authentic CCHFV IbAr10200, which they claim doesn't incorporate apoE onto the virions (as described above). Moreover, Xu *et al.*, (2024) observed only a slight decrease in the CCHFV RNA level detected in HEK293T knocked out for VLDL-R (no assessment of the VLDL-R expression published). In contrast, they observed no increase in the infection in DLD1 cells overexpressing the receptor (cells with a low-level of LDL-R at their surface) (Table 6). With all these results, we cannot exclude that VLDL-R may interact with the apoE on CCHFV particles and help for the CCHFV – LDL-R interaction, and thus, facilitate the virus entry in LDL-R expressing cells.

### c. LRP1

Even if there are some differences between the three papers, they demonstrate that CCHFV does not require LRP1 for its entry. This observation is surprising since the virus uses apoE to bind its entry factor, and apoE is a common ligand for the core members of the LDL-R family, including LRP1.

Interestingly, LRP1 was identified as a receptor for other bunyaviruses such as La Crosse virus (LACV), OROV, RVFV and Sandfly fever Sicilian virus (SFSV) (Devignot *et al.*, 2023; Ganaie *et al.*, 2021; Schwarz *et al.*, 2022). Furthermore, when RVFV and Ebinur Lake Virus (EBIV; *Peribunyaviridae*) were tested for LDL-R usage, it was shown that both viruses do not require the receptor for their entry, suggesting that the viruses using LRP1 do not use LDL-R (Monteil *et al.*, 2024; Xu *et al.*, 2024). The use of two distinct receptors from the same family in the *Bunyaviricetes* class is interesting. We can hypothesize that the distinction is a result of the viral adaptation to different vectors which express different orthologues of LDL-R (lipophorin receptor for mosquitoes and vitellogenin receptor for ticks). Indeed, CCHFV is a tick-borne virus while RVFV, LACV, OROV, SFSV and EBIV are transmitted by mosquitoes.

Similar results were observed for alphaviruses. The Venezuelan equine encephalitis virus (VEEV) was shown to use LDLRAD3 (non-core member of LDL receptor family) but not LDL-R, VLDL-R or apoER2. In contrast, Getah Virus (GETV) and Eastern equine encephalitis virus (EEEV) were shown to enter through LDL-R, VLDL-R, apoER2 but not LDLRAD3. Interestingly, VEEV mainly circulates in mosquitoes and rodents, while GETV mainly infects cattle and horses (Wang *et al.*, 2024). These results prove that even closely related virus may have different entry factors, possibly a result of their adaptation to their hosts.

In the same study as cited above, the authors investigated the key residues of LDL receptors recognised by several alphaviruses (Wang *et al.*, 2024). They observed that key residues for GETV (infecting mainly mammals and few birds) interaction with LDL-R were well-conserved among mammals but differed in the avian orthologue. In contrast, the key residues for EEEV (infecting mainly birds and few mammals), are the ones conserved in the avian orthologue. This suggests that even for viruses using the same receptor, small differences between receptor orthologues can impact the host range.

	Xu et al., 2024			Monteil et al., 2024			Ritter et al., 2024		
	Virus	Producer cells	Assay	Virus	Producer cells	Assay	Virus	Producer cells	Assay
LDL-R	Authentic YL16070 strain	VeroE6	KO, OE in DLD1 cells, KD in LDLR KO cells	VSV-CCHFV, authentic IbAr10200 strain	HEK293T (VSV-CCHFV), SW-13	KO, competition assay, blocking with soluble LDL-R	CCHFV_tecVLPs, authentic IbAr10200 strain	Huh-7.5	Neutralisation, blocking with soluble LDL-R, OE
VLDL-R	Authentic YL16070 strain	VeroE6	KO, OE in DLD1 cells, KD in LDLR KO cells	VSV-CCHFV, authentic IbAr10200 strain	HEK293T (VSV-CCHFV), SW-13	Blocking with soluble VLDL-R	CCHFV_tecVLPs	Huh-7.5	OE
ApoER2	Authentic YL16070 strain	VeroE6	KO, OE in DLD1 cells, KD in LDLR KO cells	VSV-CCHFV (not confirmed in authentic IbAr10200 strain)	HEK293T	Blocking with soluble apoER2			
LRP1	Authentic YL16070 strain	VeroE6	KO, OE in DLD1 cells, KD in LDLR KO cells				CCHFV_tecVLPs	Huh-7.5	KD
LRP1B	Authentic YL16070 strain	VeroE6	KO, OE in DLD1 cells, KD in LDLR KO cells						
LRP2	Authentic YL16070 strain	VeroE6	KO, OE in DLD1 cells, KD in LDLR KO cells						

**Table 6: Summarised results from the Xu et al., Monteil et al., and Ritter et al..** The core members of the LDL receptors family tested in the three papers are summarised in this table. VSV-CCHFV: VSVΔG pseudotyped particles bearing the CCHFV GPs. DLD1 cells: colorectal adenocarcinoma expressing a low-level of LDL-R. KO: knockout. KD: knockdown. OE: overexpression. In green, the receptors that were shown in their respective paper to be a proviral factor for CCHFV entry. In red, factors that are not involved in the virus entry. In grey, factors that were not tested.

## B. Role of apolipoproteins in CCHFV infection

### 1. Incorporation onto particles

#### a. Incorporation during production or after secretion?

In the results presented above, I demonstrated that apoE increases CCHFV entry and that the protein was incorporated onto the particles. This observation was confirmed in (Monteil *et al.*, 2024) using hepatocytes knocked out for apoE expression (HepG2 ApoE KO) to produce CCHFV and anti-apoE antibody to neutralise the virus before infection. The incorporation of apoE could have happened after secretion of the particles, meaning that free apoE from hepatocytes (human in my case) or free apoE from the serum (bovine serum) could have been incorporated onto the particles.

For HCV, it was determined that HCV can incorporate apoE after secretion. In Bankwitz *et al.*, (2017), the authors incubated HCV particles with apoE enriched supernatant (from Huh-7.5 overexpressing apoE3) or control supernatant (from Huh-7.5 knocked down for apoE) before infection. They observed that the percentage of infectivity increased in a dose-dependent manner when particles are incubated with apoE enriched supernatant. To test this hypothesis with CCHFV, I tried to produce CCHFV\_tecVLPs from apoE-free cells (HEK293T), or from Huh-7.5 hepatocytes knocked down for apoE, in media without serum. The particles would then have been incubated either with human serum (with physiologic concentration of human apoE), with media from hepatocytes grown for 3 days in OptiMEM (to mimic the apoE secreted by the usual hepatocyte producer cells), or OptiMEM (apoE-free medium). Then after incubation, I would have infected Huh-7.5 and assessed the infectivity of the particles and done an anti-apoE neutralisation assay. If particles incubated with human serum or hepatocyte media showed a higher infectivity and/or an increase sensitivity to the anti-apoE antibody, it would have meant that apoE can be incorporated after secretion. In contrast, if the incubation with apoE-containing media did not improve CCHFV infectivity, it would have suggested that apoE incorporation happens during the production of CCHFV particles. However, at the time, I had experimental issues and was not able to observe any infectious particles from neither HEK293T nor Huh-7.5 apoE KD. Now that the issue has been solved, it would be interesting to attempt the experiment again.

In our paper, we assessed the incorporation of apoE onto CCHFV\_tecVLPs using electron microscopy (EM) and immunogold labelling with anti-apoE and anti-Gc, but we did not assess the incorporation of apoB. It would have been interesting to verify it since apoB requires the activity of the microsomal triglyceride transfer protein (an ER protein) to be incorporated onto LDL. If we validate the incorporation of apoB onto CCHFV virions, it will mean that the incorporation would happen in the ER during the production of the particles near to the assembly site, without excluding a possible incorporation after secretion for apoE.

However, it was also shown by Bio-layer interferometry using recombinant Gn and Gc and immobilised sLDL-R that Gc, but not Gn, can directly bind to the receptor with  $K_D = 42.6$  nM (IbAr10200 strain), which is comparable to the binding between VSV-G and LDL-R ( $K_D = 54.3$  nM) (Xu *et al.*, 2024). These results were confirmed in Monteil *et al.*, (2024) by competition assays using Gc and Gn to interfere with LDL binding to LDL-R, and prove that both interactions, through Gc or apoE can occur.

#### b. Linked lipoproteins or apoE incorporation?

Another mystery is that we do not know whether apoE is incorporated onto viral particles or whether total lipoproteins are linked to viral proteins, and if so, how (see Figure 39). It would be interesting to assess precisely the factors present onto CCHFV virions. To start, we could establish the density of authentic CCHFV particles produced from hepatocytes or apolipoproteins-free cells (HEK293T) using Iodixanol density gradients. Iodixanol was shown to preserve lipoprotein-virus complexes. We could assess in the different fractions the viral RNA load and the presence of different proteins such as viral Gc and NP proteins, and host factors, such as apoB, apoC, apoE, cholesterol and triglyceride. The presence of those factors and a concentration of the infectious particles in the low-density fraction would indicate an association with lipoproteins and not only apolipoproteins.

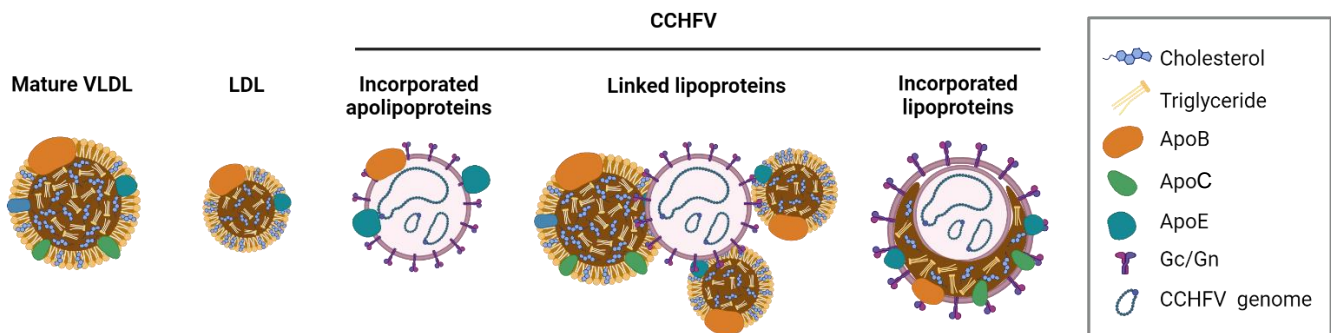


**Figure 39: Possible models of CCHFV particles, associated to apolipoproteins and/or lipoproteins.** CCHFV particles exact association with apolipoprotein remains unknown. Here, 3 models are proposed. The first model shows incorporation of only apolipoproteins. The second, complete lipoprotein non-covalently linked to the particles and the last, complete lipoprotein incorporated in the lipid bilayer of CCHFV particles. Created with BioRender.com.

While there is no study published to date on CCHFV, it was demonstrated on SARS-Co2 that the particles are associated to cholesterol through a binding to the S protein (Wei *et al.*, 2020). In the paper, the authors identified in the sequence of the S protein, cholesterol recognition amino acid consensus (CRAC) motifs adjacent to the inverted cholesterol recognition motif (CARC). CRAC is defined by the (L/V)-X1-5-(Y)-X1-5-(K/R) sequence, and CARC by the (K/R)-X1-5-(Y/F)-X1-5-(L/V) sequence. The close vicinity of both motifs suggests a high affinity, lipid specific, cholesterol-recognition (Di Scala *et al.*, 2017). Using the sequence of CCHFV IbAr10200 GPC (UniProt Q8JSZ3) and PROTTOR, I highlighted that the combination CARC-CRAC motifs was present 3-times in GP38, twice in Gn ectodomain and 4 times in Gc ectodomain (Figure 40). This suggests that an interaction with cholesterol, and maybe lipoproteins, is possible.

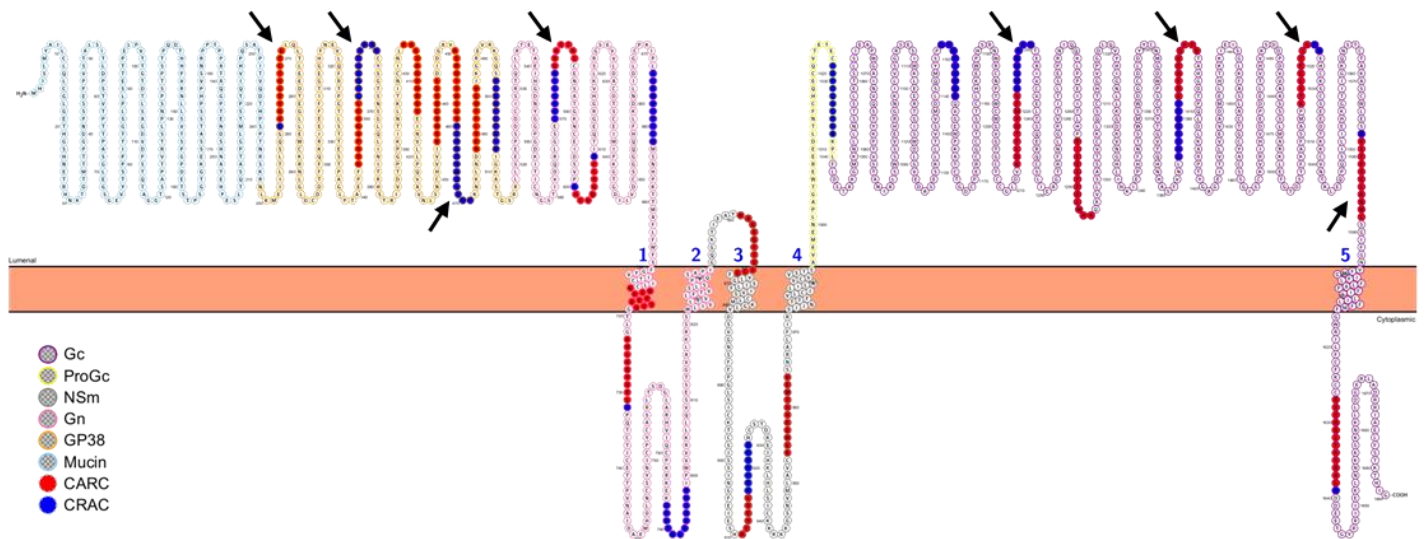


**Figure 40: Schematic representation of CCHFV IbAr10200 GPC and highlight on the CARC-CRAC motifs.** Sequence from UniProt Q8JSZ3 was represented on PROTTER. MLD sequence is represented in light blue, GP38 sequence in orange, Gn sequence in pink, NSm sequence in grey, Gc sequence in purple with the preGc in yellow. CARC motifs: (K/R)-X1-5-(Y/F)-X1-5-(L/V) in red and CRAC motifs: (L/V)-X1-5-(Y)-X1-5-(K/R) in dark blue. Dark arrows represent the sequences where CARC and CRAC motifs are in close vicinity, in the proteins ectodomains. Created with Protter.

## 2. Role of apolipoproteins in the production of CCHFV particles

Furthermore, using Huh-7.5 knocked down for apoE for the production of CCHFV\_tecVLPs, we observed a decrease of 2 log in the infectious titer and 1 log in the number of mgRNA in the supernatant compared to WT cells (Ritter *et al.*, 2024). We verified that the decrease in infectivity was not caused by a decrease in the transfection or expression of NP plasmid. However, we did not assess the fitness or viability of the Huh-7.5 LDL-R KD. Our results still suggest that apoE is involved not only in the entry of the virus but also in its production in hepatocytes, as it is the case for HCV (Chang *et al.*, 2007; Jiang and Luo, 2009). To gain more insight on the impact of apoE on the production of infectious particles, it would have been interesting to assess the intracellular infectivity in apoE knocked down cells. Indeed, the authors knocked down apoE, using siRNA, in HCV infected cells and observed a decrease of intracellular and extracellular vRNA. They also observed no changes in the capacity of HCV RNA to replicate, using a replicon assay, suggesting that the decrease observed in intracellular and extracellular RNA was the consequence of a production impairment.

It is important to note that production of CCHFV\_tecVLPs could be achieved in cells not expressing apoE (such as HEK293T) and without serum, meaning that the production is not



strictly dependant on apoE and can differ according to the producer cell type. Thus, the characterisation of the particle composition (lipids and apolipoproteins) described above would have to be done on hepatocytes and cells not producing lipoproteins. Moreover, it would be interesting to investigate the CCHFV particles produced in tick cell (detailed in Chapter IV.C.3). Indeed, since the viral membrane is acquired at the assembly site (ER / Golgi), it would make sense that the viral envelope depends on the host membrane properties. Thus, there could be different production possibilities. One independent of apoE in cells that do not express it, and the second incorporating the apolipoproteins, expressed at the assembly site, onto the particles and giving the virus some advantages, such as a broader tropism (described in the following section).

### 3. Impact of apolipoproteins incorporation

#### a. Cell-cell transmission

Another possible effect of the incorporation of apolipoproteins for the virus is to increase its ability to perform cell-to-cell transmission. Indeed, it was demonstrated for HCV that apoE plays a role in the transmission of the virus (Hueging *et al.*, 2014). The authors used Huh-7.5 cells, or 293T cells expressing apoE or not, to produce HCV by transfection with the HCV Jc1 RNA (genome allowing a production of HCV infection particles with high titers). Then, these cells were mixed with fresh Huh-7.5 containing a reporter tagRFP, fluorescent upon infection. The cell mixture was overlaid with medium containing agarose and neutralising HCV AR4A antibody. In this setting, the authors are blocking the possibility of released particles to infect cells. However, in this experiment, they still observed a spread of the infection, but only in Huh-7.5 or 293T expressing apoE, suggesting a cell-to-cell transmission allowed by the presence of apoE. However, the percentages are low (1 to 3 % of cell-to-cell spread), and were not reproduced in (Fauvelle *et al.*, 2016). The increase of the cell-cell transmission can be explained by the production of extracellular vesicles (formed from apoE-containing lipoproteins), which were shown to contain HCV viral RNA, and appear to be transmitted to neighbouring cells (Bukong *et al.*, 2014; Dreux *et al.*, 2012; Pham *et al.*, 2023). We can hypothesize that CCHFV RNA may be packaged in extracellular vesicles in a similar manner and thus, apoE would increase the transmission to nearby cells.

### b. Hiding CCHFV epitopes

In HCV, it was also shown that the apoE could hide the virus epitopes and increase the virus resistance to neutralising antibodies. Indeed, after addition of secreted apoE on HCV Jc1 supernatant, Hueging *et al.*, (2014) incubated the virus with several monoclonal neutralising antibodies targeting E1 and E2. The authors observed a 10 fold increase of the half-maximal inhibitory concentration. The impact of apoE was also observed in Fauvelle *et al.*, (2016). The authors observed that viruses produced from apoE-depleted hepatocytes were 4-17 times more sensitive to neutralisation by patient sera than virus produced by WT cells. Sensitivity to neutralisation was almost totally restored in virus produced in apoE-depleted but rescued cells (transduced to produce apoE). Interestingly, the authors did not observe an effect of apoB in the neutralising antibody escape, supporting a central role of apoE in the immune escape. These experiments done on HCV could be reproduced on CCHFV in order to assess the role of apoE in the immune escape and thus, opening the possibility for new treatments targeting the apolipoproteins.

### c. Indirect treatments against CCHFV

The incorporation of apolipoproteins onto the particles, the possible incorporation of cholesterol and the effect of both during the production of CCHFV could lead to new therapeutic treatments. Indeed, drugs were developed for people having well characterised diseases, such as familial hypercholesterolemia or diabetes that could be used for CCHFV infected people. If indeed cholesterol is involved in CCHFV infectivity, then targeting its synthesis or its uptake could decrease the virus infection.

Statins are inhibitors of the 3-hydroxy-3-methyl-glutaryl-coenzyme A reductase required for the cholesterol synthesis and allow to reduce the cholesterol concentration in the blood. This drug was tested for its effect on HCV and Dengue virus notably. *In vitro*, the treatment was shown to decrease the level of intracellular RNA by interfering at the assembly step (Delang *et al.*, 2009; Martínez-Gutierrez *et al.*, 2011; Moriguchi *et al.*, 2010). However, no strong evidence of the anti-viral effect was observed *in vivo* (Whitehorn *et al.*, 2016).

The cholesterol uptake can also be targeted. Ezetimibe is a commercialised drug known to inhibit the internalisation of the cell surface cholesterol-sensing receptor NPC1L1 (Chang and Chang, 2008). Ezetimibe was shown to decrease HCV and HBV internalisation and thus their infectivity *in vitro* (Lucifora *et al.*, 2013; Sainz *et al.*, 2012). Here again, the clinical evidence is weak. It was however demonstrated that uninfected transplant recipients receiving organs from HCV-infected donor, and treated with Ezetimibe, had a lower viral load and, combined with other drugs (glecaprevir-pibrentasvir), could prevent the establishment of a chronic infection (Azhar *et al.*, 2021; Feld *et al.*, 2020).

Finally, apoB, the apolipoprotein required for LDL formation, could be targeted. This can be achieved by silencing its mRNA with mipomersen, an antisense inhibitor of apoB shown to decrease secretion of LDL safely (Neely and Bassendine, 2010; Raal *et al.*, 2010). It can also be done by inhibiting the MTP activity with drugs such as lomitapide also used to treat familial hypercholesterolemia (Larrey *et al.*, 2023).

Should they exhibit an anti-viral effect against CCHFV, these inhibitors, as they are already clinically tested and commercialised, could be a faster way to bring a treatment to the market.

### C. Relevance in non-human hosts

In the previous chapters, I described the possible receptors and co-factors involved in the dissemination in human cells. However, CCHFV infects a wide range of hosts and during my PhD I observed a different pattern in bovine cells, suggesting that CCHFV requires specific entry factors depending on the host. In the following section, I will replace my results in a more global context.

#### 1. Murine hosts

In Xu *et al.*, (2024), the authors validated the role of LDL-R in LDL-R-deficient mice that were also suppressed for the type I IFN response with anti IFNAR1 antibody (the precise mice used

is not described). Mice knocked out for LDL-R had a better survival compared to WT mice (70% and 10%, respectively). This suggests that in mice, LDL-R is a proviral entry factor for CCHFV. The authors supported their results by quantification of the viral genome in different organs, such as liver and spleen, as well as in the serum, where they observed a decrease of 1 to 3 log, between the KO and the WT, at day 5 post-infection. Moreover, they treated WT C57BL/6 mice (pre-treated with anti-IFNAR1 antibody) with an anti-LDL-R antibody, 1 day before, at the time of infection and up to 4 days after infection and observed a survival rate of 100% (against 20% for mock treated mice). In Monteil *et al.*, (2024), the authors also used mice knocked out for LDLR (B6.129S7Ldlrm1Her/J), but they only observed 15% survival (against 0% for WT mice), 5 days post-infection. The differences between the two mice experiments can be explained by the fact that in Monteil *et al.*, (2024), the authors injected a higher viral dose per mouse of a different strain. These results demonstrate that LDL-R is a proviral factor not only in humans but also in mice.

## 2. Bovine hosts

However, this effect was not observed in bovine cells. As previously described, we did not observe any inhibition of CCHFV\_tecVLPs infection when bovine cells were incubated with the anti-LDL-R neutralising antibody. This can be due to the antibody I used. AF2148 is an antibody produced in goat immunised with human LDL-R antigen, and it is possible that it does not recognise the bovine LDL-R with sufficient affinity to block CCHFV\_tecVLPs entry into bovine cells. However, Apoorv Gandhi obtained preliminary data where he neutralised CCHFV\_tecVLPs using anti-apoE antibodies or soluble LDL-R and observed no inhibitory effect on the bovine cells, contrary to the human cells.

Thus, it is possible that CCHFV does not rely on LDL-R in bovine cells and uses a different entry pathway. It was indeed suggested that the virus could spread more efficiently by cell-to-cell transmission in bovine cells compared to human cells, and more efficiently by cell-free transmission in human cells compared to human cells (Földes *et al.*, 2020). In the paper, it was described that in human kidney cells, the copies of viral RNA increased over time intracellularly and extracellularly, suggesting an efficient replication and release of viral particles in the media. However, it was not the case in bovine cells that showed a slight

increase intracellularly, but no changes extracellularly, suggesting a low replication rate and no detectable release. Moreover, the authors infected both human and bovine cells and did a staining against CCHFV (using human antiserum) at day 1, 2, 3, 5, and 7 post-infection to observe the infected cells. In this experiment, they observed that infected bovine cells formed islet-like cell clusters, meaning that the infected cells are in close contact with each other, contrary to infected human cells, which were more spread. These two experiments suggest that the virus do not use the same transmission pathway in both hosts and so, may have different co-factors of entry.

Finally, CCHFV may acquire host factors, such as apoE during its production, giving the virus a certain host specificity. In our case, the production of CCHFV\_tecVLPs used for the blocking experiment in bovine cells was from human hepatocytes. It would have been interesting to produce CCHFV\_tecVLPs in bovine cells and use them for the blocking experiment in bovine and human cells. During my PhD, I did try to use EBL and MDBK as producer cells, but I did not reach a transfection level sufficient to observe a production of infectious particles. This could have been improved by optimising the transfection by testing different reagents or methods (such as microporation) and assessing the supernatant for its infectivity at different time after transfection.

### 3. Ticks, main vector of CCHFV

The involvement of human LDL-R in CCHFV entry and dissemination is now demonstrated but it would be interesting to assess its involvement in the main vector of the virus, the tick. Indeed, ticks are evolutionary distant from humans. The LDL-R-encoding gene is not conserved in ticks, and they are cholesterol auxotroph, meaning that they do not produce cholesterol. However, ticks express LDL-type-A-repeat-containing proteins, such as the vitellogenin receptor (VtgR) (Figure 41) (Seixas *et al.*, 2018), and take their cholesterol from their blood meal. VtgR expression in tick seems to be species-, sex- and tissue-specific, being more expressed in the ovaries of mated ticks (Mitchell *et al.*, 2007), which is one of the organs where the virus replicates (Dickson and Turell, 1992). It would be interesting to study

the impact of VtgR for CCHFV replication cycle, by modulating its RNA expression with RNA interference (as it was done in Mitchell *et al.*, (2007)).

In Monteil *et al.*, (2024), the authors produced CCHFV in tick cells and incubated the particles with a soluble LDL-R or a soluble apoER2. They observed an inhibition of the infection only when they used soluble LDL-R. They suggested that particles produced by tick cells do not incorporate apoE and thus, would not bind to apoE receptors, such as apoER2. In this experiment, it would have been interesting to assess the level of apoE in the supernatant (by ELISA for example) to be sure that tick cells do not secrete apolipoproteins.

The identification of the VtgR/Vtg role in CCHFV replication in ticks could lead to the development of an anti-tick approach targeting Vtg or using recombinant VtgR. This vaccine could deliver soluble VtgR that would inhibit the virus entry and block the virus transmission.

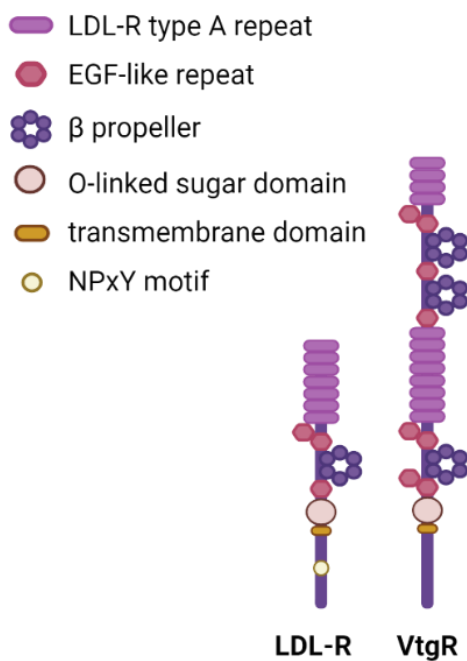


*Figure 41: Comparison of LDL-R and VtgR structures. Created with BioRender.com.*

## Chapter V. General conclusion

Throughout this manuscript I was able to gain more insight on CCHFV entry. At the time I started my PhD, no entry receptor was identified and characterised for the virus. Using CCHFV\_tecVLPs but also the WT virus, I demonstrated that LDL-R was an entry factor for the virus.

The impact of LDL-R was demonstrated on several human cell lines (rhabdosarcoma, hepatocytes, lung epithelial) and more important on primary cells (PHH). However, LDL-R does not seem to be involved in CCHFV entry in bovine cells. This can be explained by different ways of entry and cellular transmission, involving other factors.

Then, using a retrograde transport inhibitor, I showed that LDL-R was involved in the binding and the endocytosis of CCHFV.

Furthermore, I was able to better characterise the virus interaction with its co-factor of entry. Using neutralising antibodies targeting apoE, I highlighted the involvement of the apolipoprotein in the virus entry. Then by co-immunoprecipitation, I showed that apoE, is incorporated onto the particles. These results suggest that apolipoproteins are incorporated during production but can also be incorporated after secretion in the extracellular media, and could mediate the interaction with the receptors, such as described for HCV. However, these results do not exclude a possible direct interaction with LDL-R. This results open new possibilities for therapeutic treatments.

An important point to consider is that the results that I presented indicate that LDL-R is not the sole entry factor for CCHFV. Indeed, the total inhibition was never achieved. This suggest that other factors can be involved in the entry and are still to be identified, maybe by high-throughput screening.

Finally, while we were in the reviewing process of our paper, two papers were published that corroborate my findings. Together, these publications showed that LDL-R is an important entry factor for CCHFV, which interacts with the receptor either through Gc or through apoE incorporated onto the particle. The papers also indicate that LDL-R is not the only factor involved and that more research is still required to understand CCHFV entry and infection.

These findings are summarised in Figure 42.

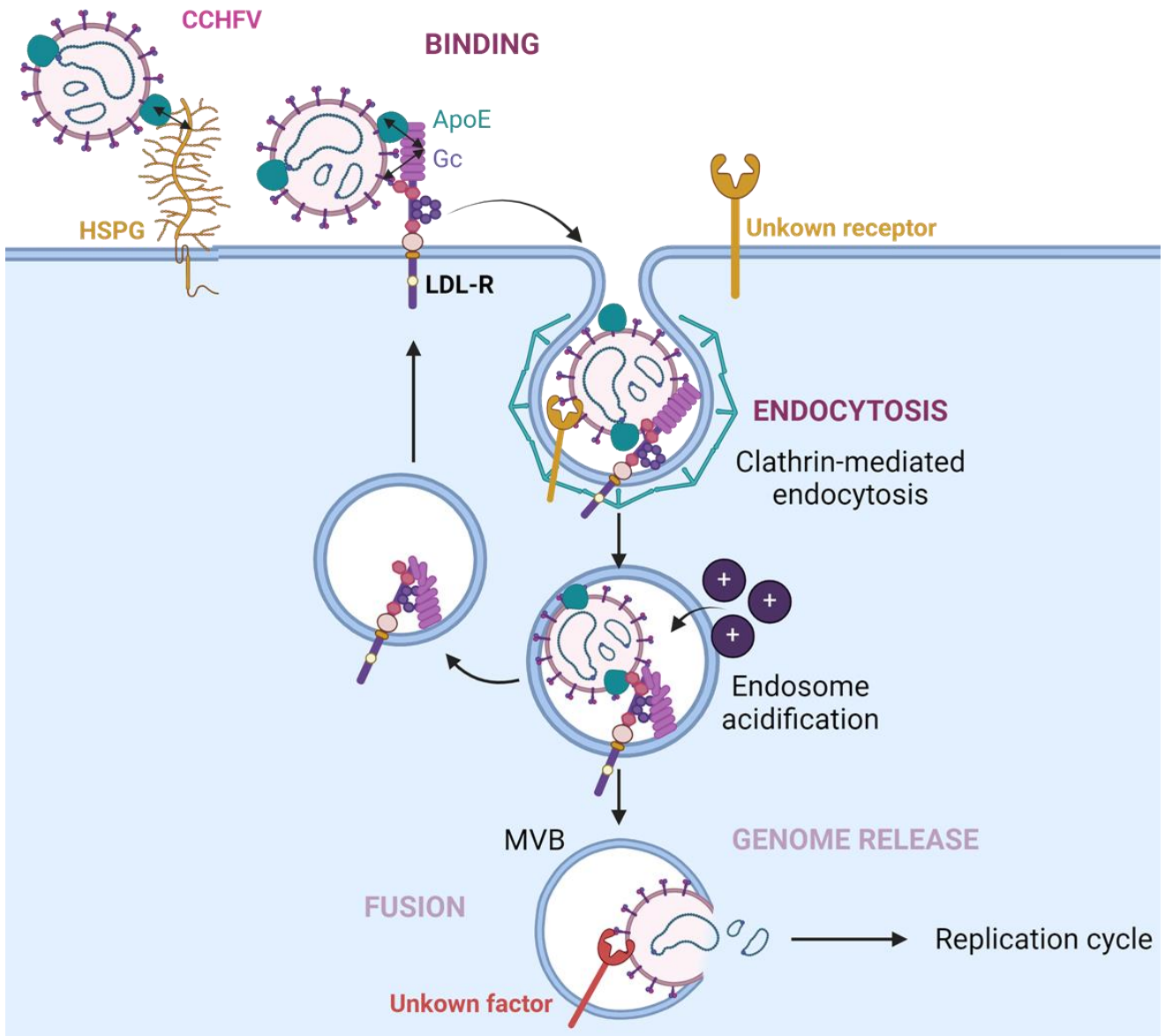


**Figure 42: Schematic representation of the factors involved in CCHFV entry into human cells.** CCHFV particles binds to LDL-R through interaction with CCHFV Gc or through apoE incorporated onto the particle. The apoE associated may also mediate the binding to HSPG, involve in the weak attachment. Once bound to LDL-R, CCHFV is internalised, and upon endosome acidification, the viral genome is released into the cytoplasm, where the replication cycle can start. In parallel, LDL-R is recycled to the cell surface. During CCHFV entry, some unknown factors can be involved in the binding, the endocytosis, and the fusion that are still to be identified. Created with BioRender.com.





## Chapter VI. Material and methods

### Cells.

Huh-7.5 cells (kind gift from Charles Rice), HEK-293T kidney cells (ATCC CRL-1573), TE-671 cells (ATCC CRL8805), A549 cells (kind gift from P. Boulanger), VeroE6 cells (ATCC CRL-1587), EBL cells (kind gift from Fabienne Archer), MDBK cells (European Collection of Authenticated Cell Cultures) were grown in Dulbecco's modified minimal essential medium (DMEM, Invitrogen, France) supplemented with 100U/mL of penicillin, 100µg/mL of streptomycin and 10% of foetal bovine serum. PHH (BD Biosciences) were centrifuged in F12-HAM medium (Sigma Aldrich) and seeded overnight in collagen-coated plates in BD Gentest seeding medium supplemented with 5% FBS. PHH were washed 16h later and cultured with a culture medium for PHH (DMEM F12, Sigma Aldrich) supplemented with 10% FCS, 1 µg/mL bovine serum albumin, 5 µg/mL bovine insulin,  $1 \times 10^{-6}$  M Dexamethasone (Sigma Aldrich),  $1 \times 10^{-8}$  M 3,3,5-triiodo-L-thyronin, 5 µg/mL apotransferrin, 1% of non-essential amino acids (Gibco), 1% of Glutamin (Gibco) and 1% Penicillin-Streptomycin solution (Gibco).

### Plasmids.

The constructs encoding WT CCHFV strain IbAr10200 L polymerase (pCAGGS-V5-L), NP nucleoprotein (pCAGGS-NP), M segment (pCAGGS-M), T7 RNA polymerase (pCAGGS-T7), NanoLuc luciferase (NLuc)-expressing minigenome flanked by L NCR under the control of a T7 promoter (pSMART-LCK\_L-Luc), GFP expressing minigenome flanked by L 5' and 3' UTRs under the control of a T7 promoter (pT7\_vL\_GFP), and an empty vector (pCAGGS) were described previously (Bergeron *et al.*, 2010; Devignot *et al.*, 2015) (all kind gifts from Friedemann Weber and Eric Bergeron). psPAX2, phCMV-G (kind gifts from Didier Trono and Jane Burns, respectively), and phCMV\_HIV\_GFP were used for VSV pseudoparticles production. psPAX2, phCMV\_HIV\_GFP and phCMV-4070A (Sandrin *et al.*, 2002) were used for MLV pseudoparticle production. pFK-JFH1/J6/C-846\_Δp7, constructed from pFK-JFH1/J6/C-846 by deletion of p7 and addition of EMCV IRES between E2 and NS2, and phCMV-noSPp7(J6) were used for HCVtcp production. pMK-RQ-HAZV resQ S EGFP P2A, pMK-RQ-HAZV M, pMK-RQ-HAZV L (kind gift from John N. Barr) were used for production of rescued HAZV rHAZV-eGFP. For the down-regulation assays, TRC1\_pLKO\_shapoE

(TRCN0000010913; Sigma-Aldrich) was used for generation of lentivirus in combination with phCMV-G and psPAX2.

**Antibodies.** See table below:

*Table 7: List of the antibodies.*

Primary antibodies		
Targets	Dilution	Company (catalog number)
NCL (mouse)	Blocking assay 1-4µg/mL	Santa Cruz (sc-8031)
LDL-R (goat)	IF 20mg/mL; FACS 40mg/mL; WB 2mg/mL; blocking assay 0.25-1-4µg/mL	R&D systems (AF2148)
apoE (goat)	IP 10mL	Sigma-Aldrich (AB947)
apoE (goat)	WB 1:2000; EM 1:100; neutralization assay 1:200-1:100-1:50; FACS 1:2000	AbD Serotec (AHP2177)
Actin (mouse)	WB 1:10000	Sigma-Aldrich (AC-74)
CCHFV Gc 11E7 (mouse)	WB 1:1000	BEI Resources (NR-40277)
CCHFV NP 9D5 (mouse)	WB 1:1000	BEI Resources (NR-40277)
CCHFV NP 2B11 (mouse)	Immunostaining 1:250	BEI Resources (NR-40257)
HCV NS5A 9E10 (mouse)	Immunostaining 1:800	Kind gift from C. Rice
HAZV NP (sheep)	WB 1:3000	Kind gift from J.N.Barr
Goat IgG	FACS 40ug/mL; blocking assay 0.25-14ug/mL	ThermoFisher (02-3636202)
Goat serum	neutralization assay 1:200-1:100-1:50	Viomed (79S094)
Secondary antibodies		
Donkey anti-mouse Alexa Fluor 555	IF 1:2000	ThermoFisher (A-31570)
Donkey anti-goat Alexa Fluor 488	IF 1:2000	ThermoFisher (A-11055)
Goat anti-Mouse-HRP	Immunostaining (HCV) 1:1000	Sigma-Aldrich (A4416)
Anti-Mouse IgG (whole molecule)-Peroxidase antibody	Immunostaining (CCHFV) 1:1000	Sigma-Aldrich (A5278)
Goat F(ab') <sub>2</sub> Anti-Mouse Ig, Human ads-APC	FACS 1:100	Southern Biotech (1012-11)
F(ab') <sub>2</sub> -Donkey anti-Goat IgG (H+L), PE	FACS 1:100	ThermoFisher (31860)
Anti-Goat IgG, FITC	FACS 1:100	Dako (F0250)
IRDye® 680RD Donkey antiMouse IgG	WB 1:10000	Li-COR Biosciences (926-68072)
IRDye® 800CW Goat antiMouse IgG	WB 1:10000	Li-COR Biosciences (926-32210)
IRDye® 800CW Donkey antiGoat IgG	WB 1:10000	Li-COR Biosciences (926-32214)

### **Production of viral stocks and infection assays with authentic WT CCHFV particles.**

All the experiments with authentic WT CCHFV were performed in the Jean Mérieux BSL-4 facility in Lyon, France. To produce viral stocks, Huh-7.5 cells were infected using CCHFV isolate IbAr10200 (obtained from Institut Pasteur) at MOI 0.01 and the production was harvested at 72h post-infection. Infectious titers were determined by NP immunostaining on VeroE6 cells using anti-NP (2B11) as primary antibody and viral preparations with titers ranging between  $3 \times 10^5$ - $10^6$  NP FFU/ml were used in this study.

For blocking and neutralisation assays, infections were performed with serial dilutions of viral stocks, corresponding to MOIs of 0.5 to 0.001. Viral stocks or cells were treated as described below. 24h post-infection, infected cells were lysed with TRIzol™ (ThermoFisher), allowing inactivation of virus, and RNAs were extracted according to manufacturer's protocol and level of viral RNA, reflecting the level of infection, was determined by RT-qPCR (see below). The viral titer was determined after selection of dilutions allowing a linear range of viral RNA signal.

### **Production of viral stock and infection assays with CCHFV\_tecVLPs.**

For production of tecVLPs, Huh-7.5 cells were transfected in 10cm dishes with 3.6 µg of pCAGGS-V5-L, 1.2 µg of pCAGGS-NP, 3 µg of pCAGGS-M or pCAGGS, 3 µg of pCAGGS-T7 and 1.2 µg of pSMART-LCK\_L-Luc (for NLuc\_tecVLP) or pT7-GFP (for GFP\_tecVLP), using GeneJammer transfection reagent (Agilent). Six hours post-transfection, cells were washed two times with OptiMEM before addition of OptiMEM. At 72h post-transfection, supernatant was harvested and filtered through a 0.45µm filter. Preparations of tecVLPs with titers of  $5 \times 10^5$  GFP infectious unit./ml (for GFP\_tecVLP) or  $10^8$  RLU/ml (for NLuc\_tecVLP) were used in this study.

For assays with GFP\_tecVLPs, targets cells were pre-transfected using 2.4 µg of pCAGGS-V5-L and 4.8 µg of pCAGGS-NP using GeneJammer transfection reagent. Cells were seeded in 24, 48 or 96-well plates in OptiMEM 6h post-transfection. Then, 24h post-transfection, cells were infected with serial dilutions of particles, corresponding to MOIs of 2 to 0.02, and 48h post-infection, infected cells were harvested. For each dilution, technical replicates were performed. Infected cells were fixed and the percentage of GFP positive cells was assessed

by flow cytometry (MACSQuant® VYB Flow Cytometer; Miltenyi Biotec). Data were analysed with FlowJo software (BD Biosciences). The viral titer was determined after selection of dilutions within the linear range of percentages of positive cells.

For assays with tecVLPs with a NLuc minigenome, the infection with serial dilutions of viral supernatant, corresponding to RLU-per-cell of 100 to 0.01, was done on Huh-7.5 cells stably expressing firefly luciferase (FLuc) and the level of infection was quantified 24h post-infection, by lysing the cells with passive lysis buffer (Promega) for 10min at room temperature and measurement of luciferase signal using Nano-Glo® Dual-Luciferase® Reporter Assay System (Promega). For each dilution, technical replicates were performed. The viral titer was determined after selection of dilutions within a linear range of NLuc signals.

For intracellular and extracellular infectivity assays used for stability of CCHFV\_tecVLPs particles and Gn and Gc mutants: Intracellular tecVLPs were released upon producer cells lysis by three repeated freeze-thaw cycles, followed by clarification by centrifugation. Extracellular particles were produced as described previously. At 24h post-infection, infected cells were fixed and the percentage of GFP positive cells was assessed by flow cytometry (MACSQuant® VYB Flow Cytometer; Miltenyi Biotec). Data were analysed with FlowJo software (BD Biosciences).

### **Production and infection assays with HAZV particles.**

For production of viral stocks, rHAZV-eGFP virus (Fuller *et al.*, 2020) was amplified in Huh-7.5 cells (MOI=0.001). At 1h post-infection, the medium was changed after a PBS wash and 72h post-infection, the supernatant was harvested and clarified by centrifugation 5min at 750xg. Preparations of rHAZV-eGFP (termed HAZV in the text and figures) with titers of 10<sup>6</sup> eGFP i.u./ml were used in this study. For infection assays, Huh-7.5 cells were inoculated with serial dilutions of viral supernatant, corresponding to MOIs of 0.5 to 0.001, before PBS wash and medium change, 1h post-infection. Level of infection was detected 16h post-infection by quantification of eGFP positive cells by flow cytometry (MACSQuant® VYB Flow Cytometer; Miltenyi Biotec). Data were analysed with FlowJo software (BD Biosciences). The viral titer was determined after selection of dilutions allowing a linear range of percentage of positive cells.

### **Production and infection assays with HCV *trans*-complemented particles (HCVtcp).**

For production of viral stocks, Huh-7.5 cells were electroporated with 2µg of phCMV-noSPp7 DNA and 10µg of Jc1 Δp7 *in vitro* transcribed RNA as described previously (Denolly *et al.*, 2019). Media was changed 6h post-electroporation and supernatant was harvested and filtered (0.45µm) 72h later. Preparations of HCVtcp with titers of 10<sup>3</sup> NS5A FFU/ml were used in this study.

For infection assays, Huh-7.5 cells were inoculated with serial dilutions of viral supernatant, corresponding to MOIs of 2 to 0.02, and were fixed using ethanol 48h post-infection and focus-forming units were determined by counting NS5A immunostained foci. The viral titer was determined after selection of dilutions allowing a linear range of foci.

### **Production and infection assays with VSV or MLV pseudoparticles.**

Retroviral vectors encoding GFP sequence and bearing VSV-G (VSVpp) or amphotropic MLV Env glycoprotein (MLVpp) were produced in HEK-293T cells by transfection of phCMV\_HIV\_GFP, psPAX2 and phCMV-G or phCMV-4070A using calcium phosphate precipitation. The medium was replaced 16h later and the supernatant was harvested and filtered (0.45µm) 24h later. Preparations of VSVpp and MLVpp with titers of 2x10<sup>6</sup> and 6x10<sup>5</sup> GFP i.u./ml, respectively, were used in this study.

For infection assays, Huh-7.5 cells were infected with serial dilutions of viral supernatants, corresponding to MOIs of 2 to 0.02, and were fixed 48h post-infection. The percentage of GFP positive cells was assessed by flow cytometry (MACSQuant® VYB Flow Cytometer; Miltenyi Biotec). Data were analysed with FlowJo software (BD Biosciences). The viral titer was determined after selection of dilutions allowing a linear range of percentage of positive cells.

### **Blocking with anti-NCL antibody.**

Huh-7.5 cells were grown in DMEM, 10%FCS and incubated with 1 or 4 µg/mL of anti-NCL (mouse), and 4 µg/mL of anti-LDL-R (goat), control IgG mouse and goat for 1h at 37°C. Then the viral inoculum was added to cells in presence of antibodies, and the medium was

replaced with DMEM, 10% FCS, 3h post-infection. The experiment was performed with serial dilution of viral supernatants. For NLuc\_tecVLPs or lentiviral pseudoparticles, cells were harvested 48h post-infection and the level of infection was quantified by lysing the cells with passive lysis buffer (Promega) and measuring the of luciferase signal using the Nano-Glo® Luciferase Assay System (Promega). Viral titers were determined as described above.

### **Blocking with anti-LDL-R antibody.**

All cell lines were grown in OptiMEM and were incubated with different doses of anti-LDL-R or control IgG for 1h at 37°C. Then the viral inoculum was added to cells in presence of antibodies, and the medium was replaced with DMEM, 10% FCS, 3h post-infection. All experiments were performed with serial dilution of viral supernatants. For GFP\_tecVLPs or retroviral pseudoparticles, cells were harvested 48h post-infection, and the level of infection was determined by flow cytometry and titers were obtained as described above; for authentic virus, cells were harvested 24h post-infection and infectious titers were determined by RT-qPCR as described above; for HAZV, cells were harvested 16h post-infection and infectious titer was determined by flow cytometry as described above. When testing different cell lines (EBL, MDBK, A549, TE-671), cells were infected with NLuc\_tecVLPs, and the level of infection was quantified 48h post-infection, by lysing the cells with passive lysis buffer (Promega) and measurement of luciferase signal using Nano-Glo® Luciferase Assay System (Promega). Viral titer was determined as described above. For analysis of incubation kinetics, Huh-7.5 cells were incubated with LDL-R antibody either 1h before infection, at the time of infection or 2h, 4h, 6h post-infection. The antibody-containing medium was replaced by fresh medium at 2h or at 24h post-infection depending on the conditions. Cells were harvested at 48h post-infection, and the viral titers were determined after detection of positive cells by flow cytometry as described above.

For infection of PHH, at 24h post-seeding, cells were washed and incubated in their culture medium, with different doses of anti-LDL-R or control IgG for 1h at 37°C before infection with serial volumes of NLuc\_tecVLPs in presence of antibodies. Then, 3h post-infection, the medium was changed, and the level of infection was assessed 24h post-infection, as described above.

### **Neutralisation assays with sLDL-R or anti-apoE antibody.**

Serial dilutions of inoculate were incubated for 1h at room temperature with different doses of soluble LDL-R (sLDL-R), CD81\_6His\_LEL, anti-apoE serum, or control goat serum and then added to Huh-7.5 cells grown in OptiMEM. All the infections were performed with serial dilutions. At 3h post-infection, the medium was replaced with DMEM, 10% FCS. For GFP\_tecVLPs or retroviral pseudoparticles, cells were harvested 48h post-infection and the level of infection was determined by flow cytometry and the viral titers were determined as described above; for WT CCHFV virus, cells were harvested 24h post-infection and the level of infectivity was determined by RT-qPCR as described above. For HAZV, infected cells were harvested 16h post-infection and the level of infectivity was determined by flow cytometry. For HCV, cells were fixed 48h post-infection and level of infectivity was determined by immunostaining as described above.

### **Cell surface staining of LDL-R.**

For flow cytometry, cells were washed and detached with Versene (Invitrogen), before fixation with 2% paraformaldehyde (Sigma-Aldrich) for 15min. Cells were then incubated for 1h at 4°C with primary anti-LDL-R antibody (AF2148) or control isotype at 40µg/mL in PBS + 2% FCS, with regular shaking. After 3 washes, cells were incubated with secondary antibody for 1h at 4°C in PBS + 2% FCS, with regular shaking. After 3 washes, cells were resuspended in PBS +2% FCS and analysed by flow cytometry (MACSQuant® VYB Flow Cytometer; Miltenyi-Biotec).

### **Live imaging analysis.**

Cells were seeded on µ-slide 8 wells IbiTreat (IBIDI) and treated according to the description. Live imaging analysis were performed using AxioObserver Z1 (Zeiss) equipped with a 20X objective and a CSU-X1 confocal spinning disk head (Yokogawa) under controlled atmosphere (37°C, 5% CO<sub>2</sub>). Multiple fields were defined, and image acquisition was performed on 5 Z-stacks (2µm) at intervals of 5 minutes for 3h. To measure the fluorescence, a max intensity projection of the Z-stacks was performed. Then, for each time-point, the mean intensity was calculated using FIJI software.



### **Co-immunoprecipitation assay.**

CCHFV\_tecVLPs were incubated with apoE antibodies (AB947; Sigma-Aldrich) or control goat IgG overnight at 4°C. Then 1.5 mg of Dynabeads protein G magnetic beads (ThermoFisher) were added during 1h at room temperature. The beads were then washed 3 times with PBS. For the elution, beads were resuspended in TriReagent and the supernatant was transferred into a new tube for RNA extraction, following the manufacturer's protocol before determination of the level of co-captured CCHFV minigenome by RT-qPCR (see below).

### **Detection of viral genomes by RT-qPCR.**

After extraction following the manufacturer's protocol, RNA was reverse transcribed (iScript cDNA synthesis kit; Bio-Rad). In the case of tecVLPs samples, RNA was treated with DNase (Invitrogen) according to the manufacturer's protocol. The level of cDNA was then quantified by qPCR. For tecVLPs minigenome, the quantification was done by detection of the NLuc minigenome for CCHFV: 5'-TAGTCGATCATGTTCGGCGT-3' and 5'-ACCCTGTGGATGATCATCACT-3' with 5'-GATTACCAGTGTGCCATAGTGCAGGATCAC-3' as a probe, using TaqMan™ Gene Expression Master Mix (ThermoFisher). For WT CCHFV, the quantification was done using FastStart Universal SYBR (Roche) with the following primers 5'-CCCCACACCCCAAGATAATA-3' and 5'-ACTACTCTGCATTCTCCTCA-3' targeting the L UTR.

For titration of WT CCHFV, viral RNA levels were normalised with respect to glyceraldehyde-3-phosphate dehydrogenase (GAPDH) RNA levels, detected using FastStart Universal SYBR (Roche) and specific primers 5'-AGGTGAAGGTCGGAGTCAACG-3' and 5'-TGGAAGATGGTGATGGGATTC-3'.

As an internal control of extraction, an exogenous RNA from the linearised Triplescript plasmid pTRI-Xef (Invitrogen) was added into the supernatant prior to extraction and quantified with specific primers (5'-CGACGTTGTCACCGGGCACG-3' and 5'-ACCAGGCATGGTGGTTACCTTTGC-3'). This signal was used for normalization of signal for crude supernatant, as well as capture and IP assays.

All analyses were done on a Quantstudio real-time PCR apparatus.

### **Drug treatment.**

For TyrA23, three different protocols were used. For a short treatment, Huh-7.5 cells pre-transfected with NP and L expression plasmids were treated with DMSO and TyrA23 (100 $\mu$ M) and infected 30min later with GFP\_tecVLP in the presence of fresh drug. The medium was removed 3h p.i. and the cells were harvested at 24h p.i. for determination of the levels of infection by flow cytometry. For long-treatment, Huh-7.5 cells pre-transfected with NP and L expression plasmids were treated for with DMSO or TyrA23 (100 $\mu$ M) and infected 24h later with GFP\_tecVLP. Media was removed 3h p.i. and the cells were harvested at 24h p.i. for determination of the levels of infection by flow cytometry. For long-treatment with addition of fresh drug, Huh-7.5 cells pre-transfected with NP and L expression plasmids were treated with DMSO or TyrA23 (100 $\mu$ M) for 24h before GFP\_tecVLP infection, with addition of fresh drug or DMSO. Media was removed 3h p.i. and the cells were harvested at 24h p.i. for determination of the levels of infection by flow cytometry. Cell viability was assessed at the time of harvesting, as described below, while level of LDL-R at cell surface was assessed at the time of infection.

### **Cell viability measurement.**

The cell viability was assessed using Cytotox-Glo Cytotoxicity Assay (Promega) according to the manufacturer's protocol.

### **Down-regulation of apoE.**

Lentiviral vectors expressing shRNA targeting apoE or control shRNA were produced in HEK-293T cells. Huh-7.5 cells were transduced with lentiviral vector. Cells were transfected with plasmid allowing tecVLPs production 24h post-transduction. Then, 72h post-transfection, supernatants were harvested and used for infectivity and RNA level assessment. The level of down-regulation was checked by apoE intracellular FACS staining. Cells were fixed and permeabilised with Cytofix/CytoPerm (BD Biosciences) according to manufacturer instructions. Cells were incubated with primary antibody (AHP2177, 1/2000) diluted in Perm/Wash buffer (BD Biosciences) for 1h at 4°C with regular shaking. After three washes with Perm/Wash buffer, cells were incubated for 1h at 4°C with secondary antibody. Cells

were washed three times with Perm/Wash buffer before resuspension in PBS and flow cytometry acquisition (MACSQuant® VYB Flow Cytometer; Miltenyi Biotec). Data were analysed with FlowJo software (BD Biosciences).

#### **Western blot analysis of cell lysates and pellets.**

For cell lysates, cells were lysed with lysis buffer (20 mM Tris [pH 7.5], 1% Triton X-100, 0.05% sodium dodecyl sulfate, 150 mM NaCl, 0.5% Na deoxycholate) supplemented with protease/phosphatase inhibitor cocktail (Roche) and lysates were clarified from the nuclei by centrifugation at 13,000×g for 10 min at 4°C for quantitative western blot analysis. For purification of particles, supernatants were harvested and filtered through a 0.45µm filter and centrifuged through a 20% sucrose cushion at 28,000 rpm for 2h at 4°C with a SW41 rotor and Optima L-90 centrifuge (Beckman). Pellets were resuspended in PBS prior to use for western blot. Proteins obtained in total cell lysates or pellets were denatured in Laemmli buffer (250mM Tris-HCL pH 6.8, 10% SDS, 50% glycerol, 500mM β-mercapto-ethanol, bromophenol blue) at 95°C for 5 min separated by SDS-PAGE, and then transferred onto nitrocellulose membranes and revealed with specific primary antibodies, followed by the addition of IRdye secondary antibodies, and imaging with an Odyssey infrared imaging system CLx (Li-Cor Biosciences). In the case of Gc detection, proteins in total cell lysates or pellets were loaded in non-denaturing, non-reducing buffer (250mM Tris-HCL pH 6.8, 5% SDS, 50% glycerol, bromophenol blue).

#### **Statistical analysis.**

Significance values were calculated by applying tests indicated in the figure legends using the GraphPad Prism 10 software (GraphPad Software, USA). P values under 0.05 were considered statistically significant and the following denotations were used: \*\*\*\*, P<0.0001; \*\*\*, P<0.001; \*\*, P<0,01; \*, P<0,5; ns (non-significant), P>0,5.

## Chapter VII. References

- Adams, L.J., Raju, S., Ma, H., Gilliland, T., Reed, D.S., Klimstra, W.B., Fremont, D.H., Diamond, M.S., 2024. Structural and functional basis of VLDLR usage by Eastern equine encephalitis virus. *Cell* 187, 360–374.e19. <https://doi.org/10.1016/j.cell.2023.11.031>
- Agnello, V., Ábel, G., Elfahal, M., Knight, G.B., Zhang, Q.-X., 1999. Hepatitis C virus and other Flaviviridae viruses enter cells via low density lipoprotein receptor. *Proc. Natl. Acad. Sci.* 96, 12766–12771. <https://doi.org/10.1073/pnas.96.22.12766>
- Ahata, B., Akçapınar, G.B., 2023. CCHFV vaccine development, current challenges, limitations, and future directions. *Front. Immunol.* 14.
- Akazawa, D., Date, T., Morikawa, K., Murayama, A., Miyamoto, M., Kaga, M., Barth, H., Baumert, T.F., Dubuisson, J., Wakita, T., 2007. CD81 expression is important for the permissiveness of Huh7 cell clones for heterogeneous hepatitis C virus infection. *J. Virol.* 81, 5036–5045. <https://doi.org/10.1128/JVI.01573-06>
- Altamura, L.A., Bertolotti-Ciarlet, A., Teigler, J., Paragas, J., Schmaljohn, C.S., Doms, R.W., 2007. Identification of a novel C-terminal cleavage of Crimean-Congo hemorrhagic fever virus PreGN that leads to generation of an NSM protein. *J. Virol.* 81, 6632–6642. <https://doi.org/10.1128/JVI.02730-06>
- Amirache, F., Lévy, C., Costa, C., Mangeot, P.-E., Torbett, B.E., Wang, C.X., Nègre, D., Cosset, F.-L., Verhoeven, E., 2014. Mystery solved: VSV-G-LVs do not allow efficient gene transfer into unstimulated T cells, B cells, and HSCs because they lack the LDL receptor. *Blood* 123, 1422–1424. <https://doi.org/10.1182/blood-2013-11-540641>
- André, P., Komurian-Pradel, F., Deforges, S., Perret, M., Berland, J.L., Sodoyer, M., Pol, S., Bréchet, C., Paranhos-Baccalà, G., Lotteau, V., 2002. Characterization of low- and very-low-density hepatitis C virus RNA-containing particles. *J. Virol.* 76, 6919–6928. <https://doi.org/10.1128/jvi.76.14.6919-6928.2002>
- Arda, B., Aciduman, A., 2007. A Historical Perspective of Infectious Diseases with Reference to Crimean-Congo Hemorrhagic Fever, in: Ergonul, O., Whitehouse, C.A. (Eds.), *Crimean-Congo Hemorrhagic Fever*. Springer Netherlands, Dordrecht, pp. 13–22. [https://doi.org/10.1007/978-1-4020-6106-6\\_2](https://doi.org/10.1007/978-1-4020-6106-6_2)
- Atkinson, B., Chamberlain, J., Logue, C.H., Cook, N., Bruce, C., Dowall, S.D., Hewson, R., 2012. Development of a real-time RT-PCR assay for the detection of Crimean-Congo hemorrhagic fever virus. *Vector Borne Zoonotic Dis. Larchmt. N* 12, 786–793. <https://doi.org/10.1089/vbz.2011.0770>
- Aydemir, O., Erdeve, O., Oguz, S.S., Dilmen, U., 2010. A healthy newborn born to a mother with Crimean-Congo hemorrhagic fever: is there protection from transplacental transmission? *Int. J. Infect. Dis.* 14, e450. <https://doi.org/10.1016/j.ijid.2009.07.001>
- Azhar, A., Binari, L.A., Joglekar, K., Tsujita, M., Talwar, M., Balaraman, V., Bhalla, A., Eason, J.D., Hall, I.E., Rofaiel, G., Forbes, R.C., Shaffer, D., Concepcion, B.P., Molnar, M.Z., 2021. Association between ezetimibe usage and hepatitis C RNA levels in uninfected kidney transplant recipients who received hepatitis C infected kidneys. *Clin. Transplant.* 35, e14485. <https://doi.org/10.1111/ctr.14485>
- Bankwitz, D., Doepke, M., Hueging, K., Weller, R., Bruening, J., Behrendt, P., Lee, J.-Y., Vondran, F.W.R., Manns, M.P., Bartenschlager, R., Pietschmann, T., 2017. Maturation of secreted HCV particles by incorporation of secreted ApoE protects from antibodies by enhancing infectivity. *J. Hepatol.* 67, 480–489. <https://doi.org/10.1016/j.jhep.2017.04.010>

- Barel, M., Hovanessian, A.G., Meibom, K., Briand, J.-P., Dupuis, M., Charbit, A., 2008. A novel receptor – ligand pathway for entry of *Francisella tularensis* in monocyte-like THP-1 cells: interaction between surface nucleolin and bacterial elongation factor Tu. *BMC Microbiol.* 8, 145. <https://doi.org/10.1186/1471-2180-8-145>
- Barnwal, B., Karlberg, H., Mirazimi, A., Tan, Y.-J., 2016. The Non-structural Protein of Crimean-Congo Hemorrhagic Fever Virus Disrupts the Mitochondrial Membrane Potential and Induces Apoptosis. *J. Biol. Chem.* 291, 582–592. <https://doi.org/10.1074/jbc.M115.667436>
- Barr, J.N., 2007. Bunyavirus mRNA synthesis is coupled to translation to prevent premature transcription termination. *RNA* 13, 731. <https://doi.org/10.1261/rna.436607>
- Barr, J.N., Elliott, R.M., Dunn, E.F., Wertz, G.W., 2003. Segment-specific terminal sequences of Bunyamwera bunyavirus regulate genome replication. *Virology* 311, 326–338. [https://doi.org/10.1016/s0042-6822\(03\)00130-2](https://doi.org/10.1016/s0042-6822(03)00130-2)
- Barrass, S.V., Butcher, S.J., 2020. Advances in high-throughput methods for the identification of virus receptors. *Med. Microbiol. Immunol. (Berl.)* 209, 309–323. <https://doi.org/10.1007/s00430-019-00653-2>
- Bates, P., Young, J.A., Varmus, H.E., 1993. A receptor for subgroup A Rous sarcoma virus is related to the low density lipoprotein receptor. *Cell* 74, 1043–1051. [https://doi.org/10.1016/0092-8674\(93\)90726-7](https://doi.org/10.1016/0092-8674(93)90726-7)
- Battini, J.L., Rodrigues, P., Müller, R., Danos, O., Heard, J.M., 1996. Receptor-binding properties of a purified fragment of the 4070A amphotropic murine leukemia virus envelope glycoprotein. *J. Virol.* 70, 4387–4393. <https://doi.org/10.1128/JVI.70.7.4387-4393.1996>
- Benelli, G., 2020. Pathogens Manipulating Tick Behavior—Through a Glass, Darkly. *Pathogens* 9, 664. <https://doi.org/10.3390/pathogens9080664>
- Bente, D.A., Alimonti, J.B., Shieh, W.-J., Camus, G., Ströher, U., Zaki, S., Jones, S.M., 2010. Pathogenesis and immune response of Crimean-Congo hemorrhagic fever virus in a STAT-1 knockout mouse model. *J. Virol.* 84, 11089–11100. <https://doi.org/10.1128/JVI.01383-10>
- Bente, D.A., Forrester, N.L., Watts, D.M., McAuley, A.J., Whitehouse, C.A., Bray, M., 2013. Crimean-Congo hemorrhagic fever: History, epidemiology, pathogenesis, clinical syndrome and genetic diversity. *Antiviral Res.* 100, 159–189. <https://doi.org/10.1016/j.antiviral.2013.07.006>
- Bereczky, S., Lindegren, G., Karlberg, H., Akerström, S., Klingström, J., Mirazimi, A., 2010. Crimean-Congo hemorrhagic fever virus infection is lethal for adult type I interferon receptor-knockout mice. *J. Gen. Virol.* 91, 1473–1477. <https://doi.org/10.1099/vir.0.019034-0>
- Bergeron, E., Albariño, C.G., Khristova, M.L., Nichol, S.T., 2010. Crimean-Congo hemorrhagic fever virus-encoded ovarian tumor protease activity is dispensable for virus RNA polymerase function. *J. Virol.* 84, 216–226. <https://doi.org/10.1128/JVI.01859-09>
- Bergeron, E., Vincent, M.J., Nichol, S.T., 2007. Crimean-Congo hemorrhagic fever virus glycoprotein processing by the endoprotease SKI-1/S1P is critical for virus infectivity. *J. Virol.* 81, 13271–13276. <https://doi.org/10.1128/JVI.01647-07>
- Bergeron, É., Zivcec, M., Chakrabarti, A.K., Nichol, S.T., Albariño, C.G., Spiropoulou, C.F., 2015. Recovery of Recombinant Crimean Congo Hemorrhagic Fever Virus Reveals a Function for Non-structural Glycoproteins Cleavage by Furin. *PLOS Pathog.* 11, e1004879. <https://doi.org/10.1371/journal.ppat.1004879>

- Bernard, C., Joly Kukla, C., Rakotoarivony, I., Duhayon, M., Stachurski, F., Huber, K., Giupponi, C., Zortman, I., Holzmüller, P., Pollet, T., Jeanneau, M., Mercey, A., Vachier, N., Lefrançois, T., Garros, C., Michaud, V., Comtet, L., Despois, L., Pourquier, P., Picard, C., Journeaux, A., Thomas, D., Godard, S., Moissonnier, E., Mely, S., Segal, M., Pannetier, D., Baize, S., Vial, L., 2024. Detection of Crimean-Congo haemorrhagic fever virus in *Hyalomma marginatum* ticks, southern France, May 2022 and April 2023. *Euro Surveill. Bull. Eur. Sur Mal. Transm. Eur. Commun. Dis. Bull.* 29, 2400023. <https://doi.org/10.2807/1560-7917.ES.2024.29.6.2400023>
- Bertolotti-Ciarlet, A., Smith, J., Strecker, K., Paragas, J., Altamura, L.A., McFalls, J.M., Frias-Stäheli, N., García-Sastre, A., Schmaljohn, C.S., Doms, R.W., 2005. Cellular localization and antigenic characterization of Crimean-Congo hemorrhagic fever virus glycoproteins. *J. Virol.* 79, 6152–6161. <https://doi.org/10.1128/JVI.79.10.6152-6161.2005>
- Bonney, L.C., Watson, R.J., Afrough, B., Mullojonova, M., Dzhuraeva, V., Tishkova, F., Hewson, R., 2017. A recombinase polymerase amplification assay for rapid detection of Crimean-Congo Haemorrhagic fever Virus infection. *PLoS Negl. Trop. Dis.* 11, e0006013. <https://doi.org/10.1371/journal.pntd.0006013>
- Boucher, P., Herz, J., 2011. Signaling through LRP1: Protection from atherosclerosis and beyond. *Biochem. Pharmacol.* 81, 1–5. <https://doi.org/10.1016/j.bcp.2010.09.018>
- Boulant, S., Stanifer, M., Lozach, P.-Y., 2015. Dynamics of virus-receptor interactions in virus binding, signaling, and endocytosis. *Viruses* 7, 2794–2815. <https://doi.org/10.3390/v7062747>
- Bouloy, M., Pardigon, N., Vialat, P., Gerbaud, S., Girard, M., 1990. Characterization of the 5' and 3' ends of viral messenger RNAs isolated from BHK21 cells infected with germiston virus (bunyavirus). *Virology* 175, 50–58. [https://doi.org/10.1016/0042-6822\(90\)90185-T](https://doi.org/10.1016/0042-6822(90)90185-T)
- Brandes, C., Kahr, L., Stockinger, W., Hiesberger, T., Schneider, W.J., Nimpf, J., 2001. Alternative splicing in the ligand binding domain of mouse ApoE receptor-2 produces receptor variants binding reelin but not alpha 2-macroglobulin. *J. Biol. Chem.* 276, 22160–22169. <https://doi.org/10.1074/jbc.M102662200>
- Brown, E.L., Lyles, D.S., 2005. Pseudotypes of vesicular stomatitis virus with CD4 formed by clustering of membrane microdomains during budding. *J. Virol.* 79, 7077–7086. <https://doi.org/10.1128/JVI.79.11.7077-7086.2005>
- Brown, M.S., Goldstein, J.L., 1986. A receptor-mediated pathway for cholesterol homeostasis. *Science* 232, 34–47. <https://doi.org/10.1126/science.3513311>
- Brown, W.V., Baginsky, M.L., 1972. Inhibition of lipoprotein lipase by an apoprotein of human very low density lipoprotein. *Biochem. Biophys. Res. Commun.* 46, 375–382. [https://doi.org/10.1016/s0006-291x\(72\)80149-9](https://doi.org/10.1016/s0006-291x(72)80149-9)
- Bu, G., 1998. Receptor-associated protein: a specialized chaperone and antagonist for members of the LDL receptor gene family. *Curr. Opin. Lipidol.* 9, 149–155. <https://doi.org/10.1097/00041433-199804000-00012>
- Bukong, T.N., Momen-Heravi, F., Kodys, K., Bala, S., Szabo, G., 2014. Exosomes from Hepatitis C Infected Patients Transmit HCV Infection and Contain Replication Competent Viral RNA in Complex with Ago2-miR122-HSP90. *PLOS Pathog.* 10, e1004424. <https://doi.org/10.1371/journal.ppat.1004424>
- Buranda, T., Wu, Y., Perez, D., Jett, S.D., BonduHawkins, V., Ye, C., Edwards, B., Hall, P., Larson, R.S., Lopez, G.P., Sklar, L.A., Hjelle, B., 2010. Recognition of DAF and  $\alpha\beta 3$  by

- inactivated Hantaviruses, towards the development of HTS flow cytometry assays. *Anal. Biochem.* 402, 151–160. <https://doi.org/10.1016/j.ab.2010.03.016>
- Burt, F.J., Swanepoel, R., Shieh, W.J., Smith, J.F., Leman, P.A., Greer, P.W., Coffield, L.M., Rollin, P.E., Ksiazek, T.G., Peters, C.J., Zaki, S.R., 1997. Immunohistochemical and in situ localization of Crimean-Congo hemorrhagic fever (CCHF) virus in human tissues and implications for CCHF pathogenesis. *Arch. Pathol. Lab. Med.* 121, 839–846.
- Calattini, S., Fusil, F., Mancip, J., Dao Thi, V.L., Granier, C., Gadot, N., Scoazec, J.-Y., Zeisel, M.B., Baumert, T.F., Lavillette, D., Dreux, M., Cosset, F.-L., 2015. Functional and Biochemical Characterization of Hepatitis C Virus (HCV) Particles Produced in a Humanized Liver Mouse Model. *J. Biol. Chem.* 290, 23173–23187. <https://doi.org/10.1074/jbc.M115.662999>
- Cao, D., Ma, B., Cao, Z., Zhang, X., Xiang, Y., 2023. Structure of Semliki Forest virus in complex with its receptor VLDLR. *Cell* 186, 2208–2218.e15. <https://doi.org/10.1016/j.cell.2023.03.032>
- Cao, W., Henry, M.D., Borrow, P., Yamada, H., Elder, J.H., Ravkov, E.V., Nichol, S.T., Compans, R.W., Campbell, K.P., Oldstone, M.B.A., 1998. Identification of  $\alpha$ -Dystroglycan as a Receptor for Lymphocytic Choriomeningitis Virus and Lassa Fever Virus. *Science* 282, 2079–2081. <https://doi.org/10.1126/science.282.5396.2079>
- Capek, M., Literak, I., Kocianova, E., Sychra, O., Najer, T., Trnka, A., Kverek, P., 2014. Ticks of the *Hyalomma marginatum* complex transported by migratory birds into Central Europe. *Ticks Tick-Borne Dis.* 5, 489–493. <https://doi.org/10.1016/j.ttbdis.2014.03.002>
- Carter, S.D., Surtees, R., Walter, C.T., Ariza, A., Bergeron, É., Nichol, S.T., Hiscox, J.A., Edwards, T.A., Barr, J.N., 2012. Structure, Function, and Evolution of the Crimean-Congo Hemorrhagic Fever Virus Nucleocapsid Protein. *J. Virol.* 86, 10914–10923. <https://doi.org/10.1128/JVI.01555-12>
- Casals, J., 1969. Antigenic Similarity between the Virus Causing Crimean Hemorrhagic Fever and Congo Virus. *Proc. Soc. Exp. Biol. Med.* 131, 233–236. <https://doi.org/10.3181/00379727-131-33847>
- Casals, J., Tignor, G.H., 2008. The Nairovirus Genus: Serological Relationships. *Intervirology* 14, 144–147. <https://doi.org/10.1159/000149175>
- CDC, Centers for Disease Control and Prevention, 2014. Outbreak Distribution Map. Available at: <https://www.cdc.gov/vhf/crimean-congo/outbreaks/distribution-map.html> (Accessed: 27 November 2023).
- Chang, K.-S., Jiang, J., Cai, Z., Luo, G., 2007. Human Apolipoprotein E Is Required for Infectivity and Production of Hepatitis C Virus in Cell Culture. *J. Virol.* 81, 13783–13793. <https://doi.org/10.1128/JVI.01091-07>
- Chang, T.-Y., Chang, C., 2008. Ezetimibe Blocks Internalization of the NPC1L1/Cholesterol Complex. *Cell Metab.* 7, 469–471. <https://doi.org/10.1016/j.cmet.2008.05.001>
- Chen, W.J., Goldstein, J.L., Brown, M.S., 1990. NPXY, a sequence often found in cytoplasmic tails, is required for coated pit-mediated internalization of the low density lipoprotein receptor. *J. Biol. Chem.* 265, 3116–3123.
- Chien, Y.-J., Chen, W.-J., Hsu, W.-L., Chiou, S.-S., 2008. Bovine lactoferrin inhibits Japanese encephalitis virus by binding to heparan sulfate and receptor for low density lipoprotein. *Virology* 379, 143–151. <https://doi.org/10.1016/j.virol.2008.06.017>
- Choi, Y., Kwon, Y.-C., Kim, S.-I., Park, J.-M., Lee, K.-H., Ahn, B.-Y., 2008. A hantavirus causing hemorrhagic fever with renal syndrome requires gC1qR/p32 for efficient cell binding and infection. *Virology* 381, 178–183. <https://doi.org/10.1016/j.virol.2008.08.035>

- Christova, I., Kovacheva, T., Georgieva, D., Ivanova, S., Argirov, D., 2009. Vaccine against congo-crimean haemorrhagic fever virus-bulgarian input in fighting the disease 37, 7–8.
- Clark, L.E., Clark, S.A., Lin, C., Liu, J., Coscia, A., Nabel, K.G., Yang, P., Neel, D.V., Lee, H., Brusic, V., Stryapunina, I., Plante, K.S., Ahmed, A.A., Catteruccia, F., Young-Pearse, T.L., Chiu, I.M., Llopis, P.M., Weaver, S.C., Abraham, J., 2022. VLDLR and ApoER2 are receptors for multiple alphaviruses. *Nature* 602, 475–480. <https://doi.org/10.1038/s41586-021-04326-0>
- Clatworthy, A.E., Stockinger, W., Christie, R.H., Schneider, W.J., Nimpf, J., Hyman, B.T., Rebeck, G.W., 1999. Expression and alternate splicing of apolipoprotein E receptor 2 in brain. *Neuroscience* 90, 903–911. [https://doi.org/10.1016/s0306-4522\(98\)00489-8](https://doi.org/10.1016/s0306-4522(98)00489-8)
- Cohen-Dvashi, H., Israeli, H., Shani, O., Katz, A., Diskin, R., 2016. Role of LAMP1 Binding and pH Sensing by the Spike Complex of Lassa Virus. *J. Virol.* 90, 10329–10338. <https://doi.org/10.1128/jvi.01624-16>
- Cohn, J.S., Tremblay, M., Batal, R., Jacques, H., Veilleux, L., Rodriguez, C., Bernier, L., Mamer, O., Davignon, J., 2002. Plasma kinetics of VLDL and HDL apoC-I in normolipidemic and hypertriglyceridemic subjects. *J. Lipid Res.* 43, 1680–1687. <https://doi.org/10.1194/jlr.M200055-JLR200>
- Colón-Ramos, D.A., Irusta, P.M., Gan, E.C., Olson, M.R., Song, J., Morimoto, R.I., Elliott, R.M., Lombard, M., Hollingsworth, R., Hardwick, J.M., Smith, G.K., Kornbluth, S., 2003. Inhibition of translation and induction of apoptosis by Bunyaviral nonstructural proteins bearing sequence similarity to reaper. *Mol. Biol. Cell* 14, 4162–4172. <https://doi.org/10.1091/mbc.e03-03-0139>
- Conde-Knape, K., Bensadoun, A., Sobel, J.H., Cohn, J.S., Shachter, N.S., 2002. Overexpression of apoC-I in apoE-null mice. *J. Lipid Res.* 43, 2136–2145. <https://doi.org/10.1194/jlr.M200210-JLR200>
- Connolly-Andersen, A.-M., Douagi, I., Kraus, A.A., Mirazimi, A., 2009. Crimean Congo hemorrhagic fever virus infects human monocyte-derived dendritic cells. *Virology* 390, 157–162. <https://doi.org/10.1016/j.virol.2009.06.010>
- Connolly-Andersen, A.-M., Magnusson, K.-E., Mirazimi, A., 2007. Basolateral Entry and Release of Crimean-Congo Hemorrhagic Fever Virus in Polarized MDCK-1 Cells. *J. Virol.* 81, 2158–2164. <https://doi.org/10.1128/JVI.02070-06>
- Cooper, A.C., Banasiak, N.C., Allen, P.J., 2003. Management and prevention strategies for respiratory syncytial virus (RSV) bronchiolitis in infants and young children: a review of evidence-based practice interventions. *Pediatr. Nurs.* 29, 452–456.
- Cosset, F.-L., Mialon, C., Boson, B., Granier, C., Denolly, S., 2020. HCV Interplay with Lipoproteins: Inside or Outside the Cells? *Viruses* 12, 434. <https://doi.org/10.3390/v12040434>
- Cross, R.W., Prasad, A.N., Borisevich, V., Geisbert, J.B., Agans, K.N., Deer, D.J., Fenton, K.A., Geisbert, T.W., 2020. Crimean-Congo hemorrhagic fever virus strains Hoti and Afghanistan cause viremia and mild clinical disease in cynomolgus monkeys. *PLoS Negl. Trop. Dis.* 14, e0008637. <https://doi.org/10.1371/journal.pntd.0008637>
- Crump, C.M., Williams, J.L., Stephens, D.J., Banting, G., 1998. Inhibition of the Interaction between Tyrosine-based Motifs and the Medium Chain Subunit of the AP-2 Adaptor Complex by Specific Tyrphostins\*. *J. Biol. Chem.* 273, 28073–28077. <https://doi.org/10.1074/jbc.273.43.28073>
- D’Addiego, J., Elaldi, N., Wand, N., Osman, K., Bagci, B.K., Kennedy, E., Pektas, A.N., Hart, E., Slack, G., Hewson, R., 2023. Investigating the effect of ribavirin treatment on genetic



- mutations in Crimean–Congo haemorrhagic fever virus (CCHFV) through next-generation sequencing. *J. Med. Virol.* 95, e28548. <https://doi.org/10.1002/jmv.28548>
- Dai, S., Wu, Q., Wu, X., Peng, C., Liu, J., Tang, S., Zhang, T., Deng, F., Shen, S., 2021. Differential Cell Line Susceptibility to Crimean-Congo Hemorrhagic Fever Virus. *Front. Cell. Infect. Microbiol.* 11.
- De Boer, S.M., Kortekaas, J., De Haan, C.A.M., Rottier, P.J.M., Moormann, R.J.M., Bosch, B.J., 2012. Heparan Sulfate Facilitates Rift Valley Fever Virus Entry into the Cell. *J. Virol.* 86, 13767–13771. <https://doi.org/10.1128/JVI.01364-12>
- De Sanctis, J.B., Blanca, I., Rivera, H., Bianco, N.E., 1998. Expression of low-density lipoprotein receptors in peripheral blood and tonsil B lymphocytes. *Clin. Exp. Immunol.* 113, 206–212. <https://doi.org/10.1046/j.1365-2249.1998.00579.x>
- de Zarate, I.B.O., Kaelin, K., Rozenberg, F., 2004. Effects of Mutations in the Cytoplasmic Domain of Herpes Simplex Virus Type 1 Glycoprotein B on Intracellular Transport and Infectivity. *J. Virol.* 78, 1540–1551. <https://doi.org/10.1128/JVI.78.3.1540-1551.2004>
- Delang, L., Paeshuyse, J., Vlieghe, I., Leyssen, P., Obeid, S., Durantel, D., Zoulim, F., Op de Beeck, A., Neyts, J., 2009. Statins potentiate the in vitro anti-hepatitis C virus activity of selective hepatitis C virus inhibitors and delay or prevent resistance development. *Hepatology* 50, 6–16. <https://doi.org/10.1002/hep.22916>
- Denolly, S., Granier, C., Fontaine, N., Pozzetto, B., Bourlet, T., Guérin, M., Cosset, F.-L., 2019. A serum protein factor mediates maturation and apoB-association of HCV particles in the extracellular milieu. *J. Hepatol.* 70, 626–638. <https://doi.org/10.1016/j.jhep.2018.11.033>
- Devignot, S., Bergeron, E., Nichol, S., Mirazimi, A., Weber, F., 2015. A Virus-Like Particle System Identifies the Endonuclease Domain of Crimean-Congo Hemorrhagic Fever Virus. *J. Virol.* 89, 5957–5967. <https://doi.org/10.1128/JVI.03691-14>
- Devignot, S., Sha, T.W., Burkard, T.R., Schmerer, P., Hagelkruys, A., Mirazimi, A., Elling, U., Penninger, J.M., Weber, F., 2023. Low-density lipoprotein receptor-related protein 1 (LRP1) as an auxiliary host factor for RNA viruses. *Life Sci. Alliance* 6, e202302005. <https://doi.org/10.26508/lsa.202302005>
- De-Zolt, S., Altschmied, J., Ruiz, P., von Melchner, H., Schnütgen, F., 2009. Gene-trap vectors and mutagenesis. *Methods Mol. Biol. Clifton NJ* 530, 29–47. [https://doi.org/10.1007/978-1-59745-471-1\\_3](https://doi.org/10.1007/978-1-59745-471-1_3)
- Di Scala, C., Baier, C.J., Evans, L.S., Williamson, P.T.F., Fantini, J., Barrantes, F.J., 2017. Relevance of CARC and CRAC Cholesterol-Recognition Motifs in the Nicotinic Acetylcholine Receptor and Other Membrane-Bound Receptors. *Curr. Top. Membr.* 80, 3–23. <https://doi.org/10.1016/bs.ctm.2017.05.001>
- Dickson, D.L., Turell, M.J., 1992. Replication and tissue tropisms of Crimean-Congo hemorrhagic fever virus in experimentally infected adult *Hyalomma truncatum* (Acari: Ixodidae). *J. Med. Entomol.* 29, 767–773. <https://doi.org/10.1093/jmedent/29.5.767>
- Dlugosz, P., Nimpf, J., 2018. The Reelin Receptors Apolipoprotein E receptor 2 (ApoER2) and VLDL Receptor. *Int. J. Mol. Sci.* 19, 3090. <https://doi.org/10.3390/ijms19103090>
- Dohm, D.J., Logan, T.M., Linthicum, K.J., Rossi, C.A., Turell, M.J., 1996. Transmission of Crimean-Congo Hemorrhagic Fever Virus by *Hyalomma impeltatum* (Acari: Ixodidae) after Experimental Infection. *J. Med. Entomol.* 33, 848–851. <https://doi.org/10.1093/jmedent/33.5.848>
- Dokuzoguz, B., Celikbas, A.K., Gök, Ş.E., Baykam, N., Eroglu, M.N., Ergönül, Ö., 2013. Severity scoring index for Crimean-Congo hemorrhagic fever and the impact of ribavirin and

- corticosteroids on fatality. *Clin. Infect. Dis. Off. Publ. Infect. Dis. Soc. Am.* 57, 1270–1274. <https://doi.org/10.1093/cid/cit527>
- Douam, F., Dao Thi, V.L., Maurin, G., Fresquet, J., Mompelat, D., Zeisel, M.B., Baumert, T.F., Cosset, F.-L., Lavillette, D., 2014. Critical interaction between E1 and E2 glycoproteins determines binding and fusion properties of hepatitis C virus during cell entry. *Hepatology* 59, 776–788. <https://doi.org/10.1002/hep.26733>
- Dreux, M., Garaigorta, U., Boyd, B., Décembre, E., Chung, J., Whitten-Bauer, C., Wieland, S., Chisari, F.V., 2012. Short-Range Exosomal Transfer of Viral RNA from Infected Cells to Plasmacytoid Dendritic Cells Triggers Innate Immunity. *Cell Host Microbe* 12, 558–570. <https://doi.org/10.1016/j.chom.2012.08.010>
- Duh, D., Saksida, A., Petrovec, M., Dedushaj, I., Avšič-Županc, T., 2006. Novel one-step real-time RT-PCR assay for rapid and specific diagnosis of Crimean-Congo hemorrhagic fever encountered in the Balkans. *J. Virol. Methods* 133, 175–179. <https://doi.org/10.1016/j.jviromet.2005.11.006>
- Dülger, A.C., Yakarişik, M., Uzun, Y.E., Şahin, A.M., 2020. Treatment of Crimean-Congo Haemorrhagic Fever by Favipiravir in a Patient with Novel Coronavirus Co-Infection. *Eur. J. Case Rep. Intern. Med.* [https://doi.org/10.12890/2020\\_002042](https://doi.org/10.12890/2020_002042)
- Elferink, J.G.R., 1979. Chlorpromazine inhibits phagocytosis and exocytosis in rabbit polymorphonuclear leukocytes. *Biochem. Pharmacol.* 28, 965–968. [https://doi.org/10.1016/0006-2952\(79\)90287-9](https://doi.org/10.1016/0006-2952(79)90287-9)
- Ergönül, Ö., 2006. Crimean-Congo haemorrhagic fever. *Lancet Infect. Dis.* 6, 203–214. [https://doi.org/10.1016/S1473-3099\(06\)70435-2](https://doi.org/10.1016/S1473-3099(06)70435-2)
- Ergönül, O., Battal, I., 2014. Potential Sexual Transmission of Crimean-Congo Hemorrhagic Fever Infection. *Jpn. J. Infect. Dis.* 67, 137–138. <https://doi.org/10.7883/yoken.67.137>
- Ergönül, O., Celikbas, A., Dokuzoguz, B., Eren, S., Baykam, N., Esener, H., 2004. Characteristics of Patients with Crimean-Congo Hemorrhagic Fever in a Recent Outbreak in Turkey and Impact of Oral Ribavirin Therapy. *Clin. Infect. Dis.* 39, 284–287. <https://doi.org/10.1086/422000>
- Ergönül, O., Celikbas, A., Yildirim, U., Zenciroglu, A., Erdogan, D., Ziraman, I., Saracoglu, F., Demirel, N., Cakmak, O., Dokuzoguz, B., 2010. Pregnancy and Crimean-Congo haemorrhagic fever. *Clin. Microbiol. Infect.* 16, 647–650. <https://doi.org/10.1111/j.1469-0691.2009.02905.x>
- Ergönül, O., Tuncbilek, S., Baykam, N., Celikbas, A., Dokuzoguz, B., 2006. Evaluation of Serum Levels of Interleukin (IL)–6, IL-10, and Tumor Necrosis Factor– $\alpha$  in Patients with Crimean-Congo Hemorrhagic Fever. *J. Infect. Dis.* 193, 941–944. <https://doi.org/10.1086/500836>
- Estrada, D.F., De Guzman, R.N., 2011. Structural Characterization of the Crimean-Congo Hemorrhagic Fever Virus Gn Tail Provides Insight into Virus Assembly. *J. Biol. Chem.* 286, 21678–21686. <https://doi.org/10.1074/jbc.M110.216515>
- Evans, M.J., von Hahn, T., Tscherne, D.M., Syder, A.J., Panis, M., Wölk, B., Hatzioannou, T., McKeating, J.A., Bieniasz, P.D., Rice, C.M., 2007. Claudin-1 is a hepatitis C virus co-receptor required for a late step in entry. *Nature* 446, 801–805. <https://doi.org/10.1038/nature05654>
- Fagbami, A.H., Tomori, O., Fabiyi, A., Isoun, T.T., 1975. Experimental Congo virus (Ib -AN 7620) infection in primates. *Virology* 26, 33–37.
- Fauvelle, C., Felmler, D.J., Crouchet, E., Lee, J., Heydmann, L., Lefèvre, M., Magri, A., Hiet, M.-S., Fofana, I., Habersetzer, F., Fong, S.K.H., Milne, R., Patel, A.H., Vercauteren, K.,

- Meuleman, P., Zeisel, M.B., Bartenschlager, R., Schuster, C., Baumert, T.F., 2016. Apolipoprotein E Mediates Evasion From Hepatitis C Virus Neutralizing Antibodies. *Gastroenterology* 150, 206–217.e4. <https://doi.org/10.1053/j.gastro.2015.09.014>
- Feingold, K.R., 2000. Introduction to Lipids and Lipoproteins, in: Feingold, K.R., Anawalt, B., Blackman, M.R., Boyce, A., Chrousos, G., Corpas, E., de Herder, W.W., Dhatariya, K., Dungan, K., Hofland, J., Kalra, S., Kaltsas, G., Kapoor, N., Koch, C., Kopp, P., Korbonits, M., Kovacs, C.S., Kuohung, W., Laferrère, B., Levy, M., McGee, E.A., McLachlan, R., New, M., Purnell, J., Sahay, R., Shah, A.S., Singer, F., Sperling, M.A., Stratakis, C.A., Trencé, D.L., Wilson, D.P. (Eds.), *Endotext*. MDText.com, Inc., South Dartmouth (MA).
- Feld, J.J., Cypel, M., Kumar, D., Dahari, H., Pinto Ribeiro, R.V., Marks, N., Kamkar, N., Bahinskaya, I., Onofrio, F.Q., Zahoor, M.A., Cerrochi, O., Tinckam, K., Kim, S.J., Schiff, J., Reichman, T.W., McDonald, M., Alba, C., Waddell, T.K., Sapisochin, G., Selzner, M., Keshavjee, S., Janssen, H.L.A., Hansen, B.E., Singer, L.G., Humar, A., 2020. Short-course, direct-acting antivirals and ezetimibe to prevent HCV infection in recipients of organs from HCV-infected donors: a phase 3, single-centre, open-label study. *Lancet Gastroenterol. Hepatol.* 5, 649–657. [https://doi.org/10.1016/S2468-1253\(20\)30081-9](https://doi.org/10.1016/S2468-1253(20)30081-9)
- Fels, J.M., Maurer, D.P., Herbert, A.S., Wirchnianski, A.S., Vergnolle, O., Cross, R.W., Abelson, D.M., Moyer, C.L., Mishra, A.K., Aguilan, J.T., Kuehne, A.I., Pauli, N.T., Bakken, R.R., Nyakatura, E.K., Hellert, J., Quevedo, G., Lobel, L., Balinandi, S., Lutwama, J.J., Zeitlin, L., Geisbert, T.W., Rey, F.A., Sidoli, S., McLellan, J.S., Lai, J.R., Bornholdt, Z.A., Dye, J.M., Walker, L.M., Chandran, K., 2021. Protective neutralizing antibodies from human survivors of Crimean-Congo hemorrhagic fever. *Cell* 184, 3486–3501.e21. <https://doi.org/10.1016/j.cell.2021.05.001>
- Filipe, A.R., Calisher, C.H., Lazuick, J., 1985. Antibodies to Congo-Crimean haemorrhagic fever, Dhori, Thogoto and Bhanja viruses in southern Portugal. *Acta Virol.* 29, 324–328.
- Finkelshtein, D., Werman, A., Novick, D., Barak, S., Rubinstein, M., 2013. LDL receptor and its family members serve as the cellular receptors for vesicular stomatitis virus. *Proc. Natl. Acad. Sci.* 110, 7306–7311. <https://doi.org/10.1073/pnas.1214441110>
- Fischer, D.G., Tal, N., Novick, D., Barak, S., Rubinstein, M., 1993. An antiviral soluble form of the LDL receptor induced by interferon. *Science* 262, 250–253. <https://doi.org/10.1126/science.8211145>
- Flanagan, M.L., Oldenburg, J., Reignier, T., Holt, N., Hamilton, G.A., Martin, V.K., Cannon, P.M., 2008. New World Clade B Arenaviruses Can Use Transferrin Receptor 1 (TfR1)-Dependent and -Independent Entry Pathways, and Glycoproteins from Human Pathogenic Strains Are Associated with the Use of TfR1. *J. Virol.* 82, 938–948. <https://doi.org/10.1128/JVI.01397-07>
- Flick, R., Flick, K., Feldmann, H., Elgh, F., 2003. Reverse genetics for crimean-congo hemorrhagic fever virus. *J. Virol.* 77, 5997–6006. <https://doi.org/10.1128/jvi.77.10.5997-6006.2003>
- Földes, K., Aligholipour Farzani, T., Ergünay, K., Ozkul, A., 2020. Differential Growth Characteristics of Crimean-Congo Hemorrhagic Fever Virus in Kidney Cells of Human and Bovine Origin. *Viruses* 12, 685. <https://doi.org/10.3390/v12060685>
- Freitas, N., Enguehard, M., Denolly, S., Levy, C., Neveu, G., Lerolle, S., Devignot, S., Weber, F., Bergeron, E., Legros, V., Cosset, F.-L., 2020. The interplays between Crimean-Congo hemorrhagic fever virus (CCHFV) M segment-encoded accessory proteins and structural proteins promote virus assembly and infectivity. *PLOS Pathog.* 16, e1008850. <https://doi.org/10.1371/journal.ppat.1008850>

- Fuller, A.O., Spear, P.G., 1987. Anti-glycoprotein D antibodies that permit adsorption but block infection by herpes simplex virus 1 prevent virion-cell fusion at the cell surface. *Proc. Natl. Acad. Sci.* 84, 5454–5458. <https://doi.org/10.1073/pnas.84.15.5454>
- Fuller, J., Álvarez-Rodríguez, B., Todd, E.J. a. A., Mankouri, J., Hewson, R., Barr, J.N., 2020. Hazara Nairovirus Requires COPI Components in both Arf1-Dependent and Arf1-Independent Stages of Its Replication Cycle. *J. Virol.* 94, e00766-20. <https://doi.org/10.1128/JVI.00766-20>
- Furuta, Y., Takahashi, K., Kuno-Maekawa, M., Sangawa, H., Uehara, S., Kozaki, K., Nomura, N., Egawa, H., Shiraki, K., 2005. Mechanism of action of T-705 against influenza virus. *Antimicrob. Agents Chemother.* 49, 981–986. <https://doi.org/10.1128/AAC.49.3.981-986.2005>
- Gan, Y., McGraw, T.E., Rodriguez-Boulan, E., 2002. The epithelial-specific adaptor AP1B mediates post-endocytic recycling to the basolateral membrane. *Nat. Cell Biol.* 4, 605–609. <https://doi.org/10.1038/ncb827>
- Ganaie, S.S., Schwarz, M.M., McMillen, C.M., Price, D.A., Feng, A.X., Albe, J.R., Wang, W., Miersch, S., Orvedahl, A., Cole, A.R., Sentmanat, M.F., Mishra, N., Boyles, D.A., Koenig, Z.T., Kujawa, M.R., Demers, M.A., Hoehl, R.M., Moyle, A.B., Wagner, N.D., Stubbs, S.H., Cardarelli, L., Teyra, J., McElroy, A., Gross, M.L., Whelan, S.P.J., Doench, J., Cui, X., Brett, T.J., Sidhu, S.S., Virgin, H.W., Egawa, T., Leung, D.W., Amarasinghe, G.K., Hartman, A.L., 2021. Lrp1 is a host entry factor for Rift Valley fever virus. *Cell* 184, 5163-5178.e24. <https://doi.org/10.1016/j.cell.2021.09.001>
- Gargili, A., Estrada-Peña, A., Spengler, J.R., Lukashev, A., Nuttall, P.A., Bente, D.A., 2017. The role of ticks in the maintenance and transmission of Crimean-Congo hemorrhagic fever virus: A review of published field and laboratory studies. *Antiviral Res.* 144, 93–119. <https://doi.org/10.1016/j.antiviral.2017.05.010>
- Garrison, A.R., 2012. Defining key entry events for Crimean-Congo hemorrhagic fever virus in mammalian cells.
- Garrison, A.R., Radoshitzky, S.R., Kota, K.P., Pegoraro, G., Ruthel, G., Kuhn, J.H., Altamura, L.A., Kwilas, S.A., Bavari, S., Haucke, V., Schmaljohn, C.S., 2013. Crimean–Congo hemorrhagic fever virus utilizes a clathrin- and early endosome-dependent entry pathway. *Virology* 444, 45–54. <https://doi.org/10.1016/j.virol.2013.05.030>
- Garrison, A.R., Shoemaker, C.J., Golden, J.W., Fitzpatrick, C.J., Suschak, J.J., Richards, M.J., Badger, C.V., Six, C.M., Martin, J.D., Hannaman, D., Zivcec, M., Bergeron, E., Koehler, J.W., Schmaljohn, C.S., 2017. A DNA vaccine for Crimean-Congo hemorrhagic fever protects against disease and death in two lethal mouse models. *PLoS Negl. Trop. Dis.* 11, e0005908. <https://doi.org/10.1371/journal.pntd.0005908>
- Garrison, A.R., Smith, D.R., Golden, J.W., 2019. Animal Models for Crimean-Congo Hemorrhagic Fever Human Disease. *Viruses* 11, 590. <https://doi.org/10.3390/v11070590>
- Gautier, T., Masson, D., De Barros, J.-P.P., Athias, A., Gambert, P., Aunis, D., Metz-Boutigue, M.-H., Lagrost, L., 2000. Human Apolipoprotein C-I Accounts for the Ability of Plasma High Density Lipoproteins to Inhibit the Cholesteryl Ester Transfer Protein Activity. *J. Biol. Chem.* 275, 37504–37509. <https://doi.org/10.1074/jbc.M007210200>
- Gavrilovskaya, I.N., Brown, E.J., Ginsberg, M.H., Mackow, E.R., 1999. Cellular entry of hantaviruses which cause hemorrhagic fever with renal syndrome is mediated by beta3 integrins. *J. Virol.* 73, 3951–3959. <https://doi.org/10.1128/JVI.73.5.3951-3959.1999>

- Gavrilovskaya, I.N., Shepley, M., Shaw, R., Ginsberg, M.H., Mackow, E.R., 1998. beta3 Integrins mediate the cellular entry of hantaviruses that cause respiratory failure. *Proc. Natl. Acad. Sci. U. S. A.* 95, 7074–7079. <https://doi.org/10.1073/pnas.95.12.7074>
- Gibbons, G.F., Wiggins, D., Brown, A.-M., Hebbachi, A.-M., 2004. Synthesis and function of hepatic very-low-density lipoprotein. *Biochem. Soc. Trans.* 32, 59–64. <https://doi.org/10.1042/bst0320059>
- Golden, J.W., Shoemaker, C.J., Lindquist, M.E., Zeng, X., Daye, S.P., Williams, J.A., Liu, J., Coffin, K.M., Olschner, S., Flusin, O., Altamura, L.A., Kuehl, K.A., Fitzpatrick, C.J., Schmaljohn, C.S., Garrison, A.R., 2019. GP38-targeting monoclonal antibodies protect adult mice against lethal Crimean-Congo hemorrhagic fever virus infection. *Sci. Adv.* 5, eaaw9535. <https://doi.org/10.1126/sciadv.aaw9535>
- Goldstein, J.L., Brown, M.S., 1974. Binding and Degradation of Low Density Lipoproteins by Cultured Human Fibroblasts: COMPARISON OF CELLS FROM A NORMAL SUBJECT AND FROM A PATIENT WITH HOMOZYGOUS FAMILIAL HYPERCHOLESTEROLEMIA. *J. Biol. Chem.* 249, 5153–5162. [https://doi.org/10.1016/S0021-9258\(19\)42341-7](https://doi.org/10.1016/S0021-9258(19)42341-7)
- Gonzalez, J.P., Camicas, J.L., Cornet, J.P., Faye, O., Wilson, M.L., 1992. Sexual and transovarian transmission of Crimean-Congo haemorrhagic fever virus in *Hyalomma truncatum* ticks. *Res. Virol.* 143, 23–28. [https://doi.org/10.1016/S0923-2516\(06\)80073-7](https://doi.org/10.1016/S0923-2516(06)80073-7)
- Gozel, M.G., Elaldi, N., Engin, A., Akkar, O.B., Bolat, F., Celik, C., 2014. Favorable Outcomes for both Mother and Baby Are Possible in Pregnant Women with Crimean-Congo Hemorrhagic Fever Disease: A Case Series and Literature Review. *Gynecol. Obstet. Invest.* 77, 266–271. <https://doi.org/10.1159/000360699>
- Grandi, G., Chitimia-Dobler, L., Choklikitumnuey, P., Strube, C., Springer, A., Albihn, A., Jaenson, T.G.T., Omazic, A., 2020. First records of adult *Hyalomma marginatum* and *H. rufipes* ticks (Acari: Ixodidae) in Sweden. *Ticks Tick-Borne Dis.* 11, 101403. <https://doi.org/10.1016/j.ttbdis.2020.101403>
- Granier, C., Toesca, J., Mialon, C., Ritter, M., Freitas, N., Boson, B., Pécheur, E.-I., Cosset, F.-L., Denolly, S., 2023. Low-density hepatitis C virus infectious particles are protected from oxidation by secreted cellular proteins. *mBio* 14, e01549-23. <https://doi.org/10.1128/mbio.01549-23>
- Guardado-Calvo, P., Rey, F.A., 2021. The Viral Class II Membrane Fusion Machinery: Divergent Evolution from an Ancestral Heterodimer. *Viruses* 13, 2368. <https://doi.org/10.3390/v13122368>
- Guo, S., Zhang, Xiaohan, Zheng, M., Zhang, Xiaowei, Min, C., Wang, Z., Cheon, S.H., Oak, M.-H., Nah, S.-Y., Kim, K.-M., 2015. Selectivity of commonly used inhibitors of clathrin-mediated and caveolae-dependent endocytosis of G protein-coupled receptors. *Biochim. Biophys. Acta BBA - Biomembr.* 1848, 2101–2110. <https://doi.org/10.1016/j.bbamem.2015.05.024>
- Guo, Y., Wang, W., Ji, W., Deng, M., Sun, Y., Zhou, H., Yang, C., Deng, F., Wang, H., Hu, Z., Lou, Z., Rao, Z., 2012. Crimean-Congo hemorrhagic fever virus nucleoprotein reveals endonuclease activity in bunyaviruses. *Proc. Natl. Acad. Sci.* 109, 5046–5051. <https://doi.org/10.1073/pnas.1200808109>
- Hackett, B.A., Yasunaga, A., Panda, D., Tartell, M.A., Hopkins, K.C., Hensley, S.E., Cherry, S., 2015. RNASEK is required for internalization of diverse acid-dependent viruses. *Proc. Natl. Acad. Sci.* 112, 7797–7802. <https://doi.org/10.1073/pnas.1424098112>

- Haddock, E., Feldmann, F., Hawman, D.W., Zivcec, M., Hanley, P.W., Saturday, G., Scott, D.P., Thomas, T., Korva, M., Avšič-Županc, T., Safronetz, D., Feldmann, H., 2018. A cynomolgus macaque model for Crimean-Congo haemorrhagic fever. *Nat. Microbiol.* 3, 556–562. <https://doi.org/10.1038/s41564-018-0141-7>
- Haferkamp, S., Fernando, L., Schwarz, T.F., Feldmann, H., Flick, R., 2005. Intracellular localization of Crimean-Congo Hemorrhagic Fever (CCHF) virus glycoproteins. *Viol. J.* 2, 42. <https://doi.org/10.1186/1743-422X-2-42>
- Halldorsson, S., Li, S., Li, M., Harlos, K., Bowden, T.A., Huiskonen, J.T., 2018. Shielding and activation of a viral membrane fusion protein. *Nat. Commun.* 9, 349. <https://doi.org/10.1038/s41467-017-02789-2>
- Hawman, D.W., Haddock, E., Meade-White, K., Nardone, G., Feldmann, F., Hanley, P.W., Lovaglio, J., Scott, D., Komeno, T., Nakajima, N., Furuta, Y., Gowen, B.B., Feldmann, H., 2020. Efficacy of favipiravir (T-705) against Crimean-Congo hemorrhagic fever virus infection in cynomolgus macaques. *Antiviral Res.* 181, 104858. <https://doi.org/10.1016/j.antiviral.2020.104858>
- Hawman, D.W., Haddock, E., Meade-White, K., Williamson, B., Hanley, P.W., Rosenke, K., Komeno, T., Furuta, Y., Gowen, B.B., Feldmann, H., 2018. Favipiravir (T-705) but not ribavirin is effective against two distinct strains of Crimean-Congo hemorrhagic fever virus in mice. *Antiviral Res.* 157, 18–26. <https://doi.org/10.1016/j.antiviral.2018.06.013>
- Hawman, D.W., Meade-White, K., Leventhal, S., Appelberg, S., Ahlén, G., Nikouyan, N., Clancy, C., Smith, B., Hanley, P., Lovaglio, J., Mirazimi, A., Sällberg, M., Feldmann, H., 2023. Accelerated DNA vaccine regimen provides protection against Crimean-Congo hemorrhagic fever virus challenge in a macaque model. *Mol. Ther. J. Am. Soc. Gene Ther.* 31, 387–397. <https://doi.org/10.1016/j.ymthe.2022.09.016>
- Hawman, D.W., Meade-White, K., Leventhal, S., Feldmann, F., Okumura, A., Smith, B., Scott, D., Feldmann, H., 2021. Immunocompetent mouse model for Crimean-Congo hemorrhagic fever virus. *eLife* 10, e63906. <https://doi.org/10.7554/eLife.63906>
- Helguera, G., Jemielity, S., Abraham, J., Cordo, S.M., Martinez, M.G., Rodríguez, J.A., Bregni, C., Wang, J.J., Farzan, M., Penichet, M.L., Candurra, N.A., Choe, H., 2012. An Antibody Recognizing the Apical Domain of Human Transferrin Receptor 1 Efficiently Inhibits the Entry of All New World Hemorrhagic Fever Arenaviruses. *J. Virol.* 86, 4024–4028. <https://doi.org/10.1128/JVI.06397-11>
- Hermo, L., Lustig, M., Lefrancois, S., Argraves, W.S., Morales, C.R., 1999. Expression and regulation of LRP-2/megalin in epithelial cells lining the efferent ducts and epididymis during postnatal development. *Mol. Reprod. Dev.* 53, 282–293. [https://doi.org/10.1002/\(SICI\)1098-2795\(199907\)53:3<282::AID-MRD4>3.0.CO;2-A](https://doi.org/10.1002/(SICI)1098-2795(199907)53:3<282::AID-MRD4>3.0.CO;2-A)
- Hewson, R., Chamberlain, J., Mioulet, V., Lloyd, G., Jamil, B., Hasan, R., Gmyl, A., Gmyl, L., Smirnova, S.E., Lukashev, A., Karganova, G., Clegg, C., 2004. Crimean-Congo haemorrhagic fever virus: sequence analysis of the small RNA segments from a collection of viruses world wide. *Virus Res.* 102, 185–189. <https://doi.org/10.1016/j.virusres.2003.12.035>
- Hirota, Y., Kubo, K., Katayama, K., Honda, T., Fujino, T., Yamamoto, T.T., Nakajima, K., 2015. Reelin receptors ApoER2 and VLDLR are expressed in distinct spatiotemporal patterns in developing mouse cerebral cortex. *J. Comp. Neurol.* 523, 463–478. <https://doi.org/10.1002/cne.23691>
- Hofer, F., Gruenberger, M., Kowalski, H., Machat, H., Huettinger, M., Kuechler, E., Blaas, D., 1994. Members of the low density lipoprotein receptor family mediate cell entry of a

- minor-group common cold virus. *Proc. Natl. Acad. Sci. U. S. A.* 91, 1839–1842.  
<https://doi.org/10.1073/pnas.91.5.1839>
- Hofmann, H., Li, X., Zhang, X., Liu, W., Kühl, A., Kaup, F., Soldan, S.S., González-Scarano, F., Weber, F., He, Y., Pöhlmann, S., 2013. Severe Fever with Thrombocytopenia Virus Glycoproteins Are Targeted by Neutralizing Antibodies and Can Use DC-SIGN as a Receptor for pH-Dependent Entry into Human and Animal Cell Lines. *J. Virol.* 87, 4384–4394. <https://doi.org/10.1128/jvi.02628-12>
- Holm, T., Kopicki, J.-D., Busch, C., Olschewski, S., Rosenthal, M., Uetrecht, C., Günther, S., Reindl, S., 2018. Biochemical and structural studies reveal differences and commonalities among cap-snatching endonucleases from segmented negative-strand RNA viruses. *J. Biol. Chem.* 293, 19686–19698.  
<https://doi.org/10.1074/jbc.RA118.004373>
- Holtzman, D.M., Pitas, R.E., Kilbridge, J., Nathan, B., Mahley, R.W., Bu, G., Schwartz, A.L., 1995. Low density lipoprotein receptor-related protein mediates apolipoprotein E-dependent neurite outgrowth in a central nervous system-derived neuronal cell line. *Proc. Natl. Acad. Sci. U. S. A.* 92, 9480–9484.
- Honig, J.E., Osborne, J.C., Nichol, S.T., 2004. Crimean–Congo hemorrhagic fever virus genome L RNA segment and encoded protein. *Virology* 321, 29–35.  
<https://doi.org/10.1016/j.virol.2003.09.042>
- Hoogstraal, H., 1979. Review Article 1: The Epidemiology of Tick-Borne Crimean-Congo Hemorrhagic Fever in Asia, Europe, and Africa. *J. Med. Entomol.* 15, 307–417.  
<https://doi.org/10.1093/jmedent/15.4.307>
- Huang, L., Li, H., Ye, Z., Xu, Q., Fu, Q., Sun, W., Qi, W., Yue, J., 2021. Berbamine inhibits Japanese encephalitis virus (JEV) infection by compromising TPRMLs-mediated endolysosomal trafficking of low-density lipoprotein receptor (LDLR). *Emerg. Microbes Infect.* 10, 1257–1271. <https://doi.org/10.1080/22221751.2021.1941276>
- Hueging, K., Doepke, M., Vieyres, G., Bankwitz, D., Frentzen, A., Doerrbecker, J., Gumz, F., Haid, S., Wölk, B., Kaderali, L., Pietschmann, T., 2014. Apolipoprotein E Codetermines Tissue Tropism of Hepatitis C Virus and Is Crucial for Viral Cell-to-Cell Transmission by Contributing to a Postenvelopment Step of Assembly. *J. Virol.* 88, 1433–1446.  
<https://doi.org/10.1128/JVI.01815-13>
- Huggins, J.W., 1989. Prospects for Treatment of Viral Hemorrhagic Fevers with Ribavirin, a Broad-Spectrum Antiviral Drug. *Rev. Infect. Dis.* 11, S750–S761.  
[https://doi.org/10.1093/clinids/11.Supplement\\_4.S750](https://doi.org/10.1093/clinids/11.Supplement_4.S750)
- Hussain, M.M., Shi, J., Dreizen, P., 2003. Microsomal triglyceride transfer protein and its role in apoB-lipoprotein assembly. *J. Lipid Res.* 44, 22–32.  
<https://doi.org/10.1194/jlr.r200014-jlr200>
- Ikegami, T., Won, S., Peters, C.J., Makino, S., 2005. Rift Valley Fever Virus NSs mRNA Is Transcribed from an Incoming Anti-Viral-Sense S RNA Segment. *J. Virol.* 79, 12106–12111. <https://doi.org/10.1128/JVI.79.18.12106-12111.2005>
- Jabbari, A., Besharat, S., Abbasi, A., Moradi, A., Kalavi, K., 2006. Crimean-Congo hemorrhagic fever: case series from a medical center in Golestan province, Northeast of Iran (2004). *Indian J. Med. Sci.* 60, 327–329.
- Jackson, R.L., Sparrow, J.T., Baker, H.N., Morrisett, J.D., Taunton, O.D., Gotto, A.M., 1974. The primary structure of apolipoprotein-serine. *J. Biol. Chem.* 249, 5308–5313.
- Jae, L.T., Raaben, M., Herbert, A.S., Kuehne, A.I., Wirchnianski, A.S., Soh, T., Stubbs, S.H., Janssen, H., Damme, M., Saftig, P., Whelan, S.P., Dye, J.M., Brummelkamp, T.R., 2014.

- Lassa virus entry requires a trigger-induced receptor switch. *Science* 344, 1506–1510.  
<https://doi.org/10.1126/science.1252480>
- Jameson, L.J., Morgan, P.J., Medlock, J.M., Watola, G., Vaux, A.G.C., 2012. Importation of *Hyalomma marginatum*, vector of Crimean-Congo haemorrhagic fever virus, into the United Kingdom by migratory birds. *Ticks Tick-Borne Dis.* 3, 95–99.  
<https://doi.org/10.1016/j.ttbdis.2011.12.002>
- Jangra, R.K., Herbert, A.S., Li, R., Jae, L.T., Kleinfelter, L.M., Slough, M.M., Barker, S.L., Guardado-Calvo, P., Román-Sosa, G., Dieterle, M.E., Kuehne, A.I., Muena, N.A., Wirchnianski, A.S., Nyakatura, E.K., Fels, J.M., Ng, M., Mittler, E., Pan, J., Bharrhan, S., Wec, A.Z., Lai, J.R., Sidhu, S.S., Tischler, N.D., Rey, F.A., Moffat, J., Brummelkamp, T.R., Wang, Z., Dye, J.M., Chandran, K., 2018. Protocadherin-1 is essential for cell entry by New World hantaviruses. *Nature* 563, 559–563.  
<https://doi.org/10.1038/s41586-018-0702-1>
- Jeeva, S., Cheng, E., Ganaie, S.S., Mir, M.A., 2017a. Crimean-Congo Hemorrhagic Fever Virus Nucleocapsid Protein Augments mRNA Translation. *J. Virol.* 91, e00636-17.  
<https://doi.org/10.1128/JVI.00636-17>
- Jeeva, S., Pador, S., Voss, B., Ganaie, S.S., Mir, M.A., 2017b. Crimean-Congo hemorrhagic fever virus nucleocapsid protein has dual RNA binding modes. *PLoS One* 12, e0184935. <https://doi.org/10.1371/journal.pone.0184935>
- Jiang, J., Luo, G., 2009. Apolipoprotein E but Not B Is Required for the Formation of Infectious Hepatitis C Virus Particles. *J. Virol.* 83, 12680–12691.  
<https://doi.org/10.1128/JVI.01476-09>
- Jin, H., Elliott, R.M., 1993. Non-viral sequences at the 5' ends of Dugbe nairovirus S mRNAs. *J. Gen. Virol.* 74, 2293–2297. <https://doi.org/10.1099/0022-1317-74-10-2293>
- Johnson, S., Henschke, N., Maayan, N., Mills, I., Buckley, B.S., Kakourou, A., Marshall, R., 2018. Ribavirin for treating Crimean Congo haemorrhagic fever. *Cochrane Database Syst. Rev.* <https://doi.org/10.1002/14651858.CD012713.pub2>
- Jones, L.D., Davies, C.R., Steele, G.M., Nuttall, P.A., 1987. A Novel Mode of Arbovirus Transmission Involving a Nonviremic Host. *Science* 237, 775–777.  
<https://doi.org/10.1126/science.3616608>
- Kahl, O., Gern, L., Eisen, L., Lane, R.S., 2002. Ecological research on *Borrelia burgdorferi* sensu lato: terminology and some methodological pitfalls. *Lyme Borreliosis Biol. Epidemiol. Control*, CABI Books 29–46.  
<https://doi.org/10.1079/9780851996325.0029>
- Karlberg, H., Tan, Y.-J., Mirazimi, A., 2011. Induction of Caspase Activation and Cleavage of the Viral Nucleocapsid Protein in Different Cell Types during Crimean-Congo Hemorrhagic Fever Virus Infection. *J. Biol. Chem.* 286, 3227–3234.  
<https://doi.org/10.1074/jbc.M110.149369>
- Kawano, Y., Yoshida, T., Hieda, K., Aoki, J., Miyoshi, H., Koyanagi, Y., 2004. A Lentiviral cDNA Library Employing Lambda Recombination Used To Clone an Inhibitor of Human Immunodeficiency Virus Type 1-Induced Cell Death. *J. Virol.* 78, 11352–11359.  
<https://doi.org/10.1128/JVI.78.20.11352-11359.2004>
- Kim, B., Bae, M., Park, Y.-K., Ma, H., Yuan, T., Seeram, N.P., Lee, J.-Y., 2018. Blackcurrant anthocyanins stimulated cholesterol transport via post-transcriptional induction of LDL receptor in Caco-2 cells. *Eur. J. Nutr.* 57, 405–415.  
<https://doi.org/10.1007/s00394-017-1506-z>
- Kim, D.H., Iijima, H., Goto, K., Sakai, J., Ishii, H., Kim, H.J., Suzuki, H., Kondo, H., Saeki, S., Yamamoto, T., 1996. Human apolipoprotein E receptor 2. A novel lipoprotein



- receptor of the low density lipoprotein receptor family predominantly expressed in brain. *J. Biol. Chem.* 271, 8373–8380. <https://doi.org/10.1074/jbc.271.14.8373>
- Knott, T.J., Pease, R.J., Powell, L.M., Wallis, S.C., Rall, S.C., Innerarity, T.L., Blackhart, B., Taylor, W.H., Marcel, Y., Milne, R., 1986. Complete protein sequence and identification of structural domains of human apolipoprotein B. *Nature* 323, 734–738. <https://doi.org/10.1038/323734a0>
- Korolev, M.B., Donets, M.A., Rubin, S.G., Chumakov, M.P., 1976. Morphology and morphogenesis of Crimean Hemorrhagic Fever Virus. *Arch. Virol.* 50, 169–172. <https://doi.org/10.1007/BF01318011>
- Kosenko, T., Golder, M., Leblond, G., Weng, W., Lagace, T.A., 2013. Low Density Lipoprotein Binds to Proprotein Convertase Subtilisin/Kexin Type-9 (PCSK9) in Human Plasma and Inhibits PCSK9-mediated Low Density Lipoprotein Receptor Degradation. *J. Biol. Chem.* 288, 8279–8288. <https://doi.org/10.1074/jbc.M112.421370>
- Krautkrämer, E., Zeier, M., 2008. Hantavirus causing hemorrhagic fever with renal syndrome enters from the apical surface and requires decay-accelerating factor (DAF/CD55). *J. Virol.* 82, 4257–4264. <https://doi.org/10.1128/JVI.02210-07>
- Kuhn, J.H., Abe, J., Adkins, S., Alkhovsky, S.V., Avšič-Županc, T., Ayllón, M.A., Bahl, J., Balkema-Buschmann, A., Ballinger, M.J., Kumar Baranwal, V., Beer, M., Bejerman, N., Bergeron, É., Biedenkopf, N., Blair, C.D., Blasdell, K.R., Blouin, A.G., Bradfute, S.B., Briese, T., Brown, P.A., Buchholz, U.J., Buchmeier, M.J., Bukreyev, A., Burt, F., Büttner, C., Calisher, C.H., Cao, M., Casas, I., Chandran, K., Charrel, R.N., Kumar Chaturvedi, K., Chooi, K.M., Crane, A., Dal Bó, E., Carlos de la Torre, J., de Souza, W.M., de Swart, R.L., Debat, H., Dheilly, N.M., Di Paola, N., Di Serio, F., Dietzgen, R.G., Digiaro, M., Drexler, J.F., Duprex, W.P., Dürrwald, R., Easton, A.J., Elbeaino, T., Ergünay, K., Feng, G., Firth, A.E., Fooks, A.R., Formenty, P.B.H., Freitas-Astúa, J., Gago-Zachert, S., Laura García, M., García-Sastre, A., Garrison, A.R., Gaskin, T.R., Gong, W., Gonzalez, J.-P.J., de Bellocq, J., Griffiths, A., Groschup, M.H., Günther, I., Günther, S., Hammond, J., Hasegawa, Y., Hayashi, K., Hepojoki, J., Higgins, C.M., Hongō, S., Horie, M., Hughes, H.R., Hume, A.J., Hyndman, T.H., Ikeda, K., Jiāng, D., Jonson, G.B., Junglen, S., Klempa, B., Klingström, J., Kondō, H., Koonin, E.V., Krupovic, M., Kubota, K., Kurath, G., Laenen, L., Lambert, A.J., Li, J., Li, J.-M., Liu, R., Lukashevich, I.S., MacDiarmid, R.M., Maes, P., Marklewitz, M., Marshall, S.H., Marzano, S.-Y.L., McCauley, J.W., Mirazimi, A., Mühlberger, E., Nabeshima, T., Naidu, R., Natsuaki, T., Navarro, B., Navarro, J.A., Neriya, Y., Netesov, S.V., Neumann, G., Nowotny, N., Nunes, M.R.T., Ochoa-Corona, F.M., Okada, T., Palacios, G., Pallás, V., Papa, A., Paraskevopoulou, S., Parrish, C.R., Pauvolid-Corrêa, A., Pawęska, J.T., Pérez, D.R., Pfaff, F., Plemper, R.K., Postler, T.S., Rabbidge, L.O., Radoshitzky, S.R., Ramos-González, P.L., Rehanek, M., Resende, R.O., Reyes, C.A., Rodrigues, T.C.S., Romanowski, V., Rubbenstroth, D., Rubino, L., Runstadler, J.A., Sabanadzovic, S., Sadiq, S., Salvato, M.S., Sasaya, T., Schwemmler, M., Sharpe, S.R., Shi, M., Shimomoto, Y., Kavi Sidharthan, V., Sironi, M., Smither, S., Song, J.-W., Spann, K.M., Spengler, J.R., Stenglein, M.D., Takada, A., Takeyama, S., Tatara, A., Tesh, R.B., Thornburg, N.J., Tian, X., Tischler, N.D., Tomitaka, Y., Tomonaga, K., Tordo, N., Tu, C., Turina, M., Tzanetakis, I.E., Maria Vaira, A., van den Hoogen, B., Vanmechelen, B., Vasilakis, N., Verbeek, M., von Bargen, S., Wada, J., Wahl, V., Walker, P.J., Waltzek, T.B., Whitfield, A.E., Wolf, Y.I., Xia, H., Xylogianni, E., Yanagisawa, H., Yano, K., Ye, G., Yuan, Z., Zerbini, F.M., Zhang, G., Zhang, S., Zhang, Y.-Z., Zhao, L., Økland, A.L., 2023. Annual (2023) taxonomic update of RNA-directed RNA polymerase-encoding negative-sense RNA

- viruses (realm Riboviria: kingdom Orthornavirae: phylum Negarnaviricota). *J. Gen. Virol.* 104, 001864. <https://doi.org/10.1099/jgv.0.001864>
- Kumar, B., Manjunathachar, H.V., Ghosh, S., 2020. A review on Hyalomma species infestations on human and animals and progress on management strategies. *Heliyon* 6, e05675. <https://doi.org/10.1016/j.heliyon.2020.e05675>
- Kwon, O.Y., Hwang, K., Kim, J.-A., Kim, K., Kwon, I.C., Song, H.K., Jeon, H., 2010. Dab1 binds to Fe65 and diminishes the effect of Fe65 or LRP1 on APP processing. *J. Cell. Biochem.* 111, 508–519. <https://doi.org/10.1002/jcb.22738>
- Lagace, T.A., Curtis, D.E., Garuti, R., McNutt, M.C., Park, S.W., Prather, H.B., Anderson, N.N., Ho, Y.K., Hammer, R.E., Horton, J.D., 2006. Secreted PCSK9 decreases the number of LDL receptors in hepatocytes and in livers of parabiotic mice. *J. Clin. Invest.* 116, 2995–3005. <https://doi.org/10.1172/JCI29383>
- Larrey, D., D’Erasmus, L., O’Brien, S., Arca, M., 2023. Long-term hepatic safety of lomitapide in homozygous familial hypercholesterolaemia. *Liver Int.* 43, 413–423. <https://doi.org/10.1111/liv.15497>
- Lavanya, M., Cuevas, C.D., Thomas, M., Cherry, S., Ross, S.R., 2013. siRNA screen for genes that affect Junin virus entry uncovers voltage-gated calcium channels as a therapeutic target. *Sci. Transl. Med.* 5, 204ra131. <https://doi.org/10.1126/scitranslmed.3006827>
- Lavillette, D., Ruggieri, A., Boson, B., Maurice, M., Cosset, F.-L., 2002. Relationship between SU subdomains that regulate the receptor-mediated transition from the native (fusion-inhibited) to the fusion-active conformation of the murine leukemia virus glycoprotein. *J. Virol.* 76, 9673–9685. <https://doi.org/10.1128/jvi.76.19.9673-9685.2002>
- Léger, P., Tetard, M., Youness, B., Cordes, N., Rouxel, R.N., Flamand, M., Lozach, P.-Y., 2016. Differential Use of the C-Type Lectins L-SIGN and DC-SIGN for Phlebovirus Endocytosis. *Traffic Cph. Den.* 17, 639–656. <https://doi.org/10.1111/tra.12393>
- Leventhal, S.S., Wilson, D., Feldmann, H., Hawman, D.W., 2021. A Look into Bunyavirales Genomes: Functions of Non-Structural (NS) Proteins. *Viruses* 13, 314. <https://doi.org/10.3390/v13020314>
- Leveringhaus, E., Poljakovic, R., Herrmann, G., Roman-Sosa, G., Becher, P., Postel, A., 2024. Porcine low-density lipoprotein receptor plays an important role in classical swine fever virus infection. *Emerg. Microbes Infect.* 13, 2327385. <https://doi.org/10.1080/22221751.2024.2327385>
- Li, N., Rao, G., Li, Z., Yin, J., Chong, T., Tian, K., Fu, Y., Cao, S., 2022. Cryo-EM structure of glycoprotein C from Crimean-Congo hemorrhagic fever virus. *Virol. Sin.* 37, 127–137. <https://doi.org/10.1016/j.virs.2022.01.015>
- Li, Y., Cam, J., Bu, G., 2001. Low-density lipoprotein receptor family: endocytosis and signal transduction. *Mol. Neurobiol.* 23, 53–67. <https://doi.org/10.1385/MN:23:1:53>
- Li, Y., Lu, W., Bu, G., 2005. Striking differences of LDL receptor-related protein 1B expression in mouse and human. *Biochem. Biophys. Res. Commun.* 333, 868–873. <https://doi.org/10.1016/j.bbrc.2005.05.170>
- Li, Y., Luo, G., 2021. Human low-density lipoprotein receptor plays an important role in hepatitis B virus infection. *PLOS Pathog.* 17, e1009722. <https://doi.org/10.1371/journal.ppat.1009722>
- Li, Z., Li, Y., Bi, Y., Zhang, H., Yao, Y., Li, Q., Cun, W., Dong, S., 2017. Extracellular Interactions between Hepatitis C Virus and Secreted Apolipoprotein E. *J. Virol.* 91, e02227-16. <https://doi.org/10.1128/JVI.02227-16>

- Lindeborg, M., Barboutis, C., Ehrenborg, C., Fransson, T., Jaenson, T.G.T., Lindgren, P.-E., Lundkvist, Å., Nyström, F., Salaneck, E., Waldenström, J., Olsen, B., 2012. Migratory Birds, Ticks, and Crimean-Congo Hemorrhagic Fever Virus - Volume 18, Number 12—December 2012 - Emerging Infectious Diseases journal - CDC.  
<https://doi.org/10.3201/eid1812.120718>
- Liu, C.-X., Li, Y., Obermoeller-McCormick, L.M., Schwartz, A.L., Bu, G., 2001. The Putative Tumor Suppressor LRP1B, a Novel Member of the Low Density Lipoprotein (LDL) Receptor Family, Exhibits Both Overlapping and Distinct Properties with the LDL Receptor-related Protein. *J. Biol. Chem.* 276, 28889–28896.  
<https://doi.org/10.1074/jbc.M102727200>
- Liu, C.X., Musco, S., Lisitsina, N.M., Forgacs, E., Minna, J.D., Lisitsyn, N.A., 2000. LRP-DIT, a putative endocytic receptor gene, is frequently inactivated in non-small cell lung cancer cell lines. *Cancer Res.* 60, 1961–1967.
- Liu, K., Xiao, C., Xi, S., Hameed, M., Wahaab, A., Shao, D., Li, Z., Li, B., Wei, J., Qiu, Y., Miao, D., Zhu, H., Ma, Z., 2020. Mosquito Defensins Enhance Japanese Encephalitis Virus Infection by Facilitating Virus Adsorption and Entry within the Mosquito. *J. Virol.* 94, e01164-20. <https://doi.org/10.1128/JVI.01164-20>
- Lorenzo Juanes, H., C, C., Bf, S., A, L.-B., A, B., A, O., Cv, L., Ms, L., Ai, N., B, R.-A., Br, B., Mp, S.-S., JI, M.B., A, M., M, B.-G., 2023. Crimean-Congo Hemorrhagic Fever, Spain, 2013–2021. *Emerg. Infect. Dis.* 29. <https://doi.org/10.3201/eid2902.220677>
- Lozach, P.-Y., Kühbacher, A., Meier, R., Mancini, R., Bitto, D., Bouloy, M., Helenius, A., 2011. DC-SIGN as a receptor for phleboviruses. *Cell Host Microbe* 10, 75–88.  
<https://doi.org/10.1016/j.chom.2011.06.007>
- Lucifora, J., Esser, K., Protzer, U., 2013. Ezetimibe blocks hepatitis B virus infection after virus uptake into hepatocytes. *Antiviral Res.* 97, 195–197.  
<https://doi.org/10.1016/j.antiviral.2012.12.008>
- Ma, H., Adams, L.J., Raju, S., Sariol, A., Kafai, N.M., Janova, H., Klimstra, W.B., Fremont, D.H., Diamond, M.S., 2024. The low-density lipoprotein receptor promotes infection of multiple encephalitic alphaviruses. *Nat. Commun.* 15, 246.  
<https://doi.org/10.1038/s41467-023-44624-x>
- Ma, M., Kersten, D.B., Kamrud, K.I., Wool-Lewis, R.J., Schmaljohn, C., González-Scarano, F., 1999. Murine leukemia virus pseudotypes of La Crosse and Hantaan Bunyaviruses: a system for analysis of cell tropism. *Virus Res.* 64, 23–32.  
[https://doi.org/10.1016/s0168-1702\(99\)00070-2](https://doi.org/10.1016/s0168-1702(99)00070-2)
- Macleod, J.M.L., Marmor, H., García-Sastre, A., Frias-Staheli, N., 2015. Mapping of the interaction domains of the Crimean–Congo hemorrhagic fever virus nucleocapsid protein. *J. Gen. Virol.* 96, 524–537. <https://doi.org/10.1099/vir.0.071332-0>
- MacPhee, C.E., Hatters, D.M., Sawyer, W.H., Howlett, G.J., 2000. Apolipoprotein C-II39-62 Activates Lipoprotein Lipase by Direct Lipid-Independent Binding. *Biochemistry* 39, 3433–3440. <https://doi.org/10.1021/bi992523t>
- Mancuso, E., Toma, L., Polci, A., d’Alessio, S.G., Luca, M.D., Orsini, M., Domenico, M.D., Marcacci, M., Mancini, G., Spina, F., Goffredo, M., Monaco, F., 2019. Crimean-Congo Hemorrhagic Fever Virus Genome in Tick from Migratory Bird, Italy - Volume 25, Number 7—July 2019 - Emerging Infectious Diseases journal - CDC.  
<https://doi.org/10.3201/eid2507.181345>
- Mangia, A., Santoro, R., Minerva, N., Ricci, G.L., Carretta, V., Persico, M., Vinelli, F., Scotto, G., Bacca, D., Annese, M., Romano, M., Zechini, F., Sogari, F., Spirito, F., Andriulli, A.,

2005. Peginterferon alfa-2b and ribavirin for 12 vs. 24 weeks in HCV genotype 2 or 3. *N. Engl. J. Med.* 352, 2609–2617. <https://doi.org/10.1056/NEJMoa042608>
- Marinó, M., Andrews, D., Brown, D., McCluskey, R.T., 2001. Transcytosis of retinol-binding protein across renal proximal tubule cells after megalin (gp 330)-mediated endocytosis. *J. Am. Soc. Nephrol. JASN* 12, 637–648. <https://doi.org/10.1681/ASN.V124637>
- Marinò, M., Zheng, G., Chiovato, L., Pinchera, A., Brown, D., Andrews, D., McCluskey, R.T., 2000. Role of Megalin (gp330) in Transcytosis of Thyroglobulin by Thyroid Cells: A NOVEL FUNCTION IN THE CONTROL OF THYROID HORMONE RELEASE\*. *J. Biol. Chem.* 275, 7125–7137. <https://doi.org/10.1074/jbc.275.10.7125>
- Marlovits, T.C., Abrahamsberg, C., Blaas, D., 1998. Very-Low-Density Lipoprotein Receptor Fragment Shed from HeLa Cells Inhibits Human Rhinovirus Infection. *J. Virol.* 72, 10246–10250.
- Martínez-Gutierrez, M., Castellanos, J.E., Gallego-Gómez, J.C., 2011. Statins Reduce Dengue Virus Production via Decreased Virion Assembly. *Intervirology* 54, 202–216. <https://doi.org/10.1159/000321892>
- Marzolo, M.-P., Farfán, P., 2011. New Insights into the Roles of Megalin/LRP2 and the Regulation of its Functional Expression. *Biol. Res.* 44, 89–105. <https://doi.org/10.4067/S0716-97602011000100012>
- Matthys, V.S., Gorbunova, E.E., Gavrilovskaya, I.N., Mackow, E.R., 2010. Andes Virus Recognition of Human and Syrian Hamster  $\beta$ 3 Integrins Is Determined by an L33P Substitution in the PSI Domain. *J. Virol.* 84, 352–360. <https://doi.org/10.1128/JVI.01013-09>
- Mehand, M.S., Al-Shorbaji, F., Millett, P., Murgue, B., 2018. The WHO R&D Blueprint: 2018 review of emerging infectious diseases requiring urgent research and development efforts. *Antiviral Res.* 159, 63–67. <https://doi.org/10.1016/j.antiviral.2018.09.009>
- Mercer, J., Schelhaas, M., Helenius, A., 2010. Virus Entry by Endocytosis. *Annu. Rev. Biochem.* 79, 803–833. <https://doi.org/10.1146/annurev-biochem-060208-104626>
- Merz, A., Long, G., Hiet, M.-S., Brügger, B., Chlanda, P., Andre, P., Wieland, F., Krijnse-Locker, J., Bartenschlager, R., 2011. Biochemical and morphological properties of hepatitis C virus particles and determination of their lipidome. *J. Biol. Chem.* 286, 3018–3032. <https://doi.org/10.1074/jbc.M110.175018>
- Messina, J.P., Pigott, D.M., Golding, N., Duda, K.A., Brownstein, J.S., Weiss, D.J., Gibson, H., Robinson, T.P., Gilbert, M., William Wint, G.R., Nuttall, P.A., Gething, P.W., Myers, M.F., George, D.B., Hay, S.I., 2015. The global distribution of Crimean-Congo hemorrhagic fever. *Trans. R. Soc. Trop. Med. Hyg.* 109, 503–513. <https://doi.org/10.1093/trstmh/trv050>
- Midilli, K., Gargili, A., Ergonul, O., Sengöz, G., Ozturk, R., Bakar, M., Jongejan, F., 2007. Imported Crimean-Congo hemorrhagic fever cases in Istanbul. *BMC Infect. Dis.* 7, 54. <https://doi.org/10.1186/1471-2334-7-54>
- Mikhailenko, I., Battey, F.D., Migliorini, M., Ruiz, J.F., Argraves, K., Moayeri, M., Strickland, D.K., 2001. Recognition of alpha 2-macroglobulin by the low density lipoprotein receptor-related protein requires the cooperation of two ligand binding cluster regions. *J. Biol. Chem.* 276, 39484–39491. <https://doi.org/10.1074/jbc.M104382200>
- Mishra, A.K., Hellert, J., Freitas, N., Guardado-Calvo, P., Haouz, A., Fels, J.M., Maurer, D.P., Abelson, D.M., Bornholdt, Z.A., Walker, L.M., Chandran, K., Cosset, F.-L., McLellan, J.S., Rey, F.A., 2022. Structural basis of synergistic neutralization of Crimean-Congo

- hemorrhagic fever virus by human antibodies. *Science* 375, 104–109.  
<https://doi.org/10.1126/science.abl6502>
- Mitchell, R.D., Ross, E., Osgood, C., Sonenshine, D.E., Donohue, K.V., Khalil, S.M., Thompson, D.M., Michael Roe, R., 2007. Molecular characterization, tissue-specific expression and RNAi knockdown of the first vitellogenin receptor from a tick. *Insect Biochem. Mol. Biol.* 37, 375–388. <https://doi.org/10.1016/j.ibmb.2007.01.005>
- Moestrup, S.K., Holtet, T.L., Etzerodt, M., Thøgersen, H.C., Nykjaer, A., Andreasen, P.A., Rasmussen, H.H., Sottrup-Jensen, L., Gliemann, J., 1993. Alpha 2-macroglobulin-proteinase complexes, plasminogen activator inhibitor type-1-plasminogen activator complexes, and receptor-associated protein bind to a region of the alpha 2-macroglobulin receptor containing a cluster of eight complement-type repeats. *J. Biol. Chem.* 268, 13691–13696.
- Mohr, S., Bakal, C., Perrimon, N., 2010. Genomic screening with RNAi: results and challenges. *Annu. Rev. Biochem.* 79, 37–64. <https://doi.org/10.1146/annurev-biochem-060408-092949>
- Monteil, V., Salata, C., Appelberg, S., Mirazimi, A., 2020. Hazara virus and Crimean-Congo Hemorrhagic Fever Virus show a different pattern of entry in fully-polarized Caco-2 cell line. *PLoS Negl. Trop. Dis.* 14, e0008863.  
<https://doi.org/10.1371/journal.pntd.0008863>
- Monteil, V.M., Wright, S.C., Dyczynski, M., Kellner, M.J., Appelberg, S., Platzer, S.W., Ibrahim, A., Kwon, H., Pittarokoilis, I., Mirandola, M., Michlits, G., Devignot, S., Elder, E., Abdurahman, S., Bereczky, S., Bagci, B., Youhanna, S., Aastrup, T., Lauschke, V.M., Salata, C., Elaldi, N., Weber, F., Monserrat, N., Hawman, D.W., Feldmann, H., Horn, M., Penninger, J.M., Mirazimi, A., 2024. Crimean-Congo haemorrhagic fever virus uses LDLR to bind and enter host cells. *Nat. Microbiol.*  
<https://doi.org/10.1038/s41564-024-01672-3>
- Morales, C.R., Igdoura, S.A., Wosu, U.A., Boman, J., Argraves, W.S., 1996. Low density lipoprotein receptor-related protein-2 expression in efferent duct and epididymal epithelia: evidence in rats for its in vivo role in endocytosis of apolipoprotein J/clusterin. *Biol. Reprod.* 55, 676–683. <https://doi.org/10.1095/biolreprod55.3.676>
- Mora-Rillo, M., Díaz-Menéndez, M., Crespillo-Andujar, C., Arribas, J.R., 2018. Autochthonous Crimean-Congo haemorrhagic fever in Spain: So much to learn. *Enfermedades Infecc. Microbiol. Clínica* 36, 202. <https://doi.org/10.1016/j.eimc.2017.05.004>
- Moriguchi, H., Chung, R.T., Sato, C., 2010. New translational research on novel drugs for hepatitis C virus 1b infection by using a replicon system and human induced pluripotent stem cells. *Hepatology* 51, 344–345. <https://doi.org/10.1002/hep.23378>
- Morikawa, S., Qing, T., Xinqin, Z., Saijo, M., Kurane, I., 2002. Genetic Diversity of the M RNA Segment among Crimean-Congo Hemorrhagic Fever Virus Isolates in China. *Virology* 296, 159–164. <https://doi.org/10.1006/viro.2002.1387>
- Morrow, J.A., Segall, M.L., Lund-Katz, S., Phillips, M.C., Knapp, M., Rupp, B., Weisgraber, K.H., 2000. Differences in Stability among the Human Apolipoprotein E Isoforms Determined by the Amino-Terminal Domain. *Biochemistry* 39, 11657–11666.  
<https://doi.org/10.1021/bi000099m>
- Mou, D.L., Wang, Y.P., Huang, C.X., Li, G.Y., Pan, L., Yang, W.S., Bai, X.F., 2006. Cellular entry of Hantaan virus A9 strain: Specific interactions with  $\beta$ 3 integrins and a novel 70kDa protein. *Biochem. Biophys. Res. Commun.* 339, 611–617.  
<https://doi.org/10.1016/j.bbrc.2005.11.049>

- Murakami, S., Takenaka-Uema, A., Kobayashi, T., Kato, K., Shimojima, M., Palmarini, M., Horimoto, T., 2017. Heparan Sulfate Proteoglycan Is an Important Attachment Factor for Cell Entry of Akabane and Schmallenberg Viruses. *J. Virol.* 91, e00503-17. <https://doi.org/10.1128/JVI.00503-17>
- Neels, J.G., van Den Berg, B.M., Lookene, A., Olivecrona, G., Pannekoek, H., van Zonneveld, A.J., 1999. The second and fourth cluster of class A cysteine-rich repeats of the low density lipoprotein receptor-related protein share ligand-binding properties. *J. Biol. Chem.* 274, 31305–31311. <https://doi.org/10.1074/jbc.274.44.31305>
- Neely, R.D.G., Bassendine, M.F., 2010. Antisense technology to lower LDL cholesterol. *Lancet Lond. Engl.* 375, 959–961. [https://doi.org/10.1016/S0140-6736\(10\)60364-9](https://doi.org/10.1016/S0140-6736(10)60364-9)
- Negredo, A., Sánchez-Ledesma, M., Llorente, F., Pérez-Olmeda, M., Belhassen-García, M., González-Calle, D., Sánchez-Seco, M.P., Jiménez-Clavero, M.Á., 2021. Retrospective Identification of Early Autochthonous Case of Crimean-Congo Hemorrhagic Fever, Spain, 2013 - Volume 27, Number 6—June 2021 - *Emerging Infectious Diseases journal - CDC*. <https://doi.org/10.3201/eid2706.204643>
- Nestel, P.J., Fidge, N.H., 1982. Apoprotein C metabolism in man. *Adv. Lipid Res.* 19, 55–83. <https://doi.org/10.1016/b978-0-12-024919-0.50008-4>
- Nielsen, S.U., Bassendine, M.F., Burt, A.D., Martin, C., Pumeechockchai, W., Toms, G.L., 2006. Association between hepatitis C virus and very-low-density lipoprotein (VLDL)/LDL analyzed in iodixanol density gradients. *J. Virol.* 80, 2418–2428. <https://doi.org/10.1128/JVI.80.5.2418-2428.2006>
- Nikolic, J., Belot, L., Raux, H., Legrand, P., Gaudin, Y., Albertini, A., 2018. Structural basis for the recognition of LDL-receptor family members by VSV glycoprotein. *Nat. Commun.* 9, 1029. <https://doi.org/10.1038/s41467-018-03432-4>
- Nimpf, J., Schneider, W.J., 2000. From cholesterol transport to signal transduction: low density lipoprotein receptor, very low density lipoprotein receptor, and apolipoprotein E receptor-2. *Biochim. Biophys. Acta* 1529, 287–298. [https://doi.org/10.1016/s1388-1981\(00\)00155-4](https://doi.org/10.1016/s1388-1981(00)00155-4)
- Nuttall, P.A., Labuda, M., 2004. Tick–host interactions: saliva-activated transmission. *Parasitology* 129, S177–S189. <https://doi.org/10.1017/S0031182004005633>
- Oestereich, L., Rieger, T., Neumann, M., Bernreuther, C., Lehmann, M., Krasemann, S., Wurr, S., Emmerich, P., Lamballerie, X. de, Ölschläger, S., Günther, S., 2014. Evaluation of Antiviral Efficacy of Ribavirin, Arbidol, and T-705 (Favipiravir) in a Mouse Model for Crimean-Congo Hemorrhagic Fever. *PLoS Negl. Trop. Dis.* 8, e2804. <https://doi.org/10.1371/journal.pntd.0002804>
- Oka, K., Ishimura-Oka, K., Chu, M.J., Sullivan, M., Krushkal, J., Li, W.H., Chan, L., 1994. Mouse very-low-density-lipoprotein receptor (VLDLR) cDNA cloning, tissue-specific expression and evolutionary relationship with the low-density-lipoprotein receptor. *Eur. J. Biochem.* 224, 975–982. <https://doi.org/10.1111/j.1432-1033.1994.00975.x>
- Olson, G.E., Winfrey, V.P., Hill, K.E., Burk, R.F., 2008. Megalin mediates selenoprotein P uptake by kidney proximal tubule epithelial cells. *J. Biol. Chem.* 283, 6854–6860. <https://doi.org/10.1074/jbc.M709945200>
- Olson, G.E., Winfrey, V.P., Nagdas, S.K., Hill, K.E., Burk, R.F., 2007. Apolipoprotein E receptor-2 (ApoER2) mediates selenium uptake from selenoprotein P by the mouse testis. *J. Biol. Chem.* 282, 12290–12297. <https://doi.org/10.1074/jbc.M611403200>
- Orlando, R.A., Rader, K., Authier, F., Yamazaki, H., Posner, B.I., Bergeron, J.J., Farquhar, M.G., 1998. Megalin is an endocytic receptor for insulin. *J. Am. Soc. Nephrol. JASN* 9, 1759–1766. <https://doi.org/10.1681/ASN.V9101759>

- Owen, D.M., Huang, H., Ye, J., Gale, M., 2009. Apolipoprotein E on hepatitis C virion facilitates infection through interaction with low-density lipoprotein receptor. *Virology* 394, 99–108. <https://doi.org/10.1016/j.virol.2009.08.037>
- Pak.TP, 1970. Epidemiology of Crimean hemorrhagic fever in Tadjik SSR. NAMRU-T1188. Inst PolioVirus Entsef, Akad Med Nauk SSSR Moskva. 1970. p. 26.
- Palomar, A.M., Portillo, A., Santibáñez, S., García-Álvarez, L., Muñoz-Sanz, A., Márquez, F.J., Romero, L., Eiros, J.M., Oteo, J.A., 2017. Molecular (ticks) and serological (humans) study of Crimean-Congo hemorrhagic fever virus in the Iberian Peninsula, 2013–2015. *Enfermedades Infecc. Microbiol. Clínica* 35, 344–347. <https://doi.org/10.1016/j.eimc.2017.01.009>
- Panda, D., Cherry, S., 2012. Cell-based genomic screening: elucidating virus-host interactions. *Curr. Opin. Virol.* 2, 778–786. <https://doi.org/10.1016/j.coviro.2012.10.007>
- Papa, A., Papadimitriou, E., Christova, I., 2011. The Bulgarian vaccine Crimean-Congo haemorrhagic fever virus strain. *Scand. J. Infect. Dis.* 43, 225–229. <https://doi.org/10.3109/00365548.2010.540036>
- Patel, A.A., Dalal, Y.D., Parikh, A., Gandhi, R., Shah, A., 2023. Crimean-Congo Hemorrhagic Fever: An Emerging Viral Infection in India, Revisited and Lessons Learned. *Cureus*. <https://doi.org/10.7759/cureus.43315>
- Pettersson, R., Kääriäinen, L., 1973. The ribonucleic acids of Uukuniemi virus, a noncubical tick-borne arbovirus. *Virology* 56, 608–619. [https://doi.org/10.1016/0042-6822\(73\)90062-7](https://doi.org/10.1016/0042-6822(73)90062-7)
- Pettersson, R.F., von Bonsdorff, C.H., 1975. Ribonucleoproteins of Uukuniemi virus are circular. *J. Virol.* 15, 386–392. <https://doi.org/10.1128/JVI.15.2.386-392.1975>
- Pham, M.-T., Lee, J.-Y., Ritter, C., Thielemann, R., Meyer, J., Haselmann, U., Funaya, C., Laketa, V., Rohr, K., Bartenschlager, R., 2023. Endosomal egress and intercellular transmission of hepatic ApoE-containing lipoproteins and its exploitation by the hepatitis C virus. *PLOS Pathog.* 19, e1011052. <https://doi.org/10.1371/journal.ppat.1011052>
- Pietrantonì, A., Fortuna, C., Remoli, M., Ciufolini, M., Superti, F., 2015. Bovine Lactoferrin Inhibits Toscana Virus Infection by Binding to Heparan Sulphate. *Viruses* 7, 480–495. <https://doi.org/10.3390/v7020480>
- Piper, R.C., Katzmann, D.J., 2007. Biogenesis and Function of Multivesicular Bodies. *Annu. Rev. Cell Dev. Biol.* 23, 519–547. <https://doi.org/10.1146/annurev.cellbio.23.090506.123319>
- Pitas, R.E., Boyles, J.K., Lee, S.H., Foss, D., Mahley, R.W., 1987. Astrocytes synthesize apolipoprotein E and metabolize apolipoprotein E-containing lipoproteins. *Biochim. Biophys. Acta BBA - Lipids Lipid Metab.* 917, 148–161. [https://doi.org/10.1016/0005-2760\(87\)90295-5](https://doi.org/10.1016/0005-2760(87)90295-5)
- Polz, E., Kotite, L., Havel, R.J., Kane, J.P., Sata, T., 1980. Human apolipoprotein C-I: Concentration in blood serum and lipoproteins. *Biochem. Med.* 24, 229–237. [https://doi.org/10.1016/0006-2944\(80\)90017-4](https://doi.org/10.1016/0006-2944(80)90017-4)
- Príncipe, C., Dionísio de Sousa, I.J., Prazeres, H., Soares, P., Lima, R.T., 2021. LRP1B: A Giant Lost in Cancer Translation. *Pharmaceuticals* 14, 836. <https://doi.org/10.3390/ph14090836>
- Pshenichnaya, N.Y., Sydenko, I.S., Klinovaya, E.P., Romanova, E.B., Zhuravlev, A.S., 2016. Possible sexual transmission of Crimean-Congo hemorrhagic fever. *Int. J. Infect. Dis.* 45, 109–111. <https://doi.org/10.1016/j.ijid.2016.02.1008>

- Punch, E.K., Hover, S., Blest, H.T.W., Fuller, J., Hewson, R., Fontana, J., Mankouri, J., Barr, J.N., 2018. Potassium is a trigger for conformational change in the fusion spike of an enveloped RNA virus. *J. Biol. Chem.* 293, 9937–9944. <https://doi.org/10.1074/jbc.RA118.002494>
- Qi, X., Lan, S., Wang, W., Schelde, L.M., Dong, H., Wallat, G.D., Ly, H., Liang, Y., Dong, C., 2010. Cap binding and immune evasion revealed by Lassa nucleoprotein structure. *Nature* 468, 779–783. <https://doi.org/10.1038/nature09605>
- Qiao, L., Luo, G.G., 2019. Human apolipoprotein E promotes hepatitis B virus infection and production. *PLOS Pathog.* 15, e1007874. <https://doi.org/10.1371/journal.ppat.1007874>
- Raaben, M., Jae, L.T., Herbert, A.S., Kuehne, A.I., Stubbs, S.H., Chou, Y.-Y., Blomen, V.A., Kirchhausen, T., Dye, J.M., Brummelkamp, T.R., Whelan, S.P., 2017. NRP2 and CD63 Are Host Factors for Lujo Virus Cell Entry. *Cell Host Microbe* 22, 688–696.e5. <https://doi.org/10.1016/j.chom.2017.10.002>
- Raal, F.J., Santos, R.D., Blom, D.J., Marais, A.D., Charng, M.-J., Cromwell, W.C., Lachmann, R.H., Gaudet, D., Tan, J.L., Chasan-Taber, S., Tribble, D.L., Flaim, J.D., Crooke, S.T., 2010. Mipomersen, an apolipoprotein B synthesis inhibitor, for lowering of LDL cholesterol concentrations in patients with homozygous familial hypercholesterolaemia: a randomised, double-blind, placebo-controlled trial. *Lancet Lond. Engl.* 375, 998–1006. [https://doi.org/10.1016/S0140-6736\(10\)60284-X](https://doi.org/10.1016/S0140-6736(10)60284-X)
- Radoshitzky, S.R., Abraham, J., Spiropoulou, C.F., Kuhn, J.H., Nguyen, D., Li, W., Nagel, J., Schmidt, P.J., Nunberg, J.H., Andrews, N.C., Farzan, M., Choe, H., 2007. Transferrin receptor 1 is a cellular receptor for New World haemorrhagic fever arenaviruses. *Nature* 446, 92–96. <https://doi.org/10.1038/nature05539>
- Raftery, M.J., Lalwani, P., Krautkrämer, E., Peters, T., Scharffetter-Kochanek, K., Krüger, R., Hofmann, J., Seeger, K., Krüger, D.H., Schönrich, G., 2014.  $\beta$ 2 integrin mediates hantavirus-induced release of neutrophil extracellular traps. *J. Exp. Med.* 211, 1485–1497. <https://doi.org/10.1084/jem.20131092>
- Raju, R., Kolakofsky, D., 1989. The ends of La Crosse virus genome and antigenome RNAs within nucleocapsids are base paired. *J. Virol.* 63, 122–128. <https://doi.org/10.1128/JVI.63.1.122-128.1989>
- Raju, R., Kolakofsky, D., 1987. Translational requirement of La Crosse virus S-mRNA synthesis: in vivo studies. *J. Virol.* 61, 96–103. <https://doi.org/10.1128/jvi.61.1.96-103.1987>
- Rall Jr, S.C., Mahley, R.W., 1992. The role of apolipoprotein E genetic variants in lipoprotein disorders. *J. Intern. Med.* 231, 653–659. <https://doi.org/10.1111/j.1365-2796.1992.tb01254.x>
- Randolph, S.E., Rogers, D.J., 2007. Ecology of Tick-Borne Disease and the Role of Climate, in: Ergonul, O., Whitehouse, C.A. (Eds.), *Crimean-Congo Hemorrhagic Fever: A Global Perspective*. Springer Netherlands, Dordrecht, pp. 167–186. [https://doi.org/10.1007/978-1-4020-6106-6\\_14](https://doi.org/10.1007/978-1-4020-6106-6_14)
- Rasmussen, I., Vilhardt, F., 2014. Macropinocytosis Is the Entry Mechanism of Amphotropic Murine Leukemia Virus. *J. Virol.* 89, 1851–1866. <https://doi.org/10.1128/JVI.02343-14>
- Reddy, S.S., Connor, T.E., Weeber, E.J., Rebeck, W., 2011. Similarities and differences in structure, expression, and functions of VLDLR and ApoER2. *Mol. Neurodegener.* 6, 30. <https://doi.org/10.1186/1750-1326-6-30>



- Riblett, A.M., Blomen, V.A., Jae, L.T., Altamura, L.A., Doms, R.W., Brummelkamp, T.R., Wojcechowskyj, J.A., 2016. A Haploid Genetic Screen Identifies Heparan Sulfate Proteoglycans Supporting Rift Valley Fever Virus Infection. *J. Virol.* 90, 1414–1423. <https://doi.org/10.1128/JVI.02055-15>
- Ritter, M., Canus, L., Gautam, A., Vallet, T., Zhong, L., Lalande, A., Boson, B., Gandhi, A., Bodoirat, S., Burlaud-Gaillard, J., Freitas, N., Roingard, P., Barr, J.N., Lotteau, V., Legros, V., Mathieu, C., Cosset, F.-L., Denolly, S., 2024. The low-density lipoprotein receptor and apolipoprotein E associated with CCHFV particles mediate CCHFV entry into cells. *Nat. Commun.* 15, 4542. <https://doi.org/10.1038/s41467-024-48989-5>
- Ritter, P., Yousefi, K., Ramirez, J., Dykxhoorn, D.M., Mendez, A.J., Shehadeh, L.A., 2018. LDL Cholesterol Uptake Assay Using Live Cell Imaging Analysis with Cell Health Monitoring. *J. Vis. Exp. JoVE.* <https://doi.org/10.3791/58564>
- Rodriguez, S.E., Cross, R.W., Fenton, K.A., Bente, D.A., Mire, C.E., Geisbert, T.W., 2019. Vesicular Stomatitis Virus-Based Vaccine Protects Mice against Crimean-Congo Hemorrhagic Fever. *Sci. Rep.* 9, 7755. <https://doi.org/10.1038/s41598-019-44210-6>
- Rusnati, M., Vicenzi, E., Donalisio, M., Oreste, P., Landolfo, S., Lembo, D., 2009. Sulfated K5 *Escherichia coli* polysaccharide derivatives: A novel class of candidate antiviral microbicides. *Pharmacol. Ther.* 123, 310–322. <https://doi.org/10.1016/j.pharmthera.2009.05.001>
- Russo, L.M., Sandoval, R.M., McKee, M., Osicka, T.M., Collins, A.B., Brown, D., Molitoris, B.A., Comper, W.D., 2007. The normal kidney filters nephrotic levels of albumin retrieved by proximal tubule cells: retrieval is disrupted in nephrotic states. *Kidney Int.* 71, 504–513. <https://doi.org/10.1038/sj.ki.5002041>
- Saijo, M., Tang, Q., Shimayi, B., Han, L., Zhang, Y., Asiguma, M., Tianshu, D., Maeda, A., Kurane, I., Morikawa, S., 2005. Antigen-capture enzyme-linked immunosorbent assay for the diagnosis of crimean-congo hemorrhagic fever using a novel monoclonal antibody. *J. Med. Virol.* 77, 83–88. <https://doi.org/10.1002/jmv.20417>
- Sainz, B., Barretto, N., Martin, D.N., Hiraga, N., Imamura, M., Hussain, S., Marsh, K.A., Yu, X., Chayama, K., Alrefai, W.A., Uprichard, S.L., 2012. Identification of the Niemann-Pick C1-like 1 cholesterol absorption receptor as a new hepatitis C virus entry factor. *Nat. Med.* 18, 281–285. <https://doi.org/10.1038/nm.2581>
- Saito, H., Dhanasekaran, P., Baldwin, F., Weisgraber, K.H., Phillips, M.C., Lund-Katz, S., 2003. Effects of Polymorphism on the Lipid Interaction of Human Apolipoprotein E\*. *J. Biol. Chem.* 278, 40723–40729. <https://doi.org/10.1074/jbc.M304814200>
- Saksida, A., Duh, D., Wraber, B., Dedushaj, I., Ahmeti, S., Avsic-Zupanc, T., 2010. Interacting roles of immune mechanisms and viral load in the pathogenesis of crimean-congo hemorrhagic fever. *Clin. Vaccine Immunol. CVI* 17, 1086–1093. <https://doi.org/10.1128/CVI.00530-09>
- Salata, C., Monteil, V., Karlberg, H., Celestino, M., Devignot, S., Leijon, M., Bell-Sakyi, L., Bergeron, É., Weber, F., Mirazimi, A., 2018. The DEVD motif of Crimean-Congo hemorrhagic fever virus nucleoprotein is essential for viral replication in tick cells. *Emerg. Microbes Infect.* 7, 190. <https://doi.org/10.1038/s41426-018-0192-0>
- Sanchez, A.J., Vincent, M.J., Erickson, B.R., Nichol, S.T., 2006. Crimean-Congo Hemorrhagic Fever Virus Glycoprotein Precursor Is Cleaved by Furin-Like and SKI-1 Proteases To Generate a Novel 38-Kilodalton Glycoprotein. *J. Virol.* 80, 514–525. <https://doi.org/10.1128/JVI.80.1.514-525.2006>

- Sanchez, A.J., Vincent, M.J., Nichol, S.T., 2002. Characterization of the Glycoproteins of Crimean-Congo Hemorrhagic Fever Virus. *J. Virol.* 76, 7263–7275. <https://doi.org/10.1128/jvi.76.14.7263-7275.2002>
- Sandrin, V., Boson, B., Salmon, P., Gay, W., Nègre, D., Le Grand, R., Trono, D., Cosset, F.-L., 2002. Lentiviral vectors pseudotyped with a modified RD114 envelope glycoprotein show increased stability in sera and augmented transduction of primary lymphocytes and CD34+ cells derived from human and nonhuman primates. *Blood* 100, 823–832. <https://doi.org/10.1182/blood-2001-11-0042>
- Sanson, K.R., Hanna, R.E., Hegde, M., Donovan, K.F., Strand, C., Sullender, M.E., Vaimberg, E.W., Goodale, A., Root, D.E., Piccioni, F., Doench, J.G., 2018. Optimized libraries for CRISPR-Cas9 genetic screens with multiple modalities. *Nat. Commun.* 9, 5416. <https://doi.org/10.1038/s41467-018-07901-8>
- Santé Publique France, 2023. Fièvre Hémorragique de Crimée-Congo : première détection du virus sur des tiques dans le sud de la France. (no date). Accueil. Available at: <https://www.santepubliquefrance.fr/les-actualites/2023/fievre-hemorragique-de-crimée-congo-première-détection-du-virus-sur-des-tiques-collectées-dans-des-elevages-bovins-dans-le-sud-de-la-france> (Accessed: 27 November 2023).
- Scholte, F.E.M., Spengler, J.R., Welch, S.R., Harmon, J.R., Coleman-McCray, J.D., Freitas, B.T., Kainulainen, M.H., Pegan, S.D., Nichol, S.T., Bergeron, É., Spiropoulou, C.F., 2019. Single-dose replicon particle vaccine provides complete protection against Crimean-Congo hemorrhagic fever virus in mice. *Emerg. Microbes Infect.* 8, 575–578. <https://doi.org/10.1080/22221751.2019.1601030>
- Scholte, F.E.M., Zivcec, M., Dzimianski, J.V., Deaton, M.K., Spengler, J.R., Welch, S.R., Nichol, S.T., Pegan, S.D., Spiropoulou, C.F., Bergeron, É., 2017. Crimean-Congo Hemorrhagic Fever Virus Suppresses Innate Immune Responses via a Ubiquitin and ISG15 Specific Protease. *Cell Rep.* 20, 2396–2407. <https://doi.org/10.1016/j.celrep.2017.08.040>
- Schwarz, M.M., Price, D.A., Ganaie, S.S., Feng, A., Mishra, N., Hoehl, R.M., Fatma, F., Stubbs, S.H., Whelan, S.P.J., Cui, X., Egawa, T., Leung, D.W., Amarasinghe, G.K., Hartman, A.L., 2022. Oropouche orthobunyavirus infection is mediated by the cellular host factor Lrp1. *Proc. Natl. Acad. Sci. U. S. A.* 119, e2204706119. <https://doi.org/10.1073/pnas.2204706119>
- Schwarz, T.F., Nsanze, H., Ameen, A.M., 1997. Clinical features of Crimean-Congo haemorrhagic fever in the United Arab Emirates. *Infection* 25, 364–367. <https://doi.org/10.1007/BF01740819>
- Seidah, N.G., Benjannet, S., Wickham, L., Marcinkiewicz, J., Jasmin, S.B., Stifani, S., Basak, A., Prat, A., Chrétien, M., 2003. The secretory proprotein convertase neural apoptosis-regulated convertase 1 (NARC-1): Liver regeneration and neuronal differentiation. *Proc. Natl. Acad. Sci. U. S. A.* 100, 928–933. <https://doi.org/10.1073/pnas.0335507100>
- Seixas, A., Alzugaray, M.F., Tirloni, L., Parizi, L.F., Pinto, A.F.M., Githaka, N.W., Konnai, S., Ohashi, K., Yates III, J.R., Termignoni, C., da Silva Vaz Jr., I., 2018. Expression profile of *Rhipicephalus microplus* vitellogenin receptor during oogenesis. *Ticks Tick-Borne Dis.* 9, 72–81. <https://doi.org/10.1016/j.ttbdis.2017.10.006>
- Shahhosseini, N., Wong, G., Babuadze, G., Camp, J.V., Ergonul, O., Kobinger, G.P., Chinikar, S., Nowotny, N., 2021. Crimean-Congo Hemorrhagic Fever Virus in Asia, Africa and Europe. *Microorganisms* 9, 1907. <https://doi.org/10.3390/microorganisms9091907>
- Sheehan, K.C.F., Lai, K.S., Dunn, G.P., Bruce, A.T., Diamond, M.S., Heutel, J.D., Dungo-Arthur, C., Carrero, J.A., White, J.M., Hertzog, P.J., Schreiber, R.D., 2006. Blocking Monoclonal

- Antibodies Specific for Mouse IFN- $\alpha/\beta$  Receptor Subunit 1 (IFNAR-1) from Mice Immunized by In Vivo Hydrodynamic Transfection. *J. Interferon Cytokine Res.* 26, 804–819. <https://doi.org/10.1089/jir.2006.26.804>
- Shepherd, A.J., Leman, P.A., Swanepoel, R., 1989a. Viremia and antibody response of small African and laboratory animals to Crimean-Congo hemorrhagic fever virus infection. *Am. J. Trop. Med. Hyg.* 40, 541–547. <https://doi.org/10.4269/ajtmh.1989.40.541>
- Shepherd, A.J., Swanepoel, R., Cornel, A.J., Mathee, O., 1989b. Experimental Studies on the Replication and Transmission of Crimean-Congo Hemorrhagic Fever Virus in some African Tick Species. *Am. J. Trop. Med. Hyg.* 40, 326–331. <https://doi.org/10.4269/ajtmh.1989.40.326>
- Shepherd, A.J., Swanepoel, R., Leman, P.A., 1989c. Antibody Response in Crimean-Congo Hemorrhagic Fever. *Rev. Infect. Dis.* 11, S801–S806. [https://doi.org/10.1093/clinids/11.Supplement\\_4.S801](https://doi.org/10.1093/clinids/11.Supplement_4.S801)
- Shimajima, M., Kawaoka, Y., 2012. Cell surface molecules involved in infection mediated by lymphocytic choriomeningitis virus glycoprotein. *J. Vet. Med. Sci.* 74, 1363–1366. <https://doi.org/10.1292/jvms.12-0176>
- Shimajima, M., Ströher, U., Ebihara, H., Feldmann, H., Kawaoka, Y., 2012. Identification of Cell Surface Molecules Involved in Dystroglycan-Independent Lassa Virus Cell Entry. *J. Virol.* 86, 2067–2078. <https://doi.org/10.1128/JVI.06451-11>
- Shtanko, O., Nikitina, R.A., Altuntas, C.Z., Chepurinov, A.A., Davey, R.A., 2014. Crimean-Congo Hemorrhagic Fever Virus Entry into Host Cells Occurs through the Multivesicular Body and Requires ESCRT Regulators. *PLoS Pathog.* 10, e1004390. <https://doi.org/10.1371/journal.ppat.1004390>
- Simon, Melinda, Johansson, C., Lundkvist, Å., Mirazimi, A., 2009. Microtubule-dependent and microtubule-independent steps in Crimean-Congo hemorrhagic fever virus replication cycle. *Virology* 385, 313–322. <https://doi.org/10.1016/j.virol.2008.11.020>
- Simon, M., Johansson, C., Mirazimi, A., 2009. Crimean-Congo hemorrhagic fever virus entry and replication is clathrin-, pH- and cholesterol-dependent. *J. Gen. Virol.* 90, 210–215. <https://doi.org/10.1099/vir.0.006387-0>
- Smith, D.R., Shoemaker, C.J., Zeng, X., Garrison, A.R., Golden, J.W., Schellhase, C.W., Pratt, W., Rossi, F., Fitzpatrick, C.J., Shamblin, J., Kimmel, A., Zelko, J., Flusin, O., Koehler, J.W., Liu, J., Coffin, K.M., Ricks, K.M., Voorhees, M.A., Schoepp, R.J., Schmaljohn, C.S., 2019. Persistent Crimean-Congo hemorrhagic fever virus infection in the testes and within granulomas of non-human primates with latent tuberculosis. *PLoS Pathog.* 15, e1008050. <https://doi.org/10.1371/journal.ppat.1008050>
- Soares-Weiser, K., Thomas, S., Thomson, G., Garner, P., 2010. Ribavirin for Crimean-Congo hemorrhagic fever: systematic review and meta-analysis. *BMC Infect. Dis.* 10, 207. <https://doi.org/10.1186/1471-2334-10-207>
- Spengler, J.R., Bente, D.A., Bray, M., Burt, F., Hewson, R., Korukluoglu, G., Mirazimi, A., Weber, F., Papa, A., 2018. Second International Conference on Crimean-Congo Hemorrhagic Fever. *Antiviral Res.* 150, 137–147. <https://doi.org/10.1016/j.antiviral.2017.11.019>
- Spengler, J.R., Bergeron, É., Rollin, P.E., 2016. Seroepidemiological Studies of Crimean-Congo Hemorrhagic Fever Virus in Domestic and Wild Animals. *PLoS Negl. Trop. Dis.* 10, e0004210. <https://doi.org/10.1371/journal.pntd.0004210>
- Spengler, J.R., Kelly Keating, M., McElroy, A.K., Zivcec, M., Coleman-McCray, J.D., Harmon, J.R., Bollweg, B.C., Goldsmith, C.S., Bergeron, É., Keck, J.G., Zaki, S.R., Nichol, S.T., Spiropoulou, C.F., 2017. Crimean-Congo Hemorrhagic Fever in Humanized Mice

- Reveals Glial Cells as Primary Targets of Neurological Infection. *J. Infect. Dis.* 216, 1386–1397. <https://doi.org/10.1093/infdis/jix215>
- Spengler, J.R., Patel, J.R., Chakrabarti, A.K., Zivcec, M., García-Sastre, A., Spiropoulou, C.F., Bergeron, É., 2015. RIG-I Mediates an Antiviral Response to Crimean-Congo Hemorrhagic Fever Virus. *J. Virol.* 89, 10219–10229. <https://doi.org/10.1128/JVI.01643-15>
- Spengler, J.R., Welch, S.R., Scholte, F.E.M., Coleman-McCray, J.D., Harmon, J.R., Nichol, S.T., Bergeron, É., Spiropoulou, C.F., 2019. Heterologous protection against Crimean-Congo hemorrhagic fever in mice after a single dose of replicon particle vaccine. *Antiviral Res.* 170, 104573. <https://doi.org/10.1016/j.antiviral.2019.104573>
- Stehle, T., Casasnovas, J.M., 2009. Specificity switching in virus-receptor complexes. *Curr. Opin. Struct. Biol.* 19, 181–188. <https://doi.org/10.1016/j.sbi.2009.02.013>
- Su, P.-Y., Wang, Y.-F., Huang, S.-W., Lo, Y.-C., Wang, Y.-H., Wu, S.-R., Shieh, D.-B., Chen, S.-H., Wang, J.-R., Lai, M.-D., Chang, C.-F., n.d. Cell Surface Nucleolin Facilitates Enterovirus 71 Binding and Infection. *J. Virol.* 89, 4527–4538. <https://doi.org/10.1128/JVI.03498-14>
- Suda, Y., Fukushi, S., Tani, H., Murakami, S., Saijo, M., Horimoto, T., Shimojima, M., 2016. Analysis of the entry mechanism of Crimean-Congo hemorrhagic fever virus, using a vesicular stomatitis virus pseudotyping system. *Arch. Virol.* 161, 1447–1454. <https://doi.org/10.1007/s00705-016-2803-1>
- Sumpter, R., Loo, Y.-M., Foy, E., Li, K., Yoneyama, M., Fujita, T., Lemon, S.M., Gale, M., 2005. Regulating intracellular antiviral defense and permissiveness to hepatitis C virus RNA replication through a cellular RNA helicase, RIG-I. *J. Virol.* 79, 2689–2699. <https://doi.org/10.1128/JVI.79.5.2689-2699.2005>
- Sun, Y., Qi, Y., Liu, C., Gao, W., Chen, P., Fu, L., Peng, B., Wang, H., Jing, Z., Zhong, G., Li, W., 2014. Nonmuscle Myosin Heavy Chain IIA Is a Critical Factor Contributing to the Efficiency of Early Infection of Severe Fever with Thrombocytopenia Syndrome Virus. *J. Virol.* 88, 237–248. <https://doi.org/10.1128/JVI.02141-13>
- Surdo, P.L., Bottomley, M.J., Calzetta, A., Settembre, E.C., Cirillo, A., Pandit, S., Ni, Y.G., Hubbard, B., Sitlani, A., Carfi, A., 2011. Mechanistic implications for LDL receptor degradation from the PCSK9/LDLR structure at neutral pH. *EMBO Rep.* 12, 1300–1305. <https://doi.org/10.1038/embor.2011.205>
- Swanepoel, R., Gill, D.E., Shepherd, A.J., Leman, P.A., Mynhardt, J.H., Harvey, S., 1989. The clinical pathology of Crimean-Congo hemorrhagic fever. *Rev. Infect. Dis.* 11 Suppl 4, S794-800. [https://doi.org/10.1093/clinids/11.supplement\\_4.s794](https://doi.org/10.1093/clinids/11.supplement_4.s794)
- Swertfeger, D.K., Hui, D.Y., 2001. Apolipoprotein E Receptor Binding *Versus* Heparan Sulfate Proteoglycan Binding in Its Regulation of Smooth Muscle Cell Migration and Proliferation\*. *J. Biol. Chem.* 276, 25043–25048. <https://doi.org/10.1074/jbc.M102357200>
- Tani, H., Shimojima, M., Fukushi, S., Yoshikawa, T., Fukuma, A., Taniguchi, S., Morikawa, S., Saijo, M., 2016. Characterization of Glycoprotein-Mediated Entry of Severe Fever with Thrombocytopenia Syndrome Virus. *J. Virol.* 90, 5292–5301. <https://doi.org/10.1128/JVI.00110-16>
- Tayyari, F., Marchant, D., Moraes, T.J., Duan, W., Mastrangelo, P., Hegele, R.G., 2011. Identification of nucleolin as a cellular receptor for human respiratory syncytial virus. *Nat. Med.* 17, 1132–1135. <https://doi.org/10.1038/nm.2444>

- Tignor, G.H., Hanham, C.A., 1993. Ribavirin efficacy in an in vivo model of Crimean-Congo hemorrhagic fever virus (CCHF) infection. *Antiviral Res.* 22, 309–325. [https://doi.org/10.1016/0166-3542\(93\)90040-P](https://doi.org/10.1016/0166-3542(93)90040-P)
- Tonello, F., Massimino, M.L., Peggion, C., 2022. Nucleolin: a cell portal for viruses, bacteria, and toxins. *Cell. Mol. Life Sci.* 79, 271. <https://doi.org/10.1007/s00018-022-04300-7>
- Ujino, S., Nishitsuji, H., Hishiki, T., Sugiyama, K., Takaku, H., Shimotohno, K., 2016. Hepatitis C virus utilizes VLDLR as a novel entry pathway. *Proc. Natl. Acad. Sci.* 113, 188–193. <https://doi.org/10.1073/pnas.1506524113>
- Uppal, S., Postnikova, O., Villasmil, R., Rogozin, I.B., Bocharov, A.V., Eggerman, T.L., Poliakov, E., Redmond, T.M., 2023. Low-Density Lipoprotein Receptor (LDLR) Is Involved in Internalization of Lentiviral Particles Pseudotyped with SARS-CoV-2 Spike Protein in Ocular Cells. *Int. J. Mol. Sci.* 24, 11860. <https://doi.org/10.3390/ijms241411860>
- van Eeden, P.J., van Eeden, S.F., Joubert, J.R., King, J.B., van de Wal, B.W., Michell, W.L., 1985. A nosocomial outbreak of Crimean-Congo haemorrhagic fever at Tygerberg Hospital. Part II. Management of patients. *South Afr. Med. J. Suid-Afr. Tydskr. Vir Geneesk.* 68, 718–721.
- Vincent, M.J., Sanchez, A.J., Erickson, B.R., Basak, A., Chretien, M., Seidah, N.G., Nichol, S.T., 2003. Crimean-Congo hemorrhagic fever virus glycoprotein proteolytic processing by subtilase SKI-1. *J. Virol.* 77, 8640–8649. <https://doi.org/10.1128/jvi.77.16.8640-8649.2003>
- Wang, L.H., Rothberg, K.G., Anderson, R.G., 1993. Mis-assembly of clathrin lattices on endosomes reveals a regulatory switch for coated pit formation. *J. Cell Biol.* 123, 1107–1117. <https://doi.org/10.1083/jcb.123.5.1107>
- Wang, N., Merits, A., Veit, M., Lello, L.S., Kong, S., Jiao, H., Chen, J., Wang, Y., Dobrikov, G., Rey, F.A., Su, S., 2024. LDL receptor in alphavirus entry: structural analysis and implications for antiviral therapy. *Nat. Commun.* 15, 4906. <https://doi.org/10.1038/s41467-024-49301-1>
- Wang, X., Li, B., Guo, Y., Shen, S., Zhao, L., Zhang, P., Sun, Y., Sui, S.-F., Deng, F., Lou, Z., 2016. Molecular basis for the formation of ribonucleoprotein complex of Crimean-Congo hemorrhagic fever virus. *J. Struct. Biol.* 196, 455–465. <https://doi.org/10.1016/j.jsb.2016.09.013>
- Wang, Y., Dutta, S., Karlberg, H., Devignot, S., Weber, F., Hao, Q., Tan, Y.J., Mirazimi, A., Kotaka, M., 2012. Structure of Crimean-Congo Hemorrhagic Fever Virus Nucleoprotein: Superhelical Homo-Oligomers and the Role of Caspase-3 Cleavage. *J. Virol.* 86, 12294–12303. <https://doi.org/10.1128/JVI.01627-12>
- Wei, C., Wan, L., Yan, Q., Wang, Xiaolin, Zhang, J., Yang, Xiaopan, Zhang, Y., Fan, C., Li, D., Deng, Y., Sun, J., Gong, J., Yang, Xiaoli, Wang, Y., Wang, Xuejun, Li, J., Yang, H., Li, H., Zhang, Z., Wang, R., Du, P., Zong, Y., Yin, F., Zhang, W., Wang, N., Peng, Y., Lin, H., Feng, J., Qin, C., Chen, W., Gao, Q., Zhang, R., Cao, Y., Zhong, H., 2020. HDL-scavenger receptor B type 1 facilitates SARS-CoV-2 entry. *Nat. Metab.* 2, 1391–1400. <https://doi.org/10.1038/s42255-020-00324-0>
- Weidmann, M., Avsic-Zupanc, T., Bino, S., Bouloy, M., Burt, F., Chinikar, S., Christova, I., Dedushaj, I., El-Sanousi, A., Elaldi, N., Hewson, R., Hufert, F.T., Humolli, I., Jansen van Vuren, P., Koçak Tufan, Z., Korukluoglu, G., Lyssen, P., Mirazimi, A., Neyts, J., Niedrig, M., Ozkul, A., Papa, A., Paweska, J., Sall, A.A., Schmaljohn, C.S., Swanepoel, R., Uyar, Y., Weber, F., Zeller, H., 2016. Biosafety standards for working with Crimean-Congo hemorrhagic fever virus. *J. Gen. Virol.* 97, 2799–2808. <https://doi.org/10.1099/jgv.0.000610>

- Welch, S.R., Scholte, F.E.M., Flint, M., Chatterjee, P., Nichol, S.T., Bergeron, É., Spiropoulou, C.F., 2017. Identification of 2'-deoxy-2'-fluorocytidine as a potent inhibitor of Crimean-Congo hemorrhagic fever virus replication using a recombinant fluorescent reporter virus. *Antiviral Res.* 147, 91–99. <https://doi.org/10.1016/j.antiviral.2017.10.008>
- Welch, S.R., Scholte, F.E.M., Spengler, J.R., Ritter, J.M., Coleman-McCray, J.D., Harmon, J.R., Nichol, S.T., Zaki, S.R., Spiropoulou, C.F., Bergeron, E., 2020. The Crimean-Congo Hemorrhagic Fever Virus NSm Protein is Dispensable for Growth In Vitro and Disease in Ifnar-/- Mice. *Microorganisms* 8, 775. <https://doi.org/10.3390/microorganisms8050775>
- Whitehorn, J., Nguyen, C.V.V., Khanh, L.P., Kien, D.T.H., Quyen, N.T.H., Tran, N.T.T., Hang, N.T., Truong, N.T., Hue Tai, L.T., Cam Huong, N.T., Nhon, V.T., Van Tram, T., Farrar, J., Wolbers, M., Simmons, C.P., Wills, B., 2016. Lovastatin for the Treatment of Adult Patients With Dengue: A Randomized, Double-Blind, Placebo-Controlled Trial. *Clin. Infect. Dis.* 62, 468–476. <https://doi.org/10.1093/cid/civ949>
- Whitt, M.A., 2010. Generation of VSV pseudotypes using recombinant ΔG-VSV for studies on virus entry, identification of entry inhibitors, and immune responses to vaccines. *J. Virol. Methods* 169, 365–374. <https://doi.org/10.1016/j.jviromet.2010.08.006>
- WHO, blueprint, n.d. World Health Organization. Prioritizing diseases for research and development in emergency contexts (no date). Available at: <https://www.who.int/activities/prioritizing-diseases-for-research-and-development-in-emergency-contexts> (Accessed: 29 November 2023).
- WHO, Crimean-Congo haemorrhagic fever, n.d. World Health Organization. Crimean-Congo haemorrhagic fever (no date). Available at: [https://www.who.int/health-topics/crimean-congo-haemorrhagic-fever#tab=tab\\_1](https://www.who.int/health-topics/crimean-congo-haemorrhagic-fever#tab=tab_1) (Accessed: 13 May 2024).
- WHO, fact-sheet, n.d. World Health Organization. Crimean-Congo haemorrhagic fever (no date). Available at: <https://www.who.int/news-room/fact-sheets/detail/crimean-congo-haemorrhagic-fever> (Accessed: 29 November 2023).
- Willnow, T.E., 1999. The low-density lipoprotein receptor gene family: multiple roles in lipid metabolism. *J. Mol. Med. Berl. Ger.* 77, 306–315. <https://doi.org/10.1007/s001090050356>
- Willnow, T.E., Hilpert, J., Armstrong, S.A., Rohlmann, A., Hammer, R.E., Burns, D.K., Herz, J., 1996. Defective forebrain development in mice lacking gp330/megalin. *Proc. Natl. Acad. Sci. U. S. A.* 93, 8460–8464.
- Willnow, T.E., Orth, K., Herz, J., 1994. Molecular dissection of ligand binding sites on the low density lipoprotein receptor-related protein. *J. Biol. Chem.* 269, 15827–15832. [https://doi.org/10.1016/S0021-9258\(17\)40755-1](https://doi.org/10.1016/S0021-9258(17)40755-1)
- Woodall, J.P., 2007. Personal Reflections, in: Ergonul, O., Whitehouse, C.A. (Eds.), *Crimean-Congo Hemorrhagic Fever: A Global Perspective*. Springer Netherlands, Dordrecht, pp. 23–32. [https://doi.org/10.1007/978-1-4020-6106-6\\_3](https://doi.org/10.1007/978-1-4020-6106-6_3)
- Xiao, X., Feng, Y., Zhu, Z., Dimitrov, D.S., 2011. Identification of a Putative Crimean-Congo Hemorrhagic Fever Virus Entry Factor. *Biochem. Biophys. Res. Commun.* 411, 253–258. <https://doi.org/10.1016/j.bbrc.2011.06.109>
- Xu, F., Liang, X., Tesh, R.B., Xiao, S.-Y., 2008. Characterization of cell-death pathways in Punta Toro virus-induced hepatocyte injury. *J. Gen. Virol.* 89, 2175–2181. <https://doi.org/10.1099/vir.0.2008/001644-0>
- Xu, Z.-S., Du, W.-T., Wang, S.-Y., Wang, M.-Y., Yang, Y.-N., Li, Y.-H., Li, Z.-Q., Zhao, L.-X., Yang, Y., Luo, W.-W., Wang, Y.-Y., 2024. LDLR is an entry receptor for Crimean-Congo

- hemorrhagic fever virus. *Cell Res.* 34, 140–150. <https://doi.org/10.1038/s41422-023-00917-w>
- Ye, W., Ye, C., Hu, Y., Dong, Y., Lei, Y., Zhang, F., 2022. The structure of Crimean-Congo hemorrhagic fever virus Gc is revealed; many more still need an answer. *Virol. Sin.* 37, 634–636. <https://doi.org/10.1016/j.virs.2022.05.003>
- Yokode, M., Pathak, R., Hammer, R., Brown, M., Goldstein, J., Anderson, R., 1992. Cytoplasmic sequence required for basolateral targeting of LDL receptor in livers of transgenic mice. *J. Cell Biol.* 117, 39–46. <https://doi.org/10.1083/jcb.117.1.39>
- Young, J.A., Bates, P., Varmus, H.E., 1993. Isolation of a chicken gene that confers susceptibility to infection by subgroup A avian leukosis and sarcoma viruses. *J. Virol.* 67, 1811–1816. <https://doi.org/10.1128/jvi.67.4.1811-1816.1993>
- Zeller, H.G., Cornet, J.P., Camicas, J.L., 1994. Experimental transmission of Crimean-Congo hemorrhagic fever virus by west African wild ground-feeding birds to *Hyalomma marginatum rufipes* ticks. *Am. J. Trop. Med. Hyg.* 50, 676–681. <https://doi.org/10.4269/ajtmh.1994.50.676>
- Zhai, X., Li, X., Veit, M., Wang, N., Wang, Y., Merits, A., Jiang, Z., Qin, Y., Zhang, X., Qi, K., Jiao, H., He, W.-T., Chen, Y., Mao, Y., Su, S., 2024. LDLR is used as a cell entry receptor by multiple alphaviruses. *Nat. Commun.* 15, 622. <https://doi.org/10.1038/s41467-024-44872-5>
- Zhang, W.Y., Gaynor, P.M., Kruth, H.S., 1996. Apolipoprotein E produced by human monocyte-derived macrophages mediates cholesterol efflux that occurs in the absence of added cholesterol acceptors. *J. Biol. Chem.* 271, 28641–28646. <https://doi.org/10.1074/jbc.271.45.28641>
- Zheng, G., Marino, M., Zhao, J., McCluskey, R.T., 1998. Megalin (gp330): a putative endocytic receptor for thyroglobulin (Tg). *Endocrinology* 139, 1462–1465. <https://doi.org/10.1210/endo.139.3.5978>
- Zhou, Y., Mägi, R., Milani, L., Lauschke, V.M., 2018. Global genetic diversity of human apolipoproteins and effects on cardiovascular disease risk. *J. Lipid Res.* 59, 1987–2000. <https://doi.org/10.1194/jlr.P086710>
- Zhou, Z., Wang, M., Deng, F., Li, T., Hu, Z., Wang, H., 2011. Production of CCHF virus-like particle by a baculovirus-insect cell expression system. *Virol. Sin.* 26, 338. <https://doi.org/10.1007/s12250-011-3209-6>
- Zivcec, M., Metcalfe, M.G., Albariño, C.G., Guerrero, L.W., Pegan, S.D., Spiropoulou, C.F., Bergeron, É., 2015. Assessment of Inhibitors of Pathogenic Crimean-Congo Hemorrhagic Fever Virus Strains Using Virus-Like Particles. *PLoS Negl. Trop. Dis.* 9, e0004259. <https://doi.org/10.1371/journal.pntd.0004259>
- Zivcec, M., Safronetz, D., Scott, D., Robertson, S., Ebihara, H., Feldmann, H., 2013. Lethal Crimean-Congo hemorrhagic fever virus infection in interferon  $\alpha/\beta$  receptor knockout mice is associated with high viral loads, proinflammatory responses, and coagulopathy. *J. Infect. Dis.* 207, 1909–1921. <https://doi.org/10.1093/infdis/jit061>
- Zong, M., Fofana, I., Choe, H., 2014. Human and Host Species Transferrin Receptor 1 Use by North American Arenaviruses. *J. Virol.* 88, 9418–9428. <https://doi.org/10.1128/JVI.01112-14>

## Chapter VIII. List of publications, patents, and participations to scientific events

### List of publications

2024

- **Ritter M**, Canus L, Gautam A, Vallet T, Zhong L, Lalande A, Boson B, Gandhi A, Bodoirat S, Burlaud-Gaillard J, Freitas N, Roingeard P, Barr JN, Lotteau V, Legros V, Mathieu C, Cosset FL, Denolly S.  
The low-density lipoprotein receptor and apolipoprotein E associated with CCHFV particles mediate CCHFV entry into cells. *Nat Commun*. 2024 May 28;15(1):4542. doi: 10.1038/s41467-024-48989-5. PMID: 38806525; PMCID: PMC11133370.
- Gautam A, Lalande A\*, **Ritter M\***, Freitas N\*, Lerolle S, Canus L, Amirache F, Lotteau V, Legros V, Cosset FL, Mathieu C, Boson B.  
The PACS-2 protein and trafficking motifs in CCHFV Gn and Gc cytoplasmic tails govern CCHFV assembly. *Emerg Microbes Infect*. 2024 Apr 25:2348508. doi: 10.1080/22221751.2024.2348508. PMID: 38661085.

2023

- Granier C\*, Toesca J\*, Mialon C\*, **Ritter M**, Freitas N, Boson B, Pécheur E-I, Cosset F-L, Denolly S.  
Low-density hepatitis C virus infectious particles are protected from oxidation by secreted cellular proteins. *mBio*. 2023 Oct 31;14(5):e0154923. doi: 10.1128/mbio.01549-23. Epub 2023 Sep 6. PMID: 37671888; PMCID: PMC10653866.

\* : equal participation

### List of patents

- Inhibitor of the low-density lipoprotein receptor family (LDL-R family) and/or apolipoprotein E (apoE) for use in the treatment of Crimean-Congo Hemorrhagic Fever Virus (CCHFV) infection. Inserm/ ENS Lyon/ CNRS/ Université Claude Bernard Lyon1. No. de dépôt : EP23306808.9. Date de dépôt : 16 octobre 2023.



### List of participation in scientific events

2024

- CIRI internal seminar (14.06.2024). Lyon, France :  
Oral presentation 20min: *The low-density lipoprotein receptor and apolipoprotein E mediate Crimean-Congo Hemorrhagic Fever Virus entry into human cells.*
- XXVIe Journées Francophones de Virologie (10-12.04.2024). Bruxelles, Belgium:  
Poster: *Identification du LDL-R comme cofacteur d'entrée pour le virus de la Fièvre Hémorragique de Crimée-Congo en cellules humaines.*

2023

- CIRI virology day (12.06.2023). Lyon, France:  
Poster: *Identification of a co-factor mediating CCHFV entry through cellular ligand displayed on viral particles.*  
Audience prize: Best poster presentation
- 10th European Meeting on Viral Zoonoses (23-26.09.2023). St Raphaël, France

### List of participations in popular science events

2024

- Pint Of Science (15.05.2024). Lyon, France.  
Oral presentation 30min: *Qu'est-ce qu'un virus ? Comment les étudier sans en mourir ?*

2022

- Contest : Ma thèse pour les nuls (15.10.2022). ENS de Lyon, France.  
Oral presentation 3min: *Mission virus : 3 ans pour désamorcer*

## Chapter IX. Annexe



Virology | Research Article

# Low-density hepatitis C virus infectious particles are protected from oxidation by secreted cellular proteins

Christelle Granier,<sup>1</sup> Johan Toesca,<sup>1</sup> Chloé Mialon,<sup>1</sup> Maureen Ritter,<sup>1</sup> Natalia Freitas,<sup>1</sup> Bertrand Boson,<sup>1</sup> Eve-Isabelle Pécheur,<sup>2</sup> François-Loïc Cosset,<sup>1</sup> Solène Denolly<sup>1,3</sup>

**AUTHOR AFFILIATIONS** See affiliation list on p. 22.

**ABSTRACT** Hepatitis C virus (HCV) particles secreted from cells are stable at 37°C, whether the producer cell media contain serum or not. Yet, we found that intracellular HCV particles harvested after freeze-thawing of producer cells are highly unstable upon resuspension in a serum-free medium, indicating that either HCV particles gain intrinsic stability during their secretion and egress from producer cells or, alternatively, that a factor secreted from cells can stabilize intrinsically unstable HCV particles. We aimed at investigating either possibility and unraveling the mechanisms evolved by HCV to promote the stability of its viral particles. We showed that after purification and resuspension in a serum-free medium, HCV infectious particles released in cell supernatants are quickly and specifically degraded at 37°C in comparison to other viruses that can infect hepatic cells. We also found that cell-secreted proteins, including human serum albumin and transferrin, could protect HCV particles from this loss of infectivity. Moreover, we showed that such protection mainly impacted low-density particles ( $d < 1.08$ ), suggesting a specific alteration of viral particles that are lipidated. Since we also demonstrated that neither HCV RNA nor surface glycoproteins were altered, this suggested that virion lipids are sensitive to decay, resulting in a loss of infectivity. Indeed, our results further indicated that HCV particles are sensitive to oxidation, which leads to a loss of their membrane fusion capacity. Altogether, our results indicate that HCV is highly sensitive to oxidation and highlight a specific protection mechanism evolved by HCV to prevent oxidation-mediated degradation of its lipidated particles by using secreted factors.

**IMPORTANCE** Assessments of viral stability on surfaces or in body fluids under different environmental conditions and/or temperatures are often performed, as they are key to understanding the routes and parameters of viral transmission and to providing clues on the epidemiology of infections. However, for most viruses, the mechanisms of inactivation vs stability of viral particles remain poorly defined. Although they are structurally diverse, with different compositions, sizes, and shapes, enveloped viruses are generally less stable than non-enveloped viruses, pointing out the role of envelopes themselves in virus lability. In this report, we investigated the properties of hepatitis C virus (HCV) particles with regards to their stability. We found that, compared to alternative enveloped viruses such as Dengue virus (DENV), severe acute respiratory syndrome coronavirus 2 (SARS-CoV-2), hepatitis delta virus (HDV), and Crimean–Congo hemorrhagic fever virus (CCHFV) that infect the liver, HCV particles are intrinsically labile. We determined the mechanisms that drastically alter their specific infectivity through oxidation of their lipids, and we highlighted that they are protected from lipid oxidation by secreted cellular proteins, which can protect their membrane fusion capacity and overall infectivity.

**KEYWORDS** hepatitis C virus, oxidation, virus stability

**Invited Editor** Stanley M. Lemon, University of North Carolina at Chapel Hill, Chapel Hill, North Carolina, USA

**Editor** Stephen P. Goff, Columbia University Medical Center, New York, New York, USA

Address correspondence to Solène Denolly, solene.denolly@ens-lyon.fr, or François-Loïc Cosset, flcosset@ens-lyon.fr.

Christelle Granier, Johan Toesca, and Chloé Mialon are joint first authors. C.G., J.T., and C.M. performed the majority of the experiments; hence, their joint first authorship. C.G. spent the longest time on this project; hence, she was designated as first of the joint first authors.

François-Loïc Cosset and Solène Denolly are joint last authors.

The authors declare no conflict of interest.

See the funding table on p. 23.

**Received** 17 June 2023

**Accepted** 4 July 2023

**Published** 6 September 2023

Copyright © 2023 Granier et al. This is an open-access article distributed under the terms of the Creative Commons Attribution 4.0 International license.

Viruses can be transmitted through highly divergent routes, such as direct person-to-person contacts, droplets, aerosols, or interactions with a plethora of environment-dependent factors/vectors. Assessments of viral stability on surfaces or in body fluids under different environmental conditions and/or temperatures are often performed, as they are key to understanding the routes and parameters of viral transmission and to providing clues on the epidemiology of infections. Several reports have demonstrated that the life span in different environments of coronaviruses such as severe acute respiratory syndrome coronavirus 2 (SARS-CoV-2) and Middle East Respiratory Syndrome coronavirus (MERS-CoV) is markedly higher as compared with that of other enveloped viruses, such as, e.g., influenza A virus (1). However, for most viruses, the mechanisms of inactivation vs stability of viral particles remain poorly defined. For example, although many studies have indicated that enveloped viruses are generally less stable than non-enveloped viruses (2–4), they are structurally highly diverse, with different compositions, sizes, and shapes, which may differentially impact their stability. Yet, the current data indicate that their envelopes themselves play a crucial role in virus lability. Indeed, while lipid bilayers of the envelopes provide an additional physical protection of the nucleocapsid from the environment, they are intrinsically fragile and can be easily altered. This may result in a loss of infectivity through disruption of the viral surface glycoproteins and hence, of the cell entry processes. For example, some retroviruses exhibit particularly labile envelopes due to easy shedding of the SU (surface) subunit from TM (transmembrane) subunit of their glycoprotein complexes, whereas rhabdoviruses such as vesicular stomatitis virus display particularly stable surface glycoproteins (5, 6).

Among enveloped viruses, viruses that infect the liver may have evolved specific mechanisms for maintaining their specific infectivity, as they face several challenges upon their assembly and release. On the one hand, they are produced in hepatocytes, i.e., professional secretory cells that are characterized by high and diverse metabolic activities resulting in secretion of thousands of proteins per second (7), and on the other hand, they are further exposed to a different and highly complex environment after their secretion. Indeed, the liver is a complex organ that plays a central role in metabolism homeostasis (8). Specifically, it is involved in the metabolism of lipids, with, e.g., synthesis of bile and secretion of lipoproteins, as well as in the metabolism of carbohydrates with gluconeogenesis and glycogenolysis. It is also responsible for the synthesis of a large fraction of serum proteins, such as for example albumin, apolipoproteins, alpha-1-antitrypsin, or several growth factors. Many of the above-mentioned factors are secreted via the same organelles than those that are responsible for secretion of viral particles, with particularly high concentrations, which can increase their encountering and mutual interrelations.

In this report, we sought to address the properties of hepatitis C virus (HCV) particles with regards to their stability. HCV infection is a major cause of chronic liver diseases worldwide. Direct-acting antivirals can now cure most patients but there remains major challenge in basic, translational, and clinical research (9). As an enveloped virus, the HCV particle is composed of a nucleocapsid containing the viral (+) RNA and core proteins, surrounded by a lipid bilayer in which the viral E1 and E2 surface glycoproteins are embedded. It is still unclear if the HCV p7 viroporin, which plays a crucial role in envelopment of viral particles (10), can be incorporated in virions. In addition, HCV particles are associated with neutral lipids and apolipoproteins (11–16), which is the result of direct lipid transfer of lipids from lipoproteins and protein components of the serum during secretion or after virion egress (15, 17).

HCV particles produced in cell culture (termed HCVcc) can survive in a liquid environment for some time with a stability inversely correlated to temperature (18). While some secreted components like, e.g., hepatic lipase and lipoprotein lipase may alter HCV particles, leading to a loss of infectivity (19–21), the presence of human serum in tissue culture media was shown to increase the stability of these particles (18). However, it also modulates the composition, buoyant density, and infectivity of

HCV particles (15), thereby highlighting the involvement of extracellular environment components in the lability vs protection of infectious particles.

Here, we hypothesized that some secreted factors could help HCV viral particles to survive in the liver environment and blood circulation. We therefore sought to study the stability of HCV relative to unrelated viruses that can infect hepatocytes and to determine the mechanisms by which secreted factors could protect the infectivity of HCV particles.

## RESULTS

### High instability of HCV intracellular particles at body temperature

We investigated the stability of infectious particles from different viruses that can replicate in hepatocytes, including HCV, dengue virus (DENV), SARS-CoV-2, hepatitis delta virus (HDV), and Crimean–Congo hemorrhagic fever virus (CCHFV). HCV and DENV particles were produced by electroporation of Huh7.5 cells with *in vitro*-transcribed viral genomic RNAs. SARS-CoV-2 was produced by infection of Huh-7.5 cells with viral stocks. HDV was produced by co-transfection in Huh-7.5 cells with plasmids encoding the HDV RNA genome and the hepatitis B virus (HBV) glycoproteins. For CCHFV, we produced virus-like particles called tecVLPs (22), which have the same structure and composition than full-length CCHFV (23) but whose viral genome segments are replaced by a minigenome segment encoding a reporter gene (nanoLuc). All these viruses were produced in serum-free media to allow their recovery in their most native forms from cell supernatants (Fig. 1A), i.e., by avoiding the influence of factors present in the serum that is typically added to cell culture media. Indeed, for example with HCV, the serum can induce a strong extracellular lipidation of its viral particles via lipid exchanges from lipoproteins and other factors, as shown previously (15).

First, we assessed the infectivity of HCV (Jc1 HCVcc), DENV, SARS-CoV-2, HDV, and CCHFV particles in the crude supernatants of producer cells (i.e., extra-cellular particles) upon a 6-h incubation at 37°C following their harvest (Fig. 1A). Compared to virus supernatants stored at 4°C immediately after harvest, we found that all these viruses were stable in these conditions (Fig. 1B).

Next, we sought to compare the stability of these extracellular particles with their intracellular counterparts. Indeed, since all these viruses are assembled at intracellular membrane [endoplasmic reticulum (ER) for HCV and DENV, ER-Golgi intermediate compartment (ERGIC) for HDV and SARS-CoV-2, and Golgi for CCHFV], we could readily isolate infectious intracellular viral particles by freeze-thaw lysis cycles for all viruses except for SARS-CoV-2 (Fig. 1C). We then determined the stability of isolated intracellular particles resuspended in serum-free medium upon incubation at 37°C for 6 h. In contrast to HDV and CCHFV intracellular particles that remained stable in these conditions relative to viruses kept at 4°C, we observed a strong loss of infectivity, of >30-fold, for HCV and DENV intracellular particles incubated at 37°C for 6 h (Fig. 1C).

Altogether, our results highlighted a specific feature of *Flaviviridae* intracellular particles that are unstable at 37°C, and gain stability upon secretion in the extracellular medium.

### HCV particles are intrinsically unstable and are protected by secreted factors

Next, we sought to investigate how HCV and DENV become stable upon secretion and egress. As Huh-7.5 cells secrete many factors that may influence virion stability, we sought to evaluate the stability of “purified extracellular viral particles,” i.e., obtained after separation of extracellular viral particles from medium components. Hence, we isolated particles from producer cell supernatants by ultracentrifugation (pellets) and resuspension in serum-free medium (Fig. 1A), and we subsequently analyzed their stability after a 6-h incubation at 37°C. Interestingly, while we observed a moderate decrease of infectivity for DENV of ca. threefold, we detected a profound loss of infectivity for HCV by ca. 34-fold (Fig. 1D, open bars). This suggested that while DENV nascent virions become

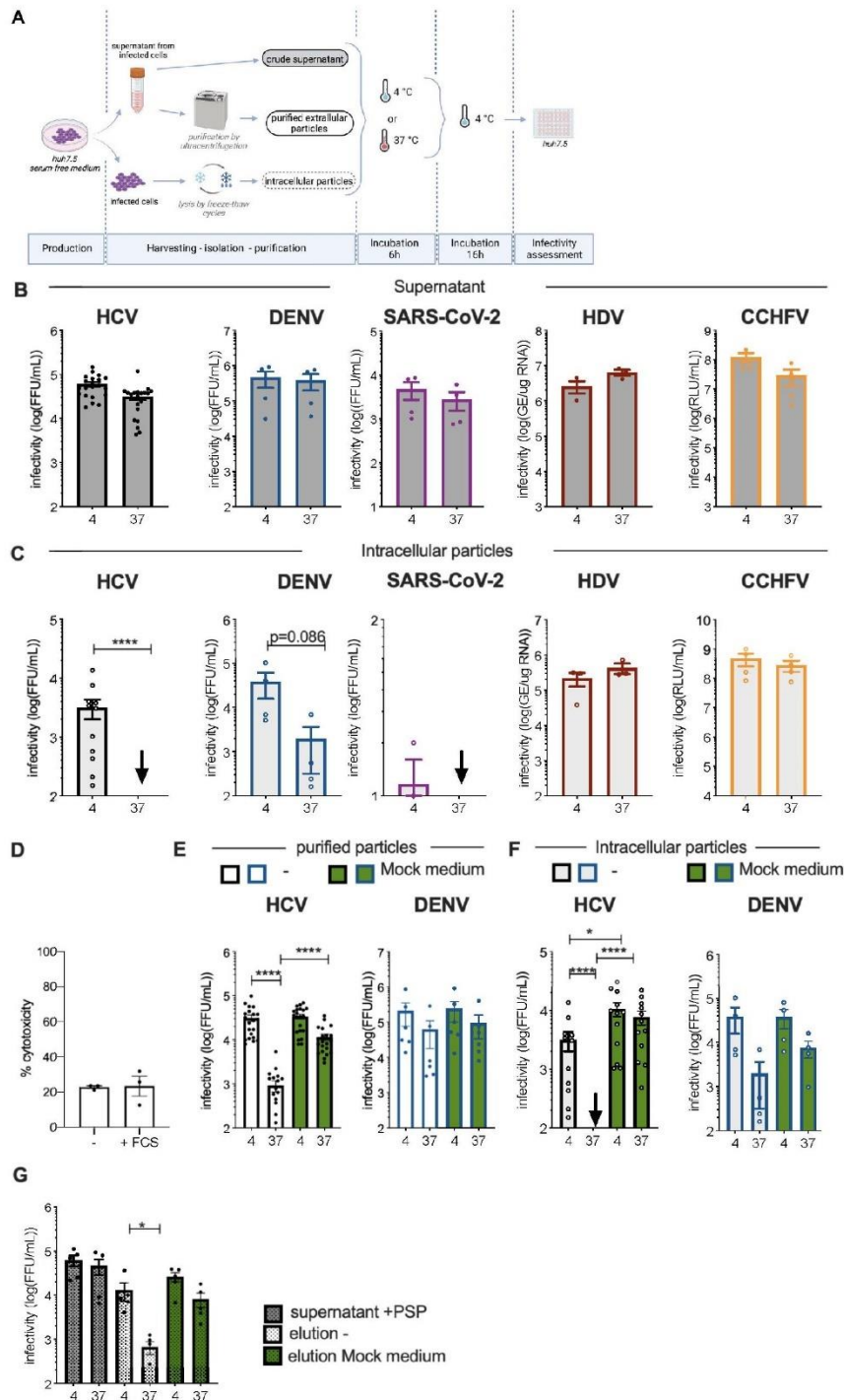


**FIG 1** Purified HCV infectious particles are protected from temperature-sensitive degradation by secreted factors. (A) Schematic representation of the protocol used to assess stability of infectious particles. Crude supernatants from producer cells were left untreated or were used for purification of viral particles via ultracentrifugation. Cells were lysed by several (Continued on next page)

FIG 1 (Continued)

freeze-thaw cycles to isolate intracellular particles. To assess the stability of virus infectivity, the different preparations of viral particles were either left at 4°C before infection or incubated for 6 h at 37°C (“4” vs “37,” in the figure panels) and then kept at 4°C before infection of naïve Huh-7.5 cells. (B) Infectivity of producer cell supernatants treated according to (A) containing HCV, DENV, SARS-CoV-2, HDV, and CCFHV particles, as indicated. (C) Infectivity of intracellular particles collected from virus-producer cells that were diluted in serum-free medium and treated as in (A). (D) Cytotoxicity assays of Huh-7.5 cells cultivated in serum-free medium with or without 10% fetal calf serum (FCS), as assessed with CytoTox-Glo kit. (E) HCV or DENV extracellular particles were purified by ultracentrifugation. Infectivity of purified extracellular particles diluted in serum-free medium (white bars) or in Mock medium (i.e., a supernatant from Huh-7.5 cells cultivated in serum-free medium for 3 days, green bars) and treated as in (A). (F) Infectivity of HCV or DENV intracellular particles diluted in serum-free medium (white bars) or in Mock medium (green bars). (G) HCV particles harboring a cleavable FLAG tag before E2 sequence, were purified by immunoprecipitation with anti-FLAG antibodies, followed by a cleavage of the FLAG tag by PreScission protease (PSP). Infectivity of crude supernatant cleaved by PSP (gray bars) or purified particles diluted in serum-free medium (white bars) vs Mock medium (green bars) left at 4°C before infection or incubated for 6 h at 37°C and then kept at 4°C before infection. The results are represented as means  $\pm$  SEM. Each dot in the graphs corresponds to the value of an individual experiment. The arrows represent the infectivity of samples that was below the threshold of detection.

stable during secretion/egress, the HCV extracellular particles are still highly sensitive to temperature, which could be assessed upon their separation from medium components.

Comparing the stability of HCV particle present in crude supernatants vs in resuspended pellets led us to hypothesize that some secreted cellular factor(s) could stabilize or protect the HCVcc particles. Thus, to investigate the effect of potential stabilizing factors secreted by virus-producer cells on stability of HCV particles, we resuspended purified extracellular or intracellular particles in a “Mock medium,” i.e., consisting of a supernatant of naïve Huh-7.5 cells incubated for 72 h in a serum-free medium, rather than directly in a serum-free medium. No cytotoxicity could be detected during production of Mock media (Fig. 1D), excluding the possibility that the Mock medium could contain some intracellular components just released from dead, lysed cells during production. Strikingly, we found that the Mock medium could fully protect both purified extracellular and intracellular HCV particles from temperature-dependent loss of infectivity (Fig. 1E and F).

To exclude any artifact that could be induced by our procedure of purification of viral particles, we analyzed the stability of HCV particles isolated by immunoprecipitation. Specifically, we used a modified Jc1 virus harboring a FLAG tag on E2 (24) that was further modified by insertion of the human rhinovirus 3C protease cleavage site (25), which, upon cleavage, could avoid interference of the FLAG tag with the infectivity of HCV particles. While the addition of this sequence did not impair infectivity, the combination of antiFLAG IP and cleavage with the PreScission protease (PSP) allowed an efficient and specific recovery of viral particles (Fig. S1). Importantly, using the eluted HCV particles, we confirmed the temperature sensitivity of isolated HCV particles and their protection by Mock medium (Fig. 1G).

Altogether, these results showed that HCV particles are characterized by their high instability at 37°C, which can be overcome by secreted factors.

### HCV-specific infectivity is altered in a genome length- and temperature-dependent manner

To further characterize the decay of infectivity of HCV particles, we titrated the extracellular HCVcc RNAs after 6 h incubation at 37°C. We found that the RNAs isolated from the viral particles from both the cell supernatants and the pellets remained stable (Fig. 2A). This highlighted a loss of HCV-specific infectivity, of ca. 30-fold, rather than a mere degradation of physical viral particles (Fig. 2B). Accordingly, resuspension of pelleted particles in Mock medium prevented the loss of specific infectivity (compare white and green bars in Fig. 2B). Aiming at determining the half-life of HCV infectivity, we harvested particles at different time points after incubation at 37°C. In contrast to the 6 h half-life of secreted HCV particles determined in producer cells supernatants, we found that both

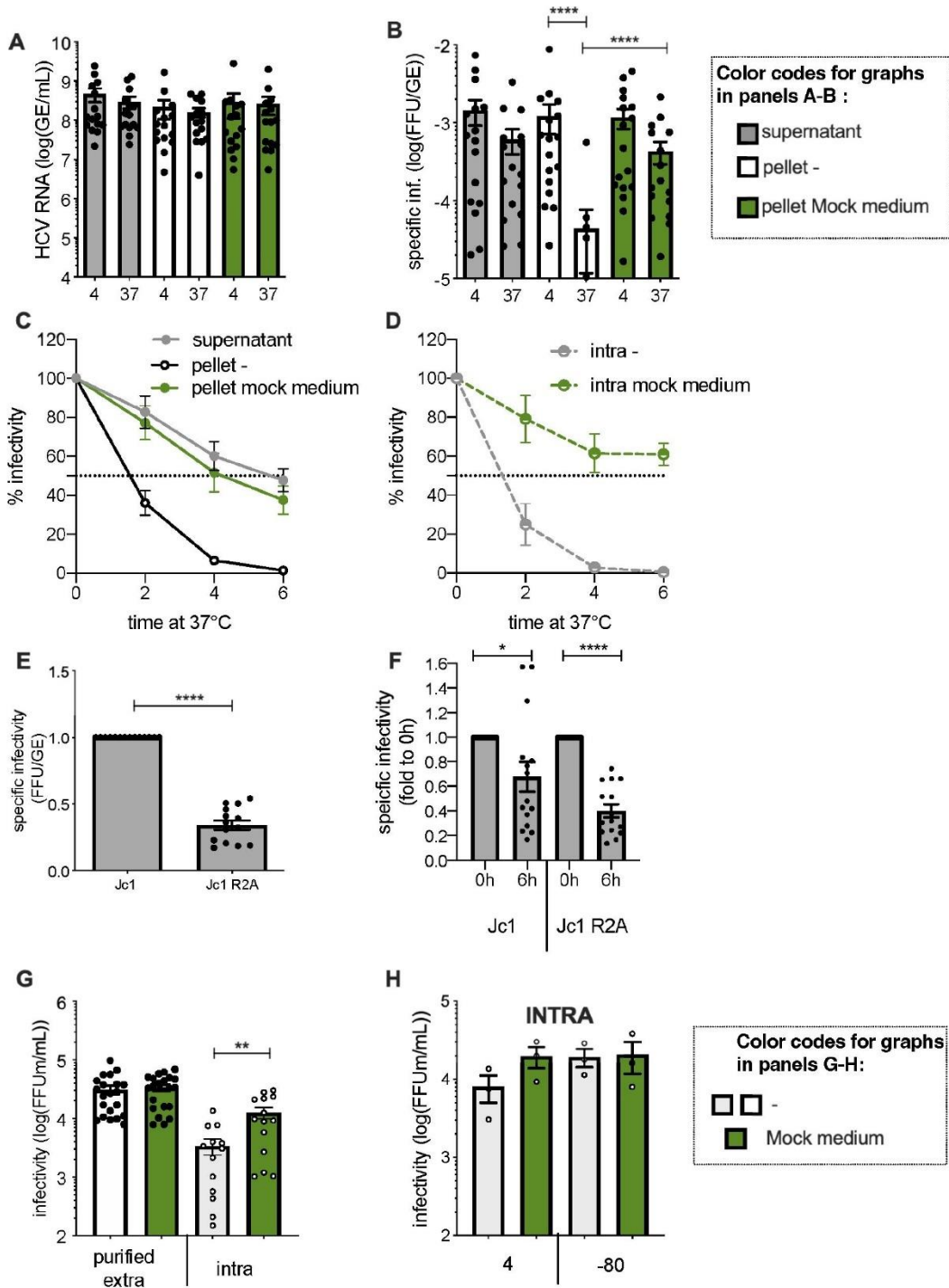


**FIG 2** The specific infectivity of purified HCV particles is quickly lost at 37°C. (A) Quantification of HCV extracellular RNA isolated from crude supernatants (gray bars) vs from purified extracellular particles diluted in serum-free medium (white bars) or in Mock medium (green bars) and treated as in Fig. 1A. (B) Specific infectivity of HCV particles treated as indicated in (A). (C) Infectivity of extracellular HCV particles from supernatants (gray lines) vs of purified extracellular HCV (Continued on next page)

FIG 2 (Continued)

particles diluted in serum-free medium (pellet –, black lines) or in Mock medium (pellet mock medium, green lines) after incubation at 37°C for the indicated times. (D) Same as (C) for intracellular particles. (E) Specific infectivity of Jc1 vs Jc1 R2A viral particles from crude supernatants of producer cells. (F) Specific infectivity of Jc1 vs Jc1 R2A from crude supernatants treated as in Fig. 1A. (G) Comparison of infectivity of purified extracellular (plain bars) vs intracellular (dashed bars) particles that were resuspended in serum-free medium (–, white bars) or in Mock medium (green bars) and maintained at 4°C before infection. (H) Infectivity of intracellular particles diluted in serum-free medium (–, white bars) or in Mock medium (green bars) and maintained at 4°C vs at –80°C before infection. The results are represented as means  $\pm$  SEM. For panels (A and B) and (E–H), each dot in the graphs corresponds to the value of an individual experiment.

purified extracellular and intracellular HCVcc particles exhibited a half-life of ca. 1.5 h (Fig. 2C and D), highlighting an intrinsically high instability of HCV particles at 37°C.

Then, since the viral RNAs remained stable under conditions where infectivity was quickly lost, we wondered if assembling viral particles with a slightly longer genome, which may induce some mechanical constraints at the level of virion conformation, maturation by lipidation, and/or cell entry, could impact HCV stability. Accordingly, we compared virus stability and specific infectivity of the Jc1 HCVcc vs the Jc1-derived R2A virus (26), which expresses a Renilla Luciferase marker that increases HCV genome length by ca. 11%. When determined in producer cell supernatants, we found that the Jc1 R2A virus exhibited a reduced specific infectivity by three- to fourfold (Fig. 2E), indicating that increasing genome length could alter HCV particle infectivity. Moreover, upon incubation for 6 h at 37°C of these viral supernatants, we found that the specific infectivity of the Jc1 R2A HCVcc was further decreased as compared to wt Jc1 virus (Fig. 2F), hence reinforcing the notion that the latter viral particles display high instability.

These results indicated that optimal genome length is a key determinant of HCV stability, which can be assessed at both 37°C and 4°C.

Finally, we sought to investigate the stability of purified extracellular and intracellular particles of HCV at low temperatures, which prevents maturation of viral particles by extracellular lipidation (15). Interestingly, we observed that the Mock medium increased the infectivity of HCVcc intracellular particles maintained at 4°C by over fourfold relative to serum-free medium, in contrast to the purified extracellular particles (Fig. 2G). This suggested that intracellular particles are not fully stable at 4°C and that a destabilizing factor can alter these particles at low temperatures. To confirm this hypothesis, we froze the intracellular particles immediately after their harvest rather than storing them at 4°C before infection. We showed that the HCVcc particles maintained at –80°C were ca. threefold more infectious than those maintained at 4°C, with an infectivity level comparable to particles incubated at 4°C with Mock medium (Fig. 2H).

These results suggested that intracellular particles are unstable at 4°C, which is not the case of extracellular particles, hence suggesting a protecting maturation event during secretion/egress.

### HCV particles are protected by different hepatocyte-specific secreted proteins

The above results prompted us to determine factor(s) expressed by Huh-7.5 cells that may protect HCV particles during their traffic through the secretory pathway. We tested human serum albumin (HSA) and iron-free transferrin (apo-Tf), apolipoprotein E (apoE), and alpha-1-antitrypsin (A1AT), which—except for apoE—are proteins that typically produced and secreted by Huh-7.5 cells (Fig. 3A). These proteins were selected because of their high secretion levels (27) and because of their properties, such as iron chelation for apo-Tf and association with HCV particles for apoE (14, 16, 28, 29). Of note, a low level of transferrin was already present in serum-free medium though at a concentration at least fourfold lower than in the Mock medium (Fig. 3A). When tested individually, we found that either factor induced some levels of protection of purified extracellular HCVcc particles, with two- to six-fold increases of viral infectivity after a 6-h incubation at 37°C (Fig. 3B). Furthermore, with the exception of apoE, either factor alone could also induce a significant protection of intracellular particles (Fig. 3C). Interestingly, when we



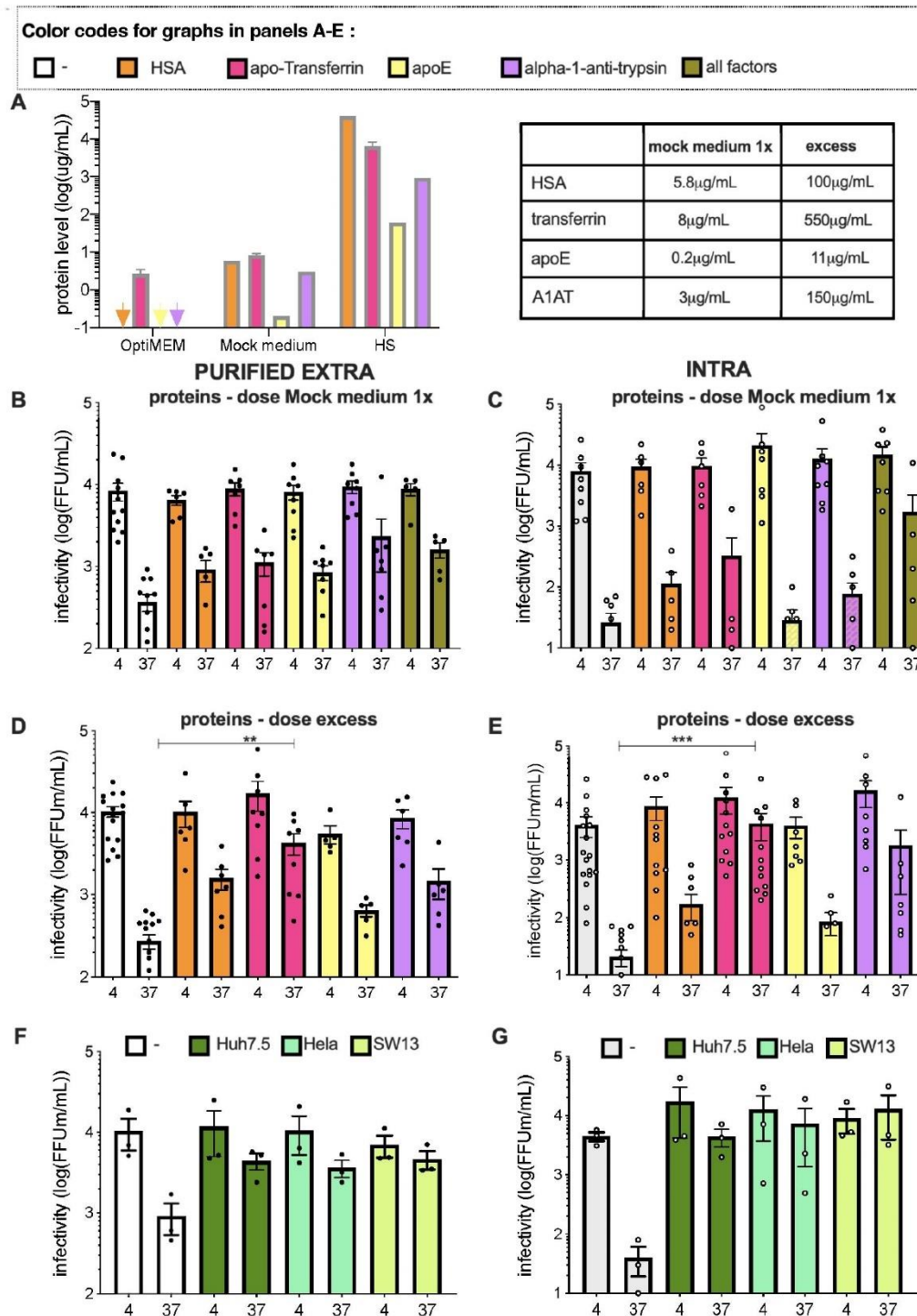


**FIG 3** Secreted hepatic factors can protect HCV particles. (A) Titers of human serum albumin (orange bars), apo-transferrin (pink bars), apoE (yellow bars), or alpha-1-antitrypsin (violet bars) as determined in serum-free medium (OptiMEM), Mock medium or human serum (HS). The arrows represent the concentration of samples that was below the threshold of detection. (B) Infectivity of purified extracellular particles diluted in serum-free medium (white bars) that were or not (Continued on next page)

**FIG 3** (Continued)

supplemented with each indicated protein alone at the levels corresponding to Mock medium (A) vs with the combination of the four proteins and treated as in Fig. 1A. (C) Same as (B) for intracellular particles. (D) Infectivity of purified extracellular particles diluted in serum-free medium supplemented with each protein alone at a 20-fold higher concentration than in Mock medium. (E) Same as (D) for intracellular particles. (F) Infectivity of purified extracellular particles diluted in serum-free medium (white bars) or in Mock media from Huh7.5, HeLa, or SW13 cells, as indicated. (G) Same as (F) for intracellular particles. For panels (B–G), the results are represented as means  $\pm$  SEM. Each dot in the graphs corresponds to the value of an individual experiment.

combined these factors together, we found that this could readily protect intracellular particles from instability (Fig. 3B and C). Yet, the protection levels were lower than that provided by the Mock medium (Fig. 1E and F), suggesting that alternative factors might also contribute to stabilize HCV infectivity. Furthermore, we found that Mock media produced from HeLa and SW13 cells could also protect purified HCV particles as well as intracellular particles (Fig. 3F and G), suggesting that different or, alternatively, ubiquitous cell-secreted factors can stabilize HCV particles.

Since the above-mentioned factors were individually tested at their concentrations detected in the Mock medium produced by Huh-7.5 cells, which are lower than those detected in human serum (Fig. 3A), we next sought to test them at higher concentrations. Interestingly, HSA, A1AT, and more particularly apo-Tf could efficiently protect purified extracellular HCVcc particles, with 4- to 15-fold increases of viral infectivity after a 6-h incubation at 37°C (Fig. 3D) while apoE remained poorly efficient. For intracellular particles, while HSA and apoE could weakly protect their infectivity, with four- to ninefold increases of viral infectivity after a 6-h incubation at 37°C, we found that A1AT and more particularly apo-Tf could fully prevent the loss of infectivity (Fig. 3E). Interestingly, we found that these factors could also enhance infectivity of HCV intracellular particles maintained at 4°C, by up to fourfold (Fig. 3E).

Altogether, these results suggested that a combination of secreted cellular factors could protect both intracellular and extracellular HCV particles from their intrinsic instability.

**Nonprotected HCV particles are sensitive to oxidation**

As cell culture media contain different ions and since HSA and transferrin can bind several cations including calcium or iron, we hypothesized that the loss of infectivity of HCV particles could be cation-dependent. To test this hypothesis, we supplemented the purified extracellular and intracellular particles with EDTA, which chelates divalent metallic cations. Interestingly, we found that EDTA could protect both purified extracellular and intracellular particles from temperature-dependent degradation (Fig. 4A and B) and that EDTA could also enhance infectivity of intracellular particles kept at 4°C (Fig. 4B). Since transferrin, which can readily protect HCV infectivity (Fig. 3), is specific to iron cation and since our serum-free medium contains Fe<sup>3+</sup> (ThermoFisher communication), we thought that Fe<sup>3+</sup> could be involved in inhibition of HCV infectivity. We therefore supplemented purified particles with two iron-specific chelators, i.e., deferoxamine (DFO) and deferiprone (DFP). Interestingly, we observed a dose-dependent protection of both purified extracellular and intracellular particles with either chelator (Fig. 4C through F), suggesting a role of iron cations in the loss of infectivity of infectious particles.

It is well known that iron can induce oxidation under specific environments and more particularly in the presence of ascorbic acid via the Fenton reaction, which results in the formation of ascorbyl radical and ultimately reactive oxygen species (ROS) (30). As our serum-free medium also contains ascorbic acid (ThermoFisher communication), we sought to investigate if infectivity of HCV particles could be specifically affected by oxidation. Hence, we supplemented medium with DFO and ascorbate oxidase (AO), a plant oxidase specific to ascorbate, i.e., the ionic form of ascorbic acid in the medium, to bypass the initial, iron-dependent steps of the Fenton reaction. We observed that AO could overcome the protecting effect of DFO on both purified extracellular and intracellular particles, and could induce a loss of their infectivity (Fig. 4G and H). This indicated that either iron/ascorbate or AO can induce similar alteration of HCV stability.

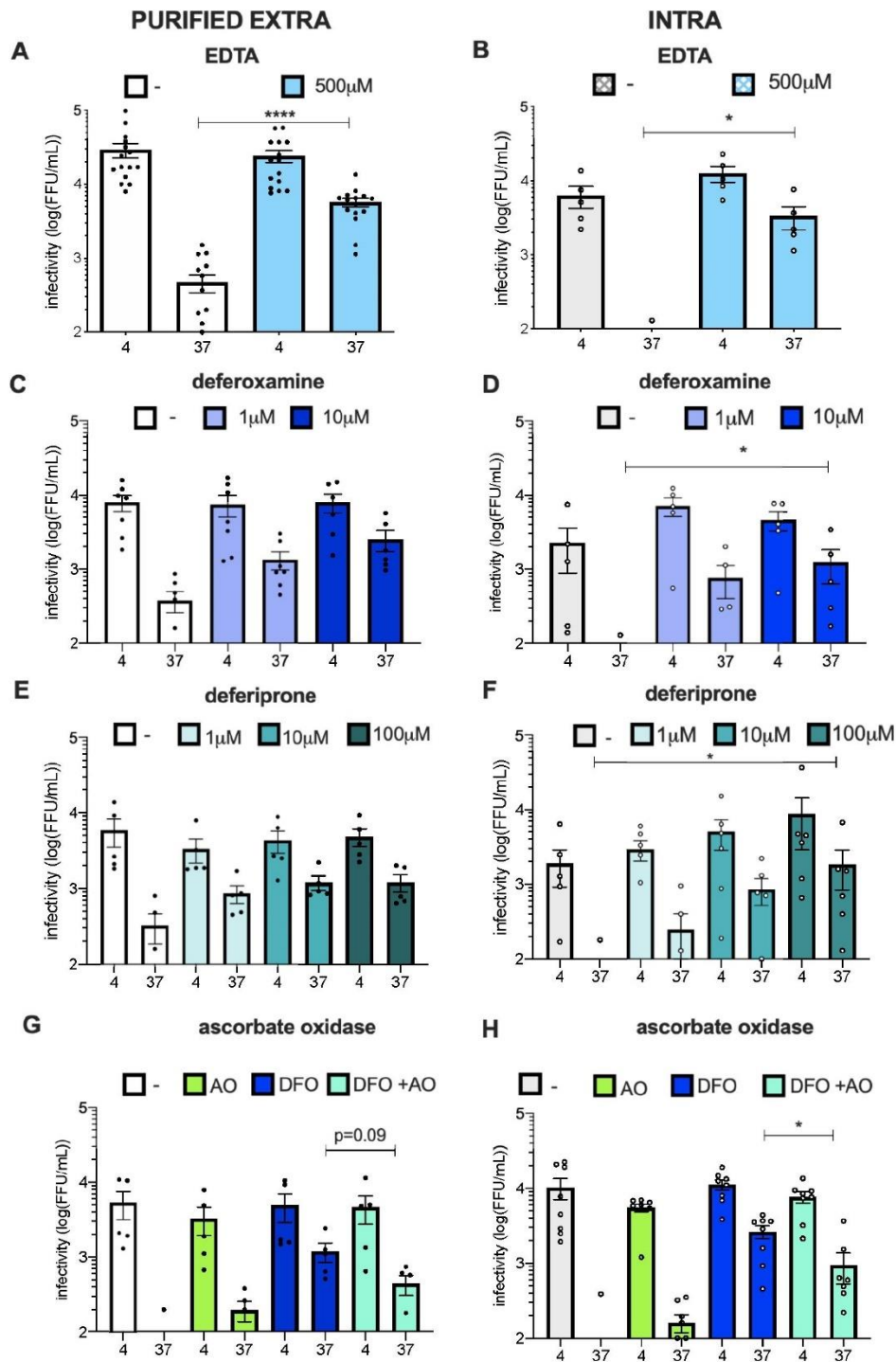


**FIG 4** HCV particles are sensitive to iron-induced oxidation. (A) Infectivity of purified extracellular particles diluted in serum-free medium (–) vs in serum-free medium supplemented with EDTA (0.5 mM) and treated as in Fig. 1A. (B) Same as (A) for intracellular particles. (C) Infectivity of purified extracellular particles diluted in serum-free medium (–) vs in serum-free medium supplemented with different concentrations of deferoxamine and treated as in Fig. 1A. (D) Same (Continued on next page)

**FIG 4 (Continued)**

as (C) for intracellular particles. (E) Infectivity of purified extracellular particles diluted in serum-free medium (–) vs in serum-free medium supplemented with different concentrations of deferiprone and treated as in Fig. 1A. (F) Same as (E) for intracellular particles. (G) Infectivity of extracellular particles diluted in serum-free medium (–) vs in serum-free medium supplemented with 10U of ascorbate oxidase (AO) in combination or not with 10  $\mu$ M of deferoxamine (DFO) and treated as in Fig. 1A. (H) Same as (G) for intracellular particles. The results are represented as means  $\pm$  SEM. Each dot in the graphs corresponds to the value of an individual experiment.

Finally, as we observed that DENV intracellular particles are unstable at 37°C (Fig. 1C), we sought to address if, like for HCV, EDTA and DFO could stabilize their infectivity. However, in contrast to HCV, such treatment with either EDTA or DFO did not restore the infectivity of intracellular DENV particles (Fig. S2), thus underscoring a different mechanism of instability.

Altogether, these results highlighted that in the absence of cell-secreted protecting factors, HCV particles are sensitive to oxidation.

**Oxidation of HCV particles prevents membrane fusion**

We next sought to determine how oxidation could alter HCV infectious particles.

Our RT-qPCR data suggested that viral RNA is not degraded after incubation of purified viral particles at 37°C (Fig. 2); yet, since qPCR amplifies a small fraction of the genome, we could not firmly conclude that the integrity of the HCV RNA was preserved. Thus, we electroporated naïve Huh-7.5 cells with the same amounts of RNA extracted from purified particles diluted in serum-free medium vs in Mock medium and incubated at 4°C vs 37°C. Indeed, should the genome remain intact, it would allow HCV replication and propagation, which we investigated by flow cytometry to assess expression of the virus core protein. Strikingly, while we observed a strong loss of infectivity of purified HCV particles incubated at 37°C, as expected, we could readily detect HCV-positive cells after electroporation of naïve cells with the RNA extracted from these particles, with an only twofold decrease of HCV-positive cells relative to cells electroporated with RNA extracted from viral particles kept at 4°C (Fig. 5A). These results indicated that the instability of purified HCV particles is not caused by a disruption of their RNA.

Then, to determine if HCV surface glycoproteins were specifically impacted, we tested if HCV pseudoparticles (HCVpp) are sensitive to oxidation. Indeed, HCVpp are retroviral particles harboring functional HCV E1E2 glycoproteins at their surface but no other HCV components (31). Interestingly, we observed that in contrast to HCVcc particles (Fig. 1E), purified HCVpp particles were stable upon incubation at 37°C (Fig. 5B). This suggested that E1 and E2 glycoproteins may not be primarily impacted by the temperature-induced oxidation.

To complement this notion, we measured the attachment to Huh-7.5 cells of purified HCVcc particles after incubation at 37°C. As shown in Fig. 5C, we found that relative to incubation at 4°C, a 6-h incubation at 37°C did not affect the attachment of purified HCVcc extracellular particles to the surface of Huh-7.5 cells.

These results together indicate that E1 and E2 glycoproteins are not impacted by oxidation and, therefore, the loss of infectivity occurs at a post-binding step.

Hence, we sought to determine how oxidation could alter the membrane fusion properties of HCV particles using an *in vitro* assay based on liposomes containing a self-quenched R18 dye (32, 33). We compared the fusion activity of purified extracellular particles relative to those present in crude producer cell supernatants. Strikingly, while incubation at 37°C did not alter the fusion efficiency of HCVcc particles from crude supernatants (Fig. 5D, top), it altered the fusion activity of purified extracellular particles, as shown by the reduction of both the maximal extent at plateau (Fig. 5D, bottom) and the initial rates (Fig. 5D and E) of membrane fusion.

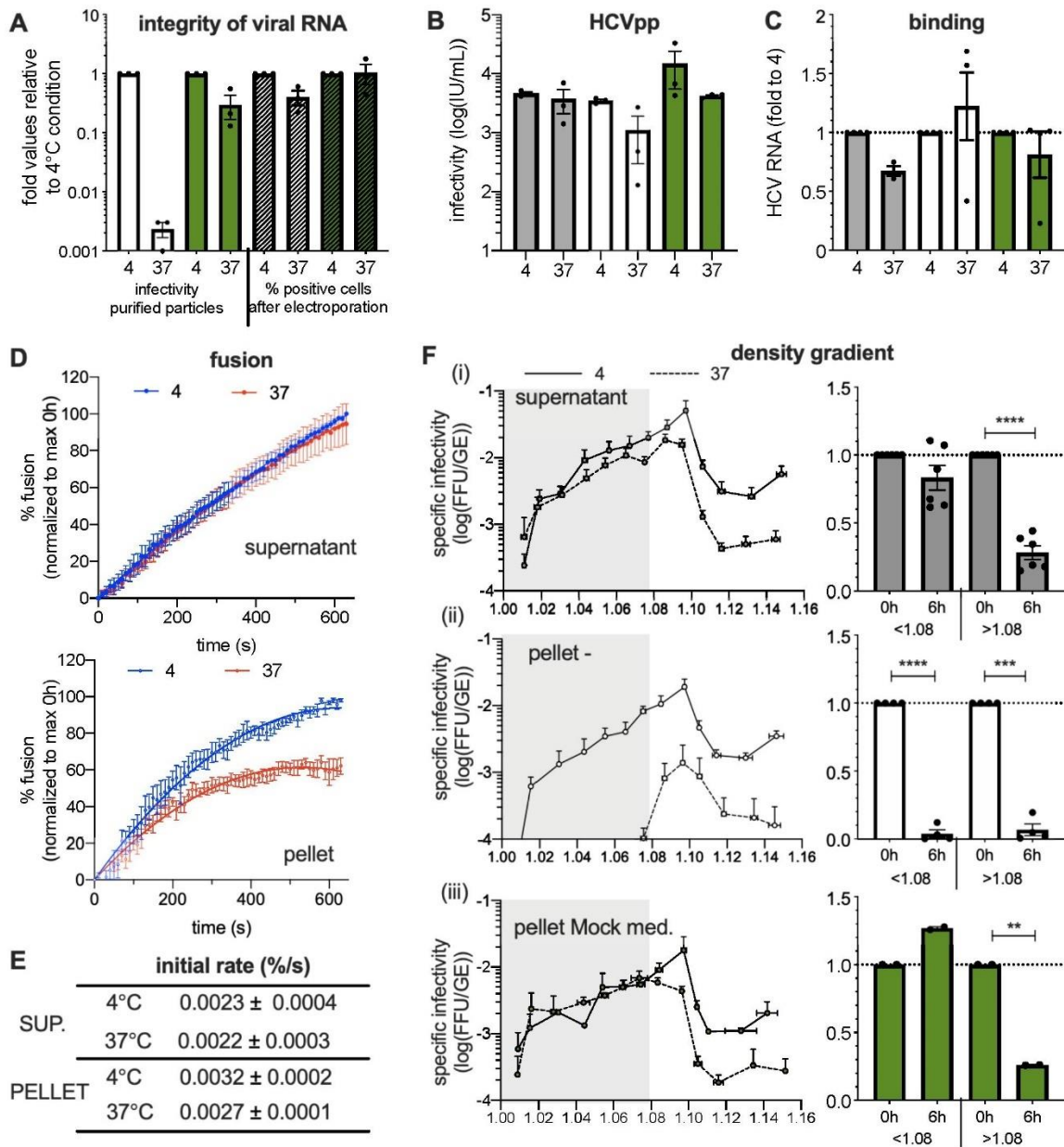


**FIG 5** Characterization of HCV properties impaired by oxidation. (A) RNA from purified particles diluted in serum-free medium vs in Mock medium and left at 4°C or incubated for 6 h at 37°C were extracted and used for electroporation of naïve cells. The left part of the graph shows the infectivity of the purified particles before extraction of RNA (white bars, viral particles left in serum-free medium; green bars, viral particles incubated in Mock medium) and the right part of the graph shows the percentage of HCV-positive cells after electroporation with extracted RNA (gray bars, percentage of positive cells electroporated with RNA extracted from viral particles left in serum-free medium for 6 h at 4°C or 37°C; green bars, percentage of positive cells electroporated with RNA extracted from viral particles incubated in Mock medium for 6 h at 4°C or 37°C). The data are represented as fold values relative to 4°C incubation. (B) Infectivity of HCV pseudoparticles (HCVpp) from crude supernatant of producer cells (gray bars) or purified by ultracentrifugation and diluted in serum-free medium (white bars) or Mock medium (green bars) that were left at 4°C or incubated for 6 h at 37°C. (C) Levels of HCV RNA attached to Huh-7.5 cells after 2 h of incubation at 4°C using crude virus producer cell supernatants (gray bars) or purified extracellular particles diluted in serum-free medium (white bars) vs in Mock medium (green bars) that were left at 4°C or incubated for 6 h at 37°C. (D) Membrane fusion assays with liposomes using either crude virus producer cell supernatants (top) or purified (Continued on next page)

FIG 5 (Continued)

extracellular particles (bottom) diluted in serum-free medium, left at 4°C (blue lines) or incubated for 6 h at 37°C (red lines). The results show the percentages of fusion relative to Triton X-100-treated liposomes and normalized to the maximum of fusion for 0 h condition for each experiment. (E) Values of the initial rates of the fusion curves. (F) Specific infectivity of HCV particles detected in fractions from buoyant density gradients of crude virus producer cell supernatant [(i), top graph] or of purified particles diluted in serum-free medium [(ii), middle graph] or in Mock medium [(iii), bottom graph] that were left at 4°C (plain lines) or incubated for 6 h at 37°C (dotted lines). The ratios of specific infectivity of each fraction upon incubation at 37°C vs 4°C were determined (right). The results show the mean of average of these ratios for fractions below and above density of 1.08. The results are represented as means  $\pm$  SEM. For panels (A–C) and F, each dot in the graphs corresponds to the value of an individual experiment.

### Lipids of HCV particles are altered by oxidation

That HCVcc particles seemed to be specifically sensitive to oxidation in comparison to other viruses (Fig. 1) or to HCVpp (Fig. 5B) suggested that their instability could be linked to a specific property of authentic HCV particles. Indeed, HCV particles from patients as well as HCVcc are known to be heterogenous in terms of buoyant density (12, 13), which reflects different levels of lipidation of these particles compared to those of HCVpp (34) or DENV (35) particles. We therefore hypothesized that the loss of infectivity due to oxidation could occur for a specific subpopulation of HCV particles. To test this hypothesis, we layered on a density gradient crude HCVcc producer cell supernatants or, alternatively, purified extracellular particles that were incubated beforehand for 6 h at 37°C vs 4°C in serum-free medium. As for crude supernatants, we observed a significant loss of specific infectivity for HCV particles of high densities though they poorly contributed to the overall infectivity (Fig. 5F, upper graphs), whereas there was no substantial loss of infectivity for viral particles of lower densities. Interestingly, for purified extracellular particles, we found a temperature-dependent decrease of specific infectivity of ca. 20-fold for all fractions (Fig. 5F, middle graphs). These results indicated that HCV particles of low densities, which correspond to lipidated virions (15), become specifically unstable upon purification and incubation at 37°C. Moreover, these results suggested that some secreted factors may specifically protect low-density particles. Accordingly, we found that incubation of purified extracellular particles for 6 h in Mock medium resulted in an explicit restoration of the specific infectivity of lipidated particles (Fig. 5F, bottom graphs). Altogether these results indicated that low-density HCV particles are specifically sensitive to oxidation.

Next, since low-density particles have a high lipid/protein ratio (15), we surmised that lipids (either phospholipids or neutral lipids) of viral particles were specifically sensitive to oxidation, which agrees with the alteration of HCV fusion activity (Fig. 5D and E). We attempted to detect lipid peroxidation by measuring the amounts of isoprostanes, as a marker of lipid oxidation (36). Unfortunately, we could not detect any increase of this marker, even when we induced oxidation with CuSO<sub>4</sub>, likely owing to too low amounts of lipids in our HCV samples. Thus, to indirectly address if our experimental conditions could induce lipid peroxidation, we used low-density lipoproteins (LDLs) diluted in serum-free medium as a surrogate model of lipidated HCV particles (12), which allowed detection of isoprostanes (Fig. 6A). Interestingly, we detected increased isoprostane levels when these LDL preparations were incubated at 37°C for 6 h (Fig. 6A, white bars). Importantly, we did not detect increase of isoprostane levels when the LDLs were diluted in either Mock medium (Fig. 6A, green bars) or in serum-free medium supplemented with DFO (Fig. 6A, blue bars). Altogether, these results confirmed that our experimental conditions could reflect lipid peroxidation.

Then, to confirm that lipids from viral particles are altered by oxidation, we sought to test if high-density lipoproteins (HDLs), which are known to protect LDLs from lipid peroxidation (37), could protect HCV particles. Hence, we supplemented purified extracellular and intracellular HCV particles with HDLs at different concentrations corresponding to 0.2%, 2%, and 10% of human serum. Interestingly, all HDL doses could readily protect HCV particles from temperature-dependent degradation (Fig. 6B and C). Furthermore, HDL could also protect intracellular particles at 4°C as we also observed an

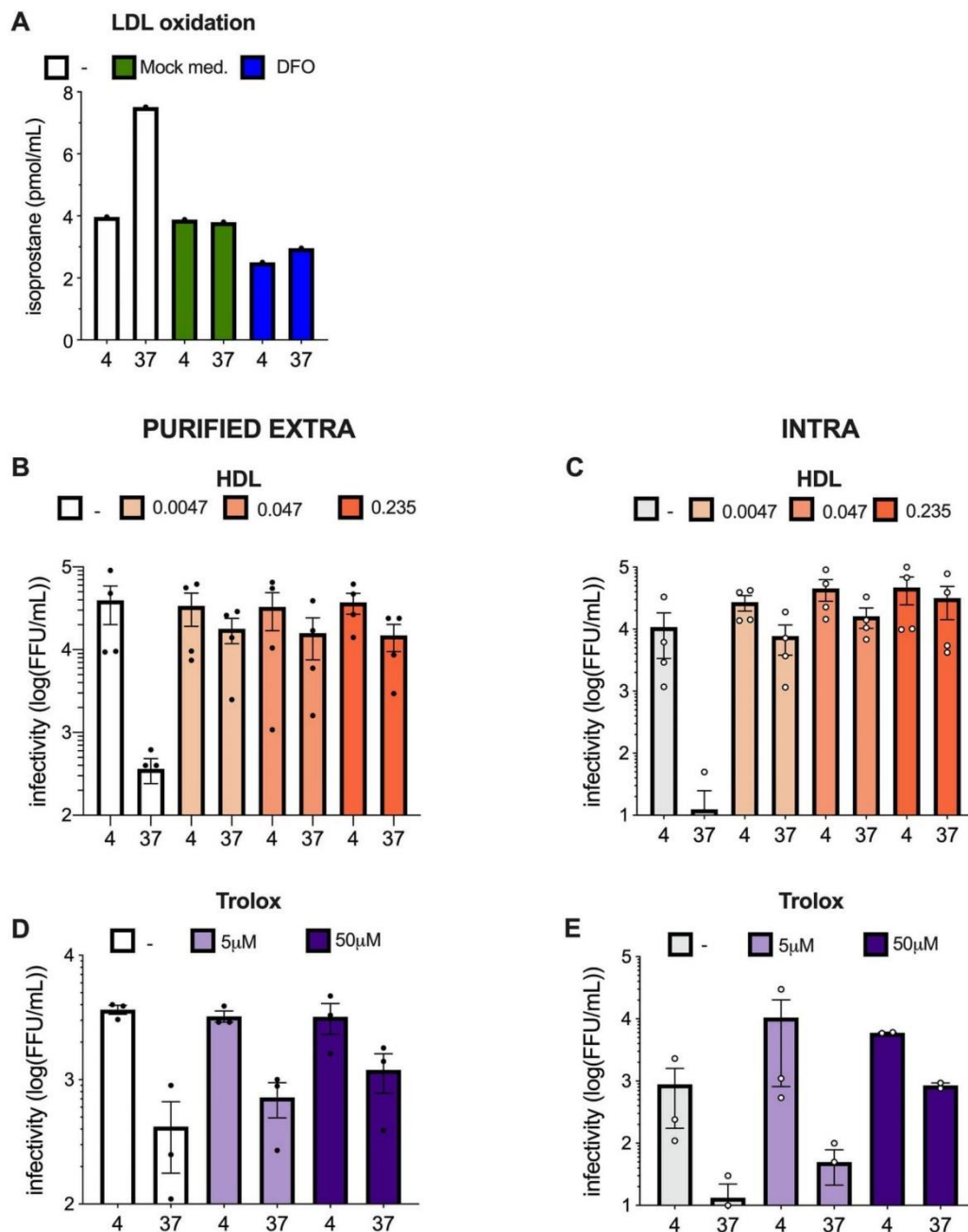


**FIG 6** HCV particles are sensitive to lipid peroxidation. (A) Amount of isoprostanones found in LDLs diluted in serum-free medium (white bars), Mock medium (green bars), or serum-free medium supplemented with deferoxamine (DFO) (blue bars) and left at 4°C or incubated for 6 h at 37°C. (B) Infectivity of purified extracellular particles diluted in serum-free medium (-, white bars) vs in serum-free medium supplemented with different concentrations of HDLs (in g/L) and treated as in Fig. 1A. (C) Same as (B) for intracellular particles. (D) Infectivity of purified extracellular particles diluted in serum-free medium vs in serum-free medium supplemented with different concentrations of Trolox and treated as in Fig. 1A. (E) Same as (D) for intracellular particles. The results are represented as means  $\pm$  SEM. Each dot in the graphs corresponds to the value of an individual experiment.

increase of infectivity when HDLs were present at 4°C (Fig. 6C). To complement this approach, we tested the lipophilic antioxidant Trolox, which is a water-soluble analog of vitamin E (38). We found that Trolox could prevent the loss of infectivity of both purified extracellular and intracellular HCV particles upon incubation at 37°C (Fig. 6D and E).

Altogether, these results confirmed that lipids of HCV particles are sensitive to peroxidation.

Finally, since HCVcc particles with a longer genome (Jc1 R2A HCVcc) appeared to be more unstable than wt virus (Fig. 2E and F), we surmised that this difference could be linked to a differential reactivity to oxidation of their lipidated particles; the characteriza-

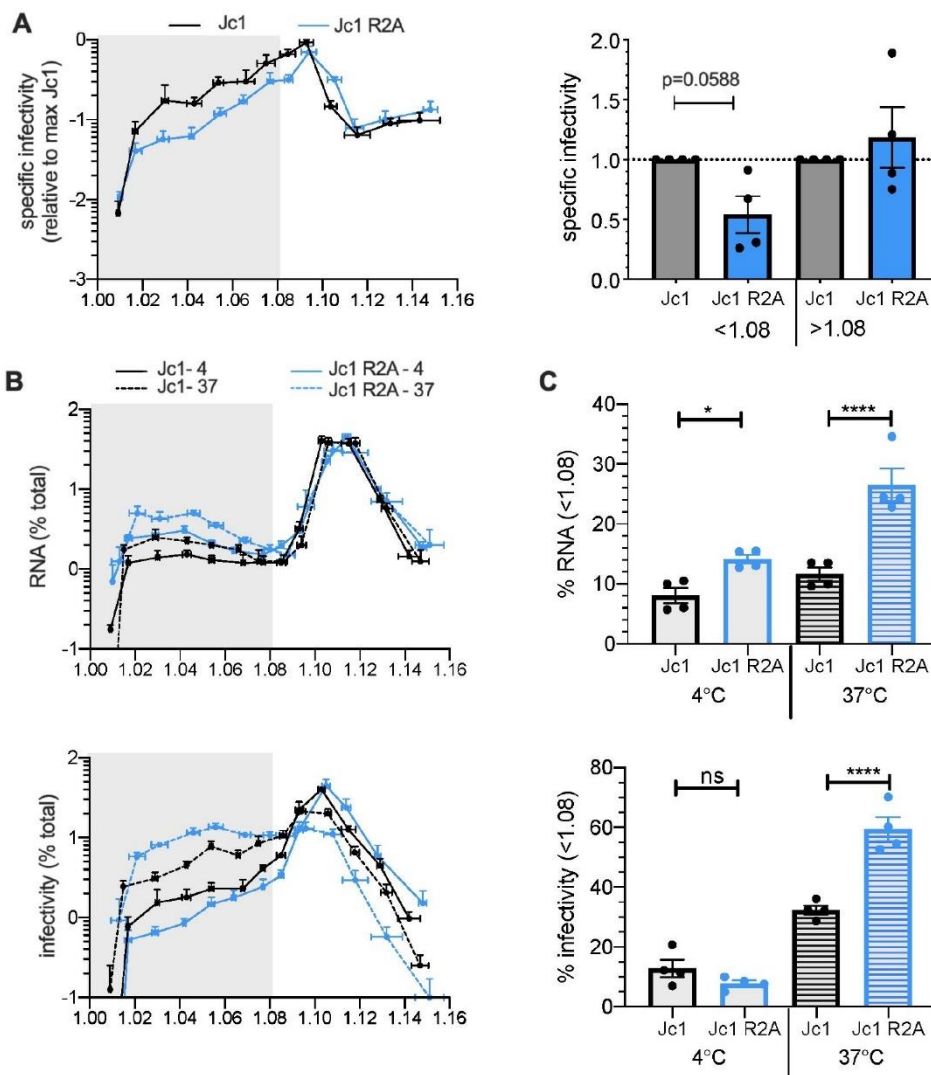


**FIG 7** The size of the HCV genome influences densities and stability of viral particles. (A) Specific infectivity of Jc1 (black line) vs Jc1 R2A (blue line) detected in fractions from buoyant density gradients of crude supernatant. The ratios of specific infectivity of each fraction upon incubation at 37°C vs 4°C were determined (right). The results show the mean of average of these ratios for fractions below and above density of 1.08. (B) Viral RNA (top) or infectivity (bottom) of Jc1 (black lines) vs Jc1 R2A (blue lines) particles detected in fractions from density gradients of crude virus producer cell supernatant after incubation at 4°C (plain lines) and 37°C (dotted lines). (C) The sum of percentage of RNA (top graph) or infectivity (bottom graph) in fractions below 1.08 from (B) is represented. The results are represented as means  $\pm$  SEM. Each dot in the graphs corresponds to the value of an individual experiment.



tion of which may provide hints to understand mechanisms evolved by HCV to mitigate the impact of oxidation after viral production.

First, we compared the stability of Jc1 R2A HCVcc with parental Jc1 virus through their analysis in density gradients. We found that compared to Jc1 HCVcc, the Jc1 R2A virus exhibited a twofold reduction of specific infectivity in its low-density fractions (Fig. 7A), indicating that Jc1 R2A low-density particles are more unstable than those of Jc1. Interestingly, compared to the Jc1 HCVcc, we also found that proportionally, the Jc1 R2A virus displayed more abundant RNA levels—reflecting viral particles—in low-density fractions (Fig. 7B, plain lines in upper graphs), which, unexpectedly, were associated to a loss of infectivity (Fig. 7B, plain lines in lower graphs). That the Jc1 R2A virus, which seems more efficiently lipidated than Jc1 HCVcc particles, had specifically lost infectivity of its lipidated fractions agreed with the hypothesis that lipidated particles are more sensitive to oxidation.

Thus, to further explore the basis of the difference between either virus for lipidation vs oxidation of viral particles, we allowed them to become lipidated by incubating their supernatants for 6 h at 37°C, which induces partial virion lipidation by lipids released from Huh-7.5 cells (Fig. S3). Accordingly, we detected significantly higher levels of viral particles in low-density fractions for both Jc1 and Jc1 R2A viruses (Fig. 7B, upper graphs). Yet, while this increase of RNA levels in lipidated fractions was similar between Jc1 and Jc1 R2A, we observed a greater increase of infectious titers for the Jc1 R2A virus (Fig. 7B, lower graphs), suggesting a higher dynamic of lipidation for this latter virus.

Altogether, these results indicated that lipidation as well as rates of lipid exchanges are linked to the stability of HCV and that genome length may modulate the above.

Overall, these results suggested that HCV particles lipids are specifically sensitive to oxidation, leading to an altered fusion capacity and thus a loss of entry capacities and infectivity.

## DISCUSSION

Summarizing, here we show first that HCV particles are intrinsically labile, which drastically alters their specific infectivity by oxidation of their lipids, and second that they are protected from lipid oxidation by secreted cellular proteins, which can preserve their membrane fusion capacity and overall infectivity.

Interestingly, our results show that HCV particles are sensitive to oxidation-mediated degradation in contrast to other tested viruses that infect hepatocytes, including a closely related member of the *Flaviviridae* family, i.e., DENV. We show that this property is due to the unique feature of HCV particles, i.e., their association with neutral lipids such as triglycerides and cholesterol esters, which results in their peculiar low density relative to other viruses (11–16). In this respect, HCV particles have a lipid composition closer to LDL than to other enveloped viral particles such as, e.g., HIV particles (24), which induces their specific and high sensitivity to oxidation, as shown in our report. Of note, we also show that HCVpp are not sensitive to oxidation. While both HCVpp and HCVcc particles harbor E1 and E2 glycoproteins at their surface, the lipid composition of either viral particle is dissimilar (34), which is due to their different assembly sites [ER for HCVcc and multi-vesicular bodies (MVBs) for HCVpp (39)] and to specific acquisition of neutral lipids by HCVcc (15, 40). This explains the link between the unique lipidic composition of authentic HCV particles and their sensitivity to oxidation.

Our results reveal that oxidation alters the fusogenicity of purified HCV particles. This agrees with a previous report showing that knock-down of GPx4, a key protector of intracellular lipid peroxidation, resulted in secretion of HCV particles with altered fusogenicity (41). While in this report, lipid peroxidation was induced inside the cells, which altered viral particles during their assembly and/or secretion, here we show that lipid oxidation could also impair fusogenicity of particles after their secretion and we highlight both the targeted viral components and the mechanisms of protection developed by HCV particles. Typically, membrane fusion involves activation of membrane surface proteins, such as viral glycoproteins, and mixing of lipids from outer and

inner membrane layers (42). Since our data indicated that HCVpp are not sensitive to oxidation and that cellular binding of HCVcc was not impaired (Fig. 5), this led us to propose that fusion impairment was caused by a defect of the lipid bilayer rather than to an alteration of the viral surface glycoproteins themselves. Formation of ROS that are free radicals that can damage organic macromolecules may occur as a product of the Fenton reaction (30), which can be initiated by the presence of ascorbate and iron in the environment. Then, ROS can react with cholesterol or with unsaturated fatty acids via their carbon-carbon double bonds and create hydroperoxide groups. This could alter properties of the viral membrane such as its fluidity or curvature, which may alter its membrane fusion properties (43). Interestingly, light-activated membrane-targeting singlet oxygen ( $^1\text{O}_2$ ) generators, leading to ROS formation, were developed as broad-spectrum antiviral compounds (43). One of such compounds, LJ001, was shown to inhibit the membrane fusion properties of HIV and HCV particles by altering lipid packing and membrane fluidity, confirming the link between lipid oxidation and viral fusion (44–46). More precisely, at the molecular level, we could speculate on the one hand, that the oxidized lipids would cluster into microdomains in order to protect the resulting polar groups from hydrophobic repulsion and on the other hand, that the surface of viral particles would inflate owing to the addition of hydroperoxide groups, both events leading to an alteration of the fusogenicity of the membrane.

Importantly, we found that several serum proteins could protect purified HCV particles from oxidation, namely apo-Tf, HSA, and A1AT that are typically secreted by hepatocytes and by lipid-free apoE that is present in serum, albeit at variable efficiency (Fig. 3), although it appears that the mechanism(s) may also involve alternative factors. As these proteins display various and non-related functions, we can only speculate about the different mechanisms by which they could induce protection of viral particles. First, transferrin could protect HCVcc particles by chelating iron cations, which is its main function, and which would therefore prevent the Fenton reaction and subsequent oxidation to occur. Second, HSA exhibits antioxidant properties as it can display binding sites for several metal ions, including iron, but also as its Cysteine at position 34 can be oxidized (47), which could therefore prevent reaction of ROS with viral particles. Indeed, HSA is primarily detected in its reduced form although about 30–40% could be variably oxidized with either reversible or irreversible modification (48). Yet, we cannot exclude the possibility that a previously described direct interaction between HSA and HCV particles (15) could, by ‘shielding’ the latter, reduce their oxidation. Third, A1AT was also shown to display antioxidant properties via its methionine residues (49), which could be oxidized instead of viral particles. Finally, apoE also has antioxidant properties (50) probably by scavenging radicals (51). Yet, we can also speculate that it could protect the viral lipid bilayer from oxidation by making a physical barrier, since apoE was shown to bind to HCV particles after secretion (28, 29). Finally, we could not exclude that alternative antioxidant factors secreted by hepatocytes or other cell types may also contribute to protect HCV particles from oxidation.

Our data reveal a different sensitivity to oxidation between intracellular particles and extracellular particles. Indeed, the loss of infectivity was ca. 10-fold higher for the former, as compared to the latter (Fig. 2). Moreover, freezing at  $-80^\circ\text{C}$  (Fig. 2H) or treatment of the former particles immediately put on ice upon harvest with the above hepatocyte factors (Fig. 1E, 2G, and 3E), chelators (Fig. 4B, D, and F), or antioxidants (Fig. 5I) could increase their infectivity by up to fivefold, as compared to the latter particles. One explanation could be due to a poorly characterized maturation process of HCV particles since HCV intracellular and extracellular particles seem to exhibit different physico-chemical properties, such as pH sensitivity (52) or buoyant density (15, 53), though the latter property may not fully explain the increased sensitivity to oxidation since intracellular particles are not or much less lipidated than extracellular particles (15). On the other hand, intracellular particles are likely to represent more native forms of infectious viral particles, i.e., before they can acquire neutral lipids, which readily occurs after egress (15). Indeed, when extracellular particles acquire neutral lipids, they also incorporate

some serum proteins, such as, e.g., apoE while they accumulate in the extracellular medium (28, 29), which results in an equilibrium between factors protecting (e.g., apoE) vs sensitizing (e.g., lipids) virions to oxidation. Note that such events may also partly occur during traffic of viral particles through the secretion pathway, after their biogenesis in the endoplasmic reticulum (11). As virions traffic via organelles that could also be used by secreted hepatocyte factors (54, 55), this co-trafficking is likely to increase their encountering and mutual interrelations, which may ultimately protect viral particles from oxidation.

Thus, altogether, our results highlight a new crossroad between HCV particles and serum components, such as proteins, but also lipoproteins since some secreted factors that promote antioxidative protection of viral particles, as shown in this report, were also shown to condition physico-chemical properties of HCV particles, such as their buoyant density. For example, HSA mediates lipidation of the viral particles by lipoproteins in the serum (15). On the other hand, secreted lipases, such as lipoprotein lipase and hepatic triglyceride lipase, have been shown to increase the density of HCV particles by removing lipids (19). Yet, whether lipase activity may promote HCV oxidation remains to be shown. Besides, other serum components can influence HCV particles infectivity and immune evasion. Indeed, HDLs as well as some lipid-free apolipoproteins, such as ApoC1 and ApoE, can promote HCV entry and inhibit neutralizing antibodies (56–58). In contrast, oxidized LDLs could decrease HCV entry (59).

Finally, our data underscore an intriguing relation between stability of HCV particles and the size of the viral genome they harbor (Fig. 6). Indeed, while a 10% increase of the size of the HCV RNA had no impact on viral replication, it strongly altered the infectivity and stability of the particles. We can only speculate at this stage on potential explanations since, clearly, additional experiments that were beyond the scope of this report are needed to fully understand the mechanisms that regulate these events. Interestingly, an allometric relationship between viral genome length and virion volumes was identified (60), suggesting that genome size could directly influence the composition or the architecture of particles and how viruses have evolved to reach the optimal genome size. We can therefore propose that the artificial extension of genome size may result in particles containing more phospholipids and/or cholesterol, as the inside of particles would need to expand. Indeed, any increase of genome size may require more core proteins to protect the HCV RNA, hence resulting in a larger particle volume and therefore requiring more fatty acids to envelope such a nucleocapsid. Yet, although more phospholipids could be recruited on virion, this may not necessarily translate in more glycoproteins being incorporated since the level of glycoproteins at the surface of viral particles is likely to be regulated by other finely tuned processes that involve, e.g., delayed cleavage between E2 and p7 (10), as well as preformed nucleocapsids (61), before envelopment steps. Overall, this could result in larger amounts of fatty acids in and/or on virions that would be more accessible to oxidation, thereby decreasing the stability of HCV particles.

## MATERIALS AND METHODS

### Cells

Huh-7.5 cells (a kind gift from Charles Rice, Rockefeller University, New York, USA), Huh-7-NTCP cells (62), and HEK-293T kidney cells (ATCC CRL-1573) were grown in Dulbecco's modified minimal essential medium (DMEM, Invitrogen, France) supplemented with 100 U/mL of penicillin, 100 µg/mL of streptomycin, and 10% of FCS (A10111-1098/RF1103719P, GE Healthcare).

### Plasmids

pFK-JFH1/J6/C-846 and pFK\_i389-Rluc\_2a\_Core\_3' plasmids encoding full-length Jc1 HCV, with or without reporter renilla luciferase, respectively, were kind gifts from

R. Bartschlagler (Heidelberg University, Germany). pFK-JFH1/J6/C-846\_FLAG-E2 was a kind gift from T. Pietschmann (Twincore, Germany) and was used to generate pFK-JFH1/J6/C-846\_FAG\_3C harboring the human rhinovirus 3C protease cleavage site between FLAG peptide and E2 sequence, by PCR mutagenesis (oligonucleotide sequences are available upon request).

The constructs encoding wild-type CCHFV strain IbAr10200 L polymerase (pCAGGS-V5-L), N nucleoprotein (pCAGGS-NP), M segment (pCAGGS-M), T7 RNA polymerase (pCAGGS-T7), nLuc-expressing minigenome flanked by L NCR under the control of a T7 promoter (pSMART-LCK\_L-Luc), and an empty vector (pCAGGS) were described previously (22, 63).

The constructs encoding HDV Ag (pSVLD3) and HBV envelope glycoproteins (pT7HB2.7) were described previously (64). The constructs encoding full-length DENV-2 strain New Guinea C (NGC) pDVWS601 was described previously (65).

### Reagents

Human serum albumin (HSA) fraction V (Sigma-Aldrich), apolipoprotein E from human plasma (Sigma-Aldrich), human apo-transferrin (Sigma-Aldrich), and alpha-1-antitrypsin from human plasma (Sigma-Aldrich) were used at concentration indicated in Fig. 3. Ascorbate Oxidase (AO) from Cucurbita sp. (Sigma-Aldrich), Deferiprone (DFP) (Sigma Aldrich), deferoxamine mesylate (DFO) (Sigma Aldrich), EDTA (Invitrogen), Trolox (Sigma Aldrich), and purified human HDLs (Sigma Aldrich) were used at the indicated concentrations.

### Protein level evaluation

Human apoB and apoE concentrations were measured in OptiMEM and in Huh-7.5 cell supernatant (Mock medium) using ELISA (Mabtech) according to manufacturer's instructions. HSA concentrations were measured using Cobas C501 analyzer (Roche Applied Science). Human transferrin and alpha-1-antitrypsin concentrations were evaluated by quantitative western blot using a standard curve made with purified apo-transferrin and alpha-1-antitrypsin.

### Cytotoxicity measurement

The cytotoxicity of cells cultured in serum-free medium was assessed 72 h post-seeding using Cytotox-Glo Cytotoxicity Assay (Promega) according to the manufacturer's protocol.

### Production of HCVcc particles

HCVcc particles were produced as described previously (15). Electroporated Huh-7.5 cells were grown in serum-free medium (OptiMEM, Invitrogen). Intracellular infectivity was determined as described previously from HCVcc producer cells following four freeze/thaw cycles. Virus-containing supernatants were collected at 3 days post-electroporation and clarified through a 0.45- $\mu$ m filter (Corning Inc, Corning, NY, USA). Viral stocks were titrated on Huh-7.5 cells by immunostaining with anti-NS5A 3E10 (kind gift from C. Rice).

### Production of DENVcc particles

Viral stocks of the DENV-2 strain New Guinea C (NGC) (AF038403) was produced using *in vitro* RNA transcripts prepared from DENV-2 infectious plasmid clone pDVWS601 plasmid (65). Briefly, plasmid was linearized with XbaI (New England Biolabs, Ipswich, MA, USA) and RNA transcripts were produced and purified using mMESSAGE mMACHINE T7 Kit (Ambion/ThermoFisher Scientific, Waltham, MA, USA). RNA transcripts were introduced into Huh-7.5 cells by electroporation (using 5  $\mu$ g RNA for  $6 \times 10^6$  cells per electroporation). Virus-containing supernatants were collected at 3 days post-electroporation and clarified through a 0.45- $\mu$ m filter (Corning Inc, Corning, NY, USA). Viral stocks were titrated on Huh-7.5 cells.

### Production of SARS-CoV-2 particles

SARS-CoV-2 particles were amplified on Vero E6 cells as described previously (66). SARS-CoV-2 virions were then produced in serum-free OptiMEM by infection of Huh-7.5 cells using this viral stock at MOI = 0.1. Supernatants containing SARS-CoV-2 particles were clarified by centrifugation for 10 min at  $5,000 \times g$  at 72 h post-infection. For titration, Huh-7.5 cells were infected with different dilutions of virus. At 6 h post-infection, the medium was replaced by DMEM/10% FCS containing 1.2% of carboxymethylcellulose (Sigma). Cells were fixed at 72 h post-infection and were immunostained with SARS-CoV-2 nucleocapsid antibodies (Sino Biological).

### Production of HDV particles

HDV virions were produced in serum-free OptiMEM culture media by co-transfection of Huh-7.5 cells with a 1:1 mixture of the pSVLD3 plasmid encoding the HDV genome and the pT7HB2.7 plasmid encoding the HBV glycoproteins using GeneJammer transfection reagent (Agilent), as described previously. Following addition of the transfection mixture, the medium was removed after a 6-h incubation and replaced with fresh serum-free medium. HDV producer cells were maintained under serum-free conditions for 10 days, with the medium replaced every second or third day. Supernatants containing HDV virions were clarified by microfiltration through 0.45  $\mu\text{m}$  filters. Infection assays were performed using Huh-7-NTCP cells. Huh-7-NTCP cells were incubated with HDV overnight and the infection medium was replaced by William's E medium (WME) (Gibco, France) supplemented with non-essential amino acids, 2 mM L-glutamine, 10 mM 4-(2-hydroxyethyl)-1-piperazineethanesulfonic acid (HEPES) buffer, 100 U/mL of penicillin, 100  $\mu\text{g}/\text{mL}$  of streptomycin, 10% fetal bovine serum, and 2% of DMSO. Infected Huh-7-NTCP cells were analyzed at day 9 post-infection by RT-qPCR (62).

### Production of CCHFV tecVLP particles

Huh-7.5 cells were washed two times with OptiMEM and seeded overnight in the same medium in 10cm dish. Cells were transfected with 3.6 $\mu\text{g}$  of pCAGGS-V5-L, 1.2 $\mu\text{g}$  of pCAGGS-NP, 3 $\mu\text{g}$  of pCAGGS-M or pCAGGS, 3 $\mu\text{g}$  of pCAGGS-T7, and 1.2 $\mu\text{g}$  of pSMART-LCK\_L-Luc, using GeneJammer transfection reagent (Agilent), as described previously (67). The transfection medium was replaced 6 h post-transfection. Seventy-two hours post-transfection, supernatant was harvested and filtered through a 0.45- $\mu\text{m}$  filter. For titration, Huh-7.5 cells were pre-transfected using 2.4  $\mu\text{g}$  of pCAGGS-V5-L and 4.8  $\mu\text{g}$  of pCAGGS-NP using GeneJammer transfection reagent. The transfection medium was replaced at 6 h post-transfection and cells were seeded in 24-well plates in OptiMEM. Twenty-four hours post pre-transfection, cells were infected and then lysed after 24 h using Passive Lysis Buffer 1x (Promega), incubated 15 min at room temperature, and the nLuc activity was assessed using the Nano-Glo Luciferase Assay System (Promega) and a Mithras LB 940.

### Production of HCV pseudoparticles

To generate HCVpp, 293T cells were transfected with expression vectors encoding the viral components, i.e., E1E2 glycoproteins, retroviral Gag-Pol proteins, and packaging-competent GFP containing retroviral transfer vectors as described previously (31).

Medium (6 mL/plate) was replaced 16 h after transfection. Supernatants containing the pseudo-particles were harvested 24 h later, filtered through 0.45  $\mu\text{m}$  pore-sized membranes, and used in infection assays. Target Huh-7.5 cells were seeded in 48-well plates at a density of  $1.5 \times 10^4$  cells per well and incubated overnight at 37°C. Dilutions of viral supernatants containing the pseudo-particles were added to the cells and the plates were incubated for 6 h. The supernatants were removed, and the cells were incubated in regular medium for 72 h at 37°C. The infectious titers, expressed as infectious units (IU) per milliliter, were deduced from the transduction efficiencies, determined as the percentage of GFP-positive cells measured by FACS analysis (BD Canto).

### Purification of viral particles by ultracentrifugation

Cell supernatant containing viral particles were harvested 72 h after electroporation and concentrated 67 times by ultracentrifugation at  $25,000 \times g$  in a Beckman SW41 rotor for 105 min at 4°C, followed by resuspension in PBS for 20 min at 4°C, before further analysis.

### Purification of viral particles by immunoprecipitation

Supernatant from cells electroporated with RNA encoding for Jc1 FLAG\_3C were incubated 6 h with antiFLAG agarose beads (Sigma-Aldrich) at 4°C under continuous agitation. The complexes were washed three times with PBS before overnight incubation with PSP (Sigma-Aldrich). The supernatant containing eluted particles, after cleavage of the FLAG peptide, was then used for stability measurement.

### Stability measurement

Stability was measured by diluting purified particles or intracellular particles 50-fold in serum-free medium supplemented, or not, with different components or with Mock medium. The samples were split in two: one part was incubated for 6 h at 37°C in the CO<sub>2</sub> incubator and the other part was left at 4°C. The samples were then stored at 4°C for 16 h before measuring infectivity or RNA or before using the particles for indicated assays.

### Determination of viral RNA by RT-qPCR

HCV RNAs were extracted (TRI Reagent, Euromedex), reverse transcribed (iScript cDNA synthesis kit, Bio-Rad), and quantified (FastStart Universal SYBR Green Master kit, Roche Applied Science) on an Applied StepOne Real-Time PCR apparatus. HCV-specific primers (U147: 5'-TCT GCG GAA CCG GTG AGT A and L277: 5'-TCA GGC AGT ACC ACA AGG C). As an internal control of extraction, an exogenous RNA from the linearized Triplescript plasmid pTRI-Xef (Invitrogen) was added into the supernatant prior to extraction and quantified with specific primers (Xef-1a 970L20: 5'-CGA CGT TGT CAC CGG GCA CG and Xef-1a 864U24: 5'-ACC AGG CAT GGT GGT TAC CTT TGC). For binding assay, GAPDH level was quantified using specific primers (GAPDH 83U: 5'-TGGAAGATGGTATGGGATTC and GAPDH 287L: 5'-AGGTGAAGTCCGAGTCAACG).

### Binding of HCVcc particles to cells

Huh-7.5 cells were plated in 12 well previously coated with collagen. One day later, cells were incubated with 1 mL of viral supernatant or purified particles for 2 h and washed twice with PBS supplemented with calcium and magnesium (0.7 mM CaCl<sub>2</sub>, 0.25 mM MgSO<sub>4</sub>). Total RNA cell lysates were extracted to quantify the level of HCV and GAPDH gene by RT-qPCR.

### Iodixanol density gradient of HCVcc particles

One milliliter of samples (supernatant or diluted pellet) was layered on top of a 0–30% continuous iodixanol gradient (Optiprep; Axis-Shield). Gradients were centrifuged for 16 h at 32,000 rpm in a SW41 swinging rotor at 4°C using an Optima L-90 K Beckmann centrifuge. Fifteen fractions of 750 µL were collected from the top and were analyzed for virus infectivity and viral RNA copies.

### Fusion of HCVcc particles with liposomes

HCVcc/liposome lipid mixing assays were performed as previously described for HCVpp and HCVcc (32, 33). All liposomes were large unilamellar vesicles (100 nm) consisting of phosphatidylcholine (from egg yolk; Sigma Aldrich), cholesterol (Sigma Aldrich), and Octadecyl rhodamine B chloride (R18; Invitrogen) (65:30:5 mol%). R18-labeled liposomes were obtained by mixing R18 and lipids as ethanol and chloroform solutions. Lipid

mixing was assessed essentially as described and monitored as the dequenching of R18. Briefly, HCVcc particles treated as indicated were added to a cuvette containing R18-labeled liposomes (final lipid concentration, 15  $\mu$ M). After temperature equilibration at pH 7.4 for 2 min, fusion was initiated by adding an appropriate volume of diluted HCl to the cuvette, and kinetics were recorded using a dual-channel PicoFluor hand-held fluorimeter (Turner Biosystems, Sunnyvale, CA, USA), operated under the "rhodamine" channel (excitation and emission wavelengths 540  $\pm$  20 and >570 nm, respectively). Maximal R18 dequenching was measured after the addition of 0.1% Triton X-100 (final concentration) to the cuvette. Initial rates of fusion were taken as the value of the slope of the tangent, drawn to the steepest part of the fusion kinetics. Final extent of lipid mixing was the value obtained when fluorescence reached a plateau.

### Electroporation of purified RNA from particles

Particles purified by ultracentrifugation were used for standard stability measurement. Samples were then concentrated using Vivaspin columns with a cut-off of 100 kDa. Viral RNA from these particles was then extracted and the amounts of copies were determined by RT-qPCR according to our protocol (see above). Same amount of viral RNA was then electroporated in Huh7.5 according to the classical protocol. Seventy-two hours post-electroporation, cells were harvested and the percentage of HCV-positive cells was determined by flow cytometry using an anti-NS5A antibody as described previously (10).

### Statistical analysis

Significance values were calculated by applying Mann–Whitney or Kruskal–Wallis and Dunn's multiple comparison tests using the GraphPad Prism nine software (GraphPad Software, USA). *P* values under 0.05 were considered statistically significant and the following denotations were used: \*\*\*\*, *P* < 0.0001; \*\*\*, *P* < 0.001; \*\*, *P* < 0.01; \*, *P* < 0.05; ns (not significant), *P* > 0.05.

### ACKNOWLEDGMENTS

We thank Vincent Legros for helpful comments. We are grateful to Ralf Bartenschlager and Thomas Pietschmann for the gift of HCVcc constructs, to Friedmann Weber for the CCHFV tecVLP constructs, to Camille Sureau for the HDV constructs, to Andrew Davidson for the NGC DENV-2 construct, and to Charles Rice for the Huh-7.5 cells and the 9E10 NS5A monoclonal antibody. We acknowledge the World Reference Center for Emerging Viruses and Arboviruses (WRCEVA) and UTMB investigator Dr. Pei Yong Shi for kindly providing the recombinant icSARS-CoV-2-mNG virus based on the 2019-nCoV/USA\_WA1/2020 isolate. We acknowledge the contribution of SFR Biosciences (UMS3444/CNRS, US8/Inserm, ENS de Lyon, UCBL) ANIRA-Genetic Analysis facility and the Functional Lipidomics platform (IBISA, GIS IMBL) of INSA-Lyon for excellent technical assistance and support.

This work was supported by a grant from the French "Agence Nationale de la Recherche sur le SIDA et les hépatites virales" (ANRS | MIE, Grant ECTZ132153 to F.-L.C. and S.D.) and by the LabEx Ecofect (ANR-11-LABX-0048) of the "Université de Lyon", within the program "Investissements d'Avenir" (ANR-11-IDEX-0007) operated by the French National Research Agency (ANR). J.T. was supported by a fellowship of the ANRS | MIE (ECTZ137779), associated to ANRS | MIE Grant ECTZ132153.

The authors declare no competing financial interests.

### AUTHOR AFFILIATIONS

<sup>1</sup>CIRI – Centre International de Recherche en Infectiologie, Univ. Lyon, Université Claude Bernard Lyon 1, Inserm, U1111, CNRS, UMR5308 ENS de Lyon, Lyon, France

<sup>2</sup>Centre Léon Bérard, Centre de Recherche en Cancérologie de Lyon, CNRS 5286, Inserm U1052, Université Claude Bernard Lyon 1, Lyon, France

<sup>3</sup>Department of Infectious Diseases, Molecular Virology, Heidelberg University, Heidelberg, Germany

#### AUTHOR ORCID*s*

Eve-Isabelle Pécheur  <http://orcid.org/0000-0002-8613-862X>

François-Loïc Cosset  <http://orcid.org/0000-0001-8842-3726>

Solène Denolly  <http://orcid.org/0000-0003-1739-0079>

#### FUNDING

Funder	Grant(s)	Author(s)
Agence Nationale de Recherches sur le Sida et les Hépatites Virales (ANRS)		Johan Toesca
Agence Nationale de Recherches sur le Sida et les Hépatites Virales (ANRS)		François-Loïc Cosset Solène Denolly
Laboratoire d'Excellence Ecofect (LabEx Ecofect)		François-Loïc Cosset

#### AUTHOR CONTRIBUTIONS

Christelle Granier, Investigation | Johan Toesca, Investigation | Chloé Mialon, Investigation | Maureen Ritter, Investigation | Natalia Freitas, Investigation | Bertrand Boson, Investigation, Writing – review and editing | Eve-Isabelle Pécheur, Investigation | François-Loïc Cosset, Conceptualization, Writing – original draft | Solène Denolly, Conceptualization, Funding acquisition, Investigation, Supervision, Writing – original draft

#### DATA AVAILABILITY

The data sets generated during the current study are available from the corresponding author upon reasonable request.

#### ADDITIONAL FILES

The following material is available [online](#).

#### Supplemental Material

**Fig. S1 (mBio01549-23-s0001.tif).** Addition of a cleavage site between FLAG and E2 sequences.

**Fig. S2 (mBio01549-23-s0002.tif).** No effect of DFO and EDTA on intracellular DENV particles.

**Fig. S3 (mBio01549-23-s0003.tif).** Effect of knock-down of apoB on density gradient of HCVcc.

**Supplemental Legends (mBio01549-23-s0004.docx).** Supplemental figure legends.

#### REFERENCES

- Hirose R, Ikegaya H, Naito Y, Watanabe N, Yoshida T, Bandou R, Daidoji T, Itoh Y, Nakaya T. 2021. Survival of severe acute respiratory syndrome Coronavirus 2 (SARS-CoV-2) and influenza virus on human skin: importance of hand hygiene in Coronavirus disease 2019 (COVID-19). *Clin Infect Dis* 73:e4329–e4335. <https://doi.org/10.1093/cid/ciaa1517>
- Kadji FMN, Kotani K, Tsukamoto H, Hiraoka Y, Hagiwara K. 2022. Stability of enveloped and nonenveloped viruses in hydrolyzed gelatin liquid formulation. *Viol J* 19:94. <https://doi.org/10.1186/s12985-022-01819-w>
- Silverman AI, Boehm AB. 2021. Systematic review and meta-analysis of the persistence of enveloped viruses in environmental waters and wastewater in the absence of disinfectants. *Environ Sci Technol* 55:14480–14493. <https://doi.org/10.1021/acs.est.1c03977>
- Firquet S, Beaujard S, Lobert P-E, Sané F, Caloone D, Izard D, Hober D. 2015. Survival of enveloped and non-enveloped viruses on inanimate surfaces. *Microbes Environ* 30:140–144. <https://doi.org/10.1264/jsme2.ME14145>
- Pinter A, Kopelman R, Li Z, Kayman SC, Sanders DA. 1997. Localization of the labile disulfide bond between SU and TM of the murine leukemia virus envelope protein complex to a highly conserved CWLC motif in SU that resembles the active-site sequence of thiol-disulfide exchange enzymes. *J Virol* 71:8073–8077. <https://doi.org/10.1128/JVI.71.10.8073-8077.1997>
- Burns JC, Friedmann T, Driever W, Burrascano M, Yee JK. 1993. Vesicular stomatitis virus G glycoprotein pseudotyped retroviral vectors:



- concentration to very high titer and efficient gene transfer into mammalian and nonmammalian cells. *Proc Natl Acad Sci U S A* 90:8033–8037. <https://doi.org/10.1073/pnas.90.17.8033>
7. Molinari M, Sitia R. 2005. The secretory capacity of a cell depends on the efficiency of endoplasmic reticulum-associated degradation. *Curr Top Microbiol Immunol* 300:1–15. [https://doi.org/10.1007/3-540-28007-3\\_1](https://doi.org/10.1007/3-540-28007-3_1)
  8. Trefts E, Gannon M, Wasserman DH. 2017. The liver. *Curr Biol* 27:R1147–R1151. <https://doi.org/10.1016/j.cub.2017.09.019>
  9. Bartenschlager R, Baumert TF, Bukh J, Houghton M, Lemon SM, Lindenbach BD, Lohmann V, Moradpour D, Pietschmann T, Rice CM, Thimme R, Wakita T. 2018. Critical challenges and emerging opportunities in hepatitis C virus research in an era of potent antiviral therapy: considerations for scientists and funding agencies. *Virus Res* 248:53–62. <https://doi.org/10.1016/j.virusres.2018.02.016>
  10. Denolly S, Mialon C, Bourlet T, Amirache F, Penin F, Lindenbach B, Boson B, Cosset F-L. 2017. The amino-terminus of the hepatitis C virus (HCV) p7 viroporin and its cleavage from glycoprotein E2-P7 precursor determine specific infectivity and secretion levels of HCV particle types. *PLoS Pathog* 13:e1006774. <https://doi.org/10.1371/journal.ppat.1006774>
  11. Cosset F-L, Mialon C, Boson B, Granier C, Denolly S. 2020. HCV interplay with lipoproteins: inside or outside the cells? *Viruses* 12:434. <https://doi.org/10.3390/v12040434>
  12. André P, Komurian-Pradel F, Deforges S, Perret M, Berland JL, Sodoyer M, Pol S, Bréchet C, Paranhos-Baccalà G, Lotteau V. 2002. Characterization of low- and very-low-density hepatitis C virus RNA-containing particles. *J Virol* 76:6919–6928. <https://doi.org/10.1128/jvi.76.14.6919-6928.2002>
  13. Thomssen R, Bonk S, Propfe C, Heermann KH, Köchel HG, Uy A. 1992. Association of hepatitis C virus in human sera with beta-lipoprotein. *Med Microbiol Immunol* 181:293–300. <https://doi.org/10.1007/BF00198849>
  14. Boyer A, Dumans A, Beaumont E, Etienne L, Roingard P, Meunier JC. 2014. The association of hepatitis C virus glycoproteins with apolipoproteins E and B early in assembly is conserved in lipoviral particles. *J Biol Chem* 289:18904–18913. <https://doi.org/10.1074/jbc.M113.538256>
  15. Denolly S, Granier C, Fontaine N, Pozzetto B, Bourlet T, Guérin M, Cosset F-L. 2019. A serum protein factor mediates maturation and apoB-association of HCV particles in the extracellular milieu. *J Hepatol* 70:626–638. <https://doi.org/10.1016/j.jhep.2018.11.033>
  16. Lee J-Y, Acosta EG, Stoek IK, Long G, Hiet M-S, Mueller B, Fackler OT, Kallis S, Bartenschlager R. 2014. Apolipoprotein E likely contributes to a maturation step of infectious hepatitis C virus particles and interacts with viral envelope glycoproteins. *J Virol* 88:12422–12437. <https://doi.org/10.1128/JVI.01660-14>
  17. Felmlée DJ, Sheridan DA, Bridge SH, Nielsen SU, Milne RW, Packard CJ, Caslake MJ, McClachlan J, Toms GL, Neely RDG, Bassendine MF. 2010. Intravascular transfer contributes to postprandial increase in numbers of very-low-density hepatitis C virus particles. *Gastroenterology* 139:1774–1783. <https://doi.org/10.1053/j.gastro.2010.07.047>
  18. Song H, Li J, Shi S, Yan L, Zhuang H, Li K. 2010. Thermal stability and inactivation of hepatitis C virus grown in cell culture. *Virol J* 7:40. <https://doi.org/10.1186/1743-422X-7-40>
  19. Shimizu Y, Hishiki T, Sugiyama K, Ogawa K, Funami K, Kato A, Ohsaki Y, Fujimoto T, Takaku H, Shimotohno K. 2010. Lipoprotein lipase and hepatic triglyceride lipase reduce the infectivity of hepatitis C virus (HCV) through their catalytic activities on HCV-associated lipoproteins. *Virology* 407:152–159. <https://doi.org/10.1016/j.virol.2010.08.011>
  20. Albecka A, Belouzard S, Op de Beeck A, Descamps V, Goueslain L, Bertrand-Michel J, Tercé F, Duverlie G, Rouillé Y, Dubuisson J. 2012. Role of low-density lipoprotein receptor in the hepatitis C virus life cycle. *Hepatology* 55:998–1007. <https://doi.org/10.1002/hep.25501>
  21. Andréo U, Maillard P, Kalinina O, Walic M, Meurs E, Martinot M, Marcellin P, Budkowska A. 2007. Lipoprotein lipase mediates hepatitis C virus (HCV) cell entry and inhibits HCV infection. *Cell Microbiol* 9:2445–2456. <https://doi.org/10.1111/j.1462-5822.2007.00972.x>
  22. Devignot S, Bergeron E, Nichol S, Mirazimi A, Weber F. 2015. A virus-like particle system identifies the endonuclease domain of crimean-congo hemorrhagic fever virus. *J Virol* 89:5957–5967. <https://doi.org/10.1128/JVI.03691-14>
  23. Zivcec M, Metcalfe MG, Albariño CG, Guerrero LW, Pegan SD, Spiropoulou CF, Bergeron É. 2015. Assessment of inhibitors of pathogenic crimean-congo hemorrhagic fever virus strains using virus-like particles. *PLoS Negl Trop Dis* 9:e0004259. <https://doi.org/10.1371/journal.pntd.0004259>
  24. Merz A, Long G, Hiet M-S, Brügger B, Chlanda P, Andre P, Wieland F, Krijnse-Locker J, Bartenschlager R. 2011. Biochemical and morphological properties of hepatitis C virus particles and determination of their lipidome. *J Biol Chem* 286:3018–3032. <https://doi.org/10.1074/jbc.M110.175018>
  25. Lee J-Y, Cortese M, Haselmann U, Tabata K, Romero-Brey I, Funaya C, Schieber NL, Qiang Y, Bartenschlager M, Kallis S, Ritter C, Rohr K, Schwab Y, Ruggieri A, Bartenschlager R. 2019. Spatiotemporal coupling of the hepatitis C virus replication cycle by creating a lipid droplet-proximal membranous replication compartment. *Cell Rep* 27:3602–3617. <https://doi.org/10.1016/j.celrep.2019.05.063>
  26. Reiss S, Rebhan I, Backes P, Romero-Brey I, Erfle H, Matula P, Kaderali L, Poenisch M, Blankenburg H, Hiet M-S, Longerich T, Diehl S, Ramirez F, Balla T, Rohr K, Kaul A, Bühler S, Pepperkok R, Lengauer T, Albrecht M, Eils R, Schirmacher P, Lohmann V, Bartenschlager R. 2011. Recruitment and activation of a lipid kinase by hepatitis C virus Ns5A is essential for integrity of the membranous replication compartment. *Cell Host Microbe* 9:32–45. <https://doi.org/10.1016/j.chom.2010.12.002>
  27. Franko A, Hartwig S, Kotzka J, Ruoß M, Nüssler AK, Königsrainer A, Häring H-U, Lehr S, Peter A. 2019. Identification of the secreted proteins originated from primary human hepatocytes and HepG2 cells. *Nutrients* 11:1795. <https://doi.org/10.3390/nu11081795>
  28. Bankwitz D, Doepke M, Hueging K, Weller R, Bruening J, Behrendt P, Lee J-Y, Vondran FWR, Manns MP, Bartenschlager R, Pietschmann T. 2017. Maturation of secreted HCV particles by incorporation of secreted APOE protects from antibodies by enhancing infectivity. *J Hepatol* 67:480–489. <https://doi.org/10.1016/j.jhep.2017.04.010>
  29. Yang Z, Wang X, Chi X, Zhao F, Guo J, Ma P, Zhong J, Niu J, Pan X, Long G, Diamond MS. 2016. Neglected but important role of apolipoprotein E exchange in hepatitis C virus infection. *J Virol* 90:9632–9643. <https://doi.org/10.1128/JVI.01353-16>
  30. Timoshnikov VA, Kobzeva TV, Polyakov NE, Kontoghiorghes GJ. 2020. Redox interactions of vitamin C and iron: inhibition of the pro-oxidant activity by deferiprone. *Int J Mol Sci* 21:3967. <https://doi.org/10.3390/ijms21113967>
  31. Bartosch B, Dubuisson J, Cosset F-L. 2003. Infectious hepatitis C virus pseudo-particles containing functional E1-E2 envelope protein complexes. *J Exp Med* 197:633–642. <https://doi.org/10.1084/jem.20021756>
  32. Haid S, Pietschmann T, Pécheur E-I. 2009. Low pH-dependent hepatitis C virus membrane fusion depends on E2 integrity, target lipid composition, and density of virus particles. *J Biol Chem* 284:17657–17667. <https://doi.org/10.1074/jbc.M109.014647>
  33. Lavillette D, Bartosch B, Nourrisson D, Verney G, Cosset F-L, Penin F, Pécheur E-I. 2006. Hepatitis C virus glycoproteins mediate low pH-dependent membrane fusion with liposomes. *J Biol Chem* 281:3909–3917. <https://doi.org/10.1074/jbc.M509747200>
  34. Flint M, Logvinoff C, Rice CM, McKeating JA. 2004. Characterization of infectious retroviral pseudotype particles bearing hepatitis C virus glycoproteins. *J Virol* 78:6875–6882. <https://doi.org/10.1128/JVI.78.13.6875-6882.2004>
  35. Smith TJ, Brandt WE, Swanson JL, McCown JM, Buescher EL. 1970. Physical and biological properties of dengue-2 virus and associated antigens. *J Virol* 5:524–532. <https://doi.org/10.1128/JVI.5.4.524-532.1970>
  36. Montuschi P, Barnes PJ, Roberts LJ. 2004. Isoprostanes: markers and mediators of oxidative stress. *FASEB J* 18:1791–1800. <https://doi.org/10.1096/fj.04-2330rev>
  37. Brites F, Martin M, Guillas I, Kontush A. 2017. Antioxidative activity of high-density lipoprotein (HDL): mechanistic insights into potential clinical benefit. *BBA Clin* 8:66–77. <https://doi.org/10.1016/j.bbaci.2017.07.002>
  38. Lúcio M, Nunes C, Gaspar D, Ferreira H, Lima JLFC, Reis S. 2009. Antioxidant activity of vitamin E and trolox: understanding of the factors that govern lipid peroxidation studies *in vitro*. *Food Biophys* 4:312–320. <https://doi.org/10.1007/s11483-009-9129-4>
  39. Sandrin V, Boulanger P, Penin F, Granier C, Cosset F-L, Bartosch B. 2005. Assembly of functional hepatitis C virus glycoproteins on infectious pseudoparticles occurs intracellularly and requires concomitant

- incorporation of E1 and E2 glycoproteins. *J Gen Virol* 86:3189–3199. <https://doi.org/10.1099/vir.0.81428-0>
40. Riva L, Dubuisson J. 2019. Similarities and differences between HCV pseudoparticle (HCVpp) and cell culture HCV (HCVcc) in the study of HCV. *Methods Mol Biol* 1911:33–45. [https://doi.org/10.1007/978-1-4939-8976-8\\_2](https://doi.org/10.1007/978-1-4939-8976-8_2)
  41. Brault C, Lévy P, Duponchel S, Michelet M, Sallé A, Pécheur E-I, Plissonnier M-L, Parent R, Véricel E, Ivanov AV, Demir M, Steffen H-M, Odenthal M, Zoulim F, Bartosch B. 2016. Glutathione peroxidase 4 is reversibly induced by HCV to control lipid peroxidation and to increase virion infectivity. *Gut* 65:144–154. <https://doi.org/10.1136/gutjnl-2014-307904>
  42. Harrison SC. 2015. Viral membrane fusion. *Virology* 479–480:498–507. <https://doi.org/10.1016/j.virol.2015.03.043>
  43. Vigant F, Santos NC, Lee B. 2015. Broad-spectrum antivirals against viral fusion. *Nat Rev Microbiol* 13:426–437. <https://doi.org/10.1038/nrmicro3475>
  44. Wolf MC, Freiberg AN, Zhang T, Akyol-Ataman Z, Grock A, Hong PW, Li J, Watson NF, Fang AQ, Aguilar HC, Porotto M, Honko AN, Damoiseaux R, Miller JP, Woodson SE, Chantasirivisal S, Fontanes V, Negrete OA, Krogstad P, Dasgupta A, Moscona A, Hensley LE, Whelan SP, Faull KF, Holbrook MR, Jung ME, Lee B. 2010. A broad-spectrum antiviral targeting entry of enveloped viruses. *Proc Natl Acad Sci U S A* 107:3157–3162. <https://doi.org/10.1073/pnas.0909587107>
  45. Vigant F, Lee J, Hollmann A, Tanner LB, Akyol Ataman Z, Yun T, Shui G, Aguilar HC, Zhang D, Meriwether D, Roman-Sosa G, Robinson LR, Juelich TL, Buczkowski H, Chou S, Castanho M, Wolf MC, Smith JK, Banyard A, Kielian M, Reddy S, Wenk MR, Selke M, Santos NC, Freiberg AN, Jung ME, Lee B, Young JAT. 2013. A mechanistic paradigm for broad-spectrum antivirals that target virus-cell fusion. *PLoS Pathog* 9:e1003297. <https://doi.org/10.1371/journal.ppat.1003297>
  46. Hollmann A, Castanho M, Lee B, Santos NC. 2014. Singlet oxygen effects on lipid membranes: implications for the mechanism of action of broad-spectrum viral fusion inhibitors. *Biochem J* 459:161–170. <https://doi.org/10.1042/BJ20131058>
  47. Fanali G, di Masi A, Trezza V, Marino M, Fasano M, Ascenzi P. 2012. Human serum albumin: from bench to bedside. *Mol Aspects Med* 33:209–290. <https://doi.org/10.1016/j.mam.2011.12.002>
  48. Ogasawara Y, Mukai Y, Togawa T, Suzuki T, Tanabe S, Ishii K. 2007. Determination of plasma thiol bound to albumin using affinity chromatography and high-performance liquid chromatography with fluorescence detection: ratio of cysteinyl albumin as a possible biomarker of oxidative stress. *J Chromatogr B Analyt Technol Biomed Life Sci* 845:157–163. <https://doi.org/10.1016/j.jchromb.2006.08.006>
  49. Stockley RA. 2015. The multiple facets of alpha-1-antitrypsin. *Ann Transl Med* 3:130. <https://doi.org/10.3978/j.issn.2305-5839.2015.04.25>
  50. Miyata M, Smith JD. 1996. Apolipoprotein E allele-specific antioxidant activity and effects on cytotoxicity by oxidative insults and beta-amyloid peptides. *Nat Genet* 14:55–61. <https://doi.org/10.1038/ng0996-55>
  51. Pham T, Kodwawala A, Hui DY. 2005. The receptor binding domain of apolipoprotein E is responsible for its antioxidant activity. *Biochem* 44:7577–7582. <https://doi.org/10.1021/bi0472696>
  52. Wozniak AL, Griffin S, Rowlands D, Harris M, Yi M, Lemon SM, Weinman SA. 2010. Intracellular proton conductance of the hepatitis C virus P7 protein and its contribution to infectious virus production. *PLoS Pathog* 6:e1001087. <https://doi.org/10.1371/journal.ppat.1001087>
  53. Gastaminza P, Cheng G, Wieland S, Zhong J, Liao W, Chisari FV. 2008. Cellular determinants of hepatitis C virus assembly, maturation, degradation, and secretion. *J Virol* 82:2120–2129. <https://doi.org/10.1128/JVI.02053-07>
  54. Syed GH, Khan M, Yang S, Siddiqui A. 2017. Hepatitis C virus lipovirions assemble in the endoplasmic reticulum (ER) and bud off from the ER to the golgi compartment in COPII vesicles. *J Virol* 91:e00499-17. <https://doi.org/10.1128/JVI.00499-17>
  55. Collier KE, Heaton NS, Berger KL, Cooper JD, Saunders JL, Randall G, Ou JJ. 2012. Molecular determinants and dynamics of hepatitis C virus secretion. *PLoS Pathog* 8:e1002466. <https://doi.org/10.1371/journal.ppat.1002466>
  56. Dreux M, Pietschmann T, Granier C, Voisset C, Ricard-Blum S, Mangeot P-E, Keck Z, Foug S, Vu-Dac N, Dubuisson J, Bartenschlager R, Lavillette D, Cosset F-L. 2006. High density lipoprotein inhibits hepatitis C virus neutralizing antibodies by stimulating cell entry via activation of the scavenger receptor BI. *J Biol Chem* 281:18285–18295. <https://doi.org/10.1074/jbc.M602706200>
  57. Voisset C, de Beek AO, Horellou P, Dreux M, Gustot T, Duverlie G, Cosset F-L, Vu-Dac N, Dubuisson J. 2006. High-density lipoproteins reduce the neutralizing effect of hepatitis C virus (HCV)-infected patient antibodies by promoting HCV entry. *J Gen Virol* 87:2577–2581. <https://doi.org/10.1099/vir.0.81932-0>
  58. Fauvel C, Felmlee DJ, Crouchet E, Lee J, Heydmann L, Lefèvre M, Magri A, Hiet M-S, Fofana I, Habersetzer F, Foug SKH, Milne R, Patel AH, Vercauteren K, Meuleman P, Zeisel MB, Bartenschlager R, Schuster C, Baumert TF. 2016. Apolipoprotein E mediates evasion from hepatitis C virus neutralizing antibodies. *Gastroenterology* 150:206–217. <https://doi.org/10.1053/j.gastro.2015.09.014>
  59. Westhaus S, Bankwitz D, Ernst S, Rohrmann K, Wappler I, Agné C, Luchtfeld M, Schieffer B, Sarrazin C, Manns MP, Pietschmann T, Ciesek S, von Hahn T. 2013. Characterization of the inhibition of hepatitis C virus entry by *in vitro*-generated and patient-derived oxidized low-density lipoprotein. *Hepatology* 57:1716–1724. <https://doi.org/10.1002/hep.26190>
  60. Cui J, Schlub TE, Holmes EC. 2014. An allometric relationship between the genome length and virion volume of viruses. *J Virol* 88:6403–6410. <https://doi.org/10.1128/JVI.00362-14>
  61. Gentzsch J, Brohm C, Steinmann E, Friesland M, Menzel N, Vieyres G, Perin PM, Frentzen A, Kaderali L, Pietschmann T, Siddiqui A. 2013. Hepatitis C virus P7 is critical for capsid assembly and envelopment. *PLoS Pathog* 9:e1003355. <https://doi.org/10.1371/journal.ppat.1003355>
  62. Pérez-Vargas J, Teppa E, Amirache F, Boson B, Pereira de Oliveira R, Combet C, Böckmann A, Fusil F, Freitas N, Carbone A, Cosset F-L. 2021. A fusion peptide in preS1 and the human protein disulfide isomerase ERp57 are involved in hepatitis B virus membrane fusion process. *Elife* 10:e64507. <https://doi.org/10.7554/eLife.64507>
  63. Bergeron E, Albariño CG, Khristova ML, Nichol ST. 2010. Crimean-congo hemorrhagic fever virus-enriched ovarian tumor protease activity is dispensable for virus RNA polymerase function. *J Virol* 84:216–226. <https://doi.org/10.1128/JVI.01859-09>
  64. Sureau C. 2010. The use of hepatocytes to investigate HDV infection: the HDV/HepaRG model. *Methods Mol Biol* 640:463–473. [https://doi.org/10.1007/978-1-60761-688-7\\_25](https://doi.org/10.1007/978-1-60761-688-7_25)
  65. Pryor MJ, Carr JM, Hocking H, Davidson AD, Li P, Wright PJ. 2001. Replication of dengue virus type 2 in human monocyte-derived macrophages: comparisons of isolates and recombinant viruses with substitutions at amino acid 390 in the envelope glycoprotein. *Am J Trop Med Hyg* 65:427–434. <https://doi.org/10.4269/ajtmh.2001.65.427>
  66. Boson B, Legros V, Zhou B, Siret E, Mathieu C, Cosset F-L, Lavillette D, Denolly S. 2021. The SARS-CoV-2 envelope and membrane proteins modulate maturation and retention of the spike protein, allowing assembly of virus-like particles. *J Biol Chem* 296:100111. <https://doi.org/10.1074/jbc.RA120.016175>
  67. Freitas N, Enguehard M, Denolly S, Levy C, Neveu G, Lerolle S, Devignot S, Weber F, Bergeron E, Legros V, Cosset F-L. 2020. The interplays between crimean-congo hemorrhagic fever virus (CCHFV) m segment-encoded accessory proteins and structural proteins promote virus assembly and infectivity. *PLoS Pathog* 16:e1008850. <https://doi.org/10.1371/journal.ppat.1008850>

### Supplemental Figure legends

#### Low density hepatitis C virus infectious particles are protected from oxidation by secreted cellular proteins

##### Running title

Co-secreted cellular factors protect HCV from oxidation

Christelle Granier<sup>1#</sup>, Johan Toesca<sup>1#</sup>, Chloé Mialon<sup>1#</sup>, Maureen Ritter<sup>1</sup>, Natalia Freitas<sup>1</sup>, Bertrand Boson<sup>1</sup>, Eve-Isabelle Pécheur<sup>2</sup>, François-Loïc Cosset<sup>1§</sup>, Solène Denolly<sup>1,3 \$,\*</sup>

##### Affiliations

<sup>1</sup>CIRI – Centre International de Recherche en Infectiologie, Univ. Lyon, Université Claude Bernard Lyon 1, Inserm, U1111, CNRS, UMR5308 ENS de Lyon, F-69007, Lyon, France.

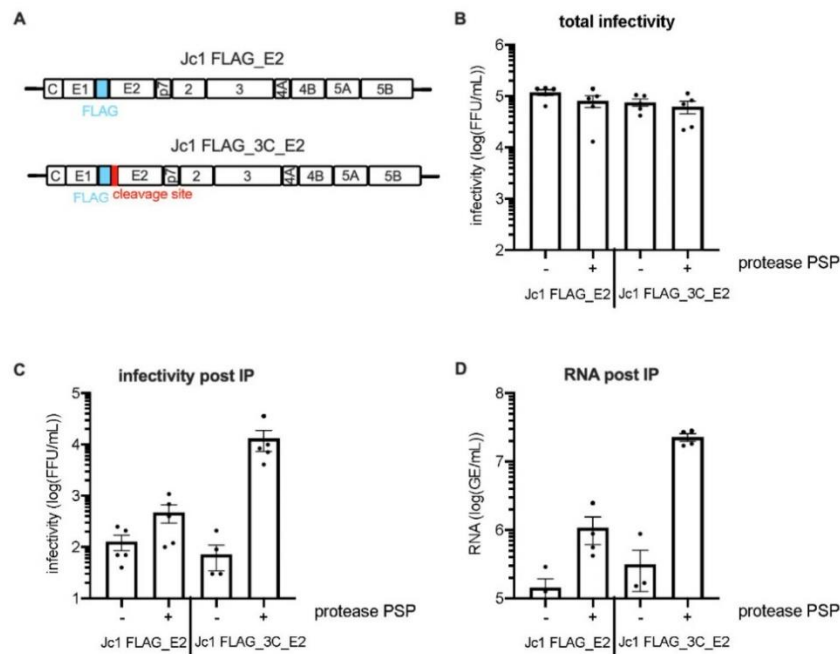
<sup>2</sup>Univ Lyon, Université Claude Bernard Lyon 1, CNRS 5286, INSERM 1052, Centre Léon Bérard, Centre de Recherche en Cancérologie de Lyon, 69008, Lyon, France.

<sup>3</sup>Department of Infectious Diseases, Molecular Virology, Heidelberg University, 69120 Heidelberg, Germany.

#co-first authors

§co-last authors

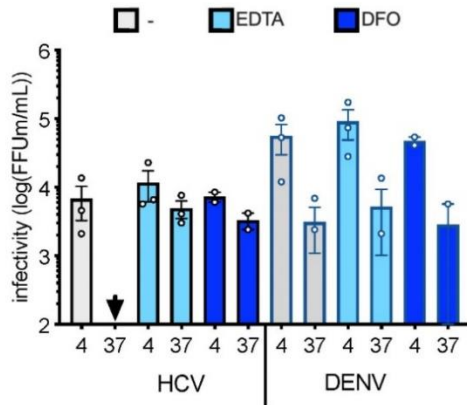
\* Corresponding author



**Supplemental Figure 1. Addition of a cleavage site between FLAG and E2 sequences.**

(A) Representation of the modified polyproteins. (B) Infectivity of crude supernatant treated or not with PreScission Protease (PSP). (C) Infectivity of Jc1 FLAG\_E2 or Jc1 FLAG\_3C\_E2 recovered after IP anti FLAG and elution using cleavage of the FLAG tag with PSP. (D) RNA of Jc1 FLAG\_E2 or Jc1 FLAG\_3C\_E2 recovered after IP anti FLAG and elution using cleavage of the FLAG tag with PSP.

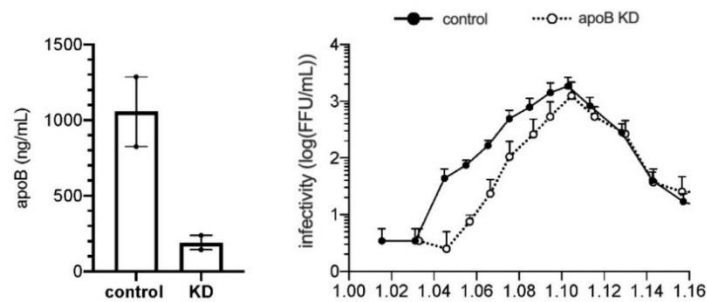
The results are represented as means  $\pm$  SEM. Each dot in the graphs corresponds to the value of an individual experiment.



**Supplemental Figure 2. No effect of DFO and EDTA on intracellular DENV particles.**

Infectivity of HCV and DENV intracellular particles diluted in serum-free medium (-) vs. in serum-free medium supplemented with EDTA (0.5mM) or DFO (10 $\mu$ M).

The results are represented as means  $\pm$  SEM. Each dot in the graphs corresponds to the value of an individual experiment.



**Supplemental Figure 3. Effect of knock-down of apoB on density gradient of HCVcc**

(A) Level of secreted apoB by Huh7.5 (control) and Huh7.5 transduced by shRNA targeting apoB (KD). (B) Infectivity of HCV particles detected in fractions from buoyant density gradients of crude virus producer cell supernatant from either Huh7.5 (full line) and Huh7.5 with knock-down of apoB (dotted line).

The results are represented as means  $\pm$  SEM.

## The PACS-2 protein and trafficking motifs in CCHFV Gn and Gc cytoplasmic domains govern CCHFV assembly

Anupriya Gautam <sup>a</sup>, Alexandre Lalande <sup>a#</sup>, Maureen Ritter <sup>a#</sup>, Natalia Freitas<sup>a#</sup>, Solène Lerolle <sup>a</sup>, Lola Canus<sup>a</sup>, Fouzia Amirache<sup>a</sup>, Vincent Lotteau<sup>b</sup>, Vincent Legros <sup>a,c</sup>, François-Loïc Cosset <sup>a</sup>, Cyrille Mathieu <sup>a</sup> and Bertrand Boson <sup>a</sup>

<sup>a</sup>CIRI – Centre International de Recherche en Infectiologie, Univ. Lyon, Université Claude Bernard Lyon 1, Lyon, France; <sup>b</sup>Laboratory P4-Jean Mérieux, Lyon, France; <sup>c</sup>Campus vétérinaire de Lyon, VetAgro Sup, Université de Lyon, Marcy-l’Étoile, France

### ABSTRACT

The Crimean-Congo hemorrhagic fever virus (CCHFV) is a tick-borne bunyavirus that causes high mortality in humans. This enveloped virus harbors two surface glycoproteins (GP), Gn and Gc, that are released by processing of a glycoprotein precursor complex whose maturation takes place in the ER and is completed through the secretion pathway. Here, we characterized the trafficking network exploited by CCHFV GPs during viral assembly, envelopment, and/or egress. We identified membrane trafficking motifs in the cytoplasmic domains (CD) of CCHFV GPs and addressed how they impact these late stages of the viral life cycle using infection and biochemical assays, and confocal microscopy in virus-producing cells. We found that several of the identified CD motifs modulate GP transport through the retrograde trafficking network, impacting envelopment and secretion of infectious particles. Finally, we identified PACS-2 as a crucial host factor contributing to CCHFV GPs trafficking required for assembly and release of viral particles.

**ARTICLE HISTORY** Received 25 January 2024; Revised 22 April 2024; Accepted 23 April 2024

**KEYWORDS** CCHFV; assembly; trafficking; glycoprotein; nucleoprotein


### Introduction

The Crimean-Congo hemorrhagic fever virus (CCHFV) belongs to the genus *Orthonairovirus* under the *Nairoviridae* family and the *Bunyavirales* order. CCHFV was first associated with the manifestation of febrile disease in Crimea in 1944 [1] and in Congo in 1956 [2], and can cause fatality rates that surpass 30%. It is now prevalent in various regions, including the Middle East, Southeast Asia, Africa, and Southern and Eastern Europe [3–5]. Ticks of the genus *Hyalomma* have been identified as the primary vector and reservoir of CCHFV, though other tick species may potentially serve as hosts for the virus in regions where it is endemic [6]. Reports have shown that CCHFV has the potential to infect various animal species, most notably livestock, without causing apparent illness. These animals facilitate the transmission of CCHFV from infected ticks to uninfected ticks through co-feeding or by feeding on viremic animals. The primary modes of transmission of CCHFV to humans are tick bites and the handling of infected livestock [7]. Subsequently, CCHFV propagates

throughout the body and target different organs, including the liver, where it induces multiple lesions, failures, and vascular dysfunction.

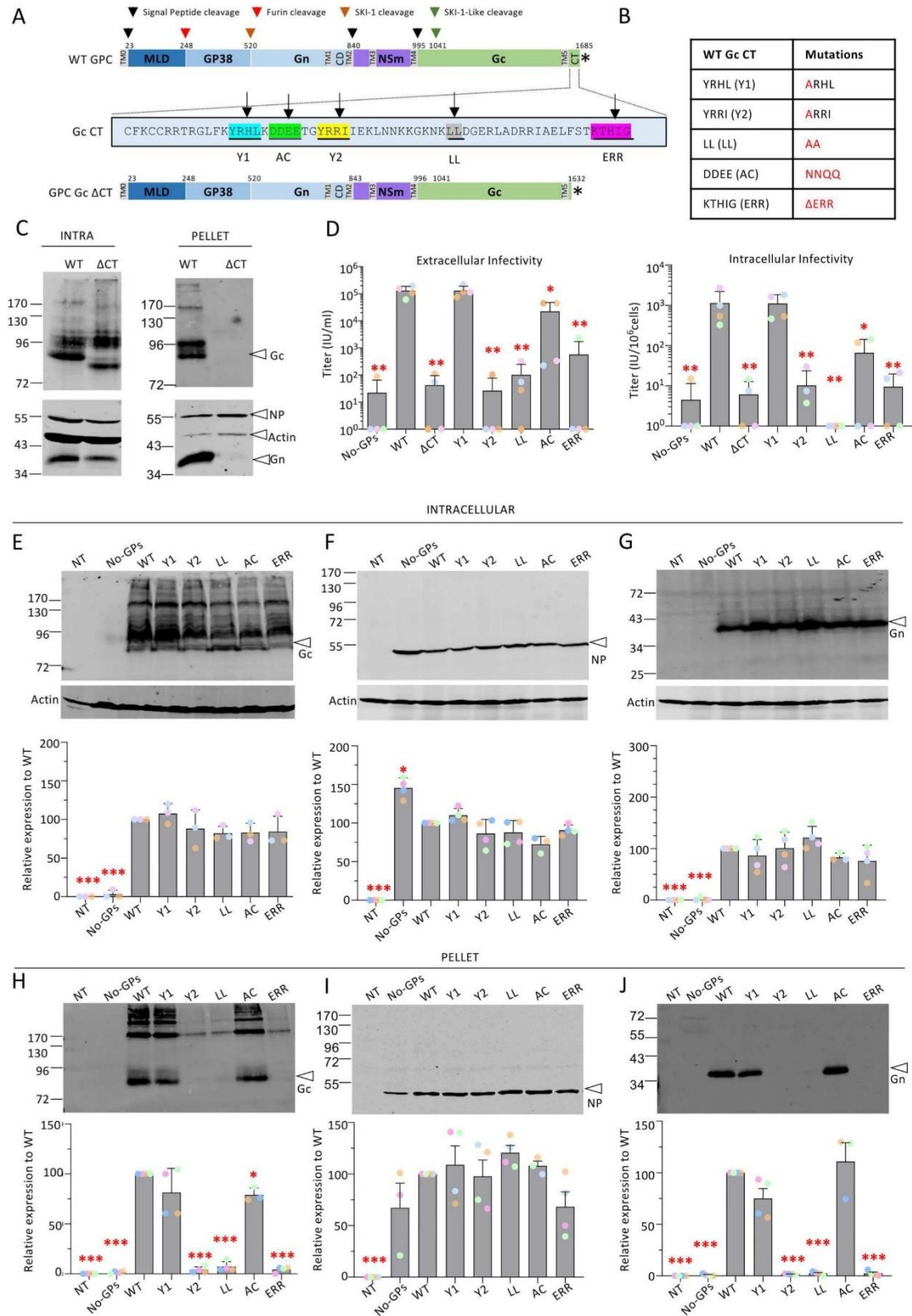
CCHFV is an enveloped virus with a tri-segmented negative – or ambisense-strand RNA genome associated with virus-encoded nucleoproteins (NP) and an RNA-dependent RNA polymerase enclosed within a host-derived lipid bilayer, at the surface of which two surface glycoproteins (GPs) – Gn and Gc heterodimer – are inserted. The three genomic RNA segments are the large (L) segment, which encodes the polymerase, the small (S) segment, which encodes NP and a non-structural protein (NSs), and the medium (M) segment, which encodes a single polyprotein precursor (Figure 1A), namely the glycoprotein precursor complex (GPC). The two surface GPs are produced by several cleavage events on GPC that also give rise to several nonstructural proteins [8,9]. Viral assembly utilizes membrane-associating determinants, featuring a leader N-terminal signal peptide (SP), two internal SPs and five transmembrane domains (TMD), two intermediate GP precursors (preGn (140 kDa)

**CONTACT** François-Loïc Cosset  [flcosset@ens-lyon.fr](mailto:flcosset@ens-lyon.fr)  CIRI – Centre International de Recherche en Infectiologie, Univ. Lyon, Université Claude Bernard Lyon 1, Inserm, U1111, CNRS, UMR5308 ENS de Lyon, Lyon F-69007, France  
<sup>#</sup>equal contribution.

 Supplemental data for this article can be accessed online at <https://doi.org/10.1080/22221751.2024.2348508>.

© 2024 The Author(s). Published by Informa UK Limited, trading as Taylor & Francis Group, on behalf of Shanghai Shangyixun Cultural Communication Co., Ltd. This is an Open Access article distributed under the terms of the Creative Commons Attribution License (<http://creativecommons.org/licenses/by/4.0/>), which permits unrestricted use, distribution, and reproduction in any medium, provided the original work is properly cited. The terms on which this article has been published allow the posting of the Accepted Manuscript in a repository by the author(s) or with their consent.

2 A. GAUTAM ET AL.



and preGc (85 kDa)), a double-membrane-spanning non-structural protein called NSm (a mucin-like protein (MLD) containing a large number of predicted O-glycosylation sites), and three secreted proteins of poorly-known functions: GP38, GP85, and GP160 (Figure 1A). PreGn is converted to Gn following the cleavage by SKI-1/S1P protease in ER-*cis* Golgi compartments, while preGc is cleaved by an unknown SKI-1-like protease to generate Gc [10]. Like for related hemorrhagic viruses such as the Severe fever with thrombocytopenia syndrome virus (SFTSV) and Bunyamwera virus (BUNV), which are from the *Bandavirus* and *Orthobunyavirus* genera (*Bunyavirales* order), respectively, the Gn/Gc GPs form multimers, suggesting that CCHFV GPs may form a complex in order to stabilize the fusion domains in the viral membrane proximal region during assembly and egress of CCHFV [11,12]. However, the site where CCHFV particles are assembled and enveloped remains undefined. Previous work on *Bunyavirales* viruses suggest that assembly occurs on the Golgi membranes [13]. Since virus GPs are synthesized in the endoplasmic reticulum (ER), a key question is about how CCHFV GPs are transported from the ER to the virion assembly site, which remains to be determined.

Protein traffic through the secretory pathway requires tight regulations and highly synchronized interactions of several cellular factors [14]. The secretory pathway is subdivided into two membrane populations: the ER/Golgi system, which is needed for oligomerization, folding, and co-

posttranslational modifications of proteins that shuttle along the secretory pathways [15,16], and the *trans*-Golgi network (TGN)/endosomal system, which is important for sorting, export, and recovery of various soluble and membrane-associated secretory proteins.

Several types of trafficking motifs are typically contained in the cytoplasmic tails (CT) or cytoplasmic domain (CD) of viral surface glycoproteins [17–19], which may also be the case for bunyaviruses [20,21], and regulate various stages of GPs, from their biogenesis to their ultimate intracellular localization. As for CCHFV, the Gn GP contains an ectodomain of 176 residues that is followed by two TMDs with, in between, a particularly long CD of 94 residues [8,10,22], which has been shown by NMR analysis to possess a unique dual CCHC-type zinc finger (ZF) fold that is capable of binding viral RNA [23]. On the other hand, the Gc glycoprotein contains an ectodomain of 481 residues [24] that is followed by a single TMD followed by a 63 residue-long CT of unknown function [25].

Several host factors can be coopted by enveloped viruses to mediate intracellular trafficking of their GPs. For example, the adaptor proteins (AP) AP-1, AP-2 and AP-3 [26] mediate different sorting events, such as internalization from plasma membrane and sorting to endosomes [27], and the COPI coatomer mediates retrograde transport of cargos from TGN to ER [28] whereas two proteins of the PACS family, PACS-1 and PACS-2, mediate retrograde transport from endosomal pathway to TGN and control the

**Figure 1. Infectivity and viral incorporation of CCHFV Gc cytoplasmic tail mutants.** (A) Schematic representation of the GPC polyprotein encoded by CCHFV wt-M cDNA (WT GPC) and mutant GPC harbouring deletion of Gc cytoplasmic tail (GPC Gc  $\Delta$ CT). The polyprotein precursor organization and positions of the first amino-acid residues after cleavage marking protein boundaries (MLD, GP38, Gn, NSm, and Gc) within the CCHFV polyprotein are shown. The stars indicate the position of the stop codon. The N-terminal signal peptide (TM0) and putative transmembrane domains (TM1 to TM5) are shown as grey boxes, signal peptidase cleavage sites are indicated by black arrows and other host protein convertase cleavage sites are indicated by red, orange and green arrows. The bottom part shows the cytoplasmic tail (CT) sequence of Gc. Several trafficking motifs were identified, underlined and boxed in different colours: two tyrosine-based motifs, Y1 and Y2 (blue and yellow); di-leucine motif, LL (grey); acidic cluster, AC, (green); endoplasmic reticulum retrieval domain, ERR (pink). Deletion of the putative trafficking motifs in the cytoplasmic tail of Gc is indicated as  $\Delta$ CT. (B) The mutations introduced in the above Gc motifs are shown in the Table. (C) Intracellular levels and processing (INTRA) and viral incorporation (PELLET) of CCHFV wild type glycoproteins compared to Gc- $\Delta$ CT GPC mutant. Lysates of Huh7.5 cells producing tc-VLPs generated with WT GPC vs. Gc- $\Delta$ CT GPC mutant were analysed by Western blotting with antibodies against the indicated proteins including Gn, Gc, NP and cellular actin. Cell supernatants containing tc-VLPs were concentrated by ultracentrifugation through 20% sucrose cushions, resuspended in Opti-MEM medium and analysed by Western blot. (D) Infectivity titres of intracellular and extracellular CCHFV tc-VLPs bearing mutant Gc CT proteins. At 72 h post-transfection, clarified supernatants and cell-associated tc-VLPs were used to infect Huh7.5 cells pre-transfected with L and N expression vectors, and titres were determined by FACS analysis at 24 h post-infection. (E-G) Intracellular levels and processing of CCHFV WT GPs compared to Gc CT mutant proteins. Representative Western blot analysis and relative quantification of intracellular Gc, NP and Gn compared to WT proteins (lower panels). Protein band intensities were quantified and normalized relative to actin and expressed as fold change compared to WT (lower panels). (H-J) tc-VLP containing cell supernatants were pelleted by ultracentrifugation through 20% sucrose cushions, resuspended in Opti-MEM medium and analysed by Western blot. Representative Western blot analysis and relative quantification of Gc, NP and Gn expressed as fold change compared to WT proteins (lower panels). Molecular weight markers are marked to the left (kDa). Statistical significance was determined using parametric student-t test compared with WT proteins. Average number of repeats for intracellular CCHFV proteins: Gn = 4, Gc = 3, NP = 4. Average number of repeats for CCHFV proteins in pellets: Gn = 4, Gc = 4, NP = 4. Average number of repeats for extracellular and intracellular infectivity assays: n = 4. The values are displayed as means  $\pm$  SEM. Each dot in the graphs corresponds to the value of an individual experiment and dots from one colour are from the same experiment.



ER localization [29], respectively, through interactions with AP-1 and AP-3 (PACS-1) and COPI (PACS-2).

How CCHFV exploits these cellular trafficking networks and cellular host components during all stages of virus assembly and/or egress remains poorly defined. Here, using both a CCHFV minigenome-reporter transcription and entry-competent virus-like particle (tc-VLP) assay [30], mimicking viral particles [31], and full length, live virus, we aimed at understanding how CCHFV GPs make use of host factors and pathways to target the site of assembly and promote envelopment of its viral particles. Through a strategy allying functional assays with biochemical and intracellular imaging analyses, we investigated the role of putative membrane trafficking motifs that we identified in the CDs of CCHFV GPs, how their mutagenesis could impact envelopment and production of infectious viral particles, and what are some cellular factors involved in the above. Altogether, our results indicate that several CCHFV GP CD motifs have specific functions to transport Gn and Gc GPs through various parts of the membrane trafficking network to the virion assembly site and that the PACS-2 connector host protein plays a crucial role in the above.

## Results

**Gc cytoplasmic determinants are essential for the formation of infectious particles.** Using consensus sequences that were determined elsewhere, such as tyrosine-based motifs (YXXΦ [Φ standing for an amino acid with a bulky hydrophobic side chain and X for any amino acid]) [32,33], dileucine motifs (DXXLL and [DE]XXXL[LI]) [26,33], acidic cluster motifs [33,34], and di-lysine motifs [28,35], we identified several putative membrane trafficking motifs in the cytoplasmic tail (CT) of CCHFV Gc glycoprotein (Figure 1A): two tyrosine-based motifs (Y1 and Y2), an acidic cluster motif (AC), a di-leucine motif (LL), and an ER retrieval motif (ERR). We noticed from multiple sequence alignment analysis that these motifs are highly conserved among various CCHFV isolates (Supplementary Fig. 1A, 1C). These potential determinants were mutated (Figure 1B) in the full context of GPC expression vectors to raise mutant Gc proteins whose properties were investigated using a CCHFV transcriptionally – and entry-competent virus-like particle (tc-VLP) production and infection assay [30,36].

We evaluated the role of these putative trafficking motifs on virion assembly, GP incorporation, and infectivity in Huh7.5 hepatoma cells, as the liver is one of the important CCHFV target organs. We first generated a mutant GPC harbouring a deletion of most Gc CT (Gc-ΔCT) that was used to produce tc-VLPs by co-transfection of Huh7.5 cells with a

CCHFV minigenome encoding GFP, CCHFV RNA polymerase (L) and nucleoprotein (NP) expression constructs together with constructs expressing either wild type (WT) GPC or Gc-ΔCT GPC (Figure 1C). Whole-cell lysates of tc-VLP producer cells (defined as “Intracellular” in all figures) and the corresponding supernatants purified by ultracentrifugation through a sucrose cushion (defined as “Pellet” in the Figures) were analysed by SDS-PAGE and Western blot at 72 h post-transfection (Figure 1C) to assess incorporation of mutant GPs on secreted viral particles. NP intracellular expression and secretion in cell supernatants were not significantly different between WT and Gc-ΔCT tc-VLPs (Figure 1C). In agreement with previous studies [10,30,31,36], the expression of WT GPC raised mature Gn protein at 37 kDa (Figure 1C) and Gc protein as a preGc precursor of 85 kDa that was converted to mature Gc (75 kDa). In contrast with WT GPC, the Gc-ΔCT GPC raised lower preGc and Gc bands due to the deletion of Gc cytoplasmic tail. Western blot analyses of pellets of tc-VLP producer cell supernatants indicated that while Gn and Gc were readily incorporated into particles for WT GPC, tc-VLPs generated with the Gc-ΔCT mutant displayed no or poor Gc and Gn levels, suggesting a defect in virion incorporation of either GP.

We examined the ability of this Gc-ΔCT GPC mutant to support the formation and release of extracellular and intracellular infectious CCHFV tc-VLPs. We used tc-VLPs generated in the absence of GPC, which does not generate infectious particles (No-GPs in Figure 1D) to set up the thresholds of infectivity assessments. In agreement with these above results, the deletion of the CT of Gc resulted in a complete loss of both extracellular and intracellular infectivity (Figure 1D), underscoring the presence of critical determinants in Gc CT that allow envelopment and production of infectious viral particles.

Next, we examined the infectivity of the GPC mutants generated in the identified Gc CT motifs (Figure 1A, B). We found that while the Y1 mutant allowed the formation and release of infectious tc-VLPs at levels identical to WT tc-VLPs, the other CT mutants yielded lower (AC mutant) or hardly detectable (Y2, LL, ERR mutants) infectivity for both intracellular and extracellular tc-VLPs. Collectively, these results indicate that several Gc CT determinants play important roles in the assembly and release of infectious tc-VLPs.

Then, to further understand the functions of Gc CT motifs, we analysed the effect of their mutation on Gn and Gc expression and processing, NP expression, and secretion of particle-associated viral proteins (Figure 1E–J). Expression of WT and mutant Gc GPC raised similar intracellular levels of NP, Gc and Gn expression (Figure 1E–G). Yet, in contrast to Y1 and AC Gc mutant GPCs whose

Gn and Gc GPs were not or only slightly less well incorporated into particles compared to WT GPC, the other Gc CT mutant GPC constructs did not allow secretion of tc-VLPs displaying Gc or Gn GPs (Figure 1H–I), which fully supported the results of infection assays (Figure 1D).

Altogether, these results indicated that the motifs identified in Gc CT regulate an early stage of virion production prior to secretion.

**Gc CT determinants play a role in cellular trafficking of CCHFV Gc glycoprotein.** The processing and maturation steps of WT GPC are initiated in the ER and are followed by PreGn and PreGc transport through the secretion pathway and ultimately to the proposed site of CCHFV assembly and envelopment, presumably near the Golgi complex [13]. Tyrosine-based motifs, di-leucine motifs, acidic clusters and ER retrieval motifs are involved in protein retrograde trafficking from plasma membrane to endosomes, from endosomes to Golgi and from Golgi to ER. Thus, we assessed the role of Gc CT determinants on Gc intracellular trafficking and localization by immunofluorescence (IF) studies using cellular markers specific for the Golgi (GM130), early (Rab5) and late (Rab7) endosomes.

As reported before [36], Gc expressed from WT GPC is localized in Huh7.5 cells throughout the secretory pathway, without significant accumulation in Golgi and late endosomes (Figure 2). Yet, in contrast to WT GP, we found that the Gc- $\Delta$ CT mutant had impaired co-localization with GM130 (Figure 2A, D) and Rab5 markers (Figure 2B, E), likely owing to the removal of intracellular trafficking motifs in Gc CT. Moreover, we found that the  $\Delta$ CT mutant displayed increased detection of Gc at the cell surface as shown by IF in non-permeabilized cells (Supplementary Fig. 2A), suggesting that this mutant accumulated at the plasma membrane (PM).

Altogether, these results underscored the role of CT motifs that allow Gc trafficking from the PM to intracellular organelles or prevent Gc exposition at the PM.

We therefore sought to address the individual contribution of the putative trafficking motifs present in Gc CT to Gc intracellular traffic and localization, and to correlate this with assembly and release of viral particles.

First, we investigated the levels of cell surface expression of the mutants by IF in non-permeabilized cells. We found that compared to WT GPC and other mutant GPCs, the Gc Y1 mutant displayed higher levels of expression at the surface (Supplementary Fig. 2A). This suggested that mutation of the Y1 motif could prevent Gc internalization, which induced its cell surface accumulation, and agreed with higher cell–cell fusion levels induced by this mutant as compared to WT GPC and other Gc CT motif mutant GPC (Supplementary Fig. 2B). Importantly, this result

argues that Gc's CT contains motifs that allow its trafficking from the PM to intracellular organelles rather than preventing its cell surface exposition.

Second, when we addressed the above determinants in Gc CT (Figure 1A, B), we found that the Gc AC mutant and, with statistical significance, the Y2 and ERR mutants exhibited reduced colocalization with GM130 marker, underscoring impaired trafficking to or within the Golgi (Figure 2A, D). Then, when we investigated Gc localization in early endosomes, we found that the Gc LL and ERR mutants exhibited a decreased co-localization with Rab5 marker, as compared to WT GPC, indicating that retrograde trafficking from early endosomes to Golgi may be impaired for these mutants (Figure 2B, E). Yet, in contrast with WT Gc, the Gc AC mutant showed slightly increased co-localization with Rab5 (Figure 2B, E). This observation suggested an impaired retrograde trafficking of the Gc AC mutant from the early endosomes to the Golgi apparatus. From early endosomal compartments, a subset of proteins can be targeted to late endosomes [37]. We thus addressed the co-localization of Gc mutants with the late endosomal marker, Rab7. In contrast to Gc expressed from WT GPC, the Y2 mutant showed increased co-localization with Rab7 (Figure 2C, F), suggesting that the mutation of its tyrosine-based motif impairs its trafficking from the late endosomes to the upstream compartment, possibly to lysosomes or lysosome-related organelles [33].

Altogether, these results indicated that in the context of GPC, several determinants of the CT domain of Gc cooperate to allow intracellular trafficking of CCHFV Gc GP from the PM to the virion assembly site.

**Mutations in Gn cytosolic determinants impact the formation of CCHFV infectious particles.** We identified several putative membrane trafficking motifs in the CD of CCHFV Gn glycoprotein (Figure 3A). Similar to Gc CT, the multiple sequence alignment analysis of Gn CD also revealed highly conserved motifs (Supplementary Fig. 1B, 1C): two tyrosine-based motifs (Y1 and Y2), an acidic cluster motif (AC) and a di-leucine motif (LL). These potential determinants were mutated in the context of the GPC expression vector to raise mutant Gn proteins upon CCHFV tc-VLP production (Figure 3B).

We found that while the mutation of the Y1 motif allowed the formation and release of infectious tc-VLPs at levels identical to WT tc-VLPs, the other CD mutants (Y2, LL, and AC mutants) yielded strongly reduced or no infectivity for both intracellular and extracellular tc-VLPs (Figure 3C). These results indicated that the latter determinants play essential roles in GP incorporation and release of infectious virions.

Then, to better understand the functions of Gn CD motifs, we analysed the effect of their mutation on Gn

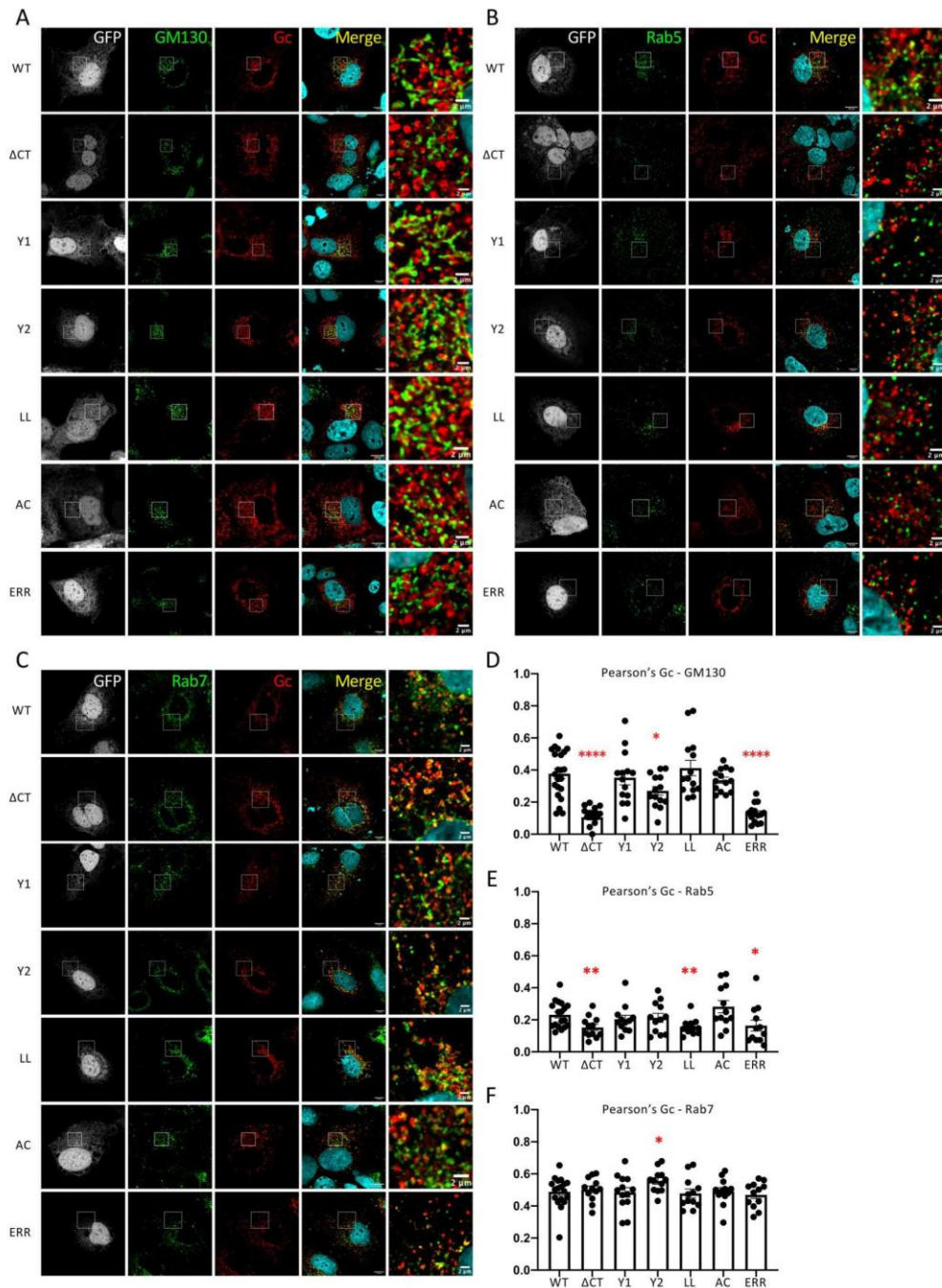


**Figure 2. Intracellular localization of CCHFV Gc cytoplasmic tail determinants.** (A, D) Golgi localization of CCHFV Gc glycoprotein. Confocal microscopy analysis of Huh7.5 cells producing tc-VLPs encoding a GFP marker that were generated with WT GPC vs. GPC harbouring Gc cytoplasmic tail mutants (ΔCT, Y1, Y2, LL, AC, ERR). At 48 h post-transfection, cells were fixed, permeabilized with Triton X-100, and stained for GFP (grey channel), Golgi (anti-GM130, green channel), Gc (11E7, red channel), and nuclei (Hoechst, blue channel). (B, E) Early endosome localization of CCHFV Gc glycoprotein. As described in (A), cells were fixed, permeabilized with Triton X-100, and stained for GFP (grey channel), Rab5 (anti-Rab5, green channel), Gc (11E7, red channel), and nuclei (Hoechst, blue channel). (C, F) Late endosome localization of CCHFV Gc glycoprotein. As described in (A), cells were fixed and stained for GFP (grey channel), Rab7 (anti-Rab7, green channel), Gc (11E7, red channel), and nuclei (Hoechst, blue channel). Scale bars represent 10 μm, zooms from squared area represent 2 μm. Pearson's coefficients were calculated using FIJI (JACoP) on 5 cells from 3 separated experiments (15 cells in total) and expressed as means ± SEM. Statistical significance was determined using non-parametric two-tailed Mann-Whitney test. The values are displayed as means ± SEM. Each dot in the graphs corresponds to the value of an individual cell.

and Gc expression and processing, NP expression and secretion of particle-associated viral proteins (Figure 3D–I). Expression of WT and mutant GPC raised similar intracellular levels of NP, Gc and Gn expression (Figure 3D–F). Yet, in sharp contrast to Gn Y1 mutant whose Gn and Gc GPs were only slightly less well incorporated into viral particles, as compared with WT GPs, the other Gn CD mutant constructs raised tc-VLPs that had no detectable Gn and/or Gc GPs (Figure 3G–I), which fully supported the results of infection assays (Figure 3C). Further, we noticed that di-leucine mutation in Gn led to less NP secretion in pellet fraction (Figure 3H).

Altogether, these results indicated that motifs identified in Gn cytosolic domain regulate an early stage of assembly before virion secretion.

To further investigate the function of these Gn determinants in assembly of viral particles, we analysed tc-VLP-producer cells by confocal microscopy using antibodies against Gc and intracellular markers. However, due to the lack of Gn antibodies suitable for IF assays, we could not perform the analysis of Gn intracellular localization.

Like for the Gc Y2 mutant (Figure 2), we found that the Gn Y2 mutant induced a defect in the distribution pattern of Gc in the Golgi (Figure 4A, D), suggesting that tyrosine domains of both Gn and Gc work in a similar way to promote CCHFV GP intracellular localization where mutations in Gn or Gc can impact traffic of the other protein [38] as they likely form a heterodimer [11,12]. Surprisingly, we also found that the Gn AC mutant induced a stronger Gc co-localization with GM130, indicating that the GP can reach the Golgi but displays impaired trafficking through the Golgi.

Finally, when we analysed Gc co-localization with early endosomes (Rab5 marker), we found that Gn Y2 and AC mutants showed a slight increase in Gc co-localization with early endosomes (Figure 4B, E). Yet, we noticed that in contrast to WT GPC, the Gn Y2 mutant exhibited increased Gc co-localization with the Rab7 late endosomal marker (Figure 4C, F).

Altogether, these results indicated that mutations of Gn CD motifs which induce GP accumulation in various cellular organelles may block retrograde transport to the trans-Golgi and prevent GP incorporation on viral particles.

**Unlike PACS-1, the PACS-2 adaptor is a critical factor controlling virion incorporation and secretion of CCHFV glycoproteins.** Our results revealed that the AC motif in Gn is important to promote CCHFV GP intracellular trafficking and/or incorporation on viral particles since its mutation induced accumulation of Gc in early endosomes and Golgi, and prevented GP assembly and release of infectious particles (Figures 3 and 4). Since some Golgi resident transmembrane proteins have been shown to use AP-1 mediated retrograde transport

from endosomes to trans-Golgi network (TGN) through binding of the cellular adaptor PACS-1 [29] to their acidic cluster, we investigated whether PACS-1 down-regulation could impair CCHFV particles assembly.

We downregulated PACS-1 through expression of a previously validated [39] short hairpin RNA (ShPACS-1) in producer cells. While we achieved a knockdown efficiency of PACS-1 of up to 80% in Huh7.5 cells (Figure 5A), this did not influence the production of infectious viral particles, as shown for both tc-VLP (Figure 5B) and full length, live CCHFV particles (Figure 5C) produced in PACS-1 downregulated Huh7.5 cells. Hence, we concluded that PACS-1 is not a crucial host factor for the transportation of CCHFV glycoproteins to the assembly site.

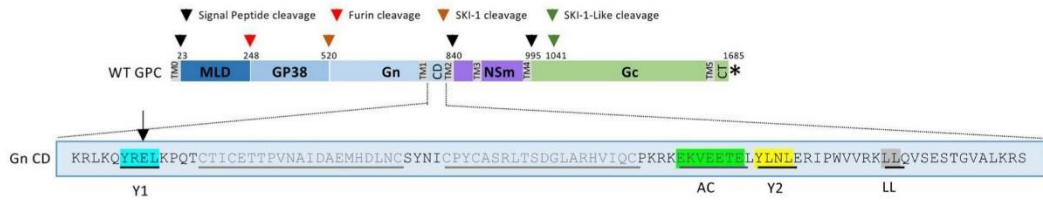
Next, we investigated the alternative possibility that the PACS-2 protein, which also binds acidic cluster motifs [40], could regulate intracellular trafficking of CCHFV GPs. We expressed in tc-VLP producer cells two distinct short hairpin RNAs (Sh103 and Sh433), which readily induced PACS-2 knockdown to up to 85% (Figure 5D). Importantly, we found that PACS-2 downregulation significantly decreased the extracellular tc-VLP infectivity with up to 10-fold reduction of the titres as compared to tc-VLPs produced in control cells (Figure 5E). Furthermore, we observed more than 10-fold reduction of intracellular infectivity of tc-VLPs produced in PACS-2 down-regulated cells (Figure 5E), which indicated that PACS-2 is important for production of infectious particles at the level of virion assembly.

We sought to confirm this result with full length, live CCHFV (Figure 5F) produced in PACS-2 knockdown vs. control cells (Figure 5D). Following infection with virus inoculate, samples from the infected cells and supernatants were collected at 24-hour following infection and analysed by qPCR on viral RNAs. Notably, we found that the extracellular CCHFV RNAs harvested from PACS-2 down-regulated cells displayed *ca.* 10-fold decrease of CCHFV RNAs as compared to controls cells (Figure 5F), which agreed with reduction of intracellular viral RNAs in producer cells (Figure 5F) and confirmed that PACS-2 is a crucial factor for production of infectious CCHFV particles.

Finally, to exclude that PACS-2 could act at the step of virus entry, notably by acting on trafficking of host entry factors, we infected PACS-2 downregulated Huh7.5 cells. We found that tc-VLPs displayed similar levels of infectivity whether PACS-2 was down-regulated or not in target cells (Figure 5G), which agreed with its involvement at the step of assembly of viral particles.

When we investigated intracellular expression of CCHFV proteins, no significant effect for NP, Gn and Gc expression could be detected upon PACS-2

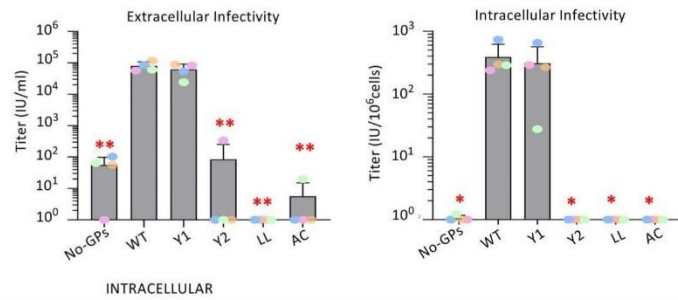
A



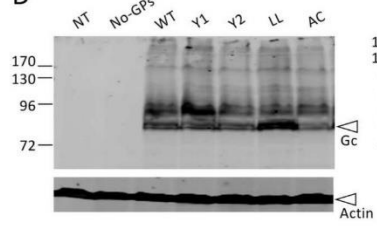
B

WT Gn CT	Mutations
YREL (Y1)	AREL
YLNL (Y2)	ALNL
LL (LL)	AA
EKVEETE (AC)	QKVQQTQ

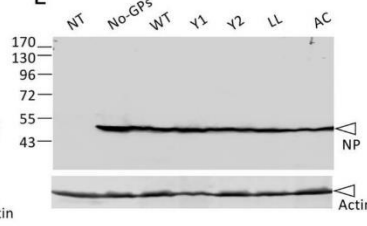
C



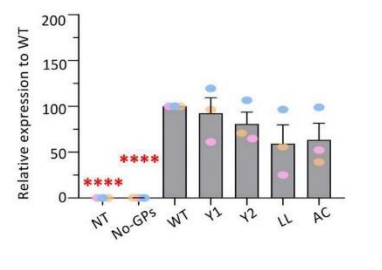
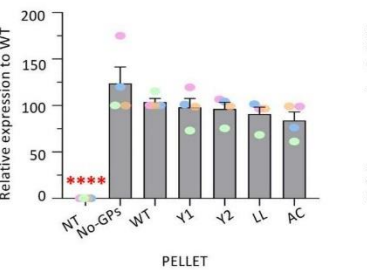
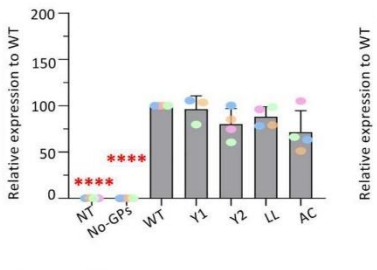
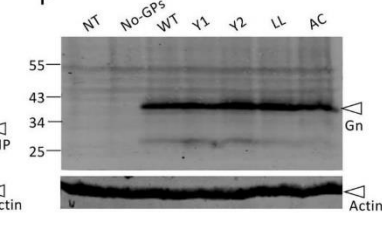
D



E

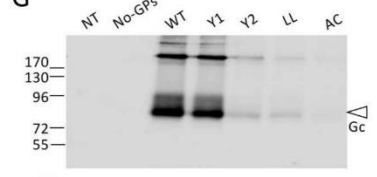


F

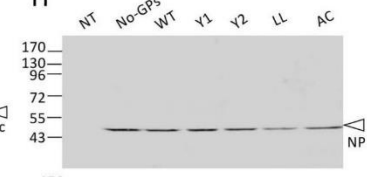


PELLET

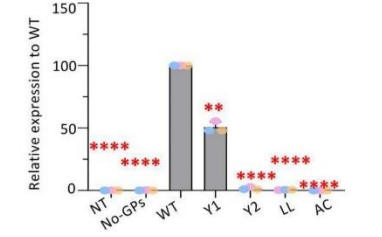
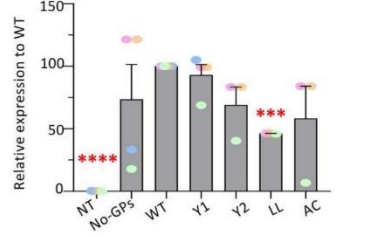
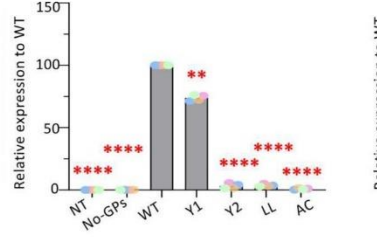
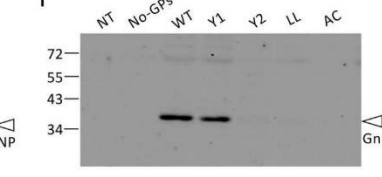
G



H



I



down-regulation, as compared to cells expressing a control short hairpin RNA (Figure 6A–C). Yet, when we analysed the pellets of ultracentrifuged supernatants of tc-VLP producer cells, we found that PACS-2 knockdown drastically reduced Gc (by *ca.* 90%) and Gn (by over 85%) secretion (Figure 6D, F). Furthermore, we found that PACS-2 downregulation also resulted in a notable reduction (by over 90%) of the secretion of NP (Figure 6E). These results suggested that PACS-2 modulates trafficking of both CCHFV GPs and NP.

To confirm these results, we subsequently investigated Gc localization in PACS-2 down-regulated cells. We found that the knockdown of PACS-2 expression induced a slight but significant increased colocalization of Gc with the Golgi marker GM130 (Figure 7A) but did not have any impact on colocalization of Gc with early or late endosomes (Supplementary Fig. 3). These results suggested that the loss of PACS-2 expression does not impact Gc trafficking from PM to Golgi, but impairs Gc trafficking through the Golgi. Interestingly, this result phenocopies the increased colocalization of Gc with GM130 that we observed for Gn AC mutant (Figure 4A, D), albeit to a lesser extent. Furthermore, we found that Gc and NP colocalization was significantly increased in PACS-2 down-regulated cells (Figure 7B), which reflected the accumulation of virion structural components when assembly was blocked.

Finally, the overexpression of PACS-2 in tc-VLP producer cells (Supplementary Fig. 4A) did not raise the production of infectious intracellular and extracellular viral particles (Supplementary Fig. 4B), which agreed with the lack of increased secretion of viral GP components (Supplementary Fig. 4C–H) and suggested that PACS-2 is not a rate limiting assembly factor for envelopment and secretion of

CCHFV particles. Note that, in contrast to Gn and Gc GPs, NP secretion was slightly increased by *ca.* 50% (Supplementary Fig. 4G).

Altogether, the above observations underscored that PACS-2 is a critical host factor modulating CCHFV GPs intracellular trafficking and CCHFV assembly and production of infectious particles.

## Discussion

Due to its high pathogenicity, CCHFV requires handling in Biosafety level 4 laboratories (BSL-4), a scarce resource in the world, which makes the study of assembly, envelopment, and secretion of CCHFV particles challenging. By comparison with other Bunyaviruses, it is currently understood that CCHFV assembly occurs at or near Golgi membranes [13]; yet, how viral proteins reach the assembly sites and which host cellular factors are involved remain open questions. One specific feature of the Gc GP of Nairoviruses is its unusually long cytoplasmic tail compared to other Bunyaviruses, which potentially contains different domains that could control distinct trafficking pathways. Taking advantage of the tc-VLP assay [30,31,36], we deleted or mutated several putative trafficking motifs in Gc and Gn cytoplasmic domains to get better insight into CCHFV envelope assembly and secretion of viral particles.

Interestingly, the removal of most (*i.e.* 85%) of the Gc CT (Gc- $\Delta$ CT GPC) increased the exposition of the GPs at the plasma membrane, as deduced by the increased formation of syncytia and GP staining in non-permeabilized cells (Supplementary Fig. 2). Moreover, this mutant GP was unable to traffic to virion assembly site and exhibited impaired Gn and Gc (but not NP) secretion as well as infectivity of tc-

**Figure 3. Infectivity and viral incorporation of CCHFV Gn cytoplasmic tail mutants.** (A) Schematic representation of the GPC polyprotein encoded by CCHFV wt-M cDNA (WT GPC). The polyprotein precursor organization and positions of the first amino-acid residues after cleavage marking protein boundaries (MLD, GP38, Gn, NSm, and Gc) within the CCHFV polyprotein are shown. The star indicates the position of the stop codon. The N-terminal signal peptide (TM0) and putative transmembrane domains (TM1 to TM5) are shown as grey boxes, signal peptidase cleavage sites are indicated by black arrows and other host protein convertase cleavage sites are indicated by red, orange and green arrows. The bottom part shows the cytoplasmic domain (CD) of Gn. Several trafficking motifs were identified, underlined and boxed in different colours: two tyrosine-based motifs, Y1 and Y2 (blue and yellow); di-leucine motif, LL (grey); acidic cluster, AC (green). (B) The mutations introduced in the above Gn motifs are shown in the Table. (C) Infectivity titres of intracellular and extracellular CCHFV tc-VLPs bearing mutant Gn CD proteins. At 72 h post-transfection, clarified supernatants and cell-associated tc-VLPs were used to infect Huh7.5 cells pre-transfected with L and N expression vectors, and titres were determined by FACS analysis at 24 h post-infection. (D–F) Intracellular levels and processing of CCHFV WT GPs compared to Gn CD mutant proteins. Representative Western blot analysis and relative quantification of intracellular Gc, NP and Gn expressed compared to WT proteins (lower panels). Protein band intensities were quantified and normalized relative to actin and expressed as fold change compared to WT (lower panels). (G–I) tc-VLP containing cell supernatants were pelleted by ultracentrifugation through 20% sucrose cushions, resuspended in Opti-MEM medium and analysed by Western blot. Representative Western blot analysis and relative quantification of Gc, NP and Gn expressed as fold change compared to WT proteins (lower panels). Molecular weight markers are marked to the left (kDa). Statistical significance was determined using parametric student-t test compared with WT proteins. Average number of repeats for intracellular CCHFV proteins: Gn = 3, Gc = 4, NP = 4. Average number of repeats for CCHFV proteins in pellets: Gn = 3, Gc = 4, NP = 4. Average number of repeats for extracellular and intracellular infectivity assays: n = 4. The values are displayed as means  $\pm$  SEM. Each dot in the graphs corresponds to the value of an individual experiment and dots from one colour are from the same experiment.

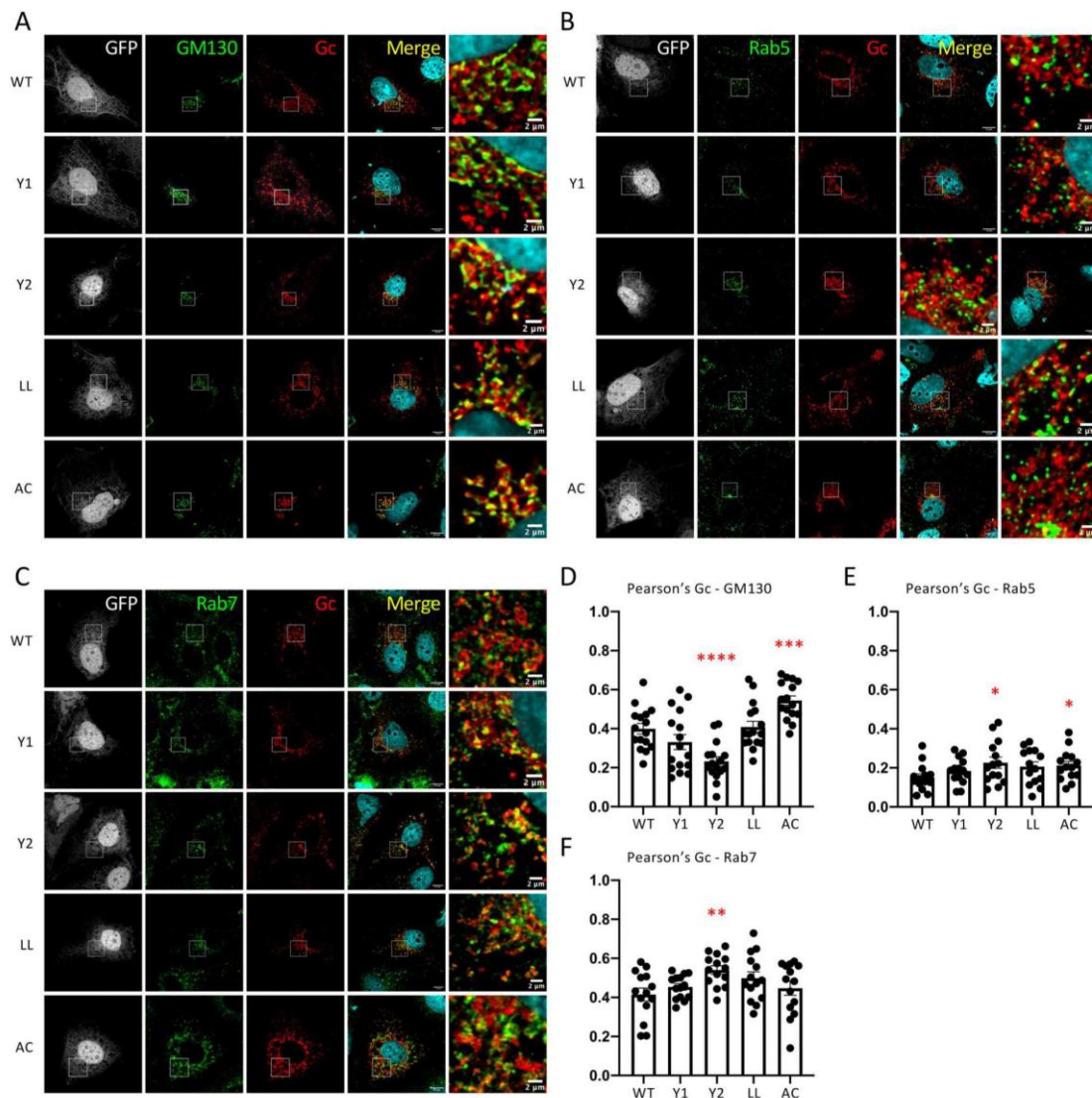
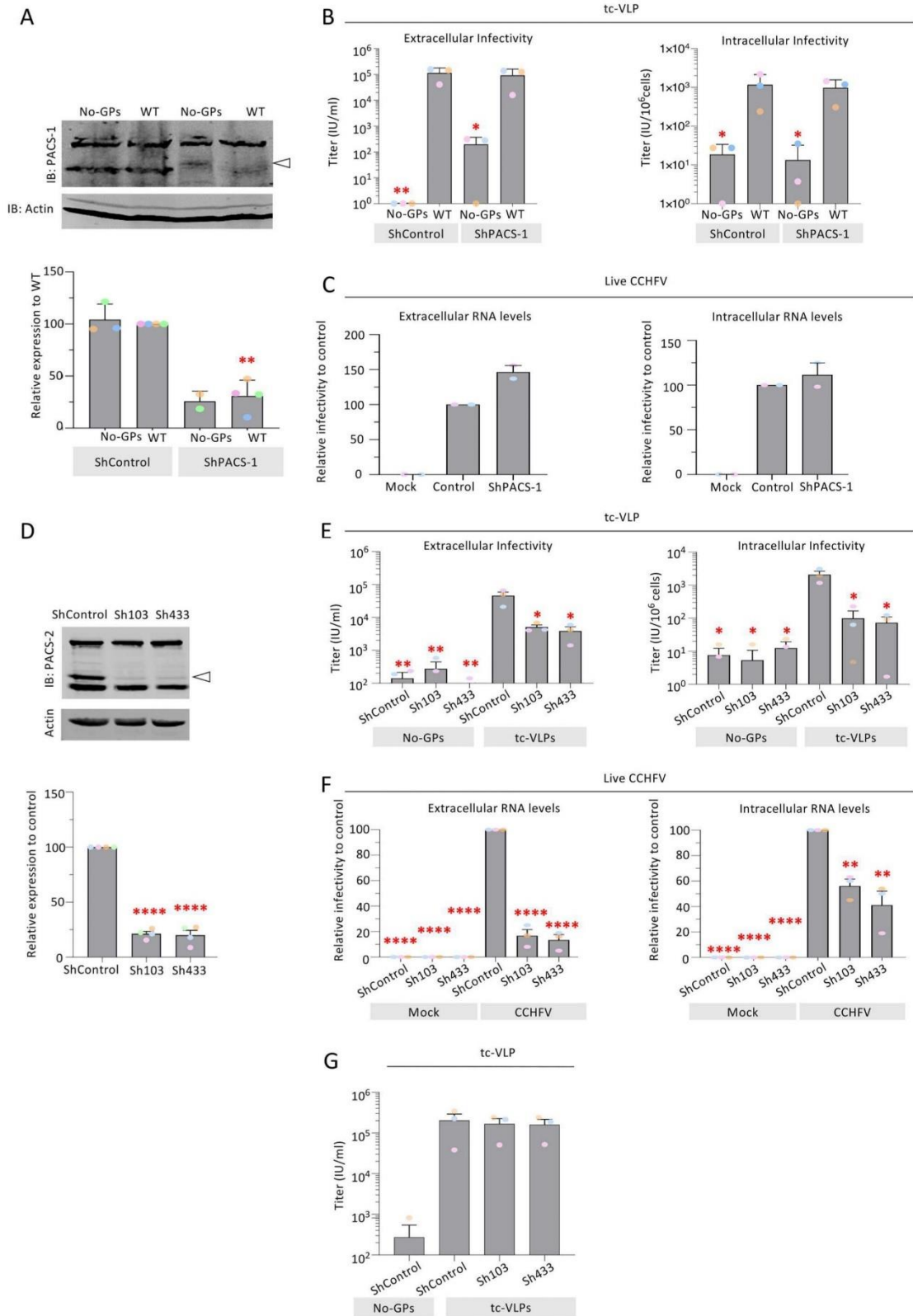


**Figure 4. Intracellular localization of CCHFV Gn cytoplasmic tail mutants. (A, D)** Golgi localization of CCHFV Gc glycoprotein. Confocal microscopy analysis of Huh7.5 cells producing tc-VLPs encoding a GFP marker that were generated with WT GPC vs. GPC harbouring Gn cytoplasmic domain mutants (Y1, Y2, LL, AC). At 48 h post-transfection, cells were fixed, permeabilized with Triton X-100, and stained for GFP (grey channel), Golgi (anti-GM130, green channel), Gc (11E7, red channel), and nuclei (Hoechst, blue channel). **(B, E)** Early endosome localization of Gc glycoprotein. As described in (A), cells were fixed, permeabilized with Triton X-100, and stained for GFP (grey channel), Rab5 (anti-Rab5, green channel), Gc (11E7, red channel), and nuclei (Hoechst, blue channel). **(C, F)** Late endosome localization of Gc glycoprotein. As described in (A), cells were fixed and stained for GFP (grey channel), Rab7 (anti-Rab7, green channel), Gc (11E7, red channel), and nuclei (Hoechst, blue channel). Scale bars represent 10  $\mu\text{m}$ , zooms from squared area represent 2  $\mu\text{m}$ . Pearson's coefficients were calculated using FIJI (JACoP) on 5 cells from 3 separated experiments (15 cells in total) and expressed as means  $\pm$  SEM. Statistical significance was determined using non-parametric two-tailed Mann-Whitney test. The values are displayed as means  $\pm$  SEM. Each dot in the graphs corresponds to the value of an individual cell.

VLPs. Overall, these results confirmed that the cytoplasmic domains of CCHFV GPs contain important trafficking signals. Accordingly, a more subtle mutant, Gc Y1, that disrupts a tyrosine-based trafficking motif, also exhibited an over-expression of Gc at the plasma membrane (Supplementary Fig. 2), which suggested that traffic to and/or exposure to the plasma

membrane is an important step for CCHFV synthesis and which implied that its GPs must return to the Golgi to reach the CCHFV assembly site (Figure 8). Although such back tracking seems counter-intuitive, this anterograde followed by retrograde trafficking is not unique as it is notably used by Golgi resident proteins such as Furin or TGN38 [33]. One possibility is





that retrograde trafficking could be essential for both proper maturation of CCHFV GPs and/or encountering/recruitment of viral RNA. Indeed, as the final maturation step of Gc involves the cleavage of preGc by an uncharacterized SKI-1/SIP protease [10], one cannot exclude that this cleavage event takes place in endosomal/lysosomal compartments since the involved proprotein convertases are active in a wide range of compartments [41]. On the other hand, cytoplasmic “condensates” that contain viral RNA and NP have been observed in CCHFV-infected cells and may represent replication sites [42], raising the possibility that Gn/Gc complex needs to use specific intracellular pathways to interact with and transport the viral RNA through Gn zinc finger domains to the assembly sites.

The above observations concerning CCHFV GPs led us first to investigate the functions of all the trafficking motifs that were detected in both Gn and Gc cytosolic domains.

Particularly, the last 5 amino acids of Gc (KTHIG), whose deletion abrogated production of infectious CCHFV tc-VLPs, would fit with a non-canonical di-lysine motif KxHxx as an ER retrieval (ERR) motif. Such a motif was first identified within an alternative viral envelope GP, the spike protein of SARS-CoV-1 [35]. Curiously, while dibasic motifs are absent in Gc proteins from Orthobunyaviruses and Tospoviruses [20], they can be detected in Gc from Phleboviruses (KKxx) and Hantaviruses (KKxx or KxKxx), suggesting different GP trafficking requirements among Bunyaviruses. These dibasic motifs (KKxx or KxKxx), present in some type I transmembrane proteins, are recognized by the COPI coatomer to achieve their retrograde transport from TGN to ER [28]. The presence of such a motif in Gc CT therefore suggests that Gc needs this motif to reach a dedicated place, probably the assembly site (Figure 8). This may be analogous to the spike protein

of coronaviruses which needs to return to the ER-Golgi Intermediate Compartment (ERGIC) to allow its incorporation into virions [43].

We also identified four putative tyrosine-based motifs, two located on Gn (YREL and YLNL, Gn Y1 and Y2 motifs, respectively) and two located on Gc (YRHL and YRRI, Gc Y1 and Y2 motifs, respectively). Tyrosine-based motifs YXXΦ are known to be involved in protein recycling from the plasma membrane *via* clathrin-mediated endocytosis [44] and in protein targeting to the lysosomes [45], endosomal compartments [46] and TGN [47]. YXXΦ motifs bind to the μ subunit of adaptor protein complexes (APs) with the highest avidity for μ2 of AP-2 complex [33].

Interestingly, our results identified distinct functional features for these different tyrosine-based motifs. As above discussed, mutations of Gc Y1 showed increased exposition of Gc at the plasma membrane, hence suggesting that this motif acts as classical endocytosis motif (Figure 8). Yet, Gn Y1 as well as Gc Y1 mutations resulted in only a mild defect, of up to two-fold of viral incorporation of either GP and had no impact on tc-VLP infectivity or on Gc localization at Golgi. This suggested that the bulk of envelope GPs were still able to reach assembly sites, owing to alternative trafficking signals or to a still active, though weaker, endocytosis mechanism, and that either motif could be important for removing exceeding GP from the plasma membrane rather than to be a limiting factor for CCHFV envelopment. In contrast to the above, the two other tyrosine-based motifs located on either envelope GP, *i.e.* Gn Y2 and Gc Y2, were shown to be crucial for virion assembly. Indeed, their individual mutation strongly impaired Gn and Gc secretion, virion envelopment, and tc-VLP infectivity. Furthermore, this correlated with

**Figure 5. Production of infectious CCHFV particles from PACS-1 or PACS-2 knockdown cells.** Downregulation of PACS-1 or PACS-2 was achieved in Huh7.5 cells *via* lentiviral vectors expressing PACS-1 (ShPACS-1), PACS-2 (Sh103, Sh433) or control shRNA (ShControl). The cells were then used to produce CCHFV tc-VLPs harbouring WT GPC or no GPC (No-GPs). **(A)** Representative Western blot analysis and relative quantification of PACS-1 expressed as fold change compared to PACS-1 levels expressed in cells transduced with a control shRNA (ShControl). **(B)** Infectivity titres of CCHFV tc-VLPs produced in the presence *vs.* in the absence of PACS-1 shRNA. At 72 h post-transfection, clarified supernatants and cell-associated tc-VLPs were used to infect Huh7.5 cells pre-transfected with L and N expression vectors, and titres were determined by FACS analysis at 24 h post-infection. **(C)** Viral characteristics of full length, live CCHFV produced in PACS-1 KD or control cells. The cells were infected with live CCHFV at an MOI of 0.01. Supernatants (extracellular) and cells (intracellular) were harvested at 24 h post infection. Viral RNA in the supernatants and cells were determined using RTqPCR. **(D)** Representative Western blot analysis and relative quantification of PACS-2 expressed as fold change compared to PACS-2 levels expressed in cells transduced with a control shRNA. **(E)** Infectivity titres of CCHFV tc-VLPs produced in the presence *vs.* in the absence of PACS-2 shRNA. At 72 h post-transfection, clarified supernatants and cell-associated tc-VLPs were used to infect Huh7.5 cells pre-transfected with L and N expression vectors, and titres were determined by FACS analysis at 24 h post-infection. **(F)** Viral characteristics of CCHFV produced in PACS-2 KD or control cells. The cells were infected with live CCHFV at an MOI of 0.01. Supernatants (extracellular) and cells (intracellular) were harvested at 24 h post infection. Viral RNA in the supernatants and cells were determined using RTqPCR. **(G)** Infectivity of tc-VLPs in PACS-2 down-regulated cells. Huh7.5 cells down-regulated for PACS-2 (Sh103, Sh433) or control shRNA (ShControl) were pre-transfected with L and N expression vectors. Twenty-four hours later, cells were infected with CCHFV tc-VLPs harbouring WT GPC or no GPC (No-GPs) and titres were determined by FACS analysis at 24 h post-infection. Average number of repeats for extracellular and intracellular infectivity assays: n = 3. The values are displayed as means ± SEM. Each dot in the graphs corresponds to the value of an individual experiment and dots from one colour are from the same experiment.

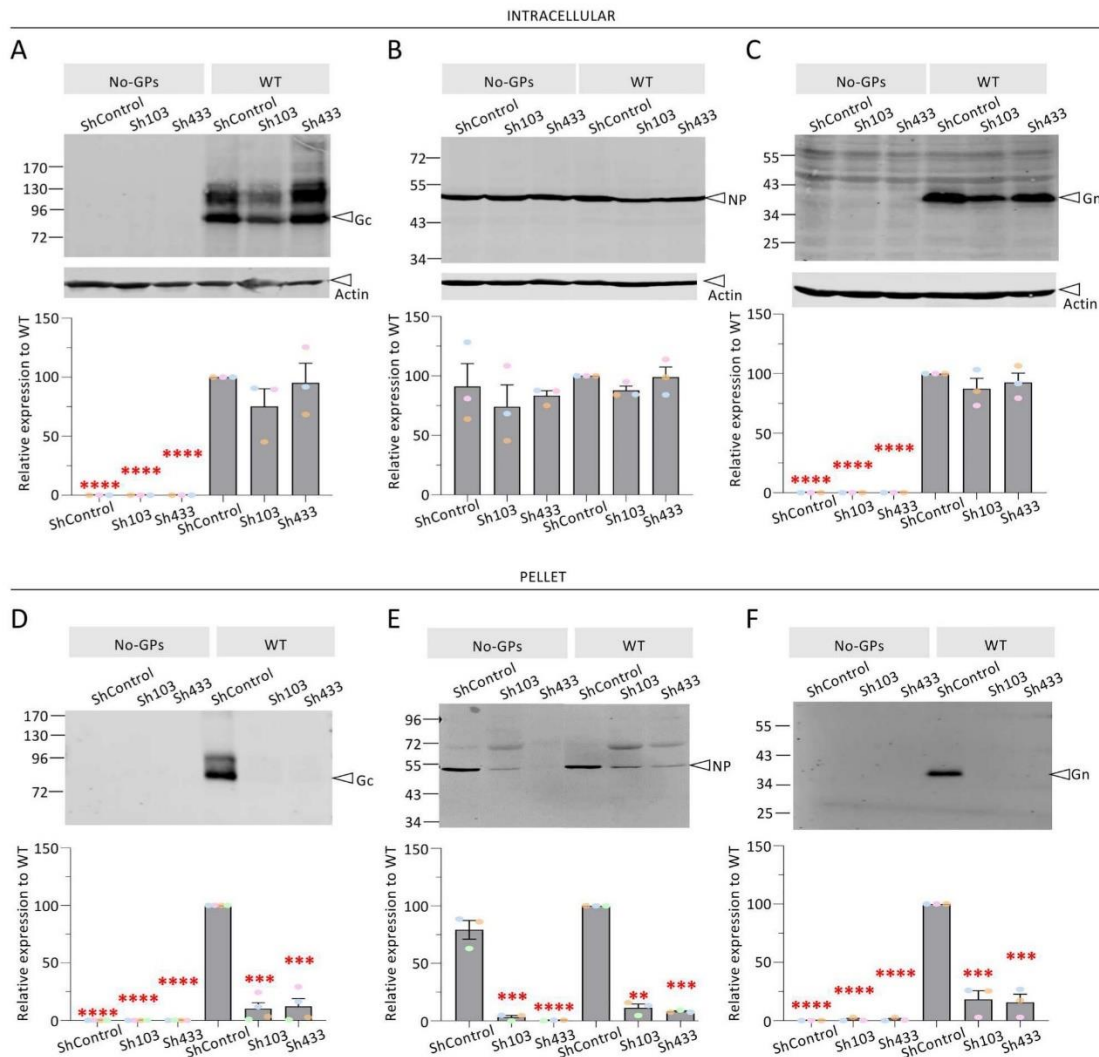


**Figure 6. Viral incorporation of CCHFV GPs in PACS-2 knockdown cells.** Downregulation of PACS-2 was achieved in Huh7.5 cells *via* a lentiviral vector expressing PACS-2 shRNAs (Sh103, Sh433) or control shRNA (ShControl). The cells were then used to produce CCHFV tc-VLPs harbouring WT GPC or no GPC (No-GPs). **(A-C)** Intracellular levels and processing of CCHFV GPs produced in the presence control shRNA vs. PACS-2 ShRNA. Representative Western blot analysis and relative quantification of intracellular Gc, NP and Gn compared to WT proteins (lower panels). Protein band intensities were quantified and normalized relative to actin and expressed as fold change compared to WT (lower panels). **(D-F)** Cell supernatants containing tc-VLPs were pelleted by ultracentrifugation through 20% sucrose cushions, resuspended in Opti-MEM medium and analysed by Western blot. Representative Western blot analysis and relative quantification of Gc, NP and Gn expressed as fold change compared to WT proteins (lower panels). Molecular weight markers are marked to the left (kDa). Statistical significance was determined using parametric student-t test compared with WT GPs. Average number of repeats for intracellular CCHFV proteins: Gn = 3, Gc = 3, NP = 3. Average number of repeats for CCHFV proteins in pellets: Gn = 3, Gc = 3, NP = 3. The values are displayed as means  $\pm$  SEM. Each dot in the graphs corresponds to the value of an individual experiment and dots from one colour are from the same experiment. Statistical significance was determined using parametric student-t test compared with WT protein in ShControl condition. The values are displayed as means  $\pm$  SEM. Each dot in the graphs corresponds to the value of an individual cell.

prevention of Gc colocalization at the Golgi, and consequently, increased Gc colocalization with late endosomes. These results suggested that these mutant GPs have impaired traffic between endosomes and Golgi (Figure 8), and thus, that Gn and Gc Y2 tyrosine-based motifs represent crucial GP intracellular trafficking domains. Notably, it was previously suggested that

tyrosine-based motifs could also act as late domains to recruit host cellular factors necessary to complete virion budding and to compensate the lack of matrix in Bunyaviruses [20]; yet, one would expect that these mutants could be blocked within the assembly sites (Golgi) and would have altered NP secretion, which was not observed in our assays.

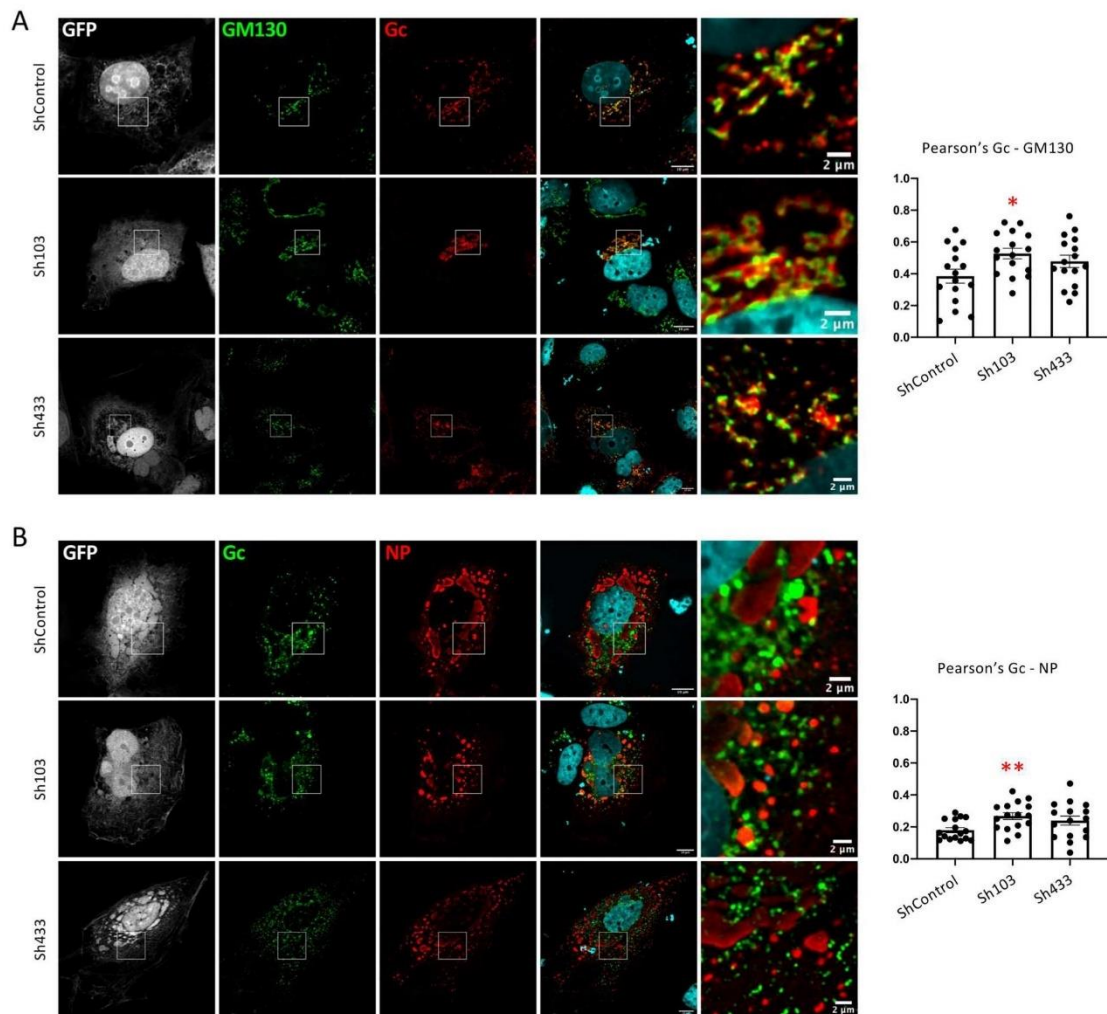


**Figure 7. CCHFV GPs trafficking in PACS-2 knockdown cells.** Downregulation of PACS-2 was achieved in Huh7.5 cells *via* a lentiviral vector expressing PACS-2 shRNAs (Sh103, Sh433) or control shRNA (ShControl). The cells were then used to produce CCHFV tc-VLPs. **(A)** Golgi localization of CCHFV Gc glycoprotein. Confocal microscopy analysis of Huh7.5 cells producing tc-VLPs encoding a GFP marker that were generated with WT GPC. At 48 h post-transfection, cells were fixed, permeabilized with Triton X-100, and stained for GFP (grey channel), Golgi (anti-GM130, green channel), Gc (11E7, red channel), and nuclei (Hoechst, blue channel). **(B)** Gc colocalization with NP. Confocal microscopy analysis of Huh7.5 cells producing tc-VLPs encoding a GFP marker that were generated with WT GPC. At 48 h post-transfection, cells were fixed, permeabilized with Triton X-100, and stained for GFP (grey channel), Gc (11E7, green channel), NP (2B11, red channel), and nuclei (Hoechst, blue channel). Scale bars represent 10  $\mu$ m. Magnification of the squared areas is shown at the right side of each condition, scale bars from squared area represent 2  $\mu$ m. Pearson's coefficients were calculated using FIJI (JACoP) and expressed as means  $\pm$  SEM. Statistical significance was determined using non-parametric two-tailed Mann-Whitney test. The values are displayed as means  $\pm$  SEM. Each dot in the graphs corresponds to the value of an individual cell.

Additionally, we identified two functional dileucine motifs either in the cytosolic domain of Gn or in the cytoplasmic tail of Gc. Di-leucine based motifs are another class of sorting motifs that act in the TGN/endosomal system. They have been shown to be recognized by AP-1, AP-2 and AP-3 [26] to mediate different sorting events, such as internalization from plasma membrane and sorting to endosomes [27]. Curiously, the substitution for alanines of a di-leucine motif in Gc strongly impaired Uukuniemi

virus (UUKV) VLPs budding, suggesting that this motif would act between assembly and secretion of UUKV VLPs [21]. In our study, we discovered that the disruption of the dileucine motif in the cytoplasmic domains of both the Gn or Gc proteins resulted in a deficiency in the envelopment and secretion of CCHFV tc-VLPs. Furthermore, our confocal microscopy analysis only revealed a slight impairment of the colocalization of Gc of the Gn LL mutant with the early endosome marker (Rab5),

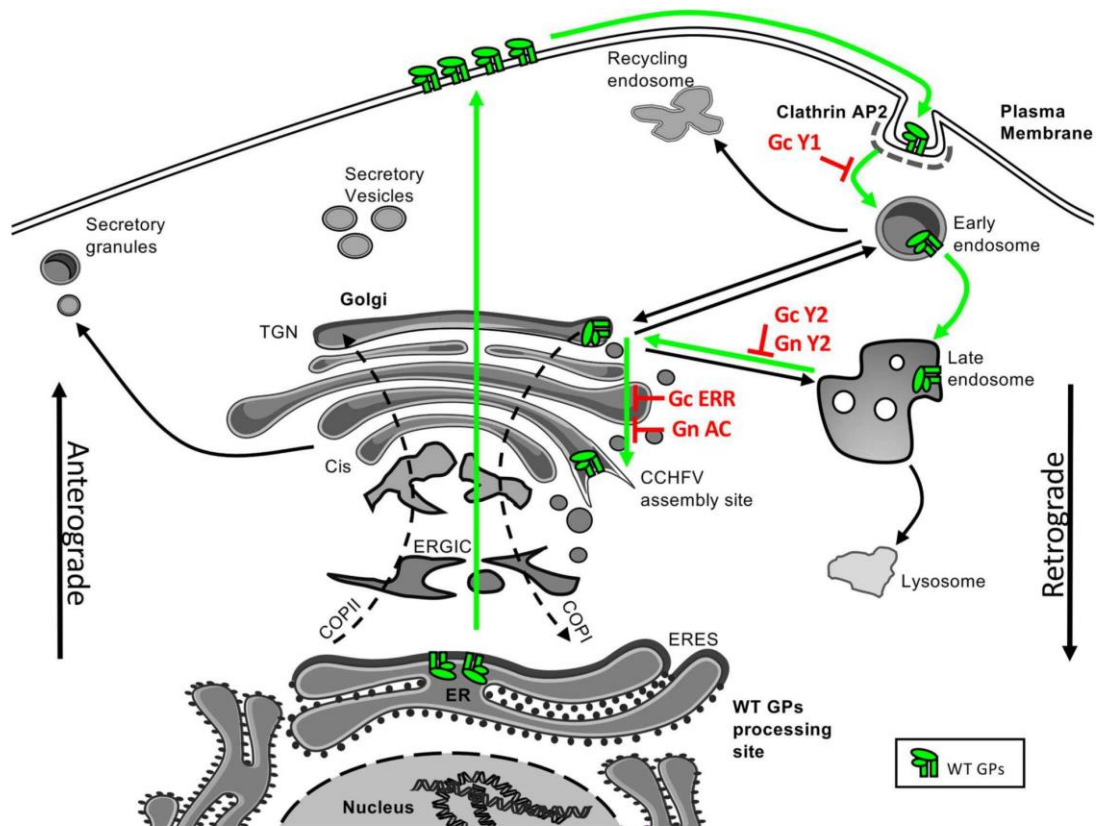


**Figure 8. Working model of CCHFV GP retrograde intracellular trafficking.** The molecular characterization of Gn and Gc CT motifs suggest that after translation, either GP follows the secretion pathway, *via* an unidentified mechanism, to reach the plasma membrane (PM). From the PM, Gc is re-endocytosed *via* its first tyrosine domain (Y1), which probably involves a clathrin-mediated endocytosis *via* AP-2 complexes. After endocytosis, Gn and Gc traffic *via* the endosomal retrograde pathway and are transferred from the late endosomes to the Golgi through the usage of their second tyrosine motif (Gn Y2 and Gc Y2 respectively). From there, Gn and Gc progress along the Golgi stacks to reach the unidentified assembly site, probably *via* COPI binding to Gc ERR motif and Gn AC motif *via* the PACS-2 protein adaptor. Interestingly, our results suggest that NP trafficking and/or assembly into particles is also dependent on PACS-2 protein.

which is likely not significant for CCHFV assembly owing to very low Pearson's coefficients for WT GPs. Thus, these results suggested that the di-leucine motifs identified in CCHFV GPs either may not be trafficking motifs *per se*, or at least may not be involved in the endosomal retrograde pathway. Indeed, consensus di-leucine motifs exhibit a negatively charged amino-acid in position - 2 or - 3 (DXXLL and [DE]XXXL[LI] respectively [33]) which is absent in CCHFV GPs. Yet, as the mutation of these LL motifs dramatically impaired tc-VLP assembly, further work would be necessary to identify at which step do they act, such as *e.g.* Gn/Gc heterodimerization, envelopment or genome packaging.

Finally, we identified putative acidic cluster (AC) motifs, which are composed of a stretch of negatively charged amino acids, in both Gn and Gc cytosolic domains [33]. While mutation of the acidic cluster of Gc GP did not seemingly alter its functions, the exchange of charged amino acids by neutral structural

homologs in the acidic cluster of Gn GP (*i.e.* substitution of EKVEETEL for QKVQQTQ) resulted in a complete loss of Gn/Gc secretion as well as of tc-VLP production and infectivity (Figure 8).

Acidic cluster motifs are often found in transmembrane proprotein convertases, such as PC6B and PC7 that are localized to the TGN and were first described in the cytosolic tail of Furin [34]. Interestingly, several viral proteins also contain such motifs including GP of KSHV [48], GP B of HCMV [49], Nef of HIV-1 [50] or TM GP of RD114 virus [39]. These acidic cluster motifs are recognized by PACS (phosphofurin acidic cluster sorting) proteins to achieve intracellular trafficking. The PACS family comprises two members, PACS-1 and PACS-2, that have similar structures but different functions [29]. The structure of PACS proteins consist of a cargo (furin)-binding region (FBR), a disordered middle region (MR) and a C-terminal region (CTR) [29]. Both proteins share 54% sequence identity, but the FBR domain of PACS-2 has 81%

sequence identity with that of PACS-1 and is believed to be critical for identifying and binding cargo proteins [29]. Widely expressed in human tissues, the biological function of PACS proteins is to sort client proteins from different organelles. The PACS-1 FBR interacts with the AP-1 and AP-3 adaptor complexes [51] and has been shown to direct the retrograde transport of numerous cellular proteins from endosomal pathway to TGN, including Furin and the cation-independent mannose-6-phosphate receptor (CI-MPR) [52], or viral proteins such as GP B of HCMV [49], the TM protein of RD114 [39], or the accessory protein Nef of HIV-1 [50]. The PACS-2 FBR binds to COPI and controls the ER localization of polycystin-2 [53] and calnexin [54], and the cell surface exposition of the metalloproteinase ADAM17 [55], but also interacts with HIV-1 Nef to trigger MHC-1 down-regulation [40]. Importantly, acidic clusters often contain serine or threonine residues that can be phosphorylated by CK2 (casein kinase 2), which confer different subcellular distribution of the cargo proteins depending on their phosphorylated state.

Our results with mutations of AC motif in CCHFV Gn GP led us to hypothesize that PACS-1 or PACS-2 could be involved in CCHFV life cycle through recognition of the Gn AC motif. Yet, we did not observe any effect neither on tc-VLP nor on live CCHFV infectivity upon PACS-1 silencing, suggesting that PACS-1 is not a crucial cellular host factor involved in production of infectious CCHFV particles.

Importantly, PACS-2 down-regulation severely impaired Gn/Gc secretion and infectivity of tc-VLPs as well as CCHFV genome expression by virus-infected cells, confirming that PACS-2 is an important proviral factor acting at the assembly/secretion level. Since silencing of PACS-2 also impaired the formation of intracellular infectious tc-VLPs, these data suggested that PACS-2 acts at assembly steps rather than secretion of CCHFV particle. Interestingly, we also observed a defect in NP secretion upon PACS-2 down-regulation. Little is known about the ligands of PACS-2, but due to its high homology with PACS-1 [29], one can imagine that PACS-2 could link several proteins at the same time, alike PACS-1 that was shown to bind within same complexes CI-MPR, CK2 and GGA3 *via* different domains contained in the FBR region [56]. It is thus tempting to speculate that PACS-2 could bind Gn *via* its acidic cluster and NP *via* an unidentified domain. This tripartite association could then help the encountering of NP with Gn or with the Gn/Gc complex, or, alternatively, could allow the co-trafficking of CCHFV GPs and NP to the assembly site. The latter would explain why the mutation of the Gn AC affects only the secretion of Gn/Gc (Figure 8), while the absence of PACS-2 impairs the secretion of both Gn/Gc and NP. Finally, we found that the mutation of the AC motif in

CCHFV Gn GP or the depletion of PACS-2 impaired the trafficking of Gc GP through the Golgi and the colocalization of Gc and NP. Since PACS-2 has been shown to adapt AC-containing proteins to COPI [53], it is reasonable to hypothesize that PACS-2 connects Gn-Gc-NP complex to COPI along the retrograde pathway through the Golgi to ultimately reach the assembly site.

In conclusion, we show that various viral determinants on CCHFV GPs and the host factor PACS-2 can induce a stepwise CCHFV GPs assembly/incorporation, egress and secretion of infectious particles.

## Materials and methods

**Cell culture and reagents.** Huh-7.5 hepato-carcinoma (kind gift from C. Rice) and HEK 293 T kidney cells were grown in Dulbecco's modified Eagle's medium (DMEM) complemented with 10% fetal bovine serum (FBS) and 1% penicillin-streptomycin. All the cells were grown in a 37°C and 5% CO<sub>2</sub> incubator.

**Plasmids and constructs.** The constructs encoding wild-type CCHFV strain IbAr10200 L polymerase (pCAGGS-V5-L), CCHFV nucleoprotein NP (pCAGGS-NP), CCHFV specific eGFP-expressing minigenome (pT7RiboSM2\_vL\_eGFP), T7 RNA polymerase (pCAGGS-T7), CCHFV M-segment polyprotein (pCAGGS-GPC), and an empty vector without viral genes (pCAGGS) were described previously [30,36,57]. Several CCHFV M segment cDNA mutants were generated using standard molecular cloning techniques and confirmed by DNA sequencing. Standard PCR and oligonucleotide-specific mutagenesis reactions were carried out with Phusion enzyme (NEBio-labs). Cytoplasmic tail mutations in Gc or Gn were introduced in the context of expression of the whole GPC. By site-directed mutagenesis, Gc tyrosine motif mutant one Y1 (YRHL/ARHL) was created by changing the tyrosine to alanine. Gc tyrosine motif mutant two Y2 (YRRI/ARRI) was generated by changing tyrosine to alanine. Gc dileucine motif (LL/AA) mutant was generated by mutagenesis. Acidic motif mutations were created (DDEE/NNQQ). ERR mutation in Gc cytoplasmic tail of GPC was generated by deletion of its last residues ( $\Delta$ KTHIG). The removal of the Gc cytoplasmic tail mutant was generated as described previously [58] for the Gc  $\Delta$ CT-expressing GPC plasmid ( $\Delta$ CT). Similarly, by using site-directed mutagenesis, Gn tyrosine motif mutant one Y1 (YREL/AREL) was created by changing the tyrosine to alanine. Gn tyrosine motif mutant two Y2 (YLNL/ALNL) was generated by changing tyrosine to alanine. Gn dileucine motif (LL/AA) mutant was generated by mutagenesis. Acidic motif mutations in Gn were created (EKVEETE/QKVQQTQ). Details of oligonucleotides used for the constructs are available upon request. The pCAG-PACS-2-HA construct was

derived from pcDNA-PACS-2-HA (kind gift of G. Thomas) [53]. Briefly, the hCMV promoter of pcDNA-PACS-2-HA was exchanged by the CAG promoter of pCAGGS-NP construct via SnaBI/EcoRI restriction and ligation following classical cloning strategy.

**Antibodies.** Anti-PreGc (clone 11E7) and anti-NP (clones 9D5 for Western blot analysis and 2B11 for immunofluorescence analysis) mouse monoclonal antibodies targeting CCHFV were received from the Joel M. Dalrymple-Clarence J. Peters USAMRIID Antibody Collection through BEI Resources, NIAID, NIH. Anti-Gn rabbit polyclonal antibody was kindly given by Ali Mirazimi (Karolinska Institute, Sweden). Monoclonal mouse anti- $\beta$ -actin AC-74 (Sigma), anti-HA (3F10, Sigma), anti-PACS-1 (A12659, Abclonal), anti-PACS-2 (ab222316, Abcam) were used at 1/1,000 for Western blotting. Anti-GM130 (ab52649, Abcam), anti-Rab5 (C8B1, Cell Signaling) and anti-Rab7 (D95F2, Cell Signaling) were used at 1/200 for immunofluorescence. All the antibodies were used according to the manufacturer's guidelines.

**Production and titration of full-length CCHFV particles.** To generate a titrated stock of live CCHFV, Huh-7.5 cells were infected in the BSL-4 laboratory (Jean Mérieux, Lyon) using CCHFV isolate IbAr10200 (obtained from Institut Pasteur) at a multiplicity of infection (MOI) of 0.01 and the production was harvested 24 h post-infection. Infectious titre was determined by NP immunostaining on VeroE6 cells.

At 24 h post-infection of Huh-7.5 cells WT or KD for PACS-1 or PACS-2 (see below) at MOI = 0.01 with this reference stock, cells and supernatants were harvested and lysed with TriReagent (Molecular Research Center, Inc. Cat. No. TR118). RNAs were extracted according to the manufacturer's protocol and level of viral RNA was determined by RT-qPCR (see below).

**Knockdown of PACS-1 and PACS-2.** Expression of specific shRNAs AGATCTGTTCAGTCGCTC through a lentiviral vector induced the PACS-1 down-regulation in producer cells [39]. Two PACS-2 shRNAs were ordered from SIGMA-ALDRICH, ref sequence NM\_015197, TRCN000135103 (sh103) (target sequence: CACCAAGGAGAAGAACAAGAA) and TRCN000137443 (sh433) (target sequence: GACCAGGCAACAGAACTTCAA). To package shRNA-expressing lentiviral vectors, HEK293 T cells were seeded in 10-cm plates and were transfected with 8  $\mu$ g of the FG12 GFP/shRNA construct or pLKO PACS-2 construct, 8  $\mu$ g of the HIV packaging construct psPAX2, and 2.7  $\mu$ g of the VSV-G glycoprotein construct phCMV-G. The vector particles were collected 48 h post-transfection by 0.45  $\mu$ m filters and aliquots were kept at  $-80^{\circ}\text{C}$  for further use. The infectious titres were determined on 293 T cells by FACS or VCN analysis. To downregulate

PACS-1 and PACS-2 in Huh7.5 cells, the shRNA lentiviral vectors were used at a MOI of 10. For PACS-1 knockdown, two days after transduction, the transduced Huh7.5 cells were seeded in 10-cm plates and transfected 24 h post-seeding with plasmids allowing production of WT tc-VLPs to perform biochemical assay either in control or knockdown cells. Similarly, for PACS-2 knockdown, 7 days after transduction, cells were used for further transfections to generate WT tc-VLPs in knockdown or control cells to perform biochemical assays. In parallel, a lentiviral vector without shRNA was used as a control. The knockdown of endogenous PACS-1 and PACS-2 was validated by immunoblotting.

For full-length virus, Huh-7.5 cells were infected after 2 days of transduction for PACS-1 or 7 days of transduction of PACS-2.

**Production of tc-VLPs.** Huh7.5 cells were seeded in 10 cm dishes and transfected with 3.6  $\mu$ g of pCAGGS-V5-L, 1.2  $\mu$ g of pCAGGS-NP, 1.2  $\mu$ g of pT7riboSM2-vS-GFP, 3  $\mu$ g of pCAGGS-GP, 3  $\mu$ g of pCAGGS-T7 by using GeneJammer transfection reagent (Agilent), as previously described [30,36]. pCAGGS plasmid was additionally transfected to keep the DNA amount uniform. For PACS-2 over-expression experiments, increasing amount of pCAG-PACS-2-HA construct, complemented or not with pCAGGS plasmid to achieve a total of 8  $\mu$ g DNA, were added to the above DNA mix prior to the transfection. The transfection media was replaced after 6 h post-transfection. Cells supernatants were harvested 72 h post-transfection and filtered through a 0.45  $\mu$ m filters and concentrated through ultracentrifugation through a 20% sucrose cushion (SW41 rotor at 28,000 rpm, 2 h,  $4^{\circ}\text{C}$ ).

**Intracellular and extracellular infectivity of tc-VLPs.** Infectivity was analysed infection of pre-transfected Huh7.5 cells expressing L and NP plasmid on Huh7.5 cells. For titration, Huh-7.5 cells were pre-transfected with 2.4  $\mu$ g of pCAGGS-V5-L and 4.8  $\mu$ g of pCAGGS-NP using GeneJammer transfection reagent. The transfection medium was replaced at 6 h post-transfection and cells were seeded in 24-well plates in DMEM. Twenty-four hours post pre-transfection, cells were infected, as previously described [30,36]. Intracellular tc-VLP particles were released upon producer cells lysis by three repeated freeze-thaw cycles, followed by clarification by centrifugation. At 24 h post-infection, the infectivity was analysed by flow cytometry (FACS) using a MACSQuant (Miltenyi Biotec) VYB apparatus. Data were then analysed using the FlowJo software. Titres were calculated according to the formula (number of seeded Huh7.5 cells  $\times$  % of GFP-positive cells)  $\times$  1000/ $\mu$ l of inoculum and expressed as infectious units per ml of supernatant (extracellular infectivity) or cell lysate (intracellular infectivity).

**RNA extraction and RT-qPCR analysis.** Viral RNAs were extracted either from infected cell (intracellular) or from the supernatant (extracellular) using TRI Reagent according to the manufacturer's instructions (Molecular Research Center). RNAs were reverse transcribed using random oligonucleotide primers with iScript (Bio-Rad). The following specific primers against S segment were used: for CCHFV RNA quantification, forward primer 5' - TGTTCCTCCACCAGAGCA and reverse primer 5'-TTCCAAATGGCCAGTGCC [59]. Quantitative PCR (qPCR) was performed using FastStart Universal SYBR Green Master (Roche) on a StepOne Real-Time PCR System (Applied Biosystems). As an internal control of extraction, in vitro-transcribed exogenous RNAs from the linearized Triplescript plasmid pTRI-Xef (Invitrogen) were added to the samples prior to RNA extraction and quantified with specific primers (5'-CGACGTTGTACCGGGCAGC and 5'-ACCAGGCATGGTGGTTACCTTTC). All values of intracellular CCHFV RNAs were normalized to glyceraldehyde 3-phosphate dehydrogenase (GAPDH) gene transcription. For GAPDH mRNA quantification, we used the forward 5'-AGGTGAAGGTCGGAGTCAACG and reverse 5'-TGGAAGATGGTGATGGATTTC primers. All extracellular CCHFV RNAs were normalized to XEF signals.

**Western blot analysis.** Huh7.5 transfected cells were washed with cold PBS and detached with Versene (Gibco). Cells were lysed in cell lysate buffer (20 mM Tris pH 7.5, 1% Triton, SDS 0.05%, sodium Deoxycholate Acid 0.5% and 150 mM NaCl) containing protease inhibitors (Roche). Cell lysates were clarified by centrifugation at 13,000 rpm for 30 min at 4°C. Pellets from ultracentrifuged supernatants were resuspended in Gibco Opti-MEM medium in 1/100 of the initial volumes. To detect the expression of NP, GC, Gn, PACS-1, PACS-2 and Actin, samples were denatured at 95°C for 5 min in reducing loading buffer (5X Blue Loading Buffer, 200 mM Tris HCl pH6.8, 10% SDS, 500 mM  $\beta$ -mercaptoethanol and 50% glycerol) and electrophoresed on 10% polyacrylamide gels. Alternatively, for detection of Gc, samples were processed in a non-reducing loading buffer (5X Blue Loading Buffer, 200 mM Tris HCl pH6.8, 5% SDS, and 50% glycerol) and electrophoresed on 10% polyacrylamide gels. Proteins were transferred to a nitrocellulose membrane by electro blotting (Bio-Rad) for 1 h at 100 V. The membrane was incubated in TBST (20 mM Tris HCl, pH 7.5, 150 mM NaCl and Tween 0.05%)-milk 5% for 1 h. Nitrocellulose membranes were incubated overnight at 4°C with primary antibodies for the detection of CCHFV protein (mouse monoclonal 9D5 anti-NP (1:1,000), mouse monoclonal 11E7 anti-Gc (1:500) and rabbit polyclonal anti-Gn (1:5,000)) diluted in TBST-milk 5%. After 3 washes using TBST, then membranes were

incubated with immunofluorophore-labelled secondary antibodies (LiCor Biosciences) at 1:10000 dilution in TBST for 1 h at room temperature, followed by imaging with Odyssey infrared imaging CLx system (LiCor Biosciences). Quantification of proteins was performed with Odyssey imaging CLx system software.

**Immunofluorescence analysis.** The procedure was described previously [60]. Briefly, Huh7.5 cells were seeded in 6-well plates on coverslips and transfected with the plasmids described above. The transfection media was replaced after 6 h post-transfection and infected with WT tc-VLPs at 24 h post-transfection. Forty-eight hours post-transfection, the cells were fixed with 4% paraformaldehyde (PFA) for 15 min at room temperature. Next, unless otherwise specified, the cells were permeabilized with 0.1% Triton X-100 for 7 min. Cells were washed 3 times with PBS and incubated for 1 h at room temperature with primary antibodies diluted in PBS/1% BSA. After 3 washes with PBS/1% BSA, cells were further incubated with Alexa Fluor-conjugated secondary antibodies (Alexa Fluor 568 and Alexa Fluor 647; Thermo Fisher) in PBS/1% BSA. After 3 washes with PBS, nuclei were stained with Hoechst 33342 (Molecular Probes), and the coverslips were mounted with Mowiol 40-88 (Sigma-Aldrich). The slides were examined using a confocal microscope LSM-800 (Zeiss). Pearson's correlation coefficients were calculated using FIJI (JACoP) and were calculated on *n* cells from 3 separate experiments and expressed as mean  $\pm$  SEM.

**Statistical analysis.** All the statistical analysis were performed using GraphPad Prism version 5.02 for Windows or Mac, GraphPad Software (San Diego, California, USA). For statistical comparisons, the Mann-Whitney or the student-t test were used. For statistical analysis, a *p*-value of 0.05 or less was considered significant. Data are presented as mean  $\pm$  standard error of the mean (SEM), and results of the statistical analysis are shown as follows: ns, not significant ( $P > 0.05$ ); \*,  $P < 0.05$ ; \*\*,  $P < 0.01$ ; and \*\*\*,  $P < 0.001$ .

## Acknowledgment

We thank Solène Denolly for critical reading of the manuscript and advises on the study. We are grateful to Charles Rice for the Huh7.5 cells, Friedmann Weber and Eric Bergeron for the tc-VLP constructs, Gary Thomas for the PACS-2 expressing construct, and Ali Mirazimi for the Gn antibody. We thank Emily Sible for helpful discussions. We acknowledge the contribution of SFR Biosciences (Université Claude Bernard Lyon 1, CNRS UAR3444, Inserm US8, ENS de Lyon): LYMIC-PLATIM-microscopie, especially Jacques Brocard, AniRA-Cytométrie and AniRA vectorology, especially Caroline Costa. We are grateful to P4 Jean Mérieux team (INSERM US03, Lyon) and the related biosafety team for their assistance for BSL4 activities, technical support, biosafety, biosecurity and for providing live CCHFV.

## Disclosure statement

No potential conflict of interest was reported by the author(s).

## Funding

This work was supported by the LabEx Ecofect (ANR-11-LABX-0048) of the “Université de Lyon”, within the program “Investissements d’Avenir” (ANR-11-IDEX-0007) operated by the French National Research Agency (ANR), the Fondation pour la Recherche Médicale (grant number: EQU202203014673 awarded to F-LC), the Agence Nationale de Recherches sur le Sida et les Hépatites Virales (ANRS/MIE [grant number: ANRS0630] awarded to F-LC), and the ANR (grant number: ANR-22-ASTR-0031 awarded to F-LC). A.G. and N.F. were supported by fellowships of the ANRS/MIE. S.L. was supported by a fellowship of the Fondation pour la Recherche Médicale. M.R. was supported by a fellowship of the LabEx Ecofect.

## Author contributions

Conceptualization, A.G., N.F., F.-L.C. and B.B.; Investigation, A.G., A.L., M.R., N.F., S.L., L.C., F.A., V.L., C.M., B.B.; Writing Original-Draft, A.G., F.-L.C. and B.B.; Supervision, F.-L.C. and B.B.; Funding Acquisition, V.L., F.L.C. and B.B.

## ORCID

Anupriya Gautam  <http://orcid.org/0000-0003-4358-8716>  
 Alexandre Lalande  <http://orcid.org/0000-0003-3917-1598>  
 Maureen Ritter  <http://orcid.org/0009-0002-7069-7790>  
 Solène Lerolle  <http://orcid.org/0000-0002-2859-4002>  
 Vincent Legros  <http://orcid.org/0000-0002-6118-7564>  
 François-Loïc Cosset  <http://orcid.org/0000-0001-8842-3726>  
 Cyrille Mathieu  <http://orcid.org/0000-0002-6682-2029>  
 Bertrand Boson  <http://orcid.org/0000-0003-1920-5172>

## References

- [1] Hoogstraal H. The epidemiology of tick-borne Crimean-Congo hemorrhagic fever in Asia, Europe, and Africa. *J Med Entomol.* 1979 May 22;15(4):307–417. doi:10.1093/jmedent/15.4.307
- [2] Simpson DI, Knight EM, Courtois G, et al. Congo virus: a hitherto undescribed virus occurring in Africa. I. Human isolations—clinical notes. *East Afr Med J.* 1967 Feb;44(2):86–92.
- [3] Messina JP, Pigott DM, Golding N, et al. The global distribution of Crimean-Congo hemorrhagic fever. *Trans R Soc Trop Med Hyg.* 2015 Aug;109(8):503–513. doi:10.1093/trstmh/trv050
- [4] Freitas N, Legros V, Cosset FL. Crimean-Congo hemorrhagic fever: a growing threat to Europe. *C R Biol.* 2022 May 11;345(1):17–36. doi:10.5802/crbio.78
- [5] Bernard C, Joly Kukla C, Rakotoarivony I, et al. Detection of Crimean-Congo haemorrhagic fever virus in *Hyalomma marginatum* ticks, southern France, May 2022 and April 2023. *Euro Surveill.* 2024 Feb;29(6):2400023. doi:10.2807/1560-7917.ES.2024.29.6.2400023
- [6] Gargili A, Estrada-Pena A, Spengler JR, et al. The role of ticks in the maintenance and transmission of Crimean-Congo hemorrhagic fever virus: A review of published field and laboratory studies. *Antiviral Res.* 2017 Aug;144:93–119. doi:10.1016/j.antiviral.2017.05.010
- [7] Spengler JR, Bergeron E, Rollin PE. Seroepidemiological Studies of Crimean-Congo Hemorrhagic Fever Virus in Domestic and Wild Animals. *PLoS Negl Trop Dis.* 2016 Jan;10(1):e0004210. doi:10.1371/journal.pntd.0004210
- [8] Altamura LA, Bertolotti-Ciarlet A, Teigler J, et al. Identification of a novel C-terminal cleavage of Crimean-Congo hemorrhagic fever virus PreGN that leads to generation of an NSM protein. *J Virol.* 2007 Jun;81(12):6632–6642. doi:10.1128/JVI.02730-06
- [9] Sanchez AJ, Vincent MJ, Nichol ST. Characterization of the glycoproteins of Crimean-Congo hemorrhagic fever virus. *J Virol.* 2002 Jul;76(14):7263–7275. doi:10.1128/JVI.76.14.7263-7275.2002
- [10] Vincent MJ, Sanchez AJ, Erickson BR, et al. Crimean-Congo Hemorrhagic Fever Virus Glycoprotein Proteolytic Processing by Subtilase SKI-1. *J Virol.* 2003 Aug;77(16):8640–8649.
- [11] Du S, Peng R, Xu W, et al. Cryo-EM structure of severe fever with thrombocytopenia syndrome virus. *Nat Commun.* 2023 Oct 10;14(1):6333. doi:10.1038/s41467-023-41804-7
- [12] Hover S, Charlton FW, Hellert J, et al. Organisation of the orthobunyavirus tripodal spike and the structural changes induced by low pH and K(+) during entry. *Nat Commun.* 2023 Sep 21;14(1):5885. doi:10.1038/s41467-023-41205-w
- [13] Spiegel M, Plegge T, Pohlmann S. The Role of Phlebovirus Glycoproteins in Viral Entry, Assembly and Release. *Viruses.* 2016 Jul 21;8(7):202. doi:10.3390/v8070202
- [14] Cole NB, Lippincott-Schwartz J. Organization of organelles and membrane traffic by microtubules. *Curr Opin Cell Biol.* 1995 Feb;7(1):55–64. doi:10.1016/0955-0674(95)80045-X
- [15] Schafer W, Stroth A, Berghofer S, et al. Two independent targeting signals in the cytoplasmic domain determine trans-Golgi network localization and endosomal trafficking of the proprotein convertase furin. *EMBO J.* 1995 Jun 1;14(11):2424–2435. doi:10.1002/j.1460-2075.1995.tb07240.x
- [16] Schekman R, Orci L. Coat proteins and vesicle budding. *Science.* 1996 Mar 15;271(5255):1526–1533. doi:10.1126/science.271.5255.1526
- [17] Beitia Ortiz de Zarate I, Kaelin K, Rozenberg F. Effects of mutations in the cytoplasmic domain of herpes simplex virus type 1 glycoprotein B on intracellular transport and infectivity. *J Virol.* 2004 Feb;78(3):1540–1551. doi:10.1128/JVI.78.3.1540-1551.2004
- [18] Byland R, Vance PJ, Hoxie JA, et al. A conserved dileucine motif mediates clathrin and AP-2-dependent endocytosis of the HIV-1 envelope protein. *Mol Biol Cell.* 2007 Feb;18(2):414–425. doi:10.1091/mbc.e06-06-0535
- [19] Lontok E, Corse E, Machamer CE. Intracellular targeting signals contribute to localization of coronavirus spike proteins near the virus assembly site. *J Virol.* 2004 Jun;78(11):5913–5922. doi:10.1128/JVI.78.11.5913-5922.2004
- [20] Strandin T, Hepojoki J, Vaheri A. Cytoplasmic tails of bunyavirus Gn glycoproteins—Could they act as matrix protein surrogates? *Virology.* 2013;437:73–80. doi:10.1016/j.virol.2013.01.001



- [21] Overby AK, Popov VL, Pettersson RF, et al. The cytoplasmic tails of Uukuniemi Virus (Bunyaviridae) G(N) and G(C) glycoproteins are important for intracellular targeting and the budding of virus-like particles. *J Virol.* 2007 Oct;81(20):11381–11391. doi:10.1128/JVI.00767-07
- [22] Haferkamp S, Fernando L, Schwarz TF, et al. Intracellular localization of Crimean-Congo Hemorrhagic Fever (CCHF) virus glycoproteins. *Virology.* 2005 Apr 25;252:42. doi:10.1186/1743-422X-2-42
- [23] Estrada DF, Boudreaux DM, Zhong D, et al. The Hantavirus Glycoprotein G1 Tail Contains Dual CCHC-type Classical Zinc Fingers. *J Biol Chem.* 2009 Mar 27;284(13):8654–8660. doi:10.1074/jbc.M808081200
- [24] Mishra AK, Hellert J, Freitas N, et al. Structural basis of synergistic neutralization of Crimean-Congo hemorrhagic fever virus by human antibodies. *Science.* 2022 Jan 7;375(6576):104–109. doi:10.1126/science.abc6502
- [25] Guardado-Calvo P, Rey FA. The Viral Class II Membrane Fusion Machinery: Divergent Evolution from an Ancestral Heterodimer. *Viruses.* 2021 Nov 26;13(12):2368. doi:10.3390/v13122368
- [26] Rapoport I, Chen YC, Cupers P, et al. Dileucine-based sorting signals bind to the beta chain of AP-1 at a site distinct and regulated differently from the tyrosine-based motif-binding site. *EMBO J.* 1998 Apr 15;17(8):2148–2155. doi:10.1093/emboj/17.8.2148
- [27] Rohn WM, Rouille Y, Waguri S, et al. Bi-directional trafficking between the trans-Golgi network and the endosomal/lysosomal system. *J Cell Sci.* 2000 Jun;113(Pt 12):2093–2101. doi:10.1242/jcs.113.12.2093
- [28] Ma W, Goldberg J. Rules for the recognition of dileucine retrieval motifs by coatomer. *EMBO J.* 2013;32:926–937. doi:10.1038/emboj.2013.41
- [29] Thomas G, Aslan JE, Thomas L, et al. Caught in the act - protein adaptation and the expanding roles of the PACS proteins in tissue homeostasis and disease. *J Cell Sci.* 2017 Jun 1;130(11):1865–1876.
- [30] Devignot S, Bergeron E, Nichol S, et al. A virus-like particle system identifies the endonuclease domain of Crimean-Congo hemorrhagic fever virus. *J Virol.* 2015 Jun;89(11):5957–5967. doi:10.1128/JVI.03691-14
- [31] Zivcec M, Scholte FE, Spiropoulou CF, et al. Molecular Insights into Crimean-Congo Hemorrhagic Fever Virus. *Viruses.* 2016 Apr 21;8(4):106. doi:10.3390/v8040106
- [32] Dell'Angelica EC, Bonifacino JS. Coatopathies: Genetic Disorders of Protein Coats. *Annu Rev Cell Dev Biol.* 2019 Oct 6;35:131–168. doi:10.1146/annurev-cellbio-100818-125234
- [33] Bonifacino JS, Traub LM. Signals for sorting of transmembrane proteins to endosomes and lysosomes. *Annu Rev Biochem.* 2003;72:395–447. doi:10.1146/annurev.biochem.72.121801.161800
- [34] Voorhees P, Deignan E, Van Donselaar E, et al. An acidic sequence within the cytoplasmic domain of furin functions as a determinant of trans-Golgi network localization and internalization from the cell surface. *EMBO J.* 1995;14:4961–4975. doi:10.1002/j.1460-2075.1995.tb00179.x
- [35] Lontok E, Corse E, Machamer CE. Intracellular Targeting Signals Contribute to Localization of Coronavirus Spike Proteins near the Virus Assembly Site. *J Virol.* 2004;78:5913–5922. doi:10.1128/JVI.78.11.5913-5922.2004
- [36] Freitas N, Enguehard M, Denolly S, et al. The interplays between Crimean-Congo hemorrhagic fever virus (CCHFV) M segment-encoded accessory proteins and structural proteins promote virus assembly and infectivity. *PLoS Pathog.* 2020 Sep;16(9):e1008850. doi:10.1371/journal.ppat.1008850
- [37] Maxfield FR, McGraw TE. Endocytic recycling. *Nat Rev Mol Cell Biol.* 2004 Feb;5(2):121–132. doi:10.1038/nrm1315
- [38] Bertolotti-Ciarlet A, Smith J, Strecker K, et al. Cellular localization and antigenic characterization of crimean-congo hemorrhagic fever virus glycoproteins. *J Virol.* 2005 May;79(10):6152–6161. doi:10.1128/JVI.79.10.6152-6161.2005
- [39] Bouard D, Sandrin V, Boson B, et al. An Acidic Cluster of the Cytoplasmic Tail of the RD114 Virus Glycoprotein Controls Assembly of Retroviral Envelopes. *Traffic (Copenhagen, Denmark).* 2007;8:835–847. doi:10.1111/j.1600-0854.2007.00581.x
- [40] Atkins KM, Thomas L, Youker RT, et al. HIV-1 Nef binds PACS-2 to assemble a multikinase cascade that triggers major histocompatibility complex class I (MHC-I) down-regulation: analysis using short interfering RNA and knock-out mice. *J Biol Chem.* 2008 Apr 25;283(17):11772–11784. doi:10.1074/jbc.M707572200
- [41] Cendron L, Rothenberger S, Cassari L, et al. Proprotein convertases regulate trafficking and maturation of key proteins within the secretory pathway. *Adv Protein Chem Struct Biol.* 2023;133:1–54. doi:10.1016/bs.apcsb.2022.10.001
- [42] Andersson C, Henriksson S, Magnusson KE, et al. In situ rolling circle amplification detection of Crimean Congo hemorrhagic fever virus (CCHFV) complementary and viral RNA. *Virology.* 2012;426:87–92. doi:10.1016/j.virol.2012.01.032
- [43] Ujike M, Taguchi F. Incorporation of spike and membrane glycoproteins into coronavirus virions. *Viruses.* 2015;7:1700–1725. doi:10.3390/v7041700
- [44] Trowbridge IS, Collawn JF, Hopkins CR. Signal-Dependent Membrane Protein Trafficking in the Endocytic Pathway. *Annu Rev Cell Biol.* 1993;9:129–161. doi:10.1146/annurev.cb.09.110193.001021
- [45] Marks MS, Roche PA, Van Donselaar E, et al. A lysosomal targeting signal in the cytoplasmic tail of the  $\beta$  chain directs HLA-DM to MHC class II compartments. *J Cell Biol.* 1995;131:351–369. doi:10.1083/jcb.131.2.351
- [46] Jackson MR, Nilsson T, Peterson PA. Retrieval of transmembrane proteins to the endoplasmic reticulum. *J Cell Biol.* 1993;121:317–333. doi:10.1083/jcb.121.2.317
- [47] Bos K, Wraight C, Stanley KK. TGN38 is maintained in the trans-Golgi network by a tyrosine-containing motif in the cytoplasmic domain. *EMBO J.* 1993;12:2219–2228. doi:10.1002/j.1460-2075.1993.tb05870.x
- [48] Mansouri M, Douglas J, Rose PP, et al. Kaposi sarcoma herpesvirus K5 removes CD31/PECAM from endothelial cells. *Blood.* 2006 Sep 15;108(6):1932–1940. doi:10.1182/blood-2005-11-4404
- [49] Tugizov S, Maidji E, Xiao J, et al. An Acidic Cluster in the Cytosolic Domain of Human Cytomegalovirus Glycoprotein B Is a Signal for Endocytosis from the Plasma Membrane. *J Virol.* 1999;73:8677–8688. doi:10.1128/JVI.73.10.8677-8688.1999

- [50] Piguet V, Wan L, Borel C, et al. HIV-1 Nef protein binds to the cellular protein PACS-1 to downregulate class I major histocompatibility complexes. *Nat Cell Biol.* 2000 Mar;2(3):163–167. doi:10.1038/35004038
- [51] Crump CM, Xiang Y, Thomas L, et al. PACS-1 binding to adaptors is required for acidic cluster motif-mediated protein traffic. *EMBO J.* 2001 May 1;20(9):2191–2201. doi:10.1093/emboj/20.9.2191
- [52] Wan L, Molloy SS, Thomas L, et al. PACS-1 defines a novel gene family of cytosolic sorting proteins required for trans-Golgi network localization. *Cell.* 1998 Jul 24;94(2):205–216. doi:10.1016/S0092-8674(00)81420-8
- [53] Kottgen M, Benzing T, Simmen T, et al. Trafficking of TRPP2 by PACS proteins represents a novel mechanism of ion channel regulation. *EMBO J.* 2005 Feb 23;24(4):705–716. doi:10.1038/sj.emboj.7600566
- [54] Myhill N, Lynes EM, Nanji JA, et al. The subcellular distribution of calnexin is mediated by PACS-2. *Mol Biol Cell.* 2008 Jul;19(7):2777–2788. doi:10.1091/mbc.e07-10-0995
- [55] Dombrowsky SL, Samsøe-Petersen J, Petersen CH, et al. The sorting protein PACS-2 promotes ErbB signalling by regulating recycling of the metalloproteinase ADAM17. *Nat Commun.* 2015 Jun 25;6:7518. doi:10.1038/ncomms8518
- [56] Scott GK, Fei H, Thomas L, et al. A PACS-1, GGA3 and CK2 complex regulates CI-MPR trafficking. *EMBO J.* 2006 Oct 4;25(19):4423–4435. doi:10.1038/sj.emboj.7601336
- [57] Bergeron E, Albarino CG, Khristova ML, et al. Crimean-Congo hemorrhagic fever virus-encoded ovarian tumor protease activity is dispensable for virus RNA polymerase function. *J Virol.* 2010 Jan;84(1):216–226. doi:10.1128/JVI.01859-09
- [58] Suda Y, Fukushi S, Tani H, et al. Analysis of the entry mechanism of Crimean-Congo hemorrhagic fever virus, using a vesicular stomatitis virus pseudotyping system. *Arch Virol.* 2016 Jun;161(6):1447–1454. doi:10.1007/s00705-016-2803-1
- [59] Peyrefitte CN, Perret M, Garcia S, et al. Differential activation profiles of Crimean-Congo hemorrhagic fever virus- and Dugbe virus-infected antigen-presenting cells. *J Gen Virol.* 2010 Jan;91(Pt 1):189–198. doi:10.1099/vir.0.015701-0
- [60] Boson B, Mialon C, Schichl K, et al. Nup98 Is Subverted from Annulate Lamellae by Hepatitis C Virus Core Protein to Foster Viral Assembly. *mBio.* 2022 Apr 26;13(2):e0292321. doi:10.1128/mbio.02923-21

**The PACS-2 protein and trafficking motifs in CCHFV Gn and Gc cytoplasmic tails govern CCHFV assembly**

**Running title**

Viral and cellular determinants involved in CCHFV assembly

**Authors**

Anupriya Gautam<sup>1</sup>, Alexandre Lalande<sup>1,\*</sup>, Maureen Ritter<sup>1,\*</sup>, Natalia Freitas<sup>1,\*</sup>, Solène Lerolle<sup>1</sup>, Lola Canus<sup>1</sup>, Fouzia Amirache<sup>1</sup>, Vincent Lotteau<sup>2</sup>, Vincent Legros<sup>1,3</sup>, François-Loïc Cosset<sup>1,\*\*</sup>, Cyrille Mathieu<sup>1</sup>, and Bertrand Boson<sup>1</sup>

**Affiliations**

<sup>1</sup>CIRI – Centre International de Recherche en Infectiologie, Univ. Lyon, Université Claude Bernard Lyon 1, Inserm, U1111, CNRS, UMR5308 ENS de Lyon, F-69007, Lyon, France.

<sup>2</sup>Laboratory P4-Jean Mérieux, Inserm, Lyon, France.

<sup>3</sup>Campus vétérinaire de Lyon, VetAgro Sup, Université de Lyon, Marcy-l’Etoile, France.

\* equal contribution

\*\* Corresponding author

**Supplementary Figures**

### Supplementary Figure legends

**Supplementary Fig. 1. Trafficking motifs identified in CCHFV Gn and Gc cytosolic domains are highly conserved between CCHFV strains.** Various CCHFV isolates were retrieved from NCBI and a multiple sequence analysis done by Clustal Omega. **(A, B)** multiple alignment of Gc (A) and Gn (B) glycoproteins. The boxes refer to the motifs investigated in this study (see Fig. 1 and Fig. 3). **(C)** The table details the various CCHFV strains that were used for this multiple alignment analysis: gene bank number, strain, host, isolation.

**Supplementary Fig. 2. Deletion of Gc cytoplasmic tail and mutation of its first tyrosine motif increases Gc exposition at the plasma membrane.** **(A)** Confocal microscopy analysis of cell surface expression of Gc in Huh7.5 cells producing tc-VLPs encoding a GFP marker that were generated with WT GPC vs. GPC harboring Gc cytoplasmic tail mutants ( $\Delta$ CT, Y1, Y2, LL, AC, ERR). At 48h post-transfection, cells were fixed, left unpermeabilized (no Triton condition), and stained for Gc expression with 11E7 antibody. As positive control for Gc staining, one slide of Gc WT was permeabilized with Triton-X100 (Triton 0.1%). Yellow arrows point cell surface detection of Gc protein. **(B)** Huh7.5 cells were transfected with WT GPC vs. GPC harboring Gc cytoplasmic tail mutants. 48 hours post-transfection, cells were fixed and syncytia formation was revealed with May-Grunwald and Giemsa stains. Pictures were acquired with an epifluorescence microscope. Yellow arrows point cell examples of syncytia.

**Supplementary Fig. 3. PACS-2 down-regulation in tc-VLP-producing cells does not influence Gc intracellular localization at early and late endosomes.** Confocal microscopy analysis of Huh7.5 cells down-regulated for PACS-2 expression using two different ShRNA (Sh103 and Sh433) and producing tc-VLPs encoding a GFP marker that were generated with WT GPC. Forty-eight hours post-transfection, cells were fixed, permeabilized with Triton X-100, and stained for GFP (grey channel), Gc (11E7, red channel), nuclei (Hoechst, blue channel) and either early endosome (anti-Rab5, green channel) or late endosome (anti-Rab7, green channel), as indicated. Scale bars represent 10  $\mu$ m. Magnification of the squared areas is shown at the right side of each condition,

scale bars from squared area represent 2 $\mu$ m. Pearson's coefficients were calculated using FIJI (JACoP) and expressed as means  $\pm$  SEM.

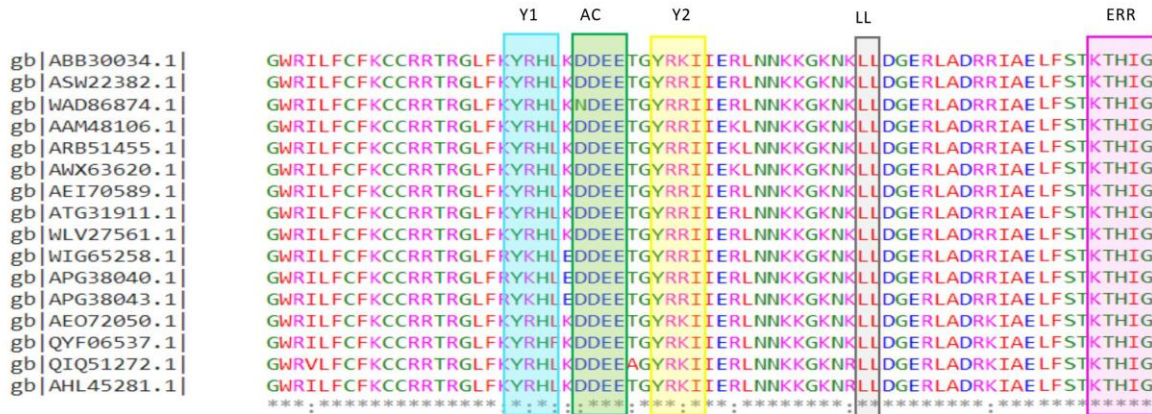
**Supplementary Fig. 4. Production of infectious CCHFV particles from cells overexpressing PACS-**

**2.** Huh7.5 were co-transfected with constructs necessary to produce tc-VLPs and with increasing amount of PACS-2 expressing construct (0, 4 or 8  $\mu$ g). **(A)** Representative Western blot analysis of HA (left panel) or PACS-2 (middle panel) and relative quantification of PACS-2 expressed as fold change compared to PACS-2 levels expressed in cells transfected with a control plasmid (0). **(B)** Infectivity titers of CCHFV tc-VLPs produced in excess of PACS-2. At 72h post-transfection, clarified supernatants and cell-associated tc-VLPs were used to infect Huh7.5 cells pre-transfected with L and NP expression vectors, and titers were determined by FACS analysis at 24h post-infection. **(C-E)** Intracellular levels and processing of CCHFV WT GPs in cells overexpressing PACS-2 compared to endogenous expression of PACS-2. Representative Western blot analysis and relative quantification of intracellular Gc, NP and Gn expressed compared to no overexpression of PACS-2 (0) (lower panels). Protein band intensities were quantified and normalized relative to actin and expressed as fold change compared to no overexpression of PACS-2 (lower panels). **(F-H)** tc-VLP containing cell supernatants were pelleted by ultracentrifugation through 20% sucrose cushions, resuspended in Opti-MEM medium and analyzed by Western blot. Representative Western blot analysis and relative quantification of Gc, NP and Gn expressed as fold change compared to no overexpression of PACS-2 (0) (lower panels).

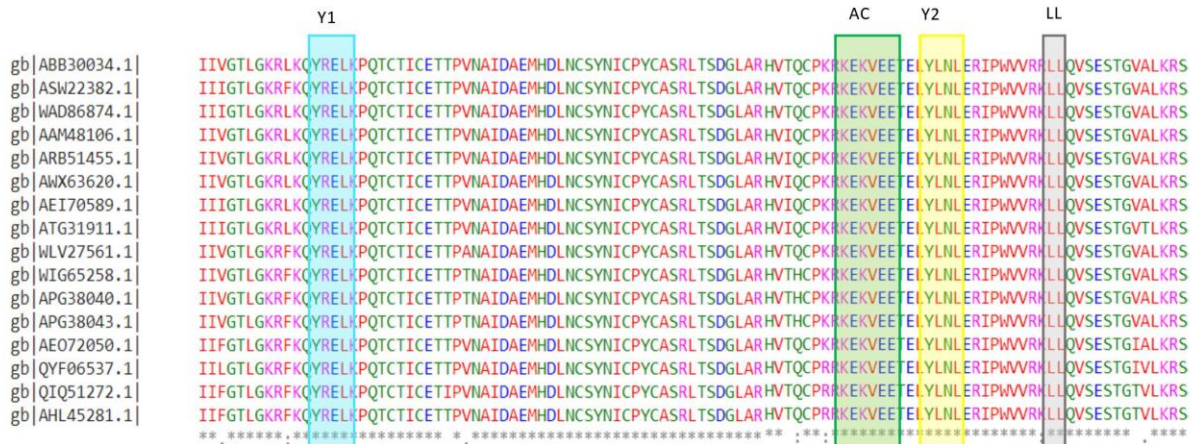
Molecular weight markers are marked to the left (kDa). Statistical significance was determined using parametric student-t test compared with WT proteins. The values are displayed as means  $\pm$  SEM. Each dot in the graphs corresponds to the value of an individual experiment and dots from one color are from the same experiment.

Supplementary Figure 1

A



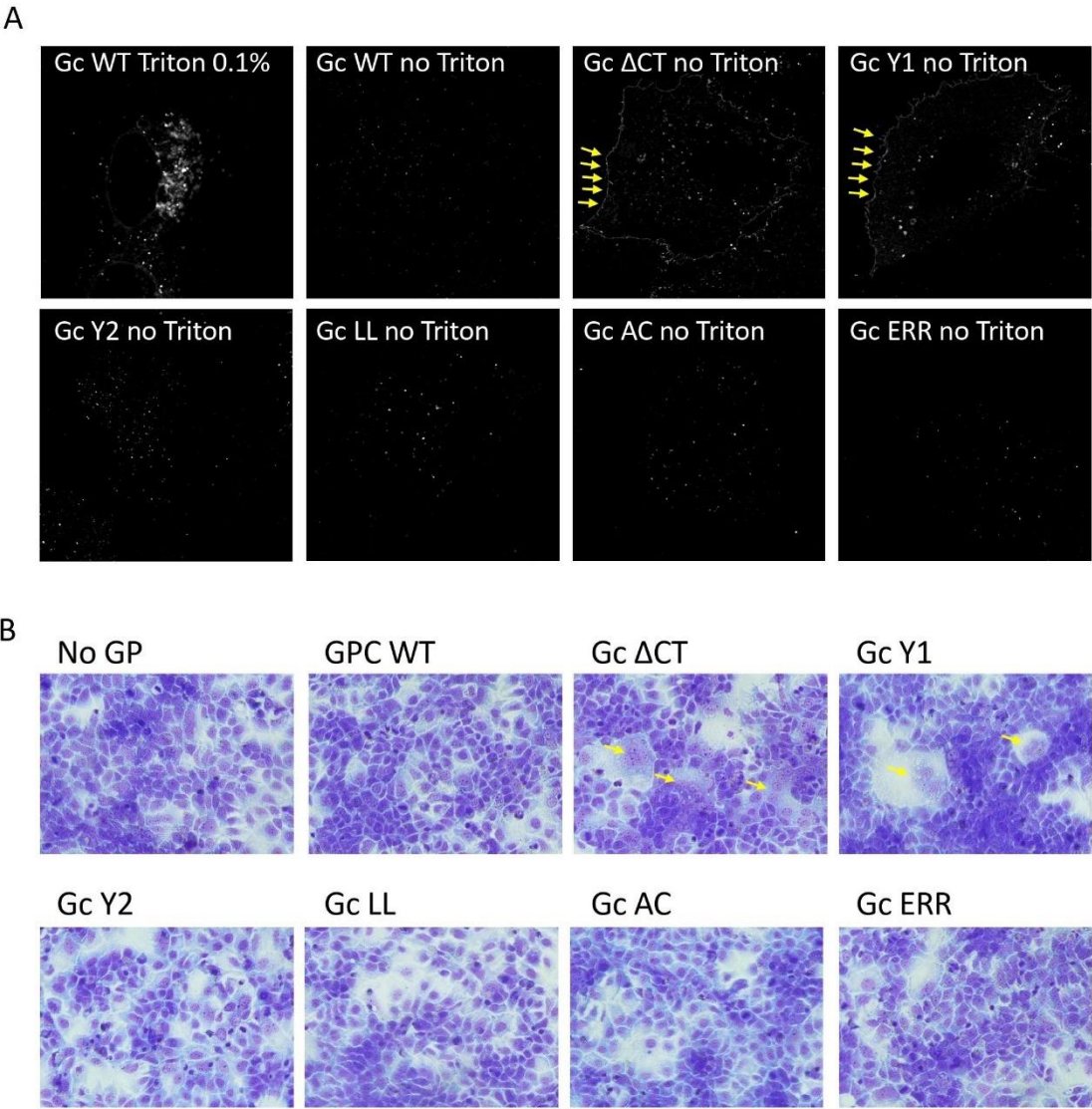
B



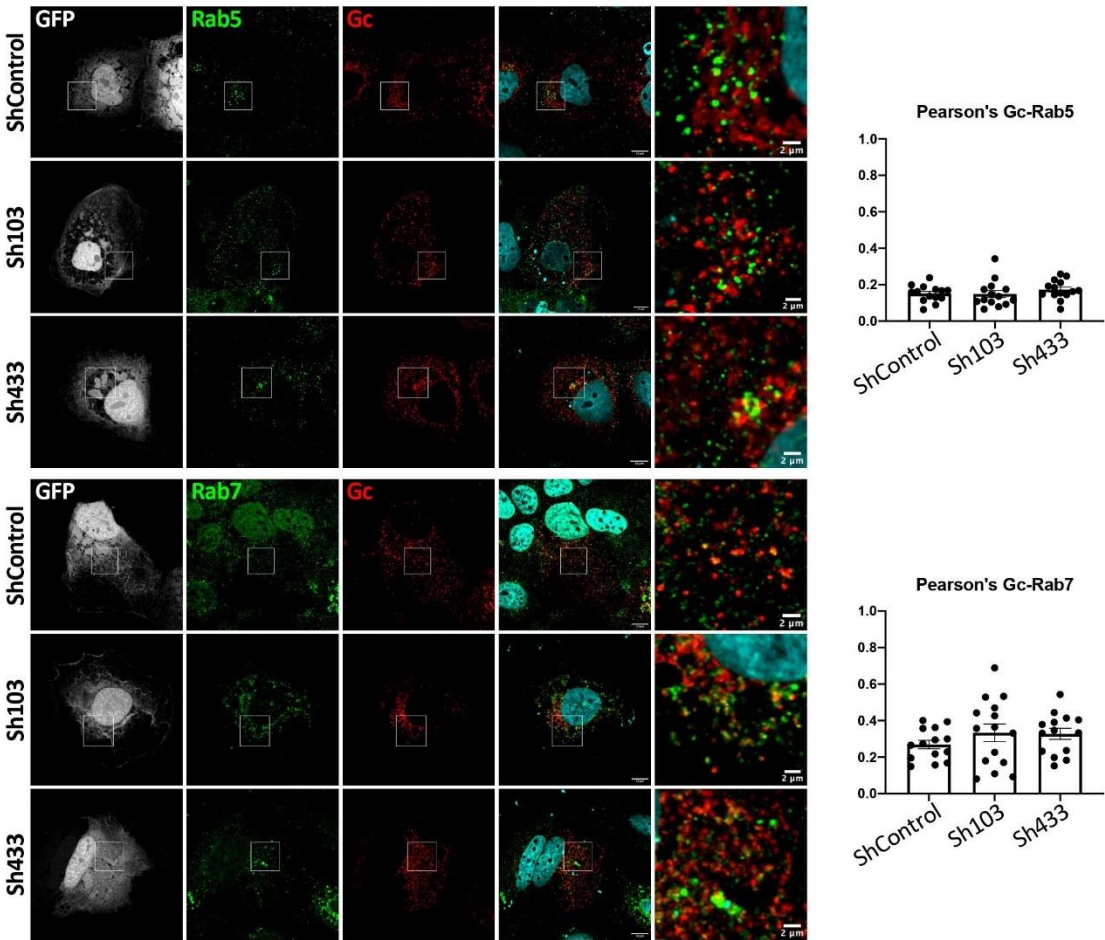
C

Genebank	strain	host	isolation
ABB30034.1	SPU103/87	Homo sapiens	
DQ211634.1	SPU134_87_813049_M	Homo sapiens	serum
WAD86874.1	Dakar8692	tick pool from ticks collected at an abattoir	
AAM48106.1	IbAr10200	Unknown tick	
ARB51455.1	IbAr10200:UCCR4401	tick	
AWX63620.1	10200	Homo sapiens	SW13 cell line
AEI70589.1	Sudan AB1-2009	Homo sapiens	sera
ATG31911.1	201643792, Spain	Homo sapiens	
WLV27561.1	BA68038	Homo sapiens	Suckling mouse brain
WIG65258.1	KAZ/18/2018	Homo sapiens	serum
APG38040.1	K168_40	tick	
APG38043.1	K168_125	tick	
AEO72050.1	NIV 112143,India	Homo sapiens	Vero E6
QYF06537.1	MCL-19-H-3154,India	Homo sapiens	
QIQ51272.1	61T/Pakistan		
AHL45281.1	Zahedan 2007, Iran		SW13 cells

Supplementary Figure 2

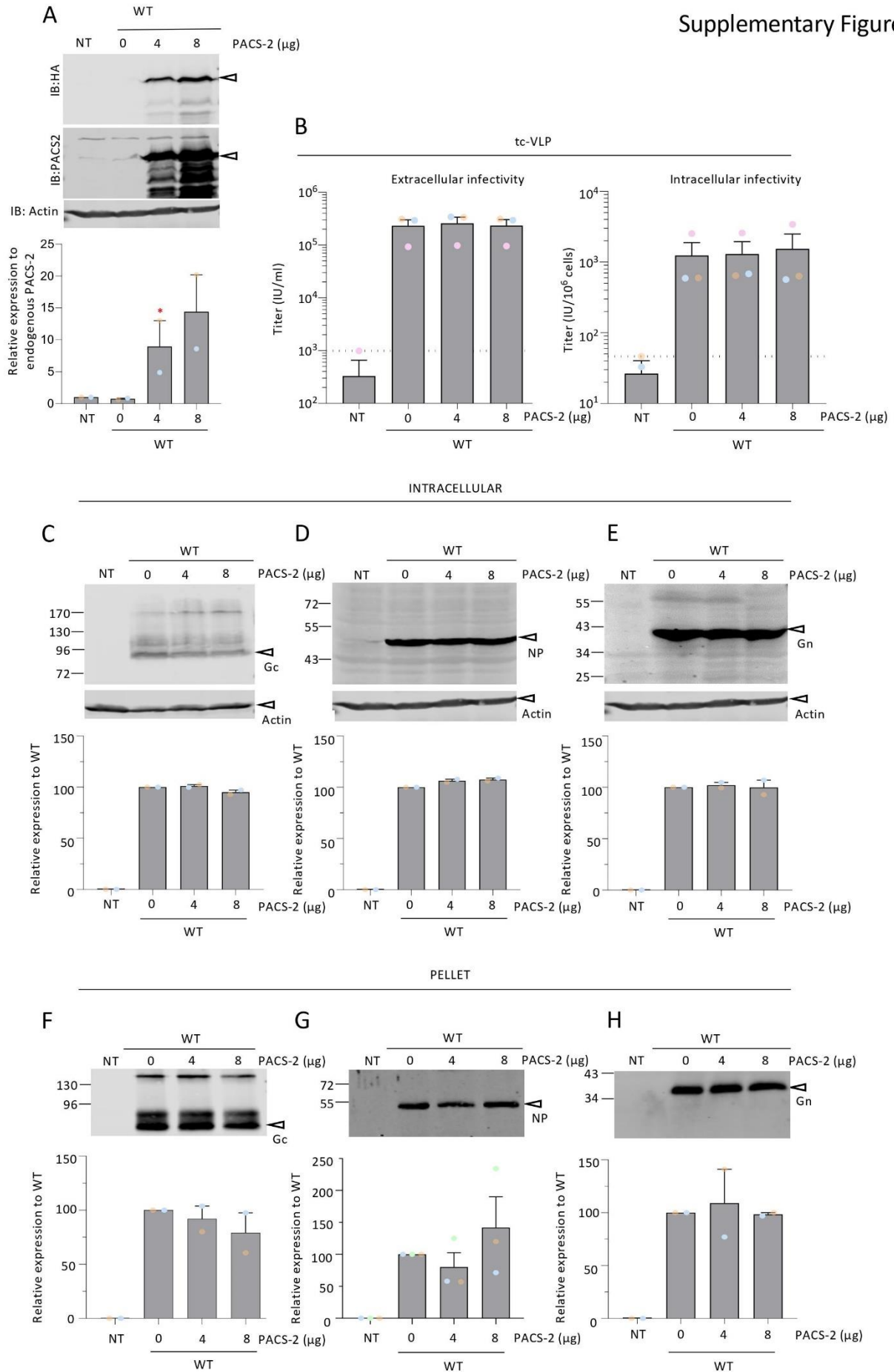


Supplementary Figure 3





Supplementary Figure 4





# The low-density lipoprotein receptor and apolipoprotein E associated with CCHFV particles mediate CCHFV entry into cells

Received: 24 October 2023

Accepted: 13 May 2024

Published online: 28 May 2024



Maureen Ritter<sup>1</sup>, Lola Canus<sup>1,7</sup>, Anupriya Gautam<sup>1,7</sup>, Thomas Vallet<sup>1,7</sup>, Li Zhong<sup>1,7</sup>, Alexandre Lalande<sup>1</sup>, Bertrand Bosen<sup>1</sup>, Apoorv Gandhi<sup>1</sup>, Sergueï Bodoirat<sup>1</sup>, Julien Burlaud-Gaillard<sup>2,3</sup>, Natalia Freitas<sup>1</sup>, Philippe Roingeard<sup>2,3</sup>, John N. Barr<sup>4</sup>, Vincent Lotteau<sup>5</sup>, Vincent Legros<sup>1,6</sup>, Cyrille Mathieu<sup>1</sup>, François-Loïc Cosset<sup>1,8</sup> ✉ & Solène Denolly<sup>1,8</sup> ✉

The Crimean-Congo hemorrhagic fever virus (CCHFV) is an emerging pathogen of the *Orthonairovirus* genus that can cause severe and often lethal hemorrhagic diseases in humans. CCHFV has a broad tropism and can infect a variety of species and tissues. Here, by using gene silencing, blocking antibodies or soluble receptor fragments, we identify the low-density lipoprotein receptor (LDL-R) as a CCHFV entry factor. The LDL-R facilitates binding of CCHFV particles but does not allow entry of Hazara virus (HAZV), another member of the genus. In addition, we show that apolipoprotein E (apoE), an exchangeable protein that mediates LDL/LDL-R interaction, is incorporated on CCHFV particles, though not on HAZV particles, and enhances their specific infectivity by promoting an LDL-R dependent entry. Finally, we show that molecules that decrease LDL-R from the surface of target cells could inhibit CCHFV infection. Our study highlights that CCHFV takes advantage of a lipoprotein receptor and recruits its natural ligand to promote entry into cells.

The Crimean-Congo hemorrhagic fever virus (CCHFV) is a tick-born zoonotic virus, responsible for severe hemorrhagic fever outbreaks in humans, with a case fatality rate of 10–40%, while being asymptomatic in non-human hosts<sup>1</sup>. CCHFV is endemic in Asia, the Middle East, Eastern Europe, Africa, and more recently, Southern Europe<sup>2,3</sup>, which corresponds to the geographic distribution of its vector and/or reservoir, mainly *Hyalomma* ticks<sup>4</sup>.

CCHFV is an enveloped virus that belongs to the *Nairoviridae* family of the *Bunyavirales* order. The viral genome consists of three single-stranded RNA segments (L, M, and S) of negative or ambisense

polarity. The RNA segments exclusively replicate in the cytosol and encode up to five non-structural proteins and four structural proteins, which are the RNA-dependent RNA polymerase L, the nucleoprotein NP, and two envelope glycoproteins (GP) Gc and Gn. The NP protein binds to genomic RNA to form, together with the viral polymerase, the pseudo-helical ribonucleoproteins (RNPs) inside the virions. Inserted on the viral envelope, the Gn and Gc GPs are responsible for the attachment of viral particles to the surface of host cells and their subsequent penetration into the cytosol (reviewed in<sup>5</sup>).

<sup>1</sup>CIRI – Centre International de Recherche en Infectiologie, Univ. Lyon, Université Claude Bernard Lyon 1, Inserm, U1111, CNRS, UMR5308, ENS de Lyon, F-69007 Lyon, France. <sup>2</sup>Inserm U1259, Morphogénèse et Antigenicité du VIH et des Virus des Hépatites (MAVIVH), Université de Tours and CHRU de Tours, 37032 Tours, France. <sup>3</sup>Université de Tours and CHRU de Tours, Plateforme IBI SA de Microscopie Electronique, Tours, France. <sup>4</sup>Faculty of Biological Sciences and Astbury Centre for Structural Molecular Biology, University of Leeds, Leeds LS2 9JT, UK. <sup>5</sup>Laboratory P4-Jean Mérieux, Inserm, Lyon, France. <sup>6</sup>Campus vétérinaire de Lyon, VetAgro Sup, Université de Lyon, Lyon, Marcy-l’Etoile, France. <sup>7</sup>These authors contributed equally: Lola Canus, Anupriya Gautam, Thomas Vallet, Li Zhong. <sup>8</sup>These authors jointly supervised this work: François-Loïc Cosset, Solène Denolly. ✉ e-mail: [francois-loic.cosset@ens-lyon.fr](mailto:francois-loic.cosset@ens-lyon.fr); [solene.denolly@inserm.fr](mailto:solene.denolly@inserm.fr)

The cellular receptors and co-factors involved in CCHFV entry to host cells remain poorly identified. Only the human C-type lectin DC-SIGN and the nuclear factor Nucleolin have been proposed to be involved in CCHFV entry<sup>6,7</sup>, but they might not be sufficient for CCHFV entry. Interestingly, a member of the low-density lipoprotein receptor (LDL-R) family, the low-density lipoprotein receptor-related protein 1 (Lrp1) was recently identified as a critical host entry factor for Rift Valley fever virus (RVFV)<sup>8,9</sup> and Oropouche orthobunyavirus (OROV)<sup>10</sup>, two members of the *Bunyvirales* order. In addition, other members of the LDL-R family, i.e., the very-low-density lipoprotein receptor (VLDL-R) and the apolipoprotein E receptor 2 (apoER2) were also recently identified as host factors for cell entry of alphaviruses<sup>11</sup>, while LDL-R was identified as host entry factor for hepatitis C virus (HCV)<sup>12–14</sup>, hepatitis B virus (HBV)<sup>15</sup>, Japanese encephalitis virus (JEV)<sup>16</sup>. Finally, several members of the LDL-R family are involved as receptors in vesicular stomatitis virus (VSV) entry<sup>17,18</sup>, suggesting that lipid transfer receptors might be used by different viral families.

We therefore sought to investigate in this study if lipid transfer receptor(s) could be used by CCHFV to promote cell entry. We used CCHF transcription and entry-competent virus-like particles (tecVLP)<sup>19</sup> that can be handled in BSL-2 and that fully mimic viral particles<sup>20</sup> as they contain all the structural proteins and a minigenome segment encoding a reporter protein (Fig. 1a). These particles were previously used for neutralization assays<sup>21</sup> or testing of inhibitors<sup>20</sup>. We also confirmed our results with wild-type (WT) virus, which needs to be manipulated in BSL-4.

Here, we show that LDL-R is a cofactor for CCHFV entry, promoting binding of viral particles to cell surface. In addition, we demonstrate that this binding occurs via apolipoprotein E (apoE), a natural ligand of LDL-R that is found to be incorporated on CCHFV particles.

## Results

### The low-density-lipoprotein receptor (LDL-R) is a cofactor of CCHFV infectivity

Lipid transfer receptors may play significant roles during cell entry for different virus families. Here, we chose Huh-7.5 cells as they are fully permissive for CCHFV infection<sup>22</sup> and express several of such receptors, including the low-density lipoprotein receptor (LDL-R), the LDL receptor-related protein 1 (Lrp1), and the scavenger receptor BI (SR-BI). While Lrp1 and LDL-R are members of the LDL-R family, SR-BI mediates lipid transfer through a different mechanism. To address whether they could be involved in CCHFV entry, we knocked down (KD) several of either lipid transfer receptor (Fig. 1b) by transduction of Huh-7.5 cells with lentiviral vectors encoding specific shRNA. We next transduced these KD cells with serial dilutions of CCHF tecVLPs harboring a nanoluciferase (nanoLuc) reporter gene (tecVLP-NanoLuc, Fig. 1a) and determined transduction levels by luciferase activity measurement. While the modulation of expression of SR-BI did not change the transduction levels of tecVLPs, we found that down-regulation of LDL-R could significantly reduce transduction of Huh-7.5 cells whereas down-regulation of Lrp1 promoted transduction of Huh-7.5 cells (Fig. 1c). Interestingly down-regulation of Lrp1 did not affect total level of LDL-R (Supplementary Fig. 1a) but induced an increase of LDL-R at cell surface (Supplementary Fig. 1b), which might explain why down-regulation of Lrp1 promoted transduction of tecVLPs.

Next, we aimed at clarifying the role of LDL-R in CCHFV infection. First, we analyzed the effect of blocking of LDL-R present at the surface of Huh-7.5 cells by using an LDL-R antibody added before transduction with serially diluted CCHF tecVLPs harboring a GFP reporter gene (tecVLP-GFP, Fig. 1a) or control particles. As positive control, we used vesicular stomatitis virus glycoprotein pseudoparticles (VSVpp), i.e., lentiviral vector particles pseudotyped with VSV-G, whose transduction depends on LDL-R for entry into cells<sup>17,18</sup>, whereas as negative control, we used lentiviral vector particles pseudotyped with the Env

glycoprotein from amphotropic murine leukemia virus (MLVpp), whose entry depends on interaction with the PiT-2, a type III sodium-dependent phosphate transporter<sup>23</sup>. The transduction titers were assessed upon determination of the percentage of positive cells by flow cytometry at 48 h post-transduction (p.t.) (Supplementary Fig. 1c). In agreement with the results of LDL-R KD, we found that LDL-R blocking inhibited transduction of both CCHF tecVLP and VSVGpp particles in an LDL-R antibody dose-dependent manner but did not affect MLVpp transduction (Fig. 1d). Then, we sought to confirm this result using WT CCHFV of the Ibar10200 strain that we produced in Huh-7.5 cells in a BSL4. Upon infection of Huh-7.5 cells with serial dilutions of infectious virus stocks and subsequent assessment of the levels of infection at 24 h post-infection (p.i.), via quantification of viral RNAs in infected cell lysates (Fig. 1a, Supplementary Fig. 1d), we confirmed that the blocking of LDL-R could dose-dependently inhibit CCHFV infection (Fig. 1e).

We also tested the dependency to LDL-R of Hazara virus (HAZV), another member of the genus *Orthonavirivirus*, using a GFP-expressing recombinant virus<sup>24</sup> produced in Huh-7.5 cells. Interestingly, the blocking of LDL-R at the surface of Huh-7.5 cells did not impair HAZV infection as assessed by flow cytometry (Fig. 1d), suggesting that LDL-R is not a pan-*Orthonavirivirus* entry factor.

LDL-R shares a highly homologous structure with the very low-density lipoprotein receptor (VLDL-R), which is widely expressed with the exception of hepatocytes, including Huh-7.5 cells, under normoxic conditions<sup>25</sup>. We therefore tested the effect of its ectopic expression on CCHF tecVLP transduction using Huh-7.5 cells transduced with a VLDL-R-encoding lentiviral vector. Interestingly, expression of VLDL-R increased the transduction levels of tecVLP-NanoLuc particles by up to 3-fold (Fig. 1f), indicating that alike the LDL-R, VLDL-R may promote CCHFV entry.

Next, we aimed at confirming the LDL-R-dependent CCHFV entry in primary human hepatocytes (PHH), which express LDL-R (Fig. 2a) and could be transduced by tecVLP-NanoLuc particles (Supplementary Fig. 1e). The read-out was performed at 24 h to maximize the level of signal in these primary cells. We found that the transduction of PHH was sensitive to LDL-R blocking (Fig. 2b). Then, we tested the involvement of LDL-R for CCHFV entry in cells from different tissues and species. First, we tested other human cells than Huh-7.5 hepatoma cells, either A549 lung epithelial cells or TE-671 rhabdomyosarcoma cells, which could readily be transduced by tecVLP-NanoLuc particles (Supplementary Fig. 1f). Interestingly, we found that transduction of both A549 and TE-671 cells, which express LDL-R (Fig. 2a), was sensitive to LDL-R blocking (Fig. 2c). Second, as CCHFV can also infect cattle, we tested the LDL-R dependency of CCHFV entry in bovine cells, either EBL embryonic lung cells or MDBK kidney cells, which were found permissive to tecVLP-NanoLuc transduction (Supplementary Fig. 1g). Yet, while the LDL-R blocking antibody could bind LDL-R expressed at the surface of bovine cells (Fig. 2a), it had no effect on tecVLP-NanoLuc transduction in these blocking assays (Fig. 2d), thus suggesting that CCHFV infection in EBL and MDBK cells may not depend on LDL-R.

Altogether, these results suggested that LDL-R is used by CCHFV for infection of human cells but not of bovine cells.

### LDL-R is involved at cell entry steps of CCHFV

Since the assessment of the levels of transduction of CCHF tecVLPs requires both cell entry of viral particles and subsequent transcription and replication of their minigenome, we sought to determine if LDL-R is involved at entry vs. transcription/replication steps. To discriminate either possibility, we added LDL-R antibody at different time points before and/or after transduction of Huh-7.5 cells (Fig. 3a). We found that while the addition of the antibody either before or concomitantly to the transduction step inhibited tecVLP-GFP transduction efficiency to up to 80%, the addition of LDL-R antibody from 2 h post-transduction had no effect on transduction efficiency (Fig. 3b),

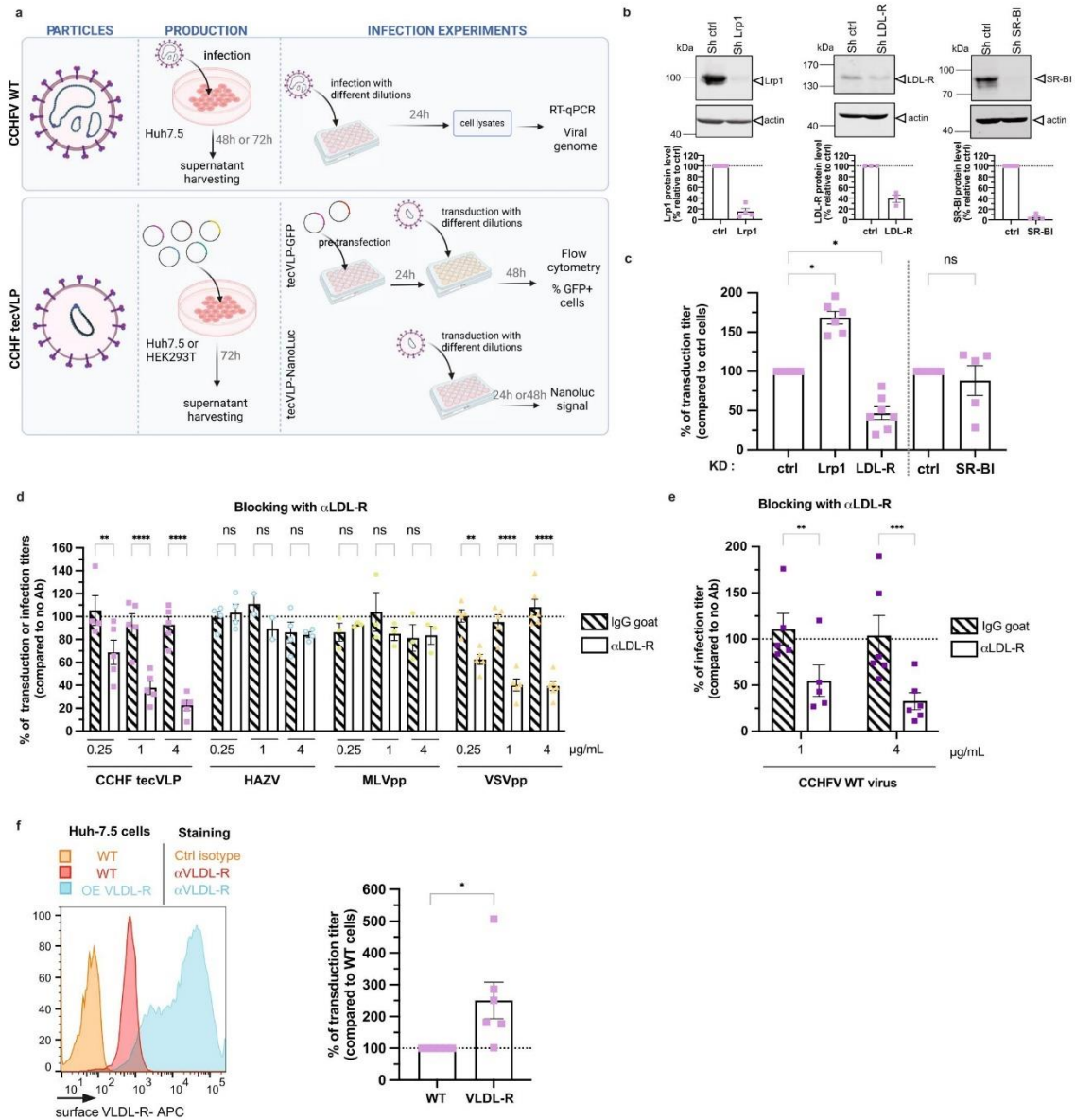


**Fig. 1 | LDL-R is a cofactor of CCHFV infectivity.** **a** WT CCHFV, manipulated in BSL4, was produced in Huh-7.5 cells, whereas CCHFV tecVLPs were produced in Huh-7.5 or HEK-293T cells. Infection or transduction assays were performed with serial dilutions. The level of infection was determined by RNA measurement in infected cells lysates. For tecVLP-GFP, target cells were pre-transfected with CCHFV NP and L expression vectors to amplify the GFP signal by minigenome replication and the level of transduction was assessed by flow cytometry. For tecVLP-NanoLuc, the level of transduction was assessed by measurement of nanoLuc levels. Created with Biorender.com. **b** Western blot analysis of cell lysates from Huh-7.5 cells transduced with lentiviral vectors allowing expression of control shRNA or shRNA targeting Lrp1 or LDL-R or SR-BI (top). Representative image of 3 experiments. Quantification of the abundance of corresponding receptors (bottom). **c** Cells described in (b) were transduced with CCHFV tecVLP-NanoLuc. Independent experiments:  $N = 5$  SR-BI;  $N = 6$  Lrp1;  $N = 7$  LDL-R. Kruskal-Wallis test with Dunn's multiple comparisons (ctrl vs. Lrp1;  $p = 0.0278$ , ctrl vs. LDL-R:  $p = 0.0498$ , ctrl vs. SR-BI:  $p > 0.9999$ ). **d** Huh-7.5 cells were incubated with different concentration of LDL-R antibody (open bars

or control isotype (IgG goat, dashed bars) for 1 h at 37 °C before transduction with CCHFV tecVLP-GFP (pink), MLVpp (green), and VSVpp (yellow) or infection with HAZV (blue). Independent experiments:  $N = 3$  MLVpp;  $N = 5$  CCHFV tecVLPs and VSVpp;  $N = 4$  HAZV (0.25  $\mu$ g/mL and 4  $\mu$ g/mL) and  $N = 2$  HAZV (1  $\mu$ g/mL). Two-way ANOVA test with Sidak's multiple comparisons ( $\alpha$ LDL-R vs. IgG: CCHFV tecVLPs, 0.25  $\mu$ g/mL  $p = 0.0091$ , 1  $\mu$ g/mL  $p < 0.0001$ , 4  $\mu$ g/mL  $p < 0.0001$ ; HAZV, 0.25  $\mu$ g/mL  $p > 0.9999$ , 1  $\mu$ g/mL  $p = 0.8951$ , 4  $\mu$ g/mL  $p > 0.9999$ ; MLVpp, 0.25  $\mu$ g/mL  $p > 0.9999$ , 1  $\mu$ g/mL  $p = 0.8343$ , 4  $\mu$ g/mL  $p > 0.9999$ ; VSVpp, 0.25  $\mu$ g/mL  $p = 0.0028$ , 1  $\mu$ g/mL  $p < 0.0001$ , 4  $\mu$ g/mL  $p < 0.0001$ ). **e** Same experiment using WT CCHFV.  $N = 4$  (1  $\mu$ g/mL) or  $N = 5$  (4  $\mu$ g/mL) independent experiments. Two-way ANOVA test with Sidak's multiple comparisons ( $\alpha$ LDL-R vs. IgG: 1  $\mu$ g/mL  $p = 0.0042$ , 4  $\mu$ g/mL  $p = 0.0004$ ). **f** Huh-7.5 cells stably expressing FLuc cells were transduced with a lentiviral vector allowing expression of VLDL-R. Surface expression of VLDL-R assessed by flow cytometry (left). Cells were then transduced with CCHFV tecVLP-NanoLuc.  $N = 6$  independent experiments. One sample t-test (two-tailed)  $p = 0.0467$ . Data are represented as means  $\pm$  SEM.

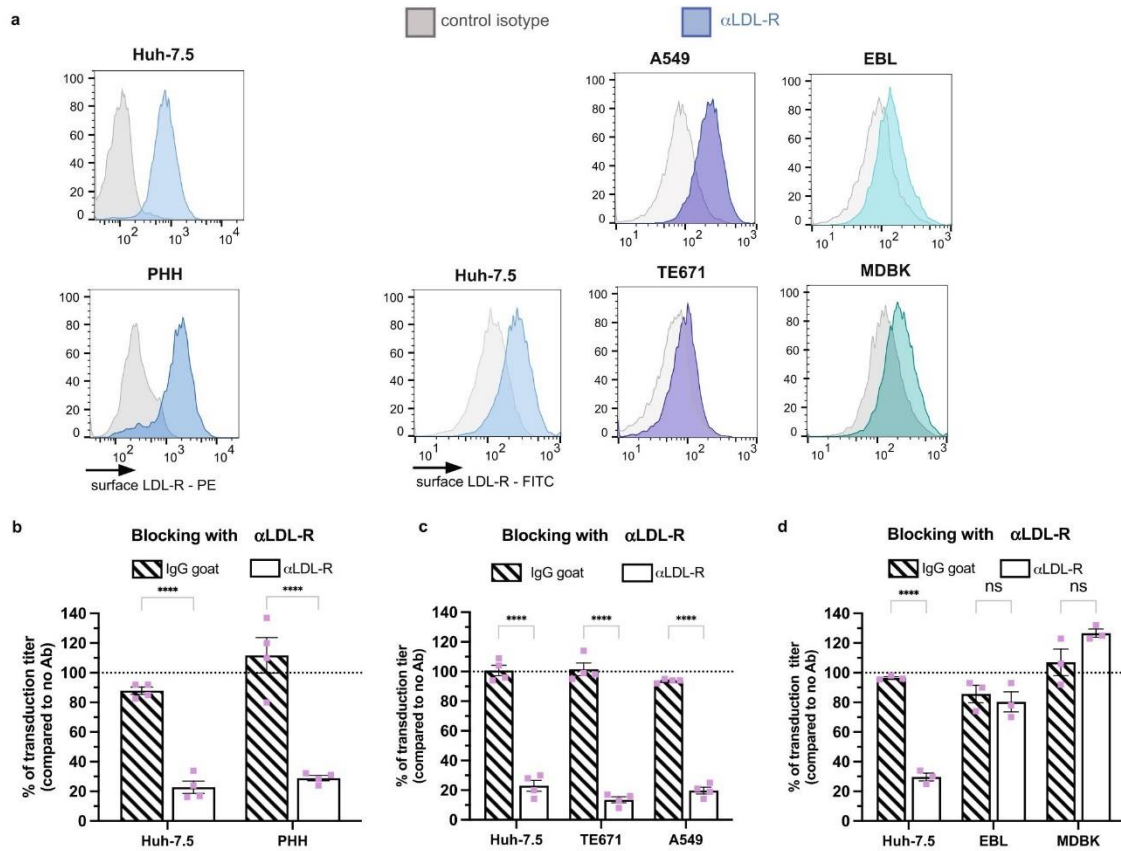


**Fig. 2 | LDL-R entry functions are conserved for infection of different human cells but not for bovine cells.** **a** Expression of LDL-R at the surface of Huh-7.5, A549, TE-671, EBL, MDBK, and PHH cells assessed by flow cytometry. **b** Huh-7.5 cells or PHH were incubated with 4µg/mL of LDL-R antibody (open bars) or IgG goat (dashed bars) for 1 h at 37 °C before transduction with CCHF tecVLP-NanoLuc.  $N = 4$  independent experiments. Two-way ANOVA test with Sidak's multiple comparisons ( $\alpha$ LDL-R vs. IgG; Huh-7.5  $p < 0.0001$ ; PHH  $p < 0.0001$ ). **c** Same as (b) with Huh-7.5,

TE-671, A549 cells with harvesting at 48 h post-transduction (p.t.).  $N = 4$  independent experiments. Two-way ANOVA test with Sidak's multiple comparisons ( $\alpha$ LDL-R vs. IgG; Huh-7.5  $p < 0.0001$ ; TE671  $p < 0.0001$ ; A549  $p < 0.0001$ ). **d** Same as (c) with Huh-7.5, EBL, MDBK cells.  $N = 3$  independent experiments. Two-way ANOVA test with Sidak's multiple comparisons ( $\alpha$ LDL-R vs. IgG; Huh-7.5  $p < 0.0001$ ; EBL  $p = 0.8740$ ; MDBK  $p = 0.0715$ ). Data are represented as means  $\pm$  SEM.

hence suggesting that LDL-R is involved at an entry step rather than at a later step of transcription/replication.

We thus hypothesized that LDL-R could serve as a CCHFV entry factor through its expression at the cell surface. To test this hypothesis, we incubated tecVLP-GFP or WT CCHFV particles with a soluble recombinant form of LDL-R (sLDL-R) before transduction or infection of Huh-7.5 cells. We used VSV pseudoparticles (VSVpp) as a positive control and amphotropic murine leukemia virus (MLV) pseudoparticles (MLVpp) as a negative control. While a soluble form of CD81 (CD81-LEL)<sup>26</sup> used as control had no effect on transduction, we found that, like for VSVpp, sLDL-R inhibited CCHFV infection in a dose-dependent manner in both tecVLP-GFP transduction (Fig. 3c) and WT CCHFV infection (Fig. 3d) assays, hence suggesting that sLDL-R could prevent cell entry through interaction with viral particles. Like for the LDL-R blocking experiment (Fig. 1d), we did not observe any impact of sLDL-R neutralization on HAZV infection (Fig. 3c). Note that while the blocking of LDL-R with an antibody impaired VSVpp and CCHF tecVLP at similar levels (Fig. 1d), sLDL-R impaired CCHFV entry at a lesser extent as compared to VSVpp (Fig. 3c, d). This difference between either virus could be due to a different role or affinity of LDL-R for the two types of viral particles. Alternatively, this could also be due to the production of CCHF tecVLPs in Huh-7.5 cells that express competitors

for binding to sLDL-R, such as apoB or apoE, which is not the case for HEK-293T cells that were used to produce VSVpp.

The above data suggested that CCHFV could bind to LDL-R. To test this hypothesis, we incubated CCHF tecVLPs with sLDL-R or CD81-LEL before the capture of these soluble receptors with Ni-NTA beads, as both soluble proteins harbor a 6xHis tag, and determination of the levels of co-captured viral genomes by qPCR. Interestingly, we found that we could capture about 7-fold more CCHF tecVLP RNAs with sLDL-R than with CD81-LEL (Fig. 3e, left). We repeated the same experiment with WT CCHFV and HAZV. While HAZV could not be captured by either protein, we confirmed that WT CCHFV RNAs could be co-captured with sLDL-R (Fig. 3e, right).

Altogether, these results indicated that LDL-R promotes CCHFV entry through the binding of viral particles.

#### The exchangeable apolipoprotein E mediates CCHFV entry

Next, we aimed to confirm the role of LDL-R in CCHFV entry using VSV pseudotyped with CCHFV glycoproteins<sup>27</sup>. Interestingly, while the blocking of LDL-R with LDL-R antibody had a strong effect on the transduction of control VSV particles pseudotyped with VSV-G with over 80% of inhibition, its inhibitory effect on VSV particles harboring CCHFV GPs, of up to 20%, was not only milder than for the former

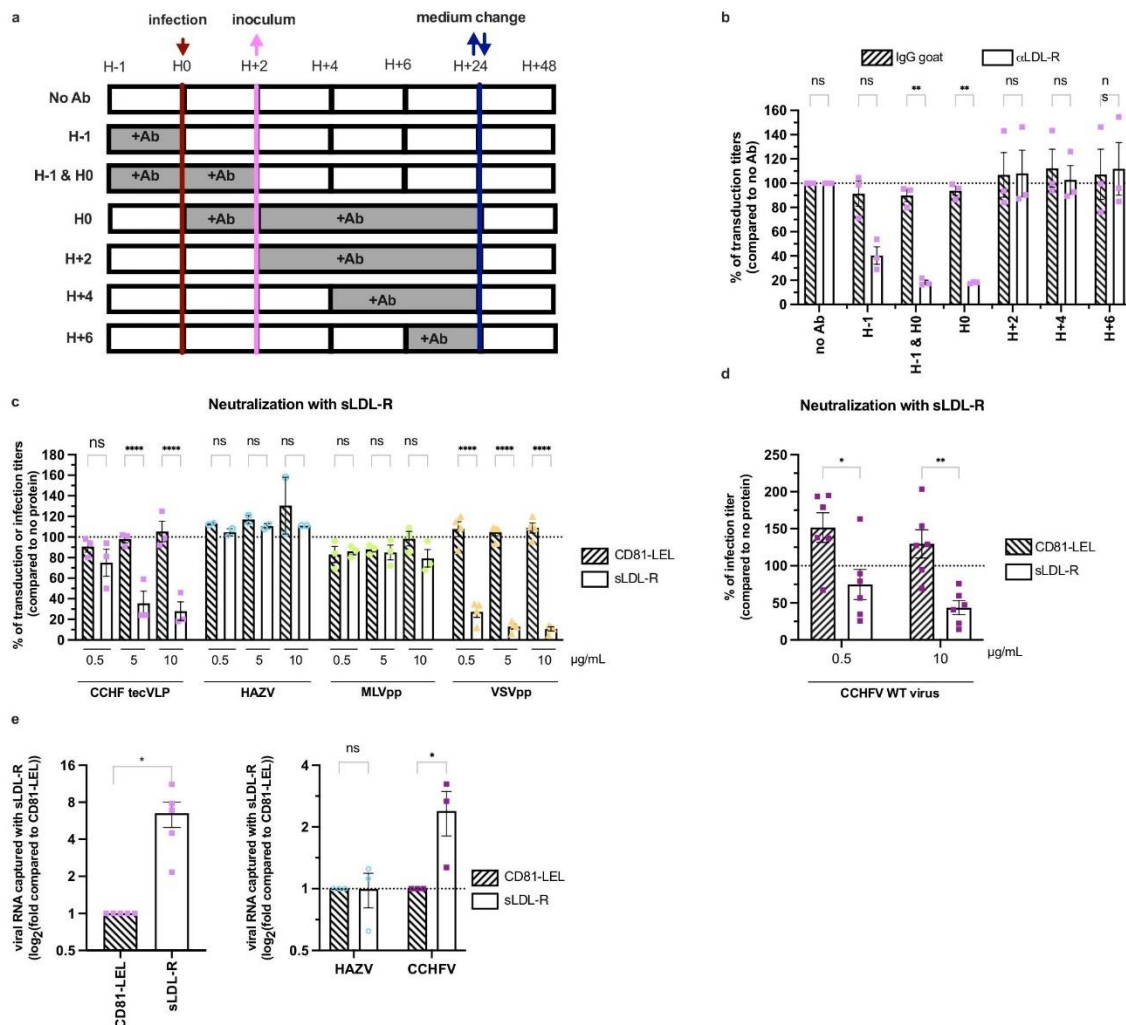


**Fig. 3 | LDL-R promotes CCHFV entry.** **a** Huh-7.5 cells were incubated with 4  $\mu\text{g}/\text{mL}$  of LDL-R antibody or control isotype before, during or after transduction with CCHF tecVLPs GFP as indicated in grey. **b** Percentage of transduction titers of CCHF tecVLP-GFP relative to control isotype as in the experimental set up described in (a).  $N = 3$  independent experiments. Two-way ANOVA test with Dunnett's multiple comparisons ( $\alpha\text{LDL-R}$  vs. IgG: no Ab  $p > 0.9999$ ; H-1  $p = 0.0505$ ; H-1 and H0  $p = 0.0026$ ; H0  $p = 0.014$ ; H + 2  $p > 0.9999$ ; H + 4  $p = 0.9980$ ; H + 6  $p > 0.999$ ). **c** CCHF tecVLP-GFP (pink), MLVpp (green), VSVpp (yellow) or HAZV (blue,  $N = 2$ ) were incubated for 1 h at room temperature with soluble LDL-R (sLDL-R, open bars) or with soluble CD81 (CD81-LEL, dashed bars) at different concentrations before transduction or infection of Huh-7.5 cells. Independent experiments:  $N = 3$  CCHF tecVLP and MLVpp;  $N = 4$  VSVpp;  $N = 2$  HAZV. Two-way ANOVA test with Sidak's multiple comparisons (sLDL-R vs. CD81-LEL: CCHF tecVLPs, 0.5  $\mu\text{g}/\text{mL}$   $p = 0.8354$ , 5  $\mu\text{g}/\text{mL}$   $p < 0.0001$ , 10  $\mu\text{g}/\text{mL}$   $p < 0.0001$ ; HAZV, 0.5  $\mu\text{g}/\text{mL}$   $p = 0.9998$ , 5  $\mu\text{g}/\text{mL}$

$p > 0.999$ , 10  $\mu\text{g}/\text{mL}$   $p = 0.8206$ ; MLVpp, 0.5  $\mu\text{g}/\text{mL}$   $p > 0.9999$ , 5  $\mu\text{g}/\text{mL}$   $p > 0.9999$ , 10  $\mu\text{g}/\text{mL}$   $p = 0.6061$ ; VSVpp, 0.5  $\mu\text{g}/\text{mL}$   $p < 0.0001$ , 5  $\mu\text{g}/\text{mL}$   $p < 0.0001$ , 10  $\mu\text{g}/\text{mL}$   $p < 0.0001$ ). **d** Same experiment using WT CCHFV. Media was removed 1 h post-infection (p.i.) and cells were lysed 24 h p.i. The level of infectivity was quantified by RT-qPCR.  $N = 6$  independent experiments. Two-way ANOVA test with Sidak's multiple comparisons (sLDL-R vs. CD81-LEL: 0.5  $\mu\text{g}/\text{mL}$   $p = 0.0125$ , 10  $\mu\text{g}/\text{mL}$   $p = 0.0053$ ). **e** CCHF tecVLPs (left) or CCHFV or HAZV (right) were incubated with sLDL-R or CD81-LEL (both expressing a 6xHis tag) for 1 h at RT before capture using magnetic beads. The levels of viral RNA co-captured were determined by RT-qPCR. One sample t-test (two-tailed) for CCHF tecVLPs ( $N = 5$  independent experiments,  $p = 0.0227$ ), two-way ANOVA test with Sidak's multiple comparisons for HAZV and CCHFV ( $N = 3$  independent experiments, HAZV  $p > 0.9999$ ; CCHFV  $p = 0.025$ ). Data are represented as means  $\pm$  SEM.

pseudotypes (Fig. 4a) but was also much lower than for CCHF tecVLPs (Fig. 4d). Since the VSV particles are produced in HEK-293T cells rather than in Huh-7.5 cells like for the CCHF tecVLPs, we wondered if the producer cell type could have an impact on either VSV or tecVLP particles and their dependency to LDL-R. We therefore produced CCHF tecVLPs in HEK-293T cells, which are fully able to produce tecVLPs (Supplementary Fig. 2a, b) albeit at a lower titer than Huh-7.5 cells. Interestingly, the blocking of LDL-R in Huh-7.5 target cells with an

LDL-R antibody had less impact on tecVLPs produced in HEK-293T cells than for tecVLPs produced from Huh-7.5 cells (Fig. 4b, left). To exclude a potential effect on cell compatibility between producer and target cells, we blocked LDL-R, which is expressed in HEK-293T cells (Supplementary Fig. 2c). Using these latter cells as targets, we found that LDL-R blocking only inhibited transduction of tecVLPs produced in Huh-7.5 cells but not those produced in HEK-293T cells (Fig. 4b, right), despite similar transduction levels (Supplementary Fig. 2d, e).

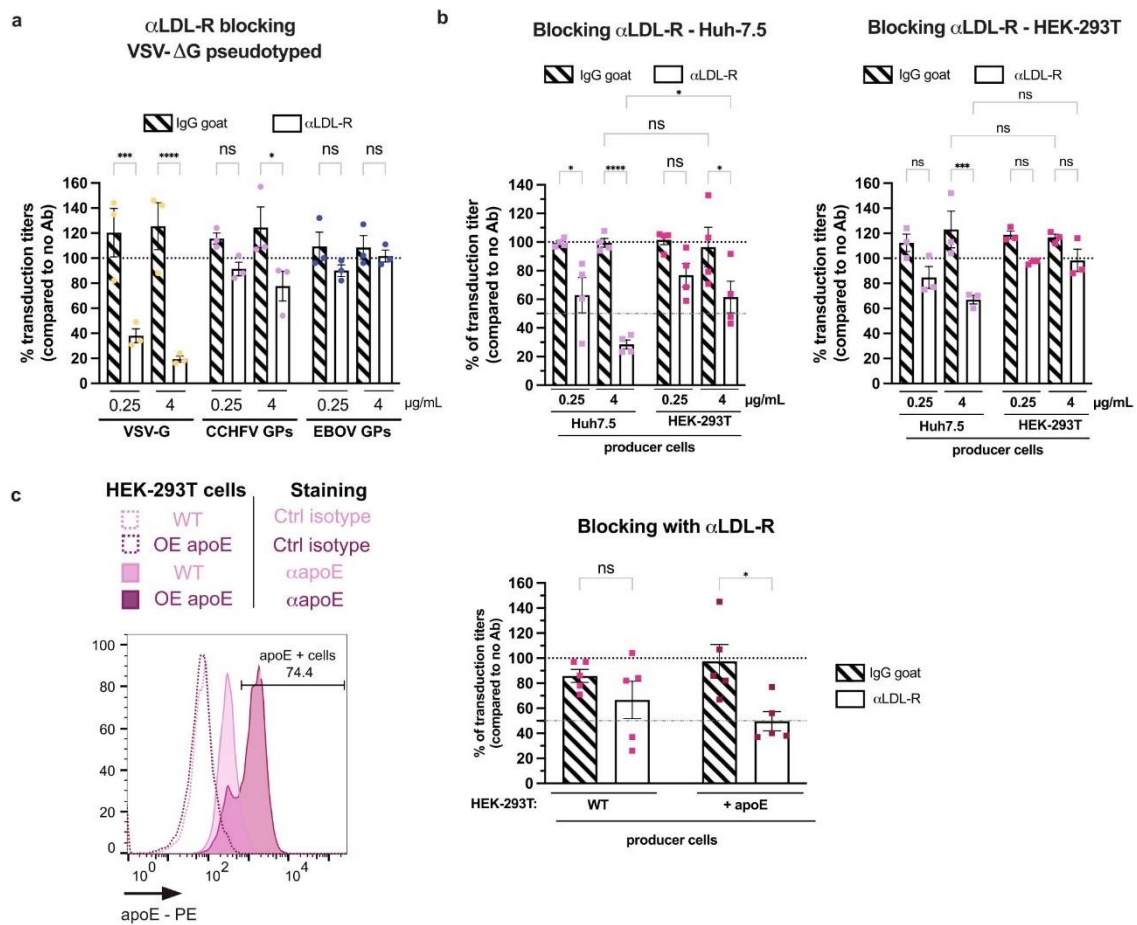


**Fig. 4 | LDL-R dependency of CCHFV entry is influenced by the virus producer cell type.** **a** Huh-7.5 cells were incubated with 0.25 µg/mL or 4 µg/mL of LDL-R antibody (open bars) or IgG goat (dashed bars) for 1 h at 37 °C before transduction with VSV-ΔG/GFP particles pseudotyped with VSV-G (yellow), CCHFV GPs (pink) or EBOV GP (blue). *N* = 3 independent experiments. Two-way ANOVA test with Sidak's multiple comparisons (αLDL-R vs. IgG: VSV-G, 0.25 µg/mL *p* = 0.0001, 4 µg/mL *p* < 0.0001; CCHFV GPs, 0.25 µg/mL *p* = 0.5799, 4 µg/mL *p* = 0.0393; EBOV, 0.25 µg/mL *p* = 0.7924, 4 µg/mL *p* > 0.9988). **b** (left) Same as (a) with CCHFV tecVLP-GFP particles produced in Huh-7.5 (pink) or HEK-293T (fuchsia) cells. *N* = 4 independent experiments. Two-way ANOVA test with Sidak's multiple comparisons (αLDL-R vs. IgG: Huh-7.5, 0.25 µg/mL *p* = 0.0106, 4 µg/mL *p* < 0.0001; HEK-293T, 0.25 µg/mL *p* = 0.1528, 4 µg/mL *p* = 0.0159; Huh-7.5 vs. HEK-293T, αLDL-R 4 µg/mL *p* = 0.0245, IgG 4 µg/mL *p* = 0.9999). (right) HEK-293T cells were incubated with 0.25 or 4 µg/mL

of αLDL-R antibody (open bars) or IgG goat (dashed bars) for 1 h at 37 °C before transduction with CCHFV tecVLP-NanoLuc particles produced in Huh7.5 (pink) or HEK-293T (fuchsia) cells. *N* = 3 independent experiments. Two-way ANOVA test with Sidak's multiple comparisons (αLDL-R vs. IgG: Huh-7.5, 0.25 µg/mL *p* = 0.1085, 4 µg/mL *p* = 0.0004, HEK-293T; 0.25 µg/mL *p* = 0.3004, 4 µg/mL *p* = 0.4791; Huh-7.5 vs. HEK-293T, αLDL-R 4 µg/mL *p* = 0.0545, IgG 4 µg/mL *p* = 0.9999). **c** Intracellular levels of apoE in HEK-293T vs. HEK-293T stably expressing apoE as assessed by flow cytometry (left). CCHFV tecVLPs produced in these cells were used for the experiment described as in (b) with 4 µg/mL of αLDL-R antibody (open bars) or IgG goat (dashed bars) (right). *N* = 5 independent experiments. Two-way ANOVA test with Sidak's multiple comparisons (HEK-293T: αLDL-R vs. IgG: 0.4196, HEK-293T + apoE: αLDL-R vs. IgG: 0.0152). Data are represented as means ± SEM.

These results therefore indicated that the LDL-R dependency of CCHFV entry could be influenced by the producer cell type. As HEK-293T cells do not express apoE, a natural ligand of LDL-R, in contrast to Huh7.5 cells (Supplementary Fig. 2f), we wondered if apoE might be responsible for the dependency of CCHFV entry to LDL-R. To test this hypothesis, we produced tecVLPs in HEK-293T cells transduced with an apoE lentiviral vector (Fig. 4c, left). Interestingly, ectopic apoE expression in HEK-293T cells increased the titers of tecVLPs (Supplementary Fig. 2g) and the effect of LDL-R blocking upon tecVLP transduction of Huh-7.5 target cells (Fig. 4c, right).

Based on these results, we wondered if and how apoE could influence the entry of CCHFV. First, we tested if apoE antibodies could neutralize CCHFV tecVLP transduction or WT CCHFV infection. As a positive control, we used HCV particles, as they can be

neutralized by apoE antibodies<sup>28</sup>, whereas we used VSVpp and MLVpp as negative controls, since VSV-G is the direct ligand of VSV for LDL-R binding<sup>29</sup> and since MLV Env binds an irrelevant receptor<sup>30</sup>. We incubated either viral particle with apoE antibodies for 1 h before transduction or infection assays. Interestingly, we found a dose-dependent inhibition for both CCHFV tecVLP-GFP (Fig. 5a) and WT CCHFV (Fig. 5b) particles by apoE antibodies, reaching up to 80% inhibition in a manner similar to HCV particles, whereas apoE antibodies did not inhibit VSVpp or MLVpp transduction (Fig. 5a). The difference of level of neutralization between CCHFV tecVLPs and WT CCHFV could be due a difference of the number of viral particles. Conversely, when we tested the apoE dependency of HAZV infection, we found that neutralization by apoE antibodies did not influence HAZV infection (Fig. 5a).

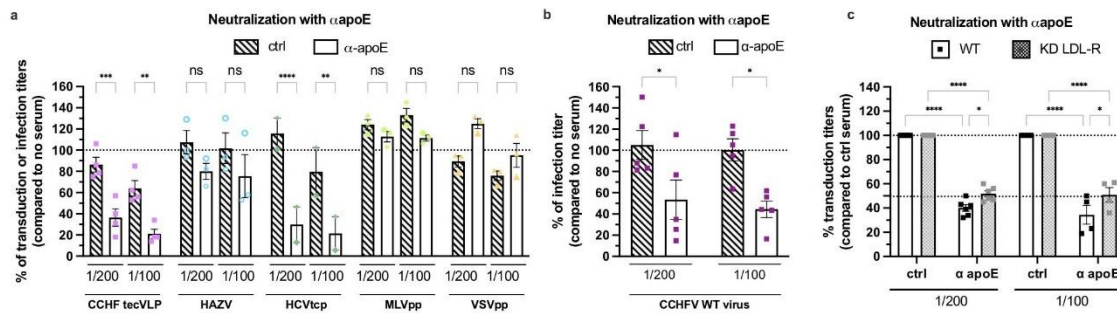


**Fig. 5 | ApoE promotes entry of CCHFV particles.** **a** CCHF tecVLPs (pink), MLVpp (light green), VSVGpp (yellow), HAZV (blue) or HCVtcp (green) were incubated for 1 h at room temperature with anti-apoE serum or control serum at different dilution before transduction or infection of Huh-7.5 cells. Independent experiments:  $N = 4$  CCHF tecVLP;  $N = 3$  MLVpp, VSVGpp, and HAZV;  $N = 2$  HCVtcp. Two-way ANOVA test with Sidak's multiple comparisons ( $\alpha$ apoE vs. ctrl serum: CCHF tecVLP, 1/200  $p = 0.0002$ , 1/100  $p = 0.0018$ ; HAZV, 1/200  $p = 0.2582$ , 1/100  $p = 0.3151$ ; HCVtcp, 1/200  $p < 0.0001$ , 1/100  $p = 0.0032$ ; MLVpp, 1/200  $p = 0.9886$ , 1/100  $p = 0.5832$ ; VSVpp, 1/200  $p = 0.0533$ , 1/100  $p = 0.7327$ ). **b** Same experiment as (a) using WT CCHFV particles.  $N = 5$  independent experiments. Two-way ANOVA test with Sidak's

multiple comparisons (ctrl vs.  $\alpha$ apoE: 1/100  $p = 0.0273$ , 1/200  $p = 0.0619$ ). **c** CCHF tecVLP-NanoLuc particles were incubated for 1 h at room temperature with an apoE serum at different dilution before transduction of Huh-7.5 cells stably expressing FLuc and transduced with lentiviral vectors allowing expression of control shRNA or shRNA targeting LDL-R as described in Fig. 1.  $N = 6$  independent experiments. Two-way ANOVA test with Sidak's multiple comparisons (WT vs. KD LDL-R: 1/200  $p = 0.012$ , 1/100  $p = 0.0383$ ; ctrl vs.  $\alpha$ apoE: WT 1/200  $p < 0.0001$ , WT 1/100  $p < 0.0001$ , KD LDL-R 1/200  $p < 0.0001$ , KD LDL-R 1/100  $p < 0.0001$ ). Data are represented as means  $\pm$  SEM.

These results suggested that apoE plays a crucial role in CCHFV infectivity. Thus, to corroborate the role of apoE in LDL-R-mediated entry, we repeated the apoE neutralization assay using Huh-7.5 target cells in which LDL-R was down-regulated. We found that under such conditions, tecVLP transduction was slightly less efficiently inhibited by apoE antibodies (Fig. 5c), hence suggesting a synergic role of apoE and LDL-R in CCHFV infection.

#### ApoE is associated with CCHFV particles and promotes their assembly/secretion and specific infectivity

ApoE is present at the surface of lipoproteins such as LDLs and VLDLs but can also exist in a lipid-free form in the extracellular environment<sup>31</sup>. Importantly, apoE belongs to the family of exchangeable apolipoproteins, implying that it can be transferred from a lipoprotein to another lipoprotein or to a viral particle, as described for HCV<sup>32,33</sup>. We therefore sought to determine if CCHF tecVLPs harbor apoE at their surface, which would promote entry of CCHFV.

First, we determined if we could capture viral particles with an apoE antibody, as previously shown for HCV<sup>34</sup>. After immunoprecipitation of CCHF tecVLPs or HAZV particles with an apoE antibody, we quantified the captured particles by detecting viral RNA by RT-qPCR. Interestingly, in contrast to HAZV, we found a 16-fold enrichment of CCHF tecVLP RNAs with apoE antibodies relative to control IgGs (Fig. 6a). In addition, we could also detect some CCHF tecVLPs in electron microscopy with immunogold labeling with anti-Gn or anti apoE (Fig. 6b). Moreover, we confirmed the association of WT CCHFV particles with apoE, since we could co-capture both viral RNA and CCHFV Gn and Gc proteins with apoE antibodies (Fig. 6c, d), suggesting an association of apoE to particles containing CCHFV glycoproteins and viral genome.

Second, we produced CCHF tecVLPs in Huh-7.5 cells transduced with a shRNA targeting apoE, which induced a robust loss of apoE expression (Fig. 6e). While apoE KD did not impair the level of expression of CCHFV NP in producer cells (Fig. 6f, top), it resulted in a strong loss of transduction efficiency of CCHF tecVLPs, with a 2-log titer decrease (Fig. 6g, top). To determine if this loss resulted from a defect in assembly *vs.* specific transduction efficiency of particles, we determined the levels of viral RNA in the supernatant. We found that apoE KD impaired by ca. 1-log the secretion of the viral genome (Fig. 6h, top), indicating that apoE plays a role in both assembly/

secretion and specific transduction efficiency of CCHF tecVLP particles. Interestingly, apoE KD had no effect on HAZV production and infectivity (Figs. 6f–h, bottom), which agreed with the results of lack of LDL-R and apoE dependency of this virus (Figs. 1c, 3c and e, 5a).

Altogether, these results indicated that CCHFV particles could incorporate apoE, which may therefore provide a ligand of LDL-R at the surface of the viral particles, and that apoE is a pro-viral factor for assembly/secretion and specific infectivity of CCHFV particles.

#### Molecules impairing LDL-R surface levels prevent CCHFV infection

Finally, we tested if molecules that regulate LDL-R surface levels could modulate CCHFV entry, aiming at proposing possible ways to prevent CCHFV infection. Using the proprotein convertase subtilisin-like kexin type 9 (PCSK9) that inhibits LDL-R recycling<sup>35</sup> and therefore decreases LDL-R exposition at the cell surface (Fig. 7a, b), without altering cell viability (Fig. 7c), we found that pre-treatment of cells with PCSK9 impaired transduction of both VSVpp and CCHF tecVLPs without affecting MLVpp transduction and HAZV infection (Fig. 7d).

We also tested Berbamine - bis-benzylisoquinoline (BBM), an alkaloid isolated from the plant *Berberis amurensis* (used in traditional Chinese medicine), that was reported to inhibit JEV by altering cell surface LDL-R level<sup>16</sup>. Again, we showed that pre-treatment of the cells with BBM decreased LDL-R levels at the cell surface (Fig. 7e, f) without altering cell viability (Fig. 7g) and impaired transduction of CCHF tecVLPs and VSVpp, without affecting transduction of MLVpp (Fig. 7h). Of note, BBM also impaired to some extent HAZV infection (Fig. 7h), which might be due to a broad effect of BBM on cellular pathways.

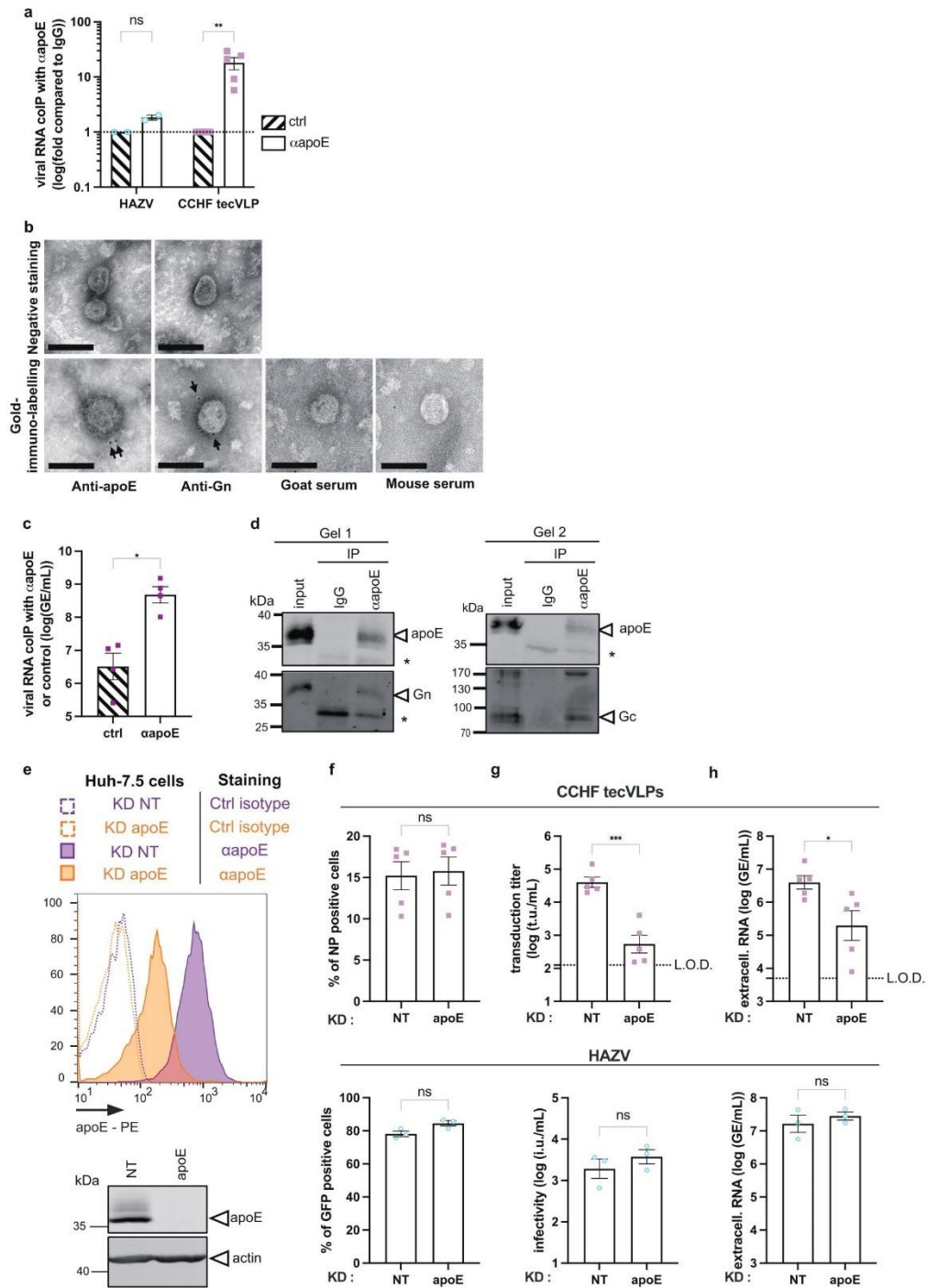
These results highlighted that molecules modulating LDL-R surface levels could be used to prevent CCHFV infection.

Altogether, our study identified LDL-R as a factor promoting CCHFV infection via binding of the viral particles. We also showed that CCHFV particles incorporate a natural ligand of LDL-R, apoE, and that this factor promotes the LDL-R-dependent entry (Fig. 8), as well as assembly of viral particles.

#### Discussion

Our results highlight the role of LDL-R and apoE as entry factors of CCHFV. Importantly, our findings using the CCHF tecVLP assay, which relies on VLPs that contain all the structural proteins but only a mini-genome segment encoding a reporter protein<sup>19,20,22</sup>, were fully





confirmed with WT CCHFV handled in BSL4. This indicates that although they do not allow full investigation of CCHFV properties, the former particles provide a bona fide assay to investigate cell entry pathways and receptors of CCHFV. In agreement with these findings, a recent study also identified LDL-R as an entry factor of CCHFV<sup>36</sup> (published while this article was in revision) using a different CCHFV strain than ours. The LDL-R is the prototype member of the 'LDL-R

family', which regroups structurally related endocytic receptors that mediate lipid transfer to cells. The ectodomains of the members of this family share high sequence similarity and capacity to bind to a large variety of ligands<sup>37</sup>. They are composed of cysteine-rich repeats, which are repeats of their ligand-binding domains, and of EGF-like modules and  $\beta$ -propellers, which are required for the pH-dependent release of their ligands following internalization.

**Fig. 6 | ApoE is associated with CCHFV particles and contribute to assembly/secretion and specific infectivity.** **a** Level of CCHFV minigenome RNA or HAZV RNA co-immunoprecipitated with an apoE serum *vs.* control IgGs and quantified by RT-qPCR. Results from  $N=2$  (HAZV) or  $N=5$  (CCHF tecVLP) independent experiments are presented as fold enrichment with apoE antibodies relative to control IgGs. Two-way ANOVA test with Sidak's multiple comparisons (HAZV  $p=0.9895$ , CCHF tecVLPs  $p=0.0036$ ). **b** Representative electron microscopy images of tecVLPs with simple negative stain (top) or with immunogold labelling with anti-Gn or anti-apoE antibodies or control antibodies (bottom). Scale bar represents 100 nm. Representative images from 2 experiments. **c** CCHFV particles were immunoprecipitated with an apoE serum *vs.* control IgGs.  $N=4$  independent experiments. Mann-Whitney test (two-tailed,  $p=0.0286$ ). **d** CCHFV particles were immunoprecipitated with an apoE serum *vs.* control IgGs and analyzed by western blot for apoE and Gn or Gc detection. Asterisks indicated unspecific bands from antibodies light chains. Representative image of 4 independent experiments.

**e** Intracellular levels of apoE as assessed by flow cytometry and Western blot of cells transduced with shRNA control (NT) or targeting apoE. Representative image of 3 independent experiments. **f** Cells described in **(e)** were used for the production of CCHF tecVLPs or HAZV particles as described in Methods. Percentage of CCHFV NP transfected cells (top) or HAZV-eGFP expressing cells (bottom). Unpaired t-test (two-tailed,  $p=0.8219$ ) for CCHFV and Mann-Whitney test (two-tailed,  $p=0.1$ ) for HAZV. **g** Transduction efficiency of CCHF tecVLPs (top) or infectivity of HAZV (bottom) particles produced in cells described in **(e)** as assessed by flow cytometry. Unpaired t-test (two-tailed,  $p=0.0003$ ) for CCHFV and Mann-Whitney test (two-tailed,  $p=0.4$ ) for HAZV. **h** Level of secreted viral RNA of tecVLPs (top) or HAZV (bottom) assessed by RT-qPCR. Unpaired t-test (two-tailed,  $p=0.0296$ ) for CCHFV and Mann-Whitney test (two-tailed,  $p=0.7$ ) for HAZV. For **(f-h)**,  $N=5$  independent experiments for CCHFV tecVLPs and  $N=3$  for HAZV. Data are represented as means  $\pm$  SEM.

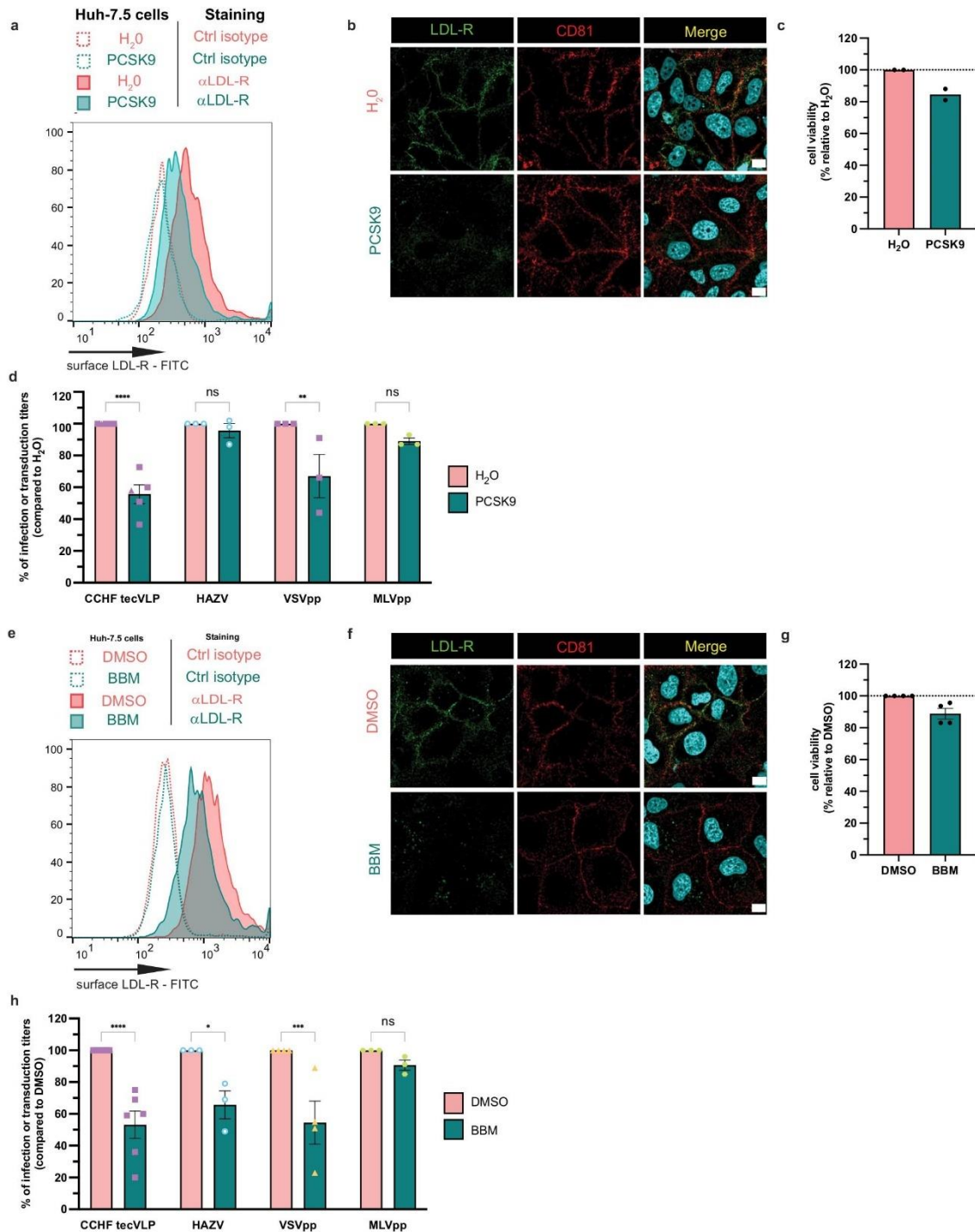
Interestingly, entry of unrelated bunyaviruses, including RVFV and OROV was recently shown to involve Lrp1, a member of the LDL-R family<sup>8-10</sup>, which does not appear to be a proviral entry factor for CCHFV (Fig. 1c). Yet, together with our results that LDL-R acts as a cofactor for CCHFV entry though not for HAZV, these findings imply that different binding and/or post-binding functions of members of the LDL-R family have been coopted by bunyaviruses in a virus-specific manner to promote their entry into cells. While LDL-R is mainly involved in the endocytosis of triglyceride- and cholesterol-containing lipoprotein particles, Lrp1 mediates the endocytosis of different types of ligands especially in the liver<sup>25</sup>. Overall, the members of the LDL-R family can bind different types of proteins or factors, suggesting that these receptors could, at least, act as capture molecules. Indeed, as above-mentioned, OROV and RVFV particles were shown to bind Lrp1 whereas we found that CCHFV particles can bind LDL-R. Furthermore, a recent study suggested that Lrp1 plays a role in RVFV endocytosis although it was unclear if this occurs via direct or indirect interactions with viral particles<sup>5</sup>.

Importantly, the usage of LDL-R family members as cell entry cofactors is not restricted to bunyaviruses since several other viruses seem to hijack members of this family, such as HCV for VLDL-R<sup>12,38</sup> and LDL-R<sup>13,14,28</sup>, HBV for LDL-R<sup>15</sup>, alphaviruses for VLDL-R and apoER2<sup>11</sup>, VSV for LDL-R<sup>17,18</sup>, Dengue virus and JEV for LDL-R<sup>16,39</sup>, as well as some rhinoviruses for LDL-R and VLDL-R<sup>40,41</sup>.

Altogether, these previous studies combined with our report underscore a wide-ranging role for receptors of the LDL-R family in virus entry. Yet, how these factors promote virus entry remains poorly defined. The current evidence suggests that overall, most of these factors may not act as bona fide viral receptors but rather, as above-discussed, as crucial co-factors of virus entry by promoting the capture of the viral particles at the cell surface or alternatively, their endocytosis. On the other hand, for some of these viruses, it is not even clear if the viral particles bind to these cofactors. While some viruses such as RVFV<sup>9</sup>, OROV<sup>10</sup> or VSV<sup>39</sup> seem to directly bind these receptors via their glycoproteins, some other viruses hijack cellular proteins like apoE as ligand cofactor for binding LDL-R, as shown in this study for CCHFV and as previously shown for HCV<sup>28</sup> and HBV<sup>42</sup>. We may therefore speculate that viruses that can replicate in hepatocytes could have evolved to easily hijack some lipoprotein components, such as apoE or alternative exchangeable apolipoproteins<sup>43,44</sup> that are produced in the same cells, either during their assembly or secretion or from the extracellular environment (see below). In contrast, other viruses could have taken advantage of the capacity of LDL-R family members to bind to a large variety of ligands via a relatively unspecific mechanism. Indeed, for some of these ligands, the interactions can involve electrostatic interactions between conserved acidic residues or tryptophans on LDL-R repeats with basic residues on the ligands (reviewed in ref. 37), as shown for human rhinovirus serotype 2 (HRV2) and VLDL-R<sup>41</sup>.

Especially, while OROV and RVFV Gn GP may directly bind Lrp1<sup>9,10</sup>, our results indicate that apoE, a natural ligand of members of the LDL-R family, is incorporated onto CCHFV particles and promotes LDL-R dependent entry (Fig. 8). On the other hand, the CCHFV Gc GP may also directly bind LDL-R<sup>36</sup>, suggesting different though not mutually exclusive mechanisms or, alternatively, a tripartite molecular interaction developed by CCHFV to interact with LDL-R and promote cell entry. This may depend on the presence of apoE as well as on other host factors that may be expressed, or not, in virus-producer cells and that could possibly directly interact with CCHFV GPs or virion surface. Association of CCHFV particles with apoE is reminiscent of the properties of HCV and HBV<sup>28,34,42,45</sup>. Indeed, in the case of HCV, previous studies indicated that apoE association with the viral particles allow them to bind different entry factors such as heparan sulphate proteoglycans (HSPG)<sup>46,47</sup>, which act as capture molecules<sup>48</sup>, but also to lipid transfer receptors such as LDL-R<sup>28</sup> and SR-BI<sup>34,45</sup>. Furthermore, binding of HCV particles to SR-BI was shown to be mediated by either ApoE or HCV E2 surface glycoprotein<sup>45</sup>, which is reminiscent of the situation with CCHFV particles that may interact with the LDL-R in a Gc-dependent manner<sup>36</sup> or, alternatively, in an apoE-dependent manner (this report). Finally, our results also underscore that species-specific determinants could be important in the above molecular interactions and their outcome in virus infectivity. For example, previous results indicated that apoE expressed in Vero cells does not allow the production of infectious HCV particles<sup>49</sup>, which could be due to a lack of interaction of this simian apoE with HCV E2 or alternatively with human LDL-R. This suggests possibilities to explain why the infectivity of CCHFV grown in Vero cells seemed to rely on the sole interaction between Gc and LDL-R<sup>36</sup> whereas the infectivity of CCHFV grown in human cells, such as Huh-7.5 cells, depends on or is strengthened by human apoE (this report).

As apoE is a high affinity ligand for most receptors of the LDL-R family<sup>50</sup>, whether it also acts as a ligand recruited by viral particles of the above-mentioned viruses that use lipid transfer receptors remains an open question. In this respect, it is surprising that only LDL-R though not Lrp1 and SR-BI acts as an entry factor of CCHFV. While further studies are needed to understand these differences, one possibility could be that Gc binds specifically to LDL-R rather than the other family members, and that apoE would stabilize this binding and promote entry through a bi-partite apoE/Gc interaction allowing productive LDL-R dependent entry. Another possibility could be that LDL-R may participate to the formation of a receptor complex through a specific association with alternative putative Gn/Gc receptor(s) (Fig. 8). On the other hand, as the location of the viral binding site on the receptor is a critical determinant of membrane fusion<sup>51</sup>, one could speculate that should apoE allow binding of CCHFV particles to Lrp1 and SR-BI, it may not provide the optimal distance between viral and target cell membranes, in agreement with a much longer extracellular domain for Lrp1 than for LDL-R<sup>32</sup>. Finally, as shown by the results with



HCV particles, whose endocytosis by LDL-R<sup>13</sup> or increasing endocytosis by SR-BI<sup>53</sup> leads to non-productive or reduced entry into cells, that Lrp1 can be endocytosed more actively than LDL-R<sup>54</sup> also raises the possibility that, even if CCHFV binds to Lrp1, this could lead to a non-productive entry. This is supported by our data suggesting that Lrp1 seems to be antiviral for CCHFV infection (Fig. 1c), though it could

also be due to a regulation of the level of LDL-R at the cell surface (Supplementary Fig. 1b).

How apoE is recruited on CCHFV particles remains ill-defined. Our results suggest that its incorporation on viral particles may occur during their production from hepatocytes in which apoE is expressed. This could involve apoE interactions with CCHFV determinants such as

**Fig. 7 | Molecules impairing LDL-R surface level impaired CCHFV infection.** **a** Cell surface expression of LDL-R of cells treated with 0 vs. 10 µg/mL of PCSK9 for 3 h at 37 °C. Control isotypes are depicted in dotted lines. Representative image of *N* = 3 independent experiments. **b** Cell surface expression of LDL-R or CD81 of cells treated with 0 vs. 10 µg/mL of PCSK9 for 3 h at 37 °C as assessed by confocal microscopy. The images provided are representative of two independent experiments. Scale bars represent 10 µm. **c** Cell viability of cells treated with PCSK9 relative to non-treated cells. *N* = 2 independent experiments. **d** Level of transduction or infection of cells treated with 0 vs. 10 µg/mL of PCSK9 for 3 h at 37 °C. The media was replaced 3 h p.i. or p.t. and the cells were harvested at 48 h p.i. or p.t. for determination of the levels of transduction or infection by flow cytometry. Independent experiments: *N* = 5 CCHFV tecVLP; *N* = 3 HAZV, VSVpp and MLVpp. Two-way ANOVA test with Sidak's multiple comparisons (H<sub>2</sub>O vs. PCSK9: CCHFV tecVLPs *p* < 0.0001, HAZV *p* = 0.9736, VSVpp *p* = 0.0023, MLVpp *p* = 0.5648). **e** Cell surface

expression of LDL-R of cells treated with 0 vs. 75 µM BBM for 2 h at 37 °C. Control isotypes are depicted in dotted lines. Representative image of 3 independent experiments. **f** Cell surface expression of LDL-R or CD81 of cells treated with 0 vs. 75 µM BBM for 2 h at 37 °C as assessed by confocal microscopy. The images provided are representative of two independent experiments. Scale bars represent 10 µm. **g** Cell viability of cells treated with 0 vs. 75 µM BBM for 2 h at 37 °C. *N* = 4 independent experiments. **h** Level of transduction or infection of cells treated with 0 vs. 75 µM BBM for 2 h at 37 °C. The media was replaced 3 h p.i. or p.t. and the cells were harvested at 48 h p.i. or p.t. for determination of the levels of transduction or infection by flow cytometry. Independent experiments: *N* = 6 CCHFV tecVLP, *N* = 3 HAZV and MLVpp, *N* = 4 VSVpp. Two-way ANOVA test with Sidak's multiple comparisons (DMSO vs. BBM: CCHFV tecVLPs *p* < 0.0001, HAZV *p* = 0.0286, VSVpp *p* = 0.0006, MLVpp *p* = 0.8694). Data are represented as means ± SEM.

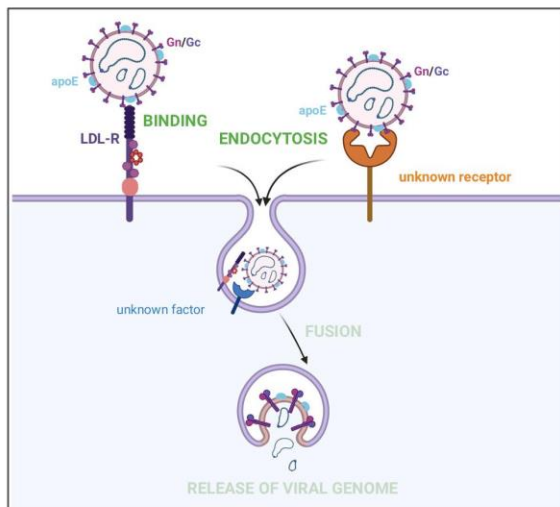


**Fig. 8 | Summary of the role of LDL-R in CCHFV entry.** CCHFV particles could incorporate apoE at their surface, which might contribute to the binding to LDL-R in addition to Gc. Followed this binding, CCHFV particles are endocytosed and then fuse with the late endosome membranes, allowing the release of viral genome. At this time, we cannot exclude the role of an additional factor (in blue) to promote endocytosis and/or fusion of CCHFV particles. In addition, an LDL-R-independent route of entry remains possible via a still unknown receptor (orange). Created with Biorender.com.

its surface GPs, which may promote assembly and secretion of viral particles in a manner reminiscent of HCV<sup>55-57</sup>. On the other hand, but not exclusively, as apoE is an exchangeable apolipoprotein<sup>58,59</sup>, its incorporation on the lipid bilayer of viral particles may occur passively during their assembly in the Golgi or other organelles of the secretory pathway<sup>60</sup>. Finally, like for HCV, for which apoE association to viral particles could also occur in the extracellular environment<sup>32</sup> as well as in the vicinity of apoE-secreting target cells<sup>33</sup>, CCHFV may recruit actively or passively apoE after virion egress.

CCHFV is detected in different organs in vivo upon infection and can infect several different cell types in vitro<sup>61</sup>, hence underscoring the need for ubiquitous cellular receptors and cofactors for cell entry. In this respect, the broad tissue distribution of LDL-R suggests that it may promote entry in a variety of CCHFV target cell types. CCHFV infection is not restricted to humans as it can infect a large diversity of mammals such as cattle, sheep, goats, rhinoceroses, and camels<sup>62</sup>, but this infection might not depend on LDL-R, at least according to our results with bovine cells. Interestingly, it seems that infection of CCHFV in mice is dependent on LDL-R<sup>36</sup>, suggesting that its entry mechanism might differ between hosts. As above-stated, this could be due to

species-specific determinants, and we could speculate a low recognition of human apoE by bovine LDL-R or a preferential usage of another LDL-R family member in non-human cells. Likewise, CCHFV also replicates in tick cells, which poses the question of species-specific entry factors *vs.* receptors conserved across arthropod and mammal species. Interestingly, the vitellogenin receptor (VgR), which is expressed in arthropod oocytes, shares the similar architecture and functions of human LDL-R<sup>63</sup>. We note that a plant virus was shown to bind vitellogenin in order to mediate cell entry via VgR in its insect host, the true bug<sup>64</sup>. In this respect, it would be interesting to know if CCHFV uses a similar mechanism in tick cells. Finally, inter-human transmission of CCHFV has been reported<sup>3</sup>, including nosocomial infections<sup>65</sup>. In that context, as incorporation of apoE on viral particles enhances infection through LDL-R (our report), apoE might play a crucial role in tropism and/or reservoir establishment in a manner dependent on tissue-specificity of apoE expression, such as in hepatocytes.

Taken together, our data identify a cellular receptor of CCHFV and its ligand incorporated within viral particles, highlighting a new and original mechanism developed by an important pathogenic bunyavirus.

## Methods

### Cells

Huh-7.5 cells (kind gift from Charles Rice), HEK-293T kidney cells (ATCC CRL-3216), TE-671 cells (ATCC CRL8805), A549 cells (kind gift from P. Boulanger), VeroE6 cells (ATCC CRL-1586), EBL cells (kind gift from Fabienne Archer), MDBK cells (European Collection of Authenticated Cell Cultures (ECACC)) were grown Dulbecco's modified minimal essential medium (DMEM, Invitrogen, France) supplemented with 100 U/mL of penicillin, 100 µg/mL of streptomycin and 10% of fetal bovine serum.

PHH (BD Biosciences) were centrifuged in F12-HAM medium (Sigma Aldrich) and seeded overnight in collagen-coated plates in BD Gentest seeding medium supplemented with 5% FCS. 16 h later, PHH were washed and cultured with a culture medium for PHH (DMEM F12, Sigma Aldrich) supplemented with 10% FCS, 1 µg/mL BSA, 5 µg/mL bovine insulin, 1 × 10<sup>-6</sup> M Dexamethasone (Sigma Aldrich), 1 × 10<sup>-8</sup> M 3.3 triiodo-L-thyronin, 5 µg/mL apotransferrin, 1% of non-essential amino acids (Gibco), 1% of Glutamin (Gibco) and 1% Penicillin-Streptomycin solution (Gibco).

### Plasmids

The constructs encoding wild-type CCHFV strain IbAr10200 L polymerase (pCAGGS-V5-L), N nucleoprotein (pCAGGS-NP), M segment (pCAGGS-M), T7 RNA polymerase (pCAGGS-T7), nanoluciferase (nanoLuc)-expressing minigenome flanked by L NCR under the control of a T7 promoter (pSMART-LCK\_L-Luc), GFP expressing minigenome flanked by L 5' and 3' UTRs under the control of a T7 promoter (pT7\_vL\_GFP), and an empty vector (pCAGGS) were described

previously<sup>19,66</sup> (all kind gifts from Friedemann Weber and Eric Bergeron). psPAX2, pHCMV-G (kind gifts from Didier Trono and Jane Burns, respectively), and pHCMV\_HIV\_GFP were used for VSV pseudoparticles production. psPAX2, pHCMV\_HIV\_GFP and pHCMV-4070A<sup>67</sup> were used for MLV pseudoparticle production. pFK-JFH1/J6/C-846\_Δp7, constructed from pFK-JFH1/J6/C-846 by deletion of p7 and addition of EMCV IRES between E2 and NS2, and pHCMV-noSpp7(J6) were used for HCVtcp production. pMK-RQ-HAZV resQ S EGFP P2A, pMK-RQ-HAZV M, pMK-RQ-HAZV L (kind gift from John N. Barr) were used for production of rescued HAZV rHAZV-eGFP. pHCMV-G, pCAGGS-M-Δ10, encoding for a CCHFV glycoprotein precursor lacking the last 53 residues of Gc<sup>6</sup>, or with pHCMV-EboV<sup>68</sup>, encoding for EBOV glycoprotein were used for production of pseudotyped VSV-ΔG. For VDL-R and apoE expression, pCSII-EF-VLDLR-HA (kind gift from Yoshiharu Matsumura) and pWPI-hApoE3 (kind gift from Ralf Bartenschlager) respectively were used for production of lentivirus in combination with pHCMV-G and psPAX2. For the down-regulation assays, TRC2\_pLKO\_shLRP1 (TRCN0000257100; Sigma-Aldrich), TRC2\_pLKO\_shLDLR (TRCN0000262146; Sigma-Aldrich); TRC1\_pLKO\_shapoE (TRCN0000010913; Sigma-Aldrich) or plasmids described in<sup>69</sup> or pHR-SIN-CSGW (empty backbone) were used for generation of lentivirus in combination with pHCMV-G and psPAX2.

#### Antibodies

The list of all antibodies used in this study is available in the Supplementary information (Supplementary Table 1).

#### Production of viral stocks and infection assays with WT CCHFV particles

All the experiments with WT live CCHFV were performed in the Jean Mérieux BSL-4 facility in Lyon, France. To produce viral stocks, Huh-7.5 cells were infected using CCHFV isolate IbAr10200 (obtained from Institut Pasteur) at MOI of 0.01 and the production was harvested at 72 h post-infection. Infectious titers were determined by NP immunostaining on VeroE6 cells<sup>70</sup> using anti-NP (2B11) as primary antibody and viral preparations with titers ranging between  $3 \times 10^5$ – $10^6$  NP FFU/ml were used in this study.

For blocking and neutralization assays, infections were performed with serial dilutions of viral stocks, corresponding to MOIs of 0.5 to 0.001. Viral stocks or cells were treated as described below. 24 h post-infection, infected cells were lysed with TRIzol<sup>TM</sup> (ThermoFisher), allowing inactivation of virus, and RNAs were extracted according to manufacturer's protocol and level of viral RNA, reflecting the level of infection, was determined by RT-qPCR (see below). The viral titer was determined after selection of dilutions allowing a linear range of viral RNA signal.

#### Production of viral stock and transduction assays with CCHFV tecVLPs

For production of tecVLPs from IbAr10200 CCHFV strain (Fig. 1a), Huh-7.5 or HEK-293T cells were transfected in 10 cm dishes with 3.6 μg of pCAGGS-V5-L, 1.2 μg of pCAGGS-NP, 3 μg of pCAGGS-M or pCAGGS, 3 μg of pCAGGS-T7 and 1.2 μg of pSMART-LCK\_L-Luc (for tecVLP-NanoLuc) or pT7-GFP (for tecVLP-GFP), using GeneJammer transfection reagent (Agilent). 6 hours post-transfection, cells were washed two times with OptiMEM before addition of OptiMEM. At 72 h post-transfection, supernatant was harvested and filtered through a 0.45 μm filter. Preparations of tecVLPs with titers of  $5 \times 10^5$  GFP transduction units (t.u./ml) (for tecVLP-GFP) or  $10^8$  RLU/ml (for tecVLP-NanoLuc) were used in this study.

For assays with tecVLP-GFP (Fig. 1a), targets cells were pre-transfected using 2.4 μg of pCAGGS-V5-L and 4.8 μg of pCAGGS-NP using GeneJammer transfection reagent. 6 hours post-transfection, cells were seeded in 24, 48 or 96-well plates in OptiMEM. 24 h post-transfection, cells were transduced with serial dilutions of particles,

corresponding to MOIs of 2 to 0.02, and 48 h post-transduction, transduced cells were harvested. For each dilution, technical replicates were performed. Transduced cells were fixed and the percentage of GFP positive cells was assessed by flow cytometry (MACSQuant<sup>®</sup> VYB Flow Cytometer; Miltenyi Biotec). Data were analyzed with FlowJo software (BD Biosciences). The viral titer was determined after selection of dilutions within the linear range of percentages of positive cells.

For assays with tecVLPs with a nanoLuc minigenome (Fig. 1a), the transduction with serial dilutions of viral supernatant, corresponding to RLU-per-cell of 100 to 0.01, was done on Huh-7.5 cells stably expressing firefly luciferase (FLuc) and the level of transduction was quantified 24 h post-transduction, by lysing the cells with passive lysis buffer (Promega) for 10 min at room temperature and measurement of luciferase signal using Nano-Glo<sup>®</sup> Dual-Luciferase<sup>®</sup> Reporter Assay System (Promega). For each dilution, technical replicates were performed. The viral titer was determined after selection of dilutions within a linear range of nanoLuc signals.

#### Production and infection assays with HAZV particles

For production of viral stocks, rHAZV-eGFP virus<sup>24</sup> was amplified in Huh-7.5 cells (MOI = 0.001). 1 h post-infection, media was changed after a PBS wash and 72 h post-infection, supernatant was harvested and clarified by centrifugation 5 min at 750 × g. Preparations of rHAZV-eGFP (termed HAZV in the text and figures) with titers of  $10^6$  eGFP infection units (i.u./ml) were used in this study.

For infection assays, Huh-7.5 cells were inoculated with serial dilutions of viral supernatant, corresponding to MOIs of 0.5 to 0.001, before PBS wash and medium change, 1 h post-infection. Level of infection was detected 16 h post-infection by quantification of eGFP positive cells by flow cytometry (MACSQuant<sup>®</sup> VYB Flow Cytometer; Miltenyi Biotec). Data were analyzed with FlowJo software (BD Biosciences). The viral titer was determined after selection of dilutions allowing a linear range of percentage of positive cells.

#### Production and infection assays with HCV trans-complemented particles (HCVtcp)

For production of viral stocks, Huh-7.5 cells were electroporated with 2 μg of pHCMV-noSpp7 DNA and 10 μg of Jc1 Δp7 in vitro transcribed RNA as described previously<sup>71</sup>. Media was changed 6 h post-electroporation and supernatant was harvested and filtered (0.45 μm) 72 h later. Preparations of HCVtcp with titers of  $10^7$  NS5A FFU/ml were used in this study.

For infection assays, Huh-7.5 cells were inoculated with serial dilutions of viral supernatant, corresponding to MOIs of 2 to 0.02, and were fixed using ethanol 48 h post-infection and focus-forming units were determined by counting NS5A immunostained foci. The viral titer was determined after selection of dilutions allowing a linear range of foci.

#### Production and transduction assays with VSV or MLV pseudoparticles

Lentiviral vectors encoding GFP sequence and bearing VSV-G (VSVpp) or amphotropic MLV Env glycoprotein (MLVpp) were produced in HEK-293T cells by transfection of pHCMV\_HIV\_GFP, psPAX2 and pHCMV-G or pHCMV-4070A using calcium phosphate precipitation. Media was replaced 16 h later and supernatant was harvested and filtered (0.45 μm) 24 h later. Preparations of VSVpp and MLVpp with titers of  $2 \times 10^6$  and  $6 \times 10^5$  GFP t.u./ml, respectively, were used in this study.

For transduction assays, Huh-7.5 cells were transduced with serial dilutions of viral supernatants, corresponding to MOIs of 2 to 0.02, and were fixed 48 h post-transduction. The percentage of GFP-positive cells was assessed by flow cytometry (MACSQuant<sup>®</sup> VYB Flow Cytometer; Miltenyi Biotec). Data were analyzed with FlowJo software (BD Biosciences). The viral titer was determined after selection of dilutions allowing a linear range of percentage of positive cells.

### Production and transduction assays with VSV-ΔG

HEK-293T cells were transfected with pHCMV-G, or with pCAGGS-M-Δ10, encoding for a CCHFV glycoprotein precursor lacking the last 53 residues of Gc<sup>6</sup>, or with pHCMV-EboV<sup>68</sup> encoding for EBOV glycoprotein. At 24 h post-transfection, cells were transduced with VSV-ΔG/GFP\*G, encoding for a GFP instead of G protein at MOI = 5. After 1 h, medium was replaced by OptiMEM in presence of anti-VSV-G 41A1. Cell supernatant was harvested 16 h post-transduction. Preparations of VSV-ΔG/GFP\*G, VSV-ΔG/GFP\*CCHFV, and VSV-ΔG/GFP\*EBOV with titers of  $2 \times 10^8$ ,  $7 \times 10^5$  and  $1.7 \times 10^5$  GFP t.u./ml, respectively, were used in this study.

For transduction assays, Huh-7.5 cells were transduced with serial dilutions of viral supernatants, corresponding to MOIs of 2 to 0.02, and were fixed 24 h post-transduction. The percentage of GFP-positive cells was assessed by flow cytometry (MACSQuant<sup>®</sup> VYB Flow Cytometer; Miltenyi Biotec). Data were analyzed with FlowJo software (BD Biosciences). The viral titer was determined after selection of dilutions allowing a linear range of percentage of positive cells.

### Down-regulation of lipid receptors

Lentiviral vectors expressing shRNA targeting LRPI, LDL-R, SRBI or control shRNA were produced in HEK-293T cells. Huh-7.5 cells stably expressing Firefly Luciferase were transduced with lentiviral vectors at MOI = 30. Four days later, cells were transduced with serial dilutions of tecVLPs with the nanoLuc minigenome. The knock-down was assessed by western blot of cell lysate generated 4 days post-transduction and using anti-LRPI, anti-LDL-R and anti-CD36L1. Level of transduction was assessed 24 h post-transduction with measurement of luciferase signals using Nano-Glo<sup>®</sup> Dual-Luciferase<sup>®</sup> Reporter Assay System (Promega) as described above.

### Down-regulation of apoE

Lentiviral vectors expressing shRNA targeting apoE or control shRNA were produced in HEK-293T cells. Huh-7.5 cells were transduced with lentiviral vector. 24 h post-transduction, cells were transfected with plasmid allowing tecVLPs production or infection of HAZV. 72 h post-transfection, supernatants were harvested and used for assessment of transduction efficiency or infectivity and RNA levels. Level of KD was checked by apoE intracellular FACS staining. Cells were fixed and permeabilized with Cytofix/CytoPerm (BD Biosciences) according to manufacturer instructions. Cells were incubated with primary antibody (AHP2177, 1/2000) diluted in Perm/Wash buffer (BD Biosciences) for 1 h at 4 °C with regular checking. After three washes with Perm/Wash buffer, cells were incubated for 1 h at 4 °C with secondary antibody. Cells were washed three times with Perm/Wash buffer before resuspension in PBS and flow cytometry acquisition (MACSQuant<sup>®</sup> VYB Flow Cytometer; Miltenyi Biotec). Data were analyzed with FlowJo software (BD Biosciences). The gating strategy is depicted in the Supplementary Fig. 4.

### Overexpression of VLDL-R

Huh-7.5 cells stably expressing Firefly luciferase, were transduced at MOI = 30 with a lentiviral vector encoding VLDL-R and transduced at 4 days post-transduction with serial dilutions of tecVLPs containing a nanoLuc expressing minigenome. The level of VLDL-R at the cell surface was assessed by flow cytometry at the day of transduction. Level of transduction was assessed 24 h post-transduction with measurement of luciferase signals using Nano-Glo<sup>®</sup> Dual-Luciferase<sup>®</sup> Reporter Assay System (Promega) as described above.

### Overexpression of apoE

HEK-293T cells were transduced with a lentiviral vector encoding apoE and were then cultivated in presence of blastidicin for selection of transduced cells. Selected cells were used for production of tecVLPs as

described above. The intracellular level of apoE was assessed by flow cytometry as described for down-regulation.

### Blocking with anti-LDL-R antibody

All cell lines were grown in OptiMEM and were incubated with different doses of anti-LDL-R or control IgG for 1 h at 37 °C. Then viral inoculum was added to cells in presence of antibodies, and media was replaced with DMEM, 10% FCS, 3 h post-transduction/infection. All experiments were performed with serial dilution of viral supernatants. For tecVLP-GFP or lentiviral pseudoparticles, cells were harvested 48 h post-transduction and level of transduction was determined by flow cytometry and titer was obtained as described above; for WT virus, cells were harvested 24 h post-infection and infectious titer was determined by RT-qPCR as described above; for HAZV, cells were harvested 16 h post-infection and infectious titer was determined by flow cytometry as described above. When testing different cell lines (EBL, MDBK, A549, TE-671, HEK-293T), cells were transduced with tecVLP-NanoLuc, the level of transduction was quantified 48 h post-transduction, by lysing the cells with passive lysis buffer (Promega) and measurement of luciferase signal using Nano-Glo<sup>®</sup> Luciferase Assay System (Promega). Viral titer was determined as described above. For analysis of incubation kinetics, Huh-7.5 cells were incubated with LDL-R antibody either 1 h before transduction, at the time of transduction or 2 h, 4 h, 6 h post-transduction. The antibody-containing media was replaced by fresh at 2 h or at 24 h post-transduction depending on the conditions (Fig. 3a). Cells were harvested at 48 h post-transduction, and the viral titer was determined after the detection of positive cells by flow cytometry as described above.

For transduction of PHH, at 24 h post-seeding, cells were washed and incubated in their culture medium, with different doses of anti-LDL-R or control IgG for 1 h at 37 °C before transduction with serial volumes of tecVLP-NanoLuc in presence of antibodies. 3 h post-transduction, medium was changed, and the level of transduction was assessed 24 h post-transduction, as described above.

### Neutralization assays with sLDL-R or apoE antibodies

Serial dilutions of inoculate were incubated for 1 h at room temperature with different doses soluble LDL-R (sLDL-R), CD81-6His-LEL, anti-apoE serum or control goat serum and then added to Huh-7.5 cells grown in OptiMEM. All the infection/transduction assays were performed with serial dilutions. At 3 h post-infection or -transduction, media was replaced with DMEM, 10% FCS. For tecVLP-GFP or lentiviral pseudoparticles, cells were harvested 48 h post-transduction and level of transduction was determined by flow cytometry and viral titer was determined as described above; for WT CCHFV virus, cells were harvested 24 h post-infection and level of infectivity was determined by RT-qPCR as described above. For HAZV, infected cells were harvested 16 h post-infection and level of infectivity was determined by flow cytometry. For HCV, cells were fixed 48 h post-infection and level of infectivity was determined by immunostaining as described above.

### Binding assays

CCHFV tecVLPs were incubated with 5 μg of sLDL-R or CD81-LEL<sup>72</sup> (both harboring a 6xHis tag) for 1 h at room temperature before incubation with Ni-particles (MagneHis<sup>™</sup> Protein Purification System, Promega), according to the manufacturer's protocol. After 3 washes, beads were resuspended in TriReagent before extraction and determination of the level of cocaptured CCHFV minigenome by RT-qPCR.

### Cell surface staining of LDL-R or VLDL-R

For flow cytometry, cells were washed and detached with Versene (Invitrogen), before fixation with 2% paraformaldehyde (PFA, (Sigma-Aldrich, France)) for 15 min. Cells were then incubated for 1 h at 4 °C with primary antibody anti-LDL-R (AF2148) or control isotype at 40 μg/mL in PBS + 2% FCS, with regular shaking. After 3 washes, cells

were incubated with secondary antibody for 1 h at 4 °C in PBS + 2% FCS, with regular shaking. After 3 washes, cells were resuspended in PBS + 2% FCS and analyzed by flow cytometry (MACSQuant® VYB Flow Cytometer; Miltenyi Biotec). The gating strategy is depicted in the Supplementary Fig. 3. For VLDL-R staining, the same protocol was used using anti-VLDLR (1H10).

For cell imaging, Huh7.5 cells were grown in 6 well plates containing coverslips. 24 h later, cells were treated as indicated in the figure. Treated cells were then fixed with 3% PFA for 15 min and directly processed for immuno-staining after 3 washes with PBS. Fixed cells were saturated with 3% bovine serum albumin (BSA)/PBS for 20 min and incubated for 1 h with anti-LDL-R (AF2148, 20 µg/mL) and anti-CD81 (JS-81, BD Pharmingen, 1/250) diluted in 1% BSA/PBS. After three washes with 1% BSA/PBS, cells were incubated for 1 h with donkey anti-goat Alexa Fluor 488 and donkey anti-mouse Alexa Fluor 555 respectively (A-11055 and A-31570 respectively, Molecular Probes) at a 1/2000 dilution in 1% BSA/PBS. Cells were washed three times with PBS, stained for nuclei with Hoechst 33342 (H3570, Molecular Probes) for 5 min in PBS, washed three times with PBS and mounted in Mowiol 40-88 (Sigma-Aldrich) before acquisition with confocal microscope LSM-800 (Zeiss) equipped with a 63X objective. Images were analyzed with the Fiji software (<https://imagej.net>).

#### Co-immunoprecipitation assay

CCHFV tecVLPs were incubated with apoE antibodies (AB947; Sigma-Aldrich) or control goat IgG overnight at 4 °C. Then 1.5 mg of Dynabeads protein G magnetic beads (ThermoFisher) were added during 1 h at room temperature. The beads were then washed 3 times with PBS. For the elution, beads were resuspended in TriReagent and the supernatant was transferred into a new tube for RNA extraction, following manufacturer's protocol before determination of the level of cocaptured CCHFV minigenome by RT-qPCR (see below).

The same procedure was used with CCHFV WT particles, with elution using Trizol LS. RNA and proteins were extracted according to the manufacturer's protocol. The level of co-captured CCHFV RNA was determined by RT-qPCR (see below) and the level of proteins was determined by western blot.

#### Capture of particles with sLDL-R or CD81-LEL

CCHFV tecVLPs or WT CCHFV or HAZV particles were incubated with 5 µg of soluble LDL-R (2148-LD-025/CF, R&D systems), or CD81-LEL for 1 h at room temperature. Then 30 µL of MagneHis Ni-Particles (Promega) were added and the samples were processed according to manufacturer's instructions. For the elution, beads were resuspended in TriReagent and the supernatant was transferred into a new tube for RNA extraction, following manufacturer's protocol before determination of the level of co-captured CCHFV or HAZV RNAs by RT-qPCR (see below).

#### Detection of viral genomes by RT-qPCR

After extraction following the manufacturer's protocol, RNA was reverse transcribed (iScript cDNA synthesis kit; Bio-Rad). In the case of tecVLPs samples, RNA was treated with DNase (Invitrogen) according to manufacturer's protocol. Level of cDNA was then quantified by qPCR. For tecVLPs minigenome, the quantification was done by detection of the nanoLuc minigenome for CCHFV: 5'-TAGTCGATCATGTTCCGGCGT-3' and 5'-ACCTGTGGATGATCATCACT-3' with 5'-GATTACCAAGTGTCCATAGTCAGGATCAC-3' as probe, using TaqMan™ Gene Expression Master Mix (ThermoFisher). For WT CCHFV, the quantification was done using FastStart Universal SYBR (Roche) with the following primers 5'-CCCCACACCCCAAGATAATA-3' and 5'-ACTACTCTGCATTCTCTCA-3' targeting L UTR. For HAZV, the quantification was done by using FastStart Universal SYBR (Roche) with the following primers 5'-CAAGCAAGCATTGCACAAC-3' and 5'-GCTTTCTCTACCCCTTTTGA-3' targeting S segment.

For titration of WT CCHFV, viral RNA levels were normalized with respect to glyceraldehyde-3-phosphate dehydrogenase (GAPDH) RNA levels, detected using FastStart Universal SYBR (Roche) and specific primers 5'-AGGTGAAGTCCGGAGTCAACG-3' and 5'-TGGAA-GATGGTATGGGATTTC-3'.

As an internal control of extraction, an exogenous RNA from the linearized Triplescript plasmid pTRI-Xef (Invitrogen) was added into the supernatant prior to extraction and quantified with specific primers 5'-CGACGTTGTACCGGGCAGC and 5'-ACCAGGCATGGTGGT-TACCTTTGC. This signal was used for normalization of signal for crude supernatant, as well as capture and IP assays.

All analyses were done on a Quantstudio real-time PCR apparatus.

#### Drug treatment

Recombinant PCSK9 (Thermo-Fisher) or Berbamine (BBM, Sigma-Aldrich) were used at the indicated concentration and time of incubation. Huh-7.5 cells were incubated with 0 vs. 10 µg/mL of PCSK9 for 3 h at 37 °C, or with 0 vs. 75 µM of Berbamine (BBM) for 2 h at 37 °C before infection or transduction with serial volume of particles. The media was replaced 3 h post-infection (p.i.) or post-transduction (p.t.) and the cells were harvested at 48 h p.i. or p.t. for determination of the levels of infection or transduction by flow cytometry. Cell viability and level of LDL-R at cell surface were assessed at the time of infection or transduction.

#### Electron microscopy

For negative staining, formvar/carbon-coated nickel grids were deposited on a drop of samples during five minutes and rinsed two times on drop of water. The negative staining was then performed with three consecutive contrasting steps using 2% uranyl acetate (Agar Scientific), before analysis under the transmission electron microscope (JEM-1400Plus).

For analysis of the particles by negative staining electron microscopy and immunogold labeling, formvar/carbon-coated nickel grids were deposited on a drop of samples during five minutes and rinsed two times with phosphate-buffered saline (PBS). Grids were then incubated on a drop of PBS/BSA 1% and then PBS containing 1:100 goat anti-apoE serum (AHP2177) and 1:100 mouse anti-Gn serum (in-house) for one hour. After six washes of five minutes with PBS, each, grids were further incubated for one hour on a drop of PBS containing 1:30 gold-conjugated (6 nm) donkey anti-goat or 1:30 gold conjugated (6 nm) goat anti-mouse (Aurion). Grids were then washed again with six drops of PBS, post-fixed in 1% glutaraldehyde and rinsed with three drops of distilled water. The negative staining was then performed with three consecutive contrasting steps using 2% uranyl acetate (Agar Scientific), before analysis under the transmission electron microscope (JEM-1400Plus).

#### Western blot analysis of cell lysates and pellets

For cell lysates, cells were lysed with lysis buffer (20 mM Tris [pH 7.5], 1% Triton X-100, 0.05% sodium dodecyl sulfate, 150 mM NaCl, 0.5% Na deoxycholate) supplemented with protease/phosphatase inhibitor cocktail (Roche) and clarified from the nuclei by centrifugation at 13,000 × g for 10 min at 4 °C for quantitative western blot analysis. For pelleting of particles, supernatants were harvested and filtered through a 0.45 µm filter and centrifuged through a 20% sucrose cushion at 28,000 rpm for 2 h at 4 °C with a SW41 rotor and Optima L-90 centrifuge (Beckman). Pellets were resuspended in PBS prior to use for western blot.

Proteins obtained in total cell lysates or pellets were denatured in Laemmli buffer (250 mM Tris-HCl pH 6.8, 10% SDS, 50% glycerol, 500 mM β-mercapto-ethanol, bromophenol blue) at 95 °C for 5 min separated by SDS-PAGE, and then transferred to nitrocellulose membrane and revealed with specific primary antibodies, followed by the addition of IRDye secondary antibodies, and imaging with an Odyssey

Article

<https://doi.org/10.1038/s41467-024-48989-5>

infrared imaging system CLx (Li-Cor Biosciences). In the case of Gc detection, proteins in total cell lysates or pellets were loaded in non-denaturing, non-reducing buffer (250 mM Tris-HCL pH 6.8, 5% SDS, 50% glycerol, bromophenol blue).

**Cell viability measurement**

The cell viability was assessed using Cytotox-Glo Cytotoxicity Assay (Promega) according to the manufacturer’s protocol.

**Statistical analysis**

Significance values were calculated by applying tests indicated in the figure legends using the GraphPad Prism 10 software (GraphPad Software, USA). P values under 0.05 were considered statistically significant and the following denotations were used: \*\*\*\* $P < 0.0001$ ; \*\*\* $P < 0.001$ ; \*\* $P < 0.01$ ; \* $P < 0.05$ ; ns (not significant),  $P > 0.05$ .

**Reporting summary**

Further information on research design is available in the Nature Portfolio Reporting Summary linked to this article.

**Data availability**

The data generated in this study are provided in the Source Data file. Source data are provided with this paper.

**References**

1. Bente, D. A. et al. Crimean-Congo hemorrhagic fever: history, epidemiology, pathogenesis, clinical syndrome and genetic diversity. *Antivir. Res* **100**, 159–189 (2013).
2. Messina, J. P. et al. A global compendium of human Crimean-Congo haemorrhagic fever virus occurrence. *Sci. Data* **2**, 150016 (2015).
3. Freitas, N., Legros, V. & Cosset, F. L. Crimean-Congo hemorrhagic fever: a growing threat to Europe. *C. R. Biol.* **345**, 17–36 (2022).
4. Gargili, A. et al. The role of ticks in the maintenance and transmission of Crimean-Congo hemorrhagic fever virus: A review of published field and laboratory studies. *Antivir. Res* **144**, 93–119 (2017).
5. Hawman, D. W. & Feldmann, H. Crimean–Congo haemorrhagic fever virus. *Nat. Rev. Microbiol.* **21**, 463–477 (2023).
6. Suda, Y. et al. Analysis of the entry mechanism of Crimean-Congo hemorrhagic fever virus, using a vesicular stomatitis virus pseudotyping system. *Arch. Virol.* **161**, 1447–1454 (2016).
7. Xiao, X., Feng, Y., Zhu, Z. & Dimitrov, D. S. Identification of a putative Crimean-Congo hemorrhagic fever virus entry factor. *Biochem Biophys. Res Commun.* **411**, 253–258 (2011).
8. Devignot, S. et al. Low-density lipoprotein receptor-related protein 1 (LRP1) as an auxiliary host factor for RNA viruses. *Life Sci. Alliance* **6**, e202302005 (2023).
9. Ganaie, S. S. et al. Lrp1 is a host entry factor for Rift Valley fever virus. *Cell* **184**, 5163–5178.e5124 (2021).
10. Schwarz, M. M. et al. Oropouche orthobunyavirus infection is mediated by the cellular host factor Lrp1. *Proc. Natl Acad. Sci. USA* **119**, e2204706119 (2022).
11. Clark, L. E. et al. VLDLR and ApoER2 are receptors for multiple alphaviruses. *Nature* **602**, 475–480 (2022).
12. Yamamoto, S. et al. Lipoprotein Receptors Redundantly Participate in Entry of Hepatitis C Virus. *PLoS Pathog.* **12**, e1005610 (2016).
13. Albecka, A. et al. Role of low-density lipoprotein receptor in the hepatitis C virus life cycle. *Hepatology* **55**, 998–1007 (2012).
14. Molina, S. et al. The low-density lipoprotein receptor plays a role in the infection of primary human hepatocytes by hepatitis C virus. *J. Hepatol.* **46**, 411–419 (2007).
15. Li, Y. & Luo, G. Human low-density lipoprotein receptor plays an important role in hepatitis B virus infection. *PLoS Pathog.* **17**, e1009722 (2021).
16. Huang, L. et al. Berbamine inhibits Japanese encephalitis virus (JEV) infection by compromising TPRMLs-mediated endolysosomal

- trafficking of low-density lipoprotein receptor (LDLR). *Emerg. Microbes Infect.* **10**, 1257–1271 (2021).
17. Finkelshtein, D., Werman, A., Novick, D., Barak, S. & Rubinstein, M. LDL receptor and its family members serve as the cellular receptors for vesicular stomatitis virus. *Proc. Natl Acad. Sci. USA* **110**, 7306–7311 (2013).
18. Amirache, F. et al. Mystery solved: VSV-G-LVs do not allow efficient gene transfer into unstimulated T cells, B cells, and HSCs because they lack the LDL receptor. *Blood* **123**, 1422–1424 (2014).
19. Devignot, S., Bergeron, E., Nichol, S., Mirazimi, A. & Weber, F. A virus-like particle system identifies the endonuclease domain of Crimean-Congo hemorrhagic fever virus. *J. Virol.* **89**, 5957–5967 (2015).
20. Zivcec, M. et al. Assessment of Inhibitors of Pathogenic Crimean-Congo Hemorrhagic Fever Virus Strains Using Virus-Like Particles. *PLoS Negl. Trop. Dis.* **9**, e0004259 (2015).
21. Fels, J. M. et al. Protective neutralizing antibodies from human survivors of Crimean-Congo hemorrhagic fever. *Cell* **184**, 3486–3501.e3421 (2021).
22. Freitas, N. et al. The interplays between Crimean-Congo hemorrhagic fever virus (CCHFV) M segment-encoded accessory proteins and structural proteins promote virus assembly and infectivity. *PLoS Pathog.* **16**, e1008850 (2020).
23. Lavillette, D., Ruggieri, A., Boson, B., Maurice, M. & Cosset, F. L. Relationship between SU subdomains that regulate the receptor-mediated transition from the native (fusion-inhibited) to the fusion-active conformation of the murine leukemia virus glycoprotein. *J. Virol.* **76**, 9673–9685 (2002).
24. Fuller, J. et al. Hazara Nairovirus Requires COPI Components in both Arf1-Dependent and Arf1-Independent Stages of Its Replication Cycle. *J. Virol.* **94**, e00766–20 (2020).
25. Go, G. W. & Mani, A. Low-density lipoprotein receptor (LDLR) family orchestrates cholesterol homeostasis. *Yale J. Biol. Med* **85**, 19–28 (2012).
26. Douam, F. et al. Critical interaction between E1 and E2 glycoproteins determines binding and fusion properties of hepatitis C virus during cell entry. *Hepatology. (Baltim., Md)* **56**, 776–788 (2014).
27. Shtanko, O., Nikitina, R. A., Altuntas, C. Z., Chepurinov, A. A. & Davey, R. A. Crimean-Congo hemorrhagic fever virus entry into host cells occurs through the multivesicular body and requires ESCRT regulators. *PLoS Pathog.* **10**, e1004390 (2014).
28. Owen, D. M., Huang, H., Ye, J. & Gale, M. Jr. Apolipoprotein E on hepatitis C virion facilitates infection through interaction with low-density lipoprotein receptor. *Virology* **394**, 99–108 (2009).
29. Nikolic, J. et al. Structural basis for the recognition of LDL-receptor family members by VSV glycoprotein. *Nat. Commun.* **9**, 1029 (2018).
30. Battini, J. L., Rodrigues, P., Muller, R., Danos, O. & Heard, J. M. Receptor-binding properties of a purified fragment of the 4070A amphotropic murine leukemia virus envelope glycoprotein. *J. Virol.* **70**, 4387–4393 (1996).
31. Zhang, W. Y., Gaynor, P. M. & Kruth, H. S. Apolipoprotein E produced by human monocyte-derived macrophages mediates cholesterol efflux that occurs in the absence of added cholesterol acceptors. *J. Biol. Chem.* **271**, 28641–28646 (1996).
32. Li, Z. et al. Extracellular Interactions between Hepatitis C Virus and Secreted Apolipoprotein E. *J. Virol.* **91**, e02227–16 (2017).
33. Bankwitz, D. et al. Maturation of secreted HCV particles by incorporation of secreted ApoE protects from antibodies by enhancing infectivity. *J. Hepatol.* **67**, 480–489 (2017).
34. Calattini, S. et al. Functional and Biochemical Characterization of Hepatitis C Virus (HCV) Particles Produced in a Humanized Liver Mouse Model. *J. Biol. Chem.* **290**, 23173–23187 (2015).
35. Zhang, D. W. et al. Binding of proprotein convertase subtilisin/kexin type 9 to epidermal growth factor-like repeat A of low density lipoprotein receptor decreases receptor recycling and increases degradation. *J. Biol. Chem.* **282**, 18602–18612 (2007).



36. Xu, Z. S. et al. LDLR is an entry receptor for Crimean-Congo hemorrhagic fever virus. *Cell Res* **34**, 140–150 (2024).
37. Blacklow, S. C. Versatility in ligand recognition by LDL receptor family proteins: advances and frontiers. *Curr. Opin. Struct. Biol.* **17**, 419–426 (2007).
38. Ujino, S. et al. Hepatitis C virus utilizes VLDLR as a novel entry pathway. *Proc. Natl Acad. Sci. USA* **113**, 188–193 (2016).
39. Chen, J. M. et al. Bovine Lactoferrin Inhibits Dengue Virus Infectivity by Interacting with Heparan Sulfate, Low-Density Lipoprotein Receptor, and DC-SIGN. *Int J. Mol. Sci.* **18**, 1957 (2017).
40. Hofer, F. et al. Members of the low density lipoprotein receptor family mediate cell entry of a minor-group common cold virus. *Proc. Natl Acad. Sci. USA* **91**, 1839–1842 (1994).
41. Verdaguer, N., Fita, I., Reithmayer, M., Moser, R. & Blaas, D. X-ray structure of a minor group human rhinovirus bound to a fragment of its cellular receptor protein. *Nat. Struct. Mol. Biol.* **11**, 429–434 (2004).
42. Qiao, L. & Luo, G. G. Human apolipoprotein E promotes hepatitis B virus infection and production. *PLoS Pathog.* **15**, e1007874 (2019).
43. Dreux, M. et al. The exchangeable apolipoprotein ApoC-I promotes membrane fusion of hepatitis C virus. *J. Biol. Chem.* **282**, 32357–32369 (2007).
44. Meunier, J. C. et al. Evidence for cross-genotype neutralization of hepatitis C virus pseudo-particles and enhancement of infectivity by apolipoprotein C1. *Proc. Natl Acad. Sci. USA* **102**, 4560–4565 (2005).
45. Dao Thi, V. L. et al. Characterization of hepatitis C virus particle subpopulations reveals multiple usage of the scavenger receptor BI for entry steps. *J. Biol. Chem.* **287**, 31242–31257 (2012).
46. Jiang, J. et al. Hepatitis C virus attachment mediated by apolipoprotein E binding to cell surface heparan sulfate. *J. Virol.* **86**, 7256–7267 (2012).
47. Lefevre, M., Felmlee, D. J., Parnot, M., Baumert, T. F. & Schuster, C. Syndecan 4 is involved in mediating HCV entry through interaction with lipoviral particle-associated apolipoprotein E. *PLoS One* **9**, e95550 (2014).
48. Dubuisson, J. & Cosset, F. L. Virology and cell biology of the hepatitis C virus life cycle - An update. *J. Hepatol.* **61**, S3–S13 (2014).
49. Murayama, A., Sugiyama, N., Wakita, T. & Kato, T. Completion of the Entire Hepatitis C Virus Life Cycle in Vero Cells Derived from Monkey Kidney. *mBio* **7**, e00273–16 (2016).
50. Herz, J. The LDL receptor gene family: (un)expected signal transducers in the brain. *Neuron* **29**, 571–581 (2001).
51. Buchholz, C. J., Schneider, U., Devaux, P., Gerlier, D. & Cattaneo, R. Cell entry by measles virus: long hybrid receptors uncouple binding from membrane fusion. *J. Virol.* **70**, 3716–3723 (1996).
52. Strickland, D. K., Gonias, S. L. & Argaves, W. S. Diverse roles for the LDL receptor family. *Trends Endocrinol. Metab.* **13**, 66–74 (2002).
53. Dreux, M. et al. Receptor complementation and mutagenesis reveal SR-BI as an essential HCV entry factor and functionally imply its intra- and extra-cellular domains. *PLoS Pathog.* **5**, e1000310 (2009).
54. Li, Y., Lu, W., Marzolo, M. P. & Bu, G. Differential functions of members of the low density lipoprotein receptor family suggested by their distinct endocytosis rates. *J. Biol. Chem.* **276**, 18000–18006 (2001).
55. Hueging, K. et al. Apolipoprotein E codetermines tissue tropism of hepatitis C virus and is crucial for viral cell-to-cell transmission by contributing to a postenvelopment step of assembly. *J. Virol.* **88**, 1433–1446 (2014).
56. Jiang, J. & Luo, G. Apolipoprotein E but not B is required for the formation of infectious hepatitis C virus particles. *J. Virol.* **83**, 12680–12691 (2009).
57. Lee, J. Y. et al. Apolipoprotein E likely contributes to a maturation step of infectious hepatitis C virus particles and interacts with viral envelope glycoproteins. *J. Virol.* **88**, 12422–12437 (2014).
58. Hatters, D. M., Peters-Libeu, C. A. & Weisgraber, K. H. Apolipoprotein E structure: insights into function. *Trends Biochem. Sci.* **31**, 445–454 (2006).
59. Nguyen, D., Dhanasekaran, P., Phillips, M. C. & Lund-Katz, S. Molecular mechanism of apolipoprotein E binding to lipoprotein particles. *Biochemistry* **48**, 3025–3032 (2009).
60. Hussain, M. M. et al. Microsomal triglyceride transfer protein in plasma and cellular lipid metabolism. *Curr. Opin. Lipido.* **19**, 277–284 (2008).
61. Dai, S. et al. Differential Cell Line Susceptibility to Crimean-Congo Hemorrhagic Fever Virus. *Front Cell Infect. Microbiol.* **11**, 648077 (2021).
62. Spengler, J. R., Bergeron, É. & Rollin, P. E. Seroepidemiological Studies of Crimean-Congo Hemorrhagic Fever Virus in Domestic and Wild Animals. *PLoS Negl. Trop. Dis.* **10**, e0004210 (2016).
63. Mitchell, R. D. 3rd, Sonenshine, D. E. & Pérez de León, A. A. Vitellogenin Receptor as a Target for Tick Control: A Mini-Review. *Front Physiol.* **10**, 618 (2019).
64. Huo, Y. et al. Insect tissue-specific vitellogenin facilitates transmission of plant virus. *PLoS Pathog.* **14**, e1006909 (2018).
65. Tsergouli, K., Karampatakis, T., Haidich, A. B., Metallidis, S. & Papa, A. Nosocomial infections caused by Crimean-Congo haemorrhagic fever virus. *J. Hosp. Infect.* **105**, 43–52 (2020).
66. Bergeron, E., Albarino, C. G., Khristova, M. L. & Nichol, S. T. Crimean-Congo hemorrhagic fever virus-encoded ovarian tumor protease activity is dispensable for virus RNA polymerase function. *J. Virol.* **84**, 216–226 (2010).
67. Sandrin, V. et al. Lentiviral vectors pseudotyped with a modified RD114 envelope glycoprotein show increased stability in sera and augmented transduction of primary lymphocytes and CD34+ cells derived from human and nonhuman primates. *Blood* **100**, 823–832 (2002).
68. Szecsi, J. et al. Targeted retroviral vectors displaying a cleavage site-engineered hemagglutinin (HA) through HA-protease interactions. *Mol. Ther.* **14**, 735–744 (2006).
69. Lavillette, D. et al. Characterization of host-range and cell entry properties of major genotypes and subtypes of hepatitis C virus. *Hepatology (Baltim., Md)* **41**, 265–274 (2005).
70. Moroso, M. et al. Crimean-Congo hemorrhagic fever virus replication imposes hyper-lipidation of MAP1LC3 in epithelial cells. *Autophagy* **16**, 1858–1870 (2020).
71. Denolly, S. et al. A serum protein factor mediates maturation and apoB-association of HCV particles in the extracellular milieu. *J. Hepatol.* **70**, 626–638 (2019).
72. Maurin, G. et al. Identification of Interactions in the E1E2 Heterodimer of Hepatitis C Virus Important for Cell Entry. *J. Biol. Chem.* **286**, 23865–23876 (2011).

### Acknowledgements

We thank Chloé Journo and Christiane Riedel for stimulating discussions. We thank Fouzia Amirache, Christelle Granier, Solène Lerolle, Chloé Mialon and Johan Toesca for their technical inputs. We are grateful to Ralf Bartenschlager for the gift of HCV and apoE constructs, Charles Rice for the Huh-7.5 cells and 9E10 NS5A monoclonal antibody, Yoshiharu Matsuura for the VLDL-R construct, Friedemann Weber and Eric Bergeron for the CCHF tecVLP constructs, Olivier Reynard for the VSV-ΔG/GFP stock, and Sandra Lacôte for the bovine cell lines. We acknowledge the contribution of SFR Biosciences (Université Claude Bernard Lyon 1, CNRS UAR3444, Inserm US8, ENS de Lyon), LYMIC-PLATIM-microscopie, AniRA-Cytométrie and AniRA vectorology, especially Caroline Costa. We are grateful to P4 Jean Mérieux team (INSERM

## Article

<https://doi.org/10.1038/s41467-024-48989-5>

USO3, Lyon) and the related biosafety team for their assistance for BSL4 activities. This work was supported by the LabEx Ecofect (ANR-11-LABX-0048 awarded to F.-L.C.) of the Université de Lyon, within the program Investissements d'Avenir (ANR-11-IDEX-0007) operated by the French National Research Agency (ANR), the Fondation pour la Recherche Médicale (FRM, Grant number: EQU202203014673 awarded to F.-L.C.), the ANRS I MIE (Grant number: ANRS0630 awarded to F.-L.C.), and the ANR (Grant number: ANR-22-ASTR-0031 awarded to F.-L.C.). S.D. and A.Gau. were supported by fellowships of the ANRS I MIE.

### Author contributions

Conceptualization, M.R., F.-L.C., and S.D.; Investigation, M.R., L.C., A.Gau., T.V., L.Z., A.L., B.B., A.Gan., S.B., J.B.G., N.F., V.Le., C.M.; Writing Original-Draft, M.R., F.-L.C., and S.D.; Writing Revised-Draft, F.-L.C. and S.D.; Supervision, F.-L.C. and S.D.; Critical reagents, P.R., J.N.B., V.Lo.; Funding Acquisition, V.Lo., V.Le., F.-L.C. and S.D.

### Competing interests

The authors declare no competing interests. A European patent application has been filed by Inserm-Transfert.

### Additional information

**Supplementary information** The online version contains supplementary material available at <https://doi.org/10.1038/s41467-024-48989-5>.

**Correspondence** and requests for materials should be addressed to François-Loïc. Cosset or Solène Denolly.

**Peer review information** *Nature Communications* thanks the anonymous, reviewer(s) for their contribution to the peer review of this work. A peer review file is available.

**Reprints and permissions information** is available at <http://www.nature.com/reprints>

**Publisher's note** Springer Nature remains neutral with regard to jurisdictional claims in published maps and institutional affiliations.

**Open Access** This article is licensed under a Creative Commons Attribution 4.0 International License, which permits use, sharing, adaptation, distribution and reproduction in any medium or format, as long as you give appropriate credit to the original author(s) and the source, provide a link to the Creative Commons licence, and indicate if changes were made. The images or other third party material in this article are included in the article's Creative Commons licence, unless indicated otherwise in a credit line to the material. If material is not included in the article's Creative Commons licence and your intended use is not permitted by statutory regulation or exceeds the permitted use, you will need to obtain permission directly from the copyright holder. To view a copy of this licence, visit <http://creativecommons.org/licenses/by/4.0/>.

© The Author(s) 2024

### Supplementary Information

#### **The low-density lipoprotein receptor and apolipoprotein E associated with CCHFV particles mediate CCHFV entry into cells**

Maureen Ritter, Lola Canus\*, Anupriya Gautam\*, Thomas Vallet\*, Li Zhong\*, Alexandre Lalande, Bertrand Boson, Apoorv Gandhi, Sergueï Bodoirat, Julien Burlaud-Gaillard, Natalia Freitas, Philippe Roingear, John N. Barr, Vincent Lotteau, Vincent Legros, Cyrille Mathieu, François-Loïc Cosset\*\*, and Solène Denolly\*\*

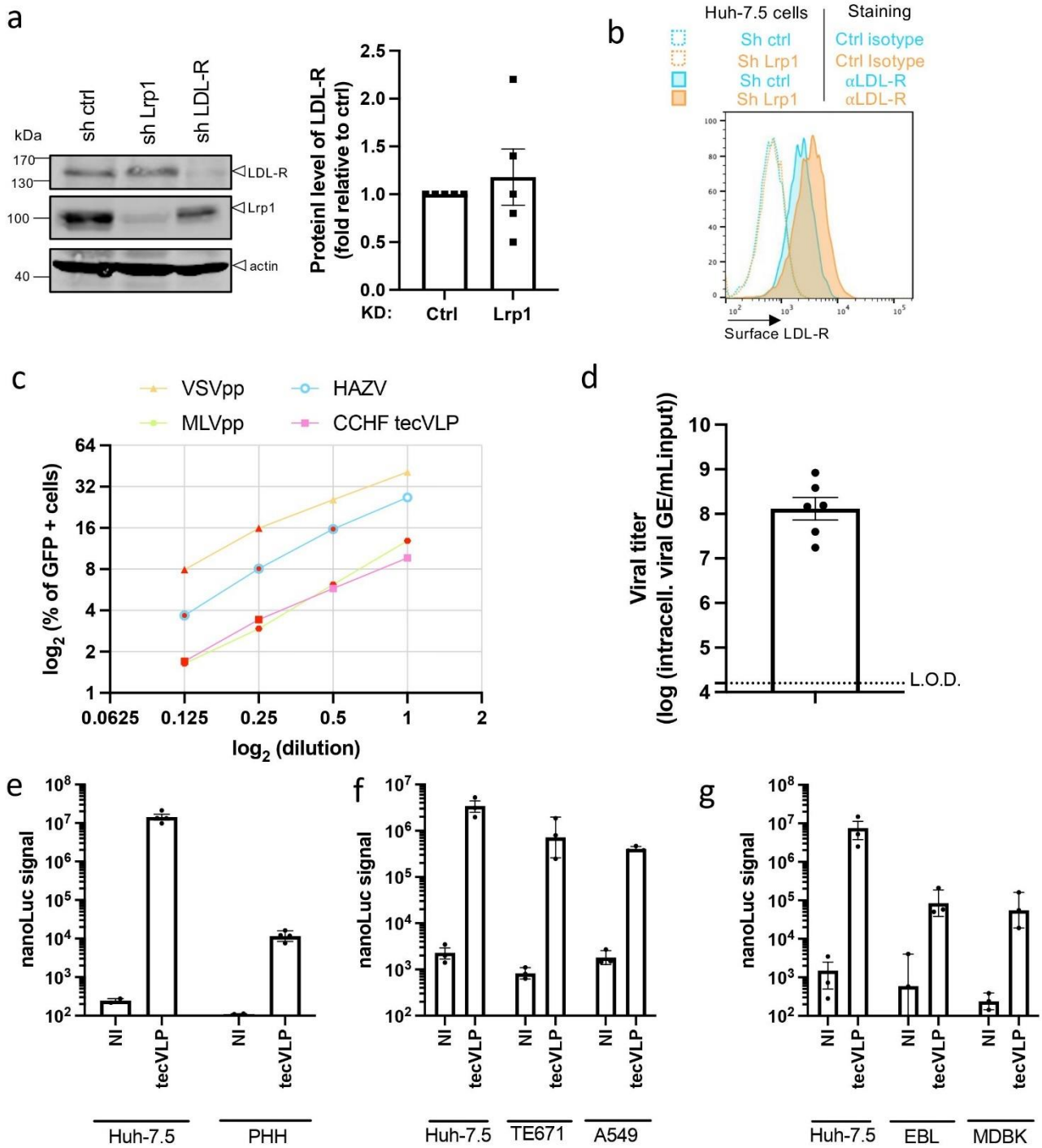
\* These authors contributed equally

\*\* These authors jointly supervised this work

Corresponding authors : [francois-loic.cosset@ens-lyon.fr](mailto:francois-loic.cosset@ens-lyon.fr); [solene.denolly@ens-lyon.fr](mailto:solene.denolly@ens-lyon.fr)

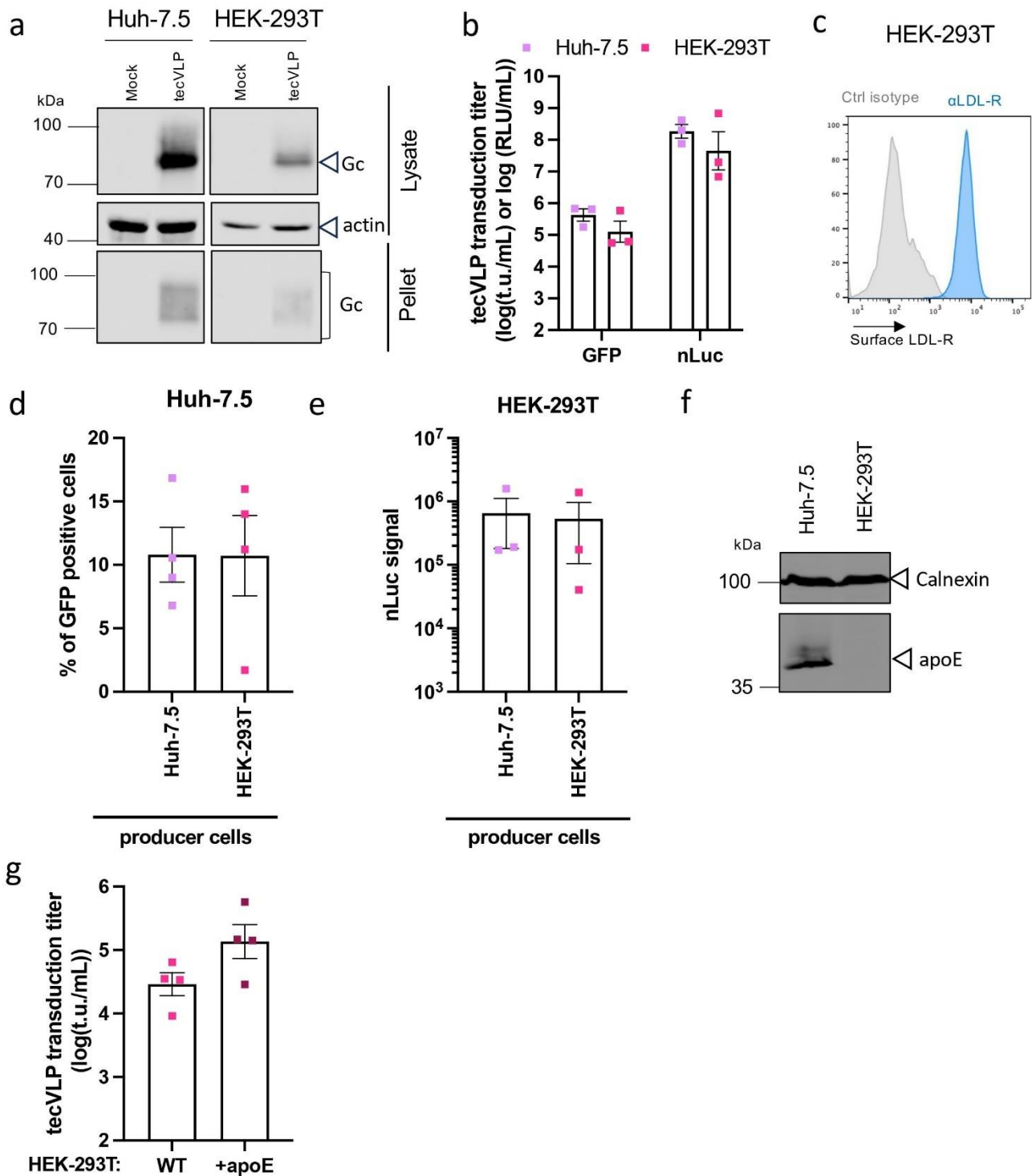
**Supplementary Table 1. Antibodies used in this study.**

<b>Primary antibodies</b>		
<b>Targets</b>	<b>Dilution</b>	<b>Company (catalog number)</b>
LDL-R (goat)	IF 20mg/mL; FACS 40mg/mL ; WB 2mg/mL; blocking assay 0.25-1-4mg/mL	R&D systems (AF2148)
Lrp1 (rabbit)	WB 1:1000	Abcam (EPR3724)
VLDL-R (mouse)	FACS 1:1000	Abcam (1H10)
SR-BI (mouse)	WB 1:200	BD biosciences (610883)
CD81 (mouse)	IF 1:250	BD Pharmingen (JS-81)
apoE (goat)	IP 10 $\mu$ L	Sigma-Aldrich (AB947)
apoE (goat)	WB 1:2000; EM 1:100; neutralization assay 1:200-1:100-1:50; FACS 1:2000	AbD Serotec (AHP2177)
Actin (mouse)	WB 1:10000	Sigma-Aldrich (AC-74)
Calnexin (rabbit)	WB 1:1000	Enzo Life sciences (ADI-SPA-865-F)
CCHFV Gc 11E7 (mouse)	WB 1:1000	BEI Resources (NR-40277 )
CCHFV Gn (mouse)	WB 1:1000 ; EM 1:100	Home-made
CCHFV NP 9D5 (mouse)	WB 1:1000	BEI Resources (NR-40277)
CCHFV NP 2B11 (mouse)	Immunostaining 1:250	BEI Resources (NR-40257)
HCV NS5A 9E10 (mouse)	Immunostaining 1:800	Kind gift from C. Rice
Anti VSV-G (mouse)	Neutralization for production 1:100	41A1 (hybridoma)
Goat IgG	FACS 40ug/mL; blocking assay 0.25-1-4ug/mL	ThermoFisher (02- 363 6202)
Goat serum	neutralization assay 1:200-1:100-1:50	Viomed (79S094)
<b>Secondary antibodies</b>		
Donkey anti-mouse Alexa Fluor 555	IF 1:2000	ThermoFisher (A-31570)
Donkey anti-goat Alexa Fluor 488	IF 1:2000	ThermoFisher (A-11055)
Goat anti-Mouse-HRP	Immunostaining (HCV) 1:1000	Sigma-Aldrich (A4416)
Anti-Mouse IgG (whole molecule)–Peroxidase antibody	Immunostaining (CCHFV) 1:1000	Sigma-Aldrich (A5278)
Goat F(ab') <sub>2</sub> Anti-Mouse Ig, Human ads-APC	FACS 1:100	Southern Biotech (1012-11)
F(ab') <sub>2</sub> -Donkey anti-Goat IgG (H+L), PE	FACS 1:100	ThermoFisher ( 31860)
Anti-Goat IgG, FITC	FACS 1:100	Dako (F0250)
IRDye® 680RD Donkey anti-Mouse IgG	WB 1:10000	Li-COR Biosciences (926-68072)
IRDye® 800CW Goat anti-Mouse IgG	WB 1:10000	Li-COR Biosciences (926-32210)
IRDye® 800CW Donkey Anti-Rabbit IgG	WB 1:10000	Li-COR Biosciences (926-32213)
IRDye® 800CW Donkey anti-Goat IgG	WB 1:10000	Li-COR Biosciences (926-32214)



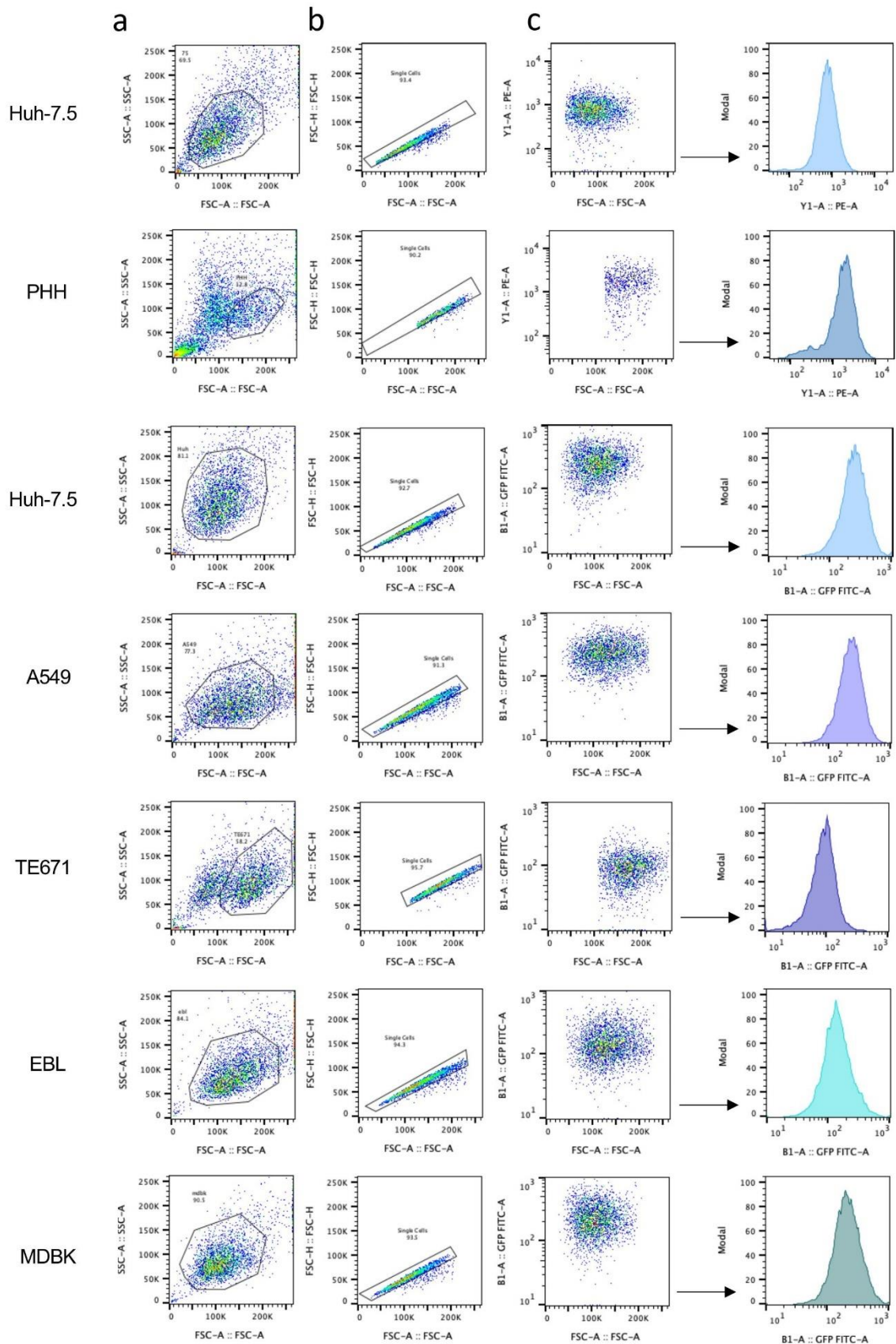
**Supplementary Figure 1. Conditions for transduction or infection with tecVLP or WT CCHFV.**

(a) Western blot analysis of cell lysates from Huh-7.5 cells stably expressing FLuc, transduced with lentiviral vectors allowing expression of control shRNA or shRNA targeting Lrp1 or LDL-R (left). Representative image of 5 independent experiments. Quantification of abundance of LDL-R in control or Lrp1 KD cells. N=5 independent experiments. (b) Cell surface expression of LDL-R of cells transduced with sh-ctrl or sh-Lrp1 as described in Figure 1b. Control isotypes are depicted in dotted lines. Representative image of 3 independent experiments (c) Representative example of the linearity of infection or transduction obtained with serial dilutions of particles. The red dots indicate the values used for calculation of the levels of infection/transduction. (d) Viral titers obtained for experiments with WT CCHFV described in Figure 1a. N=6 independent experiments. (e) Levels of nanoLuc signals detected at 24h after transduction of Huh-7.5 cells or PHH with 100 $\mu$ L of tecVLPs with minigenome encoding nanoLuc. N=4 independent experiments. (f) Levels of nanoLuc signals detected 48h after transduction of Huh-7.5, TE-671 and A549 cells with 100 $\mu$ L of tecVLPs with minigenome encoding nanoLuc. N=3 independent experiments (g) Levels of nanoLuc signals detected 48h after transduction of Huh-7.5, EBL and MDBK cells with 100 $\mu$ L of tecVLPs encoding nanoLuc. N=3 independent experiments. NI=non infected control. Data are represented as the means  $\pm$  SEM. Each dot in the graphs corresponds to the value of an individual experiment.



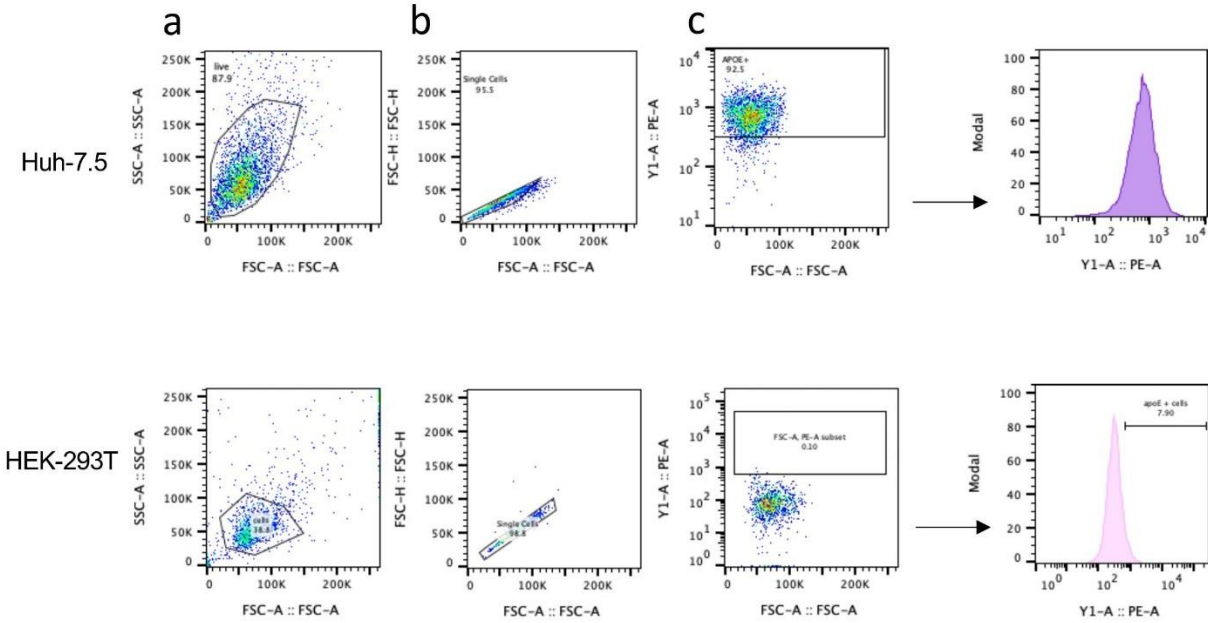
**Supplementary Figure 2. apoE influences CCHF tecVLPs infection.**

(a) Western blot of cell lysates and pellets of tecVLPs produced in Huh-7.5 or HEK-293T cells and revealed for Gc expression. Representative image of 3 independent experiments. (b) Transduction titer of tecVLP-GFP or tecVLP-NanoLuc particles produced in Huh-7.5 (violet) or HEK-293T (pink) cells. The infectivity was assessed after transduction of Huh-7.5 cells pre-transfected with NP+L expression plasmids, by flow cytometry at 24h post-transfection (p.t.) for GFP minigenome or after transduction of Huh-7.5 cells, by nanoLuc signal measurement at 24h p.t. for nanoLuc minigenome. N=3 independent experiments. (c) Cell surface staining of LDL-R at the surface of HEK-293T cells. Representative images of 3 independent experiments. (d) Percentage of GFP positive cells obtained for condition without antibodies in experiments of Figure 3b (left). N=3 independent experiments. (e) Levels of nanoLuc signal obtained for condition without antibodies in experiments of Figure 3b (right). N=3 independent experiments. (f) Western blot of cell lysates of Huh-7.5 and HEK-293T cells that were revealed for expression of apoE. Representative image of 3 independent experiments. (g) Transduction titers of tecVLP-GFP particles produced in HEK-293T cells (pink) or in HEK-293T cells ectopically expressing apoE (maroon). The infectivity was assessed after transduction of Huh-7.5 cells pre-transfected with NP+L expression plasmids, by flow cytometry at 24h p.t. for GFP minigenome. N=4 independent experiments



**Supplementary Figure 3. Gating strategy for LDL-R cell surface staining.**

(a) The population of viable cells was first identified by creating a forward vs. side scatter plot. (b) The population identified in (a) was then then gated to isolate single cells only, by plotting the forward scatter area by height and gating for cells that display a linear relationship. (c) Cells from (b) were displayed as a histogram of the fluorescent intensity of the fluorophore of interest. Strategy depicted here refers to Fig. 2a. Same strategy was used for Fig. 7.



**Supplementary Figure 4. Gating strategy for apoE intracellular staining.**

(a) The population of viable cells was first identified by creating a forward vs. side scatter plot. (b) The population identified in (a) was then then gated to isolate single cells only, by plotting the forward scatter area by height and gating for cells that display a linear relationship. (c) Cells from (b) were displayed as a histogram of the fluorescent intensity of the fluorophore of interest. Strategy depicted here refers to Fig. 4c and Fig. 6e